NASA Conference Publication 10038

NASA Computational Fluid Dynamics Conference

Volume 2: Sessions VII - XII

(NASA-CP-10038-Vol-2) NASA COMPUTATIONAL FLUID DYNAMICS CONFERENCE. VOLUME 2: SESSIONS 7-12 (NASA) 525 p CSCL 01A

N91-10646
--THRU--
N91-10901
Unclas
H1/02 0270312

Proceedings of a conference held at Ames Research Center Moffett Field, California March 7-9, 1989

NASA

NASA Conference Publication 10038

NASA Computational Fluid Dynamics Conference

Volume 2 : Sessions VII - XII

ORIGINAL CONTAINS
COLOR ILLUSTRATIONS

Proceedings of a conference sponsored by the Aerodynamics Division, Office of Aeronautics and Space Technology, NASA, held at Ames Research Center Moffett Field, California March 7-9, 1989

NASA

National Aeronautics and
Space Administration

Ames Research Center
Moffett Field, California

1989

TABLE OF CONTENTS — VOLUME 2

PREFACE ix

PANEL SESSION SUMMARY xiii

CONFERENCE COMMITTEE xv

CONFERENCE PROGRAM xvii

PAPERS

Session VII (Hypersonics/NASP) 1
A Comparative Study of Navier-Stokes Codes for High-Speed Flows
D. Rudy, J. Thomas, A. Kumar, P. Gnoffo, and S. Chakravarthy 3
Modeling of High Speed Chemically Reacting Flow Fields
J. Drummond, M. Carpenter, and H. Kamath 19
Three-Dimensional Calculation of Supersonic Reacting Flows Using an LU Scheme
S. Yu, P. Tsai, and J. Shuen 43
Progress in Computing Nozzle/Plume Flowfields
S. Ruffin, E. Venkatapathy, W. Feiereisen, and S. Lee 59
Application of CFD Codes for the Simulation of Scramjet Combustor Flowfields
T. Chitsomboon and G. Northam 75
Hypersonic CFD Applications at NASA Langley Using CFL3D and CFL3DE
P. Richardson 91

Session VIII (Space Shuttle) 115
Numerical Aerodynamic Simulation of the Space Shuttle Ascent Environment
J. Slotnick and F. Martin, Jr. 117
Computational Fluid Dynamics Analysis of Space Shuttle Main Propulsion Feed Line 17-Inch Disconnect Valves
M. Kandula and D. Pearce 133
Analysis of SSME HPOTP Bearing Inlet Cavity
P. McConnaughey 149
A Combined Eulerian-Lagrangian Two-Phase Analysis of the SSME HPOTP Nozzle Plug Trajectories
R. Garcia, P. McConnaughey, F. de Jong, J. Sabnis, and D. Pribik 161
Conjugate (Solid/Fluid) Computational Fluid Dynamics Analysis of the Space Shuttle Solid Rocket Motor Nozzle/Case and Case Field Joints
D. Doran, L. Keeton, P. Dionne, and A. Singhal 179

Session IX (Turbomachinery) 193
Simulation of Turbomachinery Flows
J. Adamczyk 195
Prediction of Turbine Rotor-Stator Interaction Using Navier-Stokes Methods
N. Madavan, M. Rai, and S. Gavali 205

PRECEDING PAGE BLANK NOT FILMED

Turbine Stage Aerodynamics and Heat Transfer Prediction
L. Griffin and H. McConnaughey 217
Automated Design of Controlled Diffusion Blades
J. Sanz 231
Numerical Analysis of Flow Through Oscillating Cascade Sections
D. Huff 245
Analysis of Three-Dimensional Viscous Flow in a Supersonic Throughflow Fan
R. Chima 259

Session X (STOVL) 273
Simulation of Powered-Lift Flows
W. Van Dalsem, K. Chawla, K. Roth, M. Smith, K. Rao, and T. Blum 275
A Numerical Study of the Hot Gas Environment Around a STOVL Aircraft in Ground Proximity
T. Van Overbeke and J. Holdeman 291
CFD Analysis for High Speed Inlets
T. Benson 311
The Use of a Navier-Stokes Code in the Wing Design Process
S. McMillin 321
Applications of a Transonic Wing Design Method
R. Campbell and L. Smith 343

Session XI (Algorithms and Tools) 359
An Embedded Grid Formulation Applied to Delta Wings
J. Thomas and S. Krist 361
Unstructured Mesh Solution of the Euler and Navier-Stokes Equations
T. Barth 379
3-D Unstructured Grids for the Solution of the Euler Equations
C. Gumbert, P. Parikh, S. Pirzadeh, and R. Löhner 395
Flux Splitting Algorithms for Two-Dimensional Viscous Flows with Finite-Rate Chemistry
J. Shuen and M. Liou 437
Visualization of Fluid Dynamics at NASA Ames
V. Watson 451
Computational Fluid Dynamics on a Massively Parallel Computer
D. Jespersen and C. Levit 467

Session XII (Hypersonics/AFE) 483
Conservation Equations and Physical Models for Hypersonic Air Flows Over the Aeroassist Flight Experiment Vehicle
P. Gnoffo 485
The Computation of Thermo-Chemical Nonequilibrium Hypersonic Flows
G. Candler 501
Aerodynamic Stability and Heating Analyses for the Aeroassist Flight Experiment Vehicle
J. McGary and C. Li 515

Aeroassist Flight Experiment Aerodynamics and Aerothermodynamics
E. Brewer 529
Direct Simulation of Rarefied Hypersonic Flows
J. Moss 545

APPENDIX: LIST OF ATTENDEES 559

TABLE OF CONTENTS — VOLUME 1

PREFACE ix

PANEL SESSION SUMMARY xiii

CONFERENCE COMMITTEE xv

CONFERENCE PROGRAM xvii

PAPERS

Session I (Center Overviews) 1
Computational Fluid Dynamics Program at NASA Ames Research Center
T. Holst 3
Computational Fluid Dynamics Research and Applications at NASA Langley Research Center
J. South, Jr. 35
Computational Fluid Dynamics at the Lewis Research Center: An Overview
R. Stubbs 49

Session II (Center Overviews Continued) 63
Marshall Space Flight Center CFD Overview
L. Schutzenhofer 65
Johnson Space Center CFD Overview
C. Li 95
NASA's CFD Validation Program
D. Satran 123

Session III (Transition and Turbulence) 135
Understanding Transition and Turbulence Through Direct Simulations
P. Spalart and J. Kim 137
Direct Simulation of Compressible Turbulence
T. Zang, G. Erlebacher, and M. Hussaini 151
Non Linear Evolution of a Second Mode Wave in Supersonic Boundary Layers
G. Erlebacher and M. Hussaini 167
Numerical Simulation of Nonlinear Development of Instability Waves
R. Mankbadi 183
More Accurate Predictions with Transonic Navier-Stokes Methods Through Improved Turbulence Modeling
D. Johnson 193

Session IV (CFD Codes) 205
Recent Advances in Runge-Kutta Schemes for Solving 3-D Navier-Stokes Equations
V. Vatsa, B. Wedan, and R. Abid 207

PRECEDING PAGE BLANK NOT FILMED

VOLUME 1 (Concluded)

Computations of Three-Dimensional Steady and Unsteady Viscous Incompressible Flows
D. Kwak, S. Rogers, S. Yoon, M. Rosenfeld, and L. Chang 223
SAGE: A 2-D Self-Adaptive Grid Evolution Code and Its Application in Computational Fluid Dynamics
C. Davies, E. Venkatapathy, and G. Deiwert 239
Time Dependent Viscous Incompressible Navier-Stokes Equations
J. Goodrich 255
CFD for Applications to Aircraft Aeroelasticity
G. Guruswamy 271
Application of Unstructured Grid Methods to Steady and Unsteady Aerodynamic Problems
J. Batina 287

Session V (Fighter Aircraft) 309
Grid Generation and Inviscid Flow Computation about Aircraft Geometries
R. Smith 311
A Zonal Navier-Stokes Methodology for Flow Simulation about a Complete Aircraft
J. Flores 327
Numerical Simulation of F-18 Fuselage Forebody Flows at High Angles of Attack
L. Schiff, R. Cummings, R. Sorenson, and Y. Rizk 345
Navier-Stokes Solutions about the F/A-18 Forebody-LEX Configuration
F. Ghaffari, J. Luckring, J. Thomas, and B. Bates 361
Navier-Stokes Solutions for Flows Related to Store Separation
O. Baysal, R. Stallings, Jr., and E. Plentovich 385
TranAir: Recent Advances and Applications
M. Madson 411

Session VI (Rotorcraft) 429
Numerical Simulation of Rotorcraft
W. McCroskey, J. Baeder, R. Border, E. Duque, G. Srinivasan and S. Stanaway 431
Calculation of the Rotor Induced Download on Airfoils
C. Lee 447
Three-Dimensional Viscous Drag Prediction for Rotor Blades
C. Chen 459
Progress Toward the Development of an Airfoil Icing Analysis Capability
M. Potapczuk, C. Bidwell, B. Berkowitz 473
The Breakup of Trailing-Line Vortices
D. Jacqmin 489

APPENDIX: LIST OF ATTENDEES 495

PREFACE

This publication is a collection of the presentations given at the NASA Computational Fluid Dynamics (CFD) Conference held at NASA Ames Research Center, Moffett Field, California, March 7-9, 1989. The objectives of the conference were to disseminate CFD research results to industry and university CFD researchers, to promote synergy among NASA CFD researchers, and to permit feedback from researchers outside NASA on issues pacing the discipline of CFD. The focus of the conference was on the application of CFD technology but also included fundamental activities. The conference was sponsored by the Aerodynamics Division, Office of Aeronautics and Space Technology (OAST), NASA Headquarters, Washington, DC 20546.

The conference consisted of twelve sessions of papers representative of CFD research conducted within NASA and three non-NASA panel sessions. For each panel session, the panel membership consisted of industry and university CFD researchers. A summary of the comments made during the panel sessions have been included in this publication.

The conference proceedings are published in two volumes. Volume 1 contains the papers presented in Sessions I-VI; Volume 2 contains those given in Sessions VII-XII. Each volume contains the same front matter, and each contains a list of attendees as an appendix.

PANEL SESSION SUMMARY

PRECEDING PAGE BLANK NOT FILMED

NASA CFD Conference
NASA Ames Research Center
March 7-9, 1989

Panel Sessions Summary

The NASA CFD Conference was held at Ames Research Center on March 7-9, 1989. To conclude each day's presentations, a panel session with participation from the audience furnished a great deal of excellent feedback from the industry and academic communities. During the conference it was evident that the panel members proffered comments only after having spent considerable time in preparing them.

The members of the panel sessions are listed below:

March 7	P. Rubbert - Boeing Commercial Airplanes R. Melnik - Grumman Aerospace Corporation D. Whitfield - Mississippi State University
March 8	I. Bhateley - General Dynamics - Fort Worth Division R. Agarwal - McDonnell Douglas Research Laboratories R. MacCormack - Stanford University
March 9	V. Shankar - Rockwell International Science Center J. Carter - United Technologies Research Center A. Jameson - Princeton University

The crucial comments from the three panel sessions have been combined and are summarized as follows:

- NASA's CFD program is now too heavily focused on applications: program balance has swung from fundamentals (1970's) to applications (1980's)

- Three critical "needs" emerged:

  (1) More algorithm research is needed; especially for Navier-Stokes solvers with unstructured grids

  (2) More research is required on geometric modelling; need rapid, accurate, and effective surface definition techniques

  (3) More research is needed on grid generation methods with the focus on speed, efficiency, and grid quality to reduce set up time and complexity

- Developers of CFD need to understand the needs of the users; designers of aerospace vehicles have requirements that are different than the CFD researchers perceptions

- Industry needs more reliable and cost effective CFD tools

PRECEDING PAGE BLANK NOT FILMED

Additional detail comments from the three panel sessions are listed below:

- CFD has matured during the last decade and is being used to solve real problems; however, industry lacks confidence in Navier-Stokes solutions

- Industry needs codes that have been validated to increase confidence in CFD technology

- Improved communality between codes would increase usability; standards are needed

- Improved data storage, networking, data transfer, and graphics required to assimilate information provided by CFD

- Improved turbulence modeling for separated flows

- Accurate prediction of drag for complete powered aerospace vehicles

- Develop multidisciplinary CFD technology with optimization capability

- NASA must maintain focus on technology development and high risk research

- Technology transfer is not complete until design engineers are using CFD codes successfully

- Industry needs NASA to improve CFD technology for codes simpler than Navier-Stokes solvers

- NAS program has been extremely helpful to industry in transferring CFD technology

- Industry needs to be more aggressive in their use of CFD

- Improved understanding of CFD by design engineers required; cooperative programs or workshops were suggested to bring CFD researchers and designers together

- Design cycle time needs to be reduced with CFD; codes must be cost effective, reliable, and useable, and robust to work at flight Reynolds Numbers

- Improved coordination/reduced overlap of CFD applications between NASA centers

Organizing Committee

General Chairman ..... Dale Satran
Administrative Chairman ..... Paul Kutler
Deputy Administrative Chairman ..... Anthony R. Gross
Conference Coordinator ..... Lyz Dunham
Administrative Associate ..... Linda Callison
Publications ..... Betty Rogers
Budget ..... Karl Talarico
Secretary & Consultant ..... Aggie Ernst

Center Focal Points

Ames Research Center ..... Terry Holst
Langley Research Center ..... Jerry South
Lewis Research Center ..... Robert Stubbs
Marshall Space Flight Center ..... Luke Schutzenhofer
Johnson Space Center ..... C. P. Li

NASA CFD CONFERENCE

March 7-9, 1989

Ames Research Center

PROGRAM

NASA CFD Conference
NASA Ames Research Center
March 7-9, 1989

Tuesday, March 7

7:30 am	Registration
8:00 am	Welcome D. Satran - Conference Chairman K. Szalai - Ames Acting Associate Director R. Graves - OAST Aerodynamics Division Director

Session I (Center Overviews) Chairman: R. Graves

8:30 am	Ames Research Center CFD Overview by T. Holst
9:10 am	Langley Research Center CFD Overview by J. South, Jr.
9:50 am	Lewis Research Center CFD Overview by R. Stubbs
10:30 am	Break

Session II (Center Overviews Continued) Chairman: P. Kutler

10:50 am	Marshall Space Flight Center CFD Overview by L. Schutzenhofer
11:20 am	Johnson Space Center CFD Overview by C. Li
11:50 am	CFD Validation Program Overview by D. Satran
12:10 pm	Lunch

PRECEDING PAGE BLANK NOT FILMED

NASA CFD CONFERENCE PROGRAM

Session III (Transition and Turbulence) Chairman: T. Pulliam

1:10 pm	Understanding Transition and Turbulence Through Direct Simulations by P. Spalart and J. Kim
1:30 pm	Direct Simulation of Compressible Turbulence by T. Zang, G. Erlebacher, and M. Hussaini
1:50 pm	Nonlinear Evolution of a Second Mode Wave in Supersonic Boundary Layers by G. Erlebacher and M. Hussaini
2:10 pm	Numerical Simulation of Nonlinear Development of Instability Waves by R. Mankbadi
2:30 pm	More Accurate Predictions with Transonic Navier-Stokes Methods Through Improved Turbulence Modeling by D. Johnson
2:50 pm	**Break**

Session IV (CFD Codes) Chairman: J. South

3:10 pm	Recent Advances in Runge-Kutta Schemes for Solving 3-D Navier-Stokes Equations by V. Vatsa, B. Wedan, and R. Abid
3:30 pm	Computations of Three-Dimensional Steady and Unsteady Viscous Incompressible Flows by D. Kwak, S. Rogers, S. Yoon, M. Rosenfeld, and L. Chang
3:50 pm	SAGE - A Self-Adaptive Grid Evolution Code and Its Application in Computational Fluid Dynamics by C. Davies, E. Venkatapathy, and G. Deiwert
4:10 pm	Time Dependent Viscous Incompressible Navier-Stokes Equations by J. Goodrich
4:30 pm	CFD for Applications to Aircraft Aeroelasticity by G. Guruswamy
4:50 pm	Application of Unstructured Grid Methods to Steady and Unsteady Aerodynamic Problems by J. Batina
5:10 pm	Break
5:20 pm	**Panel Session Chairman: P. Rubbert - Boeing Commercial** R. Melnick - Grumman Aerospace D. Whitfield - Mississippi State
6:20 pm	Adjourn to Officer's Club
6:30 pm	Cocktail Party at Moffet Field Officer's Club

NASA CFD CONFERENCE PROGRAM

Wednesday, March 8

7:50 am Administrative Announcements

Session V (Fighter Aircraft) Chairman: T. Holst

8:00 am Grid Generation and Inviscid Flow Computation about Fighter Airplanes
by R. Smith

8:20 am A Zonal Navier-Stokes Methodology for Flow Simulation about a Complete Aircraft
by J. Flores

8:40 am Numerical Simulation of F-18 Fuselage Forebody Flows at High Angles of Attack
by L. Schiff, R. Cummings, R. Sorenson, and Y. Rizk

9:00 am Navier-Stokes Solutions about the F-18 Forebody-Strake Configuration
by F. Ghaffari, J. Luckring, and J. Thomas

9:20 am Navier-Stokes Solutions for Store Separation and Related Problems
by O. Baysal, R. Stallings, Jr., and E. Plentovich

9:40 am TRANAIR: Recent Advances and Applications
by M. Madison

10:00 am Break

Session VI (Rotorcraft) Chairman: W. McCroskey

10:20 am Computations of Airloads and Acoustics of Rotorcraft
by W. McCroskey, J. Baeder, C. Chen, E. Duque, and G. Srinivasan

10:40 am Calculation of Rotor Induced Download on Airfoils
by C. Lee

11:00 am Three-Dimensional Viscous Drag Prediction for Rotor Blades
by C. Chen

11:20 am Progress Toward the Development of an Airfoil Icing Analysis Capability
by M. Potapczuk, C. Bidwell, B. Berkowitz

11:40 am The Breakup of Trailing-Line Vortices
by D. Jacqmin

12:00 pm Lunch

NASA CFD CONFERENCE PROGRAM

Session VII (Hypersonics/NASP) Chairman: D. Dwoyer

1:00 pm A Comparative Study of Navier-Stokes Codes for High-Speed Flows
by D. Rudy, J. Thomas, A. Kumar, P. Gnoffo, and S. Chakravarthy

1:20 pm Modeling of High Speed Chemically Reacting Flow Fields
by J. Drummond, M. Carpenter, and H. Kamath

1:40 pm Three-Dimensional Simulation of Supersonic Reacting Flows with Finite Rate Chemistry
by S. Yu, J. Shuen, and P. Tsai

2:00 pm Progress in Computing Nozzle/Plume Flowfields
by S. Ruffin, E. Venkatapathy, W. Feiereisen, and S. Lee

2:20 pm Application of CFD Codes for the Simulation of Scramjet Combustor Flow Fields
by T. Chitsomboon and G. Northam

2:40 pm Hypersonic CFD Applications at NASA Langley Using CFL3D and CFL3DE
by P. Richardson

3:00 pm Break

Session VIII (Space Shuttle) Chairman: L. Schutzenhofer

3:20 pm Comparison of the ARC Shuttle Ascent Simulations with Wind Tunnel and Flight Data
by J. Slotnick and F. Martin, Jr.

3:40 pm Computational Fluid Dynamics Analysis of Space Shuttle Main Propulsion Feed Line 17-Inch Disconnect Valves
by M. Kandula and D. Pearce

4:00 pm Analysis of SSME HPOTP Bearing Inlet Cavity
by P. McConnaughey

4:20 pm A Combined Eulerian-Lagrangian Two-Phase Analysis of the SSME HPOTP Nozzle Plug Trajectories
by R. Garcia, P. McConnaughey, F. de Jong, J. Sabnis, and D. Pribik

4:40 pm Conjugate (Solid/Fluid) Computational Fluid Dynamics Analysis of the Space Shuttle Solid Rocket Motor Nozzle-to-Case and Case-to-Field Joints
by D. Doran, L. Keeton, P. Dionne, and A. Singhal

5:00 pm Break

5:10 pm **Panel Session Chairman: I. Bhateley - General Dynamics**
R. Agarwal - McDonnell Douglas
R. MacCormack - Stanford University

6:10 pm Adjourn to Banquet at Santa Clara Marriott Hotel

7:00 pm Banquet at Marriott Hotel

NASA CFD CONFERENCE PROGRAM

Thursday, March 9

7:50 am Administrative Announcements

Session IX (Turbomachinery) Chairman: R. Stubbs

8:00 am Simulation of Turbomachinery Flows
by J. Adamczyk

8:20 am Prediction of Turbine Rotor-Stator Interaction Using Navier-Stokes Methods
by N. Madavan, M. Rai, and S. Gavali

8:40 am Turbine Stage Aerodynamics and Heat Transfer Prediction
by L. Griffin and H. McConnaughey

9:00 am Automated Design of Controlled Diffusion Blades
by J. Sanz

9:20 am Numerical Analysis of Flow Through Oscillating Cascade Sections
by D. Huff

9:40 am Numerical Analysis of Three-Dimensional Viscous Internal Flows
by R. Chima and J. Yokota

10:00 am Break

Session X (STOVL) Chairman: M. Liou

10:20 am Simulators of PoweredLift Flows
by W. Van Dalsem, K. Chawla, M. Smith, K. Rao, and T. Blum

10:40 am A Numerical Study of the Hot Gas Environment Around a STOVL Aircraft in Ground Proximity
by T. Van Overbeke and J. Holdeman

11:00 am CFD Analysis for High Speed Inlets
by T. Benson

11:20 am The Use of a Navier-Stokes Code in the Wing Design Process
by S. McMillin

11:40 am Application of a Transonic Wing Design Method
by R. Campbell and L. Smith

12:00 pm Lunch

NASA CFD CONFERENCE PROGRAM

Session XI (Algorithms and Tools) Chairman: J. Steger

1:00 pm	An Embedded Grid Formulation Applied to Delta Wings by J. Thomas and S. Taylor
1:20 pm	Unstructured Mesh Solution of the Euler and Navier-Stokes Equations by T. Barth
1:40 pm	3-D Unstructured Grids for the Solution of the Euler Equations by C. Gumbert, P. Parikh, S. Pirzadeh, and R. Lohner
2:00 pm	Flux Splitting Algorithms for Two-Dimensional Real Gas Flows by J. Shuen and M. Liou
2:20 pm	Visualization of Fluid Dynamics at NASA Ames by V. Watson
2:40 pm	Computational Fluid Dynamics on a Massively Parallel Computer by D. Jespersen and C. Levit
3:00 pm	Break

Session XII (Hypersonics/AFE) Chairman: C. Li

3:20 pm	Conservation Equations and Physical Models for Hypersonic Air Flows Over the Aeroassist Flight Experiment Vehicle by P. Gnoffo
3:40 pm	The Computation of Thermo-Chemical Nonequilibrium Hypersonic Flows by G. Candler
4:00 pm	Aerodynamic Heating and Stability Analyses for Aeroassist Flight Experiment Vehicle by J. McGary and C. Li
4:20 pm	Aeroassist Flight Experiment Aerodynamics and Aerothermodynamics by E. Brewer
4:40 pm	Direct Simulation of Rarefied Hypersonic Flows by J. Moss
5:00 pm	Break
5:10 pm	**Panel Session Chairman: V. Shankar - Rockwell** J. Carter - United Technology A. Jameson - Princeton University
6:10 pm	Conference Adjourned

SESSION VII

HYPERSONICS/NASP

Chairman:
Douglas L. Dwoyer
Chief, Facilities Planning Office
NASA Langley Research Center

N91-10869

A COMPARATIVE STUDY OF NAVIER-STOKES CODES FOR HIGH-SPEED FLOWS

David H. Rudy, James L. Thomas, Ajay Kumar, Peter Gnoffo
NASA Langley Research Center

and

Sukumar R. Chakravarthy
Rockwell International Science Center

A comparative study has been made with four different codes for solving the compressible Navier-Stokes equations using three different test problems. The first of these cases was hypersonic flow through the P8 inlet, which represents inlet configurations typical of a hypersonic airbreathing vehicle. The free-stream Mach number in this case was 7.4. This 2-D inlet was designed to provide an internal compression ratio of 8. Initial calculations were made using two state-of-the-art finite-volume upwind codes, CFL3D and USA-PG2, as well as NASCRIN, a code which uses the unsplit finite-difference technique of MacCormack. All of these codes used the same algebraic eddy-viscosity turbulence model. In the experiment, the cowl lip was slightly blunted; however, for the computations, a sharp cowl leading edge was used to simplify the construction of the grid. Although the overall features of the inlet flow field were predicted reasonably well, discrepancies between the computed and experimental profiles of pitot pressure and total temperature were found for all of the codes. Calculations were then made with the two finite-volume upwind codes using a patched-grid approach which allowed the use of a blunt cowl tip. This produced a more accurate location for the cowl leading-edge shock and thus an improvement in the location of the resultant shock reflections within the inlet.

The second test problem was the supersonic (Mach 3.0) flow in a three-dimensional corner formed by the intersection of two wedges with equal wedge angles of 9.48 degrees. The flow in such a corner is representative of the flow in the corners of a scramjet inlet. Calculations were made for both laminar and turbulent flow and compared with experimental data. The three-dimensional versions of the three codes used for the inlet study (CFL3D, USA-PG3, and SCRAMIN, respectively) were used for this case. For the laminar corner flow, a fourth code, LAURA, which also uses recently-developed upwind technology, was also utilized. It was found that the complex flow structure was qualitatively predicted by all of the codes. Furthermore, with a sufficiently-refined grid, all four codes gave identical results for the laminar case.

The final test case is the two-dimensional hypersonic flow over a compression ramp. In this case, the flow is laminar with a free-stream Mach number of 14.1. In the experiment, the ramp angle was varied to change the strength of the ramp shock and the extent of the viscous-inviscid interaction. Calculations have been made for the 24-degree ramp configuration which produces a large separated-flow region that extends upstream of the corner. All of the codes predicted the strong-interaction structure observed experimentally. However, a wide variation in the predicted extent of separation was found for the grid that was used.

PRECEDING PAGE BLANK NOT FILMED

DESCRIPTION OF CODES

- CFL3D
  - Written by James L. Thomas
  - Upwind-biased Roe scheme for pressure and convective terms
  - Central-difference treatment of viscous terms
  - Approximate-factorization time differencing

- USA-PG3
  - Written by Sukumar Chakravarthy
  - Roe scheme for convective and pressure terms
  - Central-difference treatment of viscous terms
  - Approximate-factorization time differencing

DESCRIPTION OF CODES

- LAURA
  - Written by Peter A. Gnoffo
  - Symmetric TVD scheme with Roe averaging
  - Alternating directional-sweep Gauss-Seidel relaxation
  - Laminar flow only at present time

- NASCRIN and SCRAMIN
  - Written by Ajay Kumar
  - Explicit unsplit MacCormack scheme

TEST PROBLEMS

- P8 Inlet
  - 2-D, transitional
  - Experimental data: Gnos et al.

- Symmetric-wedge corner
  - 3-D, laminar and turbulent
  - Experimental data: West and Korkegi

- Hypersonic compression corner
  - 2-D, laminar
  - Experimental data: Holden and Moselle

P8 INLET

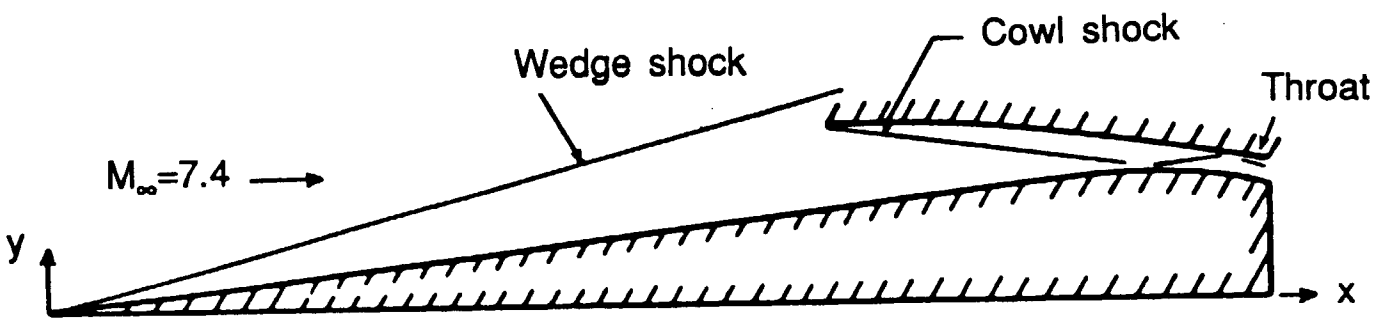

GRIDS NEAR INLET ENTRANCE

Patched-grid computations

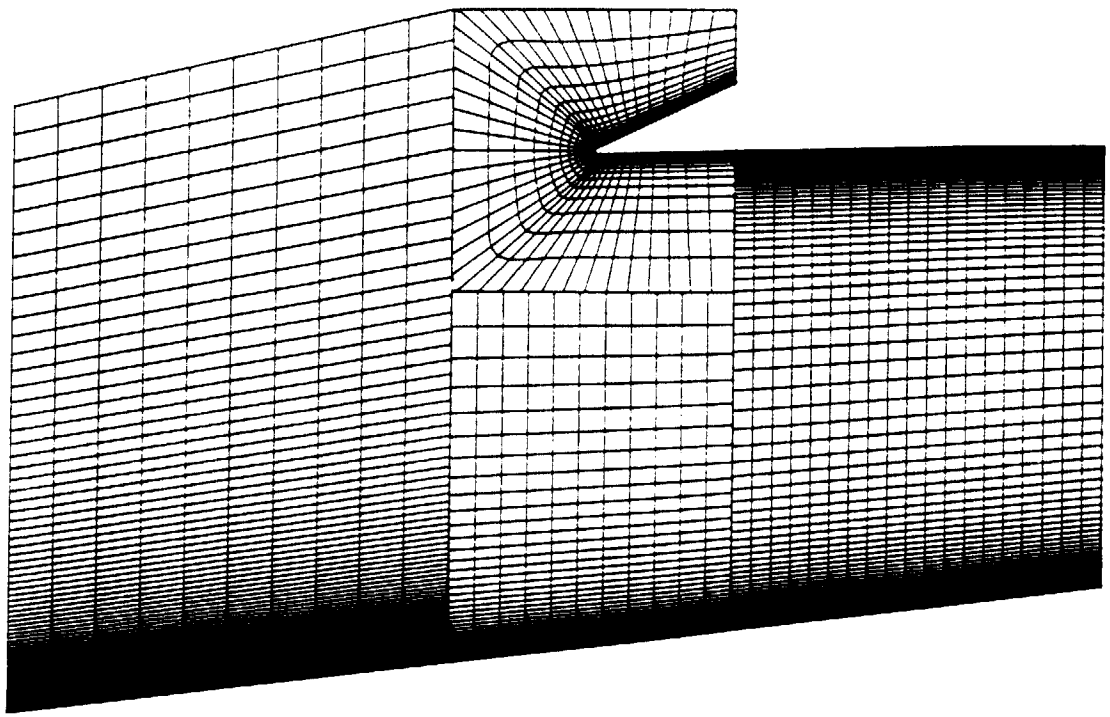

COMPUTED INLET PRESSURE

USA-PG2
Transitional computation
Sharp cowl leading edge

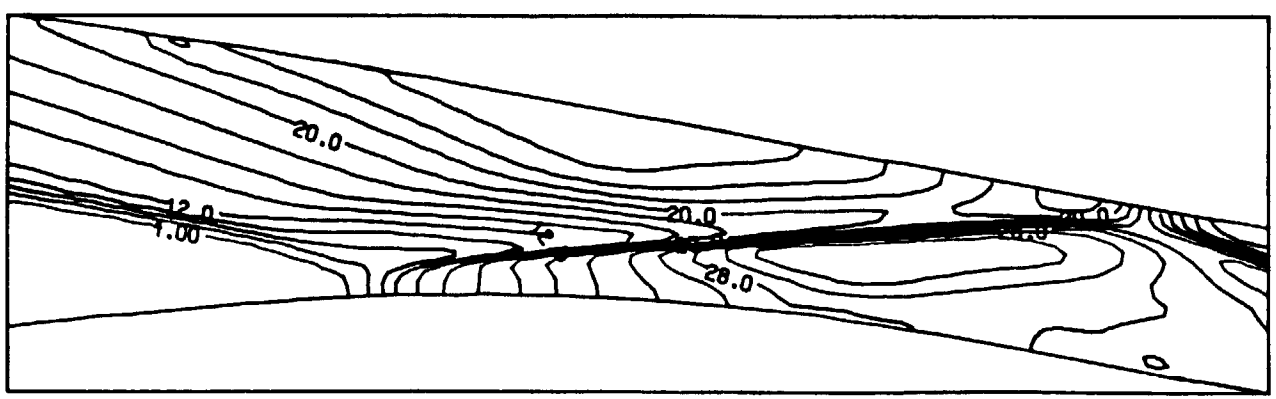

CENTERBODY PRESSURE

Blunt cowl leading edge

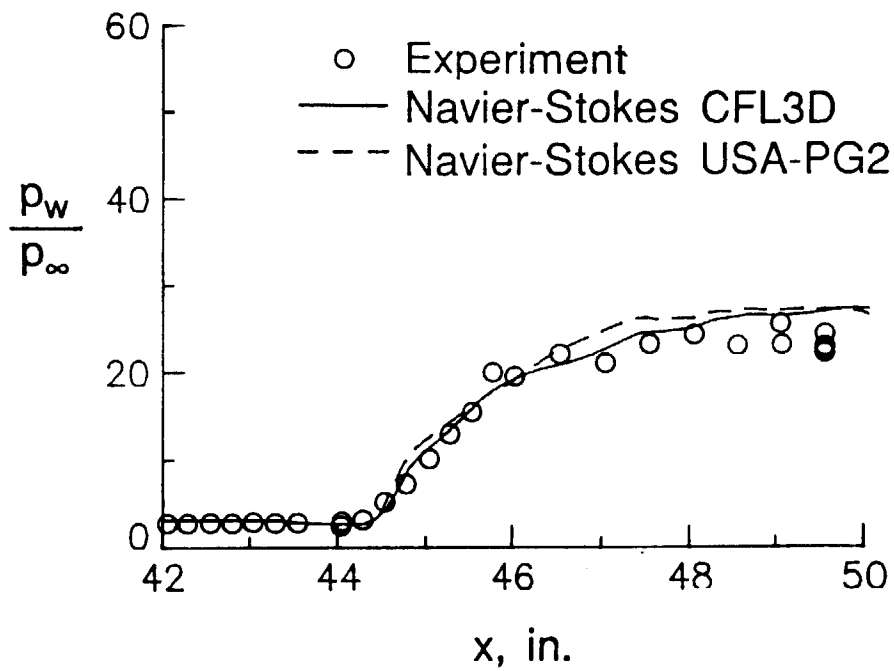

PITOT PRESSURE PROFILE

x = 40.9 in.
Blunt cowl leading edge

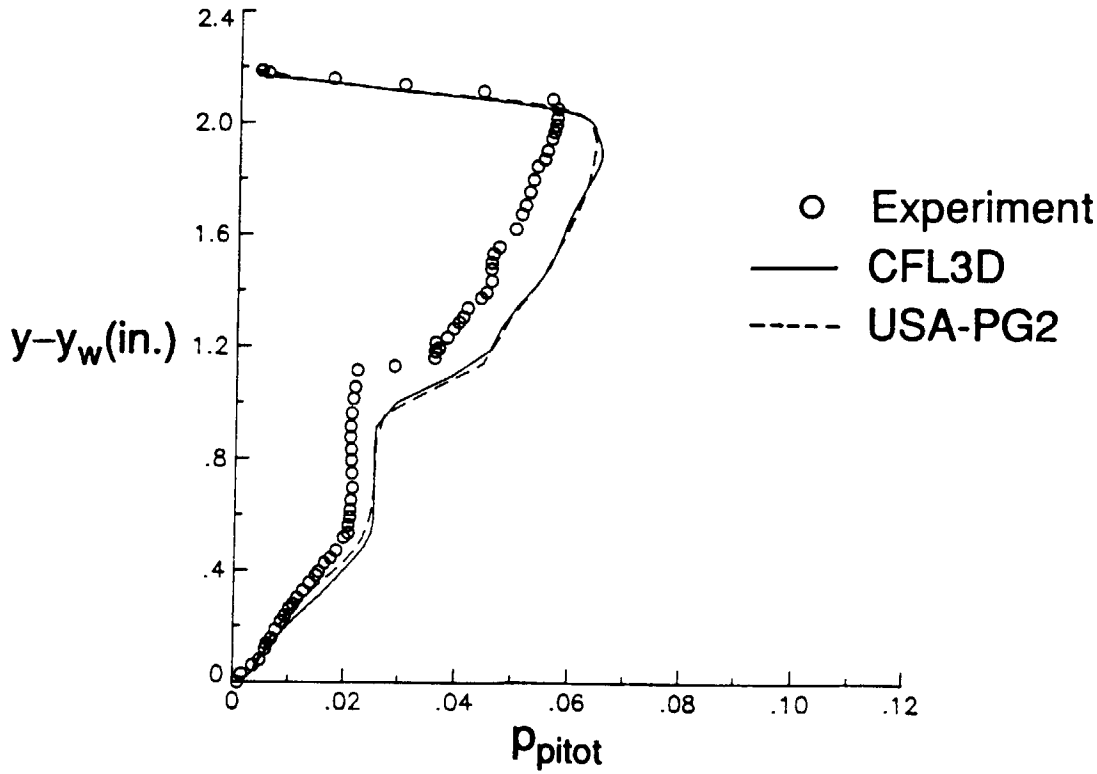

CORNER FLOW

M_∞=3.0

1 Corner shock
2 Internal shock
3 Slip line
4 Wall shock

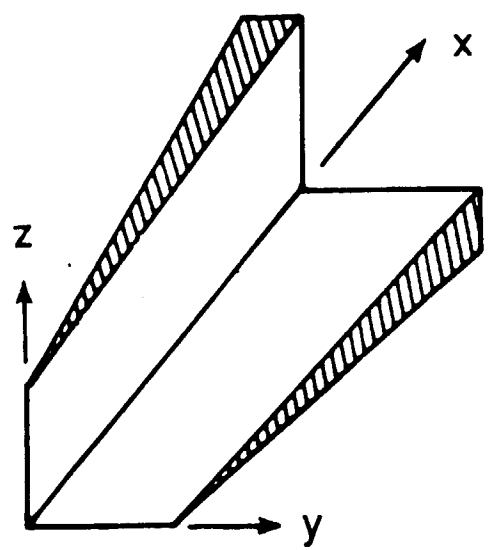

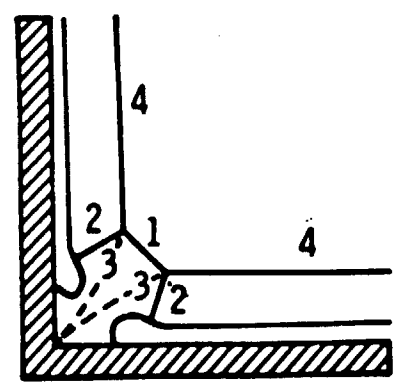

LAMINAR CORNER FLOW

x = 0.0733 m.

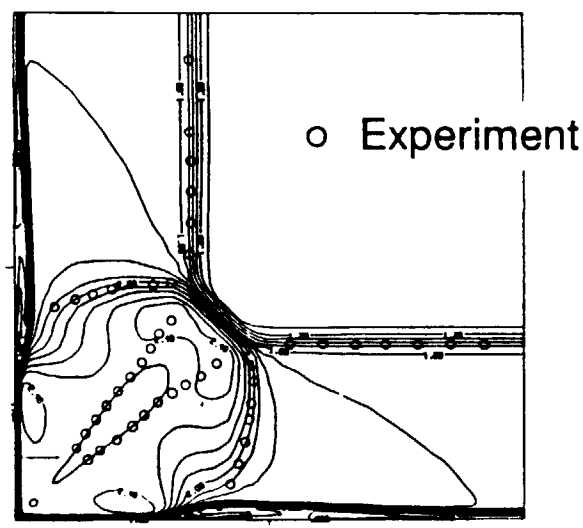

Density contours

USA-PG3

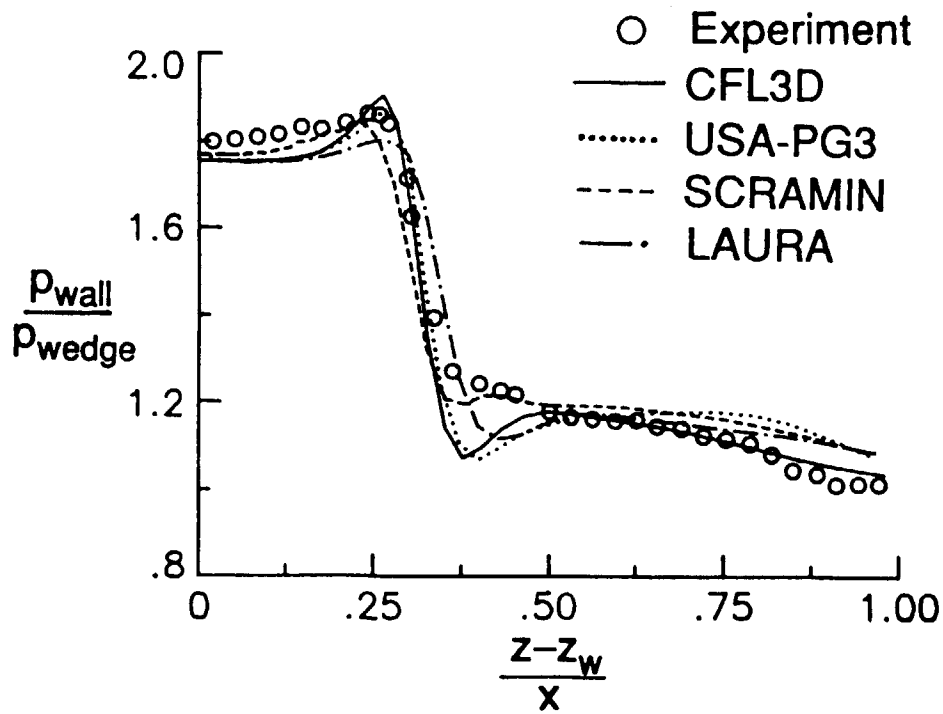

Sidewall pressure

LAMINAR CORNER FLOW

Sidewall pressure

x = 0.0733 m.

Conical flow

121 x 121 grid

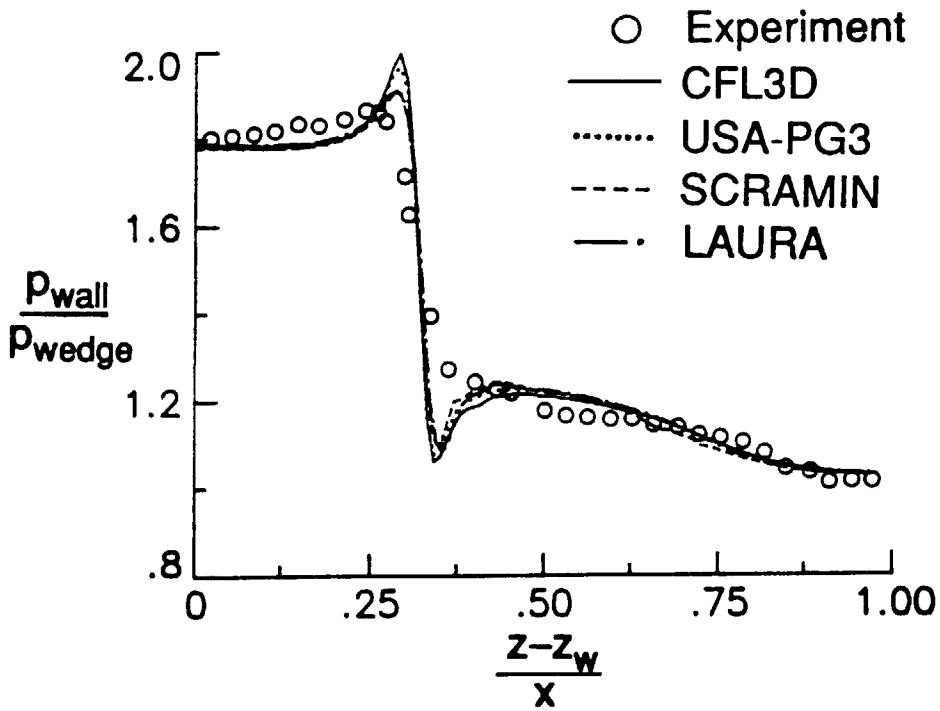

HYPERSONIC COMPRESSION CORNER

Streamlines
24-degree ramp

USA-PG2

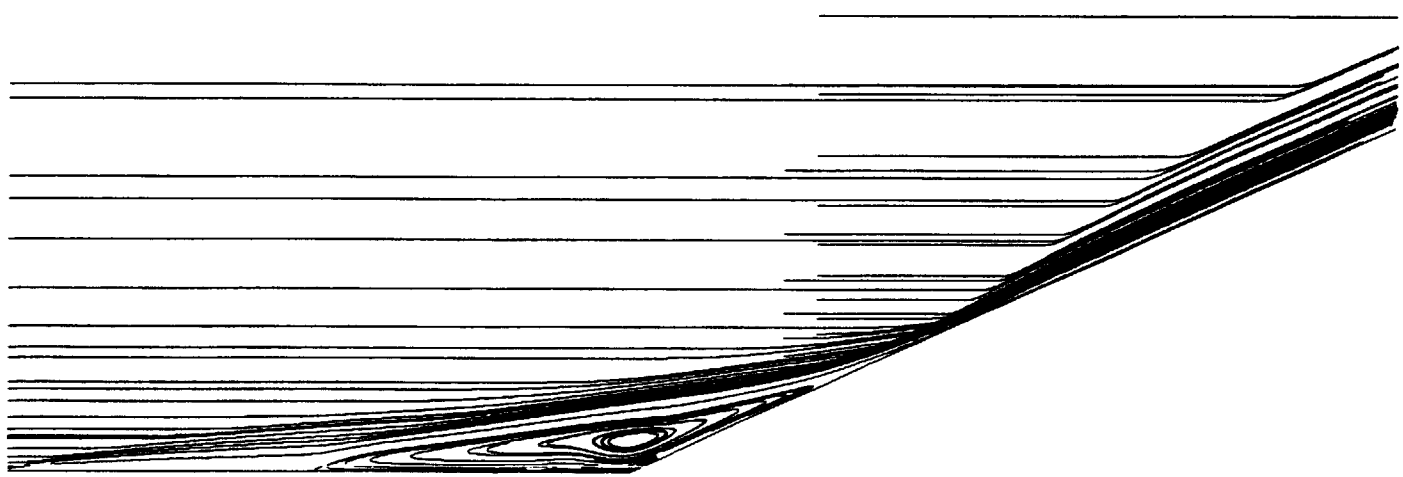

SURFACE PRESSURE

24° ramp
201 x 60 grid

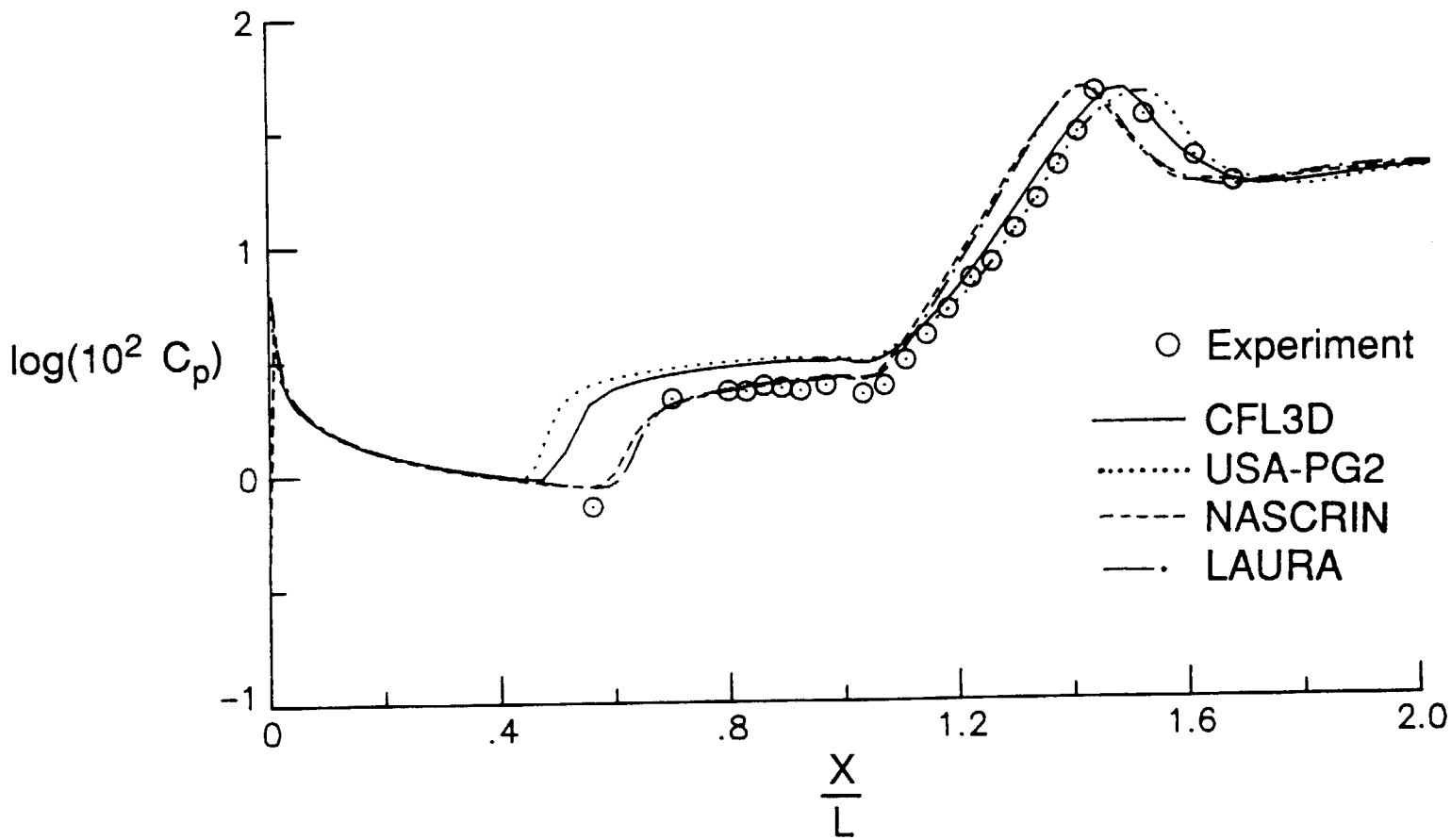

SKIN FRICTION

24° ramp
201 x 60 grid

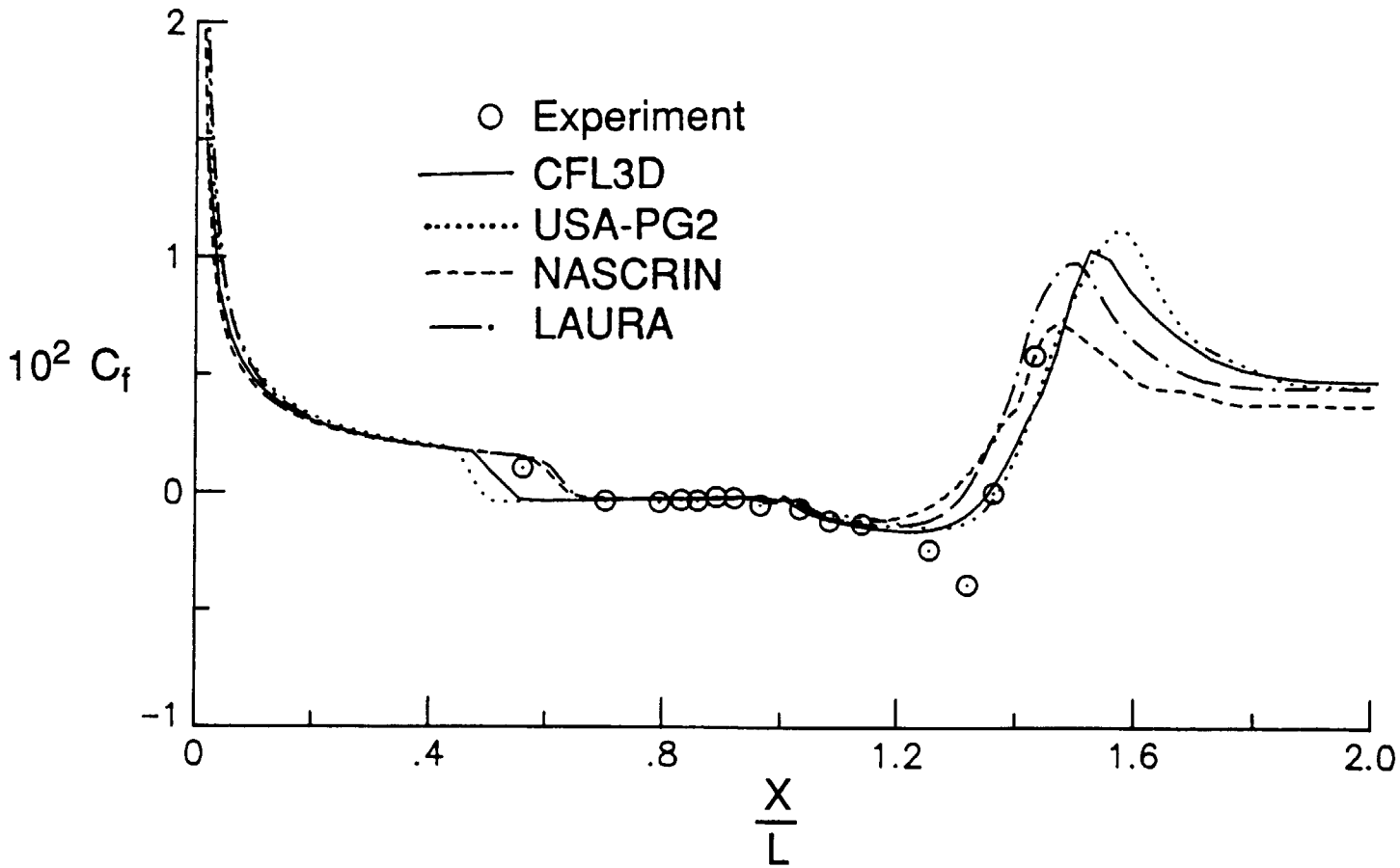

SUMMARY AND CONCLUSIONS

- A comparative study of four computer codes for the Navier-Stokes equations was performed using three test problems for high-speed flow.

- For the P8 inlet, good agreement was found between the codes. Differences between computation and experiment were possibly due to experimental effects not included.

- Flow structure in 3-D corner was predicted well by all of the codes. Good agreement was found between the solutions for all four codes.

- For the hypersonic compression ramp, the codes predicted the strong interaction structure observed experimentally. A wide variation in the predicted extent of separation was found.

N91-10870

MODELING OF HIGH SPEED CHEMICALLY REACTING FLOW-FIELDS

J. P. Drummond, M. H. Carpenter* and H. Kamath*
NASA Langley Research Center
Hampton, VA 23665

ABSTRACT

The SPARK3D and SPARK3D-PNS computer programs have been developed to model 3-D supersonic, chemically reacting flow-fields. The SPARK3D code is a full Navier-Stokes solver, and is suitable for use in scramjet combustors and other regions where recirculation may be present. The SPARK3D-PNS is a parabolized Navier-Stokes solver and provides an efficient means of calculating steady-state combustor far-fields and nozzles. Each code has a generalized chemistry package, making modeling of any chemically reacting flow possible.

Research activities by the Langley group range from addressing fundamental theoretical issues to simulating problems of practical importance. Algorithmic development includes work on higher order and upwind spatial difference schemes. Direct numerical simulations employ these algorithms to address the fundamental issues of flow stability and transition, and the chemical reaction of supersonic mixing layers and jets. It is believed that this work will lend greater insight into phenomenological model development for simulating supersonic chemically reacting flows in practical combustors. Currently, the SPARK3D and SPARK3D-PNS codes are used to study problems of engineering interest, including various injector designs and 3-D combustor-nozzle configurations. Examples, which demonstrate the capabilities of each code are presented.

*Analytical Services and Materials, Inc.

OVERVIEW

- GROUP OBJECTIVES
- DESCRIPTION OF 2 AND 3-D CODES
- 3-D FULL NAVIER-STOKES
- 3-D PARABOLIZED NAVIER-STOKES
- 2 AND 3-D MIXING ENHANCEMENT
- CONCLUSIONS AND DIRECTIONS

OBJECTIVES

- THEORETICAL ISSUES
  - NUMERICS FOR SUPERSONIC CHEMICALLY REACTING FLOWS
    - Numerical Efficiency
    - Numerical Accuracy
    - Robustness
  - PHYSICAL ISSUES
    - Mixing Enhancement and Combustion
    - Transition to Turbulence
    - Phenomenological Turbulence Models
- APPLICATIONS
  - 3-D COMBUSTORS AND NOZZLES
    - SPARK3D
    - SPARK3D-PNS

SPARK 3-D

- 3-D NAVIER-STOKES AND CHEMISTRY
- FULLY ELLIPTIC STRUCTURE
- VISCOUS OR INVISCID CAPABILITIES
- TIME-ACCURATE OR LOCAL RELAXATION
- GENERALIZED CHEMISTRY ROUTINES
- LOW STORAGE FORMAT

GENERALIZED CHEMISTRY ROUTINE

- REAL GAS THERMODYNAMICS MODELS
  - POLYNOMIAL FITS FOR C_p, C_v, S, G
  - KINETIC THEORY BASED DIFFUSION MODELS
    - Sutherlands Law for μ_i and k_i
    - Wilkes law for μ and k
    - Binary or multicomponent diffusion models
- CHEMISTRY MODELS
  - FROZEN
  - EQUILIBRIUM
  - FINITE RATE CHEMISTRY (NS=9, NR=18)

NUMERICAL METHODS

- TRANSFORMED COORDINATES (ξ,η,ζ)
  - GEOMETRIC CONSERVATION LAW TERMS INCLUDED

- TEMPORAL INTEGRATION (2ND ORDER)
  - EXPLICIT FORMULATION FOR HYDRO-DYNAMIC TERMS
    - Allows local time stepping
  - EXPLICIT/IMPLICIT FORMULATION FOR CHEMICAL SOURCE TERMS

- FINITE DIFFERENCE SPATIAL DISCRETIZATION
  - STANDARD MACCORMACK (2ND ORDER)
  - GOTTLIEB MACCORMACK (4TH ORDER)
  - COMPACT MACCORMACK (4TH ORDER AT S.S.)
  - UPWIND (3RD ORDER)

CORNER FLOW

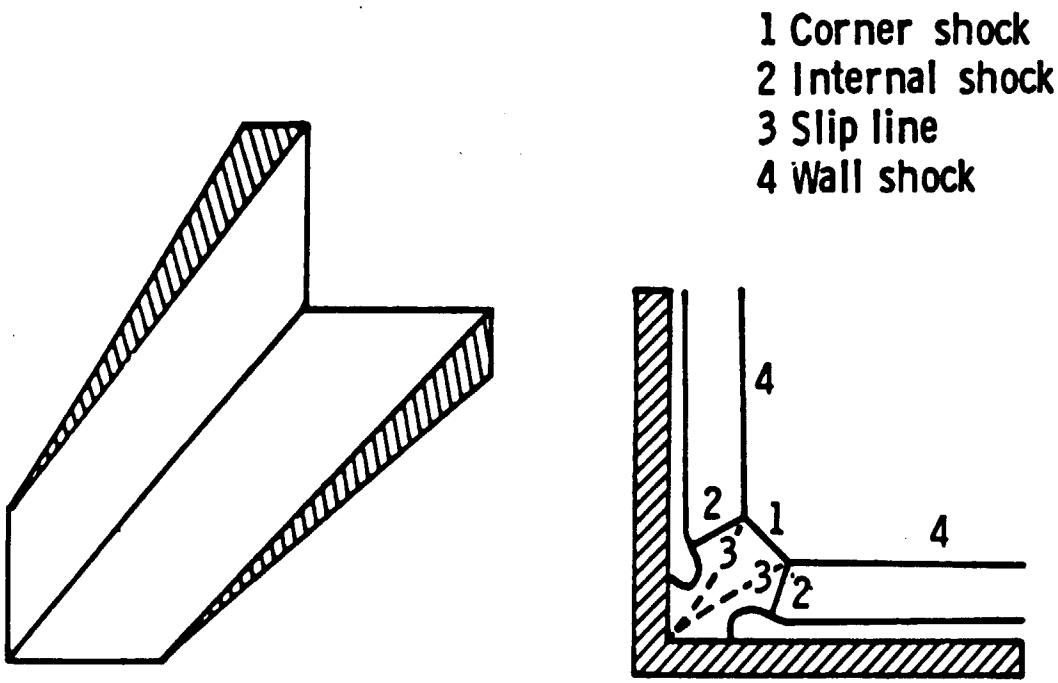

Figure 3.- Symmetric-wedge corner and schematic of corner flow.

CORNER FLOW

Symmetric-Wedge Corner

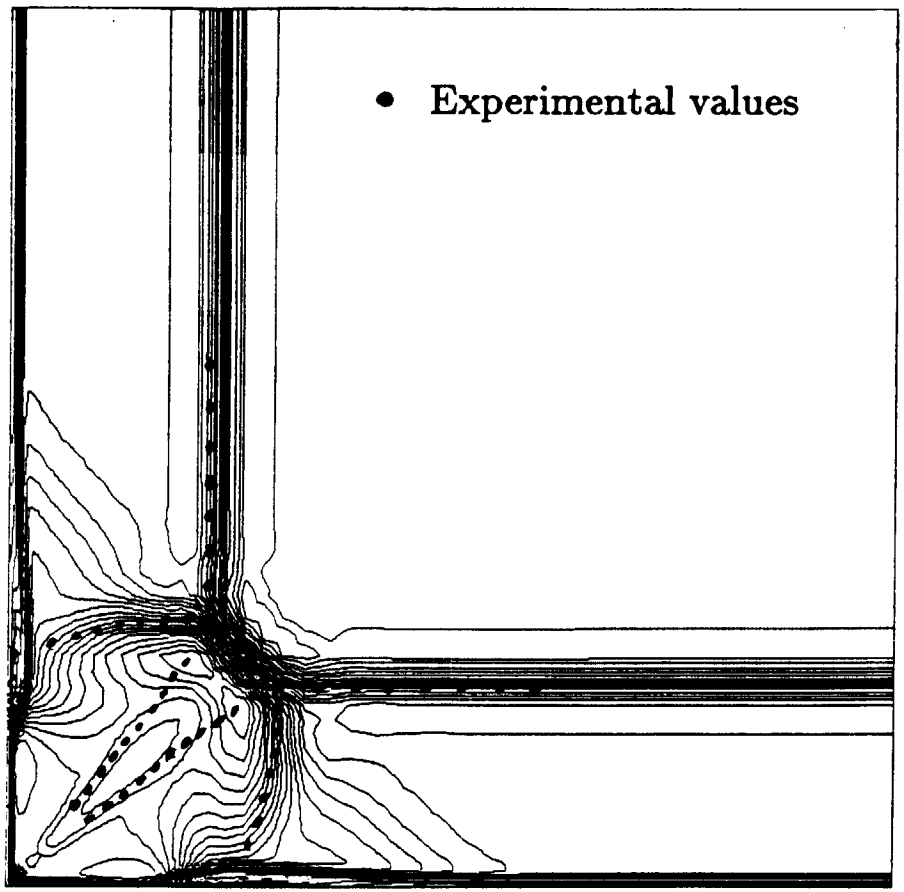

Density Contours (Laminar Flow)

REARWARD STEP

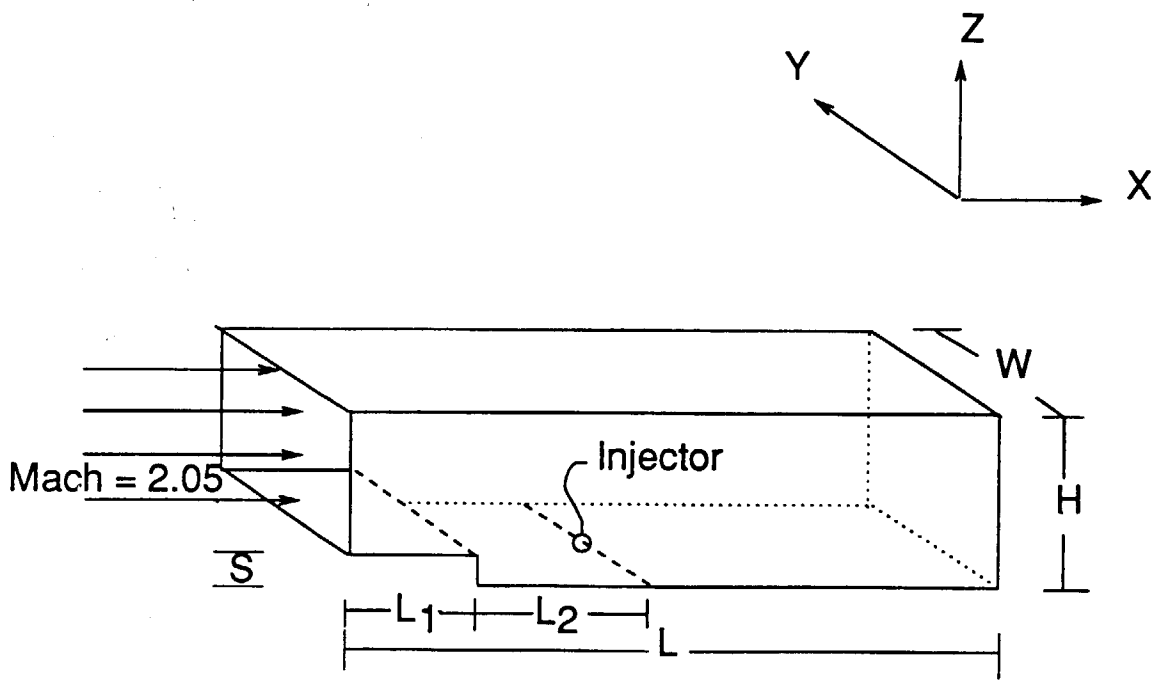

L = 7.0 cm, H = 1.8 cm, W = 2.9 cm

L_1 = 0.7 cm, L_2= 1.2 cm, S = 0.3 cm

SPARK3D
REARWARD STEP COMPARISON

Mach = 2.05

101 x 41 x 25 GRID

Qr = 0.39

JET PENETRATION IN X-Z PLANE AT Y = Y℄

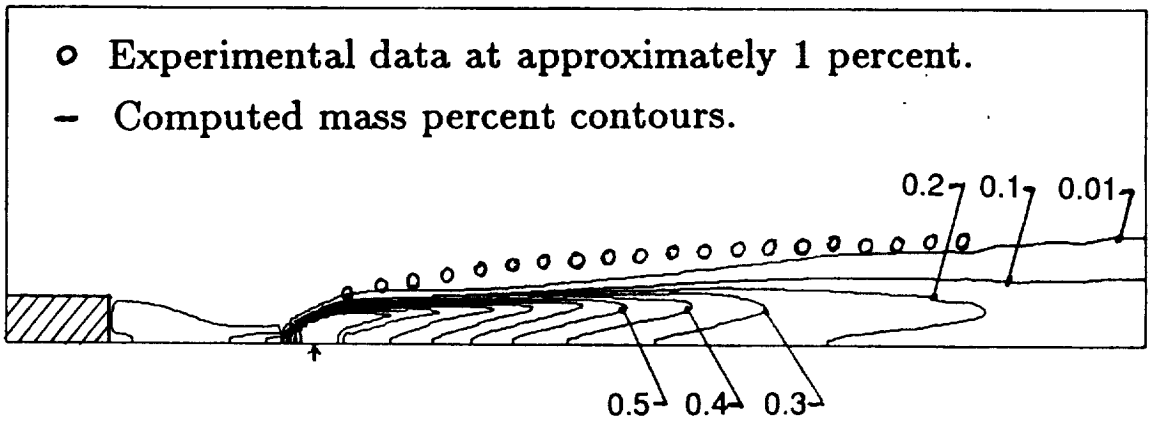

JET SPREAD IN X-Y PLANE AT Z = D

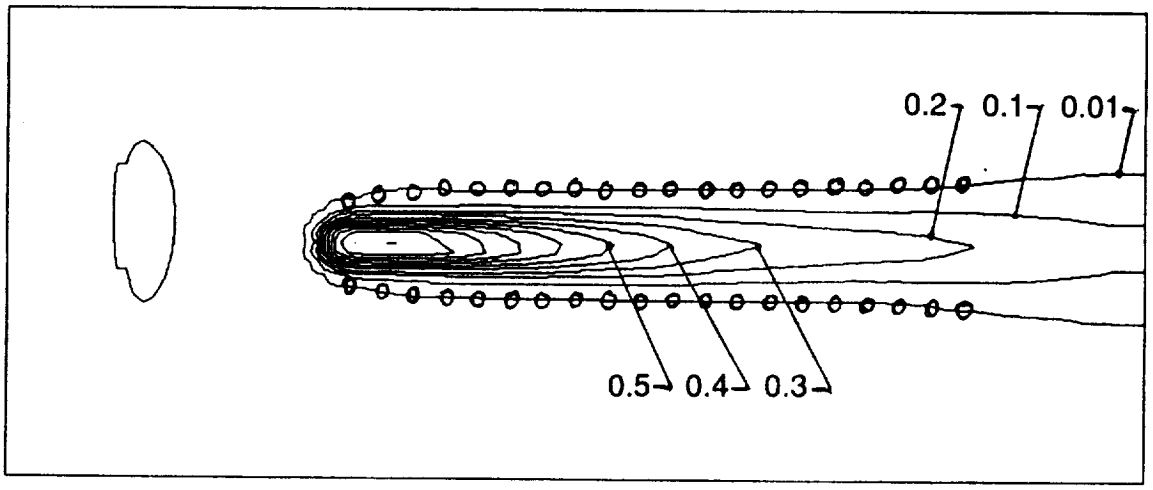

EXPERIMENTAL COMPARISON

Jet Penetration

61 x 41 x 25 GRID

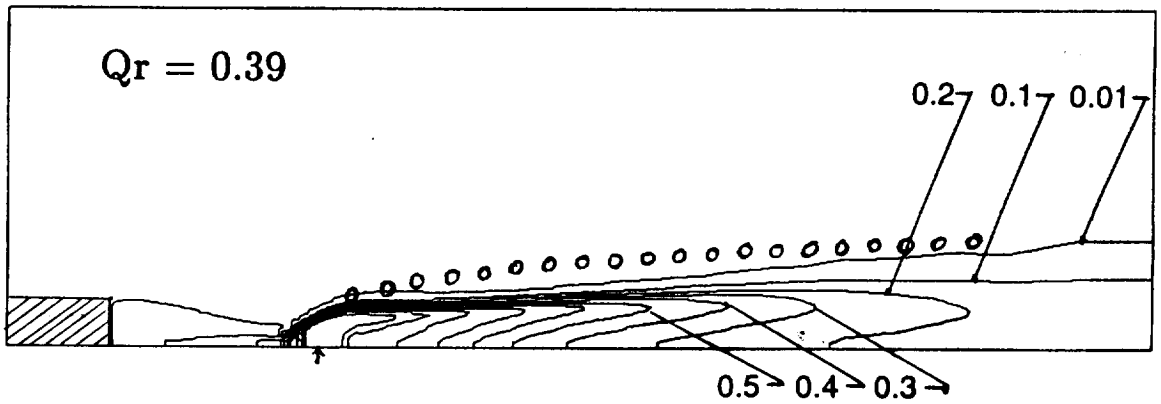

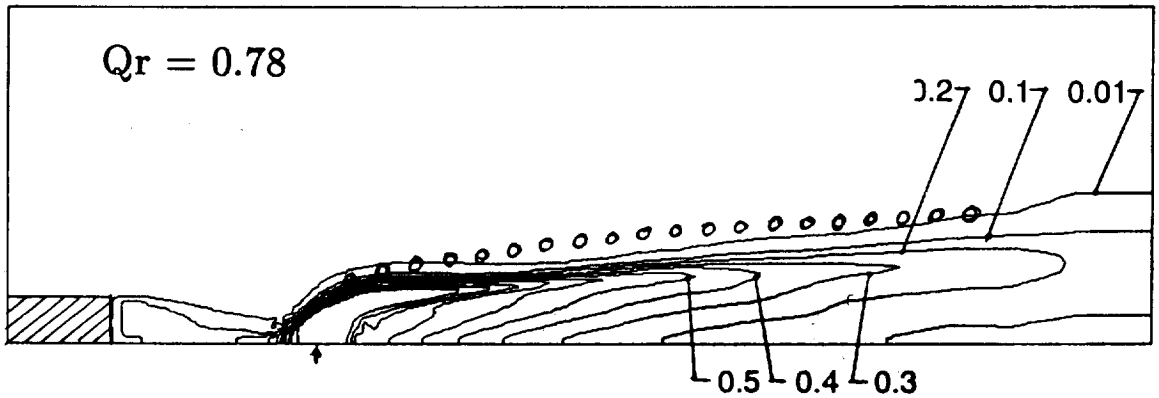

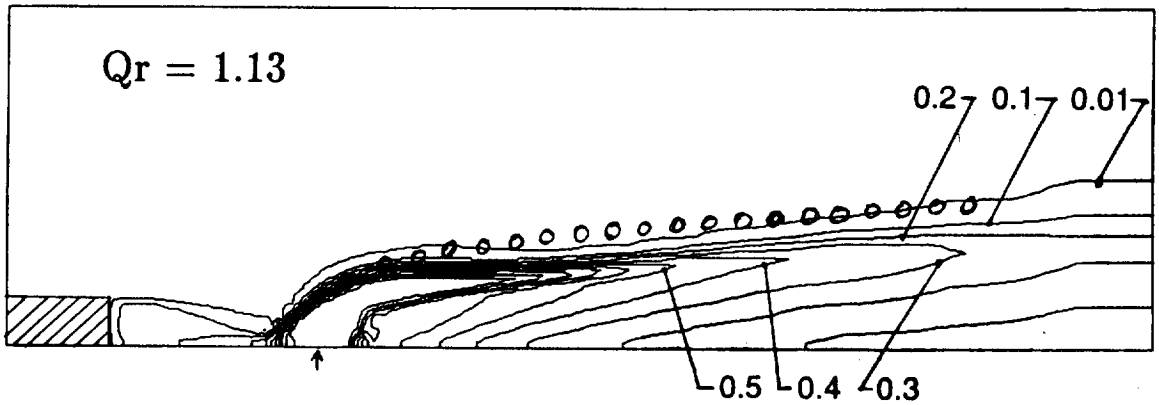

EXPERIMENTAL COMPARISON

Jet Penetration

61 x 41 x 25 GRID

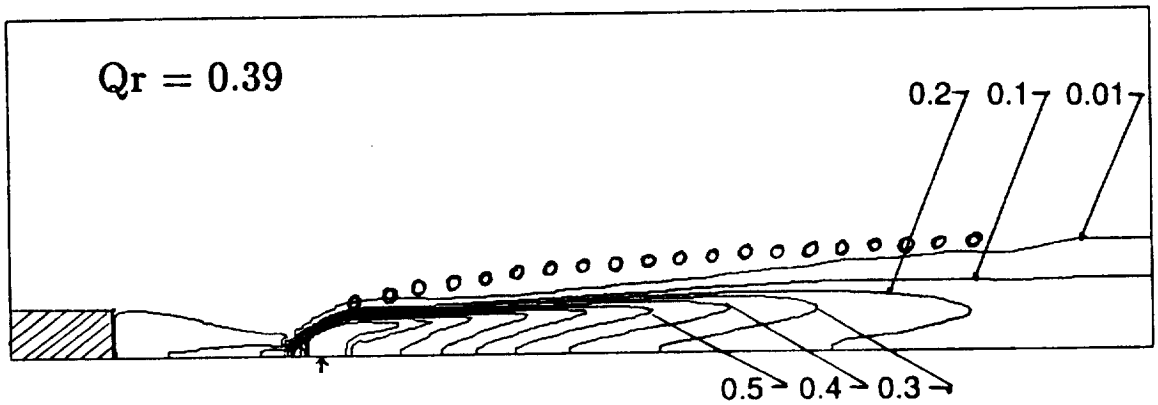

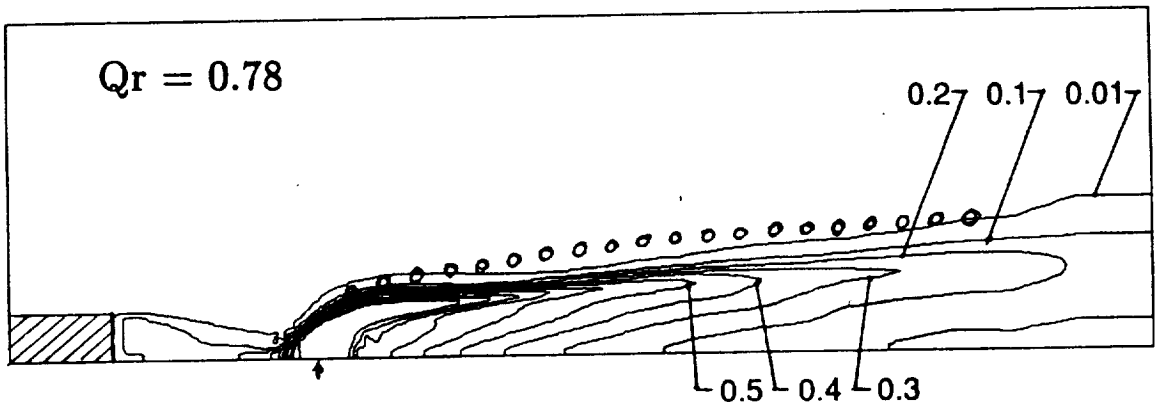

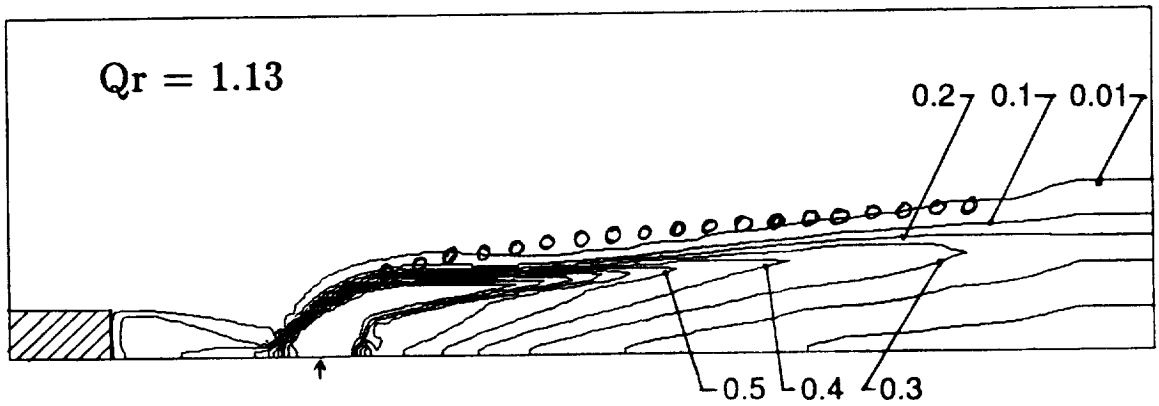

REARWARD STEP COMPARISON

Jet Spread

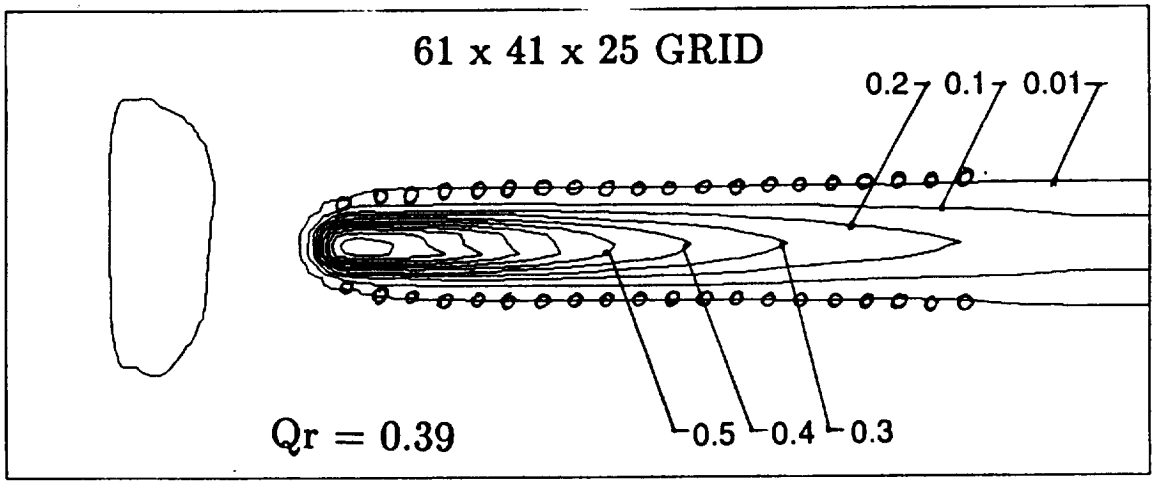

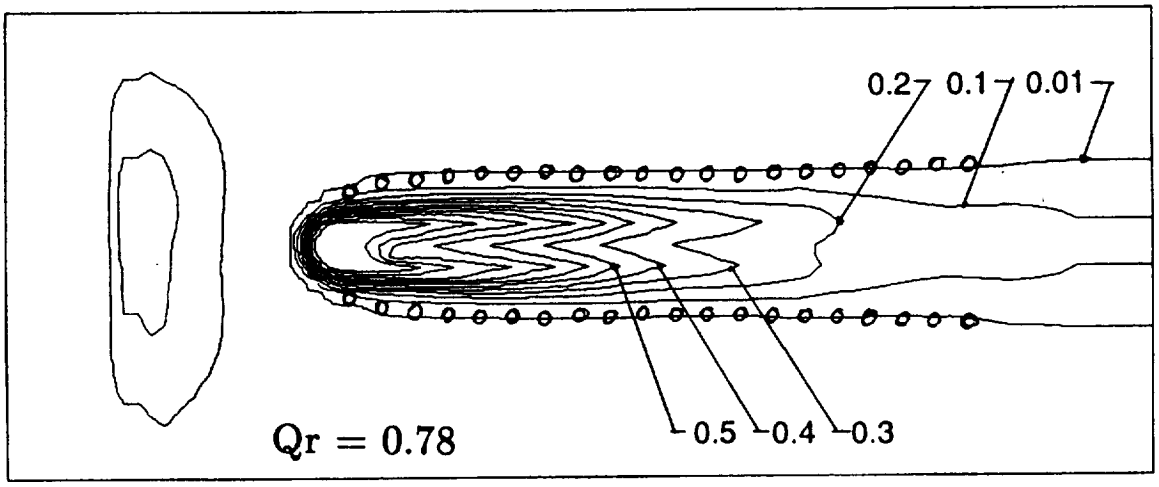

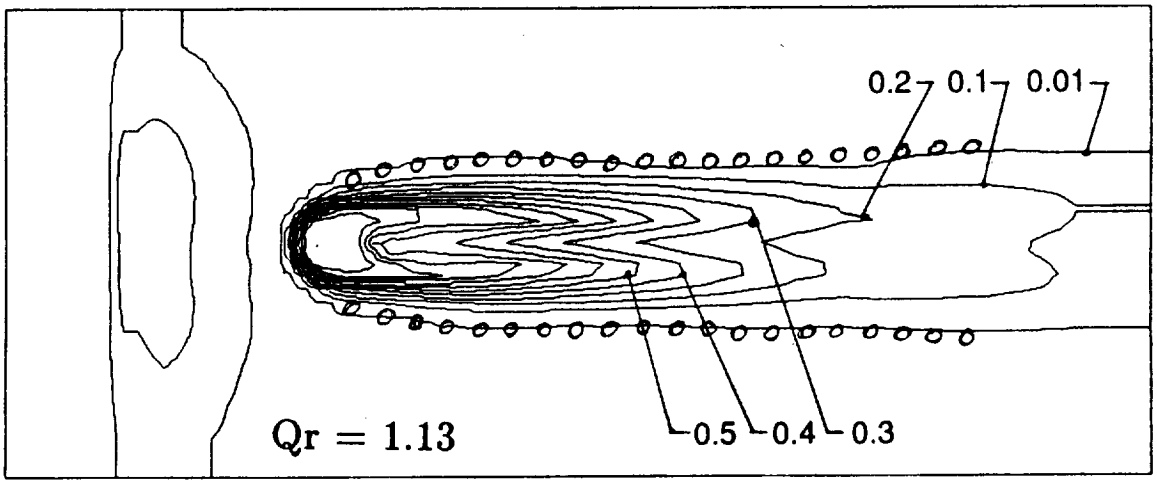

SPARK3D-PNS

- EXTENSION OF SPARK3D
- EFFICIENT SOLUTIONS OF STEADY 3-D PNS EQUATIONS
- FOR USE IN THE COMBUSTOR FAR-FIELD AND NOZZLE
- INTEGRATION SCHEME BASED ON 2ND ORDER MACCORMACK ALGORITHM

CORNER FLOW

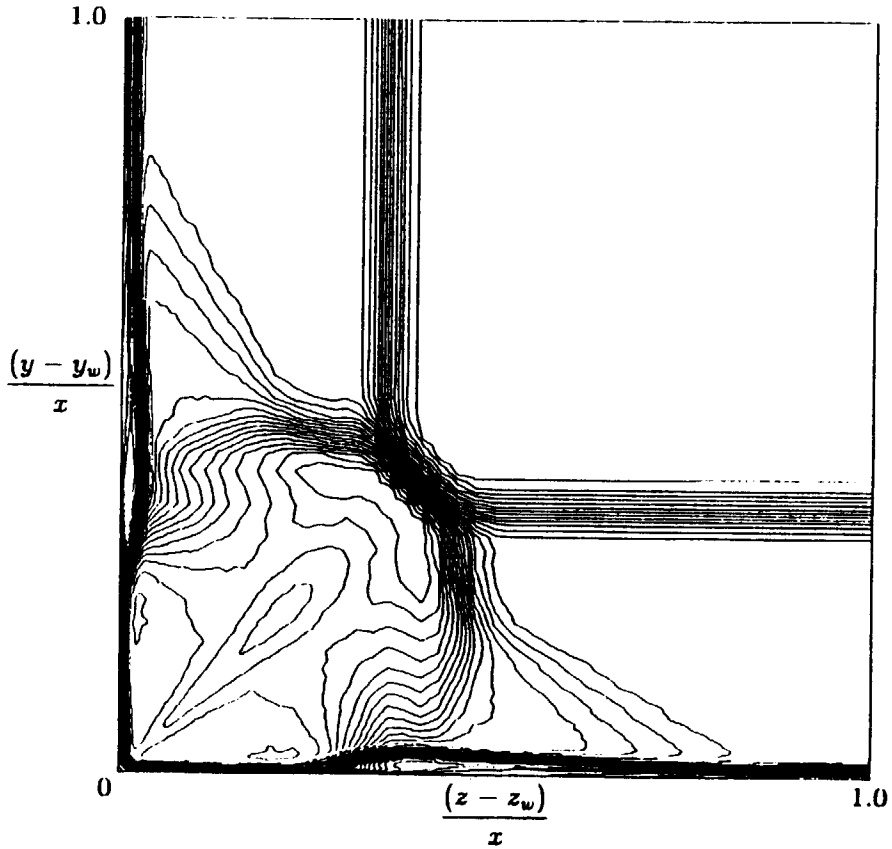

1. Computed density contours.

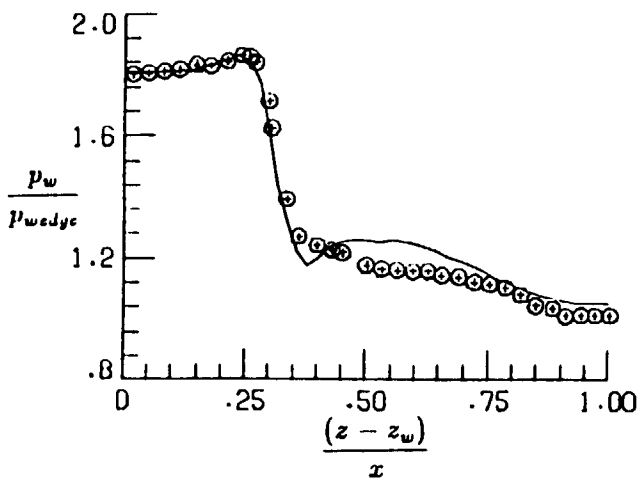

2. Wall pressure comparison.

BURROWS KURKOV

It involves Mach 1 H_2 injection in a Mach 2.44 vitiated-air stream. The flow conditions correspond to the experiments of Burrows and Kurkov. For the H_2 jet: $u = 1216$ m/s, $T = 254$ K and $f_{H_2} = 1.0$. For the vitiated-air stream: $u = 1764$ m/s, $T = 1270$ K, $f_{O_2} = 0.258$, $f_{N_2} = 0.486$ and $f_{H_2O} = 0.256$.

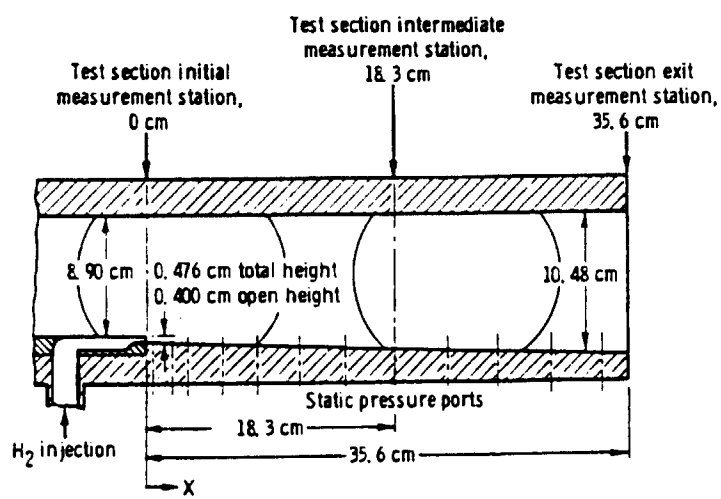

BURROWS KURKOV

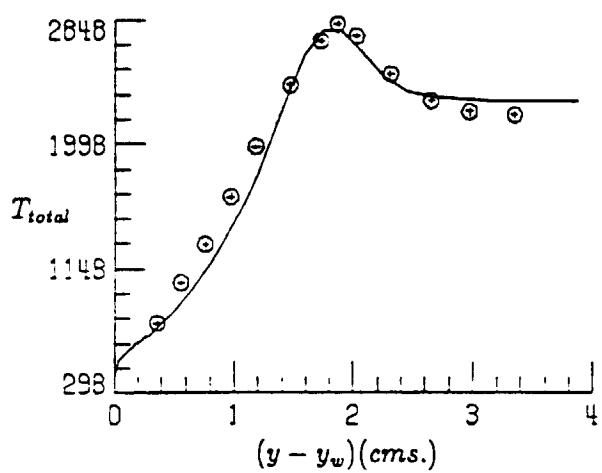

1. Total temperature comparison.

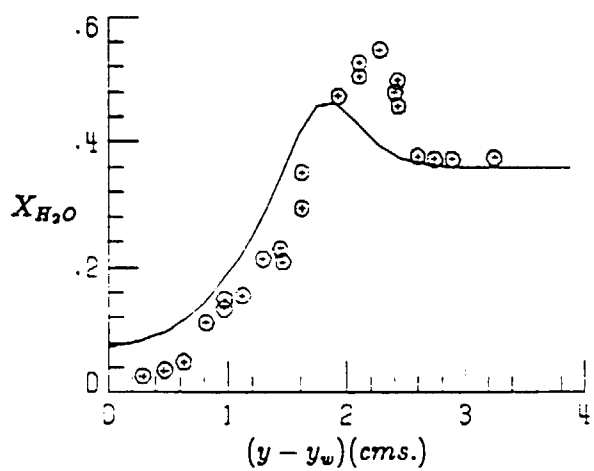

2. H_2O mole fraction comparison.

MIXING ENHANCEMENT STUDIES

- FUEL-AIR MIXING DECREASES WITH INCREASING MACH NUMBER

- MIXING ENHANCEMENT MECHANISMS ARE REQUIRED AT HIGH COMBUSTOR MACH NUMBER

  - PLANAR SHOCKS
  - CURVED SHOCKS
  - SWIRL
  - ACOUSTIC FORCING

  } EXCITATION OF UNSTABLE MODES

- ENHANCEMENT BY SHOCKS IS EXAMINED IN THIS STUDY

NASA

L-88-9164

STRUT MODIFICATION FOR IMPROVED COMBUSTION EFFICIENCY

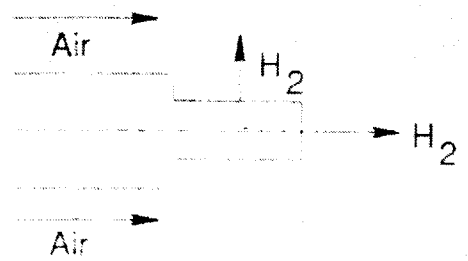

Conventional strut

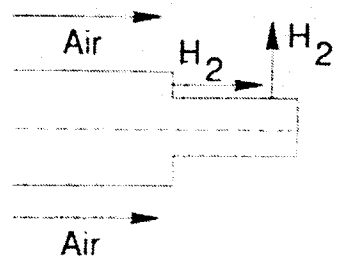

Modified strut

Water mass fraction
Conventional strut

Water mass fraction
Modified strut

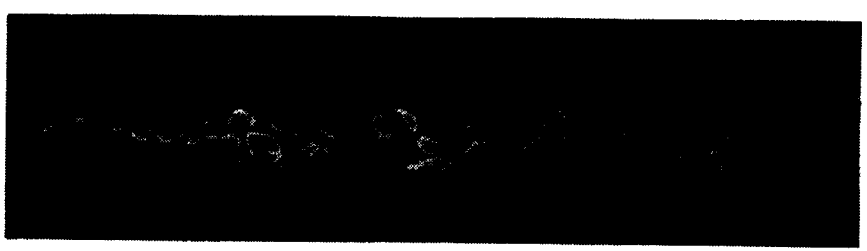

ORIGINAL PAGE IS
OF POOR QUALITY

STRUT WITH TRANSVERSE - PARALLEL JETS

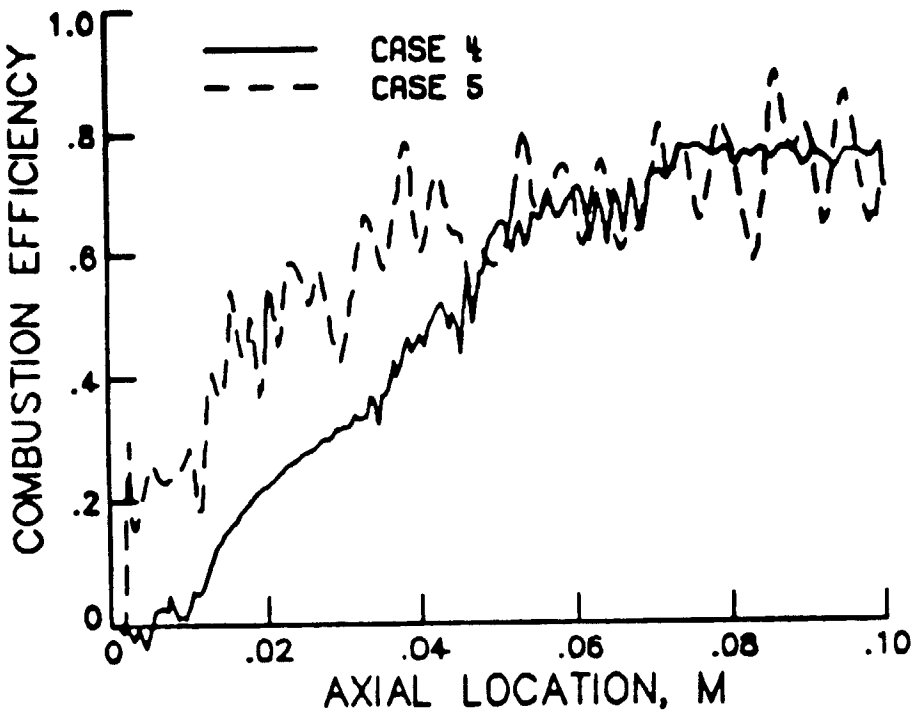

MODEL COMBUSTOR

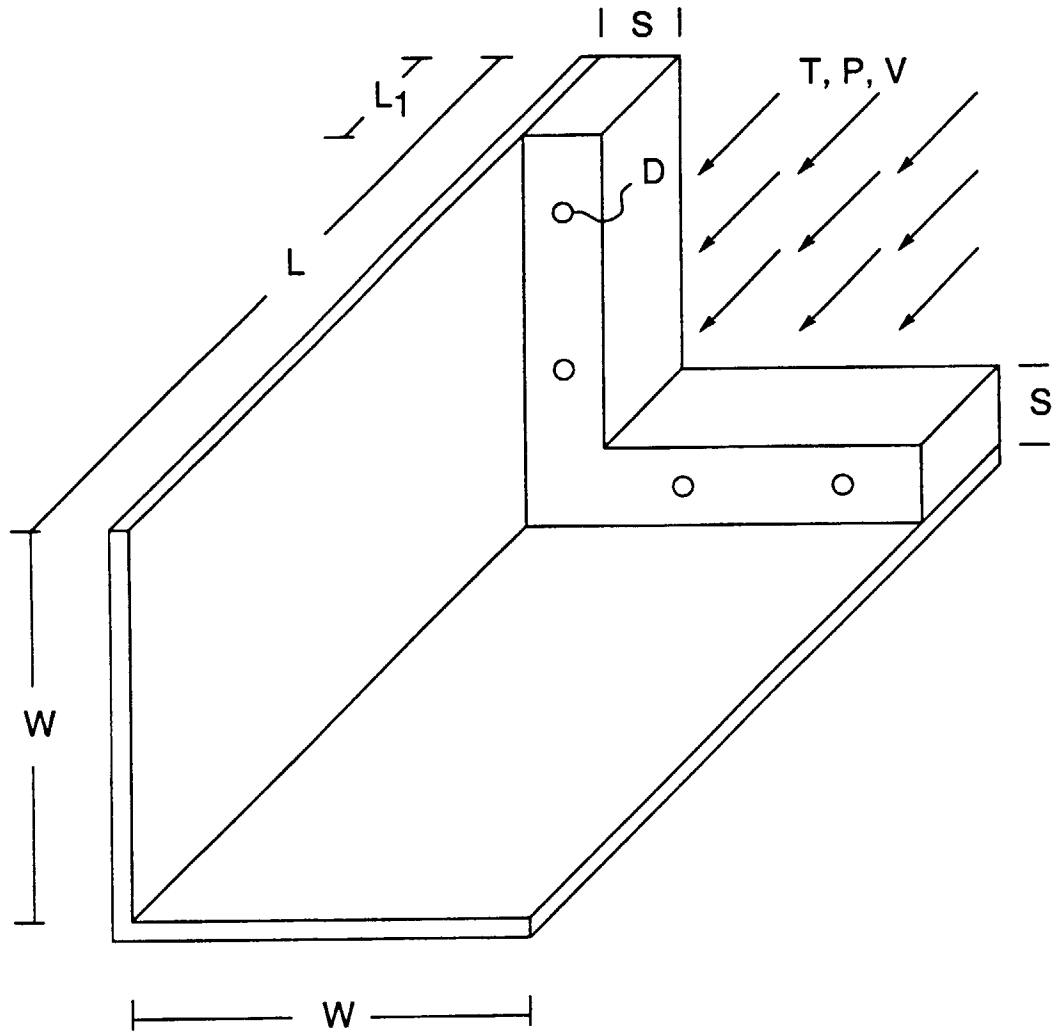

L = 20.0 cm, W = 10.0 cm

S = 2.0 cm, L_1 = 1.5 cm, D = 3.5 mm

T = 1000 K, P = 0.5 atm, V = 1500 m/s

CONCLUSIONS

- COMPUTER PROGRAMS DEVELOPED TO MODEL 3-D SUPERSONIC CHEMICALLY REACTING FLOWFIELDS.

- FAVORABLE VALIDATION AGAINST AVAILABLE EXPERIMENTAL RESULTS

- BEING USED EXTENSIVELY IN THEORETICAL STUDIES AND IN ENGINEERING ENVIRONMENTS

DIRECTIONS

- ALGORITHMS
  - HIGHER ORDER AND COMPACT
  - UPWINDING
  - PARALLEL COMPUTING
- TRANSITION - TURBULENCE MODELING
  - COMPARISON WITH LINEAR STABILITY CODES
  - DIRECT SIMULATIONS OF SUPERSONIC JETS AND MIXING LAYERS
  - "DATABASE" FOR PHENOMINOLOGICAL MODELS
- PRODUCTION CODE SUPPORT

N91-10871

Three-Dimensional Calculation of Supersonic Reacting Flows Using an LU Scheme

Sheng-Tao Yu
Y-L Peter Tsai
Jian-Shun Shuen

Sverdrup Technology, Inc.
NASA Lewis Research Center
Cleveland, Ohio

ABSTRACT

A new three-dimensional numerical program incorporated with comprehensive real gas property models has been developed to simulate supersonic reacting flows. The code employs an implicit finite volume, Lower-Upper (LU) time-marching method to solve the complete Navier-Stokes and species equations in a fully-coupled and very efficient manner. A chemistry model with nine species and eighteen reaction steps are adopted in the program to represent the chemical reaction of H_2 and air. To demonstrate the capability of the program, flow fields of underexpanded hydrogen jets transversely injected into supersonic air stream inside the combustors of scramjets are calculated. Results clearly depict the flow characteristics, including the shock structure, separated flow regions around the injector, and the distribution of the combustion products.

PRECEDING PAGE BLANK NOT FILMED

PREVIOUS WORK

- Develop fluid dynamic code to study the mixing and chemical reactions inside the combustors of ramjets.

- A two-dimensional computer code (RPLUS) using LU scheme to simulate chemical reacting flows has been developed:
  - Fully coupled and very efficient.
  - Finite rate chemistry.
  - A fast equilibrium chemistry package.

- Previous work done by using RPLUS 2D code:
  - Hypersonic inlet flows at Mach 10 and 13.
  - The combustion of a hydrogen jet transversely injected into a supersonic air stream.
  - Hydrogen air mixture passing a 10° ramp.

ANALYSIS

- 3D Navier-Stokes and N_s-1 species equations.
- Brabbs' finite rate chemistry model.
  - 9 species: H_2, H, OH, H_2O, O, O_2, HO_2, H_2O_2, and N_2.
  - 18 reaction steps.
- Implicit treatment of source terms in species equations.
- No source term in energy equation for either exothermic or endothermic reactions.
- Temperature and pressure are calculated iteratively from the following equations:

$$e = \sum_{i=1}^{N_s} Y_i h_i - \frac{p}{\rho} + \frac{1}{2}\left(u^2 + v^2 + w^2\right)$$

$$h_i = h_{fi}^o + \int_{T_{ref}}^{T} C_{pi} dT$$

$$p = \rho R_u T \sum_{i=1}^{N_s} \frac{Y_i}{M_i}$$

THERMODYNAMIC AND TRANSPORT PROPERTIES

- C_p, thermal conductivity, and viscosity of individual species are obtained from fourth order polynomial of T.
- Binary mass diffusivity is calculated using the Chapman-Enskog theory with Lennard-Jones intermolecular potential energy functions.
- Wilke's mixing rule is used for the transport properties of gas mixture.
- Mass concentration weighing is used for the C_p of gas mixture.

TURBULENCE MODEL

- Baldwin-Lomax model.
- $Sc_t = Pr_t = 0.9$

NUMERICAL SCHEME

- Time-marching LU scheme.
- Implicit treatment of source terms.

$$\frac{\partial Q}{\partial t} + \frac{\partial}{\partial x}\left(E^n + A^n \Delta Q\right) + \frac{\partial}{\partial y}\left(F^n + B^n \Delta Q\right) + \frac{\partial}{\partial z}\left(G^n + C^n \Delta Q\right)$$
$$= \frac{\partial E_v^n}{\partial x} + \frac{\partial F_v^n}{\partial y} + \frac{\partial G_v^n}{\partial z} + H^n + T^n \Delta Q$$

$$A = \frac{\partial E}{\partial Q}, \quad B = \frac{\partial F}{\partial Q}, \quad C = \frac{\partial G}{\partial Q}, \quad T = \frac{\partial H}{\partial Q}$$

$$A = A^+ + A^-$$

$$B = B^+ + B^-$$

$$C = C^+ + C^-$$

$$A^+ = 0.5(A + \gamma_A I)$$
$$A^- = 0.5(A - \gamma_A I)$$
$$B^+ = 0.5(B + \gamma_B I)$$
$$B^- = 0.5(B - \gamma_B I)$$
$$C^+ = 0.5(C + \gamma_C I)$$
$$C^- = 0.5(C - \gamma_C I)$$

$$\gamma_A \geq \max(|\lambda_A|)$$

$$\gamma_B \geq \max(|\lambda_B|)$$

$$\gamma_C \geq \max(|\lambda_C|)$$

$$\left[I + \Delta t\left(D_x^- A^+ + D_x^+ A^- + D_y^- B^+ + D_y^+ B^- + D_z^- C^+ + D_z^+ C^- - T\right)\right] \Delta Q$$
$$= \Delta t RHS$$

$$RHS = -\frac{\partial E^n}{\partial x} - \frac{\partial F^n}{\partial y} - \frac{\partial G^n}{\partial z} + \frac{\partial E_v^n}{\partial x} + \frac{\partial F_v^n}{\partial y} + \frac{\partial G_v^n}{\partial z} + H^n$$

NUMERICAL SCHEME

- Two operators for 3D calculation.
- Operation count comparable to explicit schemes.

$$
\begin{aligned}
&N\Delta Q_{ijk} - \Delta t T_{ijk}\Delta Q_{ijk} + \\
&\frac{\Delta t}{\Delta x}\left(A^-_{i+1,j,k}\Delta Q_{i+1,j,k} - A^+_{i-1,j,k}\Delta Q_{i-1,j,k}\right) + \\
&\frac{\Delta t}{\Delta y}\left(B^-_{i,j+1,k}\Delta Q_{i,j+1,k} - B^+_{i,j-1,k}\Delta Q_{i,j-1,k}\right) + \\
&\frac{\Delta t}{\Delta z}\left(C^-_{i,j,k+1}\Delta Q_{i,j,k+1} - C^+_{i,j,k-1}\Delta Q_{i,j,k-1}\right) \\
&= \Delta t RHS
\end{aligned}
$$

$$
N = I + \frac{\Delta t}{\Delta x}\left(A^+_{i,j,k} - A^-_{i,j,k}\right) + \frac{\Delta t}{\Delta y}\left(B^+_{i,j,k} - B^-_{i,j,k}\right) + \frac{\Delta t}{\Delta z}\left(C^+_{i,j,k} - C^-_{i,j,k}\right)
$$

$$
\left[N + \frac{\Delta t}{\Delta x}\left(A^-_{i+1,j,k}\right) + \frac{\Delta t}{\Delta y}\left(B^-_{i,j+1,k}\right) + \frac{\Delta t}{\Delta z}\left(C^-_{i,j+1,k}\right)\right] N^{-1}
$$

$$
\left[N - \Delta t T_{i,j} - \frac{\Delta t}{\Delta x}\left(A^+_{i-1,j,k}\right) - \frac{\Delta t}{\Delta y}\left(B^+_{i,j-1,k}\right) - \frac{\Delta t}{\Delta z}\left(C^+_{i,j,k-1}\right)\right]\Delta Q
$$

$$
= \Delta t RHS
$$

$$
N = \left(1 + \frac{\Delta t}{\Delta x}\gamma_A + \frac{\Delta t}{\Delta y}\gamma_B + \frac{\Delta t}{\Delta z}\gamma_C +\right) I
$$

PROGRAM VECTORIZATION

- LHS can be vectorized on planes normal to the sweeping direction.

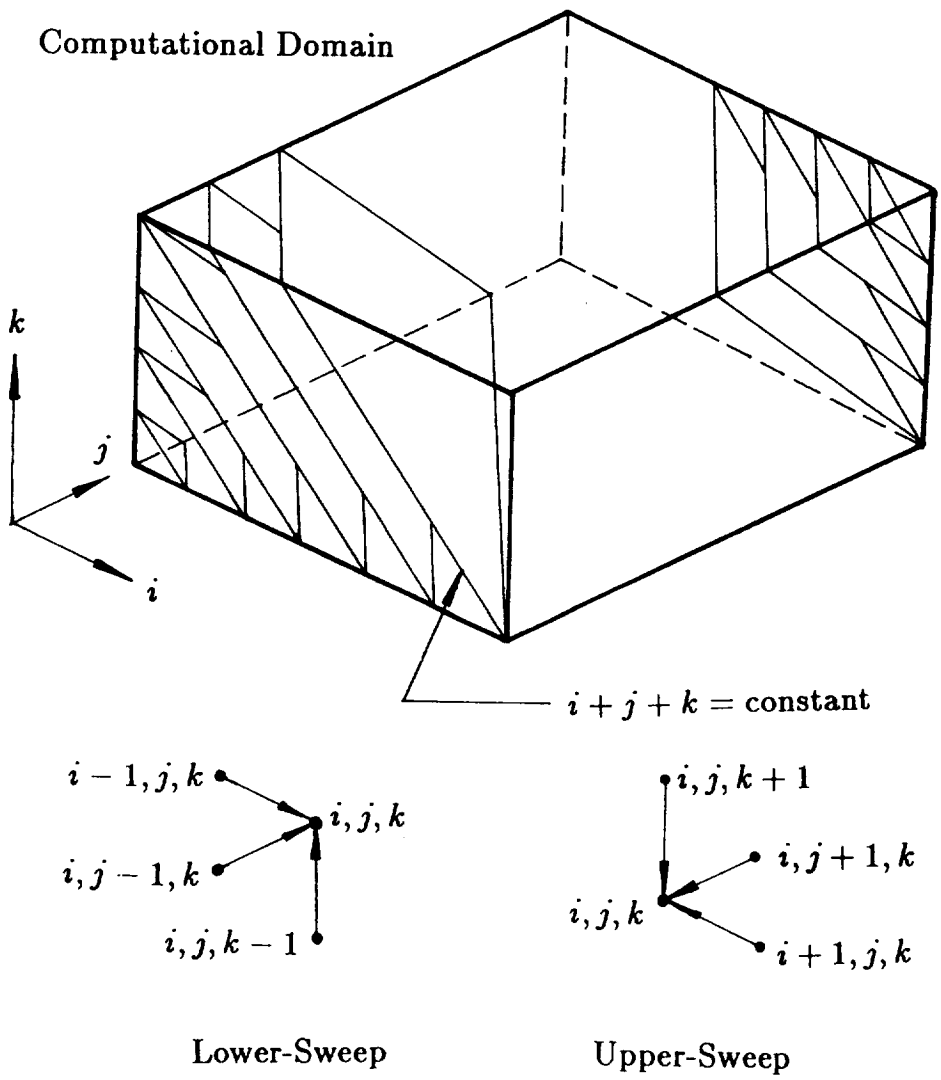

CONVERGENCE HISTORY

- Coarse grid (30x25x30)

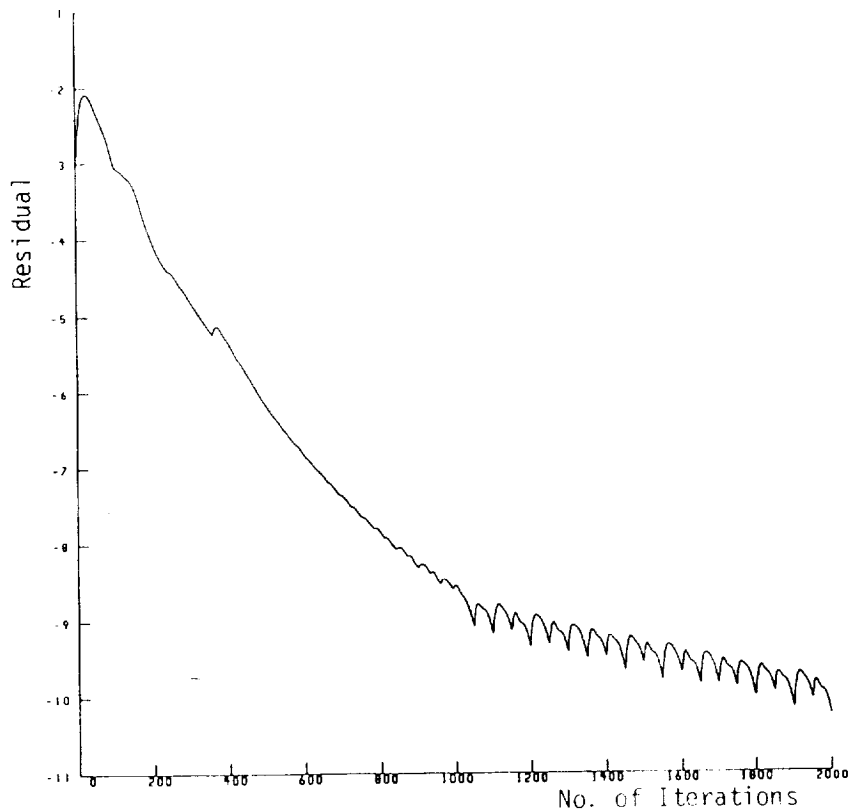

- Present calculation:
  - Residuals reduced by 4 orders of magnitude.
  - Single injection case: (61x39x43) 8 MW, 5 hrs on Cray 2.
  - Dual Injection case: (81x39x43) 11 MW, 6 hrs on Cray 2.

GEOMETRY AND FLOW CONDITION

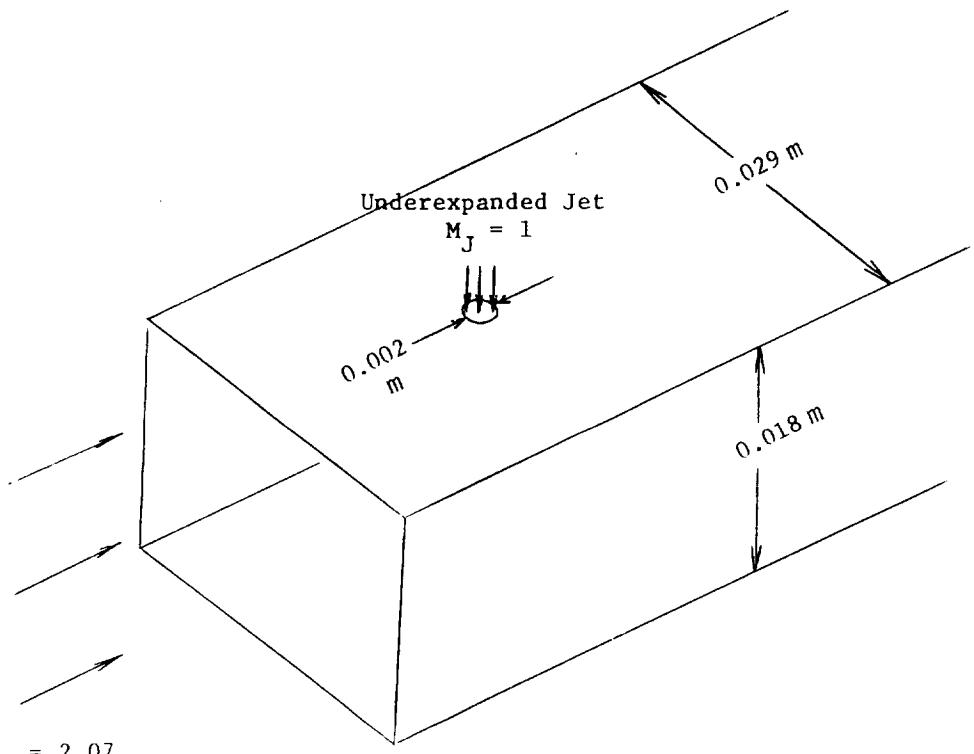

$M_{FS} = 2.07$
$P^o_{FS} = 310$ kPa
$T^o_{FS} = 298$ K

$$\bar{q} = \frac{1}{2}\rho_J u_J^2 / \frac{1}{2}\rho_{FS} u_{FS}^2$$

MASS-FRACTION CONTOUR ($\bar{Q} = 1.02, 60 \times 100 \times 50$)

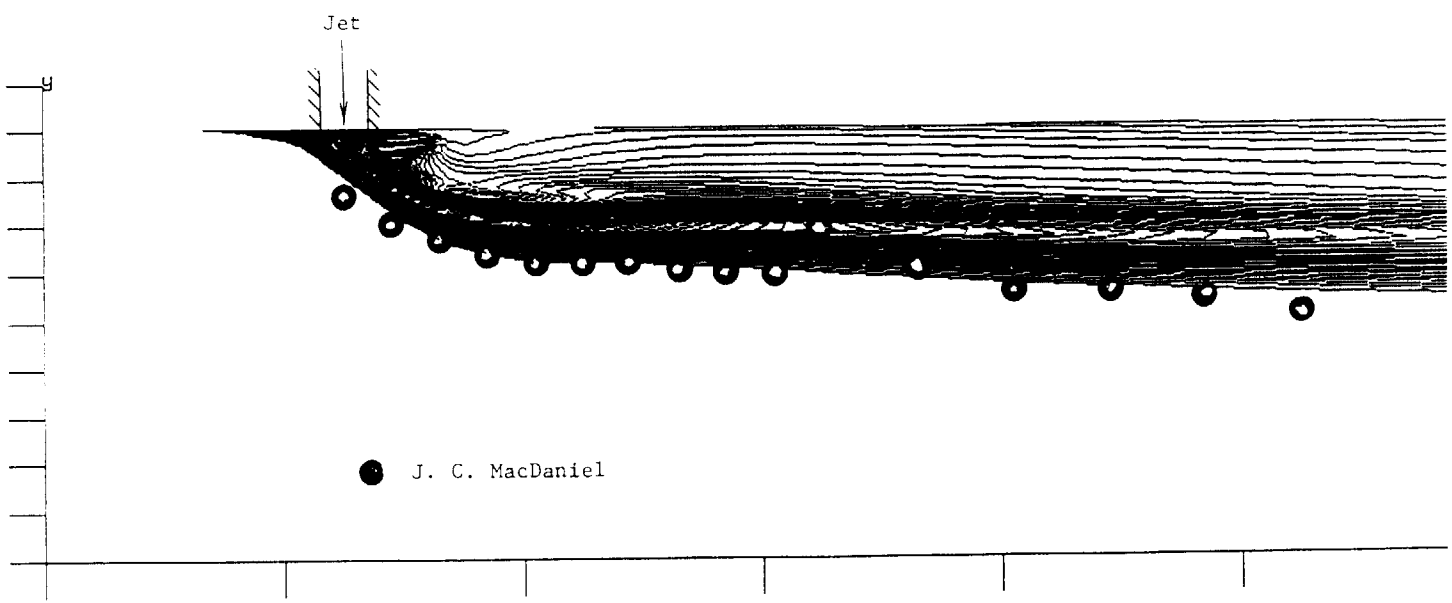

MASS-FRACTION CONTOUR (Two Ports, $\bar{Q} = 1.02$, $70 \times 100 \times 50$)

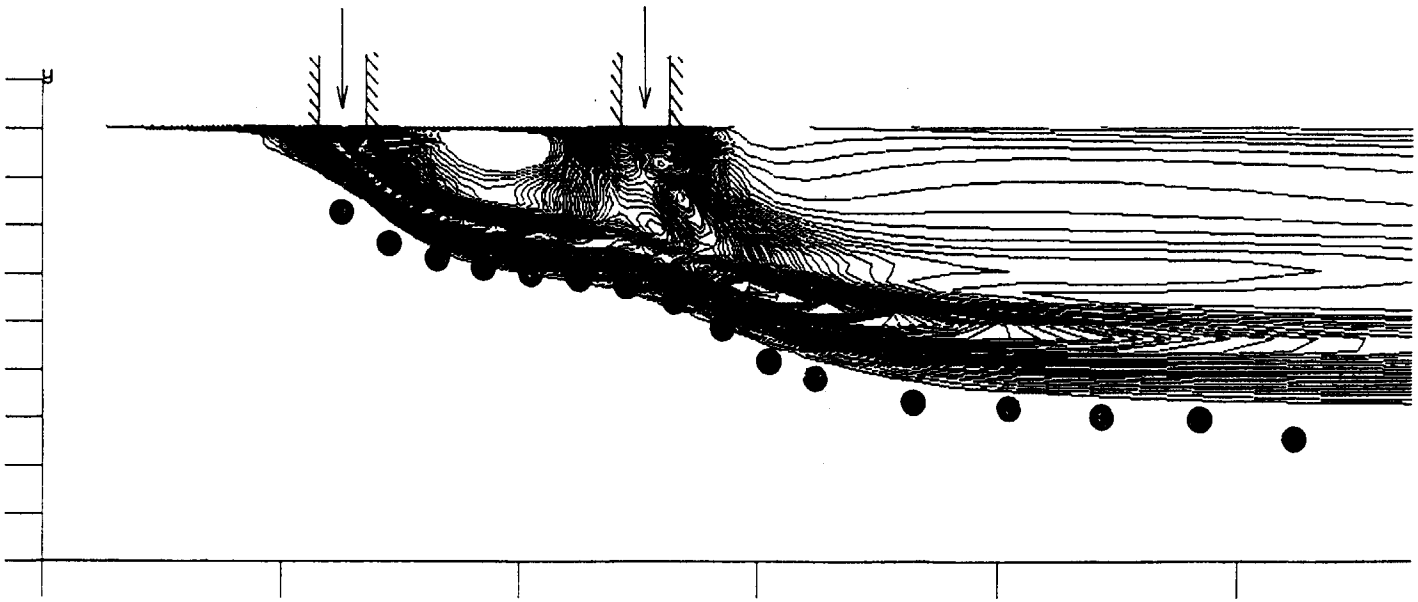

FLOW CONFIGURATION

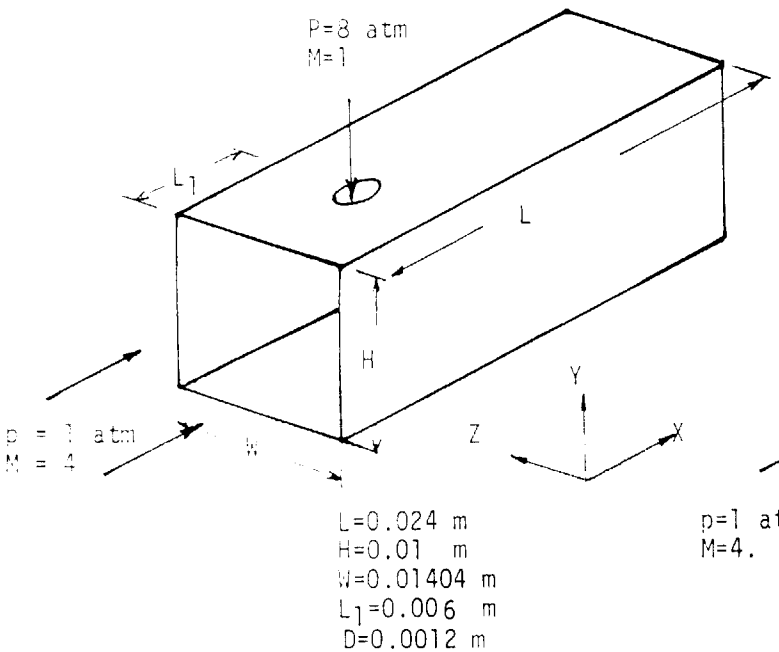

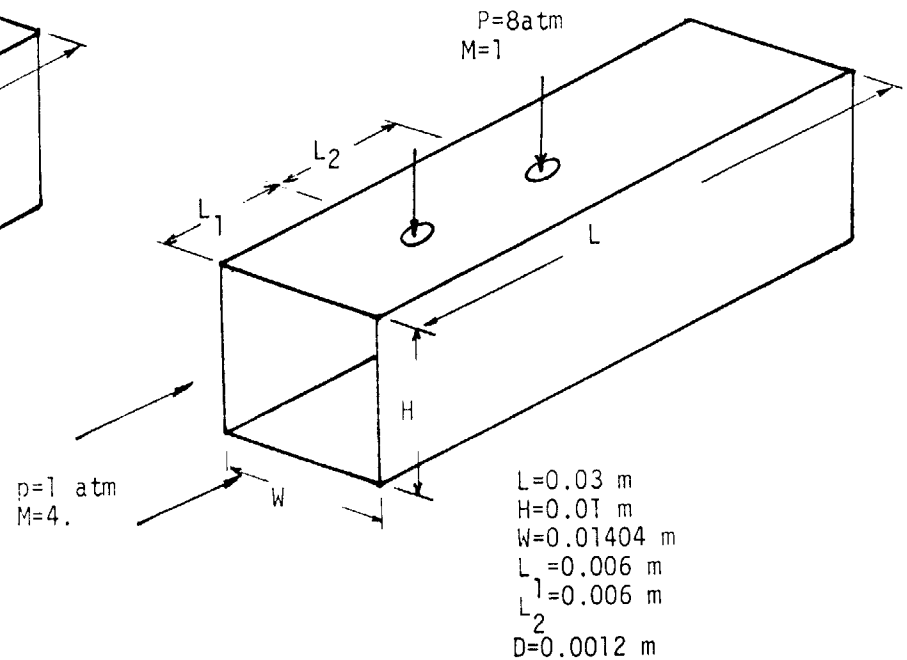

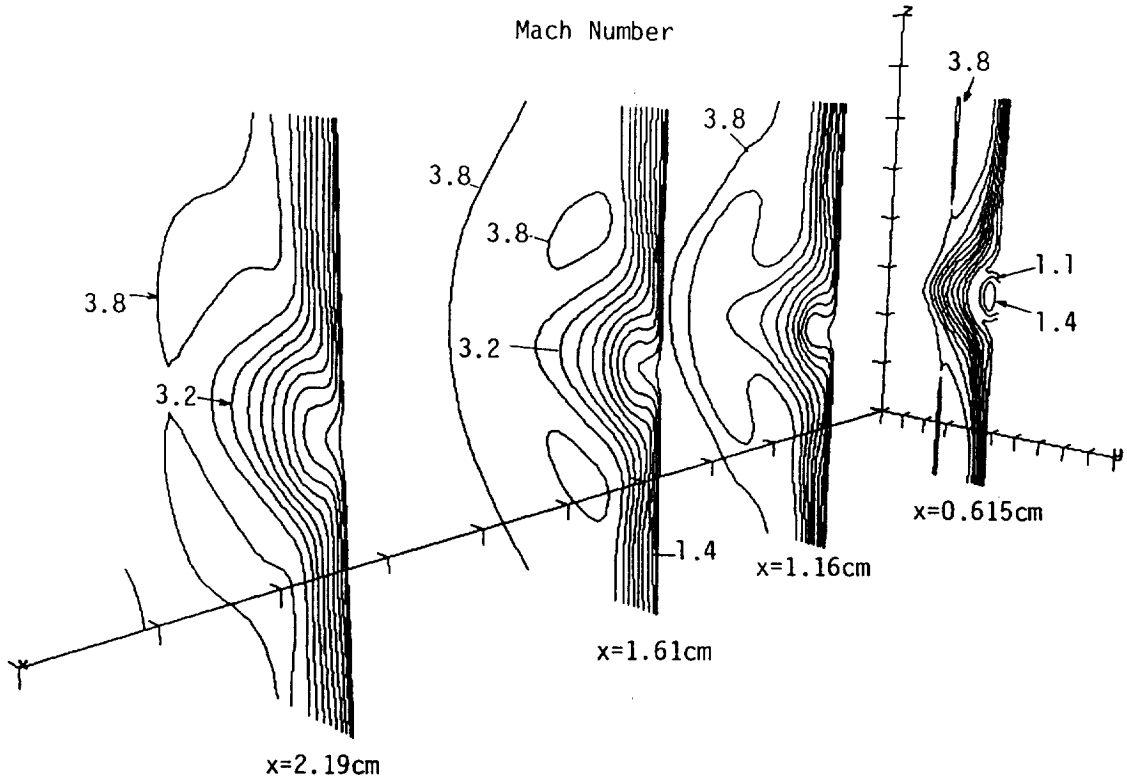
Mach Number
3.8
3.8
3.8
3.8
3.8
3.2
3.2
1.1
1.4
1.4
x=0.615cm
x=1.16cm
x=1.61cm
x=2.19cm

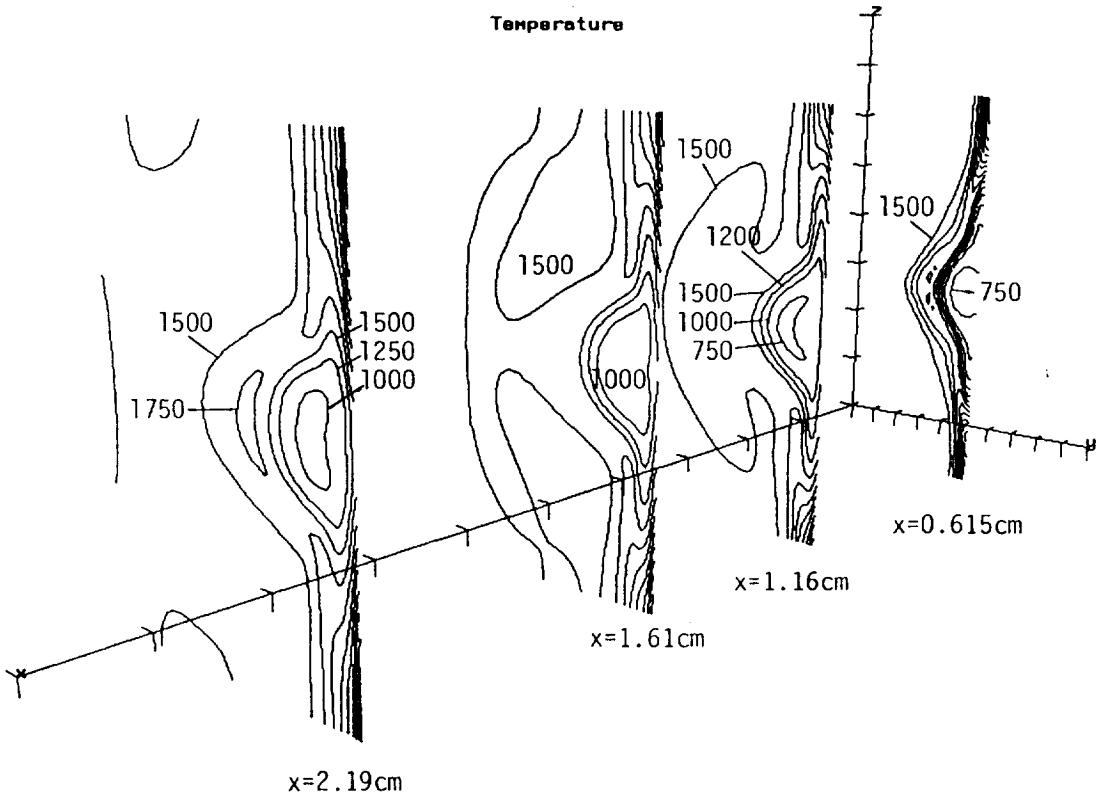
Temperature
1500
1500
1250
1000
1750
1500
1000
1500
1200
1500
1000
750
1500
750
x=0.615cm
x=1.16cm
x=1.61cm
x=2.19cm

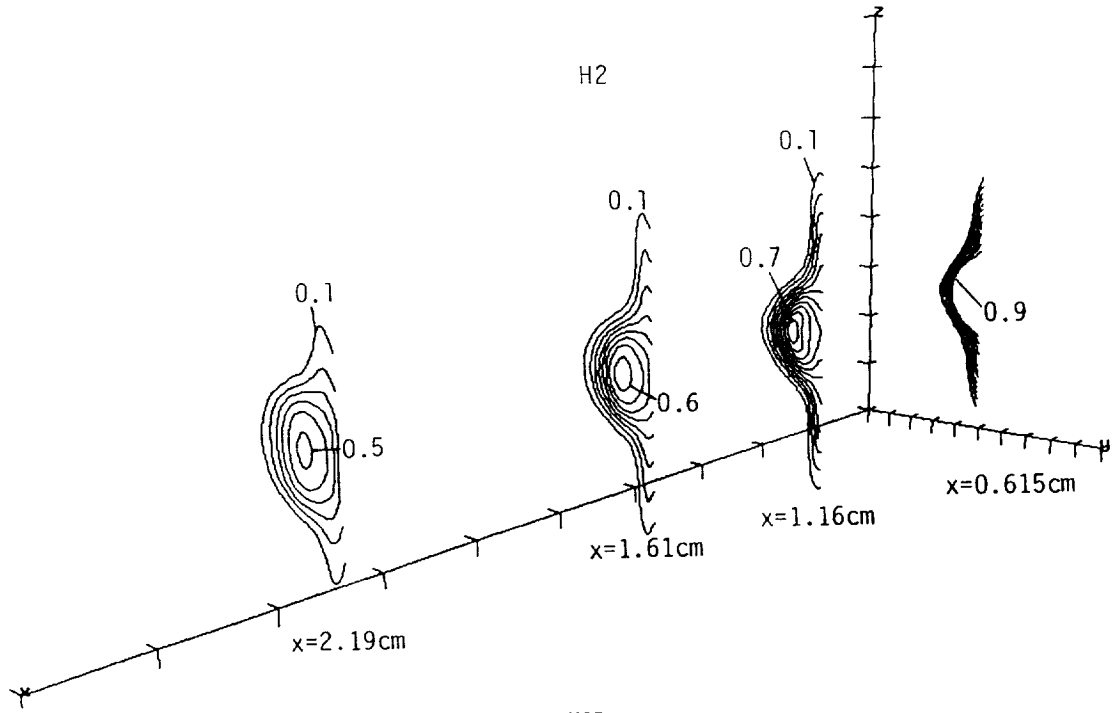
H2
0.1
0.1
0.1
0.7
0.9
0.6
0.5
x=0.615cm
x=1.16cm
x=1.61cm
x=2.19cm

H2D

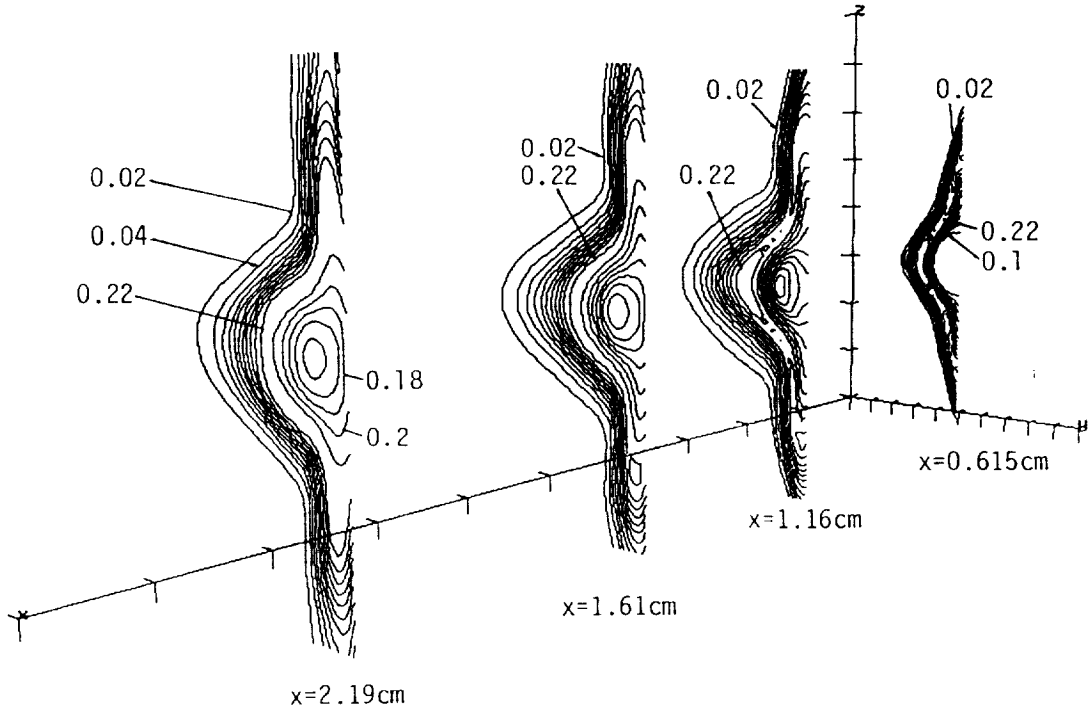
0.02
0.02
0.02
0.22
0.22
0.04
0.22
0.22
0.1
0.18
0.2
x=0.615cm
x=1.16cm
x=1.61cm
x=2.19cm

CONCLUDING REMARKS

- A new three-dimensional computer code for high speed reacting flows has been successfully developed.

- The code is very efficient because the LHS can be vectorized on the planes normal to the sweeping directions.

- The validity of the code is assessed by the comparison between the calculated results and MacDaniel's experimental data for non-reacting mixing flows.

- The code is applied to chemically reacting flows of H_2 jets transversely injected into hot airstream.
  - Results clearly depict the shock structure, recirculations, and species distribution due to chemical reaction.
  - Two-hole injection allows deeper penetration of the fuel jet and more complete combustion of H_2 and air.

N91-10872

ORIGINAL CONTAINS
COLOR ILLUSTRATIONS

Progress in Computing Nozzle/Plume Flow Fields

Stephen M. Ruffin
NASA Ames Research Center, Moffett Field, CA

Ethiraj Venkatapathy
Eloret Institute, Sunnyvale, CA

William J. Feiereisen
NASA Ames Research Center, Moffett Field, CA

Seung-Ho Lee
Eloret Institute, Sunnyvale, CA

Abstract

The long-term goal of this work is to develop the capability to predict chemically-reacting, multi-stream nozzle and plume flow fields. Two basic Navier-Stokes solvers, including the widely used F-3D code, are upgraded to include several upwind difference schemes and portable chemistry packages. Current computational capabilities for solving eqilibrium single-stream and multi-stream, frozen gas and finite rate chemistry problems are described. A variety of complex nozzle and plume flows have been computed. Solutions presented herein include axisymmetric plume flow for ideal and equilibrium air, 3-D NASP nozzle/afterbody flow, and an internal nozzle calculation comparing various finite-rate chemistry packages.

PRECEDING PAGE BLANK NOT FILMED

Motivations, Objective, and Applications

Motivations

- Flow in nozzle and propulsive plume strongly influence performance of hypersonic vehicles.
- Ground-based facilities can not fully simulate these flow fields.
- Validated, accurate and efficient flow codes are needed to design integrated propulsion systems of hypersonic vehicles.

Objective

- Develop computational ability to predict chemically reacting, multi-stream, nozzle/plume flow fields.

Applications

- NASP, Space Shuttle, general plume flows and signatures

SCHEMATIC OF AXISYMMETRIC PLUME FLOWS

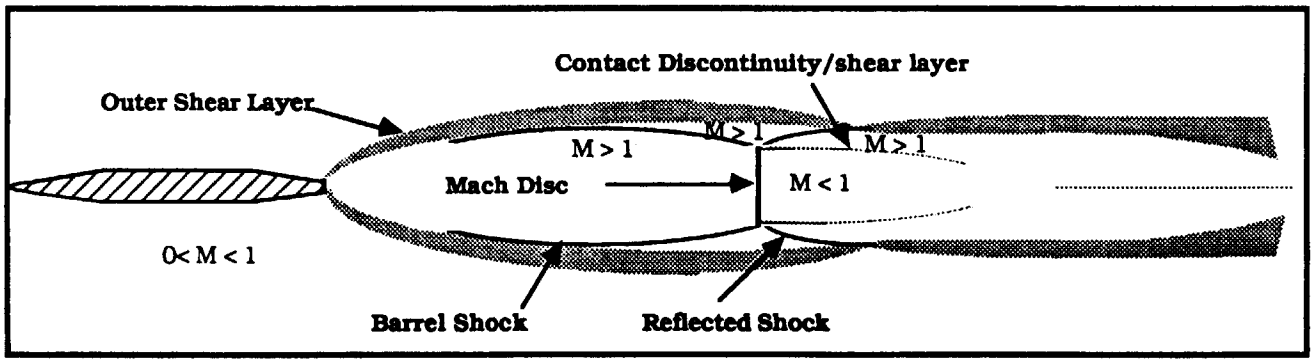

Plume Flow in Subsonic External Stream

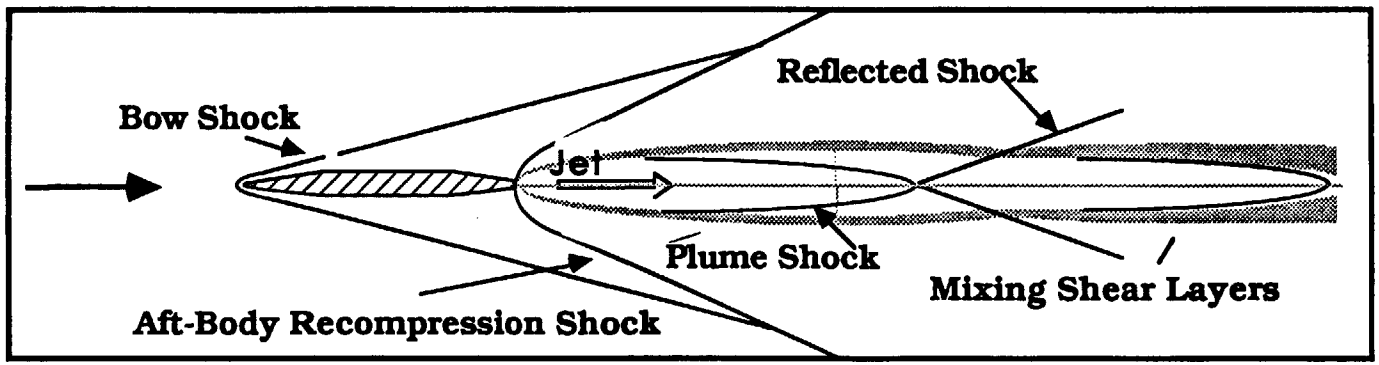

Plume Flow in Supersonic External Stream

Nozzle/Plume Flow Solvers

Difference Scheme	2-D Axisym. Eqns. Flux-Split in 2-D	3-D Eqns. Flux-Split in 1-D Central Diff. in 2-D	3-D Eqns. Roe's upwind averaging in 3-D
Implicit Soln. Algorithm	Beam & Warming in "delta form"	Two-Factor Flux-Split	LDU-ADI
Viscous Terms	in 1-D	in 1-D	in 3-D
Chemistry	Ideal Gas Equil. single-stream Equil. multi-stream Frozen	Ideal Gas Finite-Rate	Ideal Gas Equil. single-stream
Calibration	Ideal Gas: Mach disk location for jet plumes Equil. 1-stream: Shock standoff dist., and shape and species distribution for blunt body flow.	Ideal Gas: Numerous flows including Space Shuttle, Mach No., pressure and Mach disk location for plumes Finite-Rate: H_2 -air species distribution for axsymm. nozzle.	Ideal Gas: Numerous flows including Space Shuttle, Mach No., pressure and Mach disk location for plumes, plume structure in quiescent freestream

Nozzle/Plume Flow Solvers (cont.)

- All calculations performed for laminar flow
- Adaptive grid routine used for all 2-D cases
  (3-D adaptive grid routine recently completed)
- 3-D code can handle multiple, patched-grid regions and generalized specification of boundary conditions

Equilibrium and Frozen Gas Chemistry

Constant Elemental Composition (i.e., single-stream)

- Uniform gas throughout flow field

  Equilibrium Gas
  - table look-up, curve fits
  - relatively fast
  - must be pre-calculated

Variable Elemental Composition (i.e., multi-stream)

- Solution of species partial density equations allows for convection, diffusion and mixing of multiple streams

  Equilibrium Gas
  - Gordon-McBride free energy minimization
  - arbitrary gas mixtures

  Frozen Chemistry
  - No reactions

Finite Rate Chemistry

- H_2 - air chemistry currently being used
  - JANNAF plume model (Dash and Pergament, 1980)
  - 7 Species: H, H_2, H_2O, O, OH, O_2, N_2
  - 8 Reactions
- Specific heats from curve fits (Gordon and McBride data)
- Binary diffusion
  - Fick's Law with $D_{i,j}$ given by Reid, et.al., 1977)
- Non-catalytic wall
- Chemistry Coupling
  - Fully-Coupled
    Invert large matrix of order 5 + ($N_{species}$ - 1) per node
  - Loosely-Coupled
    Locally constant $\bar{\gamma}$
    P not affected by species concentration variations
    Invert two smaller matrices of order 5 and $N_{species}$ - 1 per node.

Types of Nozzle/Plume Flows Computed

Cases	Main complexity is due to: Fluid Dyn. Features	Body Geom.	Flow Chem.	References
I. Axisymmetric Single-Nozzle Plume				
A. Not including afterbody				
Ideal gas, sub. freestream ←	x			AIAA 89-0129
Ideal gas, sup. freestream	x			AIAA 88-3158
B. Including afterbody				
Ideal Gas ←	x	x		AIAA 88-2636
Equil. single-stream	x	x	x	AIAA 88-2636
Equil. multi-stream	x	x	x	in preparation
Frozen	x	x	x	in preparation
II. 3-D Multiple-Nozzle Plume				
A. Not including afterbody	x			AIAA 88-3158
B. Including afterbody	x	x		AIAA 89-0129
III. Hypersonic Nozzle/Afterbody				
A. 2-D Geometry				
Subsonic freestream	x			AIAA 89-0446
Supersonic freestream	x			AIAA 89-0446
B. 3-D Geometry				
Plume region alone	x	x		AIAA 89-0446
Complete geometry ←	x	x		AIAA 89-0446
IV. Internal Nozzle, finite rate chem. ←			x	in preparation

Axisymmetric Plume Flow in Quiscent Air
Pj/Pinf = 21.9 - Mj = 1.5

Upper Half - Computed Mach Contours with Adapted Grid

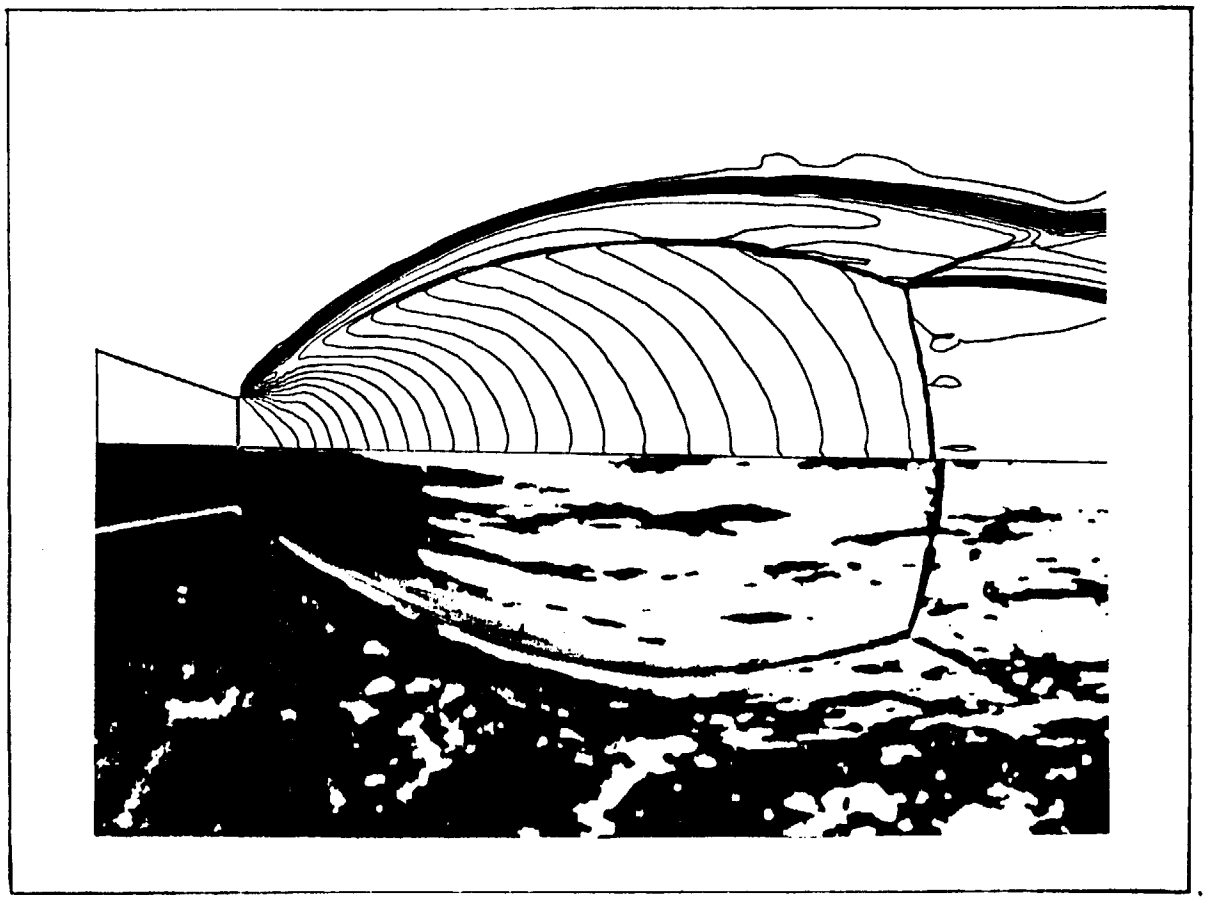

Lower Half - Experimetnal Shadowgraph - (NASA TR R 6)

Axisymmetric Plume Solutions

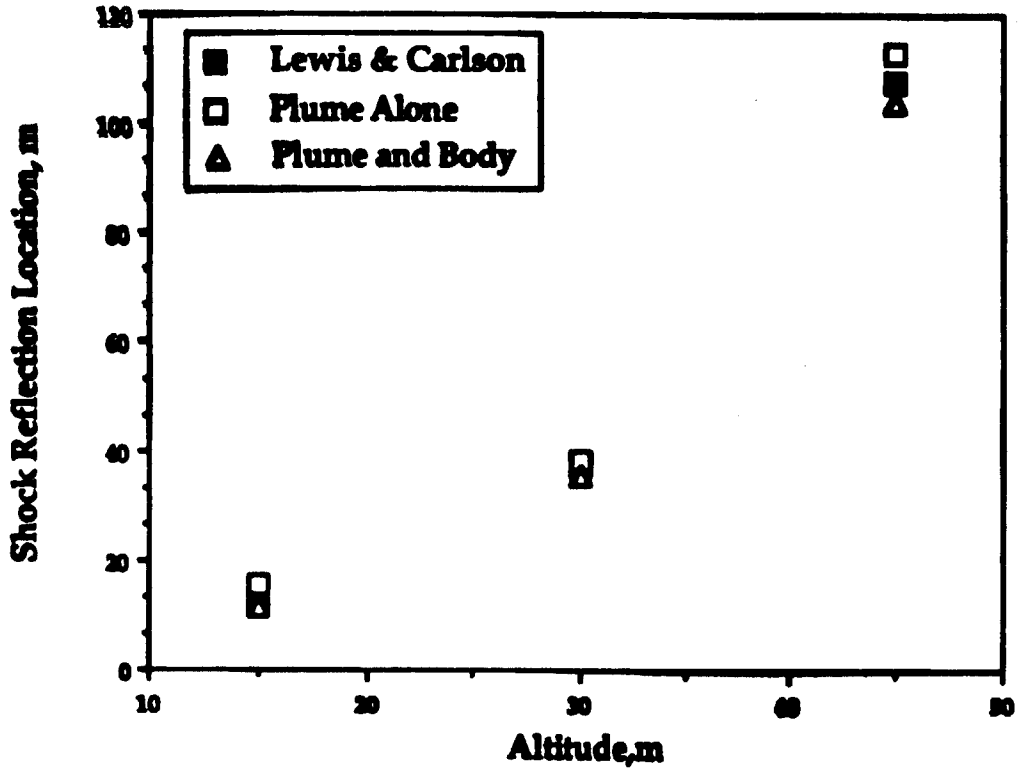

Comparison of Shock Reflection Location vs Altitude

ORIGINAL PAGE IS
OF POOR QUALITY

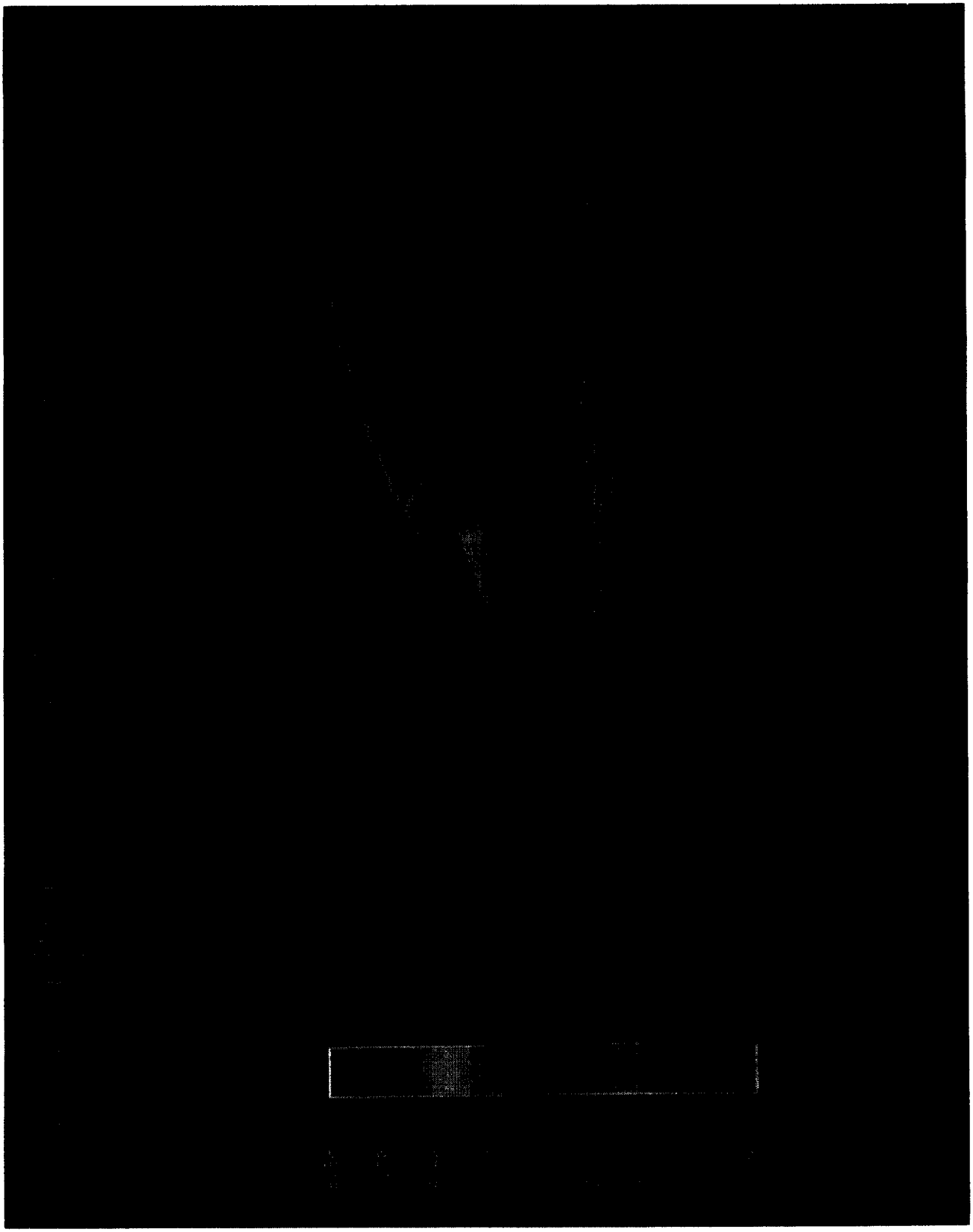

ORIGINAL PAGE IS
OF POOR QUALITY

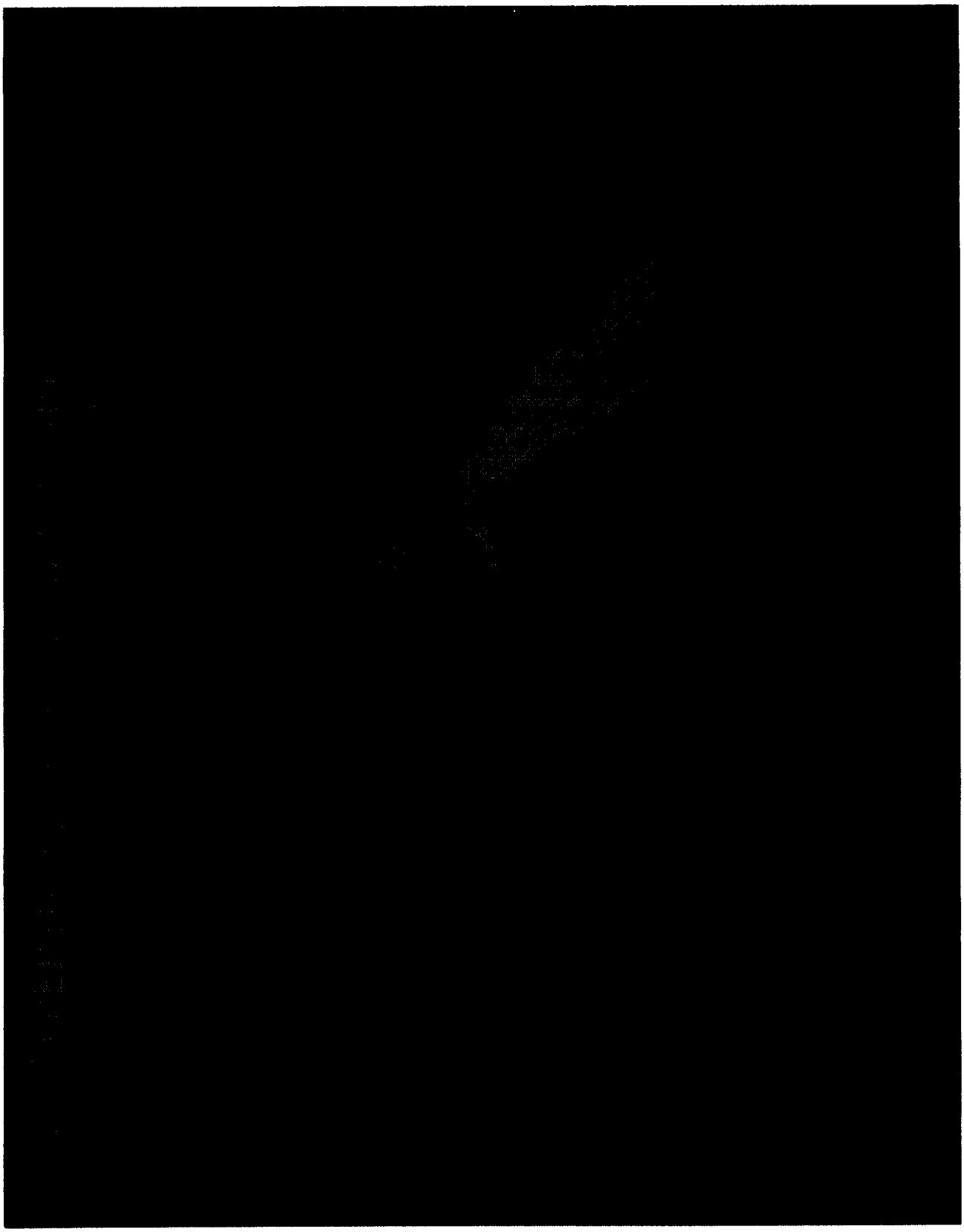

PRECEDING PAGE BLANK NOT FILMED

ORIGINAL PAGE IS
OF POOR QUALITY

NOZZLE GEOMETRY

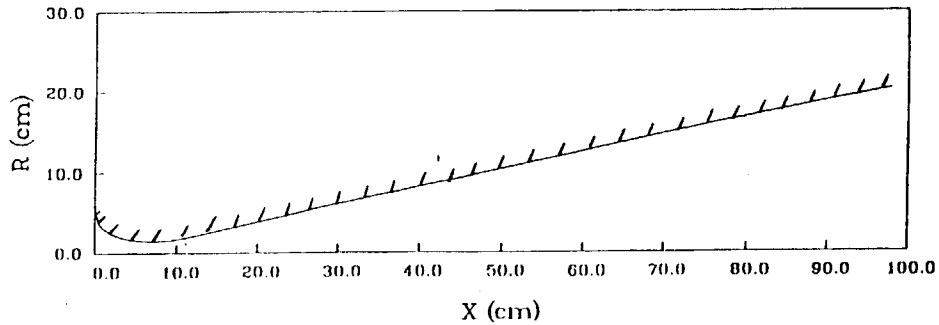

OH CONCENTRATIONS VERSUS DISTANCE ALONG NOZZLE AXIS

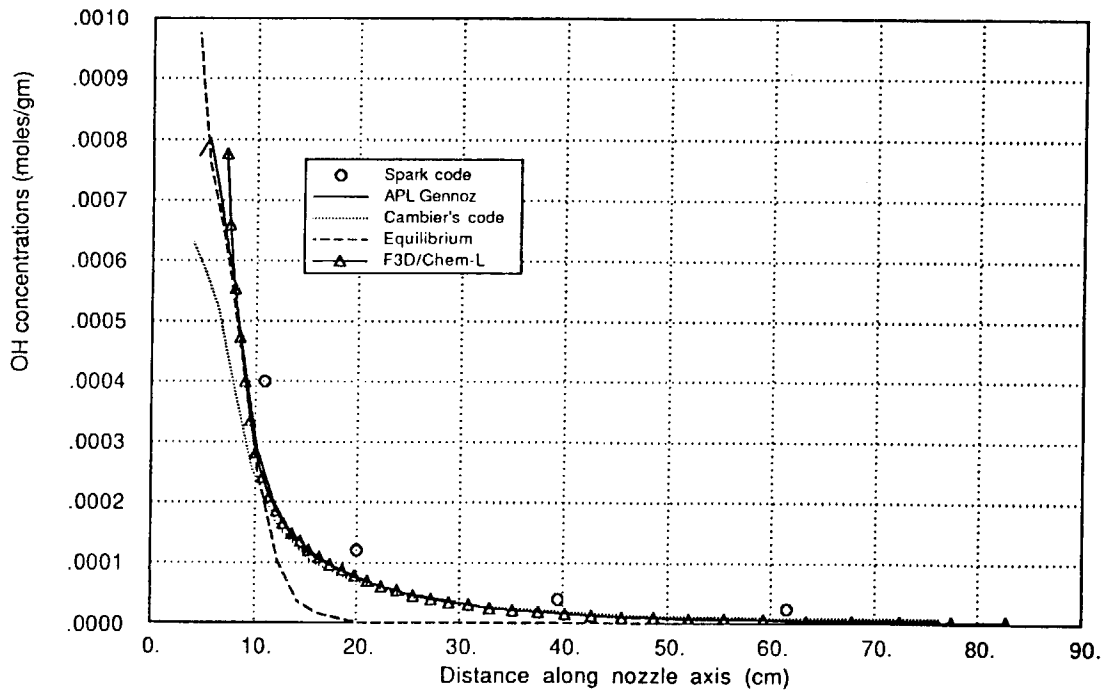

Concluding Remarks

- A variety of nozzle/plume flows have been successfully computed.
  - Complex flow structures and geometries have been studied
  - Good agreement with experimental and other computed results has been found for plume structure and Mach disk location.
- Equilibrium single-stream, equil. multi-stream, finite rate, and frozen chemistry packages have been incorporated.
- Turbulence modeling for complex plume flows is currently being studied
- 3-D code will be validated against hypersonic nozzle/afterbody experimental data
- Significant progress has been made toward goal of a single code capable of solving complex chemically reacting nozzle/plume flow fields.

N91-10873

APPLICATION OF CFD CODES FOR THE SIMULATION OF SCRAMJET COMBUSTOR FLOWFIELDS

Tawit Chitsomboom
NASA Langley Research Center/Vigyan Research Associates, Inc.
Hampton, Virginia 23665-5225

and

G. Burton Northam
NASA Langley Research Center
Hampton, Virginia 23665-5225

Office of Aeronautics and Space Technology (OAST)
NASA Computational Fluid Dynamics Conference
Mountain View, California
March 7-9, 1989

ABSTRACT

An overview of CFD activities in the Hypersonic Propulsion Branch is given. Elliptic and PNS codes that are being used for the simulation of hydrogen-air combusting flowfields for scramjet applications are discussed. Results of the computer codes are shown in comparison with those of the experiments where applicable. Two classes of experiments will be presented: (a) parallel injection of hydrogen into vitiated supersonic air flow; and (b) normal injection of hydrogen into supersonic crossflow of vitiated air.

INTRODUCTION

- A number of CFD codes are being developed and validated at the Hypersonic Propulsion Branch, Fluid Mechanics Division, NASA Langley Research Center
- These CFD codes are being applied to solving flowfields inside hydrogen-fueled scramjet combustors
- Fully elliptic codes
  - 2D, Axisymmetric, 3D
  - Global two-step finite rate combustion model
  - Use unsplit explicit MacCormack Algorithm with point-implicit chemistry source terms
- PNS Codes
  - 2D, 3D
  - Global two-step finite rate combustion model
  - Implicit, coupled space marching procedure

3D-ELLIPTIC CFD CODE

- Unsplit explicit MacCormack finite-difference algorithm
- Solve 9 PDE's by finite-difference technique
  - 1 Density
  - 3 Momentum
  - 1 Energy
  - 4 Species (O_2, H_2, H_2O, OH)
- Treat chemical source terms implicitly to alleviate stiffness associated with fast chemistry
- 2D-Layer design for efficient use of memory

COMBUSTION AND TURBULENCE MODELS

- Four-species two-step finite-rate model (Rogers-Chinitz)

$$H_2 + O_2 \underset{kb1}{\overset{kf1}{\rightleftharpoons}} 2OH$$

$$2OH + H_2 \underset{kb2}{\overset{kf2}{\rightleftharpoons}} 2H_2O$$

kf, kb = kf, kb (ϕ ,T)

- Chemical source terms are obtained by applying the law of mass action

- Prandtl mixing length hypothesis for the jet mixing process

$$\mu_t = k\rho\omega\ell^2$$

$$k \approx 0.02$$

- Baldwin-Lomax model for near-wall turbulence

RESULTS OF 2D ELLIPTIC CODE

- Supersonic coaxial burner of hydrogen-air
- Hot vitiated outer air stream co-flowing with cold inner hydrogen fuel, exiting into a quiescent air
- Use "CARS" technique to obtain data point for oxygen, nitrogen and temperature
- Compare CARS data with CFD results

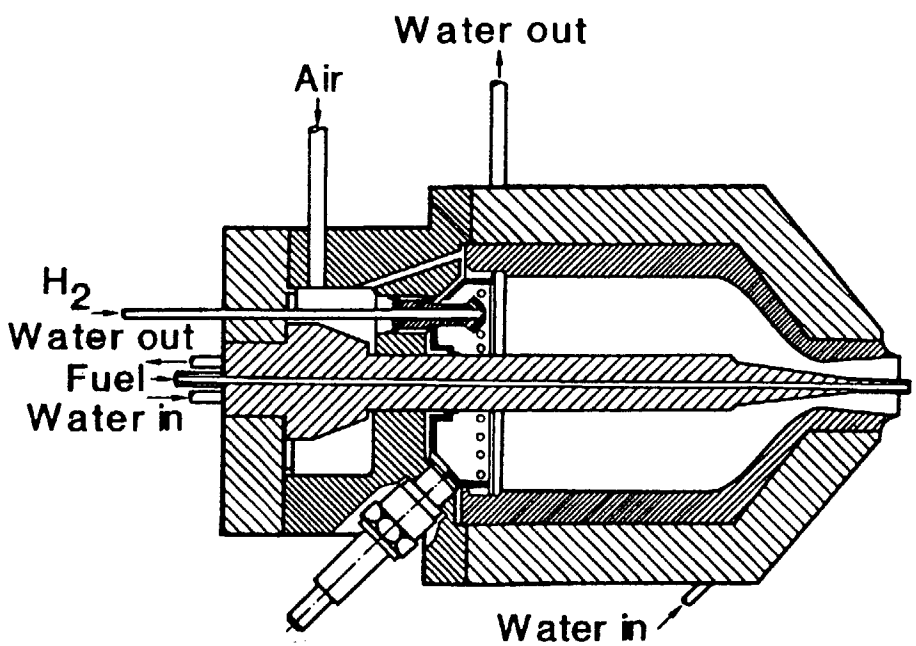

CENTERLINE DISTRIBUTION OF O_2 AND N_2 SPECIES

Symbol : CARS data
Lines : CFD data

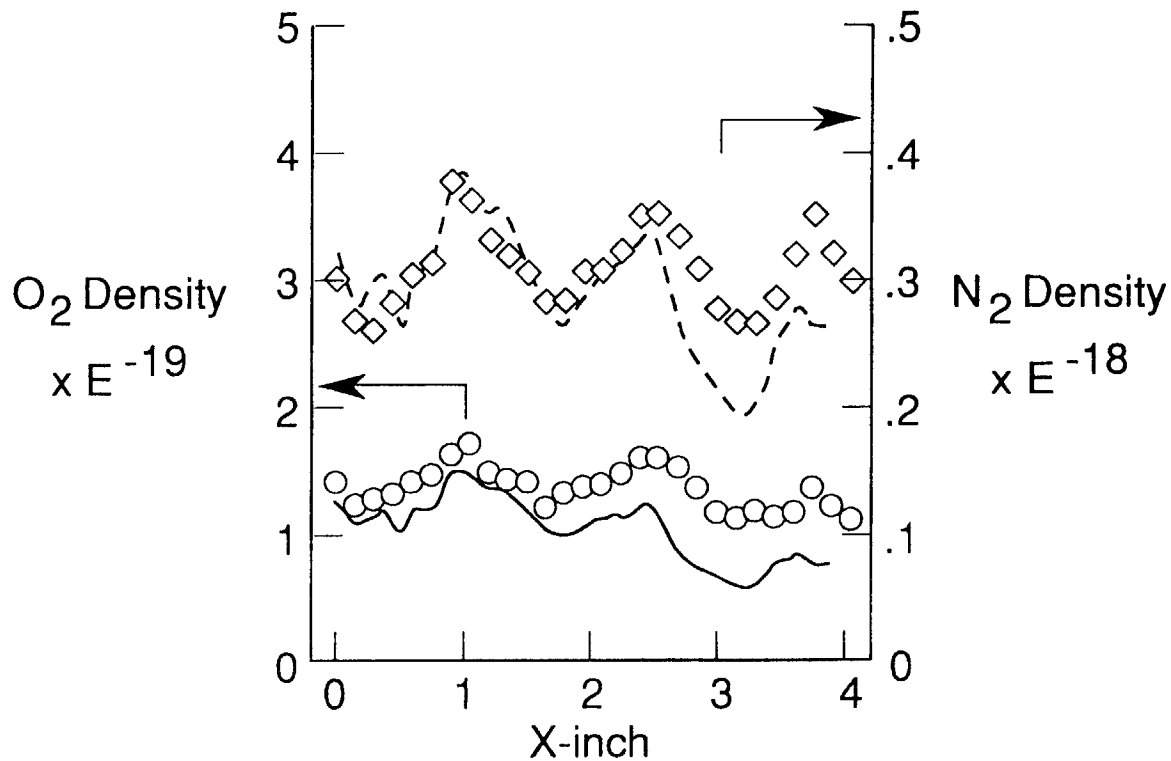

- Wavy distributions due to shock waves reflection from the free stream
- Flame was, infact, ignited by shock wave

RESULTS OF 2D ELLIPTIC CODE (CON'T)

Comparison of radial distributions at various streamwise stations

○ CARS —— CFD

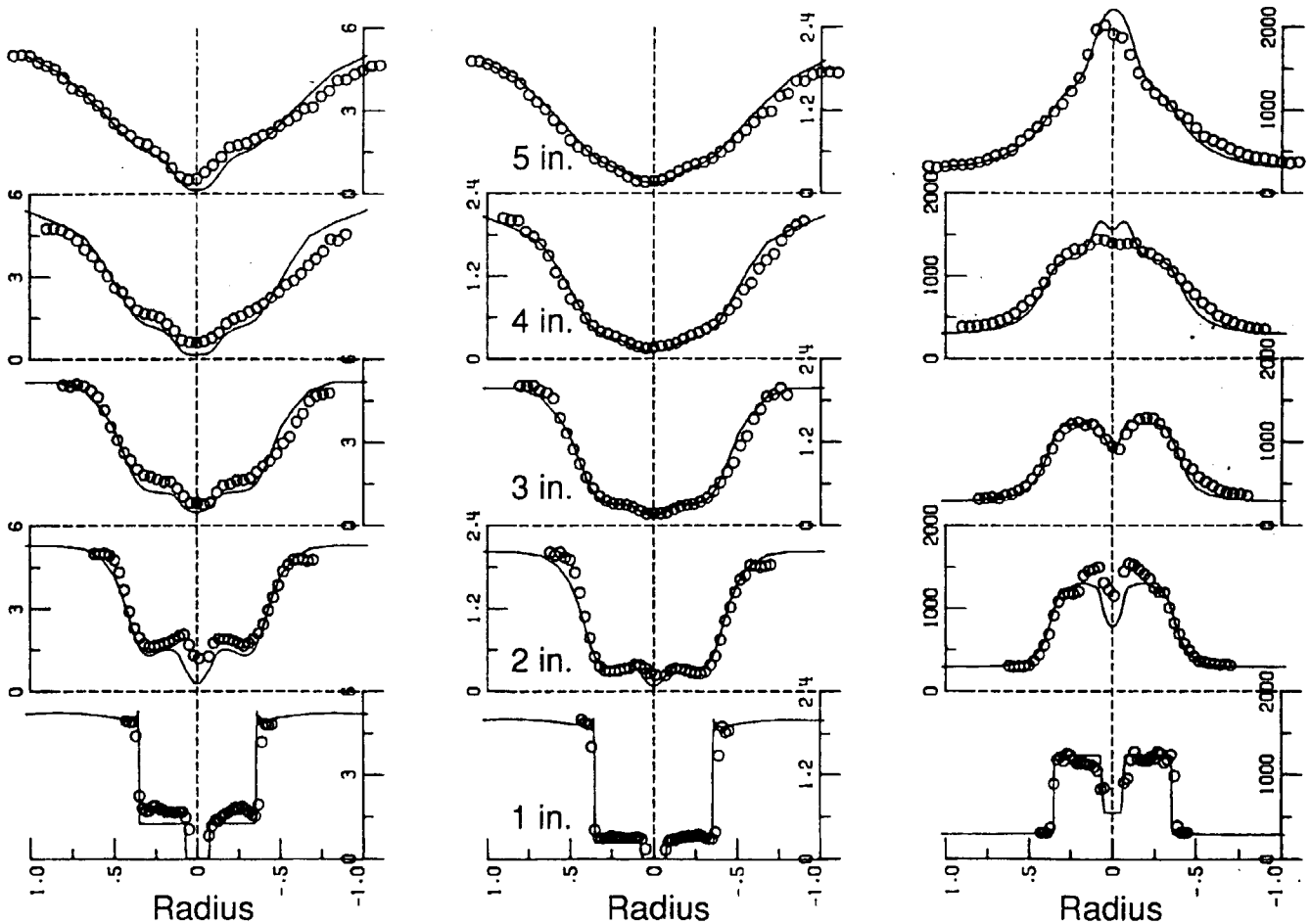

(O_2 x E^{-18}) (N_2 x E^{-19}) (Temperature, K)

ORIGINAL PAGE IS
OF POOR QUALITY

3D-CODE VALIDATION EXPERIMENT

- Subscale scramjet combustor (3.5"W, 4"L, 1.8"H) with :
  - Backward facing steps
  - Normal injections of H_2 pilot fuel, Silane ignitor fuel and H_2 primary fuel
  - 2° , Nozzle (4 ft long)
- Inflow gas was Mach 2 vitiated air at high enthalpy.
- Static pressures were measured at various points along the surfaces

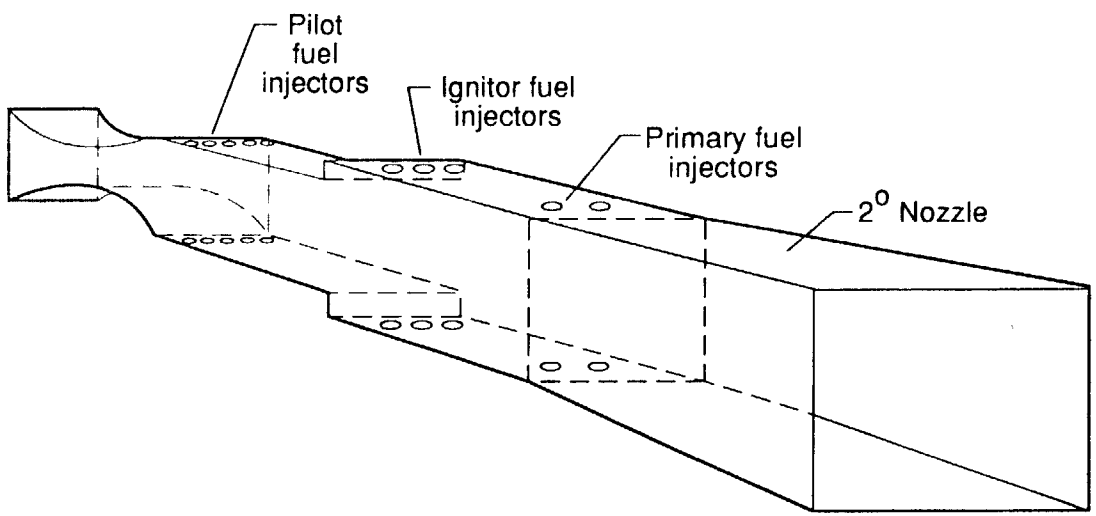

CONTOURS AND VECTORS PLOT THROUGH THE MAIN JET: NO COMBUSTION

Flow conditions: T_S = 810K, P_S = 1 atm, M = 2; ϕ = 0.43

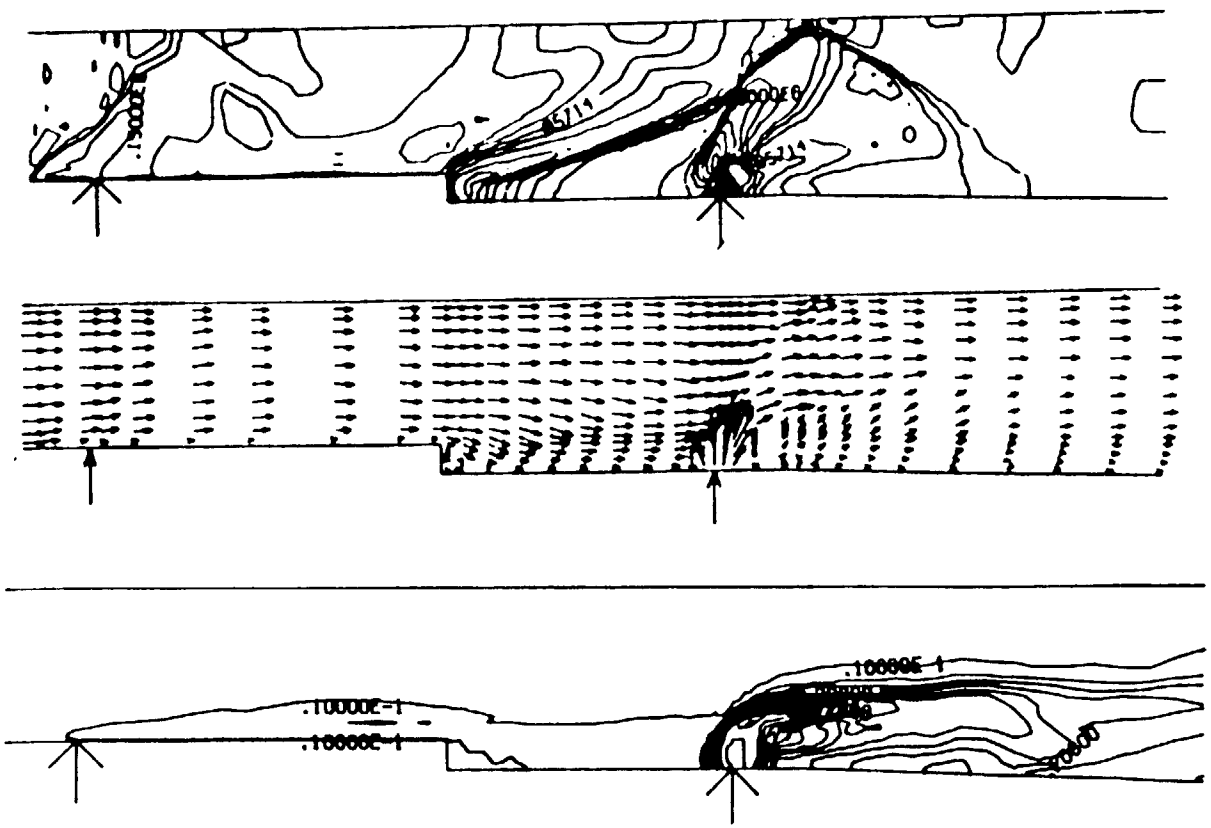

Pressure contours

Velocity vectors

Hydrogen contours

PRESSURE DISTRIBUTIONS ALONG BOTTOM WALL AT MIDPLANE

Flow conditions: T_S = 1200K, P_S = 1 atm, M = 2; ϕ = 0.48

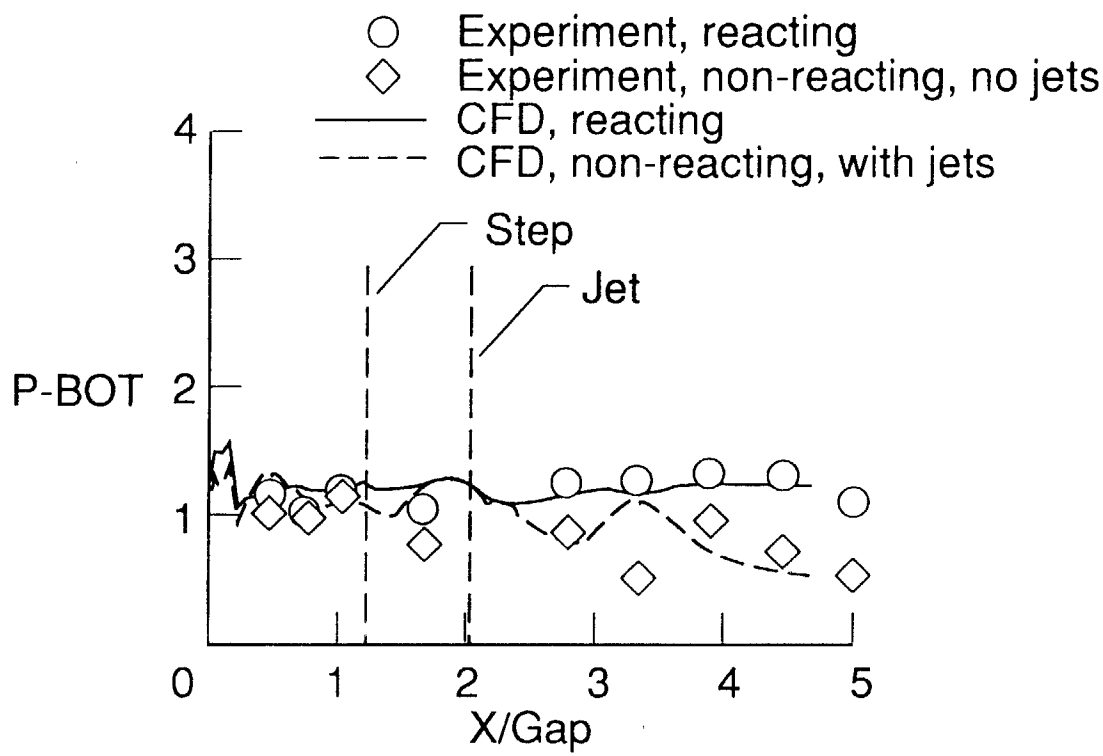

- Mixing and combustion efficiency at exit was underpredicted by 20%
- Prandtl mixing length hypothesis seems to work well

HYDROGEN CONTOURS AND VELOCITY VECTORS AT X = 1.5" DOWNSTREAM OF MAIN JET

Flow conditions: T_S = 1200K, P_S = 1 atm, M = 2; ϕ = 0.48

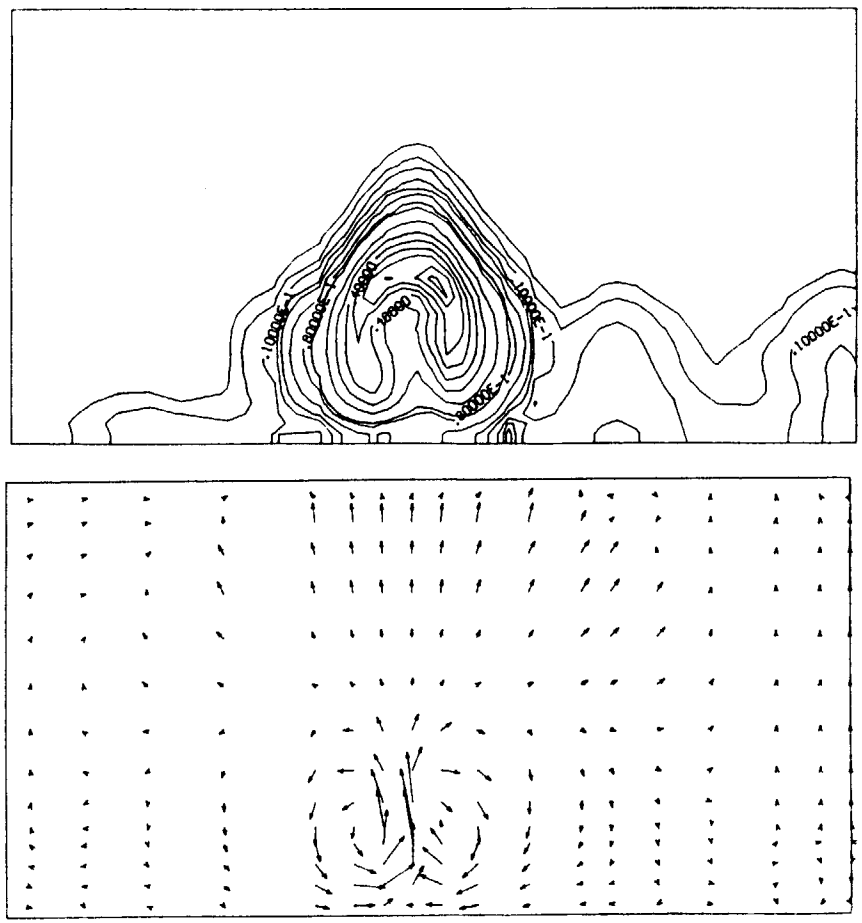

- Kidney shape profile
- Counter rotating vortices

3D-PNS CODE

- Applicable for supersonic high Reynolds number flow
- More efficient than full Navier-Stokes procedure
- Space marching technique using steady version of beam-warming algorithm (Vigneron, et al; Schiff-Steger)
- 4 Species, 2-step combustion model (Rogers-Chinitz) for hydrogen-air
- Fluid and chemical species are solved together creating block (9 x 9) tridiagonal system
- Baldwin-Lomax turbulence model
- See also AIAA Paper 84-0438

SCHEMATIC OF THE MODEL PROBLEM FOR THE 3D-PNS CODE

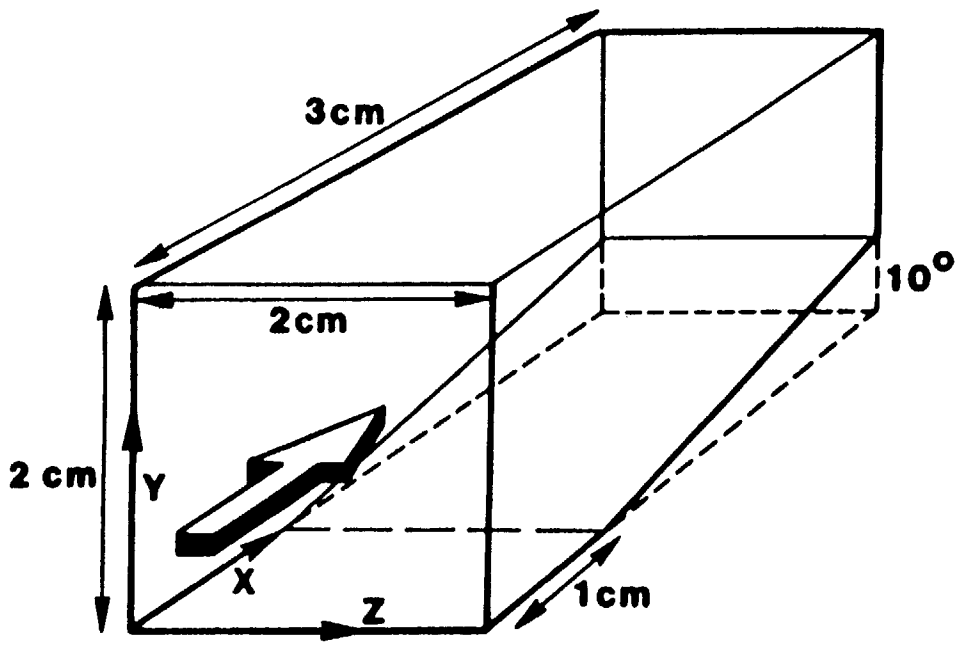

Inflow conditions: Mach = 4, T = 900K,
P = 1 atm, Equivalence ratio = 1

FLOW FIELD AT THE MIDPLANE

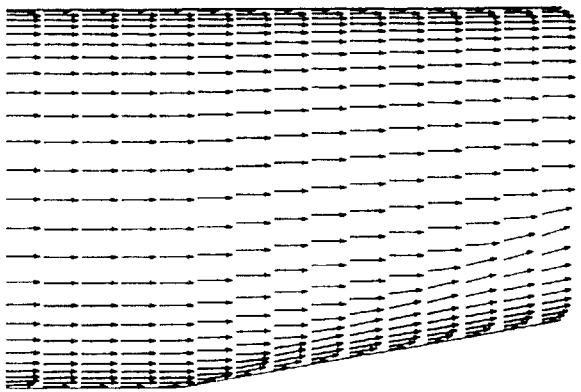

Velocity vectors

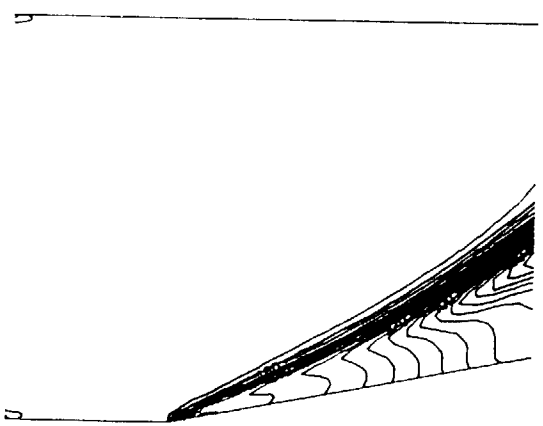

Pressure contours

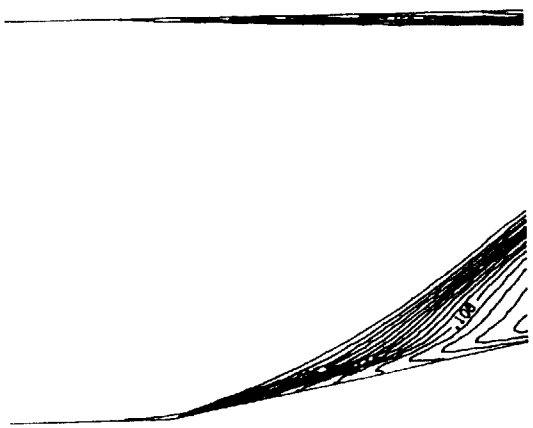

Water mass fraction contours

CONCLUDING REMARKS

- Computer codes are being developed and validated at HPB, FMD, NASA-LaRC
- Results so far have shown that MacCormack algorithm, despite some drawbacks, can give good physical results
- Simple Prandtl mixing length scheme is both viable and economical
- More sophisticated combustion and turbulence models can be used at the expense of computer time which is very costly for any 3D-reacting flow simulation
- 3D-PNS code is an economical alternative to the costly elliptic code provided that certain conditions are met
- Need to make the PNS algorithm more robust

ORIGINAL CONTAINS
COLOR ILLUSTRATIONS

HYPERSONIC CFD APPLICATIONS AT NASA LANGLEY

USING CFL3D AND CFL3DE

Pamela F. Richardson
NASA Langley Research Center
Hampton, Virginia

N91-10874

CFL3D/CFL3DE

- Time-dependent conservation law form of compressible Euler and Navier-Stokes equations
- Upwind-biased spatial differencing (Flux Vector Splitting - FVS and Flux Difference Splitting - FDS)
- Thin-layer, finite-volume implementation with algebraic turbulence model
- Zonal grids - longitudinally patched (for hypersonic flows)
  - CFL3D
    - 3-factor implicit time advancement algorithm
    - Thin-layer viscous in 3 directions - two wall corner model
  - CFL3DE
    - Streamwise-relaxation crossflow-AF, space-marching Euler or PNS, first or second order
    - Perfect gas or equilibrium air

INDUSTRY USE STATUS OF CODES

- NASP prime contractors - all instructed in code use at workshop August 2-3, 1988.
  - Production code for NASP for McDonnell Aircraft Company
  - Some use at General Dynamics
- Other industry use
  - Boeing
  - Northrup
  - United Technologies Research Center
- University use
  - Iowa State University
- Other government use
  - Naval Surface Warfare Center

SR71 - GEOMETRY DEFINITION

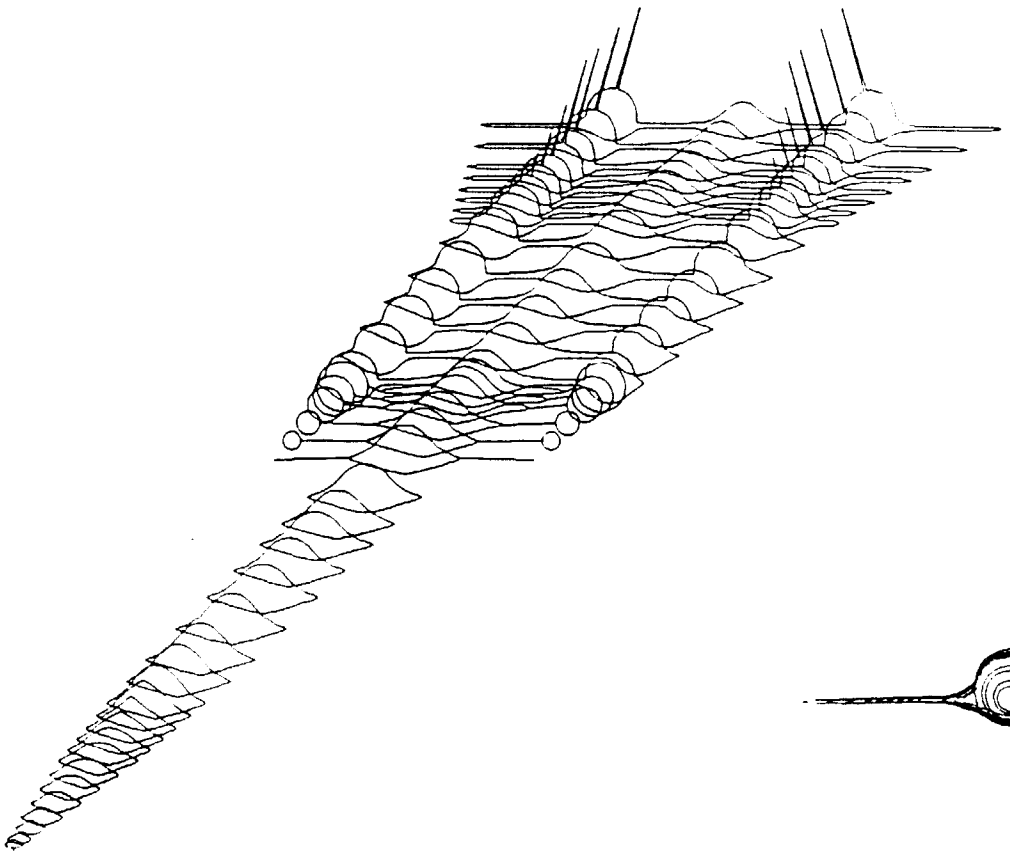

FOUR ZONES:

51X51X23
71X51X8
71X51X7
91X51X4

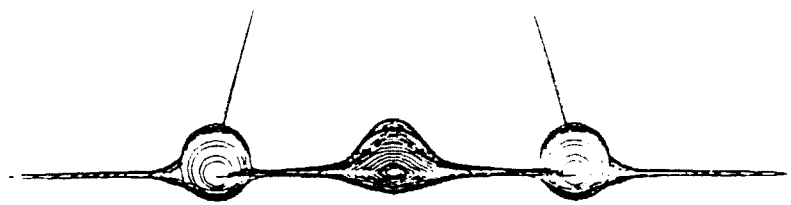

$M_\infty = 3.0 \quad \alpha = 0^o$

$\rho_\infty = 0.088 kg/m^3 \quad p_\infty = 5460 N/m^2$

SR71 - EQUILIBRIUM AIR EULER SOLUTION

CROSS-SECTION PRESSURE DISTRIBUTIONS AND GRID DEFINITIONS

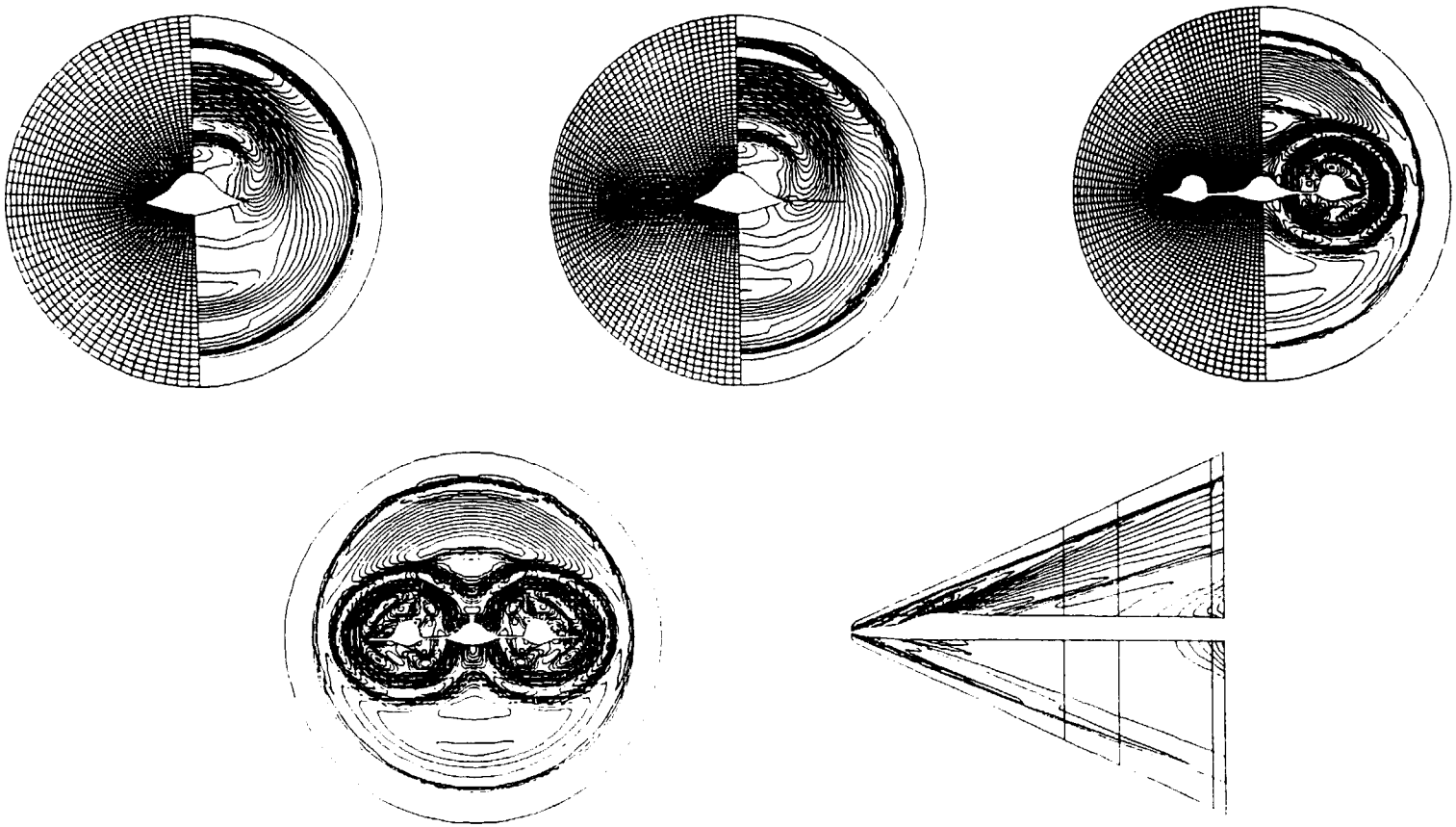

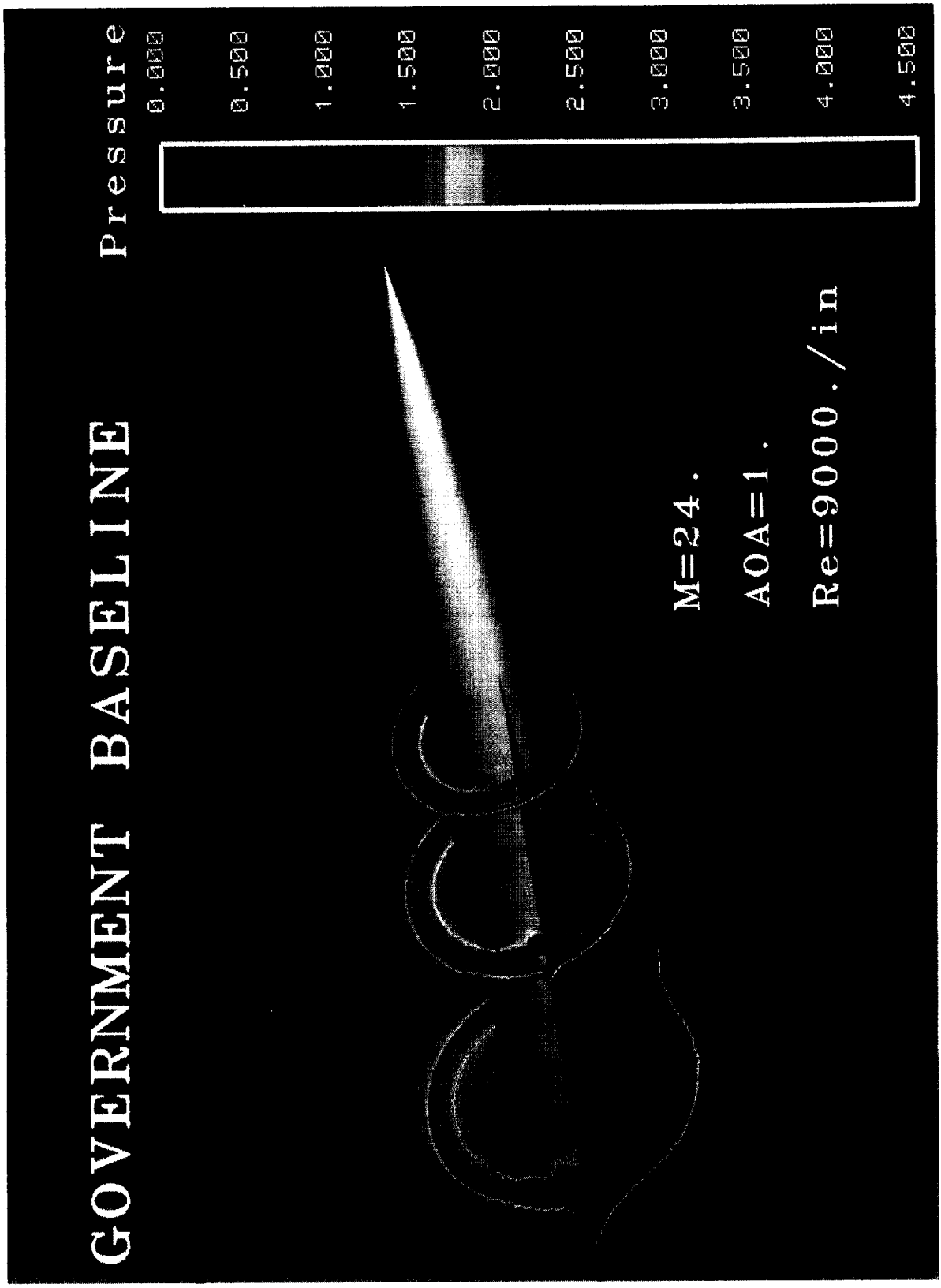

ORIGINAL PAGE IS
OF POOR QUALITY

PRECEDING PAGE BLANK NOT FILMED

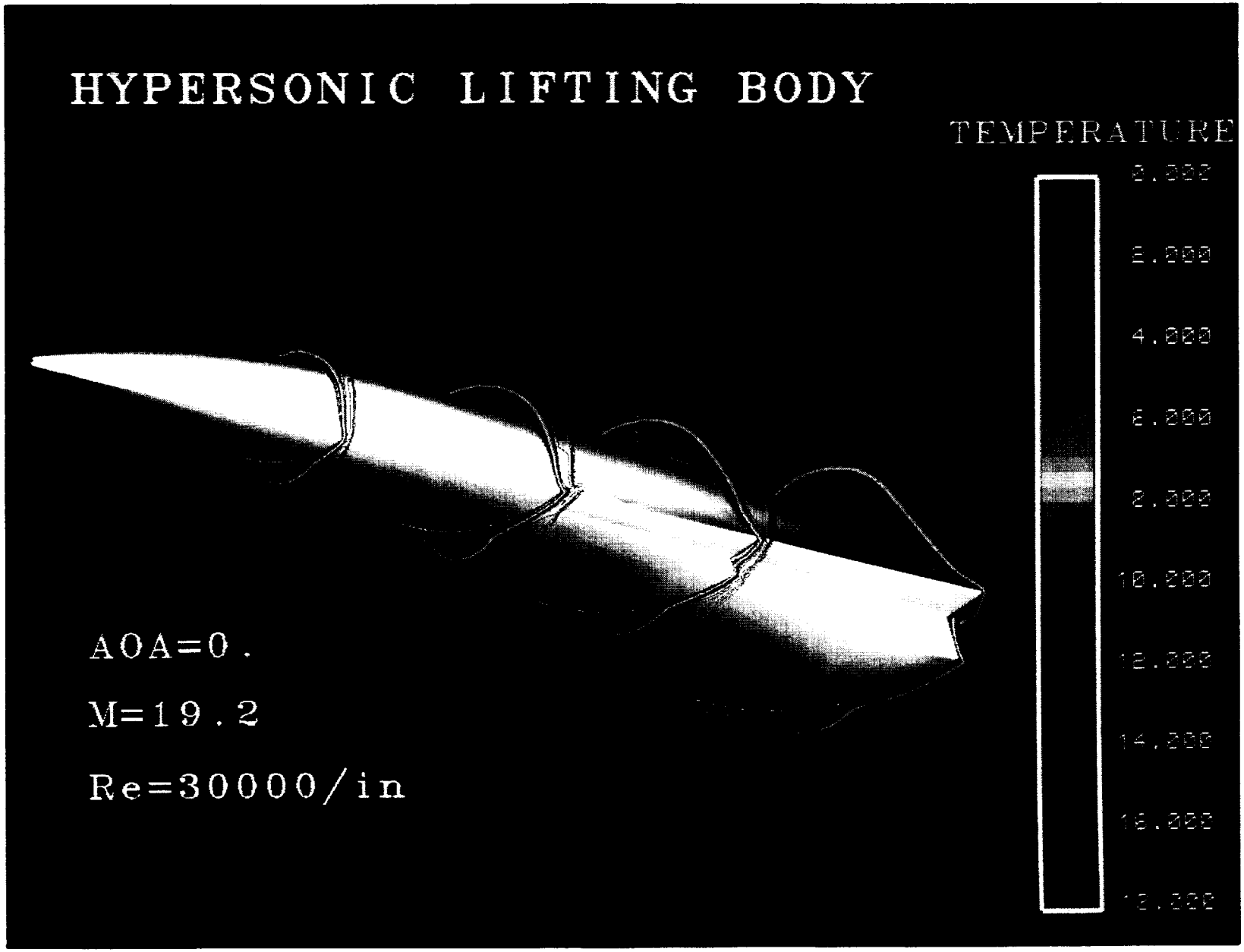

ORIGINAL PAGE IS
OF POOR QUALITY

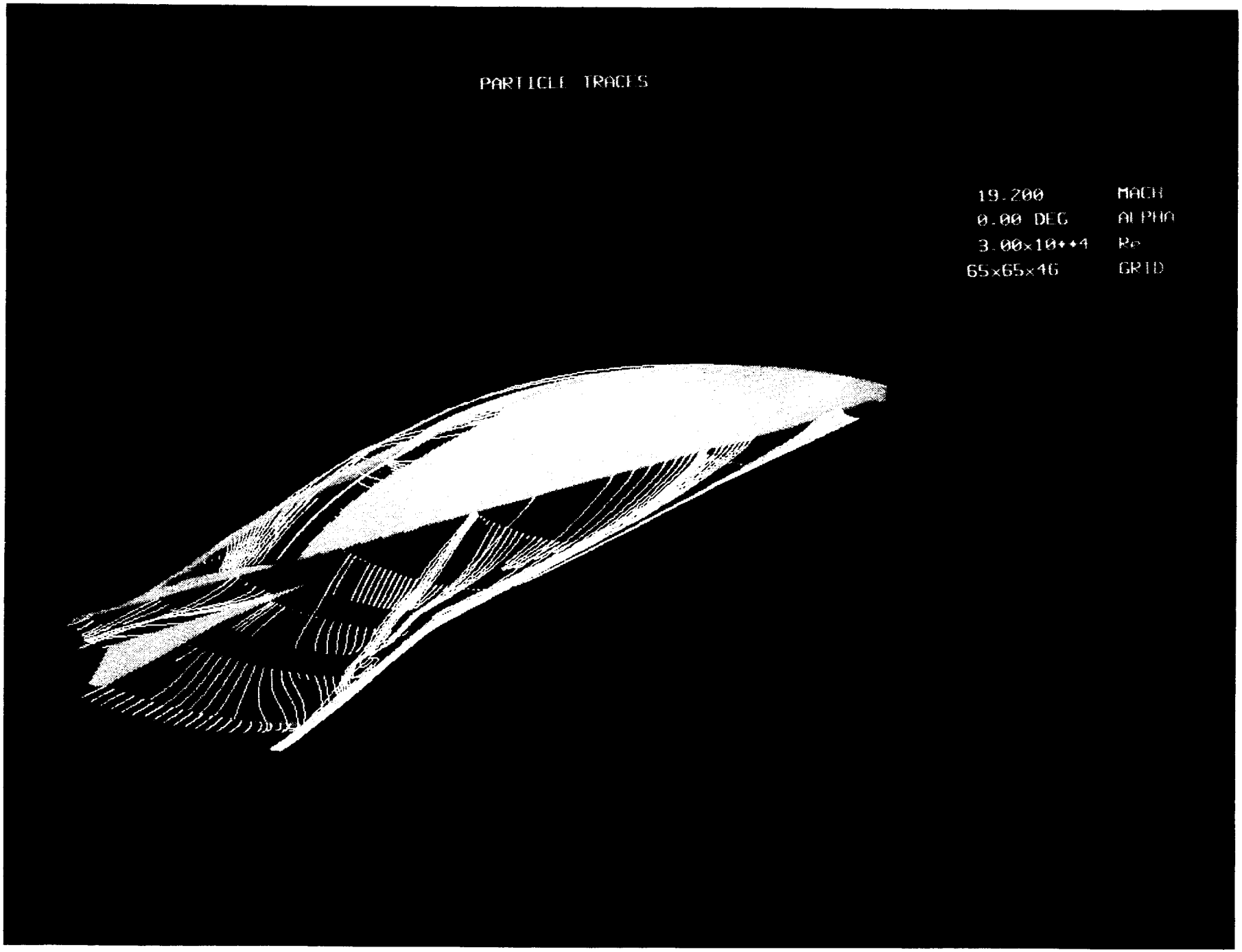
PARTICLE TRACES
19.200 MACH
0.00 DEG ALPHA
3.00x10++4 Re
65x65x46 GRID

GRID DENSITY COMPARISON

CROSS-SECTION 45 (COWL PLANE)

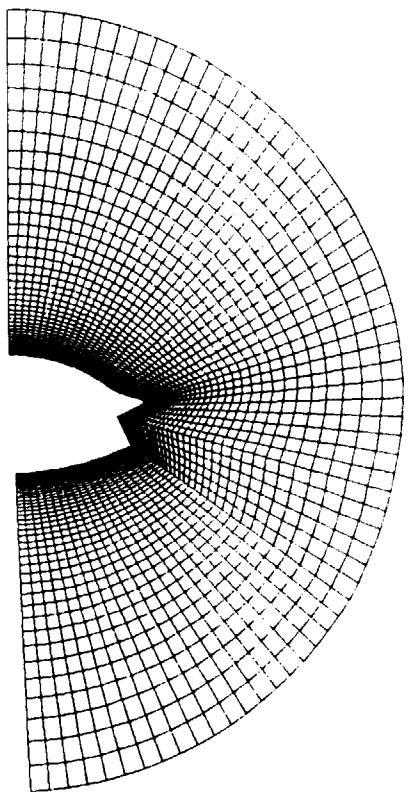

65 X 65 X 46 GRID
Y-PLUS ORDER 1.

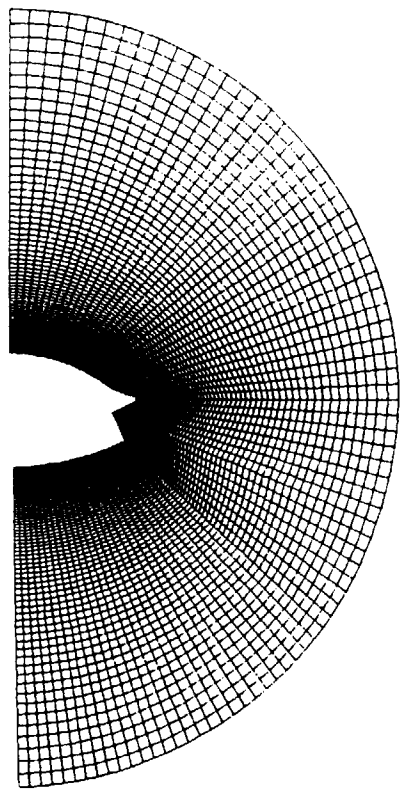

80 X 130 X 56 GRID
Y-PLUS ORDER .001

PRESSURE COMPARISONS

M = 12.55
Re = 2.7 million/ft.
Zero degrees angle of attack

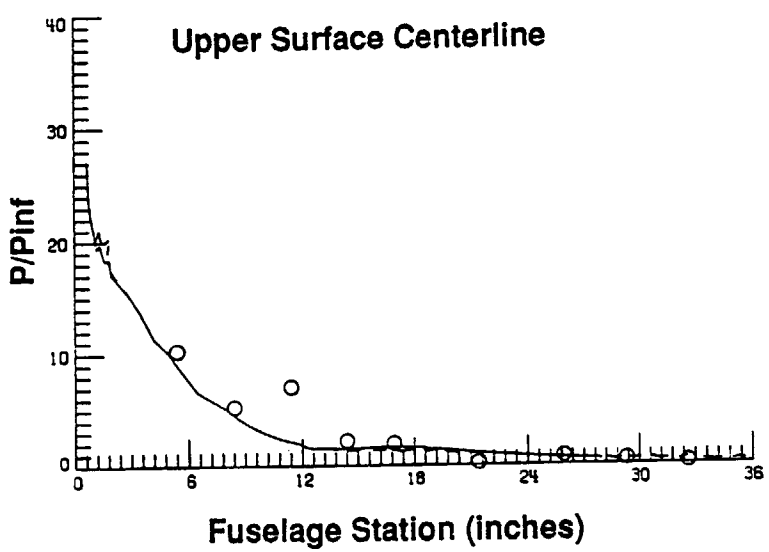

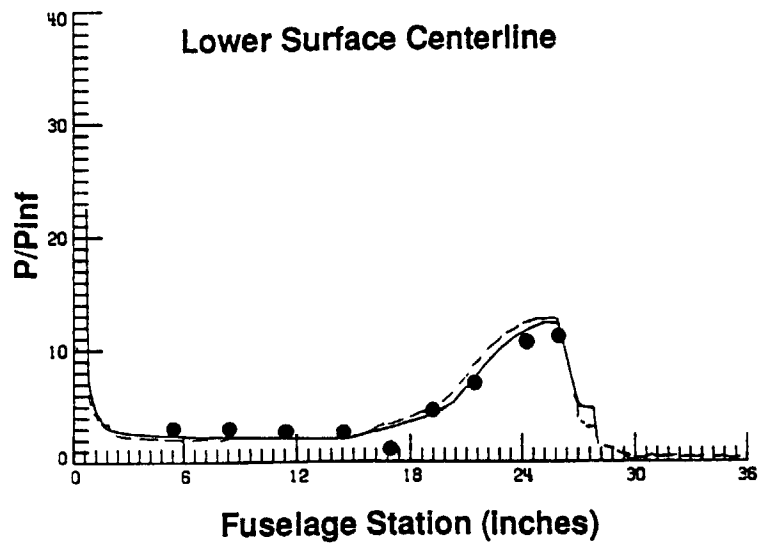

Open symbols - upper surface
Closed symbols - lower surface

HEAT TRANSFER COMPARISONS

M = 12.55
Re = 2.7 million/ft.
Zero degrees angle of attack

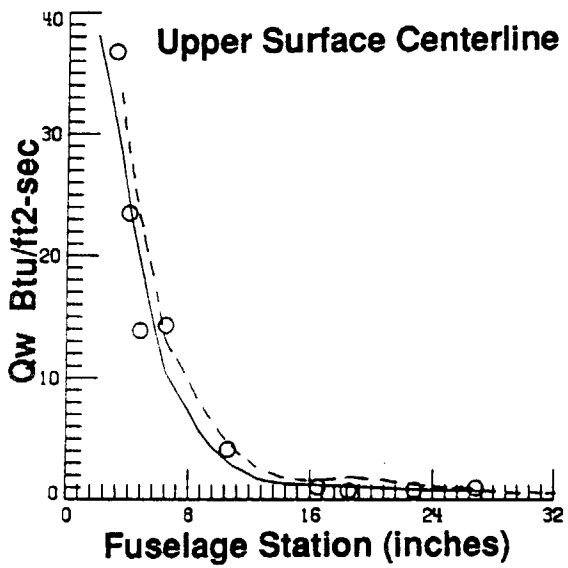

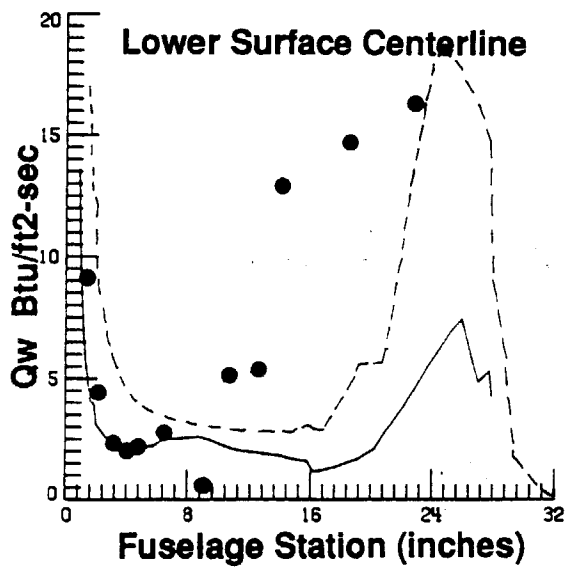

Open symbols - upper surface
Closed symbols - lower surface

AERODYNAMIC COEFFICIENTS COMPARISON MCDONNELL BLENDED WING BODY CFD AND EXPERIMENT

$M = 12.4$, $\alpha = 6^{o}$, Re/L = 930,000/ft

	CN	%ERROR	CA	%ERROR
AFWAL PNS	0.07154	3.1	0.02002	.9
MDC CFL3D	0.06956	5.8	0.01949	3.5
LARC CFL3D	0.07247	1.8	0.02154	6.6
Experiment	0.07382		0.02020	
Experimental Uncertainty		7.5		6.4

PRECEDING PAGE BLANK NOT FILMED

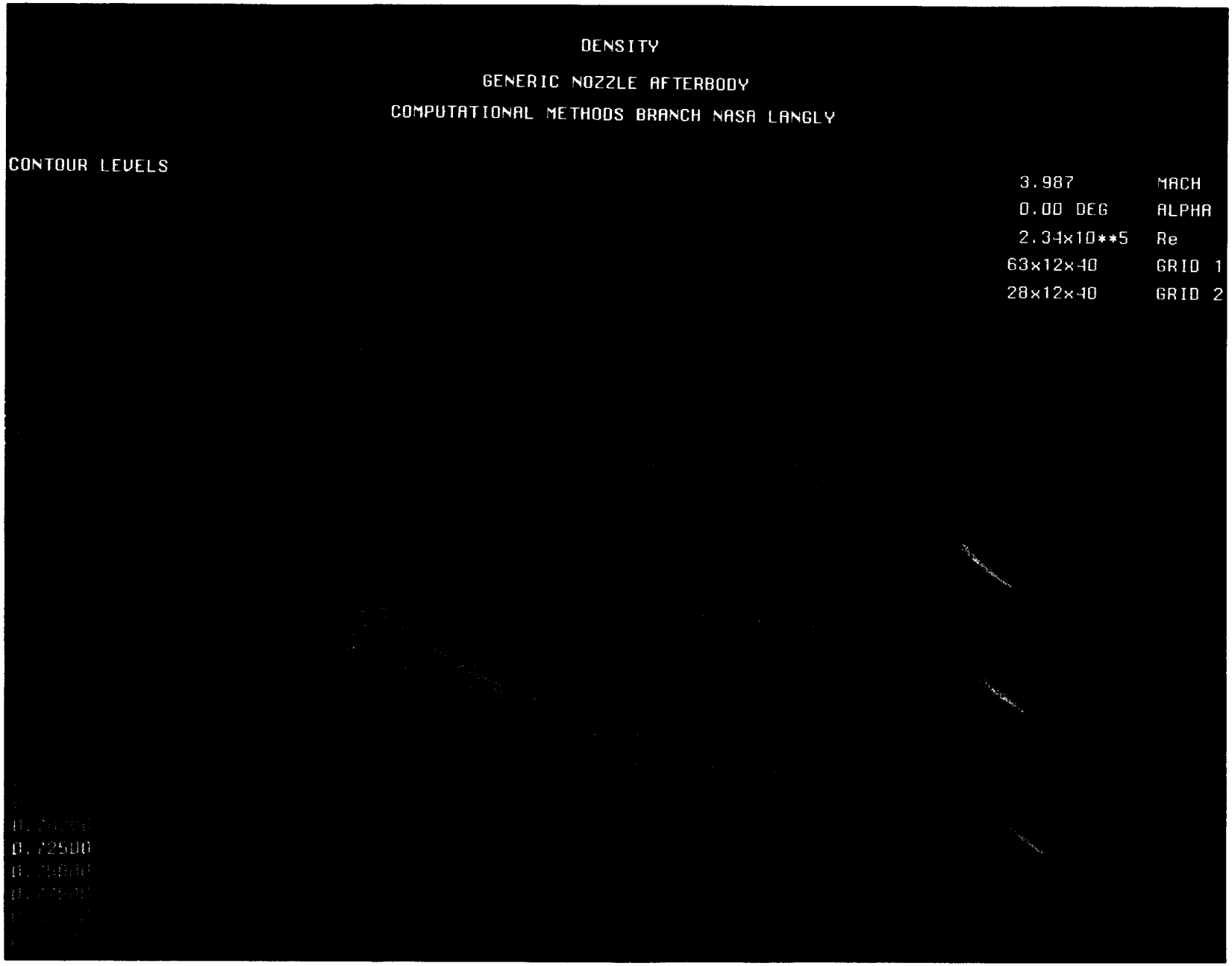

ORIGINAL PAGE IS
OF POOR QUALITY

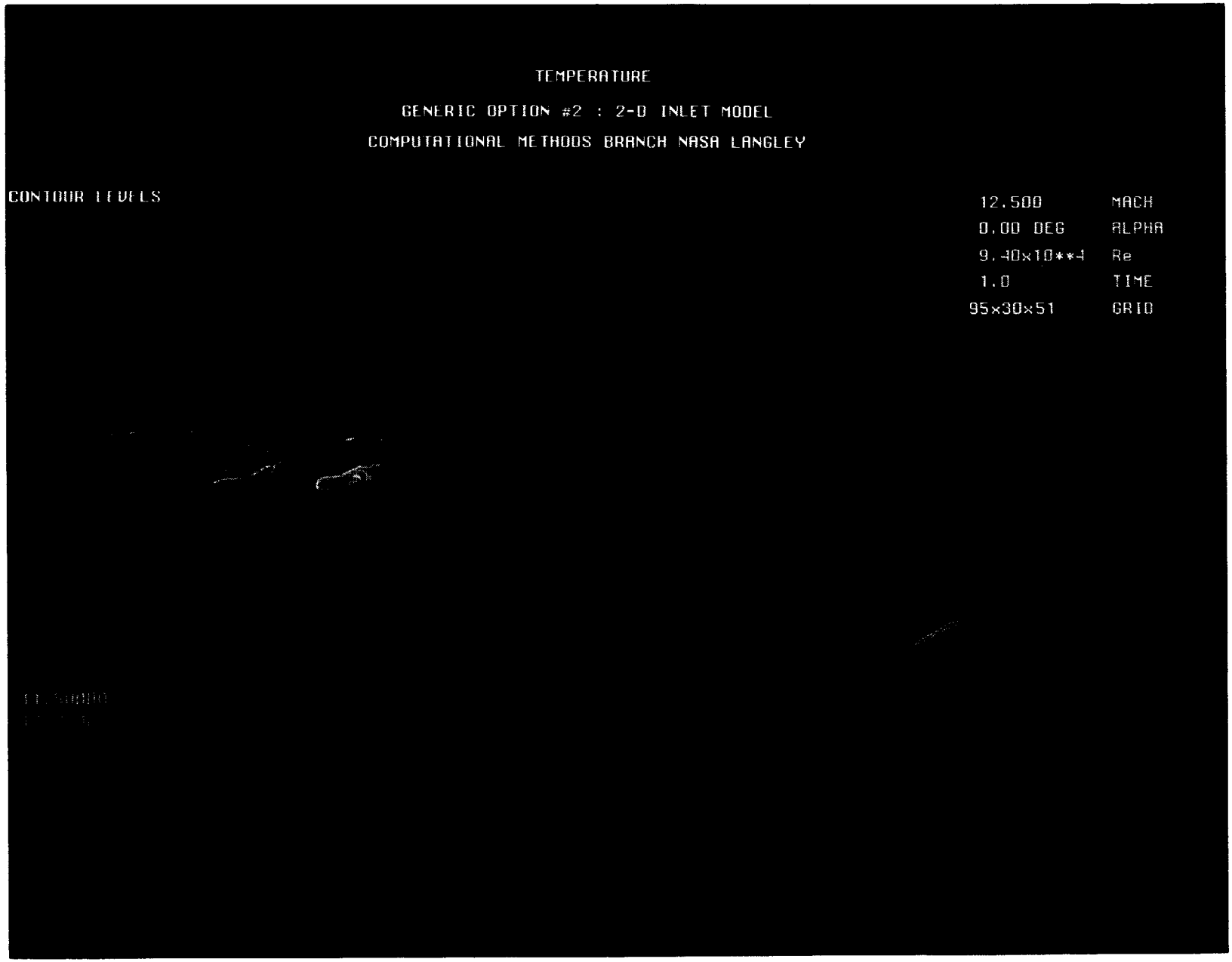
TEMPERATURE
GENERIC OPTION #2 : 2-D INLET MODEL
COMPUTATIONAL METHODS BRANCH NASA LANGLEY
CONTOUR LEVELS
12.500 MACH
0.00 DEG ALPHA
9.40x10**4 Re
1.0 TIME
95x30x51 GRID

ORIGINAL PAGE IS
OF POOR QUALITY

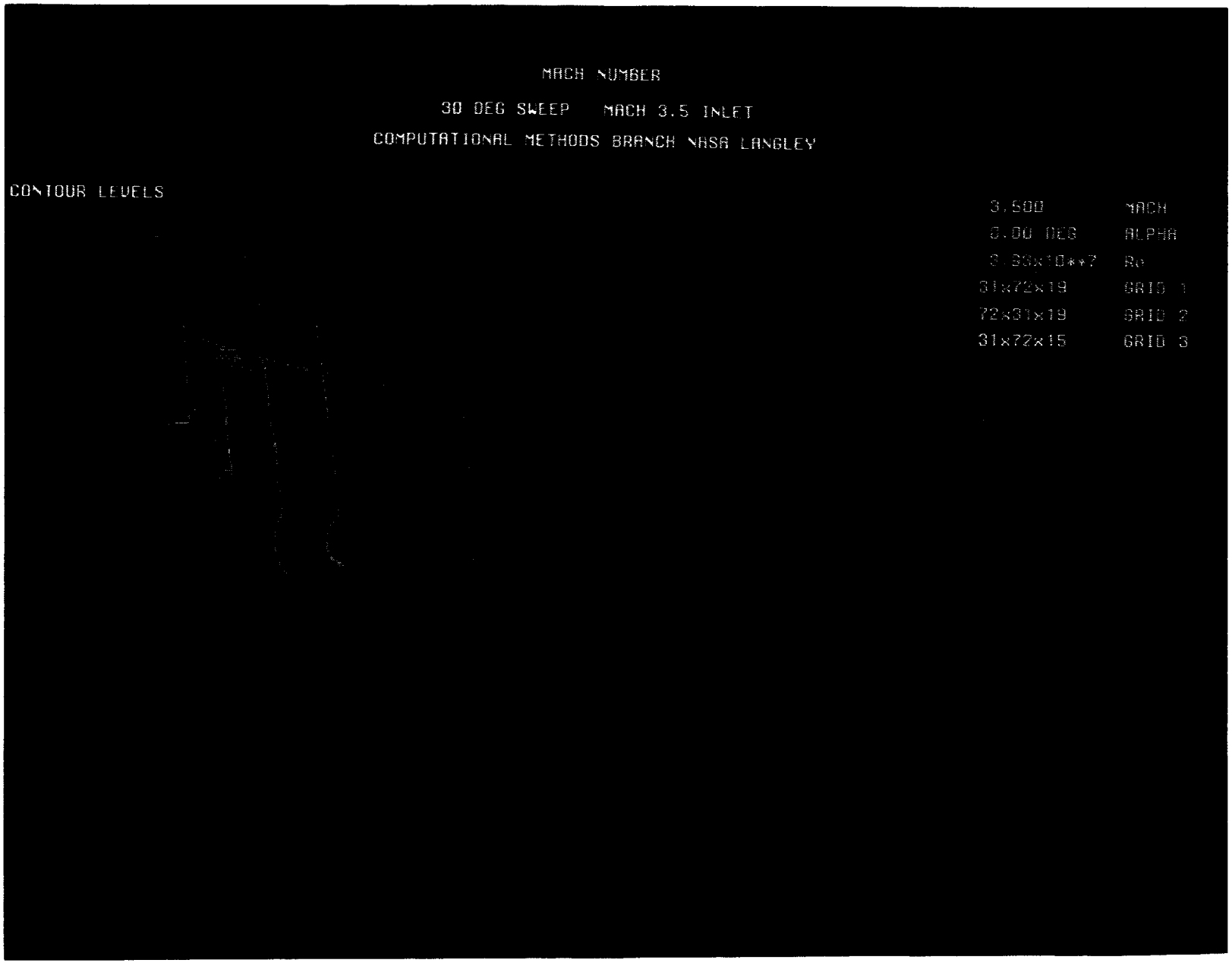

PRECEDING PAGE BLANK NOT FILMED

FUTURE PLANS RELATED TO THE NATIONAL AERO-SPACE PLANE PROGRAM

- Continue to expand the envelope of capabilities for the code to include calculations of an entire NASP-like configuration
  - Improved zonal capabilities for inlets with sweep and combustors
  - Addition of non-equilibrium chemistry for combustor and nozzle/afterbody calculations
  - All capabilities scheduled for production code by 1/90 (NASP Technology Maturation Program)

SESSION VIII

SPACE SHUTTLE

Chairman:
Luke A. Schutzenhofer
Chief, Computational Fluid Dynamics Branch
NASA Marshall Space Flight Center

PRECEDING PAGE BLANK NOT FILMED

N91-10875

NUMERICAL AERODYNAMIC SIMULATION OF THE SPACE SHUTTLE ASCENT ENVIRONMENT

J.P. Slotnick
Lockheed Engineering and Sciences Company, Houston, TX
F.W. Martin, Jr.
NASA Lyndon B. Johnson Space Center, Houston, TX

in collaboration with the

NASA Ames Space Shuttle Flow Simulation Group
P.G. Buning, I.T. Chiu, R.L. Meakin, S. Obayashi, Y.M. Rizk
S. Ben-Shmuel, J.L. Steger, and M. Yarrow
NASA Ames Research Center, Moffett Field, CA

ABSTRACT

After the STS 51-L accident, an extensive review of the Space Shuttle Orbiter's ascent aerodynamic loads uncovered several questionable areas that required further analysis. The insight gained by comparing the Shuttle ascent CFD numerical simulations, obtained by the NASA Ames Space Shuttle Flow Simulation Group led by Dr. J.L. Steger, to the current IVBC-3 aerodynamic loads database was instrumental in resolving uncertainties on the Orbiter payload bay doors and fuselage. Initial confidence in the numerical simulations was gained by comparing them with the limited flight data that had been obtained during the Orbiter Flight Test (OFT) program. Current CFD results exist for Mach numbers 0.6, 0.9, 1.05, 1.55, 2.0, and 2.5. Since the pre STS-1 wind tunnel test program (IA-105) often yields considerable differences when compared to STS-5 flight data, the M_∞=1.05 transonic case is the most investigated. The IA308 mated-vehicle hot gas plume wind tunnel test, recently completed at AEDC 16T (transonic) and Lewis (hypersonic), is also used to compare with the computation where applicable.

PRECEDING PAGE BLANK NOT FILMED

Objective

- *Joint* effort between the ARC team led by J.L. Steger and P.G. Buning and a JSC team led by F.W. Martin, Jr.

- ARC Team : Develop the technology to numerically simulate the complex launch vehicle (SSLV) geometry in a time accurate manner to
  - compute SSLV flowfield data
  - support Fast Separation Abort study
  - assist JSC with Orbiter problematic issues:
    - Crew Escape flowfield
    - STS-27 Debris Study flowfields

- JSC Team : Apply the CFD technology to gain insight into the ascent aerodynamic loads environment
  - SSLV payload bay pressure distribution
  - Orbiter Wing Loads

Jeff P. Slotnick / March 8, 1989

Scope

- ARC Team
  - Model the Orbiter ascent configuration with the *Chimera* composite grid discretization approach.
  - Overset body-conforming grids for each major component (CALSPAN *Pegasus* code).
  - Apply *F3D*, an implicit approximately factored finite-difference procedure, to solve the three-dimensional thin-layer Navier-Stokes equations.
  - Employ the NAS Cray 2 and Cray Y-MP.

- JSC Team
  - Provide technical guidance and evaluate ARC results with respect to existing databases:
    - ▷ IA-105 WTT, high resolution model.
    - ▷ IA-308 WTT, hot gas plume simulation.
    - ▷ *Limited* flight data from STS-1 through STS-5.
    - ▷ IVBC-3 operational database.

Justification

The Orbiter's modest structural capability, coupled with a complex launch vehicle configuration and severe ascent environment, places unprecendented demands on the aerodynamacist.

- Orbiter structure was designed to civil transport specifications.
  - Consistent with entry flight envelope.
  - $\bar{q} \approx 350$ psf, g_z=2.5 (g_z=2.25 as weight increases).
- Ascent environment is considerably more severe, $\bar{q}$=750-819 psf, with the simultaneous occurance of:
  - maximum $\bar{q}$
  - jet stream penetration (perturbates α, β and $\bar{q}$)
  - transonic flow field
  - maximum differential pressure, inside-outside, as the vehicle vents
  - plume/flow field interactions
  - High R_e ($\sim$ 100 million) at maximum load condition

Historical Perspective

- Discrepancies exist between aerodynamic predictions and flight experience.

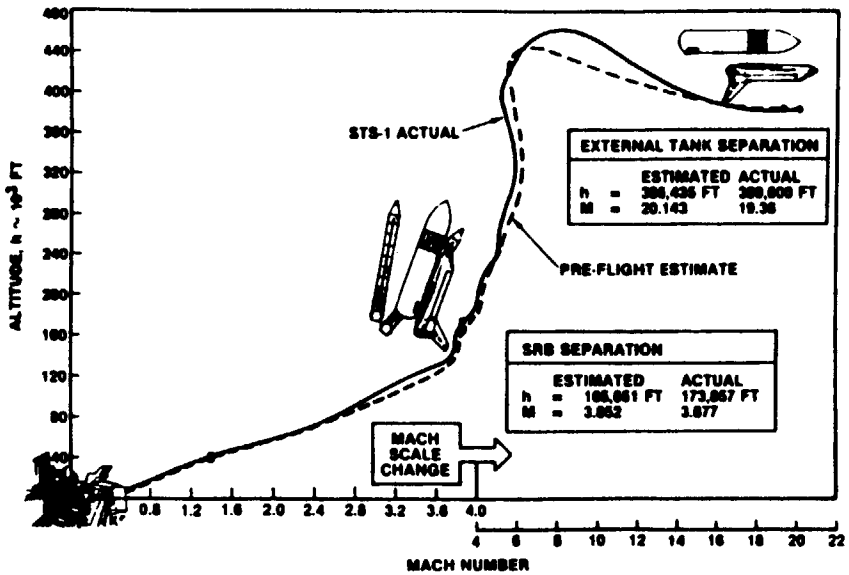

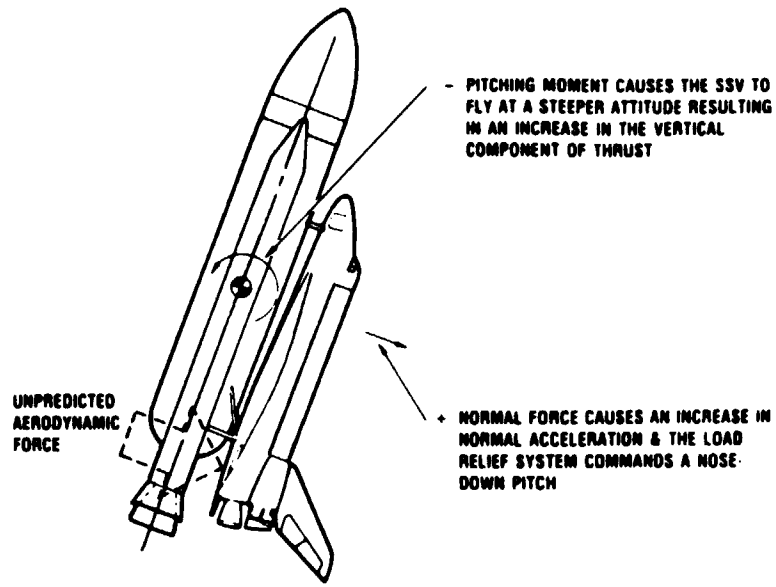

- Force and moment data was easily corrected with flight derived aerodynamic increments.
- Aerodynamic loads (pressure distribution) cannot be readily corrected because of *limited* flight pressure measurements.

ORIGINAL PAGE IS OF POOR QUALITY

Current Database

- The *I*ntegrated *V*ehicle *B*aseline *C*onfiguration (IVBC) - 3 aero loads database is a composite of
  - IA-105 WTT data
  - Flight pressure measurements
  - Flight strain measurements
  - Engineering judgement
- This resulting database contains relatively large uncertainties which have led to structural analysis predictions that were inconsistent with flight experience, especially in the payload bay door area.

Selected STS-5 Tap Points

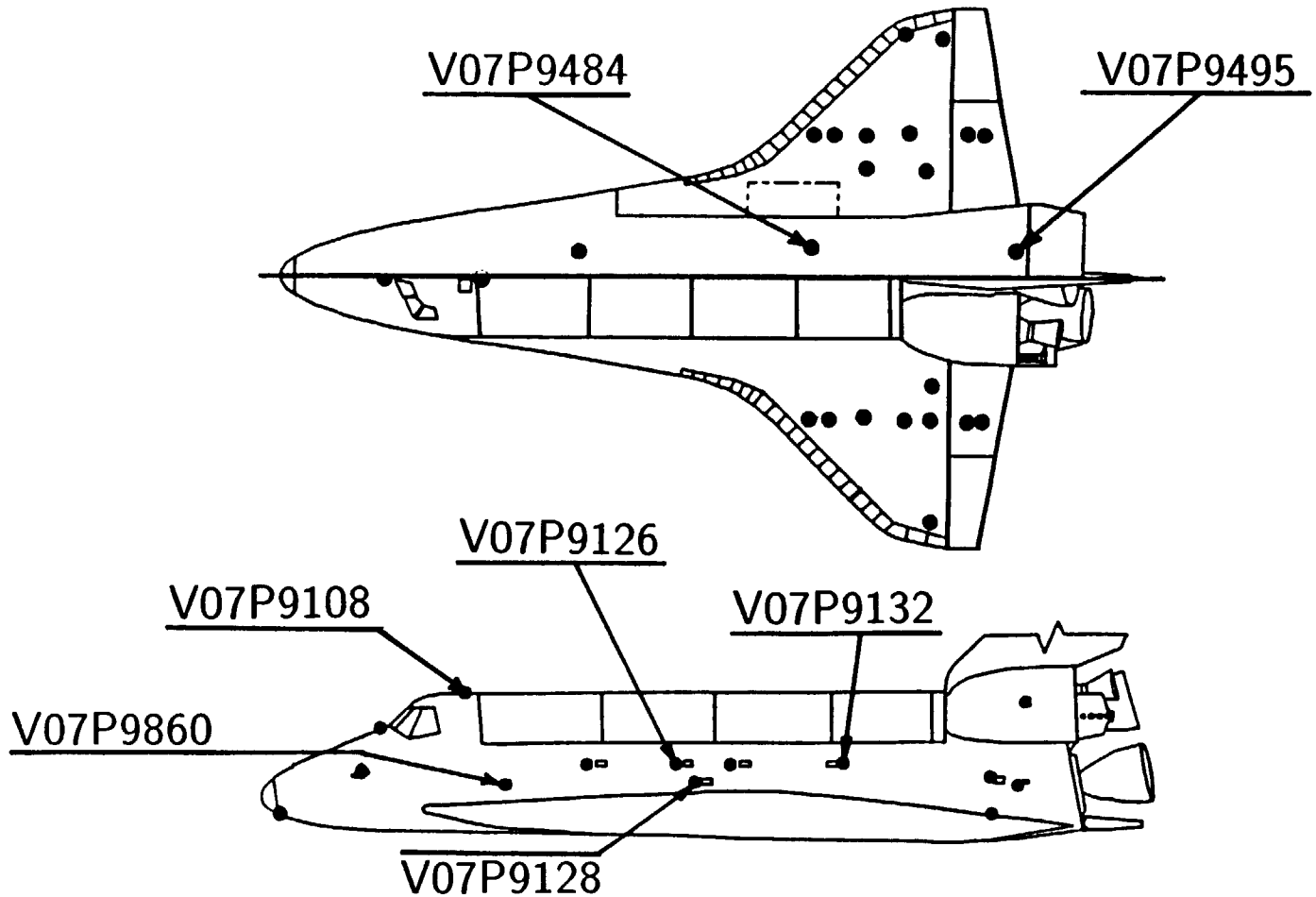

Jeff P. Slotnick / March 8, 1989

AERO DATABASE COMPARISONS

TAP V07P9108A CP HISTORY

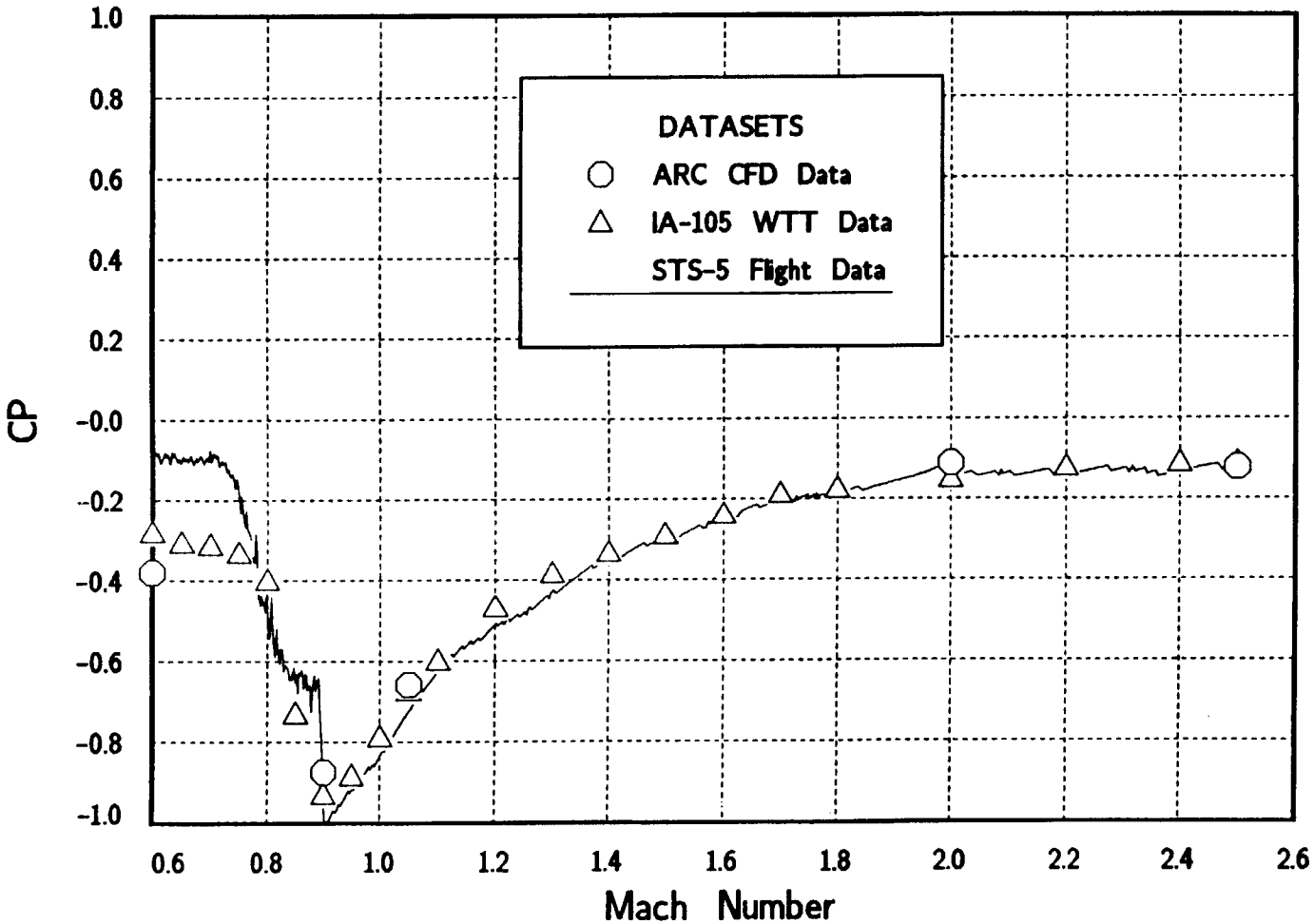

AERO DATABASE COMPARISONS

TAP V07P9495A CP HISTORY

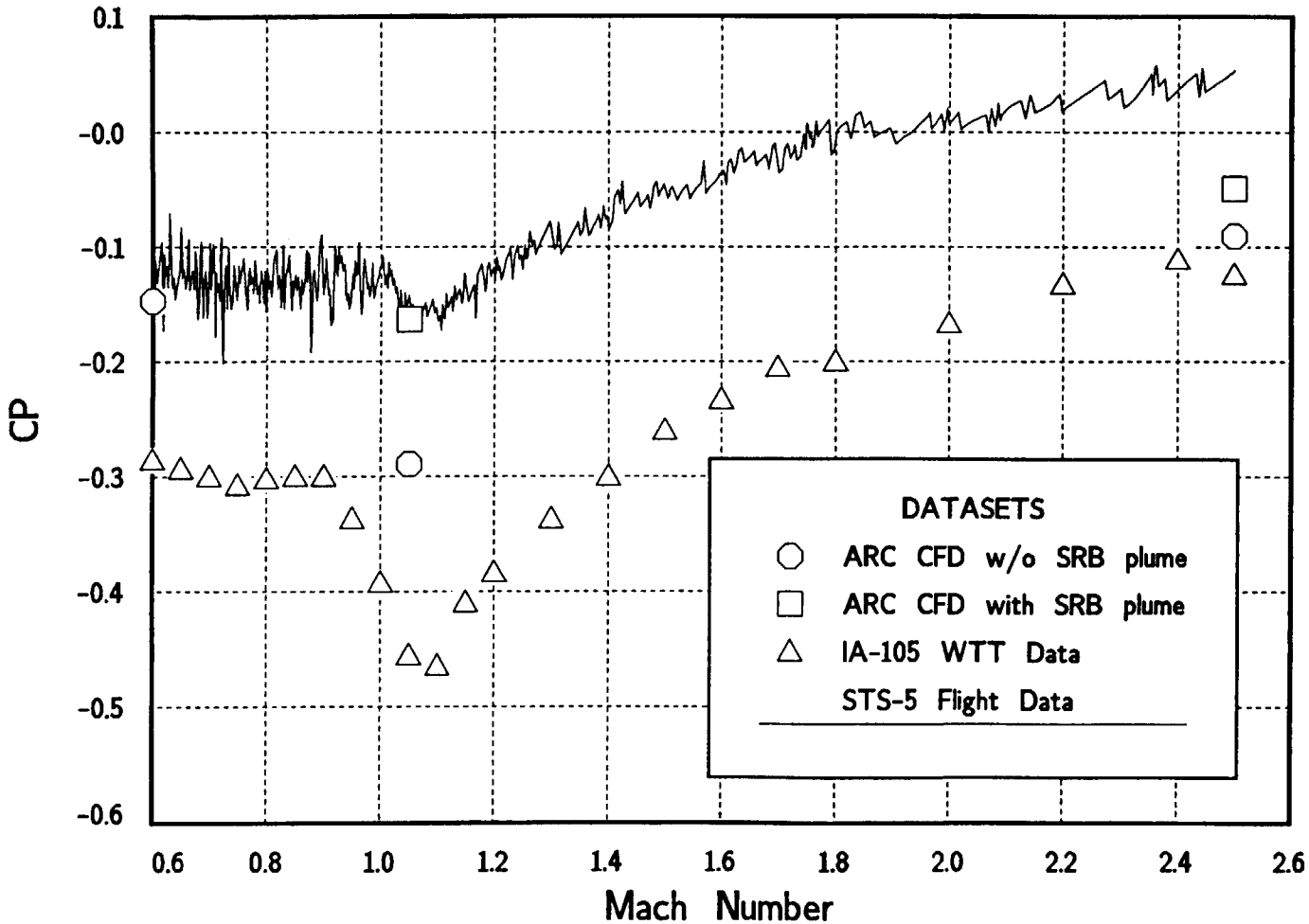

AERO DATABASE COMPARISONS

ORBITER Upper Pitch Plane CP Distributions

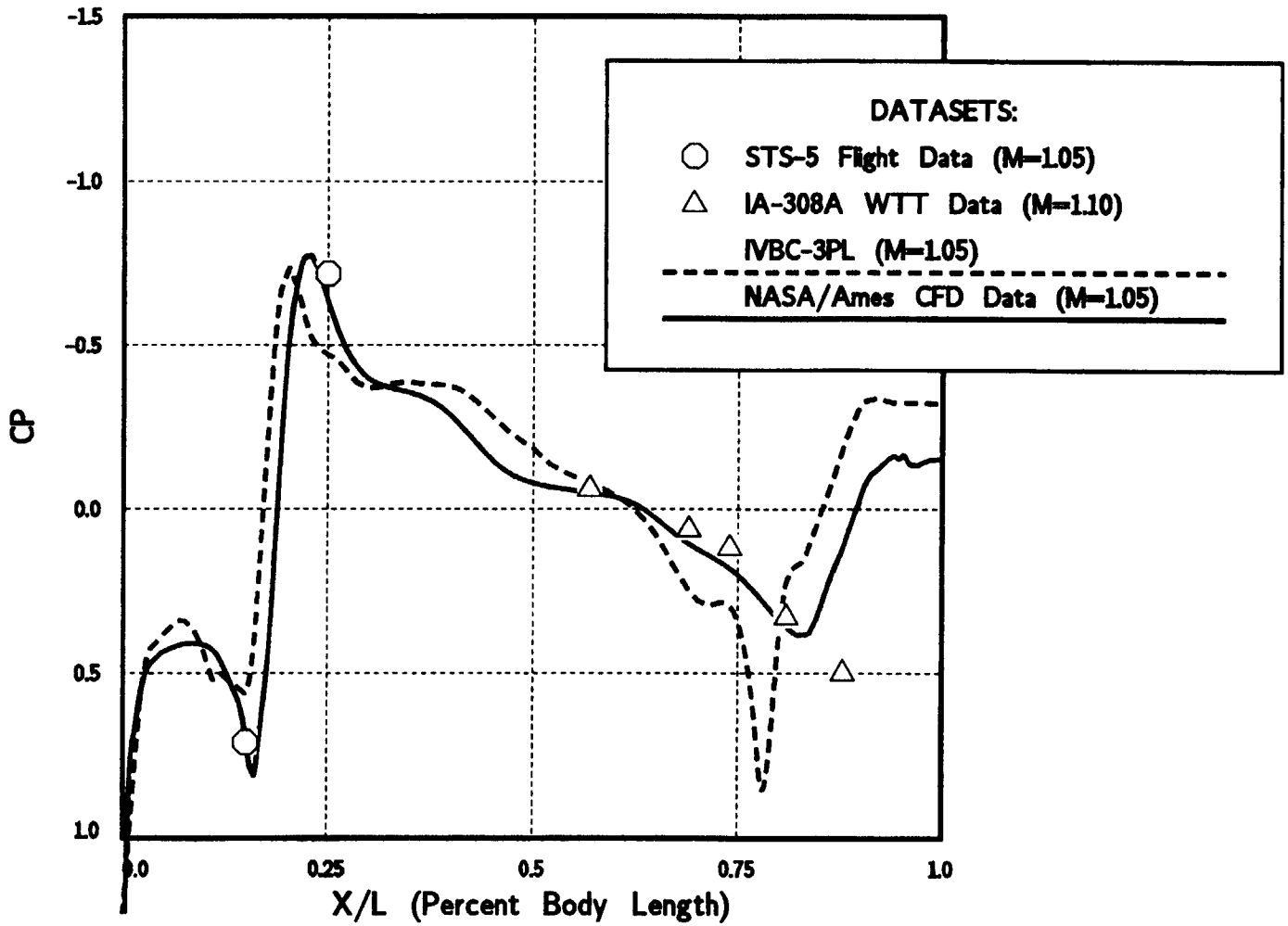

AERO DATABASE COMPARISONS

ORBITER Mid-Fuselage Region CP Distributions

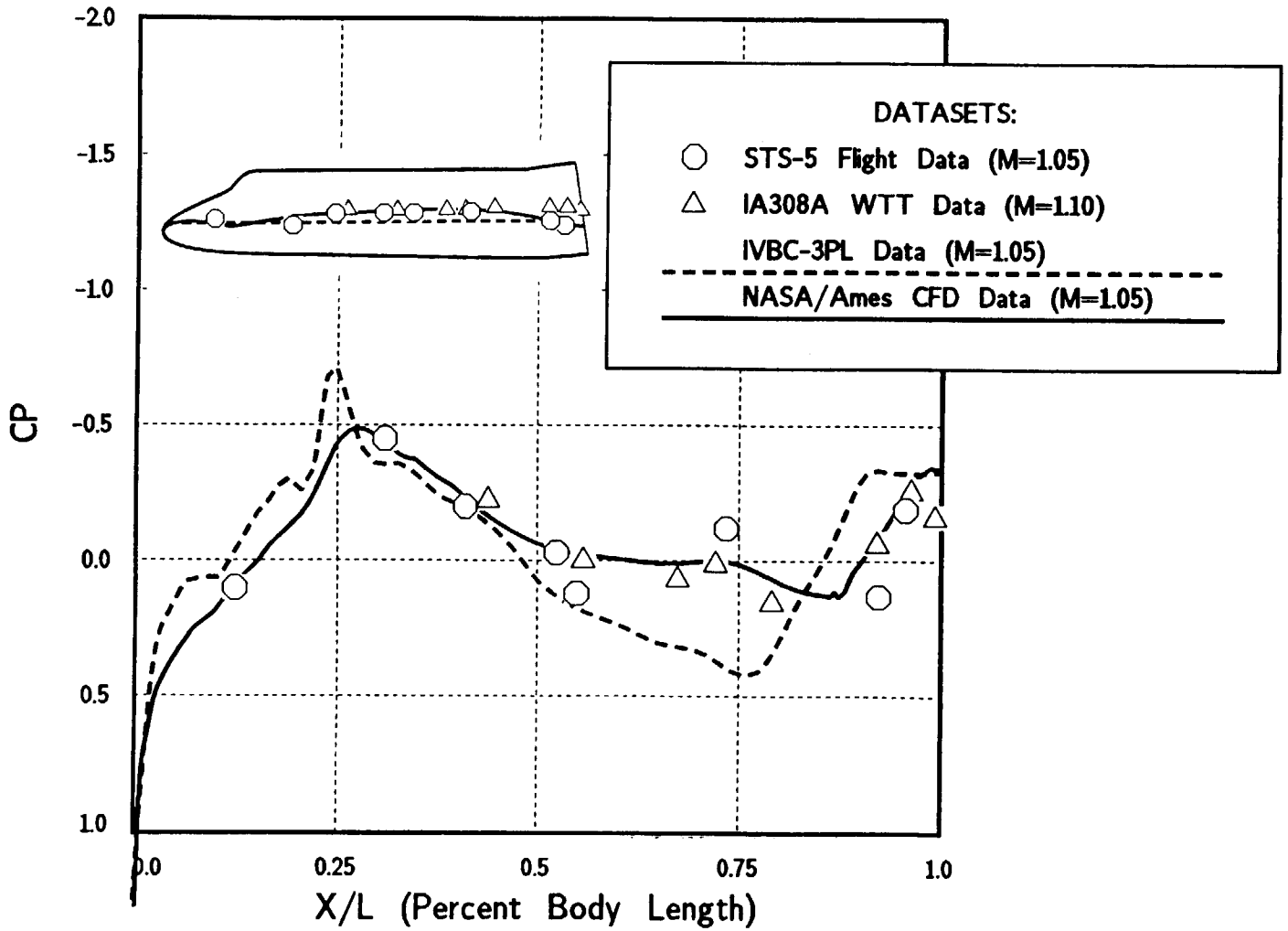

PAYLOAD BAY DOOR PRESSURE COMPARISONS

ORBITER X-STATION (X0) = 590 inches

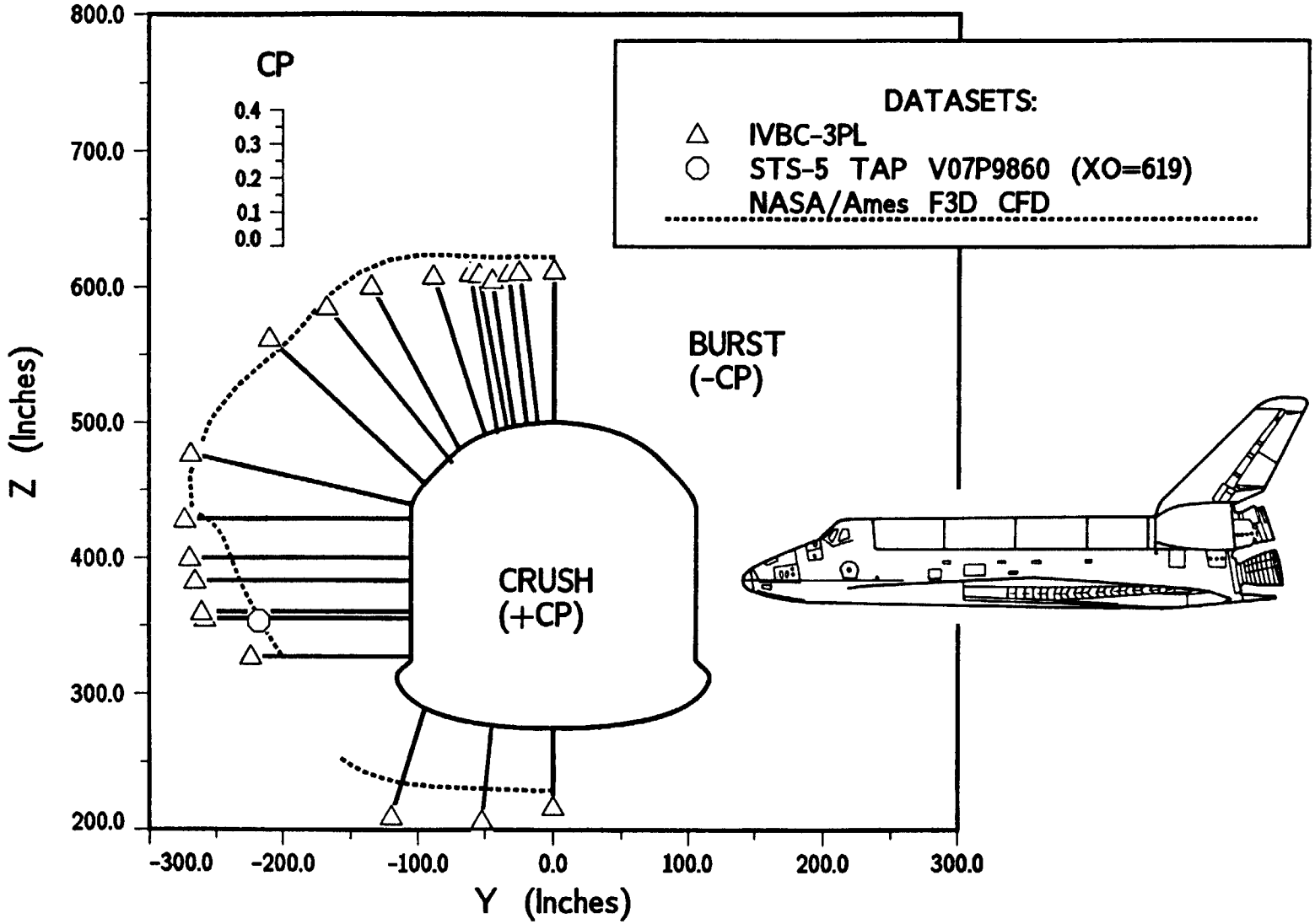

PAYLOAD BAY DOOR PRESSURE COMPARISONS
ORBITER X-STATION (X0) = 905 inches

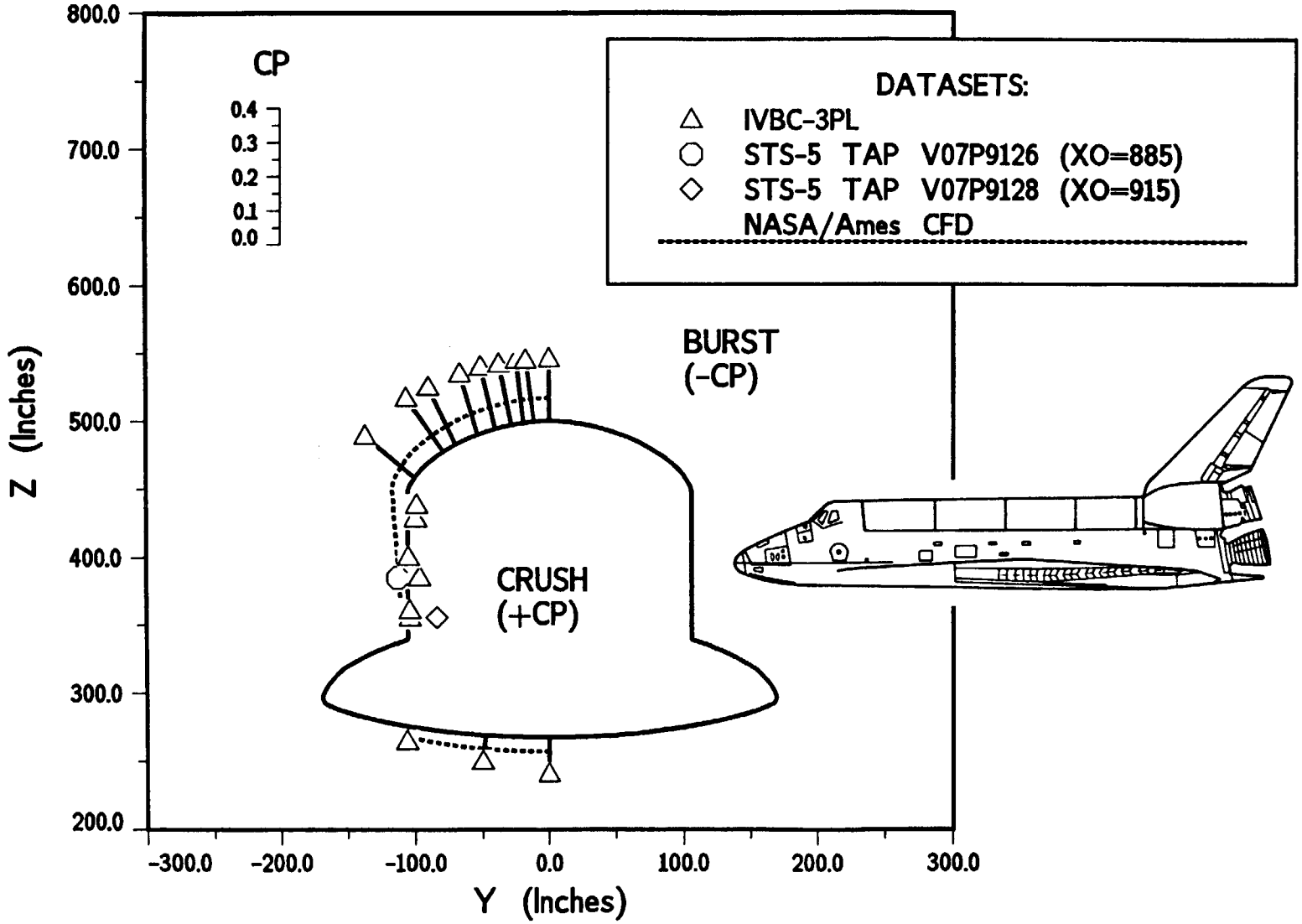

PAYLOAD BAY DOOR PRESSURE COMPARISONS

ORBITER X-STATION (X0) = 1214 inches

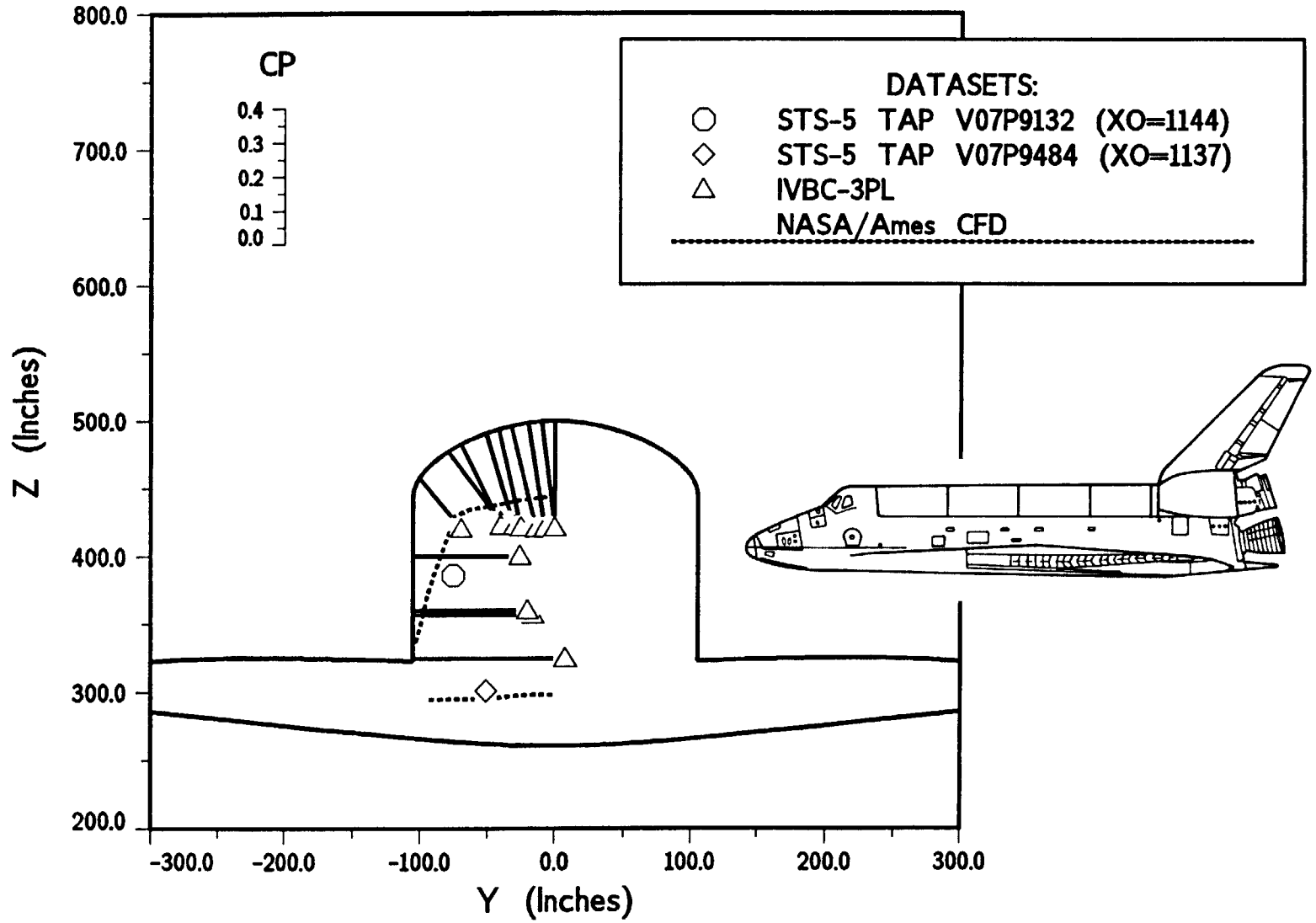

Status

- Preliminary CFD results have been instrumental in gaining insight into the present design aero database. Even with the large advances in SSLV geometry modelling, all three aero data sources (flight, wind tunnel, and CFD) are required to completely understand Shuttle ascent aerodynamics and structural loads.

- On-going CFD Activities:
  - Add the SRB attach ring and IEA box protuberances into the SSLV grid system.
  - Add more realistic aft attach hardware to the geometry model to better simulate blockage effects.
  - Add $\gamma = \gamma(T)$ to the F3D flow solver.
  - Grid the vertical tail and include in the geometry model.
  - Grid the SSMEs and incorporate the SSME plumes into the solution.

N91-10876

COMPUTATIONAL FLUID DYNAMICS ANALYSIS OF SPACE SHUTTLE MAIN PROPULSION FEED LINE 17-INCH DISCONNECT VALVES

Max Kandula* and Daniel Pearce**
Lockheed Engineering and Sciences Company
Houston, Texas

ABSTRACT

A steady incompressible three-dimensional (3-D) viscous flow analysis has been conducted for the Space Shuttle Main Propulsion External Tank (ET)/Orbiter (ORB) propellant feed line quick separable 17-inch disconnect flapper valves for liquid oxygen (LO_2) and liquid hydrogen (LH_2). The main objectives of the analyis were to predict and correlate the hydrodynamic stability of the flappers and pressure drop with available water test data.

Computational Fluid Dynamics (CFD) computer codes were procured at no cost from the public domain, and were modified and extended to carry out the disconnect flow analysis. The grid generator codes SVTGD3D and INGRID, developed by Sverdrup Technology Inc., were obtained from Arnold Air Force Station, Tennessee. NASA Ames Research Center supplied the flow solution code INS3D, and the color graphics code PLOT3D. A driver routine was developed to automate the grid generation process. Components such as pipes, elbows and flappers can be generated with simple commands, and flapper angles can be varied easily. The flow solver INS3D code was modified to treat interior flappers, and other interfacing routines were developed, which include a turbulence model, a force/moment routine, a time-step routine, and initial and boundary conditions. In particular, an under-relaxation scheme was implemented to enhance the solution stability.

Major physical assumptions and simplifications made in the analysis include the neglect of linkages (drive/follower arms), slightly reduced flapper diameter, and smooth solid surfaces. A grid size of 54x21x25 was employed for both the LO_2 and LH_2 units. Mixing length theory applied to turbulent shear flow in pipes formed the basis for the simple turbulence model.

Results of the analysis are presented for LO_2 and LH_2 disconnects. The predicted stop loads, hydrodynamic stability boundaries of the ET and orbiter flappers, and pressure drop across the valve compare well with the water test data, covering a tube Reynolds number of 3.5E06 for LO_2 unit and 2.4E06 for LH_2 unit. The ability to predict the valve performance and flapper stability over a wide range of flow rates and flapper angle combinations demonstrates the validity of the CFD model.

---

* Advanced Systems Engineering Specialist
** Engineer

PRECEDING PAGE BLANK NOT FILMED

LO_2 DISCONNECT VALVE

	WATER	FLIGHT
Re =	3.5E06	20E06

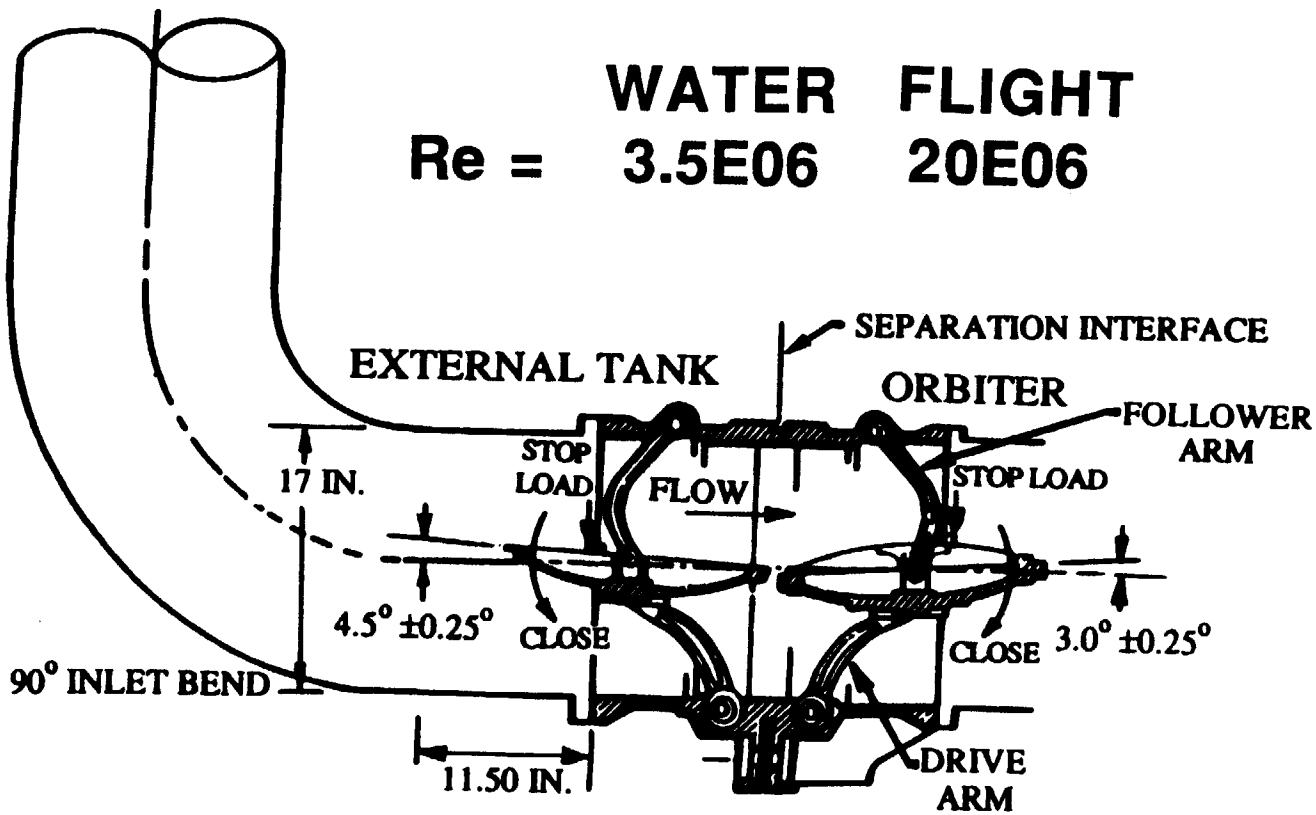

LH_2 DISCONNECT VALVE

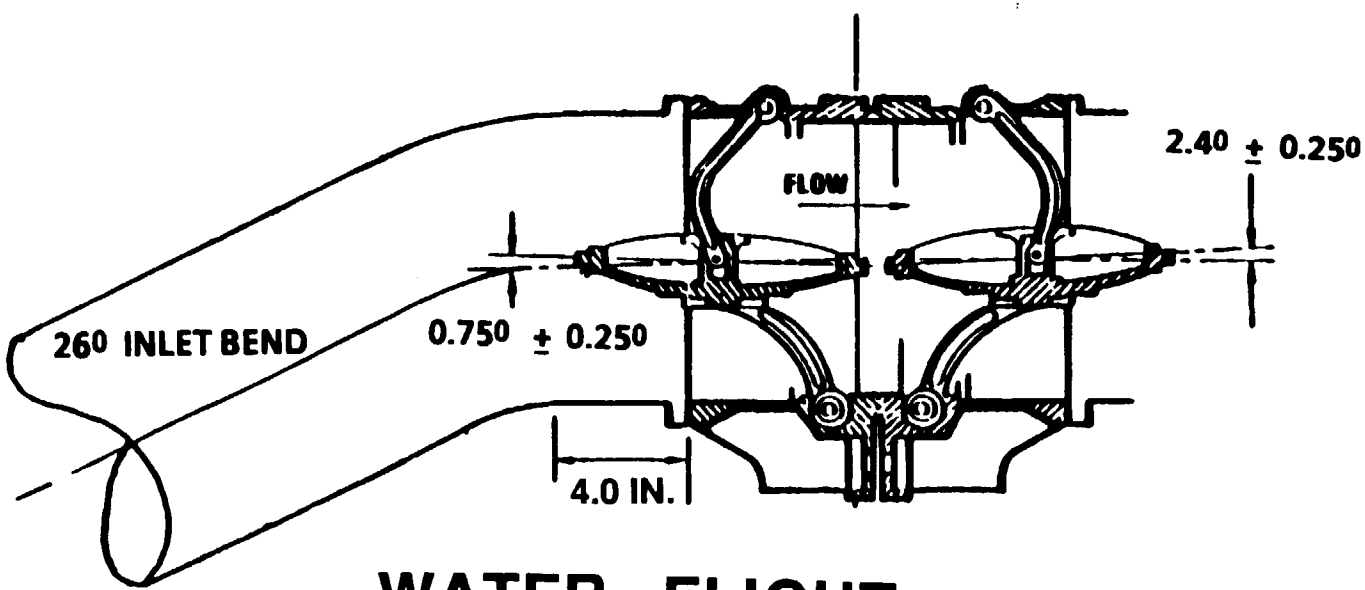

	WATER	FLIGHT
Re =	2.7E06	50E06

OBJECTIVES

- PREDICT
  - HYDRODYNAMIC STABILITY
  - PRESSURE DROP
  - CAVITATION

COMPUTATIONAL GRID

CODE : SVTGD3D (SONI ET AL. 1986)
ORG : SVERDRUP / AIR FORCE

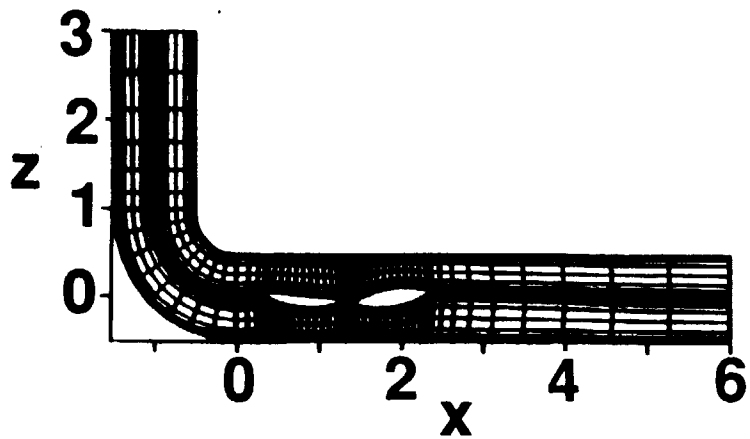

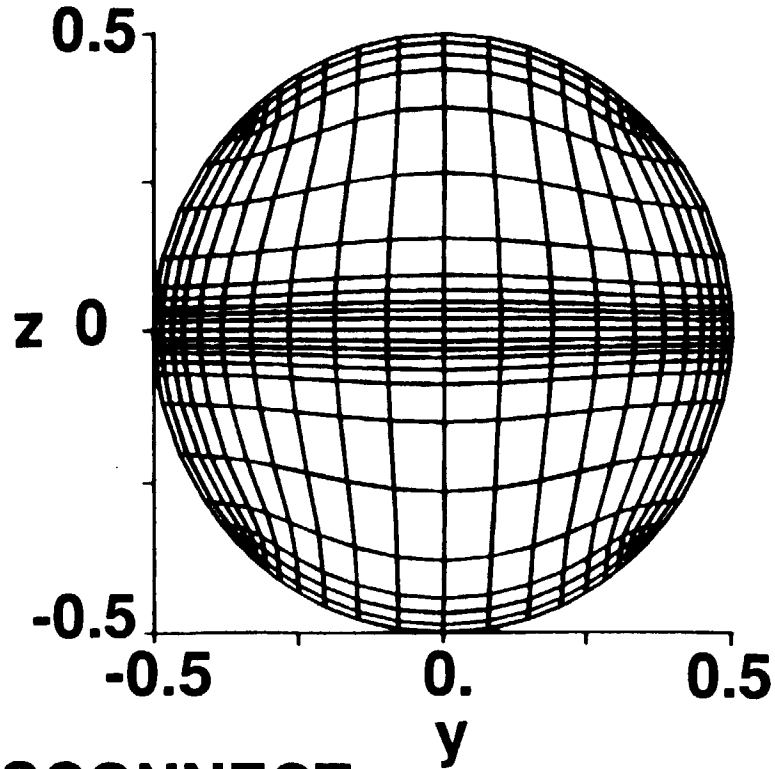

LO_2 DISCONNECT

COMPUTATIONAL GRID
LO_2 DISCONNECT

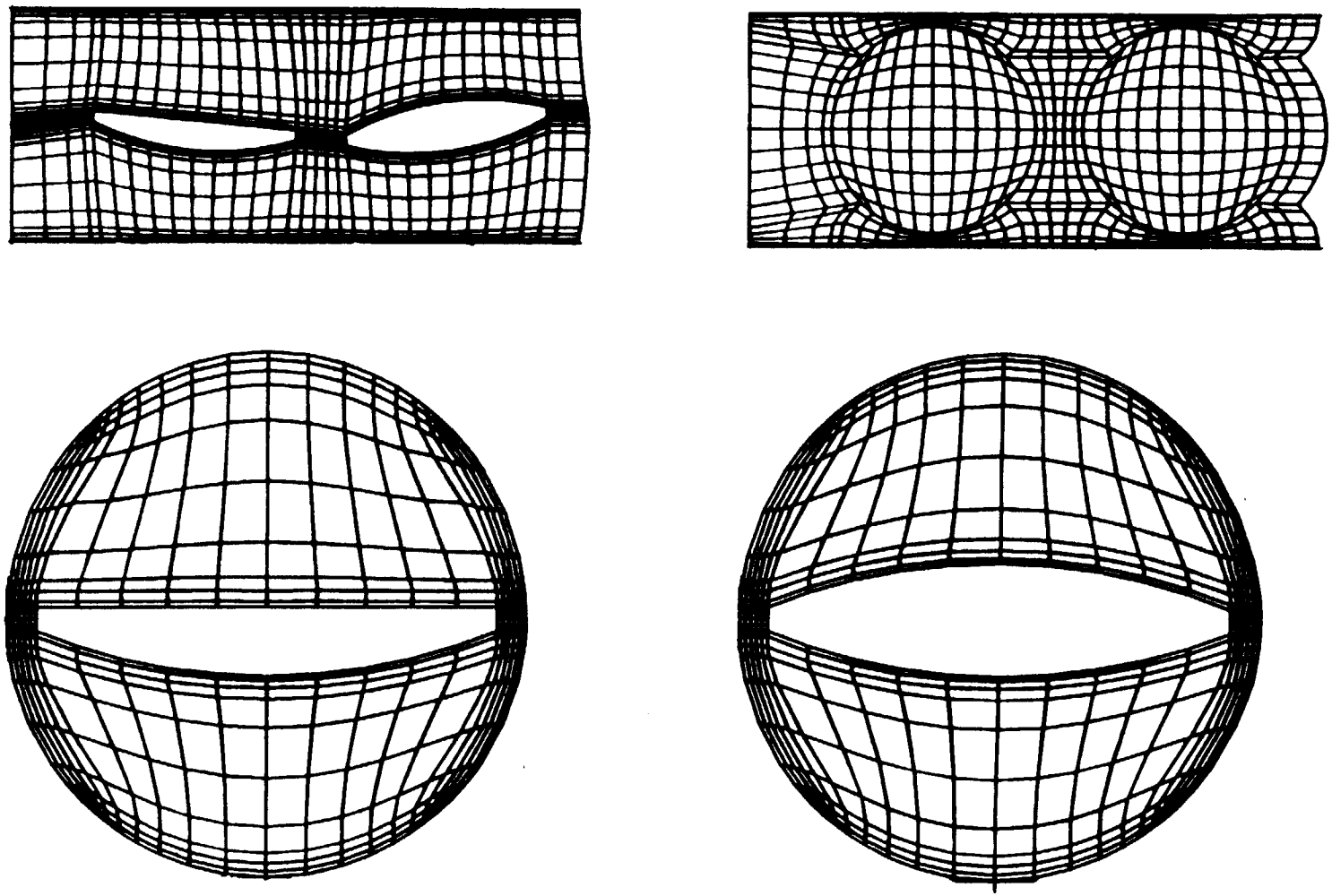

FLOW SOLUTION DEVELOPMENT

CODE : INS3D (KWAK ET AL. , 1985)
ORG : NASA AMES

- INTERNAL OBSTACLES
- TURBULENCE MODEL
- UNDER-RELAXATION

ANGLE CORRECTIONS

LO_2 :
- ET : FA = (PA+1) deg
- ORB : FA = (PA-5) deg
- PA = PRELOAD ANGLE
- FA = FLIGHT ANGLE

LH_2 : NONE

UNDER-RELAXATION

- ENHANCED STABILITY

$$Q_i^{n+1} = Q_i^{n} + \alpha r \, \Delta Q_i^{n}$$

$$Q_i = [\, p, u, v, w \,]^T$$

αr = RELAXATION FACTOR

CONVERGENCE HISTORY

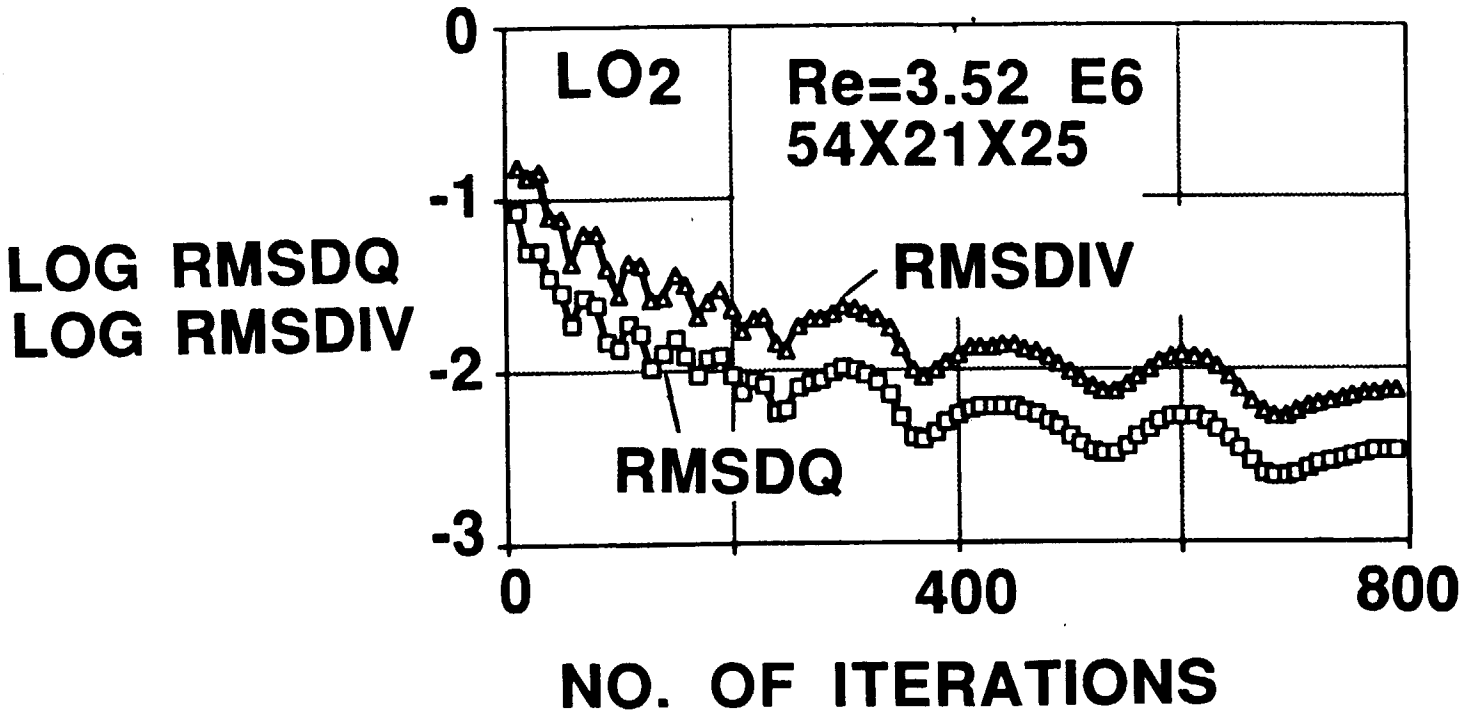

CONVERGENCE HISTORY

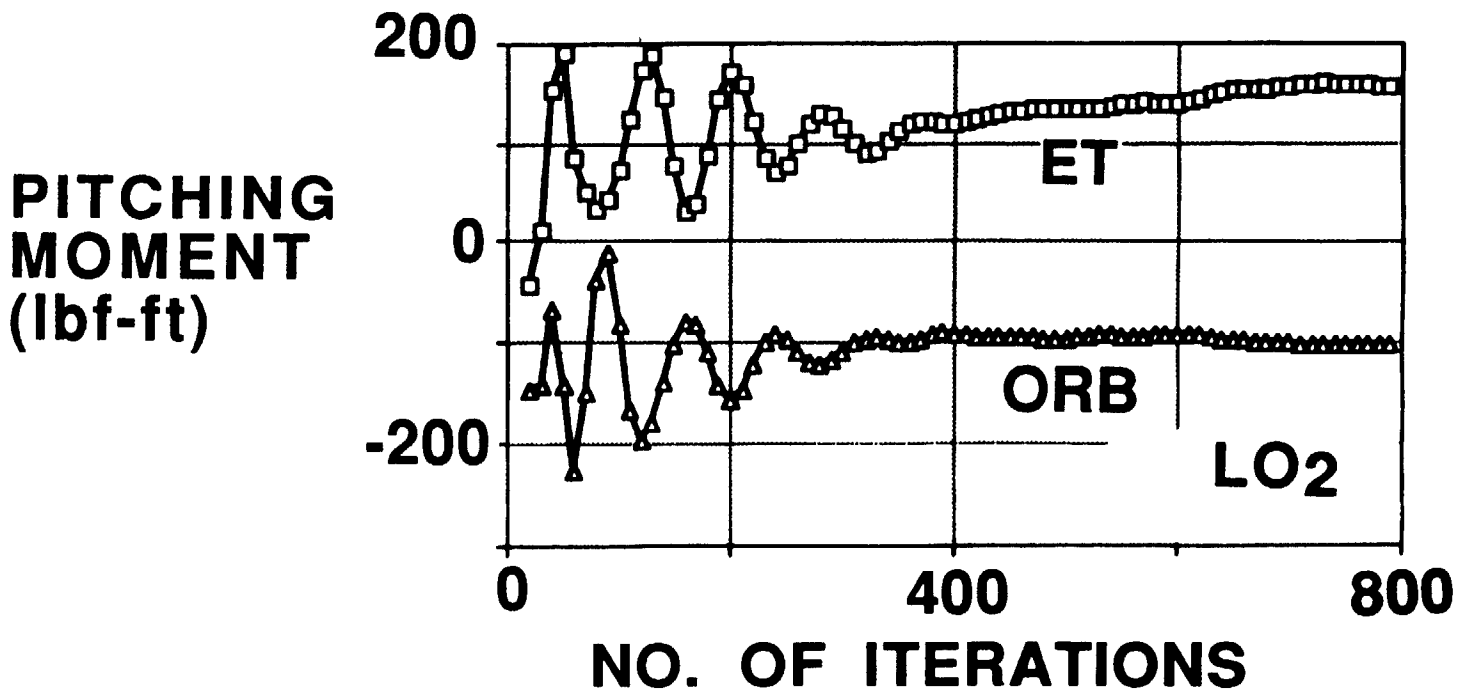

FLOW FIELD

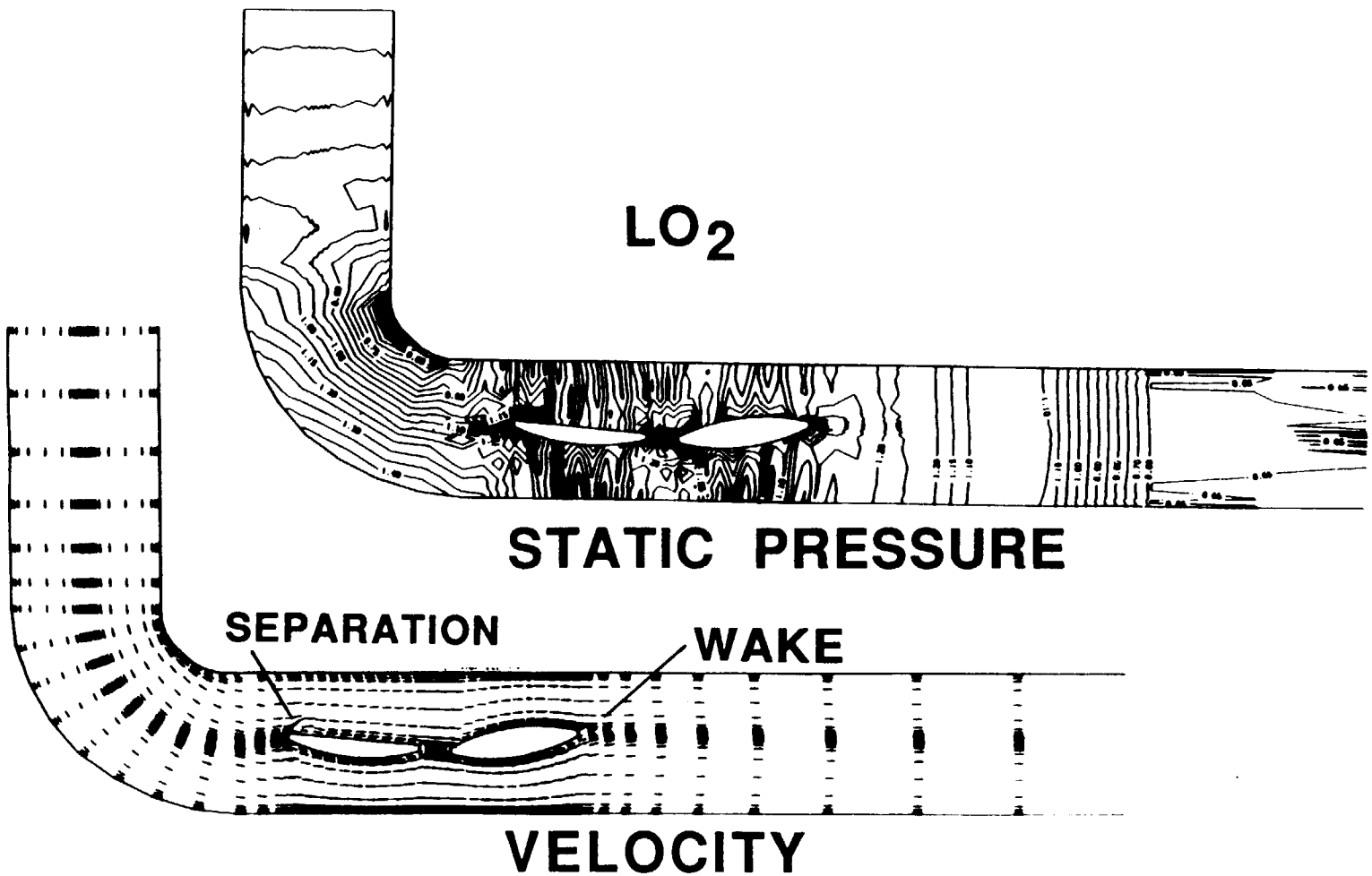

EFFECT OF FLOW RATE

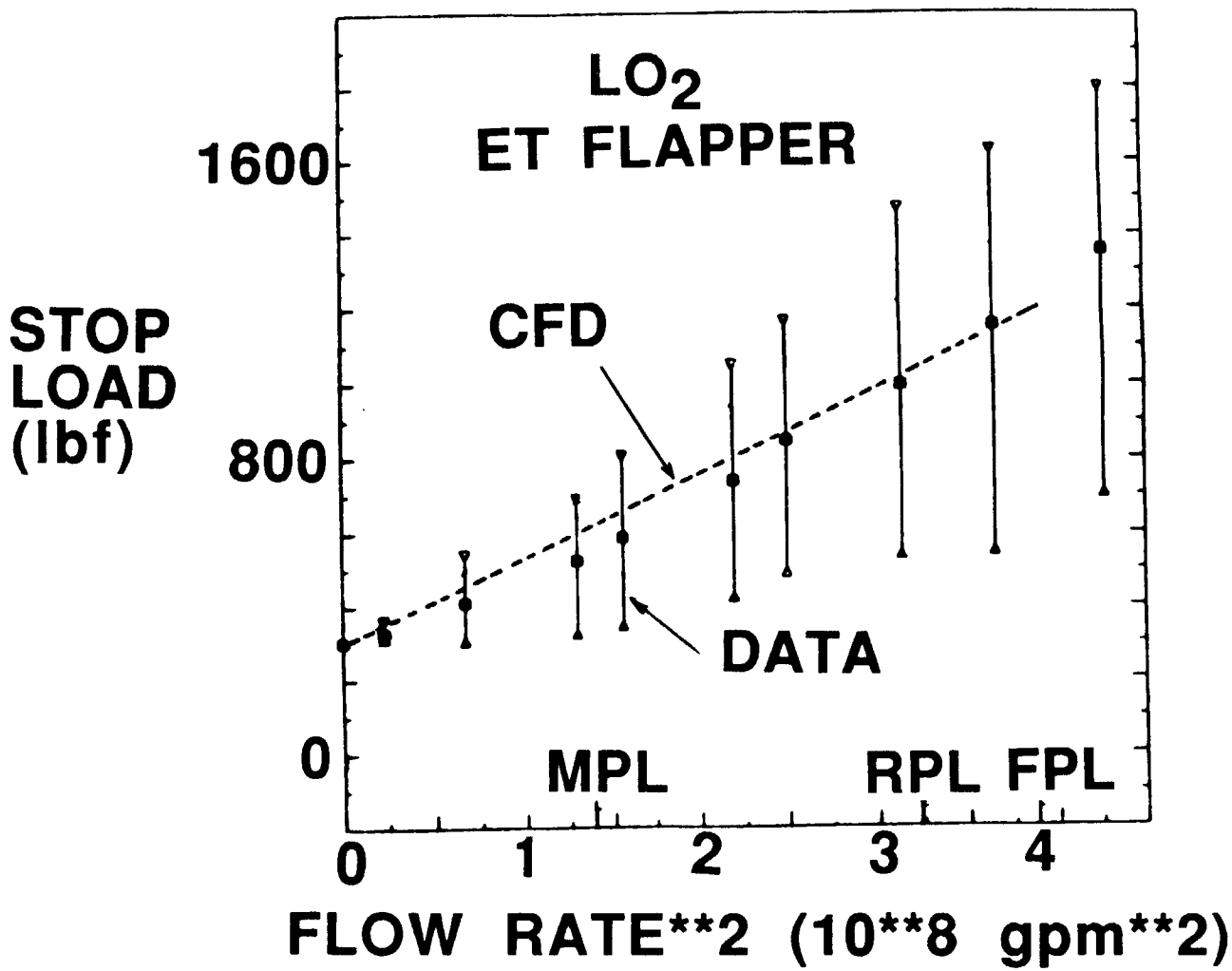

EFFECT OF FLAPPER ANGLE

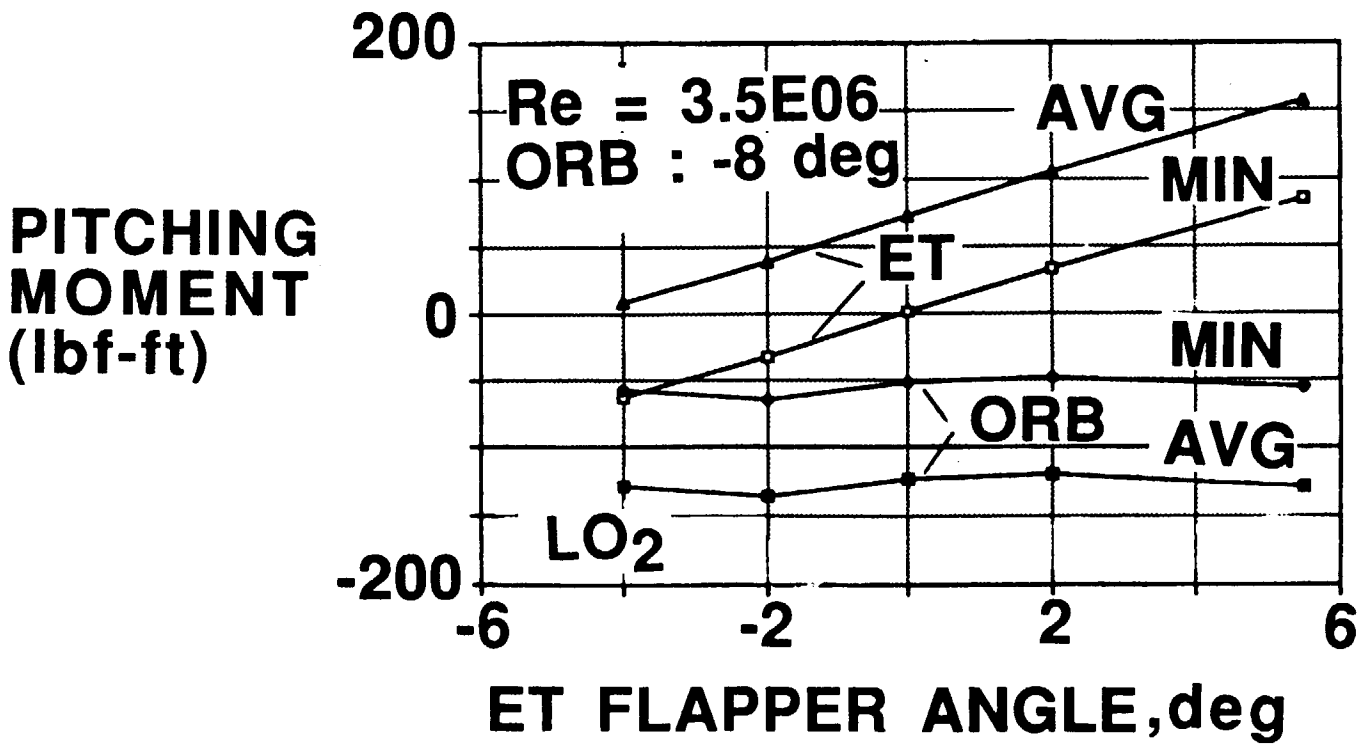

STABILITY BOUNDARIES
LO_2 DISCONNECT

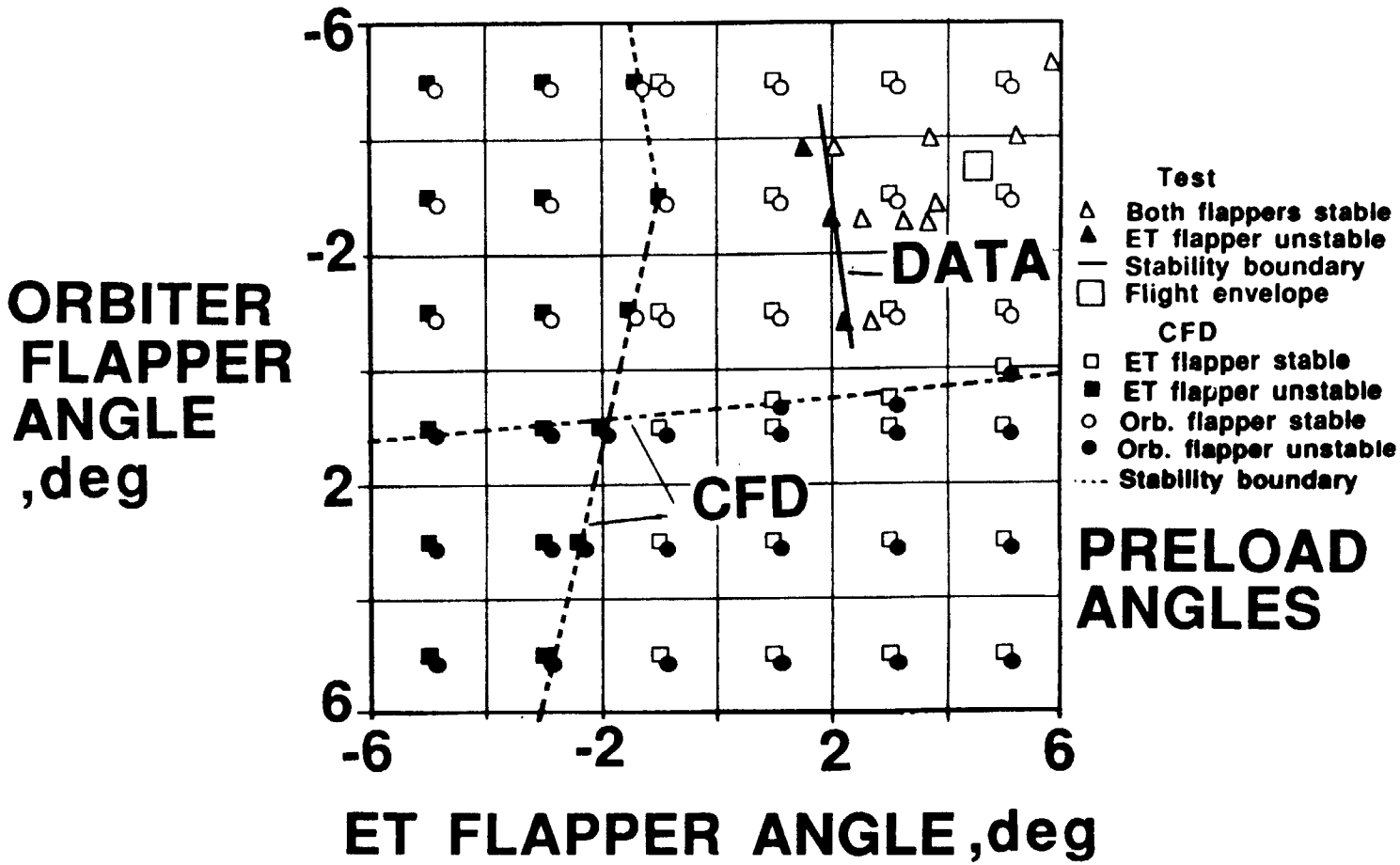

STABILITY BOUNDARIES
LH_2 DISCONNECT

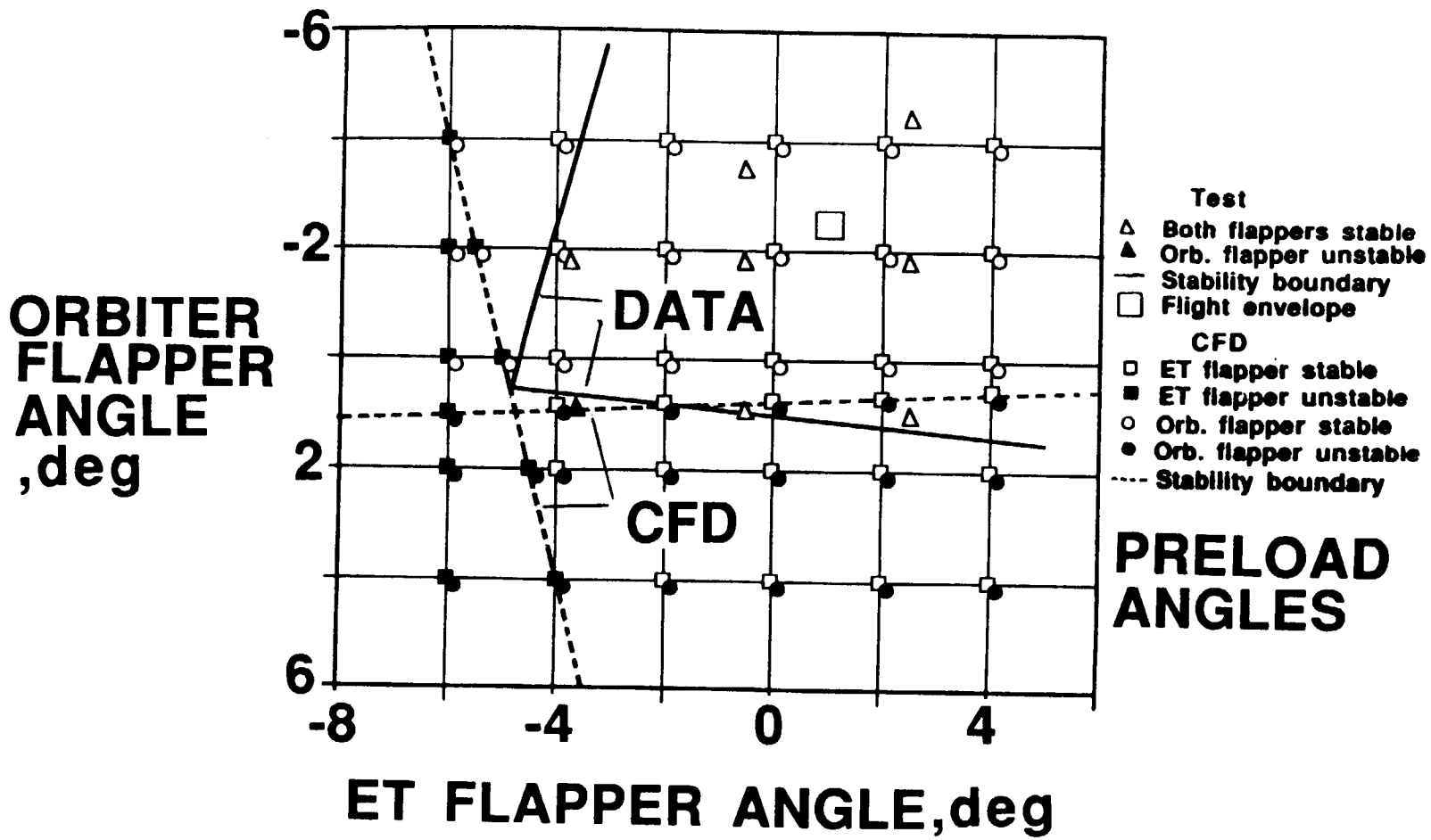

SUMMARY

- ENHACED THE STABILITY OF INS3D
- VALIDATED THE CODE WITH DATA
  - INTERNAL FLOW
  - INTERNAL OBSTACLES
  - HIGH REYNOLDS NUMBER (3.5E06)
- PREDICTED FLAPPER STABILITY
- ASSISTED IN THE VALVE REDESIGN
  - LATCH BETWEEN FLAPPERS

N91-10877

Analysis of the SSME HPOTP Bearing Inlet Cavity

P. McConnaughey, NASA/MSFC

Analysis of the flow in the Space Shuttle Main Engine (SSME) high pressure oxygen turbopump (HPOTP) bearing #1 inlet cavity has been completed in support of return-to-flight. With the incorporation of several design changes in the Phase II turbopump, rotordynamic stability of the pumps has been enhanced, but the durability and life of the LOX-cooled bearings has decreased. During the post-Challenger SSME recertification, the MSFC bearing team investigated the causes of limited bearing durability. One topic addressed by this team was the flow environment upstream of the pump-end bearing and the effect of seal exit swirl (Phase I labyrinth seal vs. Phase II damping seal) and a cavity anti-vortex rib on the bearing environment and life. The objective of the present work was to define the hydrodynamic environment upstream of the pump-end bearing and determine the effect of seal exit swirl and the anti-vortex rib on bearing inlet swirl.

The problem was posed as an axisymmetric cavity flow with the computational domain extending from the seal exit to the bearing inlet. This domain was discretized with 22800 grid points. Boundary conditions were obtained from a 1-D model of the SSME coolant path. These resulted in an axial Reynolds number of 297000 and with a seal tip speed of 29,200 rpm. The inlet Mach number was 0.19 and the problem was solved with the CMINT code utilizing the Briley-McDonald/Beam-Warming algorithm with preconditioning to speed convergence at low Mach numbers. Three parametric cases with inlet swirl of 50% shaft speed (labyrinth seal), 20% shaft speed (damping seal) and no inlet swirl were considered. Total CPU time for all analyses was 9 hours on a Cray X-MP with memory requirements of 1.7 million words.

Computational results indicate large vortical flow structures in the cavity, with the labyrinth, damping, and no-swirl cases yielding bearing inlet swirl rates of 14, 10, and 9 percent of shaft speed, respectively. These small differences are due to fluid spin-up on the shaft and inner race and indicate that upstream influences (either inlet swirl or anti-vortex ribs) have little effect on bearing inlet conditions. When these results were used as input to the SHABRETH bearing model, limited durability could not be explained by these small differences in swirl. Also, based on these results, a proposed design change for the cavity anti-vortex rib was not implemented by the SSME chief engineer.

BEARING INLET CAVITY ANALYSIS

OVERVIEW

- OBJECTIVE
- JUSTIFICATION
- APPROACH
- RESULTS
- SUMMARY AND CONCLUSIONS
- PROGRAM IMPACT

OBJECTIVES (IN SUPPORT OF RETURN-TO-FLIGHT)

- DEFINE THE HYDRODYNAMIC ENVIRONMENT FOR THE LOX BEARING #1 INLET CAVITY
  - UNDERSTAND THE SEAL EXIT/CAVITY/BEARING INLET FLOW PATH
  - QUANTIFY THE PRESSURE DROP IN THE CAVITY

- EVALUATE THE EFFECT OF SEAL EXIT SWIRL ON BEARING INLET SWIRL
  - INLET SWIRL AFFECTS VISCOUS HEAT GENERATION IN BEARING, CAGE DRAG AND PRESSURE DROP ACROSS BEARINGS

- EVALUATE EFFICACY OF THE BEARING CAVITY ANTI-VORTEX RIB

5-1631-9-104

BEARING INLET CAVITY ANALYSIS

JUSTIFICATION

- DURABILITY OF HPOTP PUMP-END BEARINGS (2000 SECOND LIMIT)
  - LOWER LIFE IN PHASE II DESIGN RELATIVE TO PHASE I DESIGN
  - CONFIGURATION CHANGES
    - DAMPING SEALS (PHASE II) VS. LABYRINTH SEALS (PHASE I)
    - INCREASED DEADBAND, INTERNAL CLEARENCES
    - ELONGATED CAGE POCKETS
- PROPOSED DESIGN CHANGE TO REMOVE ANTI-VORTEX RIB IN CAVITY

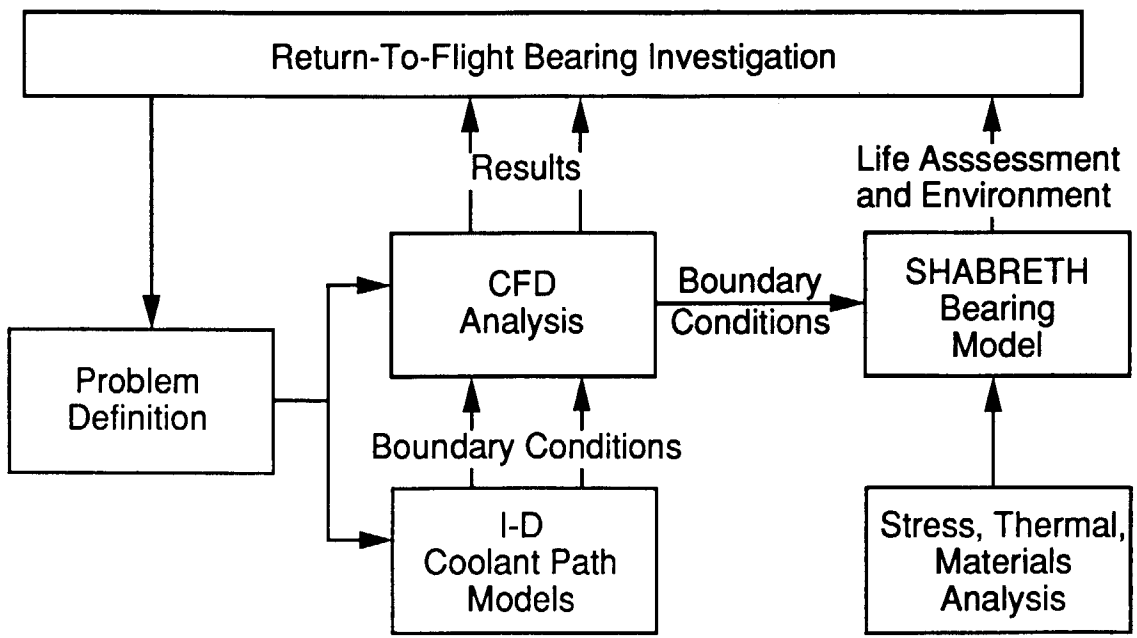

5-1619-9-104

BEARING INLET CAVITY ANALYSIS

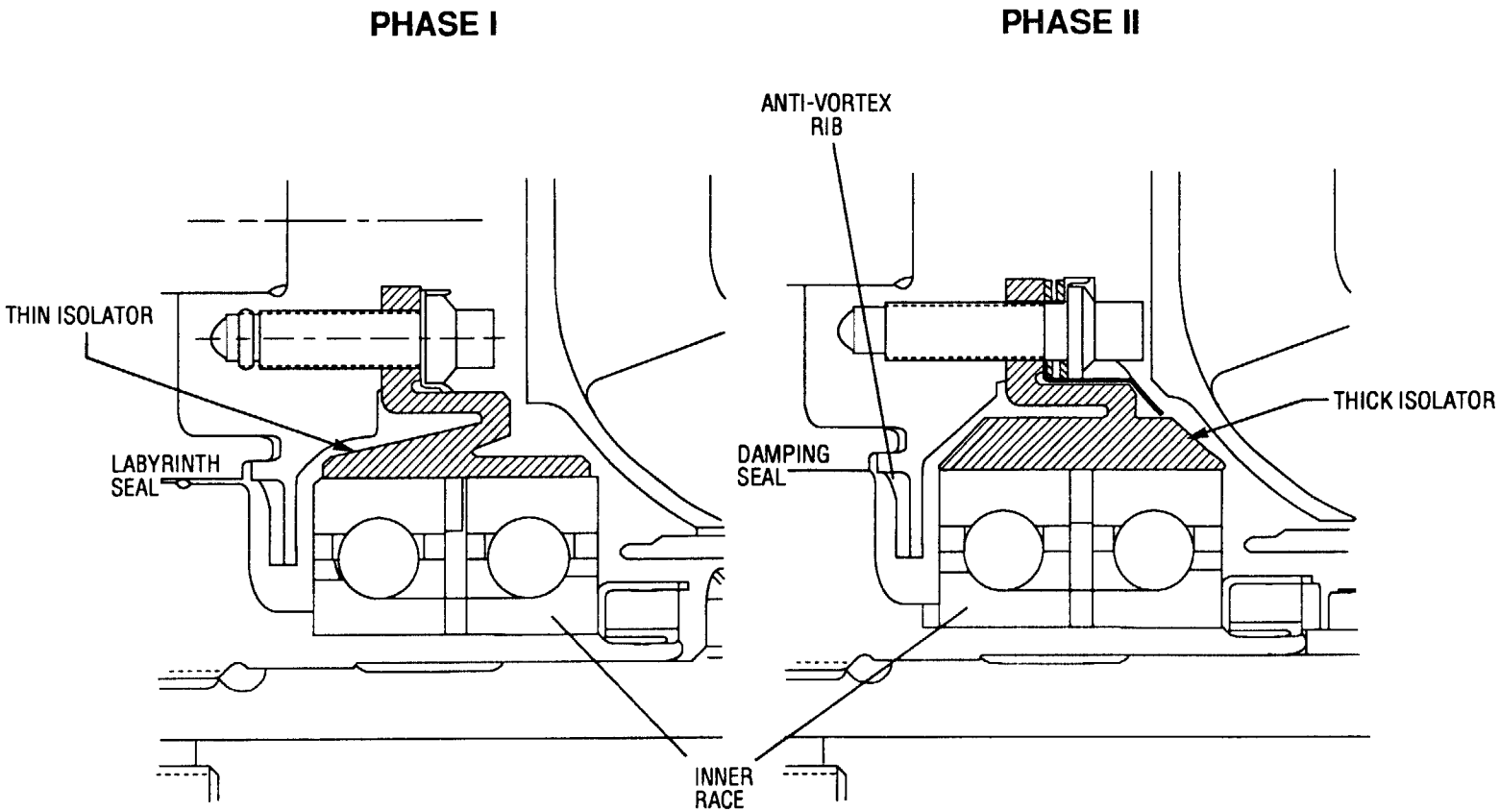

5-1616-9-98

BEARING INLET CAVITY ANALYSIS

APPROACH

PROBLEM DEFINITION

- DOMAIN FROM SEAL EXIT TO BEARING INLET
  - AXISYMMETRIC ANALYSIS (NO ANTI-VORTEX RIB)
  - LEAKAGE PATH IGNORED (1% OF FLOW)
  - ALL FLOW TO BEARING GOES BETWEEN INNER RACE AND CAGE
- Re_{ax} = 297000, Ω = 29200 rpm, M_{in} = 0.19 (109% POWER LEVEL)

METHOD OF ANALYSIS

- COMPRESSIBLE NAVIER-STOKES EQUATIONS (2-D AXISYMMETRIC WITH SWIRL)
- BRILEY-McDONALD/BEAM-WARMING WITH PRECONDITIONING
- CMINT CODE
- LOW, Re K-ε TURBULENCE MODEL
- 22800 GRID POINTS
- SOFT-START ON DOWNSTREAM STATIC PRESSURE
- 9 HOURS, 1.7 X 10^6 WORDS ON MSFC CRAY X-MP

VALIDATION OF DISK CAVITY ANALYSES

- OWEN AND PINCOMBE (JFM, 1980)
- DAILY AND NECE (1960)

5-2134-8-39

SSME HPOTP BEARING #1 INLET CAVITY ANALYSIS

120x190 Grid

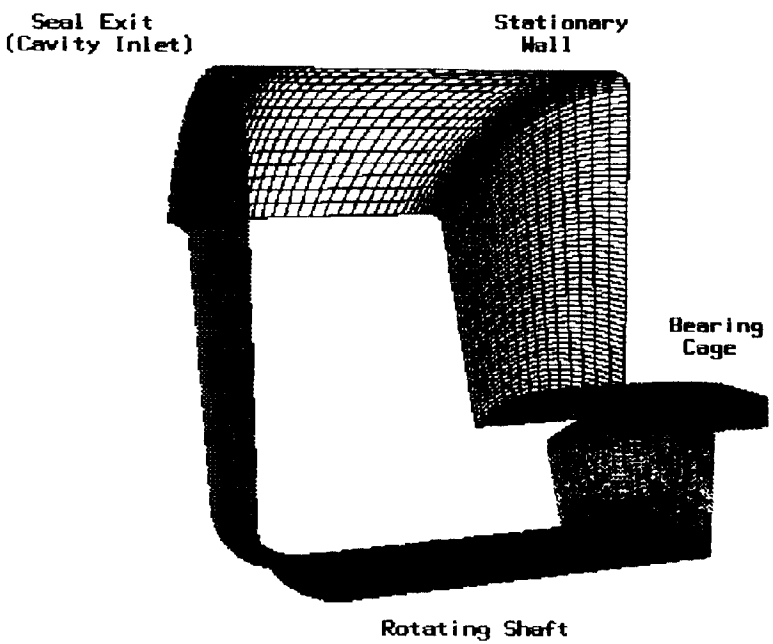

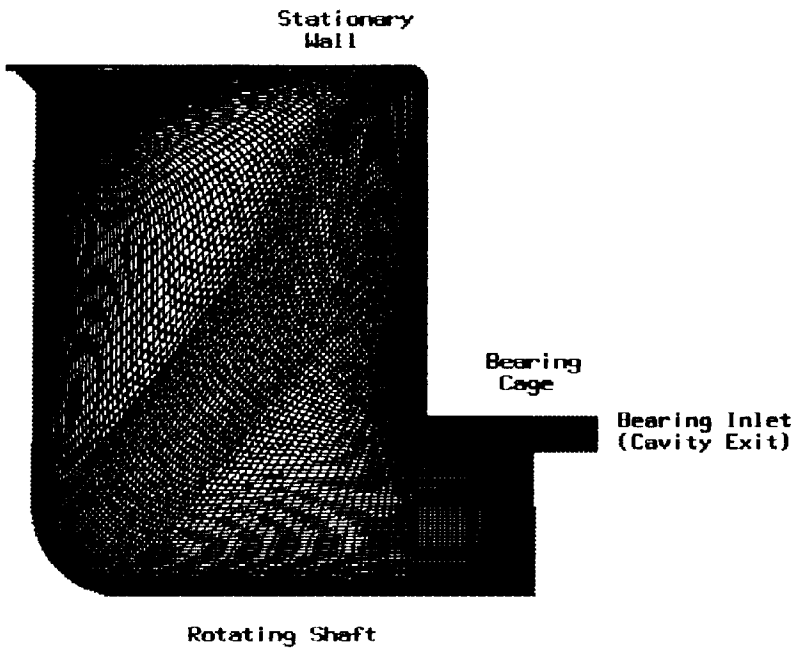

SSME HPOTP BEARING #1 INLET CAVITY ANALYSIS

120x190 Grid

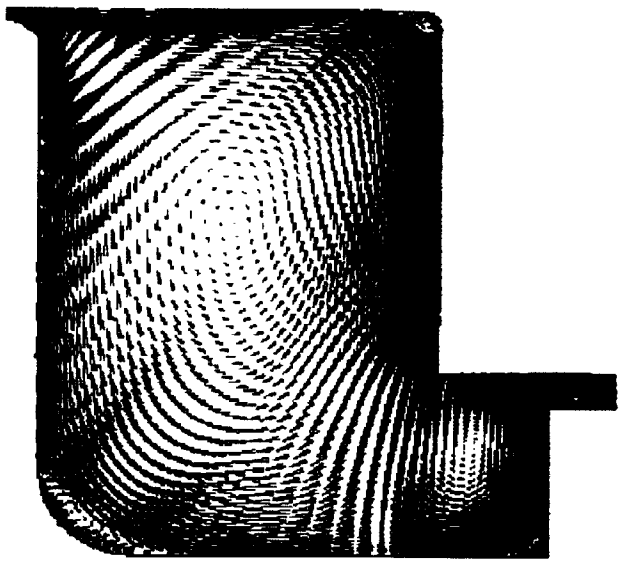

Velocity Vectors Colored
by Velocity Magnitude

Particle Traces

CONTOUR LEVELS

SWIRL VELOCITY IN HPOTP BEARING #1 INLET CAVITY

0.000 MACH
0.00 DEG ALPHA
120x1x190 GRID

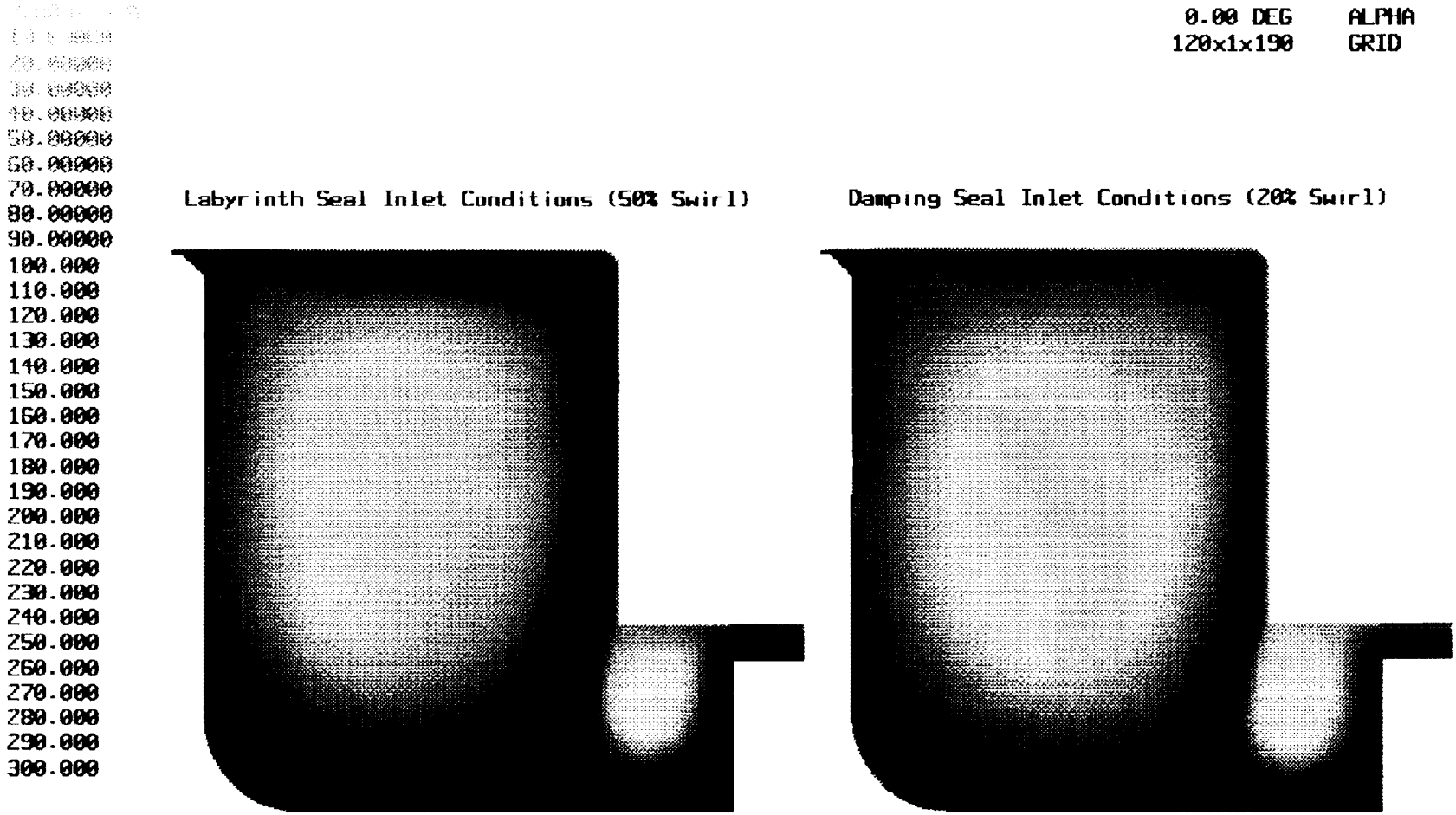

Computational Fluid Dynamics Branch, ED32

NASA / Marshall Space Flight Center

ORIGINAL PAGE IS
OF POOR QUALITY

BEARING INLET CAVITY ANALYSIS

LOX SWIRL PROFILES AT BEARING CAGE INLET

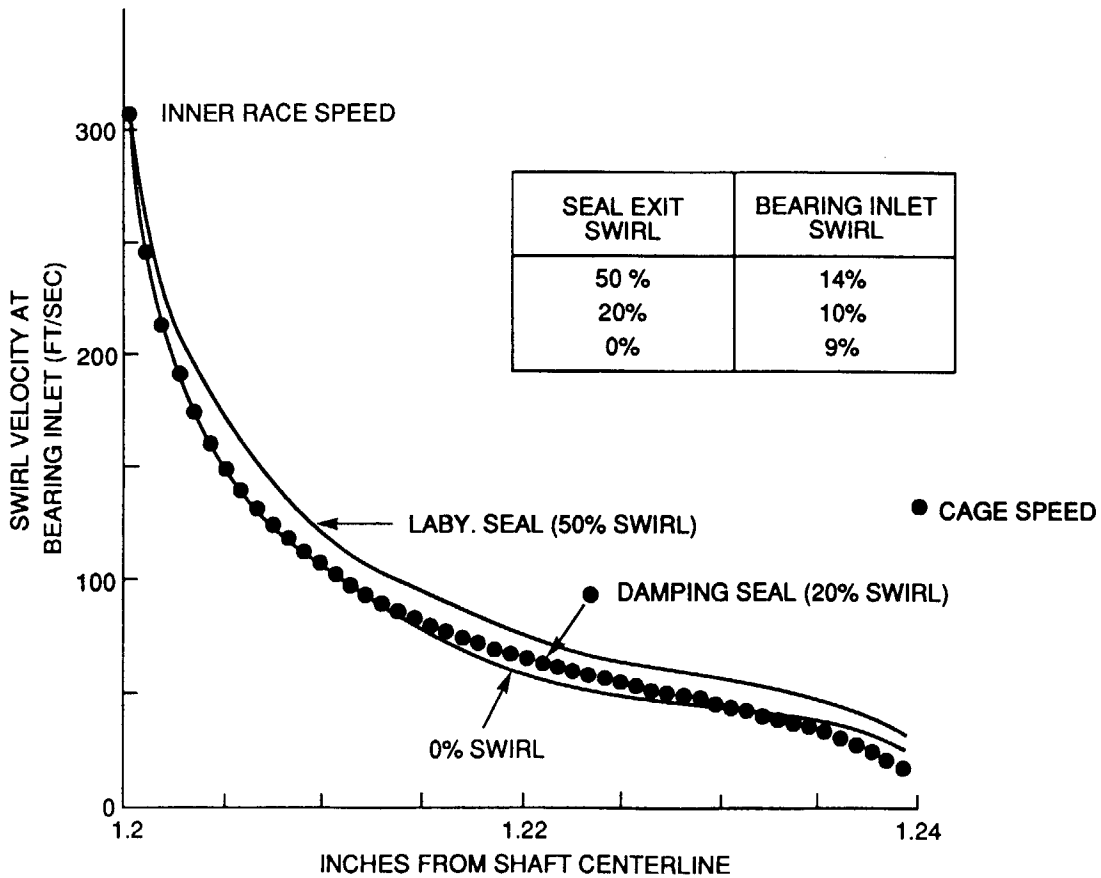

SEAL EXIT SWIRL	BEARING INLET SWIRL
50 %	14%
20%	10%
0%	9%

5-1615-9-98

BEARING INLET CAVITY ANALYSIS

SUMMARY AND CONCLUSIONS

- HYDRODYNAMIC ENVIRONMENT FOR THE SSME HPOTP BEARING #1 INLET CAVITY HAS BEEN DEFINED FOR PHASE I AND PHASE II DESIGNS
- SMALL DIFFERENCE (4%) IN BEARING INLET SWIRL BETWEEN PHASE I AND PHASE II PUMPS
- CFD RESULTS WERE USED AS INPUT INTO SHABRETH BEARING MODEL IN SUPPORT OF RETURN-TO-FLIGHT

5-1617-9-104

BEARING INLET CAVITY ANALYSIS

PROGRAM IMPACT

- DETERMINED THAT THE LIMITED DURABILITIY OF THE HPOTP PUMP-END BEARINGS IS NOT CAUSED BY CHANGES IN SWIRL ASSOCIATED WITH THE PHASE II DESIGN DAMPING SEALS
- DETERMINED THAT THE PROPOSED MODIFICATION OF THE CAVITY ANTI-VORTEX RIB WOULD HAVE LITTLE EFFECT ON SWIRL ENTERING THE BEARING. PROPOSED DESIGN CHANGE WAS NOT IMPLEMENTED BY CHIEF ENGINEERS OFFICE

5-1618-9-104

o DISK CAVITY ANALYSIS AT NASA-MSFC

	PROBLEM	CODE	TURNAROUND TIME
-	HPFTP TURBINE AFT CAVITY	PHOENICS	-
-	HPOTP BEARING # 1 INLET CAVITY	CMINT	3 MOS
-	HPFTP TURBINE FORE CAVITY	CMINT	6 MOS
-	TEST BED ENGINE CABLE CAVITY	INS3D*	3 WKS

* CODE WILL BE SET UP FOR GENERALIZED DISK CAVITY ANALYSIS

ORIGINAL CONTAINS
COLOR ILLUSTRATIONS

N91-10878

A COMBINED EULERIAN-LAGRANGIAN TWO-PHASE ANALYSIS OF THE SSME HPOTP NOZZLE PLUG TRAJECTORIES

R. Garcia, P. K. McConnaughey, NASA/MSFC
F. de Jong, J. Sabnis, Scientific Research Associates
D. Pribik, Rocketdyne Division, Rockwell International

Abstract

As a result of high cycle fatigue, hydrogen embrittlement, and extended engine use, it was observed in testing that the trailing edge on the first stage nozzle plug in the High Pressure Oxygen Turbopump (HPOTP) could detach. The objective of this study was to predict the trajectories followed by particles exiting the turbine. Experiments had shown that the heat exchanger coils, which lie downstream of the turbine, would be ruptured by particles traveling in the order of 360 ft/sec. An axisymmetric solution of the flow was obtained from the work of Lin et al [1] who used INS3D to obtain his solution. The particle trajectories were obtained using the method of de Jong et al [2] which employs Lagrangian tracking of the particle through the Eulerian flow field. The collision parameters were obtained from experiments conducted by Rocketdyne using problem specific alloys, speeds, and projectile geometries. A complete 3-D analysis using the most likely collision parameters shows maximum particle velocities of 200 ft/sec. in the heat exchanger region. Subsequent to this analysis, an engine level test was conducted in which seven particles passed through the turbine but no damage was observed on the heat exchanger coils.

References

1) Lin, S.-J. and Chang, J.L.C.: "Numerical Study of Laminar and Turbulent Flow Inside a Turnaround Duct With and Without Guide Vanes," AIAA Paper 87-0365, 1987.

2) de Jong, F.J., Sabnis, J.S., and McConnaughey, P.K.: "A Combined Eulerian-Lagrangian Two-Phase Flow Analysis of SSME HPOTP Nozzle Plug Trajectories; Part I- Methodology," To be presented at the AIAA Joint Propulsion Conference, 1989.

HIERARCHY OF ANALYSIS

- 2–D: PARTICLE EXITS TURBINE WITH NO SWIRL
- 3–D: PARTICLE WITH SWIRL, NO RADIAL STRUTS
- 3–D: PARTICLE WITH SWIRL, RADIAL STRUTS INCLUDED

PARAMETERS OF ANALYSIS

- 15 DIFFERENT PARTICLE RADIAL POSITIONS AT THE INLET TO THE DOMAIN FOR EACH RUN. (INNER TO OUTER WALL)
- DRAG COEFFICIENT OF PARTICLES – 0.4, 0.6, 0.8
  - TURBINE EXIT AXIAL VELOCITY OF PARTICLE FROM 180 TO 255 FT/SEC.
- SWIRL VELOCITY OF PARTICLE VARIED FROM ZERO TO BLADE SPEED
- LOSS OF NORMAL MOMENTUM AT THE WALLS:
  - COEFFICIENT OF RESTITUTION – 0.2, 0.4, 0.6, 0.8
- LOSS OF TANGENTIAL MOMENTUM AT THE WALLS:
  - COEFFICIENT OF SLIDING FRICTION – 0.0, 0.1, 0.2, 0.3

5-1582-9-99

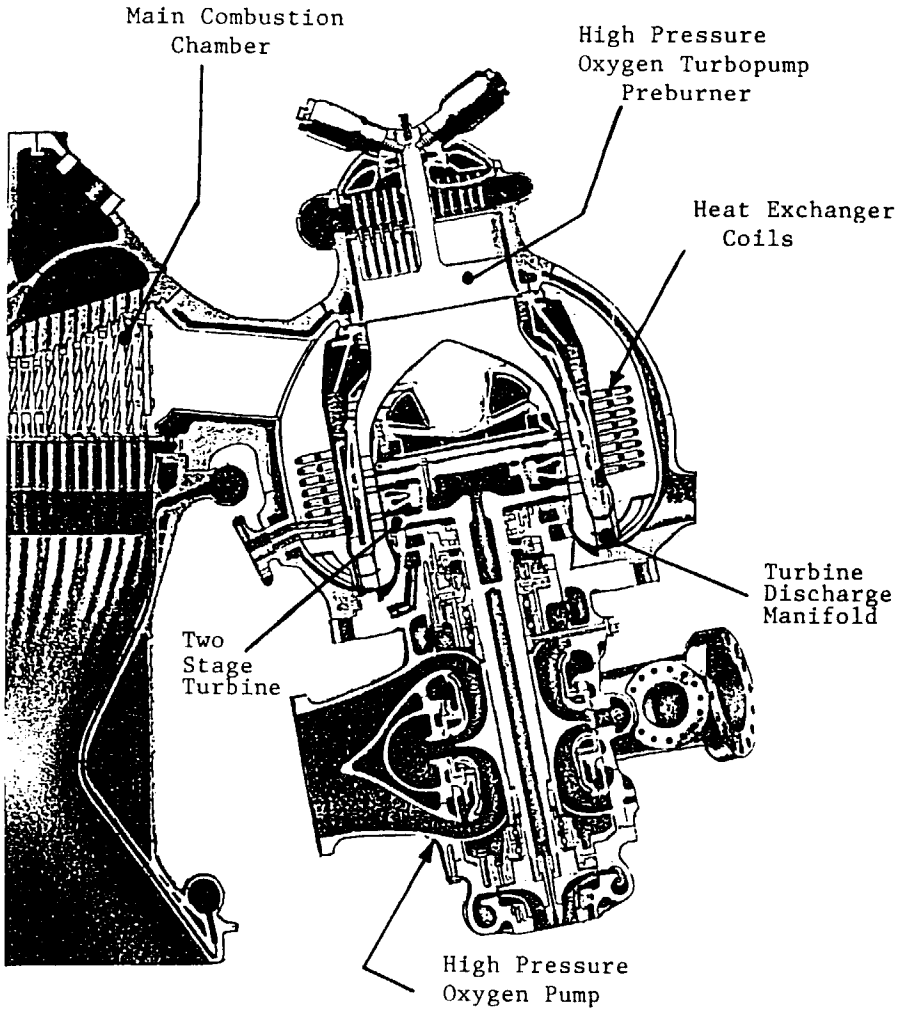

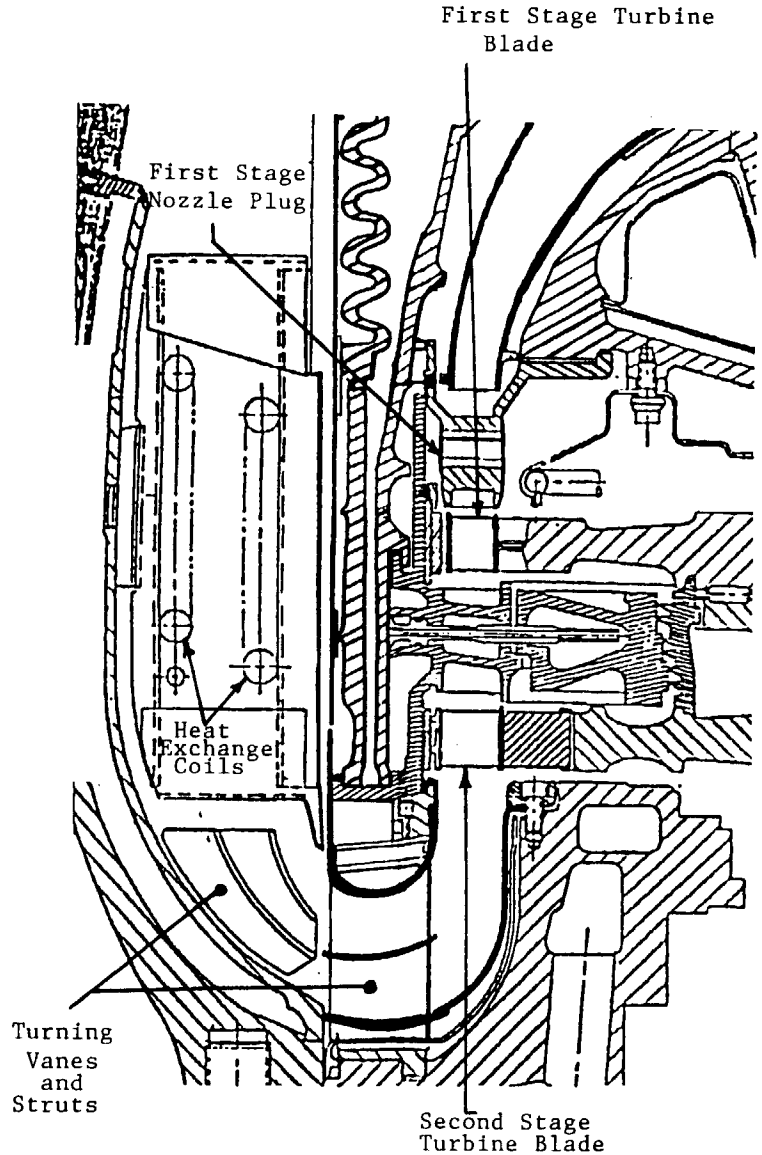

ORIGINAL PAGE IS OF POOR QUALITY

SSME HPOTP NOZZLE PLUG TRAJECTORIES

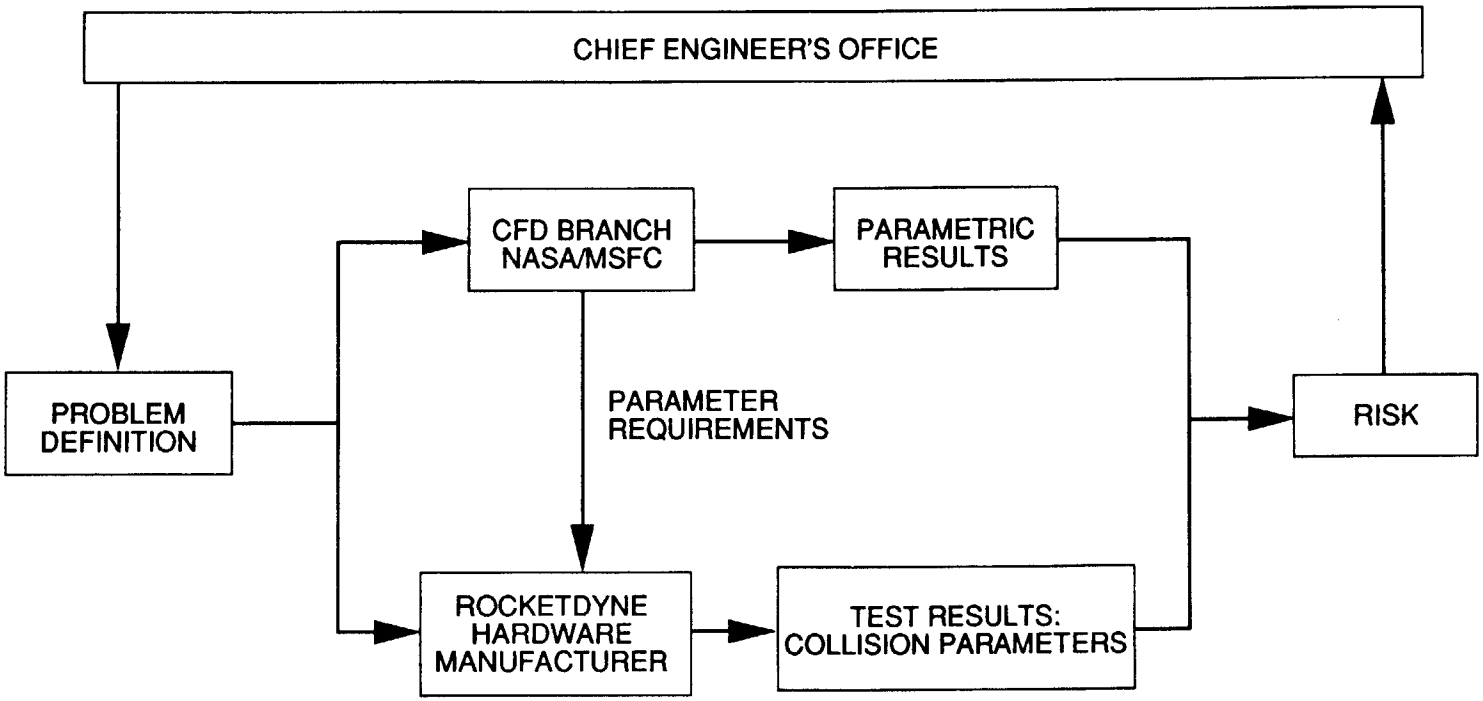

5-1625-9-94

OBJECTIVE

- TO DETERMINE THE LOCATIONS AND VELOCITIES OF NOZZLE PLUG IMPACTS ON THE HPOTP LOX HEAT EXCHANGER. TEST DATA INDICATED IMPACT VELOCITIES OF 360 FT/SEC WOULD CAUSE HEAT EXCHANGER COIL RUPTURE.

JUSTIFICATION

- RESULTS REQUESTED BY SSME CHIEF ENGINEER TO ASSESS:
  - RISK OF FULL SCALE ENGINE TEST.
  - RISK OF RETURN TO FLIGHT OF THE SPACE SHUTTLE WITH CURRENT DESIGN.

5-1580-9-99

TECHNICAL APPROACH

- USED LIN's AND CHANG's (ROCKETDYNE) AXISYMMETRIC SOLUTION OF THE FLOW IN THE HPOTP HOT GAS MANIFOLD
  - SOLUTION OBTAINED USING INS3D:
  - INCOMPRESSIBLE M = 0.1
  - $Re \cong 3 \times 10^6$, 588 FT/SEC AXIAL VELOCITY
- TRAJECTORIES CALCULATED USING LAGRANGIAN TRACKING OF THE PARTICLES THROUGH THE EULERIAN FLOW FIELD
  - METHOD OF F. J. de JONG AND J. S. SABNIS OF SRA
  - $\vec{F} = m\vec{a}$ ON THE PARTICLE THROUGH THE FLOW FIELD
  - COLLISION MODEL AT THE WALLS.
- VALIDATION
  - INS3D: COMPARED TO EXPERIMENTAL MEASUREMENTS FOR VARIOUS INCOMPRESSIBLE INTERNAL FLOWS.
  - LAGRANGIAN TRACKER: COMPARED AGAINST EXPERIMENTAL MEASUREMENTS IN A TWO-PHASE MIXING LAYER FLOW.

5-1581-9-99

SSME HPOTP NOZZLE PLUG TRAJECTORIES

OVERVIEW

- INTRODUCTION TO THE PROBLEM
- OBJECTIVES
- TECHNICAL APPROACH
- RESULTS
- CONCLUSION/IMPACT

5-1579-9-99

HPOTP Nozzle Plug Trajectories

Drag Coefficient = 0.6
Coeff. of Restitution = 0.6
Coeff. of Sliding Friction = 0.0

2-D

Swirl = 0%

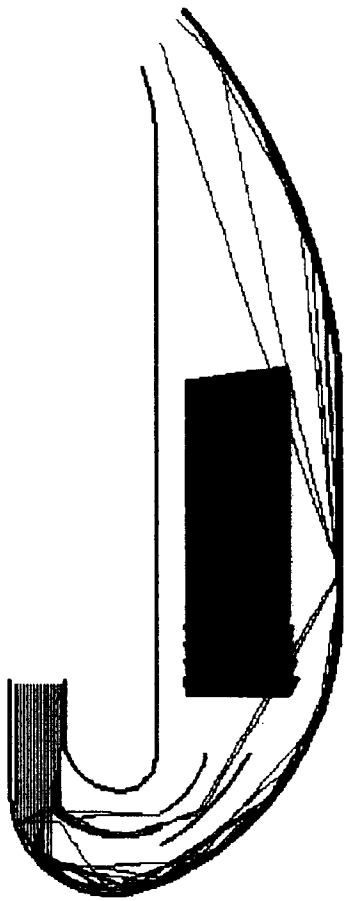

3-D

Swirl = 100%

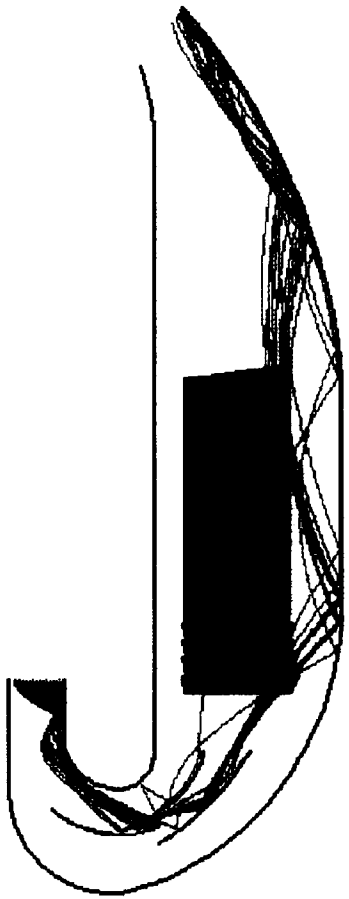

ORIGINAL PAGE IS
OF POOR QUALITY

PARTICLE VELOCITIES* AT THE HEAT EXCHANGER (FT/SEC)

FOR ALL CASES SHOWN: $C_D = 0.6$; $\mu = 0.0$

C_{RES}	2–D, $V_{SWIRL} = 0.0$	3–D, NO RADIAL STRUTS, $V_{SWIRL} = 1310$ ft/sec
0.4	192 – 152 (V_{MAX} – V_{MEAN} – V_{MIN})	635 – 610 – 572 (V_{MAX} – V_{MEAN} – V_{MIN})
0.6	204 – 200 (V_{MAX} – V_{MEAN} – V_{MIN})	672 – 611 – 435 (V_{MAX} – V_{MEAN} – V_{MIN})
0.8	224 – 167 (V_{MAX} – V_{MEAN} – V_{MIN})	765 – 683 – 465 (V_{MAX} – V_{MEAN} – V_{MIN})

*SWIRL COMPONENT NOT INCLUDED (NOT NORMAL TO COILS)

5-1583-9-99

PRECEDING PAGE BLANK NOT FILMED

3-D HPOTP Nozzle Plug Trajectories
Complete Geometry
Drag Coefficient = 0.6
Coefficient of Restitution = 0.6

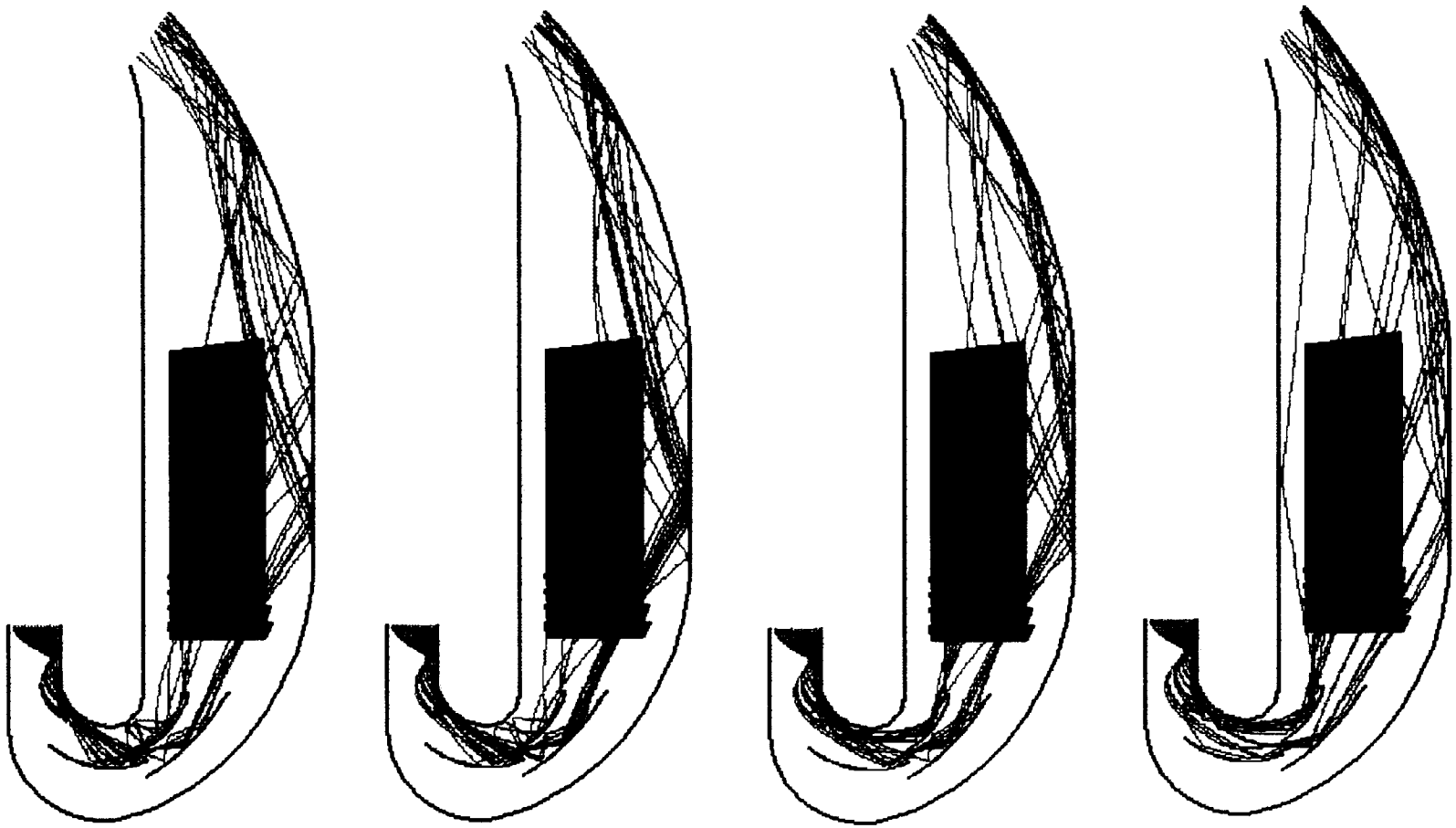

Coeff. of Sliding Friction = 0.0

Coeff. of Sliding Friction = 0.1

Coeff. of Sliding Friction = 0.2

Coeff. of Sliding Friction = 0.3

3-D ANALYSIS WITH RADIAL STRUTS (COMPLETE GEOMETRY)

PARTICLE VELOCITIES* AT HEAT EXCHANGER (FT/SEC)

$C_D = 0.6$ V_{SWIRL} = BLADE SPEED

μ (COEFF. OF SLIDING FRICTION)	$C_{RESTITUTION}$ 0.2	** 0.4	0.6	0.8	
** 0.1	150.9	130.0	156.3	210.1	$\bar{V}$
	141.1	61.5	82.3	61.7	V_{MIN}
	161.1	176.7	302.5	328.6	V_{MAX}
0.2	82.4	65.2	75.4	96.4	$\bar{V}$
	76.9	49.5	42.4	38.2	V_{MIN}
	86.3	110.2	161.8	150.7	V_{MAX}
0.3	49.5	60.5	54.6	55.2	$\bar{V}$
	43.3	51.9	26.8	21.4	V_{MIN}
	56.0	66.4	94.3	69.0	V_{MAX}

*SWIRL COMPONENT NOT INCLUDED (NOT NORMAL TO COIL)
**EXPECTED MEAN VALUE FOR COEFFICIENT BASED ON TEST DATA

5-717-9-83

PRECEDING PAGE BLANK NOT FILMED

IMPACT

- DECISION MADE TO CONDUCT FULL SCALE TEST WITH PURPOSELY CUT NOZZLE PLUGS:
  NO DAMAGE TO THE HEAT EXCHANGER

- DECISION MADE TO USE CURRENT DESIGN ON RETURN TO FLIGHT

5-1626-9-94

CONCLUSIONS

- PARTICLE MOTION DOMINATED BY COLLISION PARAMETERS
- MOST PARTICLES WILL HIT THE HEAT EXCHANGER DUE TO "FOCUSING" OF THE TURNING VANES.
- MEAN COLLISION PARAMETERS (C_{RES} = 0.6, μ = 0.1) YIELD MAXIMUM PARTICLE IMPACT VELOCITIES OF 180 FT/S
- WORST CASE STACK OF COLLISION PARAMETERS YIELDS MAXIMUM IMPACT VELOCITIES OF 300 FT/S (RUPTURE VELOCITY IS 360 FT/S).

5-1584-9-99

N91-10879

Conjugate (Solid/Fluid) Computational Fluid Dynamics Analysis of the Space Shuttle Solid Rocket Motor Nozzle/Case and Case Field Joints

D. Doran, NASA/MSFC, L. W. Keeton, P. J. Dionne, and A. K. Singhal, CFD Research Corporation

This work describes three-dimensional, conjugate (solid/fluid) heat transfer analyses of new designs of the Solid Rocket Motor (SRM) nozzle/case and case field joints.

The main focus of the study has been to predict the consequences of multiple "rips" (or debonds) in the ambient cure adhesive packed between the nozzle/case joint surfaces and the bond line between the mating field joint surfaces. The models calculate the transient temperature responses of the various materials neighboring postulated flow/leakpaths into, past and out from the nozzle/case primary O-ring cavity and case field capture O-ring cavity. These results were used to assess if the design was failsafe (i.e. no potential O-ring erosion) and reusable (i.e. no excessive steel temperatures).

The models are adaptions and extensions of the general purpose PHOENICS fluid dynamics code.

A non-orthogonal coordinate system was employed and 11,592 control cells for the nozzle/case and 20,088 for the case field joints are used with non-uniform distribution. Physical properties of both fluid and solids are temperature dependent.

A number of parametric studies were run for both joints with results showing temperature limits for reuse for the steel case on the nozzle joint being exceeded while the steel case temperatures for the field joint were not. O-ring temperatures for the nozzle joint predicted erosion while for the field joint they did not.

PRECEDING PAGE BLANK NOT FILMED

SRB NOZZLE/CASE AND CASE FIELD JOINT FLOW AND THERMAL ANALYSIS

OVERVIEW

- PROBLEM DEFINITION
- OBJECTIVES
- TECHNICAL APPROACH
- RESULTS
- PROGRAM IMPACT AND CONCLUSIONS

5-1571-9-102

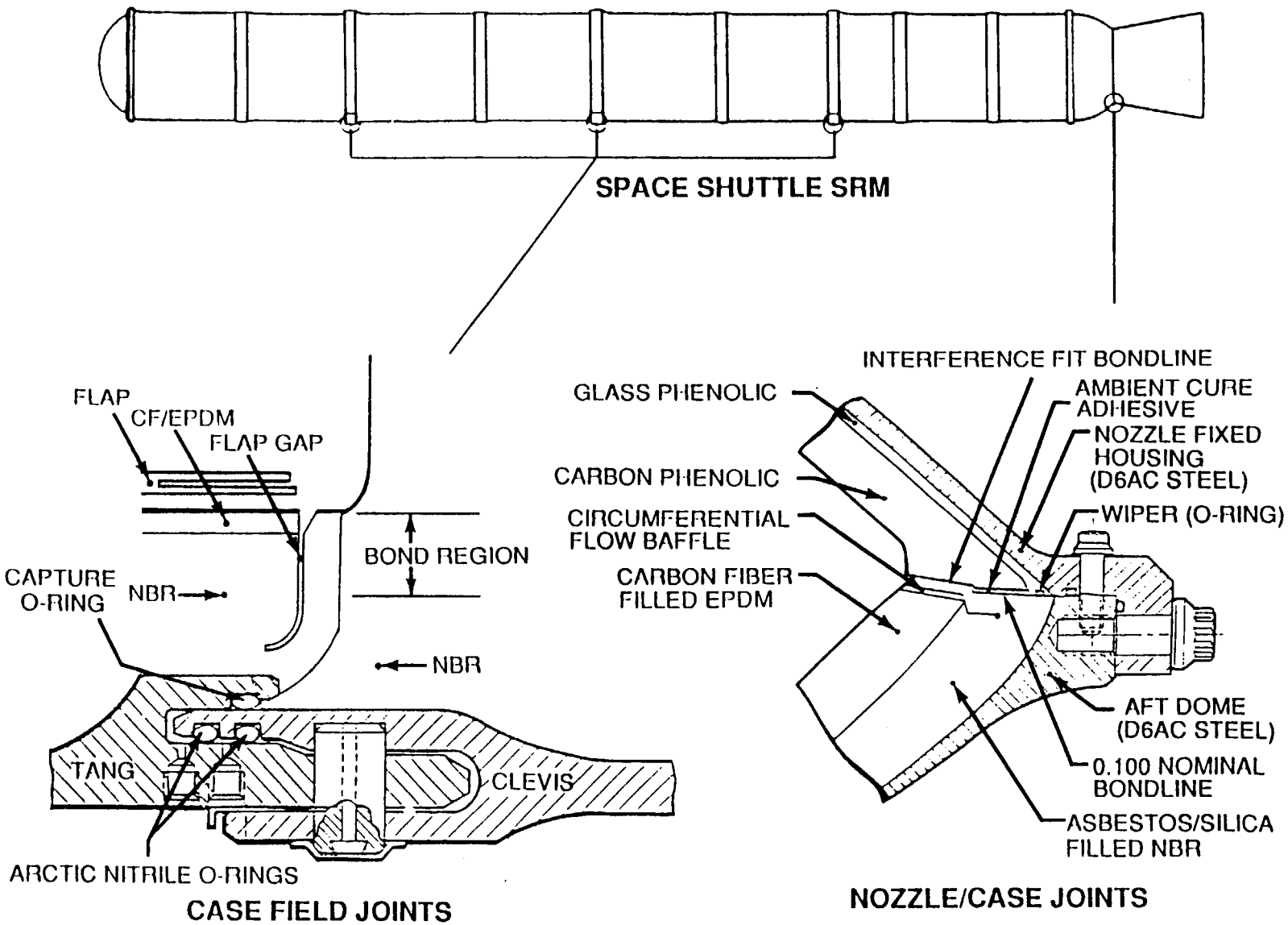
SPACE SHUTTLE SRM
FLAP
CF/EPDM
FLAP GAP
BOND REGION
CAPTURE O-RING
NBR
NBR
TANG
CLEVIS
ARCTIC NITRILE O-RINGS
CASE FIELD JOINTS
INTERFERENCE FIT BONDLINE
GLASS PHENOLIC
AMBIENT CURE ADHESIVE
NOZZLE FIXED HOUSING (D6AC STEEL)
CARBON PHENOLIC
WIPER (O-RING)
CIRCUMFERENTIAL FLOW BAFFLE
CARBON FIBER FILLED EPDM
AFT DOME (D6AC STEEL)
0.100 NOMINAL BONDLINE
ASBESTOS/SILICA FILLED NBR
NOZZLE/CASE JOINTS
ED6613

SRB NOZZLE/CASE AND CASE FIELD JOINT FLOW AND THERMAL ANALYSIS

OBJECTIVE: DEFINITION OF THE FLOW AND THERMAL ENVIRONMENTS IN THE SRB NOZZLE/CASE AND CASE FIELD JOINTS ASSUMING SEVERAL POSTULATED DOUBLE LEAKPATHS THROUGH THE NOZZLE/CASE AMBIENT CURE ADHESIVE AND THE CASE FIELD BOND LINE BETWEEN THE MATING FIELD JOINT SURFACES

JUSTIFICATION: TO DEFINE CONSERVATIVE, BUT CREDIBLE DESIGN AND FAIL-SAFE CONDITIONS AND CRITERIA FOR NOZZLE/CASE AND CASE FIELD JOINT THERMAL ANALYSIS

DESIGN - TEMPERATURES WHICH GUARANTEE REUSABILITY OF METAL PARTS AND NO EROSION OF O-RING SEALS

FAIL-SAFE - TEMPERATURES WHICH GUARANTEE A STRUCTURAL SAFETY FACTOR OF 1.0 ON METAL PARTS AND NO EROSION OF ONE SEAL

5-1572-9-102

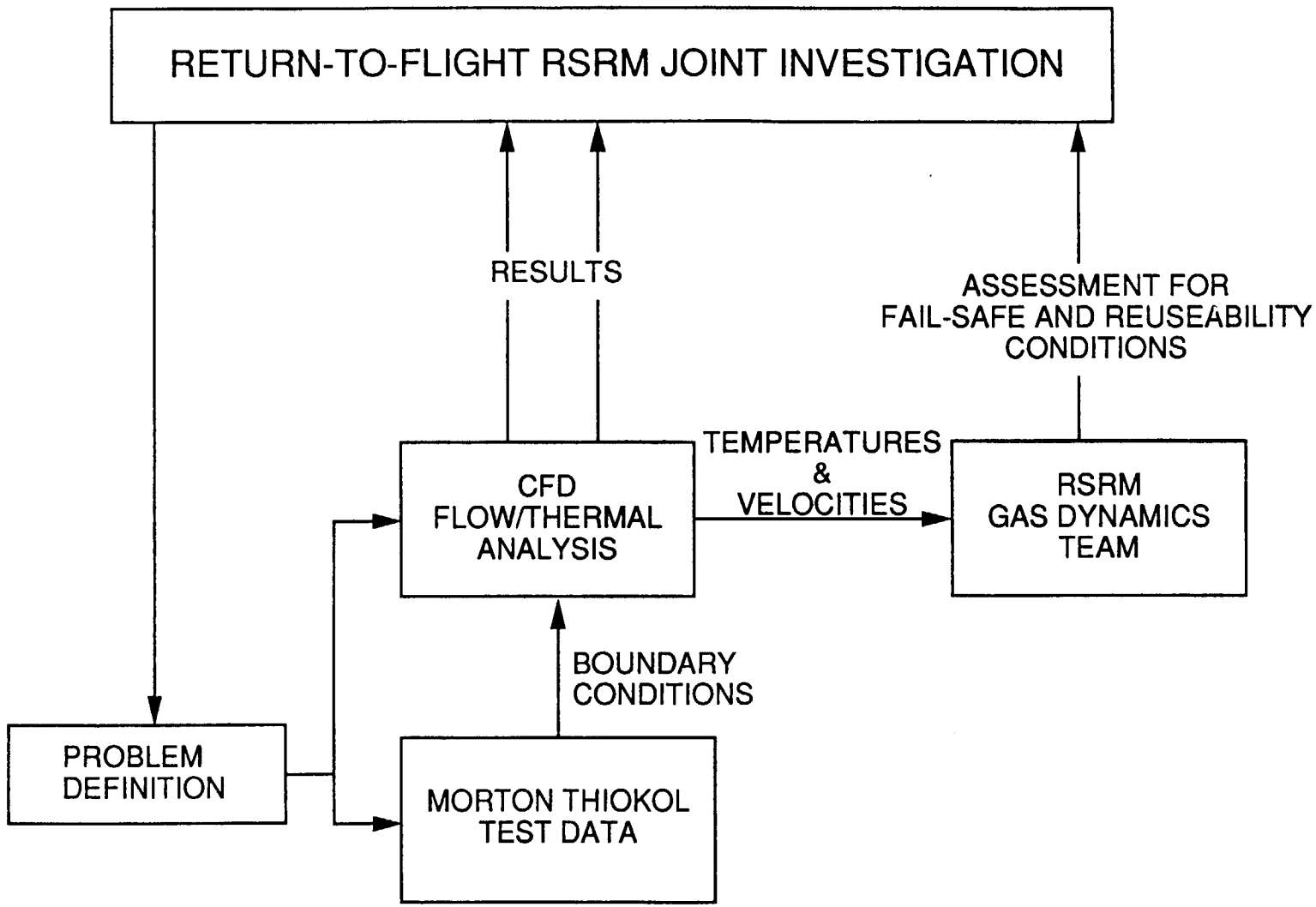
RETURN-TO-FLIGHT RSRM JOINT INVESTIGATION
RESULTS
ASSESSMENT FOR
FAIL-SAFE AND REUSEABILITY
CONDITIONS
TEMPERATURES
&
VELOCITIES
CFD
FLOW/THERMAL
ANALYSIS
RSRM
GAS DYNAMICS
TEAM
BOUNDARY
CONDITIONS
PROBLEM
DEFINITION
MORTON THIOKOL
TEST DATA

5-1624-9-103

SRB NOZZLE/CASE AND CASE FIELD JOINT FLOW AND THERMAL ANALYSIS

APPROACH: APPLICATION OF 3-D NAVIER-STOKES CODE (PHOENICS) TO FLOW IN THE DEBOND GAP AND O-RING REGIONS COUPLED WITH HEAT CONDUCTION OF THE FLUID AND NEIGHBORING "SOLIDS" (NOZZLE/CASE 11592 CELLS; CASE FIELD 20088 CELLS)

PHOENICS
- (PARABOLIC, HYPERBOLIC, OR ELLIPTIC NUMERICAL INTEGRATION CODE SERIES)

MODEL USES:
- BODY-FITTED COORDINATES
- FINITE-VOLUME FORMULATION
- 3-D TRANSIENT
- K-EPSILON TURBULENCE MODEL
- TEMPERATURE DEPENDENT SOLID AND FLUID PROPERTIES
- WALL FUNCTIONS (LOG LAW OF THE WALL)
- CHILTON-COLBURN FORM OF REYNOLDS ANALOGY FOR HEAT TRANSFER AT WALL

5-1573-9-102

GRID

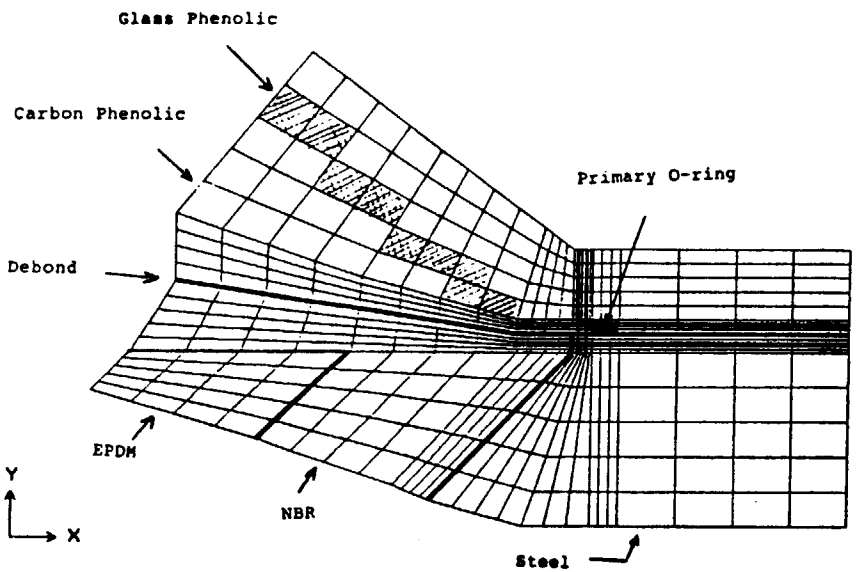

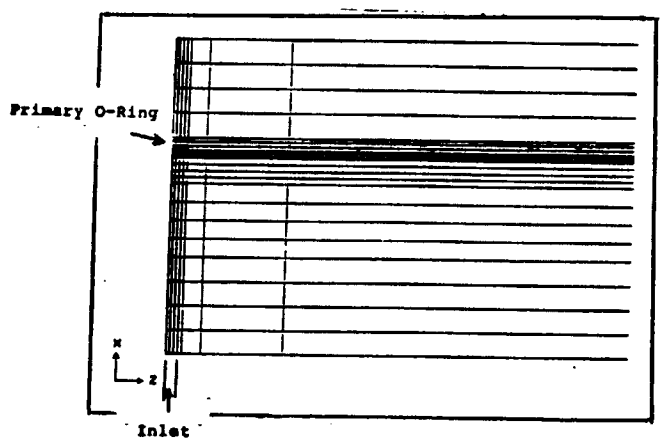

NX = 23

NY = 28

NZ = 18

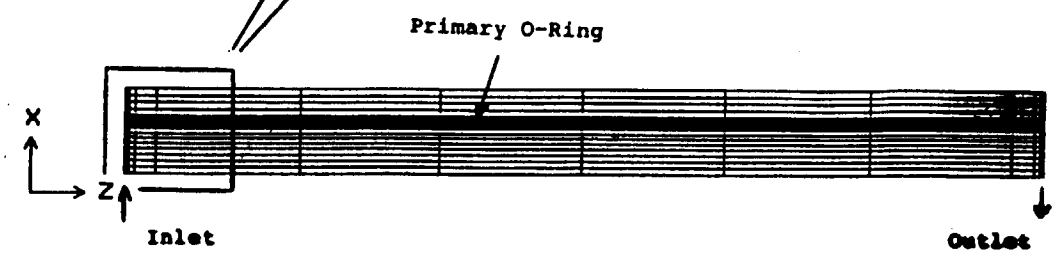

SUMMARY OF MAXIMUM TEMPERATURES FOR NOZZLE/CASE JOINT MODEL

Run No.	Insul. Gap (in.)	Steel Gap (in.)	Debond Width (5) (in.)	Diff. P (psi)	Diff. P Angle (deg)	T max Gas (deg F)	T max Steel (deg F)	T max O-ring (deg F)	Notes
1	.024	.004	F.O.	1.08	0 – 180	142	180	105	
2	.024	.010	F.O.	1.08	0 – 180	295	230	170	
3	.024	.004	3.5	1.08	0 – 180	1120	1092	769	
4	.024	.010	3.5	1.08	0 – 180	2071	1432	1423	
5	.024	.015	F.O.	envelope	0 – 180	258	132	129	
6	.100	.050	F.O.	envelope	0 – 180	1125	659	607	
7	.024	.008	3.5	envelope	0 – 180	1628	1117	885	
8	.024	.008	3.5	QM–4	0 – 180	1103	742	582	
9	.024	.008	3.5	QM–4	0 – 180	1153	769	601	1
10	.024	.008	3.5	QM–4	0 – 120	1256	852	667	1
11	.024	.008	3.5	QM–4	0 – 120	1643	1380	909	1,2
12	.050	.010	0.4	QM–4	0 – 120	2898	2320	1510	1,2
13	.050	.010	0.4	QM–4	0 – 120				1,2,3
14	.024	.008	3.5	QM–4	0 – 120	1502	1304		1,2,3
15	.046	.008	0.75	QM–4	0 – 120	2276	2352	1856	1,2,3
16	.090	.008	0.75	QM–4	0 – 120	2834	2846	2341	1,2,3
17	.046	.008	0.75	QM–4	0 – 120	2278	2359	1859	1,2,3,4
18	.046	.008	0.75	QM–4	0 – 120	2278	2351	1858	1,2,3,6
19	.046	.008	0.75	QM–4	0 – 120	2211	2252	1847	1,2,3,7
20	.046	.008	0.75	QM–4	0 – 120	2083	2353	1691	1,2,3,8
21	.046/.020	.008	0.75	QM–4	0 – 120	2089	2178	1588	1,2,3,9
22	.046/.020	.008	0.75	QM–4	0 – 120	2059	2187	1568	1,2,3,9,10
23	.046/.020	.008	0.75	QM–4	0 – 120	2053	2272	1543	1,2,3,9, 11
24	.046/.020	.008	0.75	QM–4	0 – 120	1866	2255	1509	1,2,3,9,11,12,13
25	.046/.020	.008	0.75	DM–8	0 – 120	1610	1818	1274	2, 3, 9, 11

Notes:

1. Improved modeling of QM–4 duty cycle
2. Model revised to open NBR/glass phenolic area 360 deg. and improve average material properties
3. Material properties computed as function of temperature
4. Same as Run 15 but with number of time steps doubled
5. One-half of values listed input to model due to symmetry
6. 2 X nominal number of grid nodes in Z direction
7. Increased number of grid nodes in X direction (<2 X nominal)
8. 2 X nominal number of grid nodes in X direction
9. Model regrided to provide two insulation gap width capability
10. Y grid sensitivity. Number of insulation cells increased
11. K-Epsilon turbulence model
12. Y grid sensitivity. Number of fluid cells increased by factor of 2
13. Calculation of O-ring wall temperature corrected

5-1576-9-102

NOZZLE/CASE JOINT PHOENICS RUN

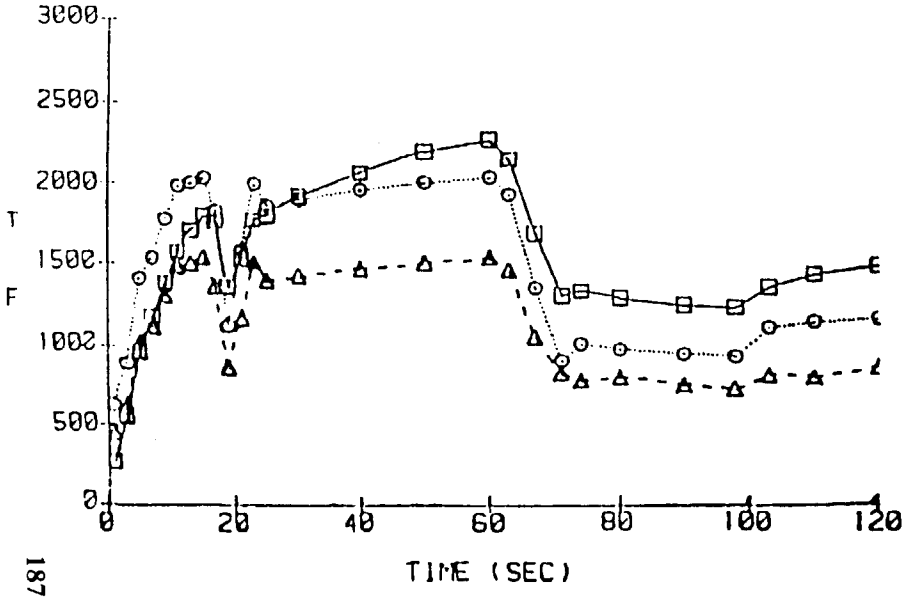

QM-4

NOZZLE/CASE JOINT PHOENICS RUN

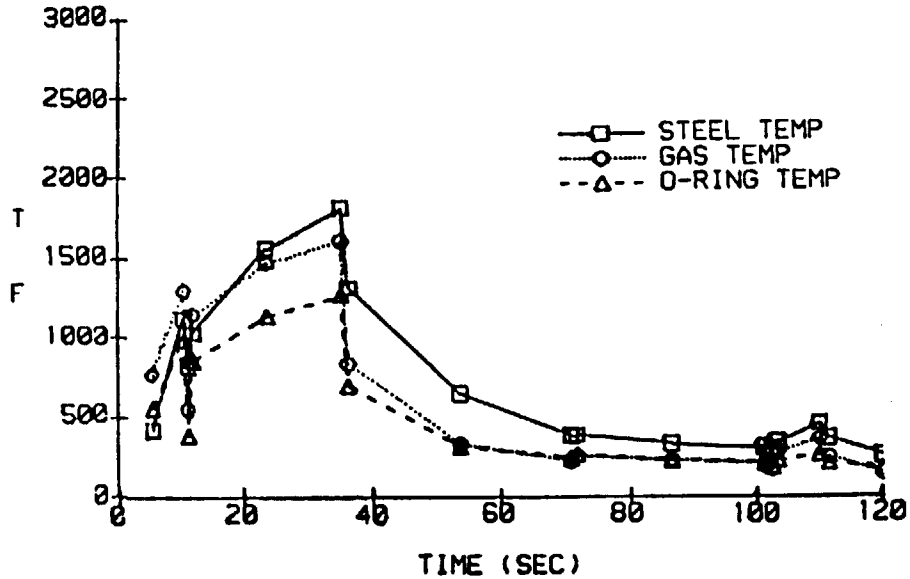

DM-8

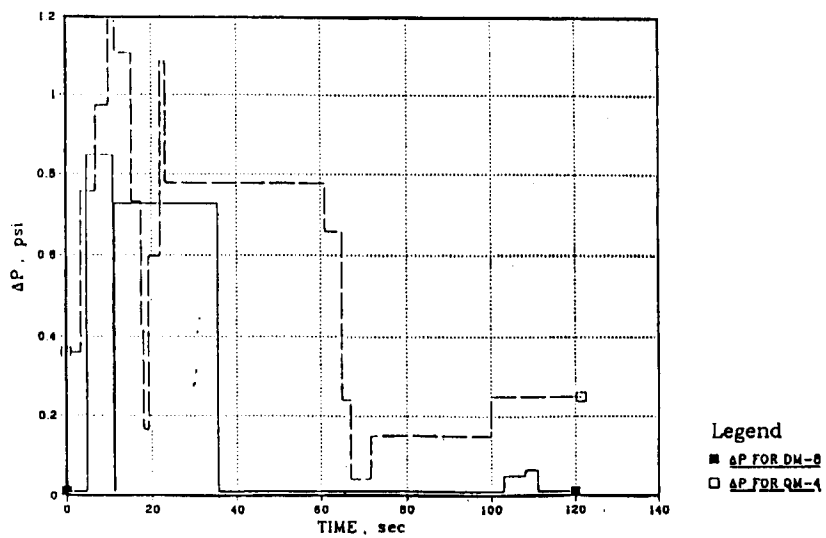

ORIGINAL PAGE IS
OF POOR QUALITY

GRID 37x32x19 GRID

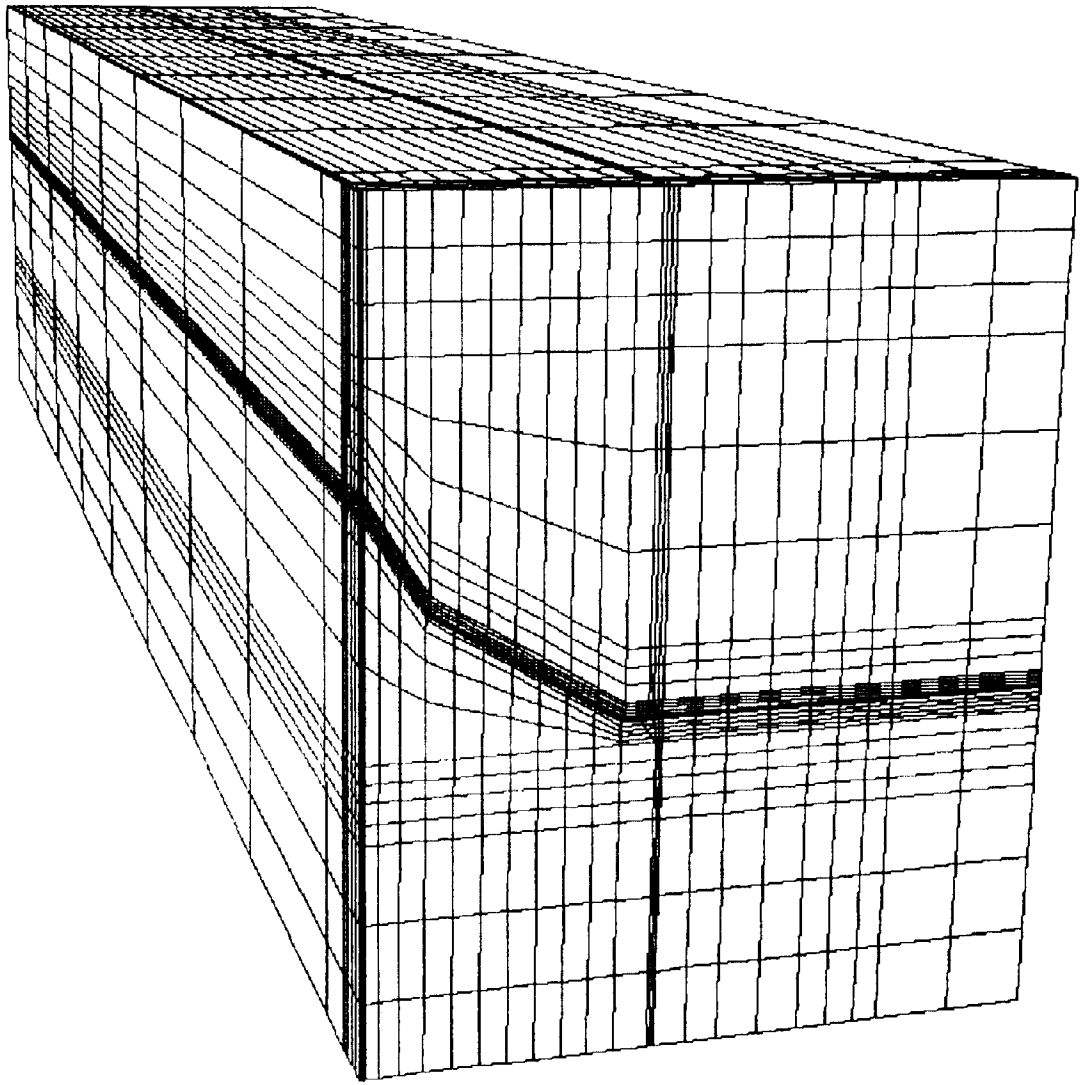

SUMMARY OF MAXIMUM TEMPERATURES FOR FIELD JOINT MODEL

RUN	SPECIFICATION				CALCULATED RESULTS		
NO.	G1 (IN)	CIRCUM. DEBOND WIDTH (IN)	CIRCUM. DEBOND ANGLE (DEG)	Δp PSI	TMAX STEEL (DEG C)	TMAX GAS (DEG C)	TMAX O-RING (DEG C)
1	0.002	2.8	120	0.5	16.1	13.9	13.6
2	0.002	2.8	15	0.5	16.2	14.1	13.7
3	0.016	0.25	120	0.5	16.5	23.3	14.2
4	0.016	0.25	15	0.5	161.7	746.6	607.4
5	0.016	0.25	15	0.1	21.0	65.4	42.3

NOTE: FOR ALL CASES G2 = 0.0264", AND G3 = 0.0241"

5-1569-9-105

CONTOUR LEVELS

[illegible]
[illegible]
[illegible]
[illegible]
[illegible]
[illegible]
[illegible]
[illegible]
[illegible]
900.000
1000.000
1100.000
1200.000
1300.000
1400.000
1500.000
1600.000
1700.000
1800.000
1900.000
2000.000
2100.000
2200.000
2300.000
2400.000
2500.000
2600.000
2700.000
2800.000
2900.000
3000.000

TEMPERATURE (DEG C)

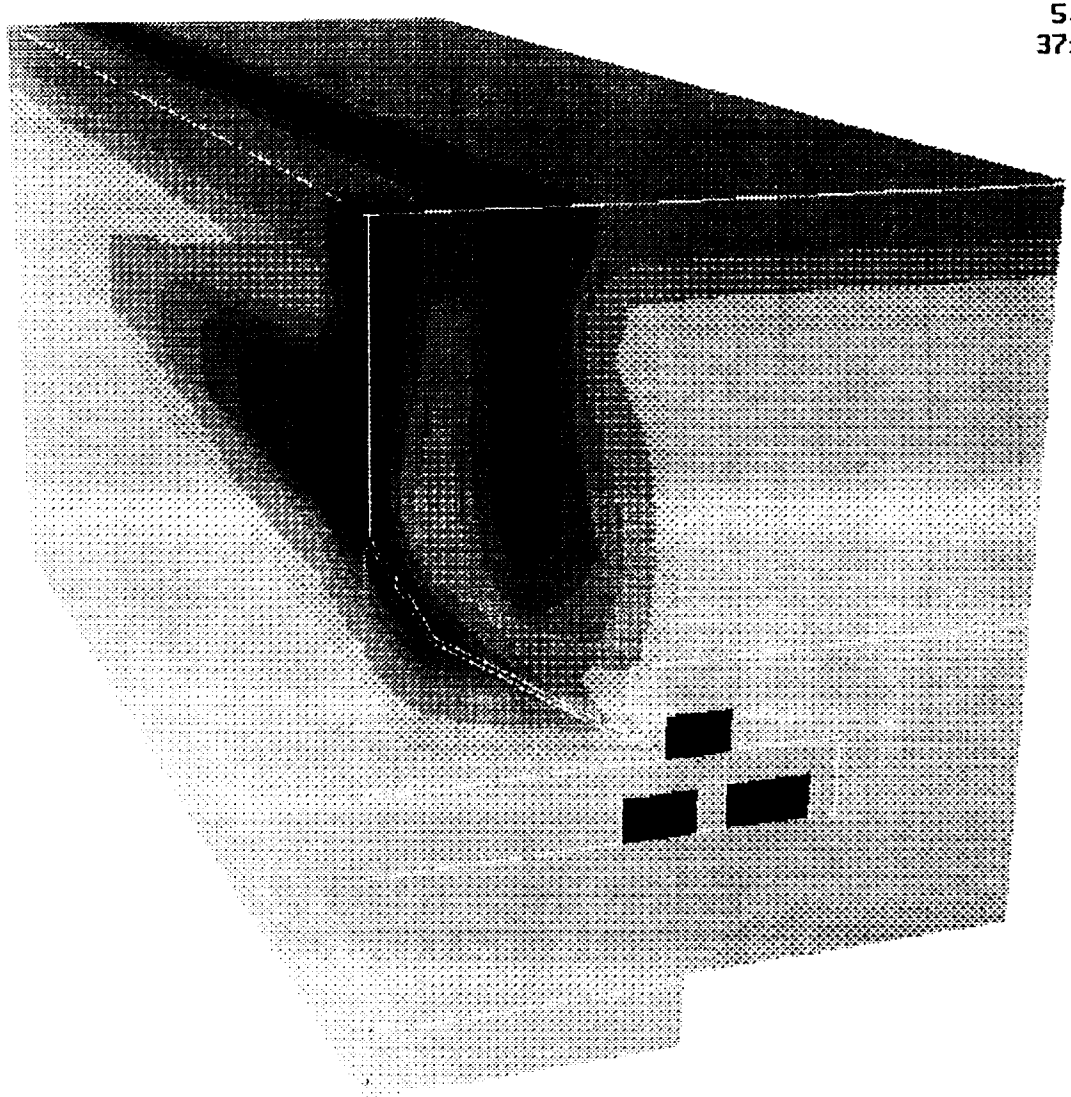

0.010	MACH
0.00 DEG	ALPHA
5.00x10 2	Re
37x32x19	GRID

ORIGINAL PAGE IS
OF POOR QUALITY

SRB NOZZLE/CASE AND CASE FIELD JOINT FLOW AND THERMAL ANALYSIS

PROGRAM IMPACT:

- STEEL CASE TEMPERATURE LIMIT FOR REUSE (1000°F)
  - EXCEEDED FOR NOZZLE/CASE JOINT (IF 2 LEAKPATHS OCCUR WHICH IS VERY UNLIKELY)
  - WITHIN LIMIT FOR CASE FIELD JOINT
- ABLATION TEMPERATURE LIMIT FOR O-RINGS (700°F)
  - EXCEEDED FOR NOZZLE/CASE JOINT (IF 2 LEAKPATHS OCCUR WHICH IS AGAIN UNLIKELY)
  - WITHIN LIMIT FOR CASE FIELD JOINT (EXCEPT ONE CASE WHERE FLOW PATH IS ONLY OVER 15°)

CONCLUSIONS:

- ANALYSIS CONSIDERED CONSERVATIVE, DUE TO WORST CASE SCENARIOS BEING ANALYZED
- ANALYSIS PERFORMED TO VERIFY OTHER ANALYSIS BEING DONE IN PARALLEL, AT MORTON THIOKOL TO SUPPORT RETURN-TO-FLIGHT STATUS
- PROBABILITY OF TWO LEAKPATHS OCCURING IS ONE IN ONE-THOUSAND SO DESIGN MEETS FAIL-SAFE AND REUSEABILITY CONDITIONS.

5-1623-9-103

SESSION IX

TURBOMACHINERY

Chairman:
Robert M. Stubbs
Chief, Computational Methods Branch
NASA Lewis Research Center

PRECEDING PAGE BLANK NOT FILMED

N91-10880

SIMULATION OF TURBOMACHINERY FLOWS

by

John J. Adamczyk
NASA Lewis Research Center

ABSTRACT

Significant advancements have been made in the last five years in the ability to model turbomachinery flows of engineering interest. This advancement can be directly attributed to the second generation of supercomputers like the Cray XMP and Cray II and advanced instrumentation techniques. Early on, the National Aeronautics and Space Administration Lewis Research Center recognized the potential gains in turbomachinery performance and life that could be achieved by taking advantage of this technology and instituted a comprehensive research program in turbomachinery flow modeling. This activity combined the areas of fluid flow analysis, computational fluid dynamics, and experimental fluid mechanics. As a result of this activity, Lewis has become an internationally recognized leader in turbomachinery flow modeling. Many of the research activities conducted under this progam have been utilized by industry. The presentation will give an overview of this program and provide sample illustration of simulation performed to date.

PRECEDING PAGE BLANK NOT FILMED

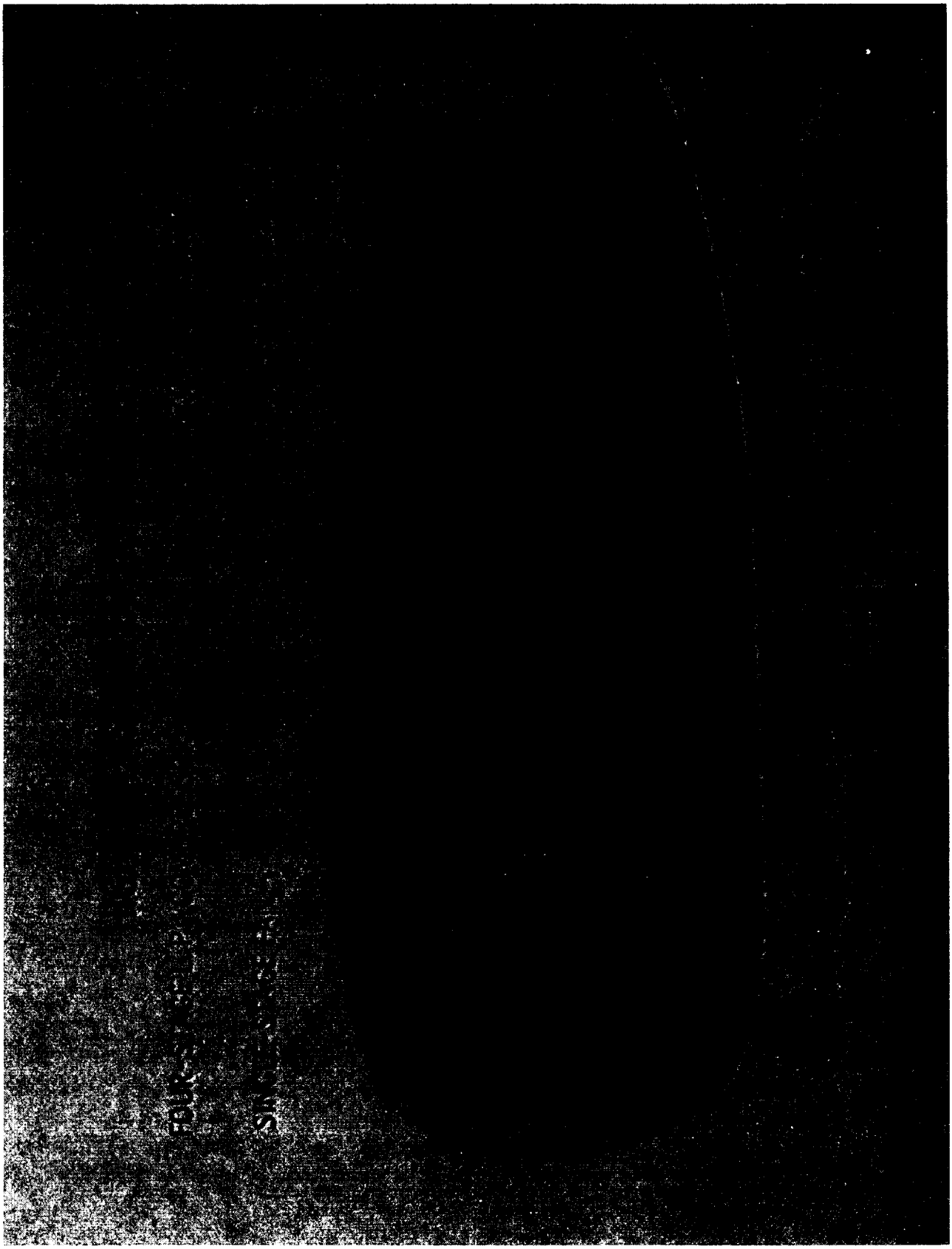

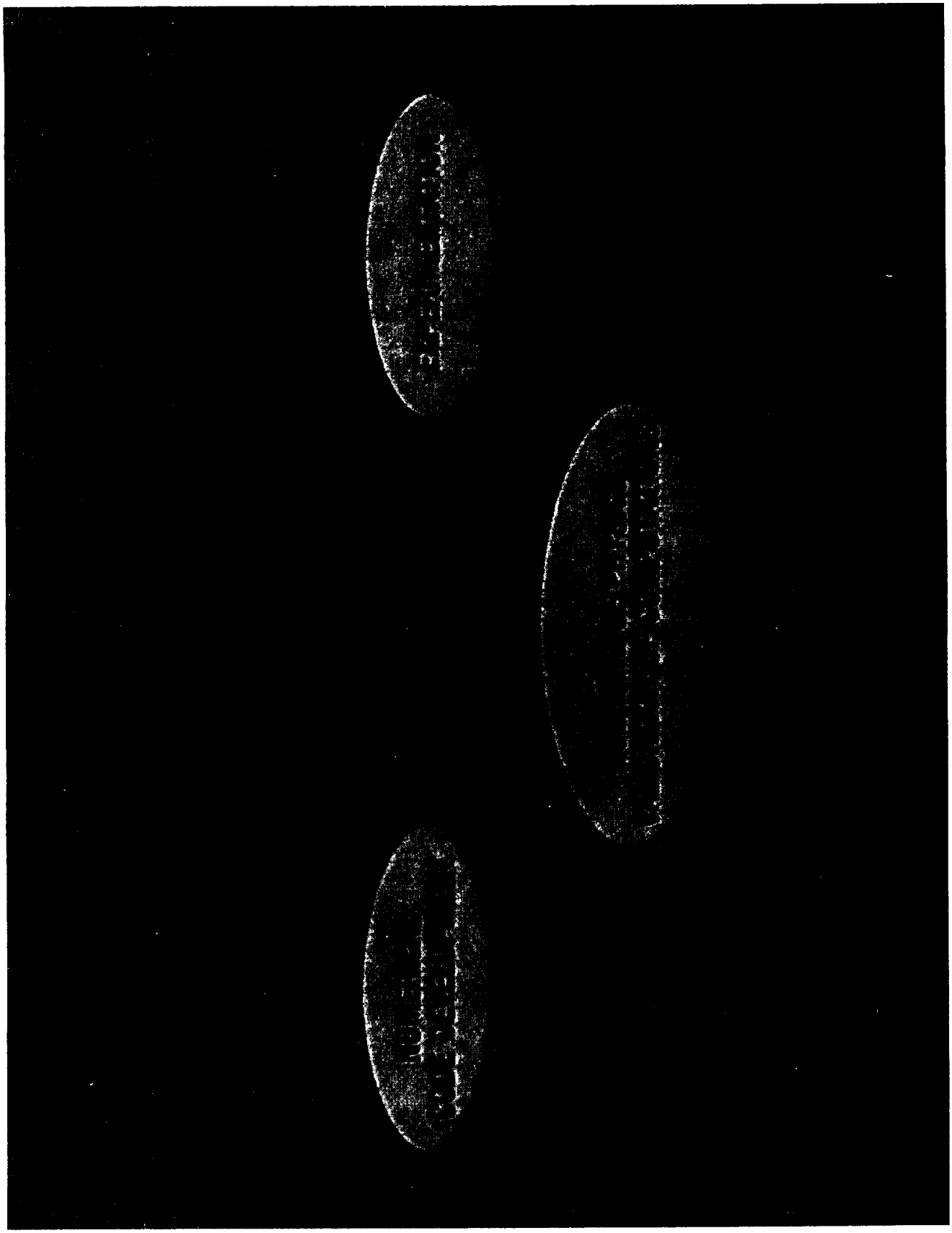

ORIGINAL PAGE IS
OF POOR QUALITY

CFD IN THE PROBLEM SOLVING PROCESS

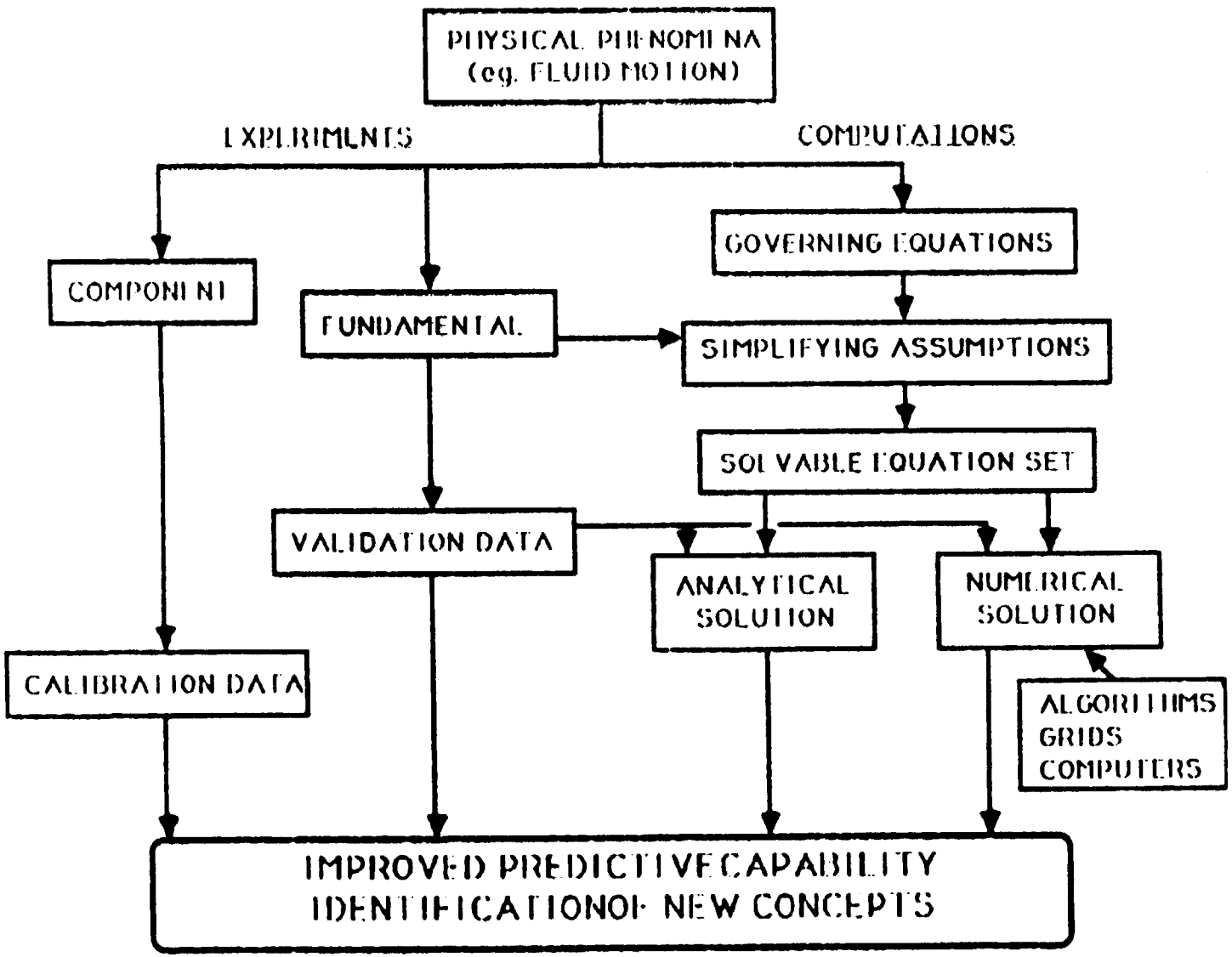

EQUATIONS HIERARCHY

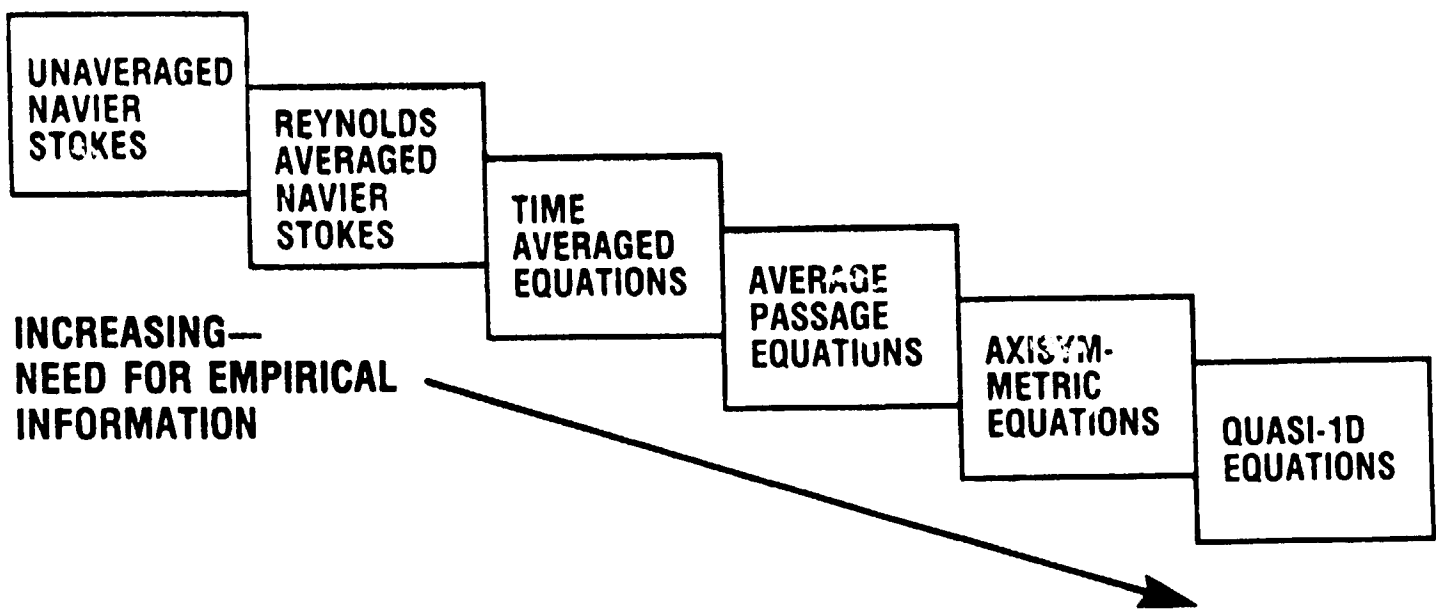

CASCADE ENDWALL FLOW STRUCTURE

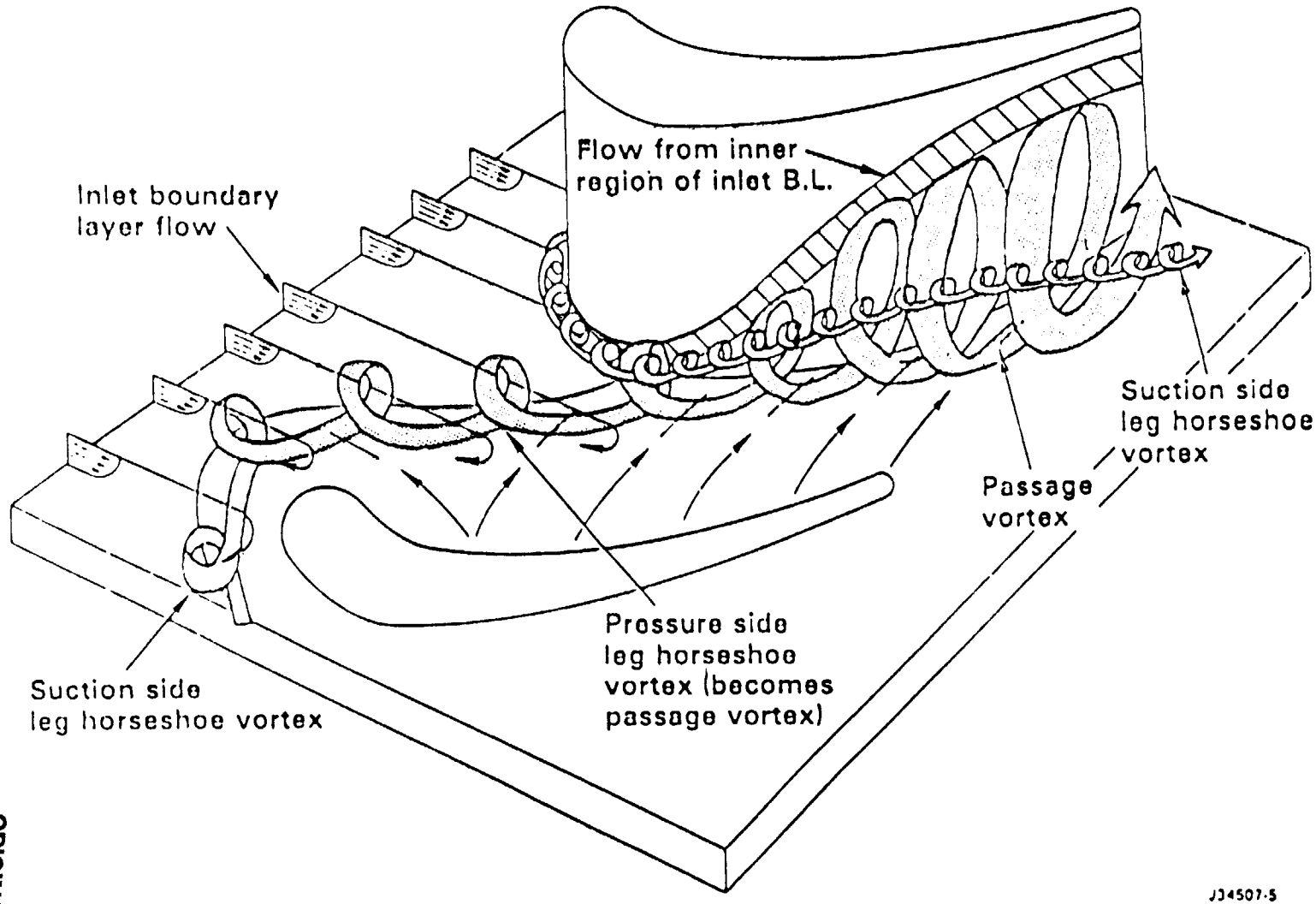

J34507-5
860606

ORIGINAL PAGE IS
OF POOR QUALITY

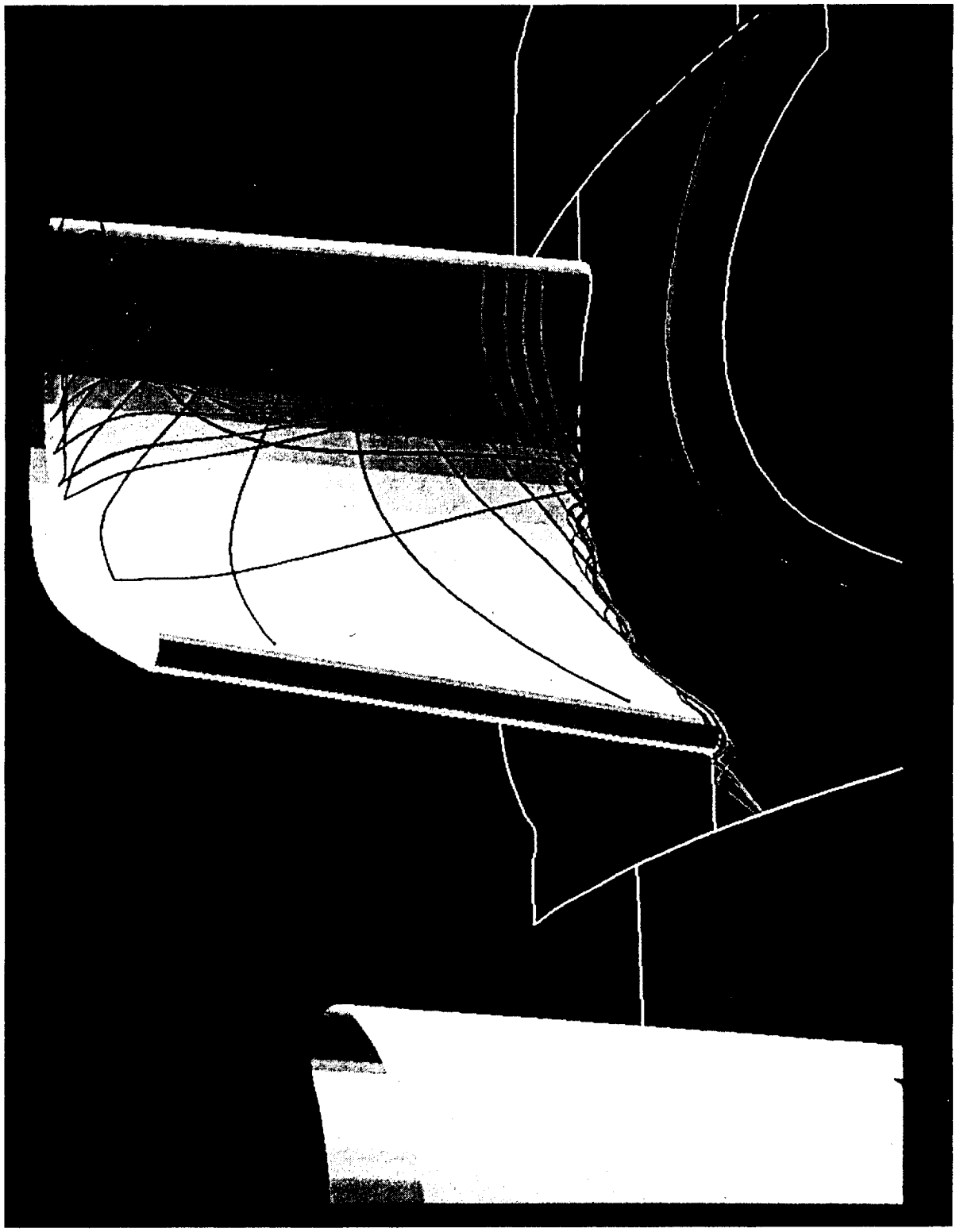

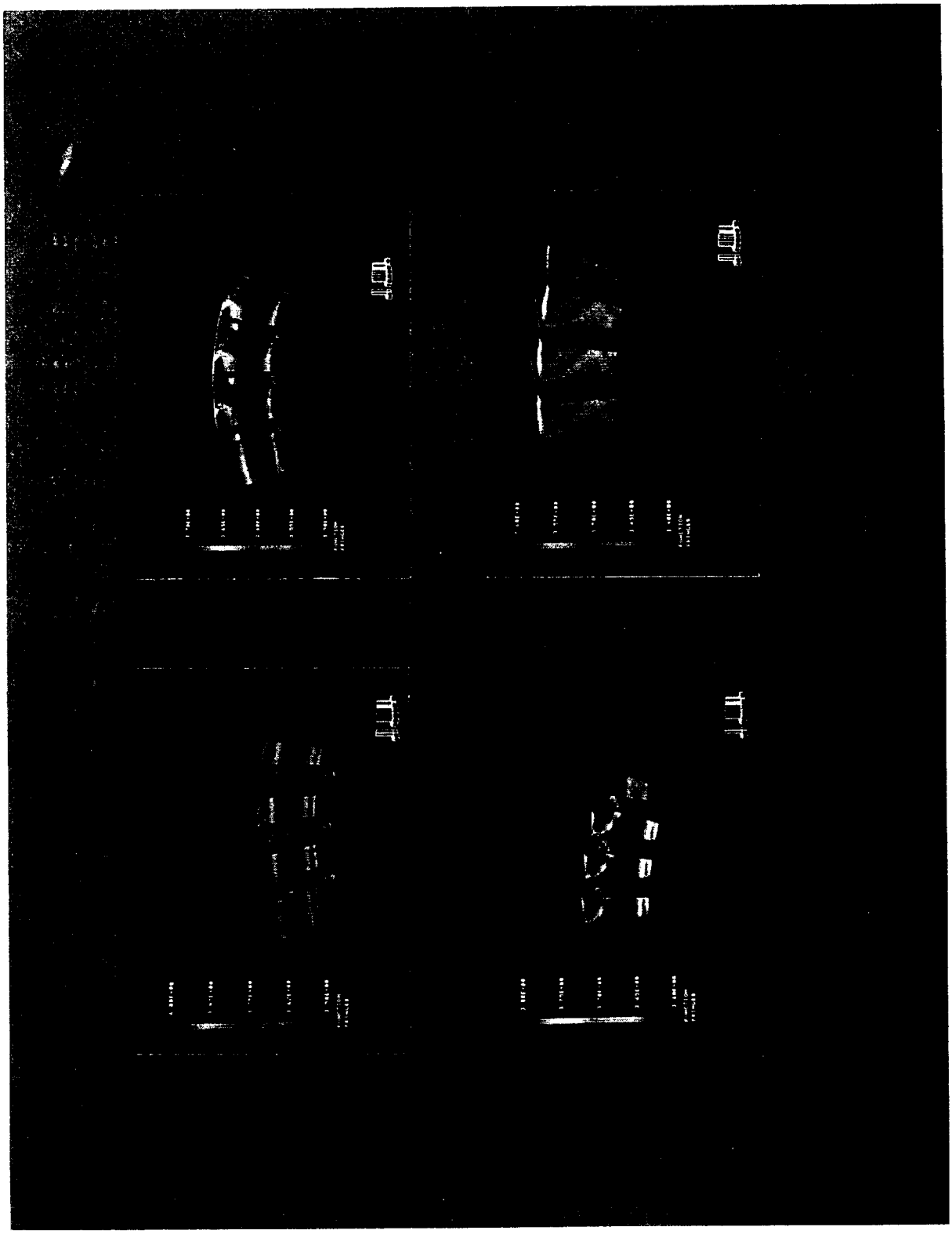

ORIGINAL PAGE IS
OF POOR QUALITY

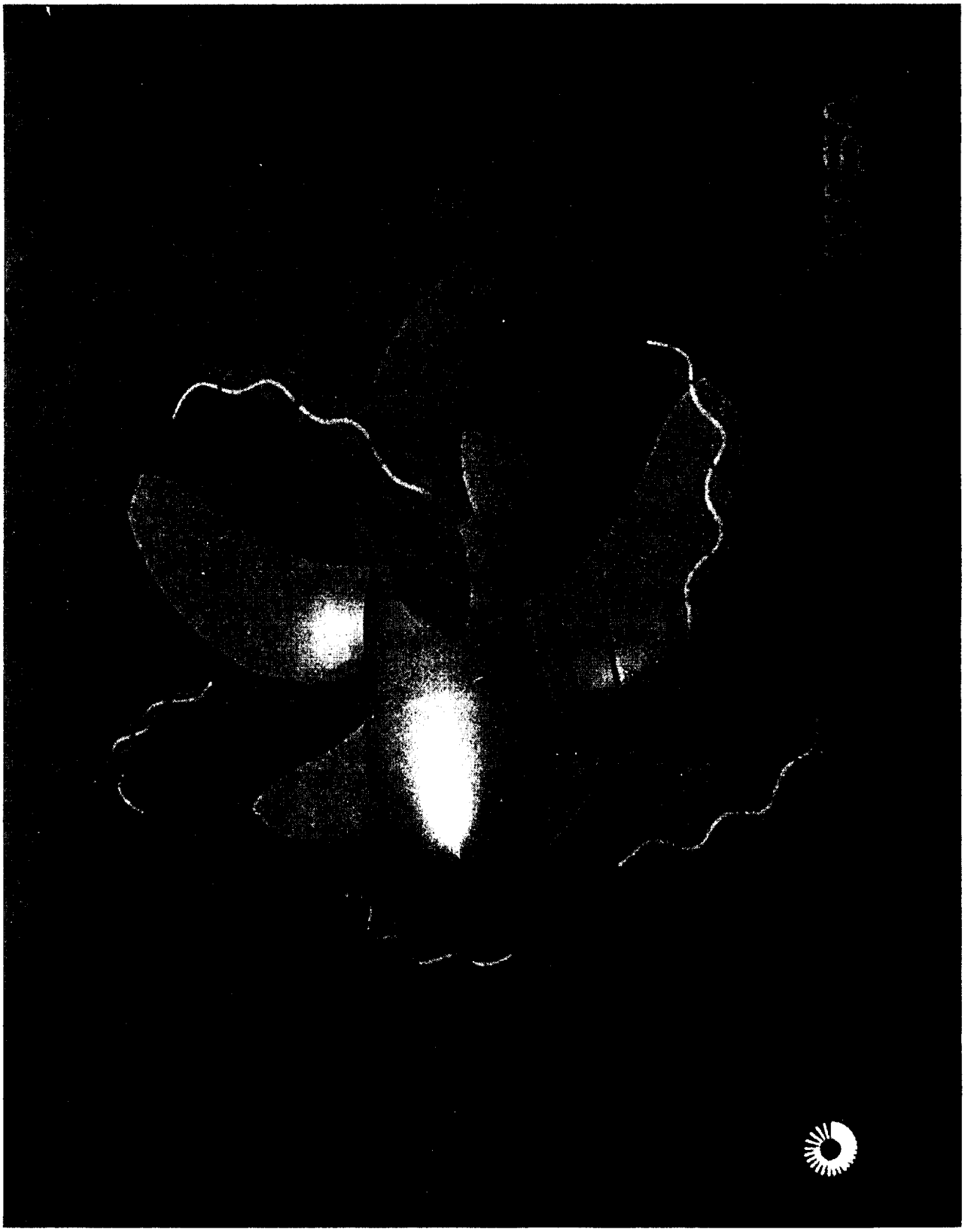

ORIGINAL PAGE IS
OF POOR QUALITY

ADVANCED CONTRA-ROTATING PROPELLER NOISE PREDICTION

2' GE F7/A7, LeRC 8x6 WIND TUNNEL, DESIGN CONDITION (M=0.72)

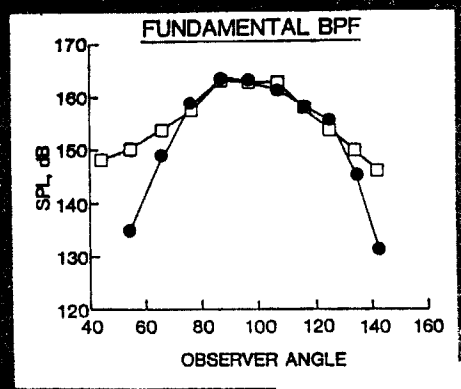

Data
Farassat

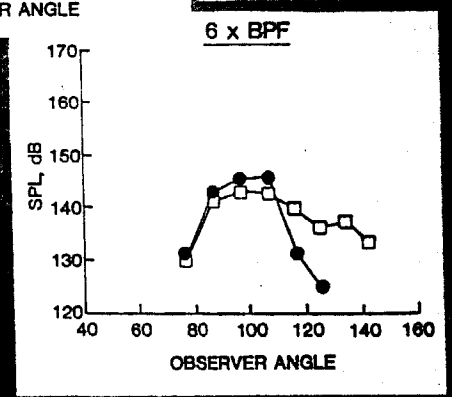

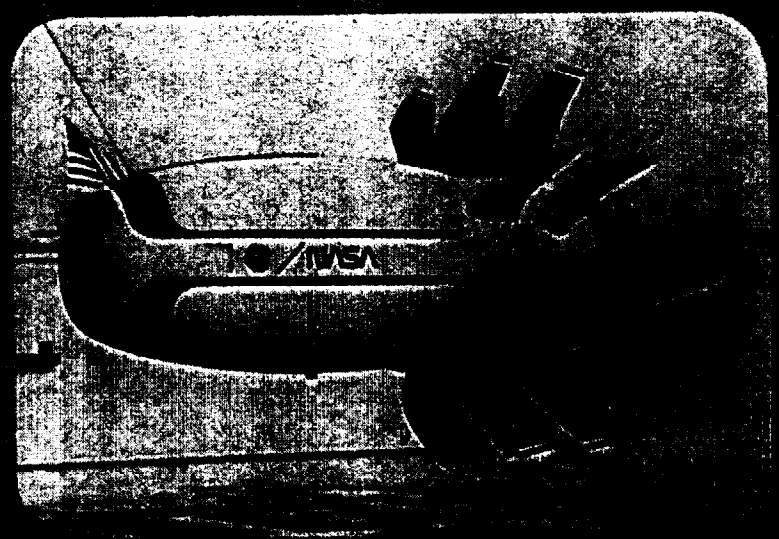

ORIGINAL PAGE IS
OF POOR QUALITY

N91-10881

PREDICTION OF TURBINE ROTOR-STATOR INTERACTION USING NAVIER-STOKES METHODS

N. K. Madavan and M. M. Rai
NASA Ames Research Center
Moffett Field, CA 94035

and

S. Gavali
Amdahl Corporation
Sunnyvale, CA 94088

Abstract

Flows in turbomachinery are generally complex and do not easily lend themselves to numerical computation. The flows are three-dimensional and inherently unsteady. The unsteadiness arises from the interaction of the downstream airfoils with the wakes and passage vortices generated upstream, from the motion of the rotors relative to the stators and from vortex shedding at blunt airfoil trailing edges. Complicated blade geometries and flow phenomena such as separation and periodic transition from laminar to turbulent flow add to the numerical complexity. Nevertheless, the accurate numerical analysis of such flows is a problem of considerable interest and practical importance to the turbomachinery community.

Much of the early work in turbomachinery flow prediction focussed on airfoil cascades. While such analyses of flows in isolated airfoil rows have helped improve our understanding of the flow phenomena and have gained widespread acceptance in the industrial community as a design tool, they do not yield any information regarding the unsteady effects arising out of rotor-stator aerodynamic interaction. These interaction effects become increasingly important as the distance between successive stator and rotor rows is decreased. Thus, the need exists for analytical tools that treat the rotor and stator airfoils as a system and provide information regarding the magnitude and the impact of the unsteady effects.

The focus of this presentation is a three-dimensional, time-accurate, thin-layer Navier-Stokes code that has been recently developed to study rotor-stator interaction problems. A system of patched and overlaid grids that move relative to each other is used to discretize the flow field and the governing equations are integrated using a third-order upwind scheme set in an iterative, implicit framework. The code has been used to simulate subsonic flow through an axial turbine configuration for which considerable experimental data exists. Grid refinement studies have also been conducted as part of the code validation process. The current status of the research, along with planned future directions, are also discussed.

INTRODUCTION

- THE PREDICTION OF FLOWS IN TURBOMACHINERY IS A PROBLEM OF CONSIDERABLE INTEREST

- THE FLOWFIELDS ARE INHERENTLY UNSTEADY DUE TO :

  MOTION OF ROTORS RELATIVE TO THE STATORS

  INTERACTION OF DOWNSTREAM AIRFOILS WITH WAKES OF UPSTREAM AIRFOILS

  VORTEX SHEDDING AT BLUNT TRAILING EDGES

- UNSTEADY (OR INTERACTION) EFFECTS PRESENT EVEN FOR AXIAL GAPS USED IN CURRENT DESIGNS (50% TO 25% CHORD)

INTRODUCTION.....CONTD.

- COMPLEX BLADE GEOMETRIES, PERIODIC TRANSITION FROM LAMINAR TO TURBULENT FLOW, FLOW SEPARATION, ETC. PRESENT ADDITIONAL COMPUTATIONAL DIFFICULTIES

- NEED EXISTS FOR A COMPUTATIONAL TOOL THAT TREATS THE COMPLETE TURBINE STAGE AS A SYSTEM AND PROVIDES INFORMATION REGARDING THE UNSTEADY EFFECTS

POSSIBLE GAINS

- IMPROVED PERFORMANCE (LOWER LOSSES, ETC.)
- IMPROVED STRUCTURAL DESIGN (STRUCTURES THAT BETTER WITHSTAND THE DYNAMIC STRESSES ASSOCIATED WITH THE UNSTEADY NATURE OF THE FLOW)
- AN UNDERSTANDING OF THE ACOUSTICS (MINIMIZATION OF ENGINE NOISE)
- PREDICTION OF UNSTEADY HEAT TRANSFER (IMPROVED COOLING TECHNOLOGY)

CURRENT STATUS

- COMPUTER CODES CAPABLE OF PREDICTING UNSTEADY FLOWFIELDS IN SINGLE–STAGE TURBOMACHINERY DEVELOPED

  ROTOR–2 ..... 2D, NAVIER–STOKES CODE

  ROTOR–3 ..... 3D, NAVIER–STOKES CODE

CURRENT STATUS.....CONTD.

- CODE CAPABILITIES DEMONSTRATED BY SIMULATING AN EXPERIMENTAL SINGLE–STAGE AXIAL TURBINE CONFIGURATION

  2D COMPUTATIONS

  3D COMPUTATIONS FULLY ACCOUNTING FOR HUB, CASING AND ROTOR TIP CLEARANCE EFFECTS

  GRID–REFINEMENT STUDIES IN 3D

- STATE–OF–THE–ART COMPUTER GRAPHICS TECHNIQUES USED FOR VISUALIZATION OF COMPUTED RESULTS

  "STEREO ANIMATION" TECHNIQUES

COMPUTATIONAL DETAILS

- HIGH–ORDER UPWIND FINITE–DIFFERENCE ALGORITHM FOR TIME–ACCURATE SOLUTION OF THE THIN–LAYER NAVIER–STOKES EQUATIONS
- ALGORITHM SET IN AN ITERATIVE, FACTORED AND IMPLICIT FRAMEWORK
- SYSTEM OF PATCHED AND OVERLAID GRIDS FOR FLOWFIELD DISCRETIZATION
- ROTOR GRIDS MOVE RELATIVE TO THE STATOR GRIDS
- BALDWIN–LOMAX TYPE TURBULENCE MODEL USED

COMPUTATIONAL GRID

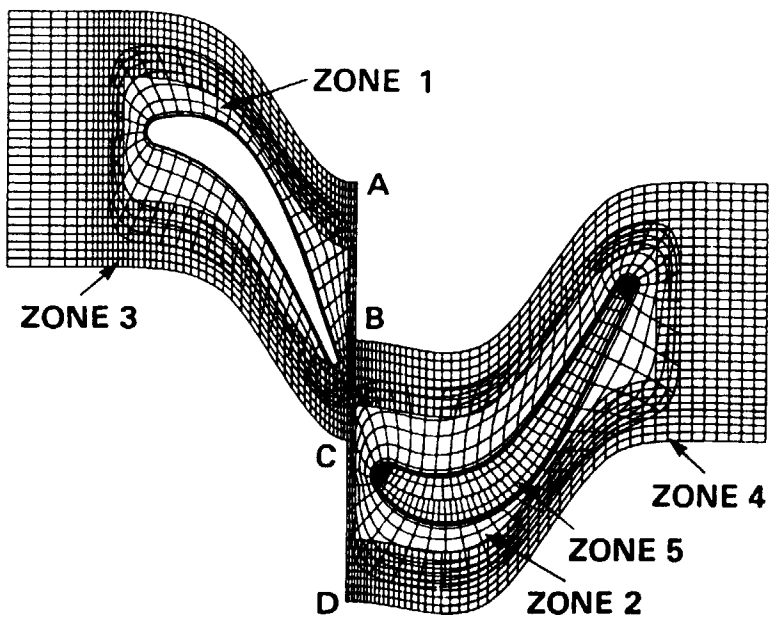

SPANWISE VARIATION OF STATOR TIME-AVERAGED PRESSURE

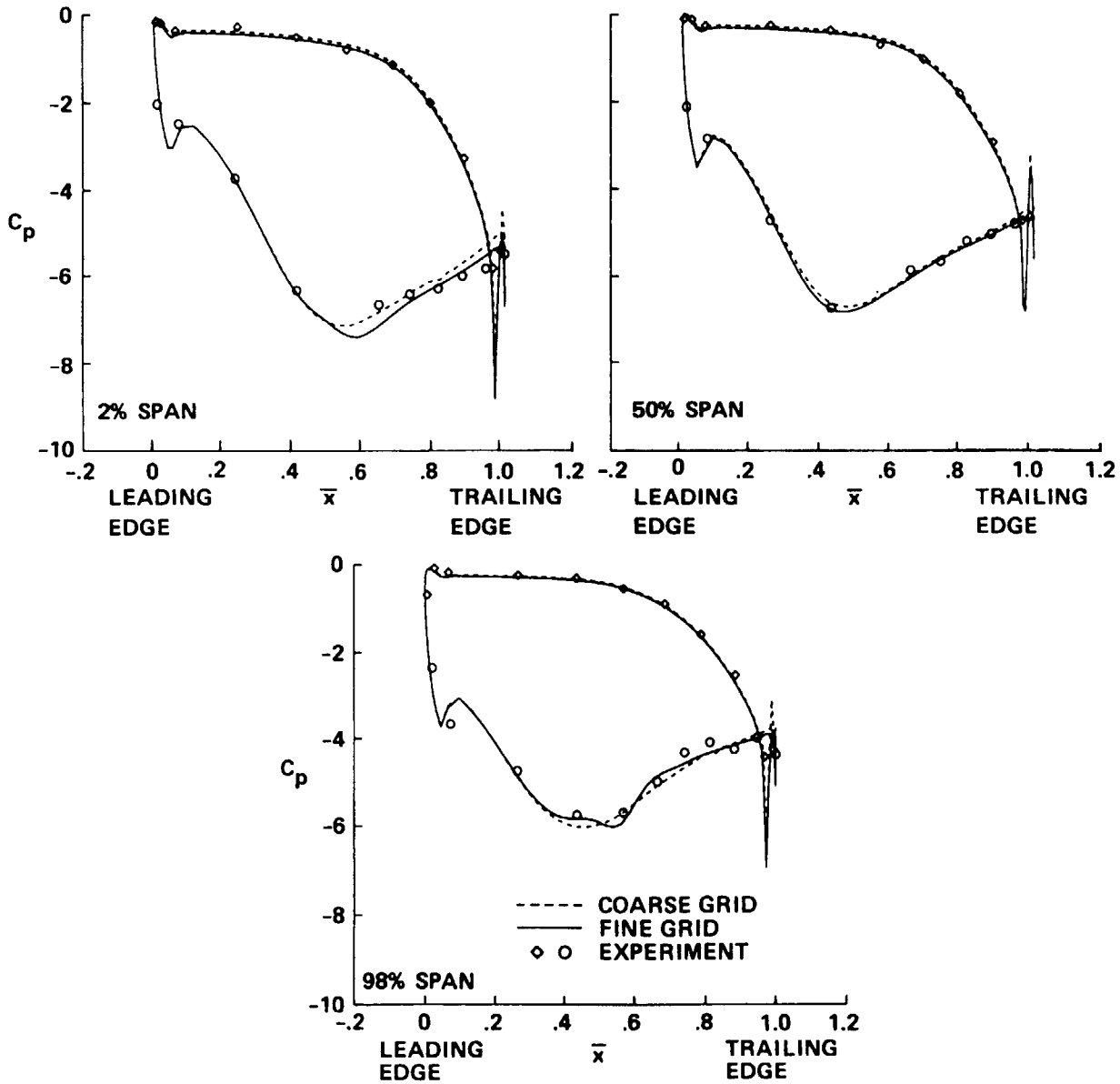

PRESSURE AMPLITUDE DISTRIBUTION ON THE STATOR

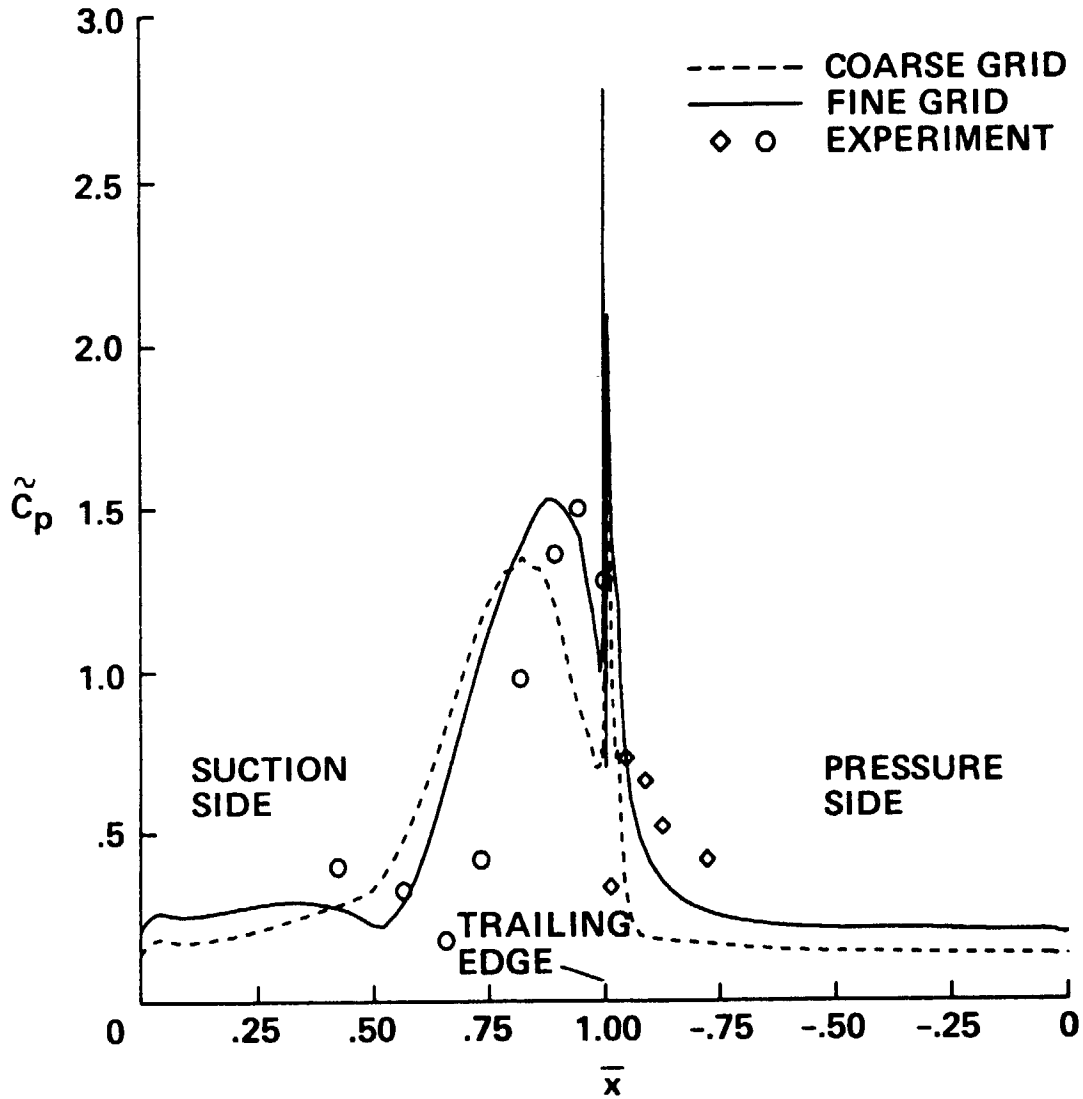

TIME-AVERAGED LIMITING STREAMLINES
ROTOR SUCTION SURFACE

FINE GRID

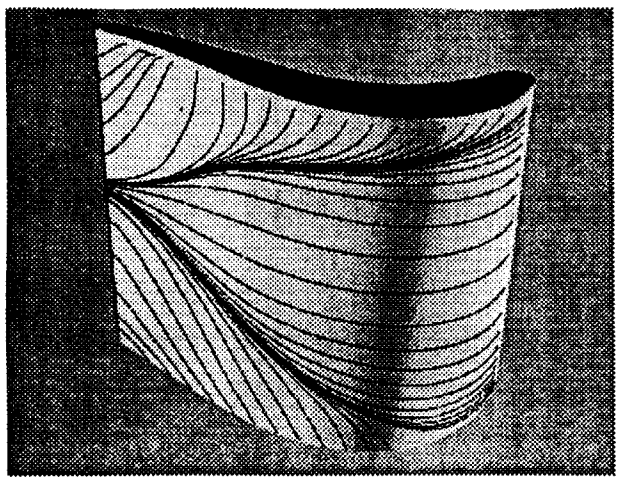

EXPERIMENTAL VISUALIZATION

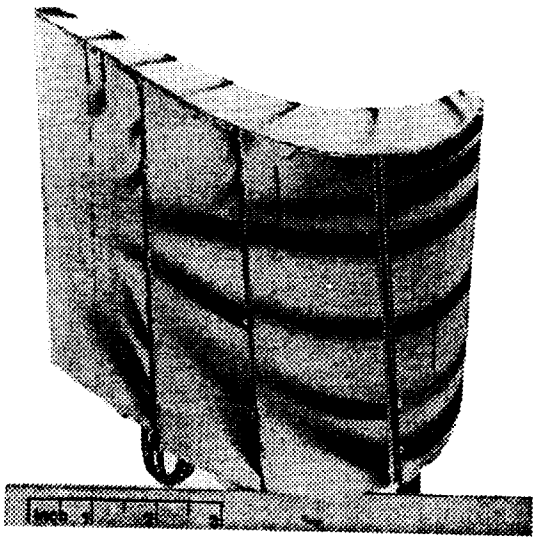

SUMMARY AND FUTURE DIRECTIONS

- 2D AND 3D UNSTEADY, THIN–LAYER NAVIER–STOKES CODES DEVELOPED TO SIMULATE ROTOR/STATOR INTERACTION IN TURBOMACHINERY

- CURRENT RESEARCH EFFORTS AND FUTURE DIRECTIONS INCLUDE :

  MULTI–BLADE COMPUTATIONS

  MULTI–STAGE COMPUTATIONS

  BOUNDARY CONDITIONS

  TURBULENCE MODELING

  CODE ACCELERATION TECHNIQUES

  GRAPHICS

N91-10882

Turbine Stage Aerodynamics And Heat Transfer Prediction

L. W. Griffin and H. V. McConnaughey
NASA/MSFC

A numerical study of the aerodynamic and thermal environment associated with axial turbine stages is presented. Computations were performed using a modification of the unsteady NASA Ames viscous code, ROTOR1, and an improved version of the NASA Lewis steady inviscid cascade system MERIDL-TSONIC coupled with boundary layer codes BLAYER and STAN5. Two different turbine stages were analyzed: the first stage of the United Technologies Research Center Large Scale Rotating Rig (LSRR) and the first stage of the Space Shuttle Main Engine (SSME) high pressure fuel turbopump turbine. The time-averaged airfoil midspan pressure and heat transfer profiles were predicted for numerous thermal boundary conditions including adiabatic wall, prescribed surface temperature, and prescribed heat flux. Computed solutions are compared with each other and with experimental data in the case of the LSRR calculations. Modified ROTOR1 predictions of unsteady pressure envelopes and instantaneous contour plots are also presented for the SSME geometry. Relative merits of the two computational approaches are discussed.

OVERVIEW

- OBJECTIVES
- MOTIVATION
- APPROACH
  - CODES
  - APPLICATIONS
- RESULTS
  - AERODYNAMIC
  - HEAT TRANSFER
- COMPUTER RESOURCES REQUIREMENTS
- IMPACT
- SUMMARY AND CONCLUSIONS

5-1556-9-105

OBJECTIVES

- DEFINITION OF STEADY AND UNSTEADY AEROTHERMAL ENVIRONMENTS FOR THE SPACE SHUTTLE MAIN ENGINE (SSME) HIGH PRESSURE FUEL TURBOPUMP (HPFTP) TURBINE

- CALIBRATION OF TURBINE ANALYSIS CODES VIA COMPARISON OF PREDICTED AND EXPERIMENTALLY MEASURED AIRFOIL LOADS IN UNITED TECHNOLOGIES RESEARCH CENTER LARGE SCALE ROTATING RIG (LSRR)

5-1557-9-105

MOTIVATION

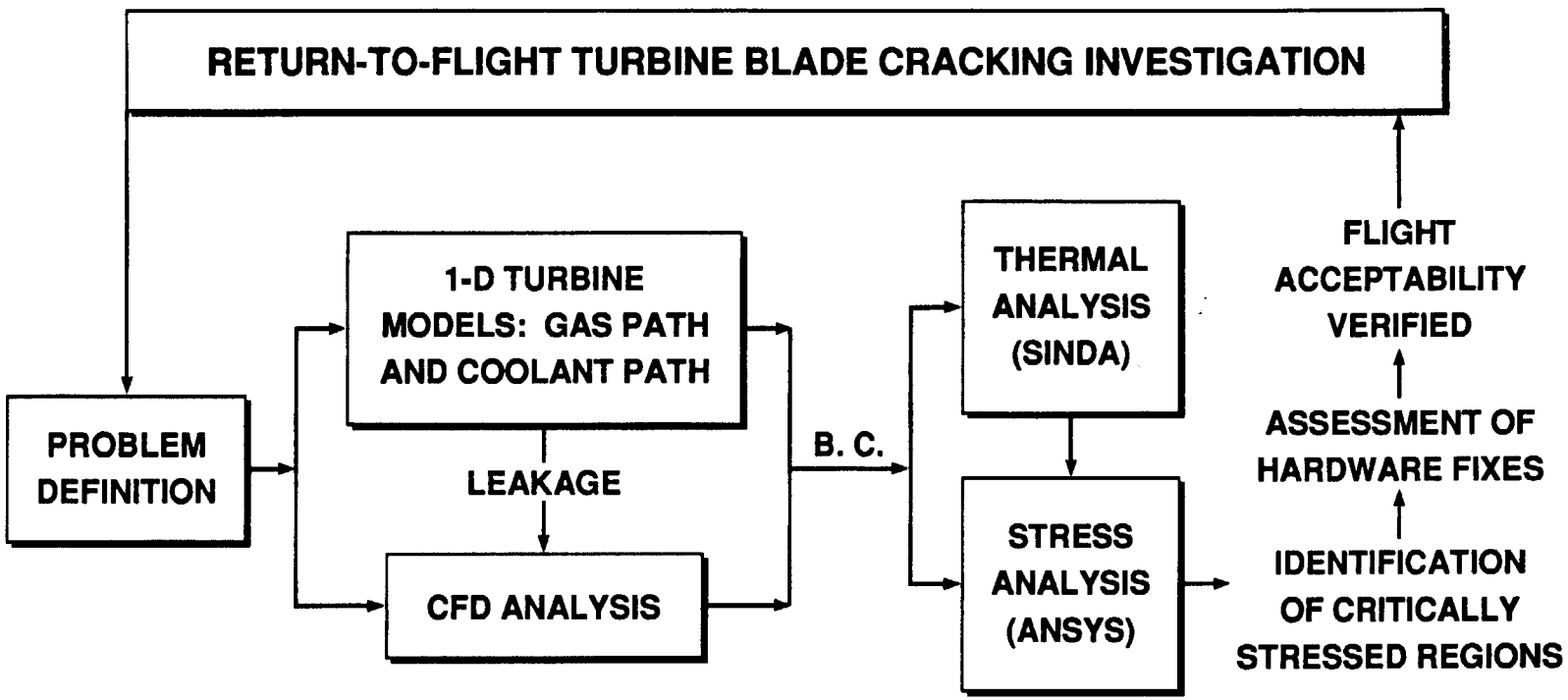

5-1629-9-103

APPROACH

CODES:

- MTSBL-STAN5 – STEADY INVISCID QUASI-3D SYSTEM MERIDL-TSONIC COUPLED WITH BOUNDARY LAYER CODES BLAYER AND STAN5. DEVELOPED AT NASA/LEWIS.
- ROTOR1 – UNSTEADY 2D SINGLE-STAGE CODE DEVELOPED AT NASA/AMES. ASSUMES EQUAL BLADE COUNT. MODIFIED TO INCORPORATE HEAT TRANSFER PREDICTION CAPABILITY

APPLICATIONS:

- LSRR – CODE CALIBRATION
- SSME HPFTP – ENVIRONMENT DEFINITION

5-1558-9-105

PRESSURE DISTRIBUTIONS FOR THE LSRR

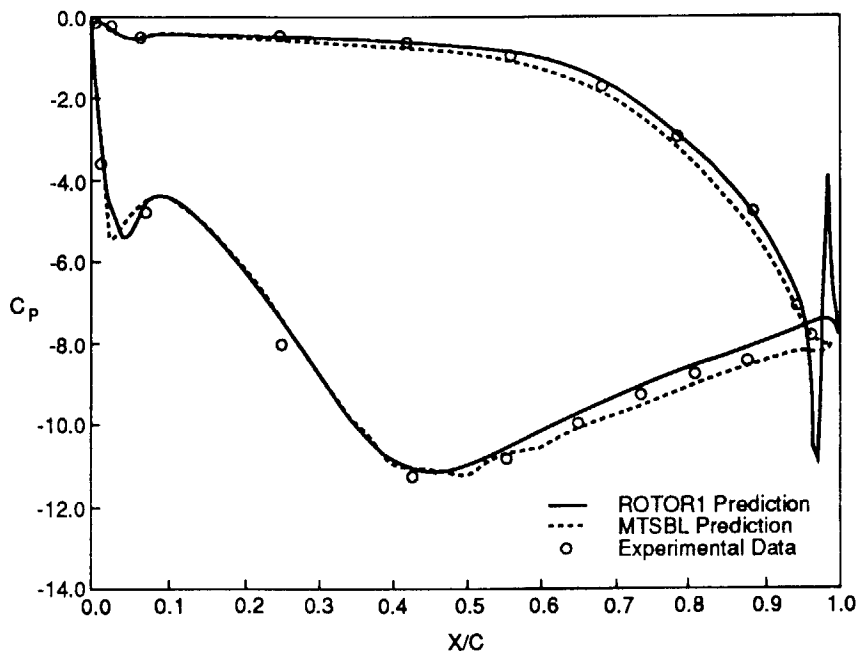

Stator

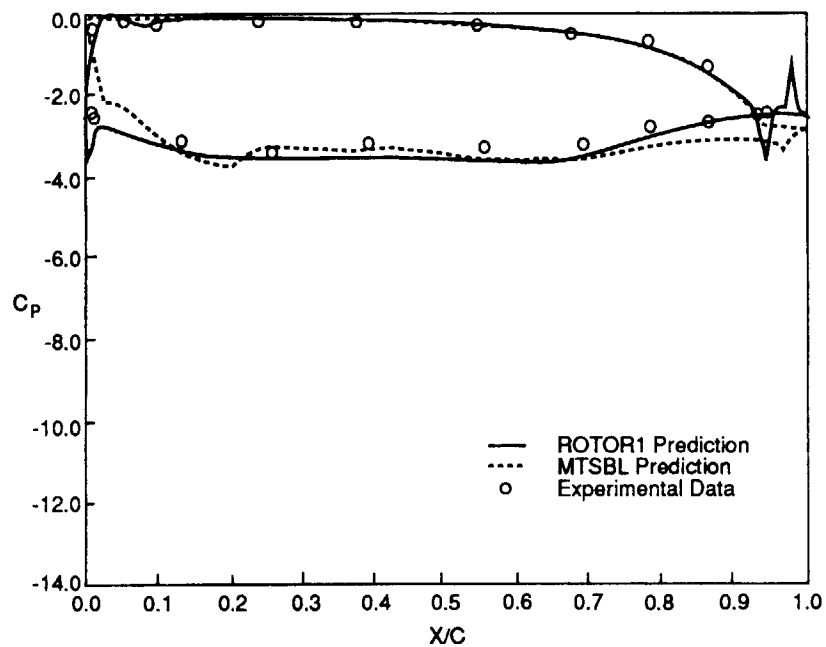

Rotor

5-1562-9-105

PRESSURE DISTRIBUTIONS FOR THE SSME HPFTP

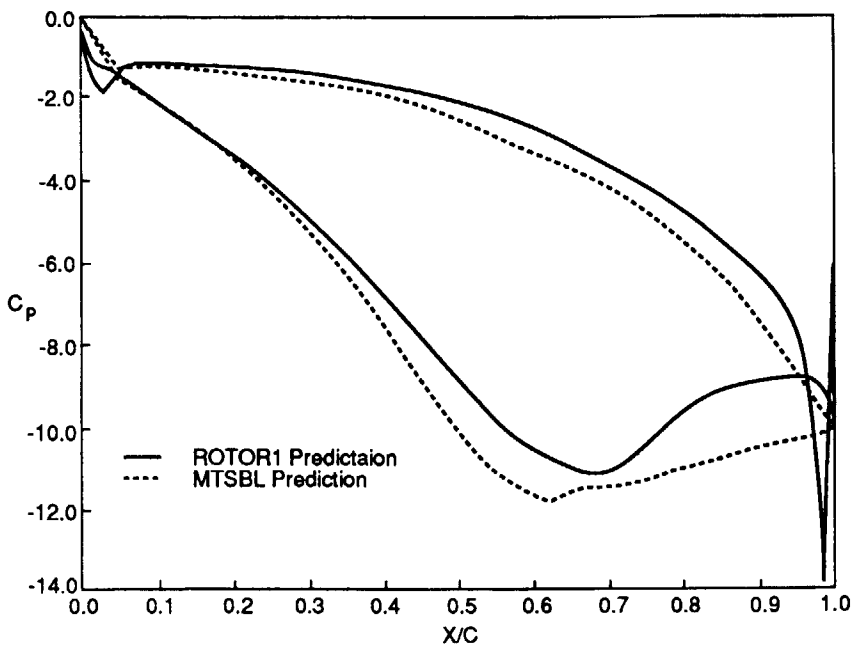

Stator

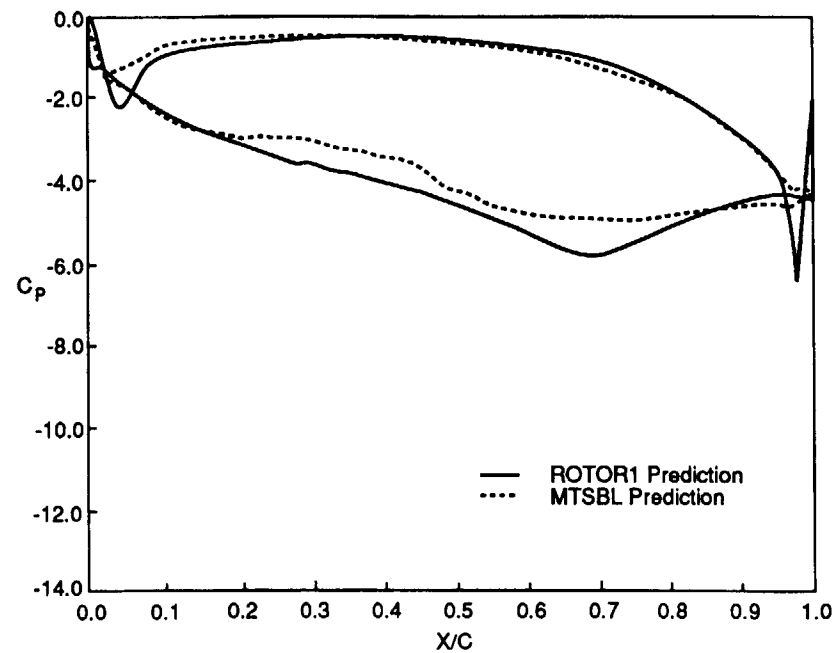

Rotor

5-1563-9-105

UNSTEADY PRESSURE DISTRIBUTIONS ON THE SSME HPFTP ROTOR

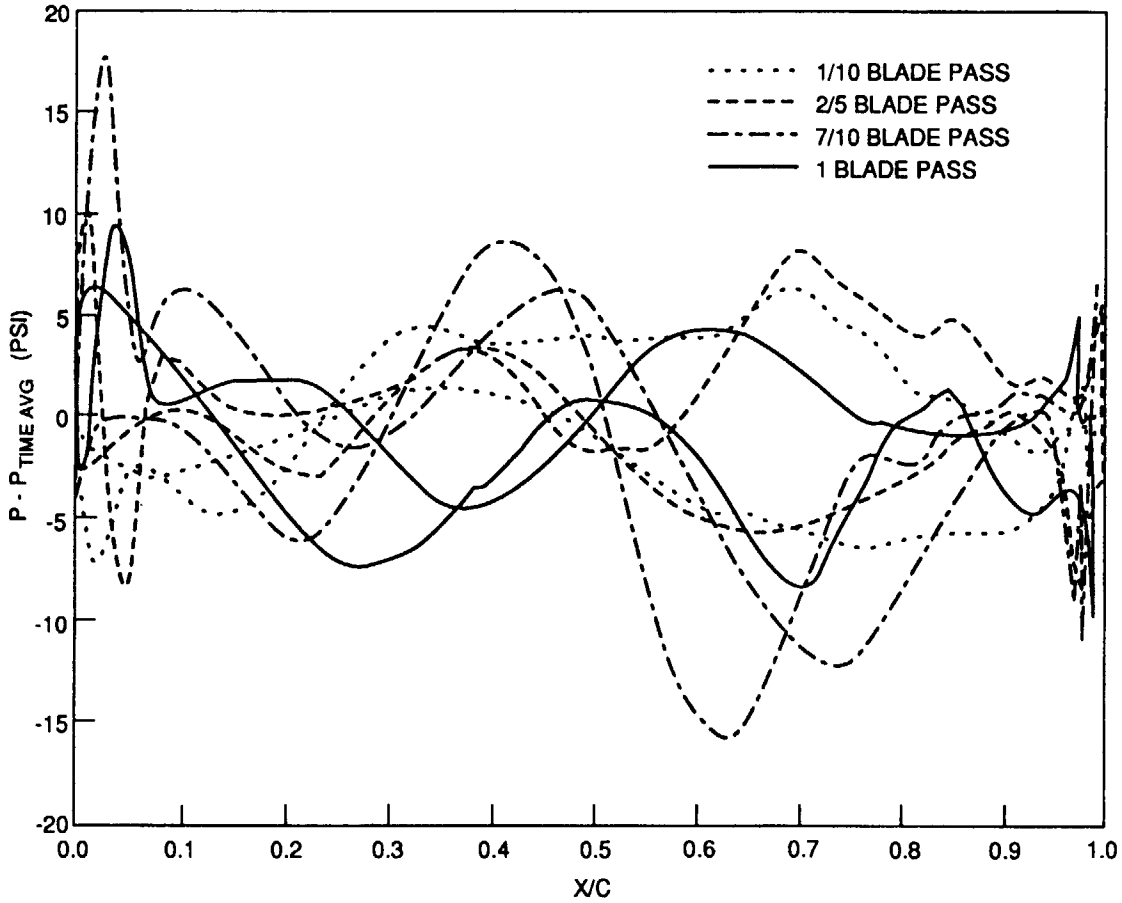

5-1592-9-105

ENTROPY CONTOURS

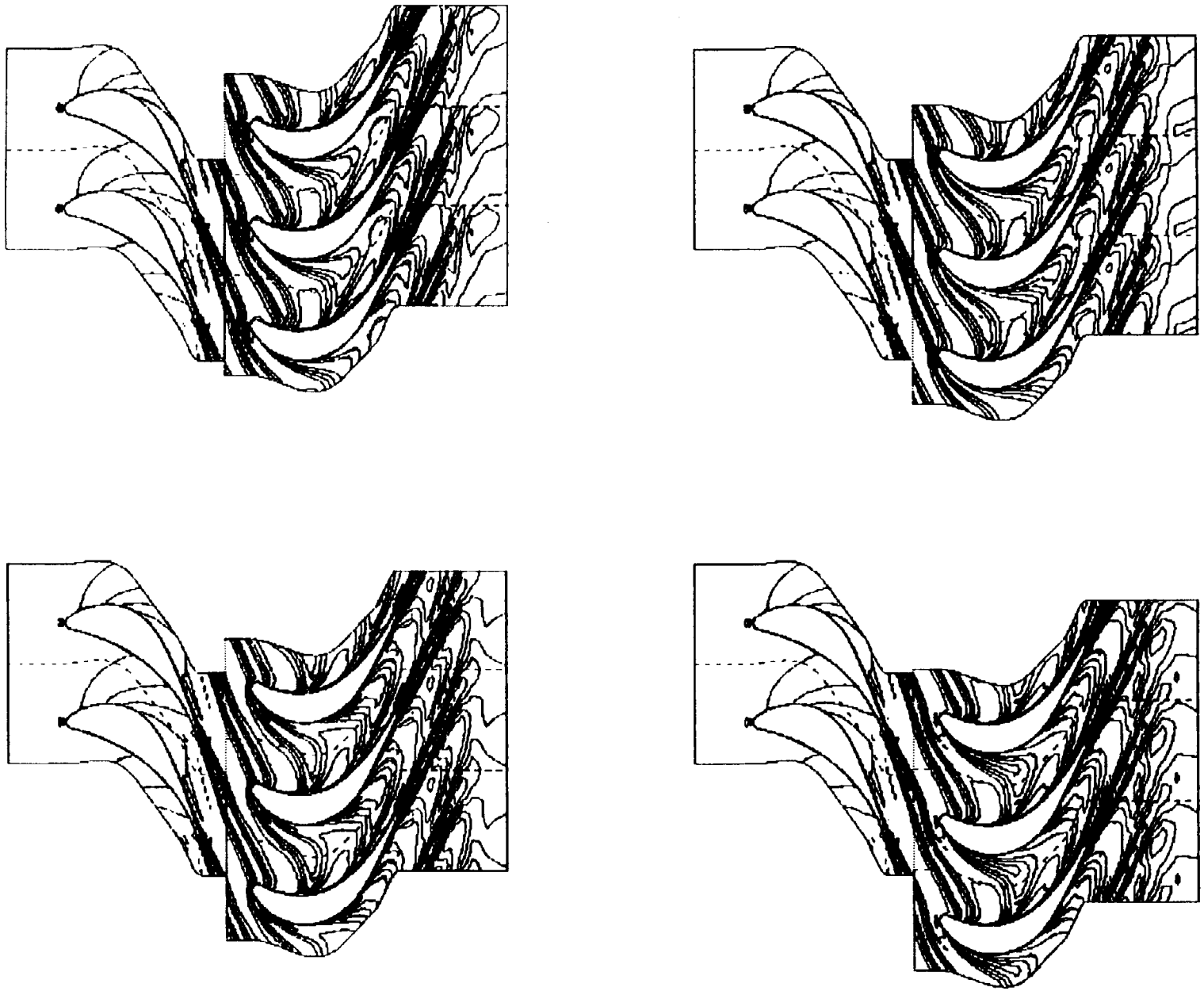

COMPARISON OF PREDICTED AND EXPERIMENTAL HEAT TRANSFER FOR THE LSRR

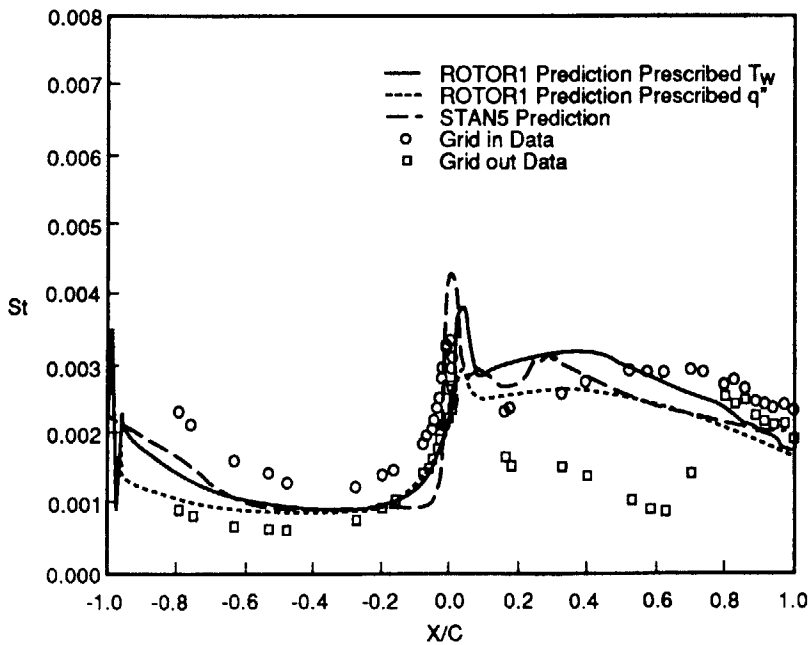

Stator

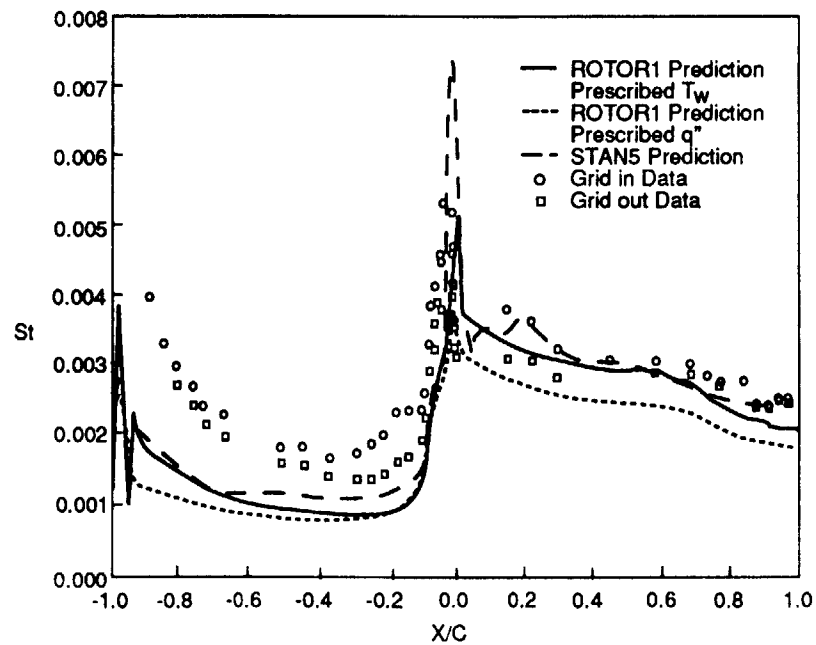

Rotor

5-1564-9-105

COMPUTER RESOURCES REQUIREMENTS

MTSBL - STAN5	– 6 CPU MINUTES,	0.9×10^6 WORDS MEMORY
ROTOR1	– 6 CPU HOURS,	2.1×10^6 WORDS MEMORY + 4.1×10^6 WORDS SSD

5-1559-9-105

IMPACT

- MSFC BENCHMARKING OF QUASI-3D TURBINE ANALYSIS SYSTEM AND UNSTEADY STAGE CODE; ASSESSMENT OF RELATIVE MERITS OF THE TWO APPROACHES.

- STEADY 3D FIRST AND SECOND STAGE BLADE LOADS WERE USED IN STRESS ANALYSIS OF HPFTP TURBINE BLADES IN SUPPORT OF RETURN TO FLIGHT; INTEGRATED LOADS PREDICT CORRECT TORQUE WITHIN 1%.

- UNSTEADY MIDSPAN PRESSURES WERE USED IN STRUCTURAL DYNAMICS ANALYSIS OF HPFTP FIRST STAGE BLADES.

5-1560-9-105

SUMMARY AND CONCLUSION

- SUPPORTED MSFC SSME PROGRAMS THROUGH CHARACTERIZATION OF THE STEADY AND UNSTEADY AEROTHERMAL ENVIRONMENTS OF THE HPFTP.
- BOTH APPROACHES YIELDED COMPARABLE STEADY OR TIME-AVERAGED AERODYNAMIC AND THERMAL RESULTS.
- AERODYNAMIC RESULTS FROM BOTH APPROACHES COMPARE WELL WITH DATA; THERMAL RESULTS EXHIBIT FAIR AGREEMENT WITH DATA.

5-1561-9-105

PRECEDING PAGE BLANK NOT FILMED

AUTOMATED DESIGN OF CONTROLLED DIFFUSION BLADES

Jose M. Sanz

NASA Lewis Research Center

ABSTRACT

A numerical automation procedure has been developed to be used in conjuction with an inverse hodograph method for the design of controlled diffusion blades.
With this procedure a cascade of airfoils with a prescribed solidity, inlet Mach No., inlet air flow angle and air flow turning can be produced automatically.
The trailing edge thickness of the airfoil, an important quantity in inverse methods, is also prescribed.

The automation procedure consists of a multi-dimensional Newton iteration in which the objective design conditions are achieved by acting on the hodograph input parameters of the underlying inverse code.

The method, although more general in scope, is applied in this paper to the design of axial flow turbomachinery blade sections, both compressors and turbines. A collaborative effort with U.S. Engine Companies to identify designs of interest to the industry will be described.

N91-10883

CURRENT APPROACH

- GUESS GEOMETRY

  - SINGLE CIRCULAR ARC
  - MULTIPLE CIRCULAR ARC
  - POLYNOMIAL SHAPES
  - NACA AIRFOILS SERIES

- ANALYZE SHAPE WITH FLOW SOLVER

  - 2-D, QUASI 3-D OR 3-D CODES
  - POTENTIAL, EULER OR NAVIER-STOKES SOLVERS

- BUILDS IN EMPIRICISM

AUTOMATION PROCEDURE

- ITERATION OF INVERSE HODOGRAPH METHOD
- PRODUCES BLADE WITH PRESCRIBED
  - SOLIDITY
  - INLET MACH NUMBER
  - INLET AIR ANGLE
  - AIR FLOW TURNING
  - TRAILING EDGE THICKNESS

BENEFITS

- REPLACE TRIAL AND ERROR PROCESS BY EXACT 2-D SOLUTION
- GREATLY REDUCES MANPOWER AND TURN AROUND TIME
- INITIALLY OPTIMIZED BLADE SECTIONS
- INNOVATIVE DESIGNS
- MAJOR IMPACT FOR DESIGNS PROBLEMS WITH NO DATA BASE

- TO IMPLEMENT AUTOMATION

  EQUATION $u = \mathcal{F}(R, M_0, \theta, q(s))$

  IS REPLACED BY

$$\bar{y} = \bar{F}(\bar{x})$$

  WHERE

$$\bar{x} = (R, M_0, \theta, Q_M, Q_{te}, S_{te})$$

$$\bar{y} = \bar{y}(\sigma, M_1, \beta_1, \Delta\beta, dn_{te}, ds_{te})$$

CD-88-33796

NEWTON ITERATION TO SOLVE VECTOR EQUATION

$$\bar{F}(x) - \bar{y}_o = 0,$$

$$\bar{y}_o = (\sigma,\ M_1,\ \beta_1,\ \Delta\beta,\ dn_{te},\ ds_{te})_o$$

IS OBJECTIVE FUNCTION.

ITERATION

$$\bar{X}_{n+1} = \bar{X}_n - J^{-1}\ (\bar{x}_n)\ (\bar{y}_n - \bar{y}_o)$$

JACOBIAN: $J = \left(\dfrac{\partial F_i}{\partial x_j}\right)$

CD-88-33797

APPLICATIONS

- ARC 40X80X120 WIND TUNNEL TURNING VANES

- SUBSONIC AND TRANSONIC (SHOCK-FREE) TURBOMACHINERY AND PROPELLER SECTIONS

- INLET GUIDE VANES FOR LARGE RANGE OF INLET AIR FLOW ANGLE - EXPERIMENTAL VERIFICATION 3/88

ARC 40X80X120 WIND TUNNEL TURNING VANES

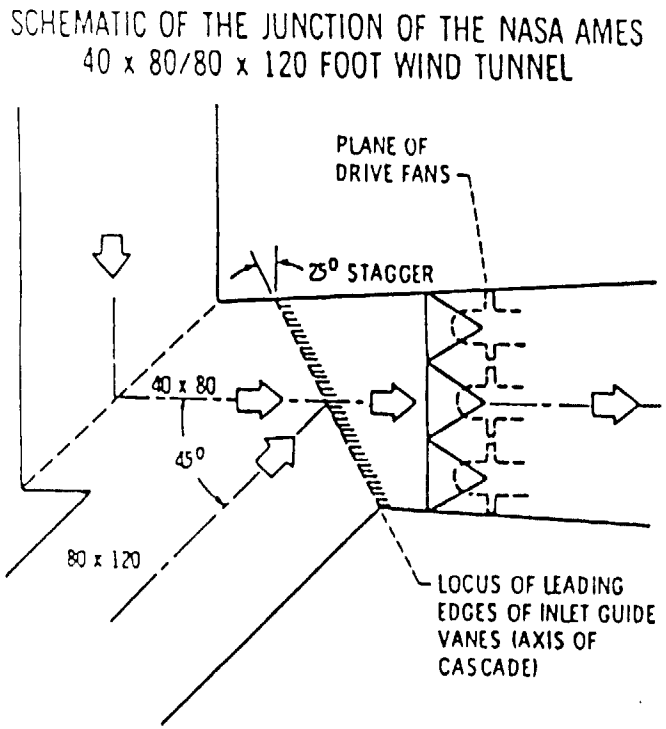

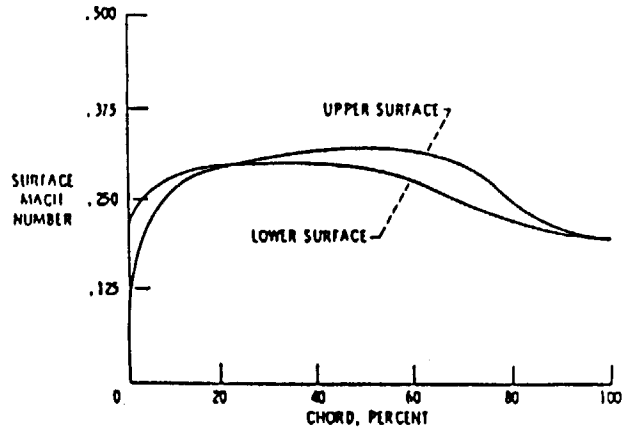

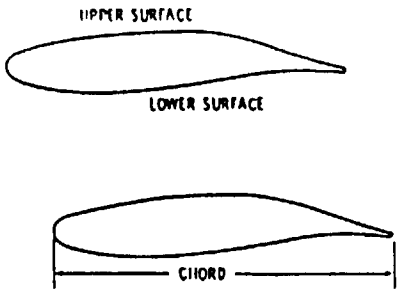

VARIABLE INLET GUIDE VANES

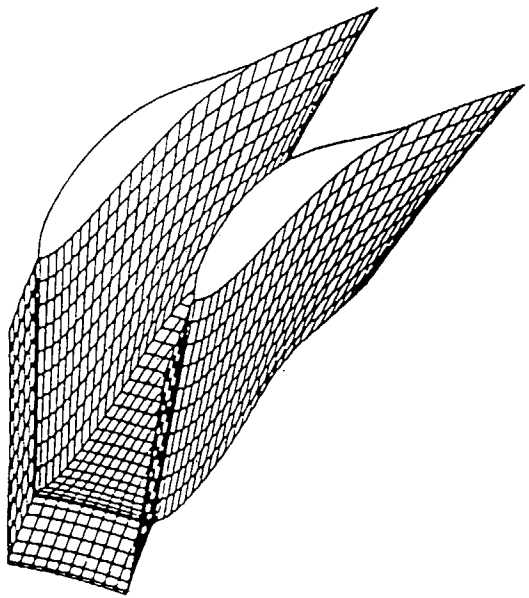

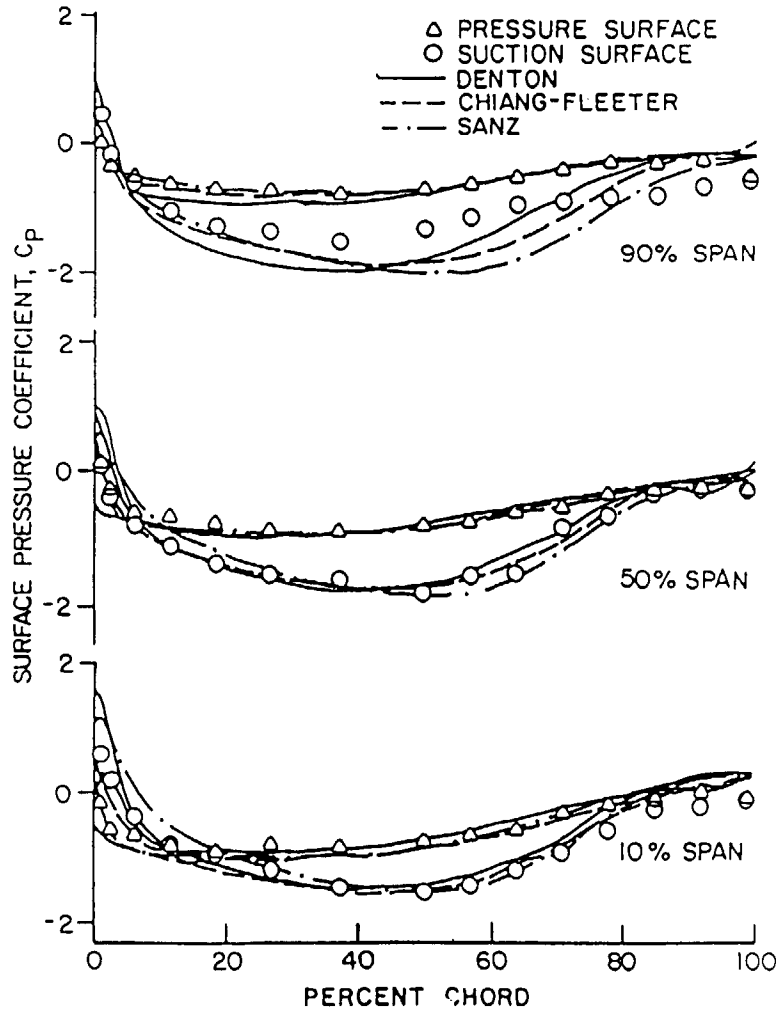

SOURCE: Neal,J.W. et al., Report ME-TSPC-88-12,PURDUE UNIVERSITY

AWT TURNING VANES

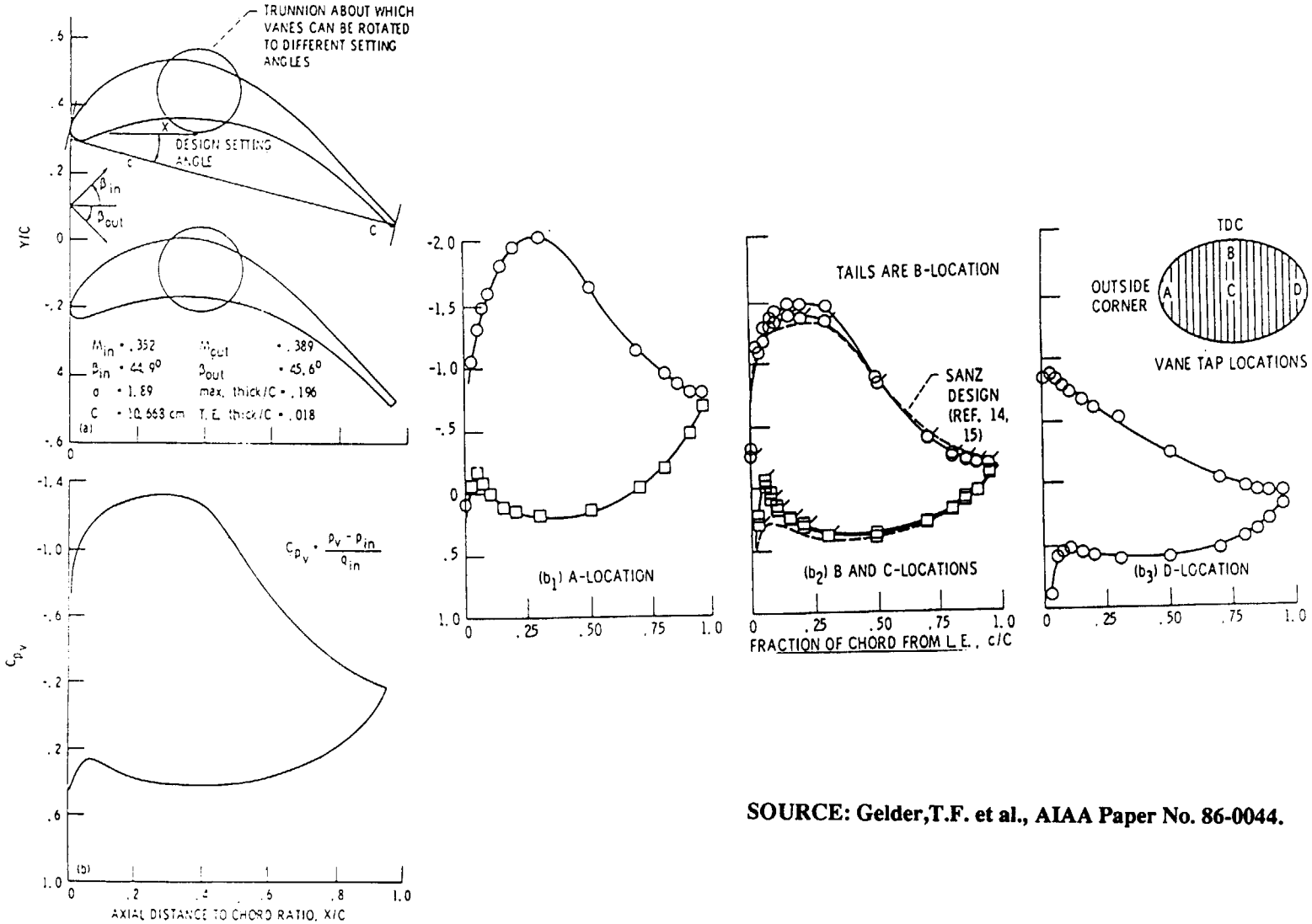

SOURCE: Gelder,T.F. et al., AIAA Paper No. 86-0044.

ORIGINAL PAGE IS OF POOR QUALITY

AUTOMATED DESIGN OF COMPRESSOR STATOR BLADE

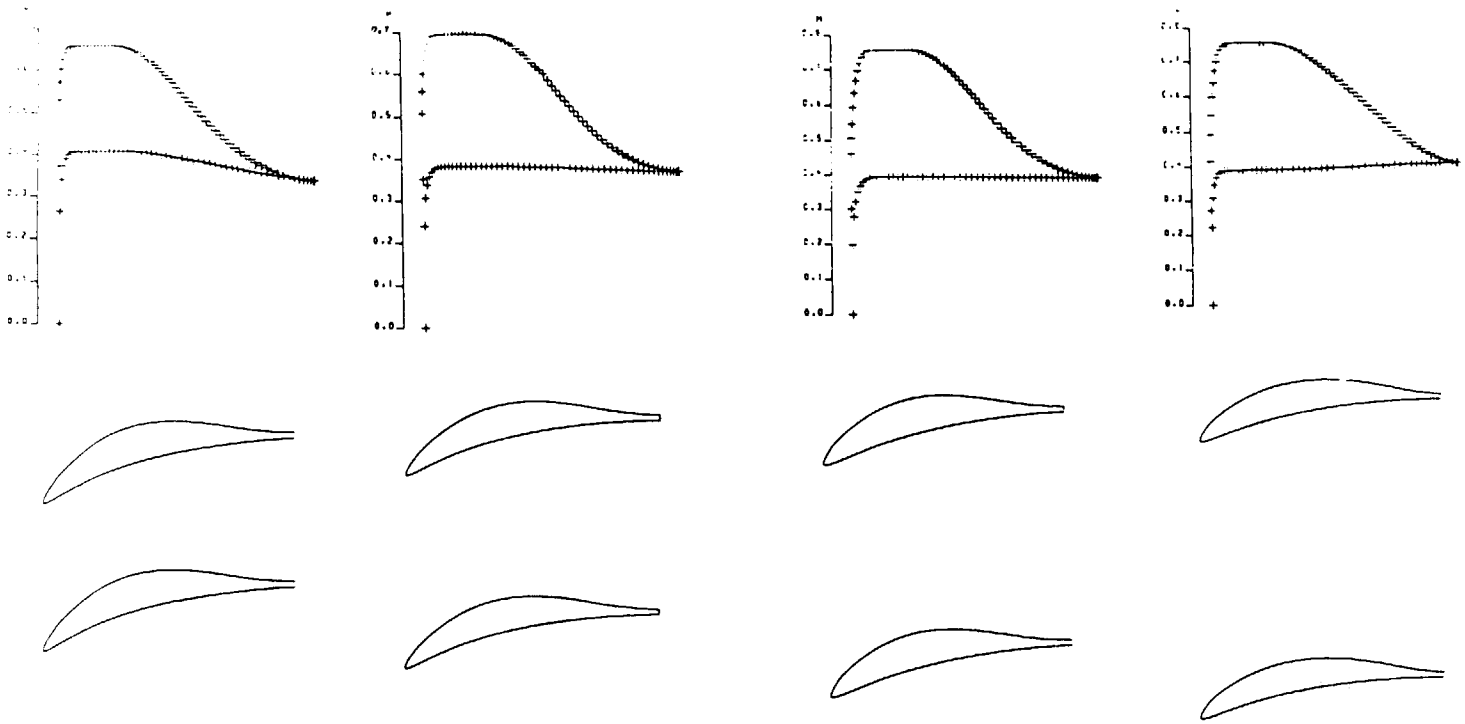

HUB SECTION

MID-HUB SECTION

MID-TIP SECTION

TIP SECTION

MID SPEED STATOR

ORIGINAL PAGE IS
OF POOR QUALITY

AUTOMATED DESIGN OF TURBINE BLADE SECTIONS

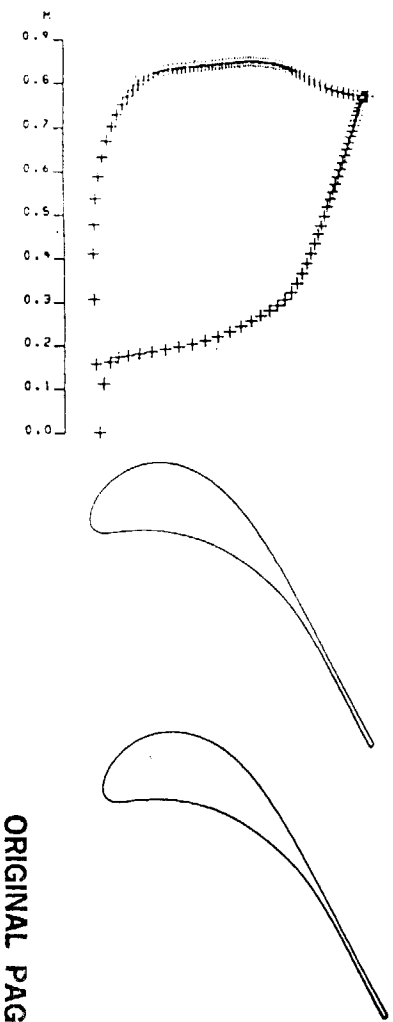

M1	0.337
BET1	36.39
M2	0.782
BET2	-61.06
DELB	97.44
SOL	1.45
THCR	0.224
DNTE	0.018
DSTE	-0.000
TEV	0.014
LOSS	0.005

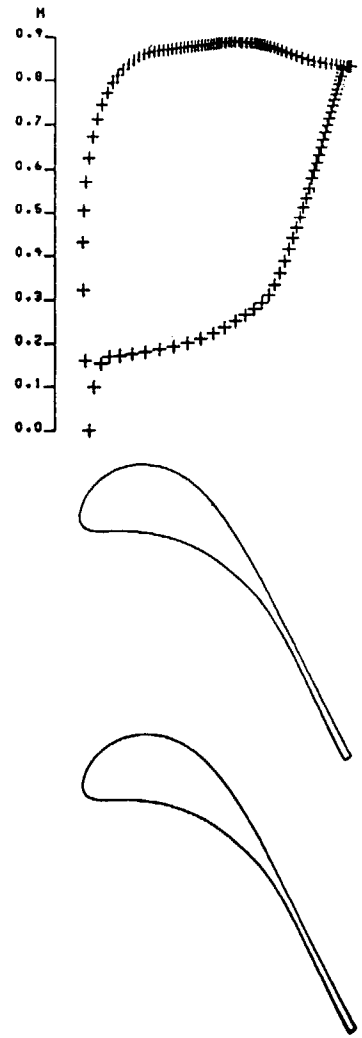

M1	0.337
BET1	36.38
M2	0.839
BET2	-61.01
DELB	97.38
SOL	1.45
THCR	0.224
DNTE	0.025
DSTE	-0.000
TEV	0.021
LOSS	0.005

ORIGINAL PAGE IS
OF POOR QUALITY

AUTOMATED DESIGN OF TURBINE BLADE SECTIONS

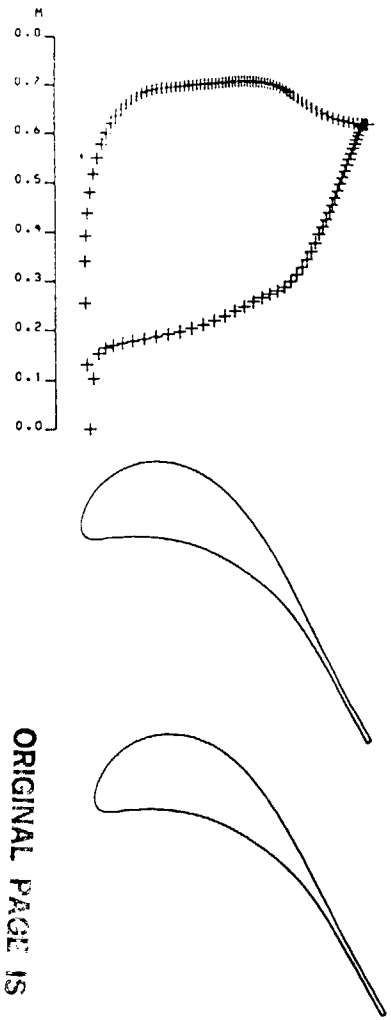

M1	0.301
BET1	36.41
M2	0.629
BET2	-61.14
DELB	97.55
SOL	1.46
THCR	0.239
DNTE	0.017
DSTE	-0.000
TEV	0.013
LOSS	0.006

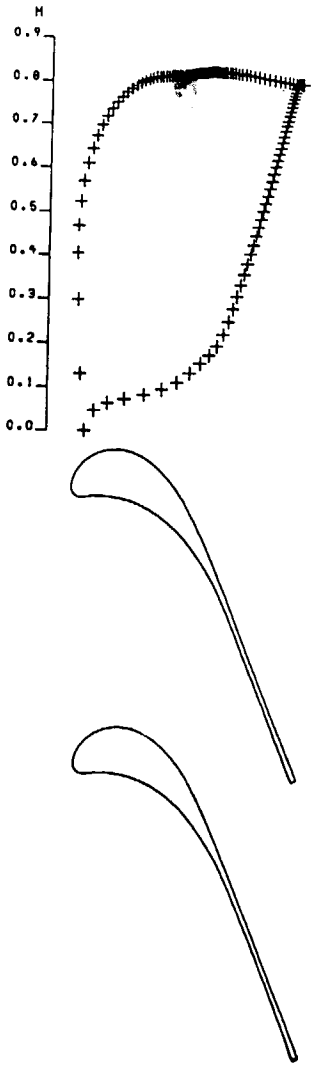

M1	0.253
BET1	32.49
M2	0.805
BET2	-66.74
DELB	99.23
SOL	1.43
THCR	0.186
DNTE	0.019
DSTE	-0.000
TEV	0.016
LOSS	0.003

ORIGINAL PAGE IS
OF POOR QUALITY

AUTOMATED DESIGN OF COMPRESSOR BLADE SECTIONS

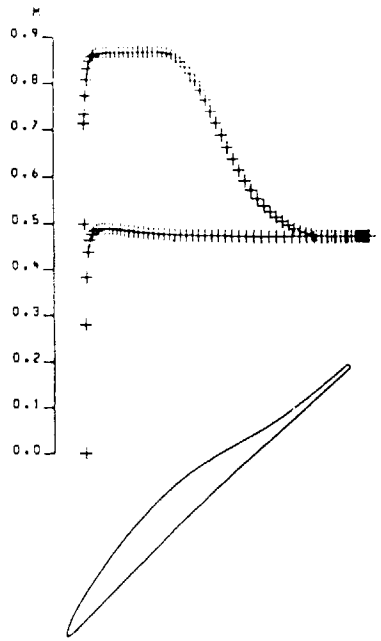

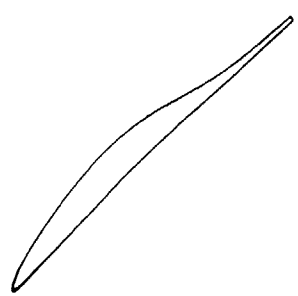

M1	0.670
BET1	52.02
M2	0.476
BET2	38.23
DELB	13.79
SOL	1.04
THCR	0.083
DNTE	0.020
DSTE	-0.000
TEV	0.012
LOSS	0.026

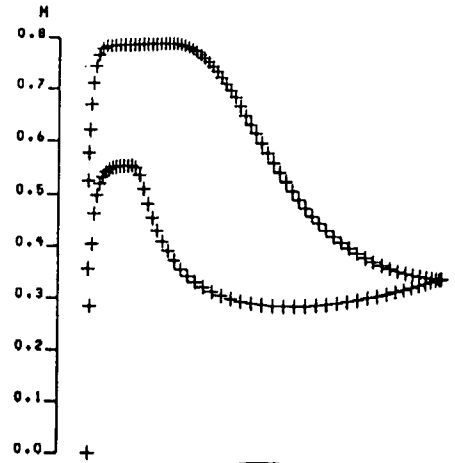

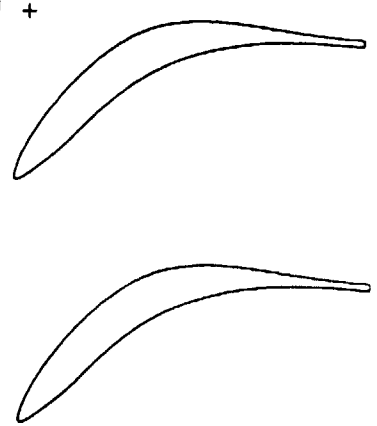

M1	0.600
BET1	51.01
M2	0.344
BET2	-3.95
DELB	54.96
SOL	1.70
THCR	0.112
DNTE	0.025
DSTE	-0.001
TEV	0.016
LOSS	0.055

ORIGINAL PAGE IS
OF POOR QUALITY

N91-10884

Numerical Analysis of Flow Through Oscillating Cascade Sections

by Dennis L. Huff

NASA Lewis Research Center

The design of turbomachinery blades requires the prevention of flutter for all operating conditions. However, flow field predictions used for aeroelastic analysis are not well understood for all flow regimes. The present research focuses on numerical solutions of the Euler and Navier-Stokes equations using an ADI procedure to model two-dimensional, transonic flow through oscillating cascades. The model prescribes harmonic pitching motions for the blade sections for both zero and non-zero inter-blade phase angles. The code introduces the use of a deforming grid technique for convenient specification of the periodic boundary conditions. Approximate nonreflecting boundary conditions have been coded for the inlet and exit boundary conditions. Sample unsteady solutions have been performed for an oscillating cascade and compared to experimental data. Also, test cases were run for a flat plate cascade to compare with an unsteady, small-perturbation, subsonic analysis.

The predictions for oscillating cascades with non-zero inter-blade phase angles are in good agreement with experimental data and small-perturbation theory. The zero degree inter-blade phase angle cases, which were near a resonant condition, differ from the experiment and theory. Studies on reflecting versus non-reflecting inlet and exit boundary conditions show that the treatment of the boundary can have a significant effect on the first harmonic, unsteady pressure distributions for certain flow conditions. This code is expected to be used as a tool for reviewing simpler models that do not include the full non-linear aerodynamics or as a final check for designs against flutter in turbomachinery.

OBJECTIVE:

- DEVELOP AN UNSTEADY, VISCOUS, TRANSONIC FLOW ANALYSIS METHOD FOR CASCADED AIRFOILS WITH PITCHING MOTIONS

TECHNIQUE:

- A COMPRESSIBLE, FULL NAVIER-STOKES, FINITE DIFFERENCE CODE IS DEVELOPED TO MODEL OSCILLATING CASCADES FOR BOTH ZERO AND NON-ZERO INTER-BLADE PHASE ANGLES

- A UNIQUE DEFORMING GRID TECHNIQUE IS INTRODUCED TO CAPTURE BLADE MOTIONS

- APPROXIMATE NON-REFLECTING BOUNDARY CONDITIONS ARE USED TO MINIMIZE WAVE REFLECTIONS FROM THE OUTER BOUNDARIES

CD-88-38197

DEFORMING GRID TECHNIQUE, SIMPLIFIED GRID WITH EXAGGERATED MOTION

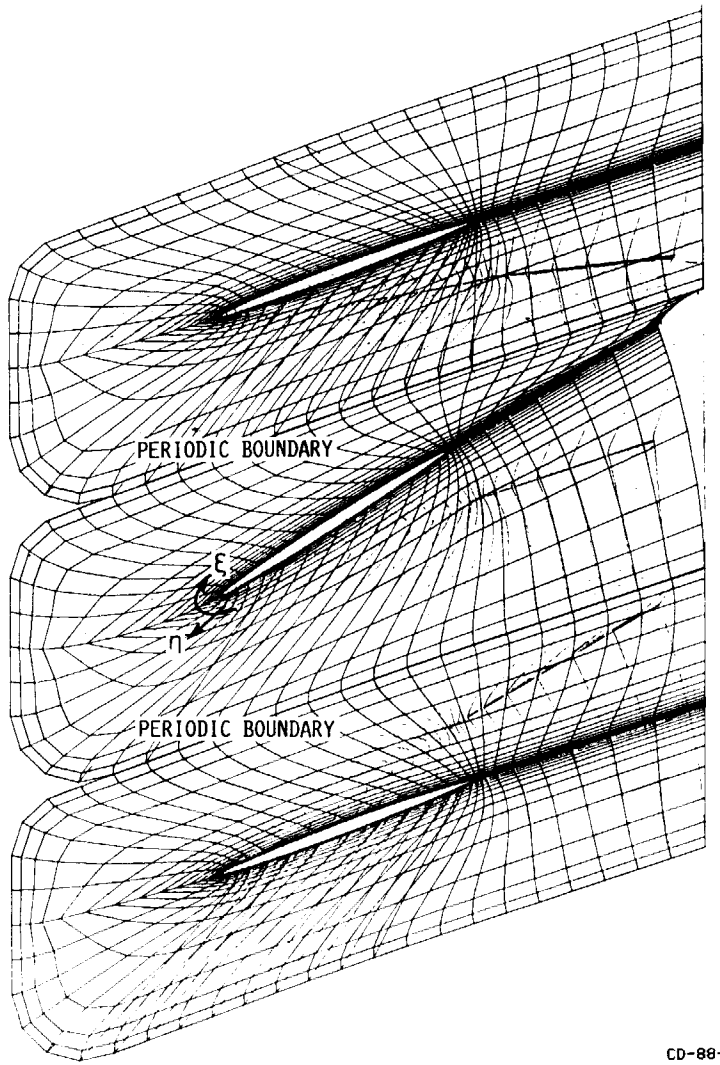

CD-88-38201

BOUNDARY CONDITIONS

INLET:

- SPECIFY DENSITY, VELOCITY, AND FLOW ANGLE
- SOLVE THE CHARACTERISTIC FORM OF THE GOVERNING EQUATIONS TO DETERMINE THE ENERGY

EXIT:

- FOR VISCOUS FLOWS, SPECIFY STATIC PRESSURE AND EXTRAPOLATE DENSITY AND VELOCITY FROM THE INTERIOR
- FOR INVISCID FLOWS, SPECIFY STATIC PRESSURE AND SOLVE THE CHARACTERISTIC FORM OF THE GOVERNING EQUATIONS TO DETERMINE DENSITY AND VELOCITY

PERIODIC BOUNDARIES FROM BLADE-TO-BLADE

SOLID WALL BOUNDARIES ON AIRFOIL SURFACE

AVERAGE FLOW PROPERTIES ACROSS THE WAKE

CD-88-38198

RESULTS

1. NACA 65-SERIES CASCADE, M = 0.17, TWO INTER-BLADE PHASE ANGLES, COMPARISONS WITH EXPERIMENT

2. FLAT PLATE CASCADE, M = 0.65 AND 0.80, THREE INTER-BLADE PHASE ANGLES, COMPARISONS WITH SMALL-PERTURBATION THEORY

3. NASA LEWIS CASCADE, M = 0.65 AND 0.80, THREE INTER-BLADE PHASE ANGLES, BOUNDARY CONDITION STUDY, NUMERICAL TIME ACCURACY STUDY, COMPARISONS WITH EXPERIMENT.

CD-88-38200

MEAN FLOW PRESSURE DISTRIBUTION FOR NACA 65-SERIES CASCADE

$M_1 = 0.17$, $\gamma = 55^0$, $g/c = 0.75$, $\tau' = 0.06$

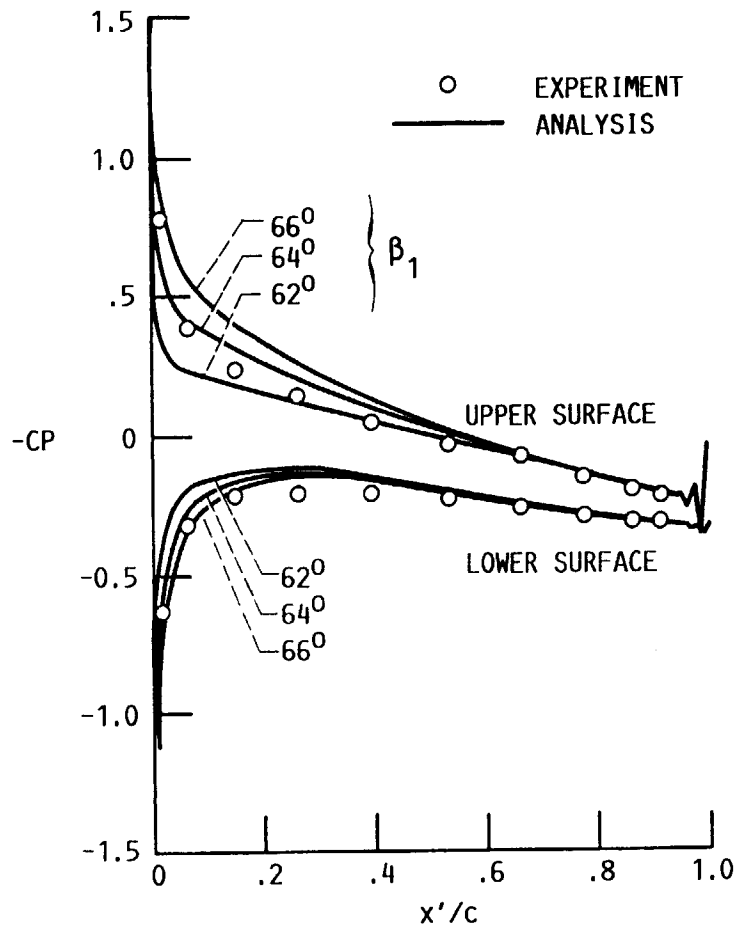

CD-88-38204

FIRST HARMONIC PRESSURE DISTRIBUTION FOR NACA 65-SERIES OSCILLATING CASCADE

$M_1 = 0.17, \beta_1 = 64^0 \pm 2^0, k = 0.123$

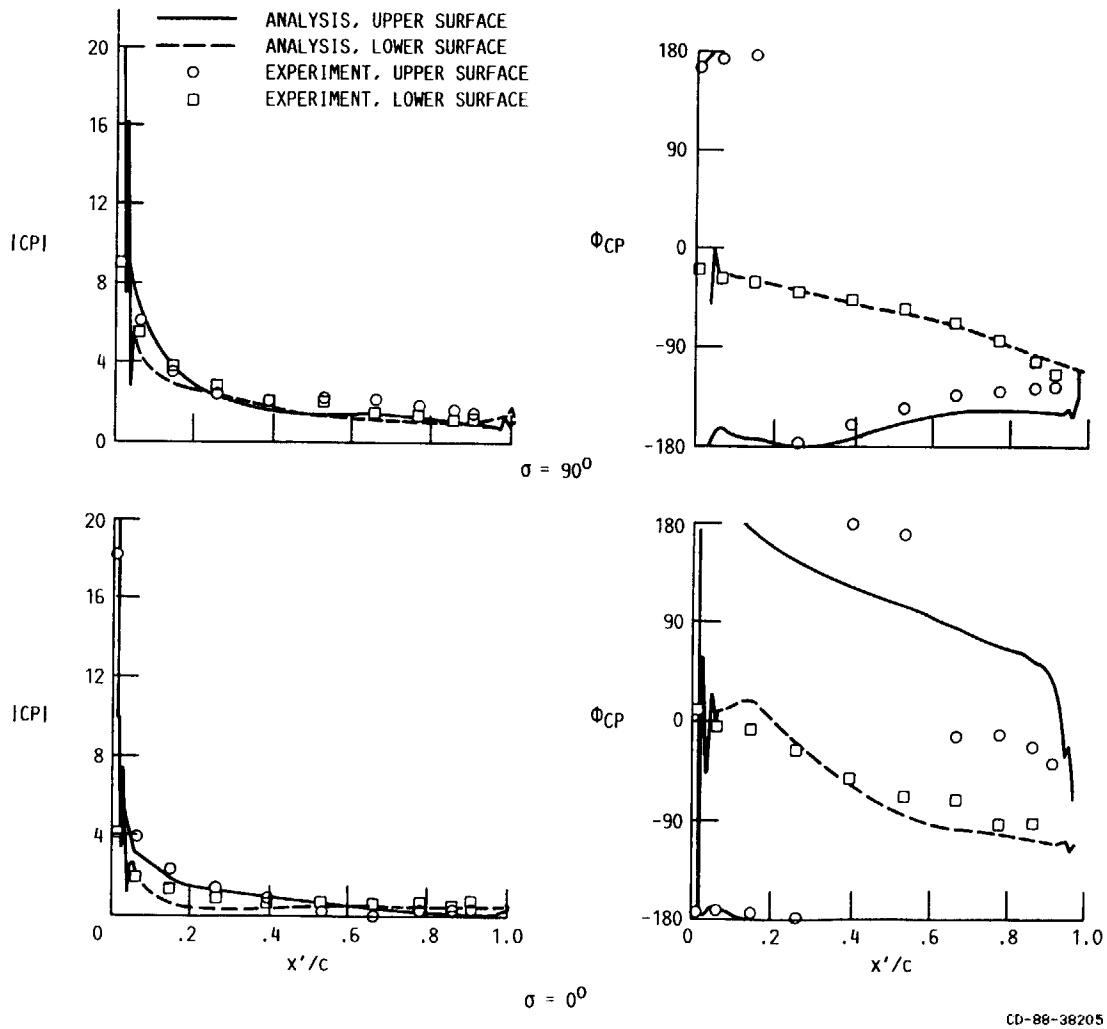

BOUNDARY CONDITION AND THEORY COMPARISON FOR FLAT PLATE CASCADE

$M_1 = 0.65$, $\beta_1 = 53^0 \pm 0.10^0$, $k = 0.221$

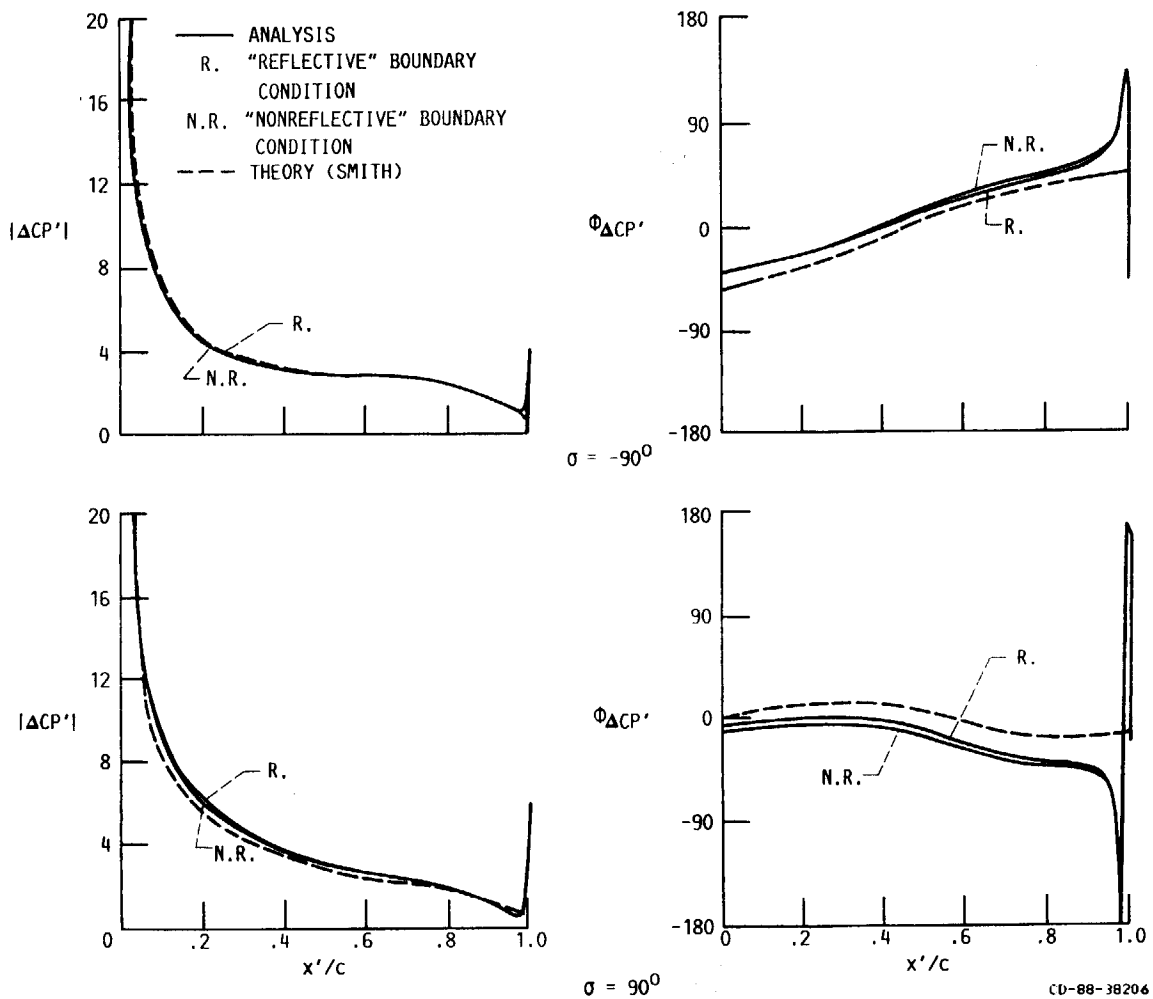

BOUNDARY CONDITION AND THEORY COMPARISON FOR FLAT PLATE CASCADE

$M_1 = 0.65$, $\beta_1 = 53^0 \pm 0.10^0$, $k = 0.221$

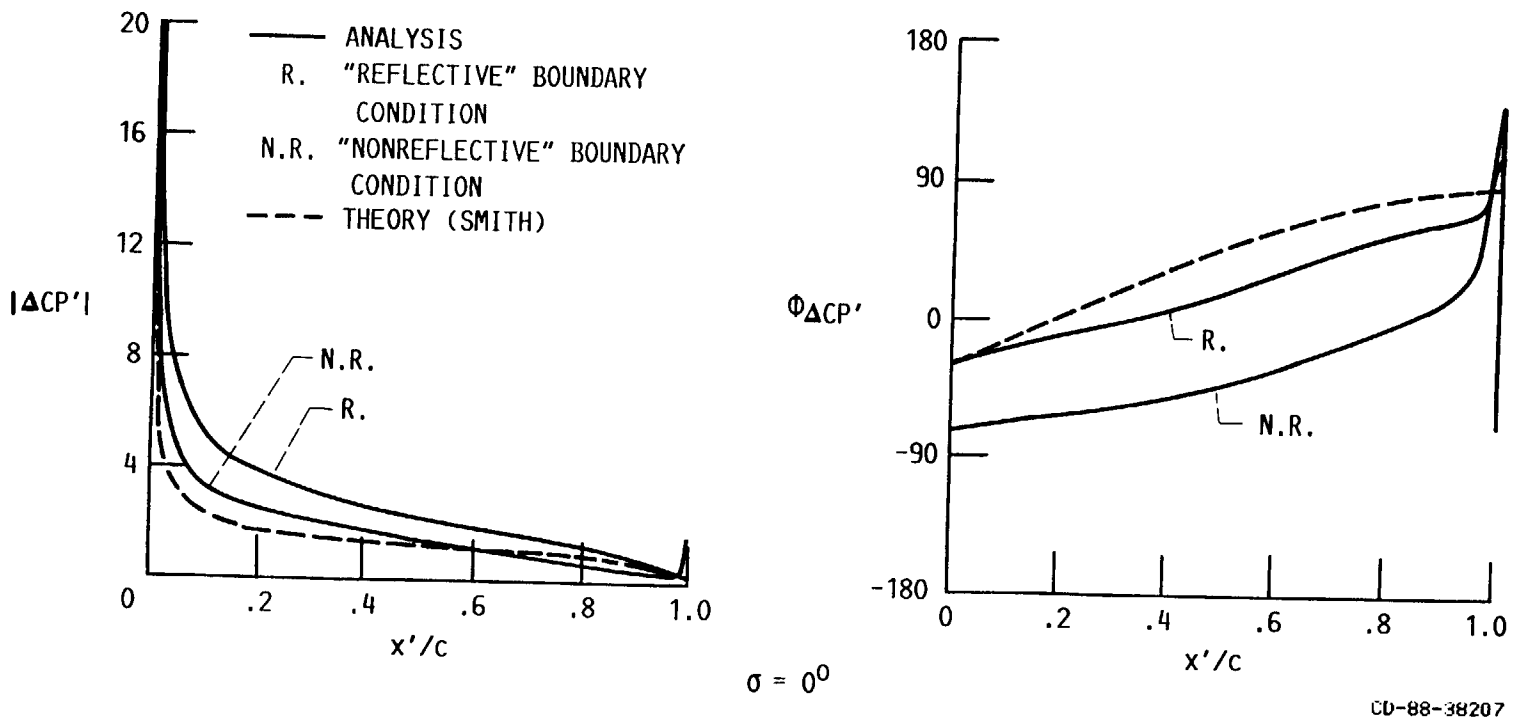

CD-88-38207

MEAN FLOW PRESSURE DISTRIBUTION FOR BICONVEX AIRFOIL CASCADE

$\beta_1 = 60^0$, $\gamma = 53^0$, $g/c = 0.767$, $\tau' = 0.07$

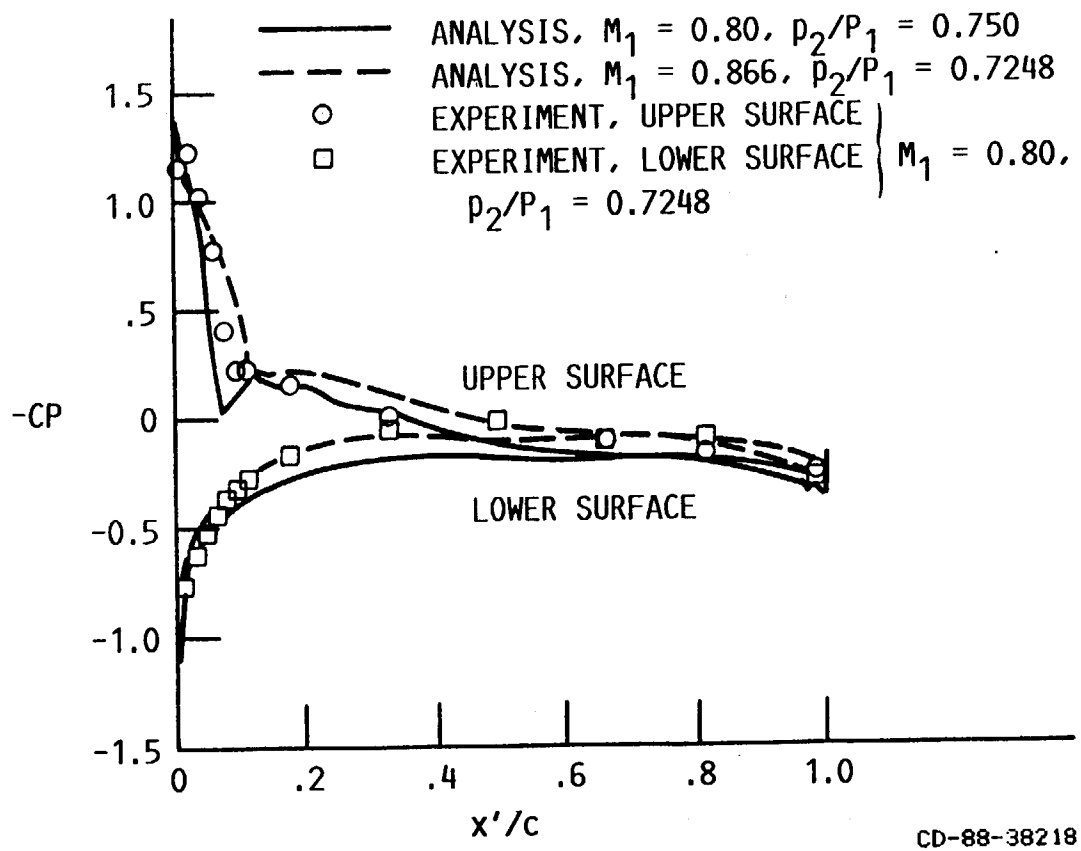

FIRST HARMONIC PRESSURE DISTRIBUTION FOR BICONVEX AIRFOIL CASCADE

$M_1 = 0.80$, $\beta_1 = 60^0 \pm 1.2^0$, $k = 0.185$, $\sigma = -90^0$

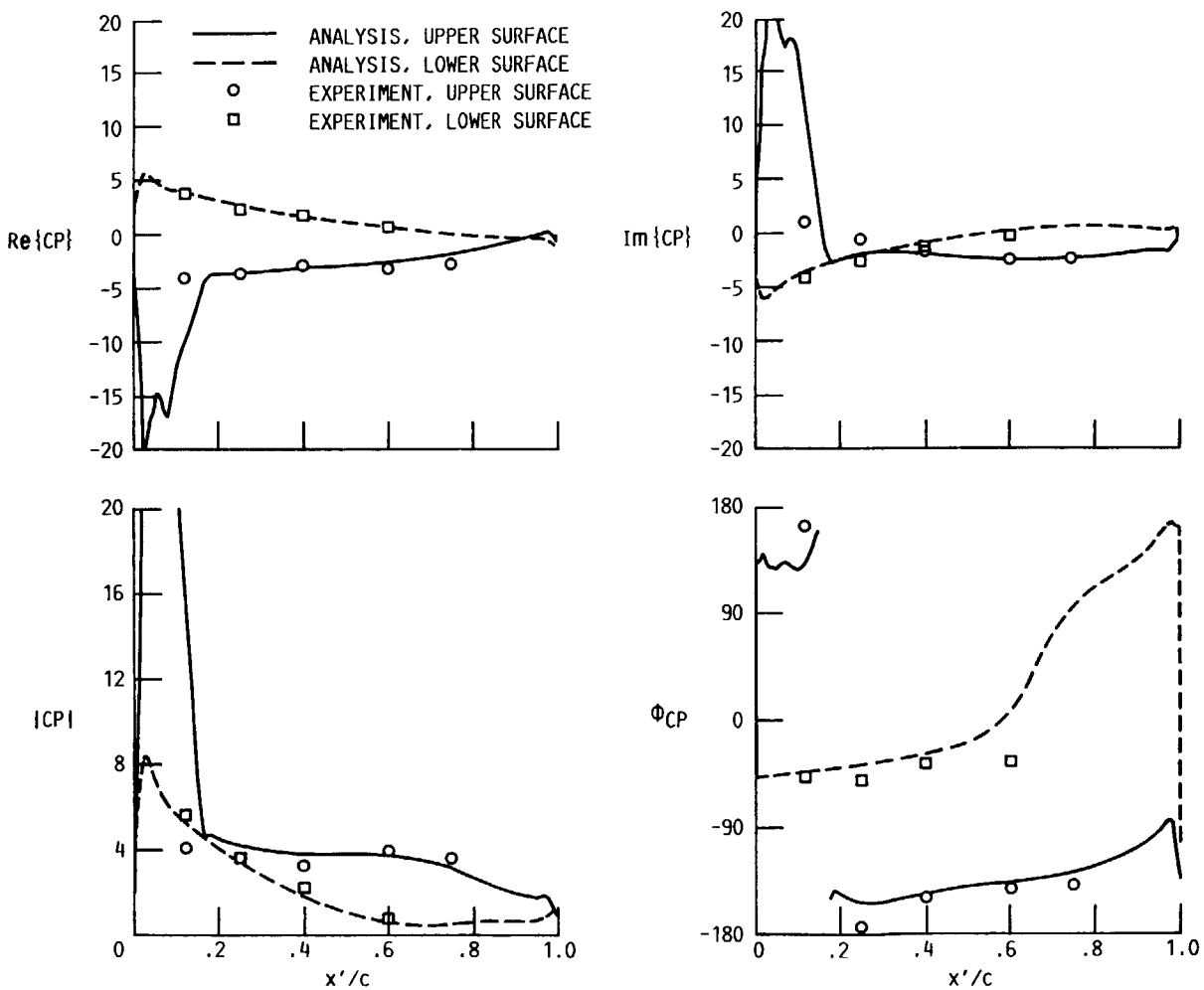

CD-88-38219

FIRST HARMONIC PRESSURE DISTRIBUTION FOR BICONVEX AIRFOIL CASCADE

$M_1 = 0.80$, $\beta_1 = 60^0 \pm 1.2^0$, $k = 0.185$, $\sigma = 0^0$

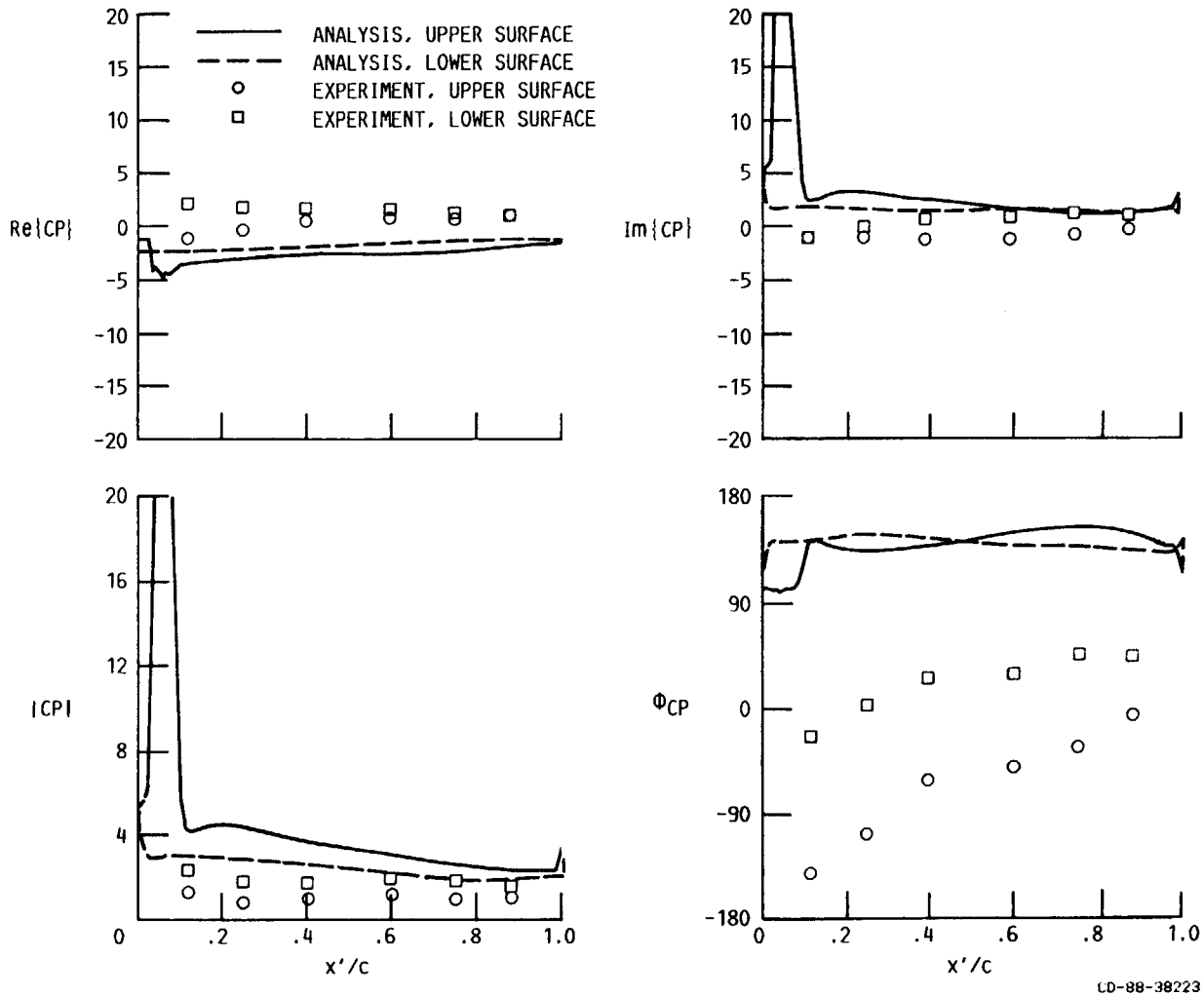

CONCLUSIONS

- A COMPRESSIBLE EULER OR NAVIER-STOKES, FINITE-DIFFERENCE CODE HAS BEEN DEVELOPED FOR THE ANALYSIS OF OSCILLATING CASCADES
- A DEFORMING GRID TECHNIQUE IS USED TO CAPTURE THE MOTION OF THE AIRFOILS FOR BOTH ZERO AND NON-ZERO INTER-BLADE PHASE ANGLES
- APPROXIMATE TWO-DIMENSIONAL, UNSTEADY CHARACTERISTIC BOUNDARY CONDITIONS ARE USED AT THE INLET AND EXIT TO MINIMIZE WAVE REFLECTIONS
- IN GENERAL, PREDICTIONS WITH NON-ZERO-INTER-BLADE PHASE ANGLES ARE IN GOOD AGREEMENT WITH THE EXPERIMENTAL DATA AND SMALL-PERTURBATION THEORY
- PREDICTIONS FOR ZERO DEGREE INTER-BLADE PHASE ANGLE CASES, WHICH WERE NEAR AN ACOUSTIC RESONANT CONDITION, DIFFER FROM THE EXPERIMENT AND THEORY
- THE TYPE OF BOUNDARY CONDITION USED AT THE INLET AND EXIT CAN HAVE A SIGNIFICANT EFFECT ON THE FIRST HARMONIC, UNSTEADY PRESSURE DISTRIBUTIONS
- FIRST-ORDER AND SECOND-ORDER TEMPORAL ACCURACY RESULTS DO NOT SHOW SIGNIFICANT DIFFERENCES IN THE UNSTEADY PRESSURE DISTRIBUTIONS

CD-88-38199

N91-10885

ANALYSIS OF THREE-DIMENSIONAL VISCOUS FLOW IN A SUPERSONIC THROUGHFLOW FAN

by

Dr. Rodrick V. Chima
NASA Lewis Research Center
Cleveland, OH 44135

Abstract

A three-dimensional Navier-Stokes code has been developed for analysis of turbomachinery blade rows and other internal flows. The Navier-Stokes equations are written in a Cartesian coordinate system rotating about the x-axis, and then mapped to a general body-fitted coordinate system. Streamwise viscous terms are neglected using the thin-layer assumption, and turbulence effects are modelled using the Baldwin-Lomax turbulence model. The equations are discretized using finite differences on stacked C-type grids and are solved using a multistage Runge-Kutta algorithm with a spatially-varying time step and implicit residual smoothing.

Calculations were made of the flow around a supersonic throughflow fan blade. The fan was designed at NASA Lewis Research Center as a key component in a supersonic cruise engine. It was designed to produce a total pressure ratio of 2.7 at an axial Mach number of 2.0. The midspan section of the blade is being tested in a supersonic linear cascade at Virginia Polytechnic Institute and will be tested in a rotating rig at Lewis in the near future. Comparisons between earlier quasi-3-D calculations and the VPI data show excellent agreement between shock locations and wake traverses.

The 3-D calculations were done on a $129 * 29 * 33$ grid and took 50 minutes of cpu time on a Cray X-MP. Comparisons with the quasi-3-D results show minor differences in loading due to 3-D effects. Particle traces show nearly 2-D flows near the pressure surface, but large secondary flows within the suction surface boundary layer. The horseshoe vortex ahead of the leading edge is clearly seen.

References

1. Chima, R. V., and Yokota, J. W. "Numerical Analysis of Three– Dimensional Viscous Internal Flows," NASA TM-100878, July, 1988.
2. Schmidt, J. F., Moore, R. D., and Wood, J. R. "Supersonic Throughflow Fan Design," NASA TM-88908, AIAA-87-1746, June, 1987.

PRECEDING PAGE BLANK NOT FILMED

RVC3D (ROTOR VISCOUS CODE 3-D)

BY R. V. CHIMA

DESCRIPTION

- EULER OR NAVIER-STOKES ANALYSIS FOR STEADY 3-D FLOWS IN TURBOMACHINERY BLADE PASSAGES

FEATURES

- STACKED C-TYPE GRIDS FOR AXIAL OR CENTRIFUGAL MACHINES
- CARTESIAN FORMULATION ROTATING ABOUT X-AXIS
  RECTANGULAR OR ANNULAR GEOMETRIES
- SOLVES NAVIER-STOKES EQUATIONS IN FINITE-DIFFERENCE FORM
  THIN-LAYER FORMULATION NEGLECTS STREAMWISE VISCOUS TERMS
  RETAINS HUB-TO-TIP & BLADE-TO-BLADE VISCOUS TERMS
  BALDWIN-LOMAX TURBULENCE MODEL
- EXPLICIT 4-STAGE RUNGE-KUTTA TIME-MARCHING SCHEME
  VARIABLE $\Delta t_{i,j}$ & IMPLICIT RESIDUAL SMOOTHING
  HIGHLY VECTORIZED FOR CRAY X-MP

RESULTS

- SUPERSONIC THROUGHFLOW FAN

GOVERNING EQUATIONS

$$\partial_t q + J[\partial_\xi \hat{E} + \partial_\eta \hat{F} + \partial_\varsigma \hat{G} - Re^{-1}(\partial_\eta \hat{F}_V + \partial_\varsigma \hat{G}_V)] = H$$

WHERE:

$$q = [\rho, \quad \rho u, \quad \rho v, \quad \rho w, \quad e]^T$$

$$H = [0, \quad 0, \quad -\Omega\rho w, \quad \Omega\rho v, \quad 0]^T$$

$$\hat{E} = J^{-1}[\rho U', \ \rho u U' + \xi_x p, \ \rho v U' + \xi_y p, \ \rho w U' + \xi_z p, \ e U' + p U]^T$$

$$\hat{F} = J^{-1}[\rho V', \ \rho u V' + \eta_x p, \ \rho v V' + \eta_y p, \ \rho w V' + \eta_z p, \ e V' + p V]^T$$

$$\hat{G} = J^{-1}[\rho W', \ \rho u W' + \varsigma_x p, \ \rho v W' + \varsigma_y p, \ \rho w W' + \varsigma_z p, \ e W' + p W]^T$$

RELATIVE VELOCITIES:

$$u' = u$$

$$v = v - \Omega z$$

$$w' = w + \Omega y$$

RELATIVE CONTRAVARIANT VELOCITIES:

$$U' = \xi_x u + \xi_y v' + \xi_z w'$$

$$V' = \eta_x u + \eta_y v' + \eta_z w'$$

$$W' = \varsigma_x u + \varsigma_y v' + \varsigma_z w'$$

ENERGY AND STATIC PRESSURE:

$$e = \rho\left[C_v T + (u^2 + v^2 + w^2)/2\right]$$

$$p = (\gamma - 1)\left[e - \rho(u^2 + v^2 + w^2)/2\right]$$

MULTISTAGE RUNGE-KUTTA ALGORITHM

GOVERNING EQUATIONS

$$\partial_t q = -J\left[R_I - (R_V + D)\right]$$

$R_I =$ INVISCID RESIDUAL

$R_V =$ VISCOUS RESIDUAL

D = ARTIFICIAL DISSIPATION TERM

MULTISTAGE SCHEME

$$q_0 = q_n$$

$$q_1 = q_0 - \alpha_1 J \Delta t \left[R_I\, q_0 - (R_V + D)\, q_0\right]$$

$$\vdots$$

$$q_k = q_0 - \alpha_k J \Delta t \left[R_I\, q_{k-1} - (R_V + D)\, q_0\right]$$

$$q_{n+1} = q_k$$

R_V & D EVALUATED AT FIRST STAGE ONLY

ARTIFICIAL DISSIPATION

NONCONSERVATIVE VERSION OF JAMESON FORMULATION

$$Dq = (D_\xi + D_\eta + D_\varsigma)\, q$$

ξ-DIRECTION OPERATOR

$$D_\xi q = C_\xi \left(V_2 q_{\xi\xi} - V_4 q_{\xi\xi\xi\xi}\right)$$

WHERE:

$$C_\xi = \frac{1}{J}\left(\frac{1}{\Delta t_\eta} + \frac{1}{\Delta t_\varsigma}\right) \simeq \frac{a}{J}\left(\frac{1}{\Delta s_\eta} + \frac{1}{\Delta s_\varsigma}\right)$$

$$V_2 = \mu_2 \max\left(\nu_{i+1}, \nu_i, \nu_{i-1}\right)$$

$$V_4 = \max\left(0, \mu_4 - V_2\right)$$

AND

$$\nu_{i,j} = \frac{|P_{i+1,j} - 2P_{i,j} + P_{i-1,j}|}{|P_{i+1,j} + 2P_{i,j} + P_{i-1,j}|}$$

$$\mu_2 = O(1)$$

$$\mu_4 = O(\tfrac{1}{16})$$

IMPLICIT RESIDUAL SMOOTHING

USE A TIME STEP GREATER THAN THE STABILITY LIMIT
MAINTAIN STABILITY BY SMOOTHING THE RESIDUAL IMPLICITLY

$$(1 - \epsilon_\xi \delta_{\xi\xi})(1 - \epsilon_\eta \delta_{\eta\eta})(1 - \epsilon_\varsigma \delta_{\varsigma\varsigma})\bar{R} = R$$

UNCONDITIONALLY STABLE IF

$$\epsilon \geq \frac{1}{4}\left[\left(\frac{\lambda}{\lambda^*}\right)^2 - 1\right]$$

WHERE
λ^* IS COURANT LIMIT OF THE UNSMOOTHED SCHEME
λ IS THE LARGER OPERATING COURANT NUMBER

SUPERSONIC FAN

(NASA LeRC ASSESSMENT STUDY)

CONVENTIONAL TURBOFAN

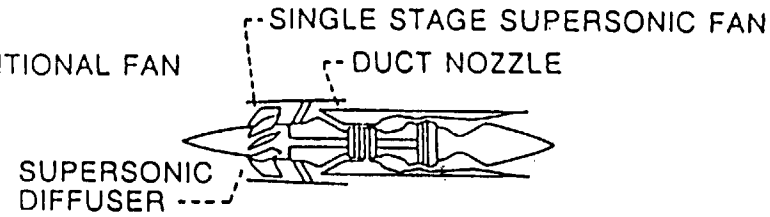

SUPERSONIC FAN ENGINE

SUPERSONIC FAN ENGINE FEATURES

- SHORT, ALL SUPERSONIC INLET
- SINGLE STAGE SUPERSONIC FAN
- BPR DECREASES WITH M_0

IMPLICATIONS

- LOWER WEIGHT, LOWER INLET DRAG
- LOWER WEIGHT AND COST, RUGGED BLADING
- HIGHER CRUISE THRUST

WEIGHT 15 TO 20% LOWER	CRUISE SFC-10 TO 20% LOWER

CO-86-19471

GEOMETRY

SUPERSONIC THROUGHFLOW FAN

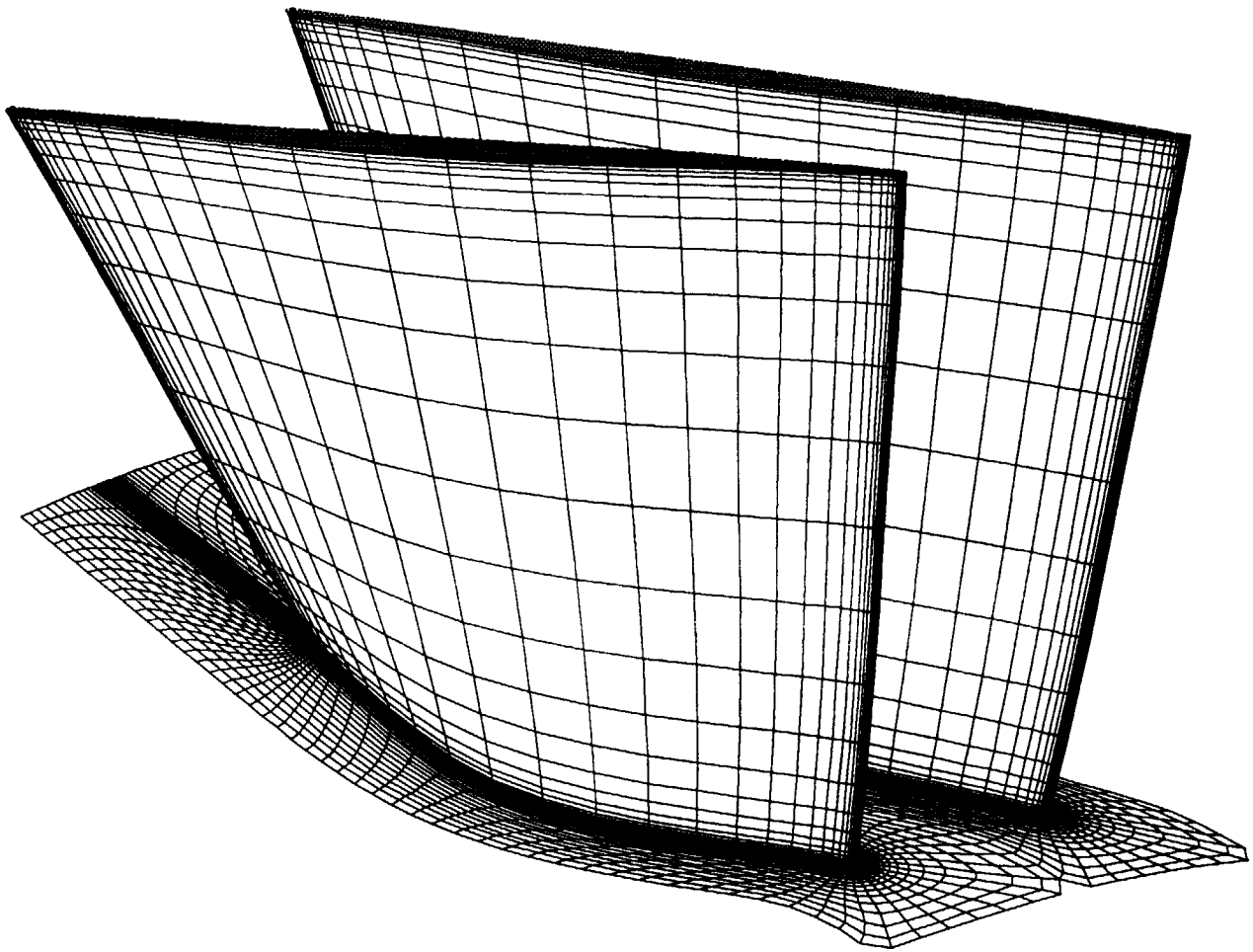

PRESSURE

SUPERSONIC THROUGHFLOW FAN, Mrel = 2.5

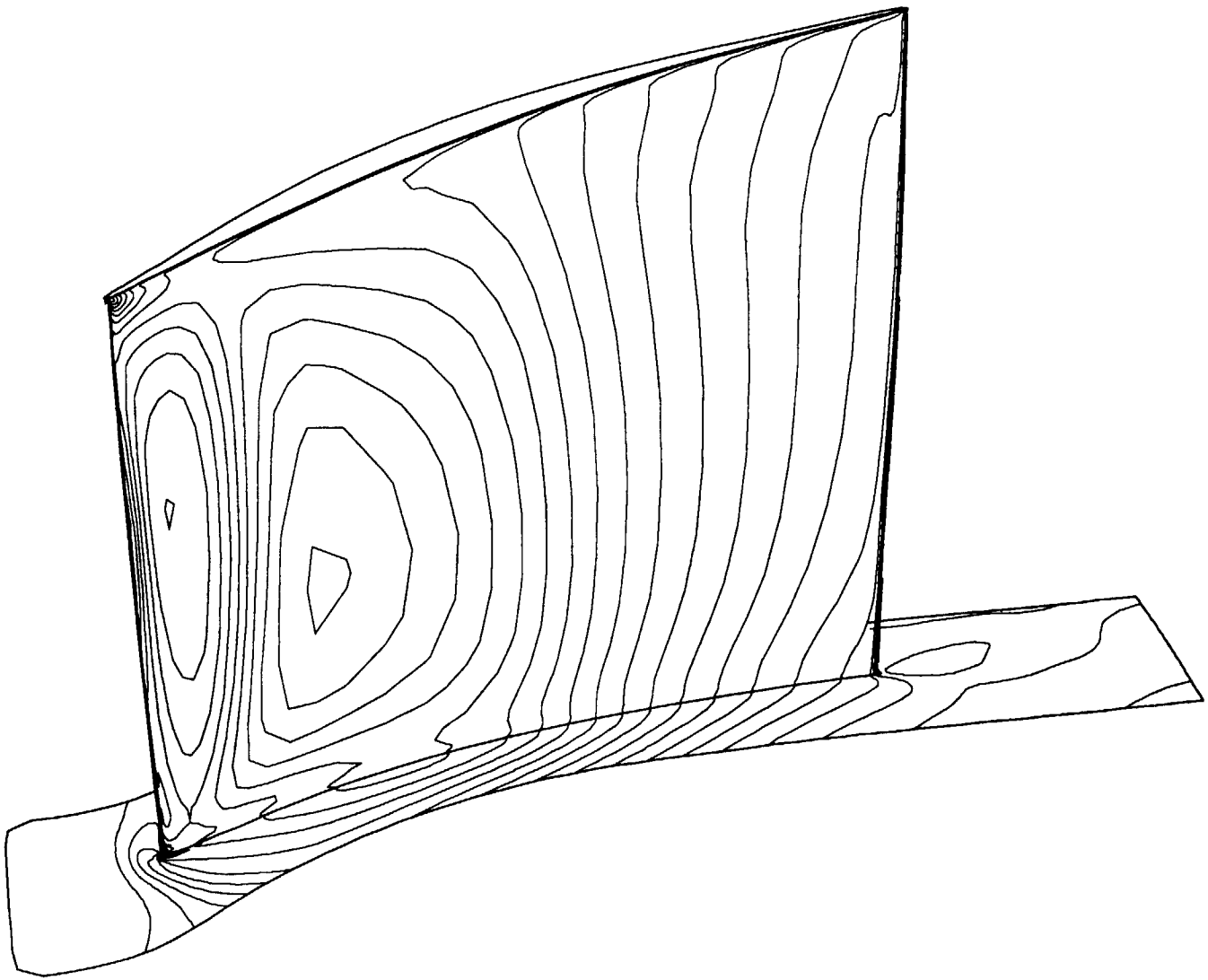

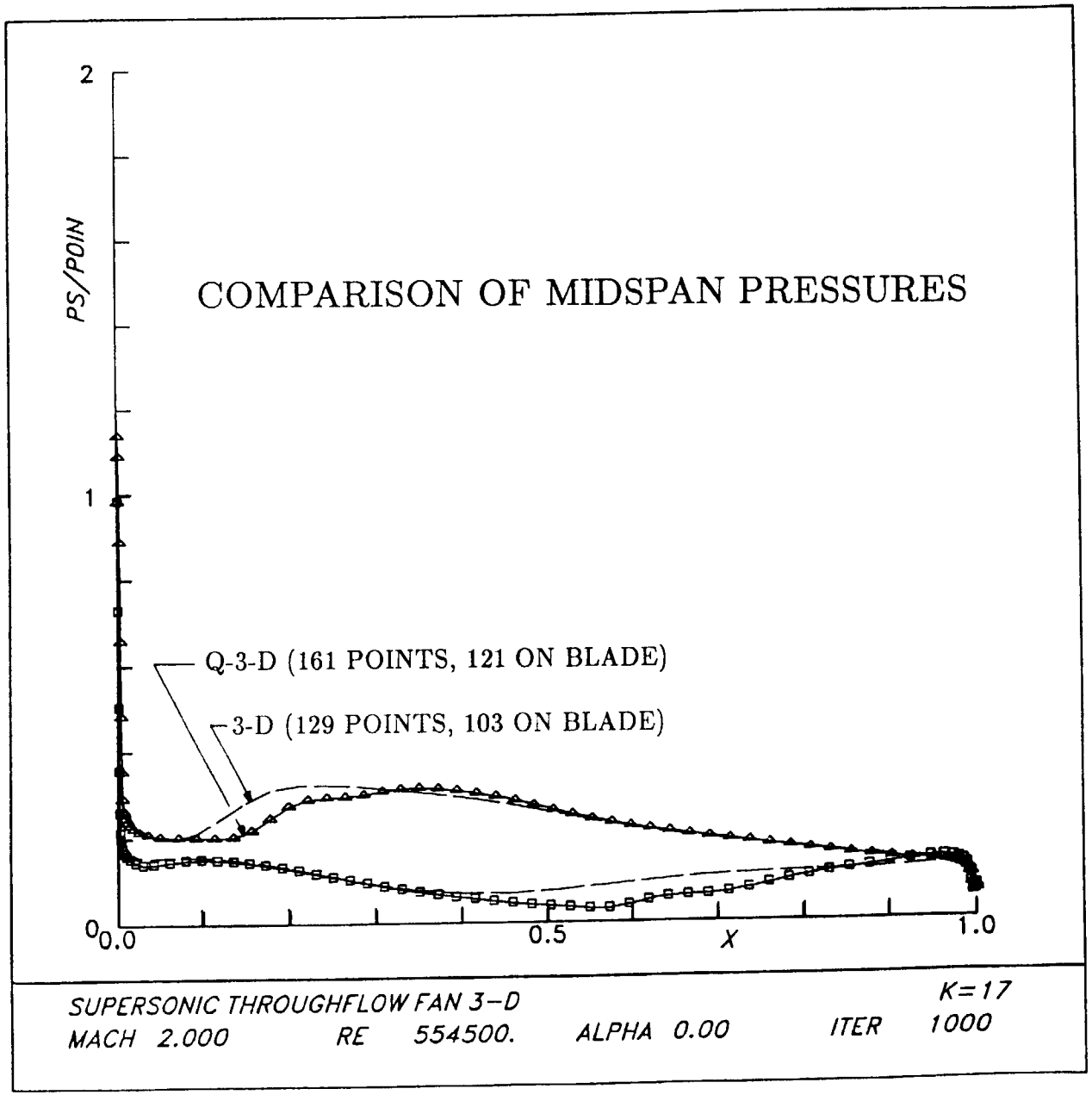
COMPARISON OF MIDSPAN PRESSURES
PS/POIN
2
1
0
0.0
0.5
X
1.0
Q-3-D (161 POINTS, 121 ON BLADE)
3-D (129 POINTS, 103 ON BLADE)
SUPERSONIC THROUGHFLOW FAN 3-D
K=17
MACH 2.000
RE 554500.
ALPHA 0.00
ITER 1000

DENSITY

SUPERSONIC THROUGHFLOW FAN, Mrel = 2.5

PARTICLE TRACES

SUPERSONIC THROUGHFLOW FAN, Mrel = 2.5

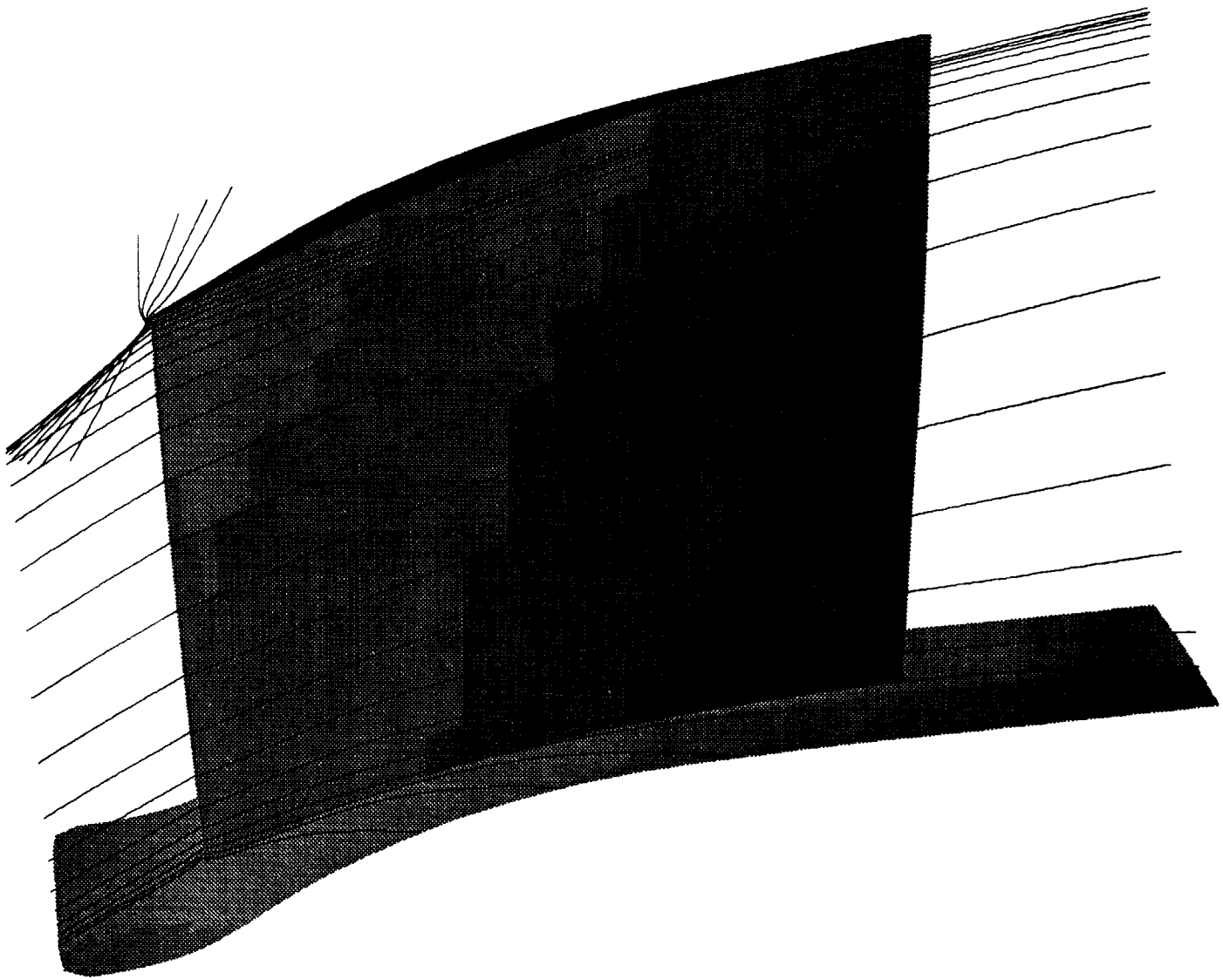

PARTICLE TRACES

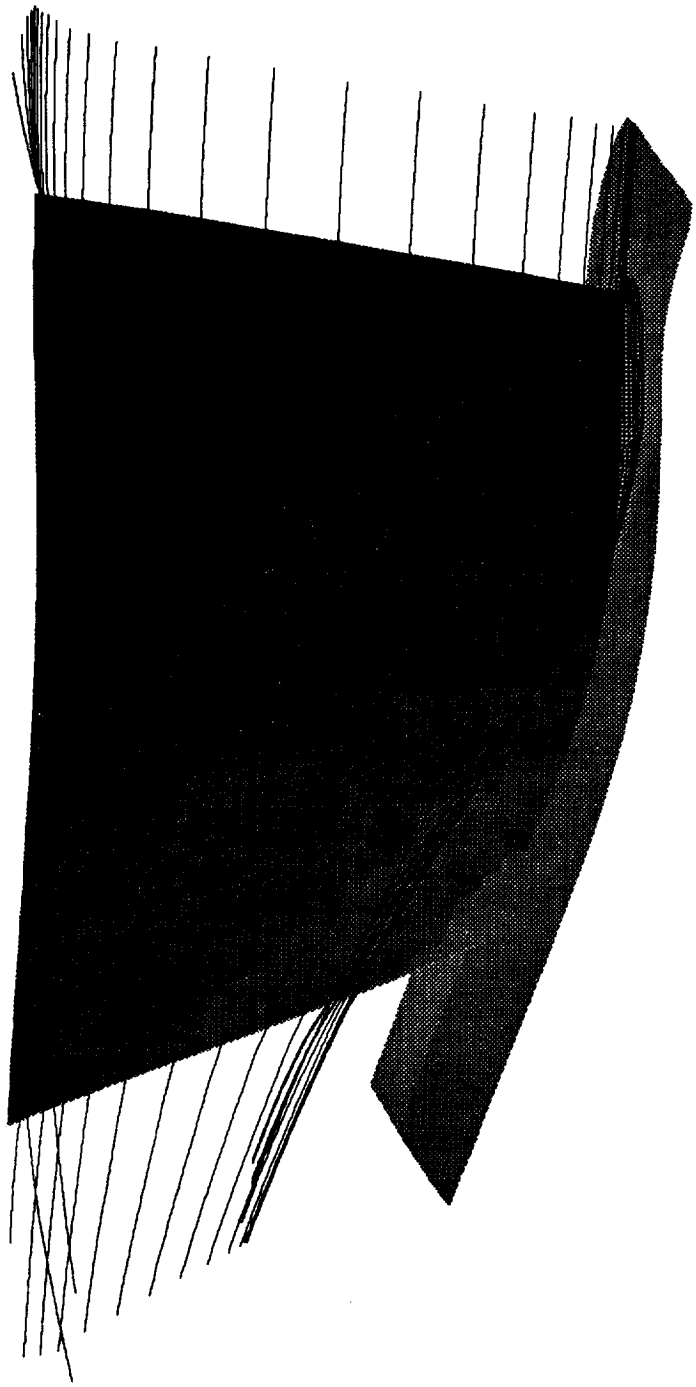

SUMMARY

PHYSICS

- 3-D NAVIER-STOKES ANALYSIS FOR STEADY INTERNAL FLOWS
- CARTESIAN FORMULATION ROTATING ABOUT X-AXIS
- THIN LAYER IN STREAMWISE DIRECTION, FULL N-S IN OTHERS
- BALDWIN-LOMAX TURBULENCE MODEL

NUMERICS

- FINITE-DIFFERENCE FORM ON GENERAL BODY FITTED GRID
- EXPLICIT MULTISTAGE RUNGE-KUTTA SCHEME
- VARIABLE $\Delta t_{i,j}$ & IMPLICIT RESIDUAL SMOOTHING

RESULTS

- SUPERSONIC THROUGHFLOW FAN
- HORSESHOE VORTEX AHEAD OF CYLINDER
- ANNULAR TURBINE CASCADE

FUTURE

- NEW FAN DESIGN WITH CONVERGING HUB, HIGH TURNING
- FINER GRIDS ON NAS
- TIP CLEARANCE
- MULTIGRID

SESSION X

STOVL

Chairman:
Meng-Sing Liou
Chief, Computational Fluid Dynamics Branch
NASA Lewis Research Center

PRECEDING PAGE BLANK NOT FILMED

N91-10886

SIMULATION OF POWERED-LIFT FLOWS

William R. Van Dalsem
Kalpana Chawla
Karlin R. Roth
Merritt H. Smith
Kuditipudi V. Rao

NASA Ames Research Center, Moffett Field, CA

Thomas C. Blum

BOEING Advanced Systems, Seattle, WA

The primary objective of this presentation is to expose government, industry, and academic scientists to work underway at NASA-Ames towards the application of CFD to the powered lift area. One goal of our research is to produce the technologies which will be required in the application of numerical techniques to, for example, the Supersonic STOVL program.

In the presentation, we will summarize our progress to date on the following specific projects:

Jet in ground effect with crossflow

Jet in a crossflow

Delta planform with multiple jets in ground effect

Integration of CFD with thermal and acoustic analyses

Improved flow visualization techniques for unsteady flows

YAV-8B Harrier simulation program

E-7 simulation program

Additional work is underway at NASA-Ames in the development of turbulence models and solution adaptive grid techniques suitable for the powered lift area, and the simulation of USB configurations. However, this work is not included here due to space constraints.

PRECEDING PAGE BLANK NOT FILMED

ORIGINAL PAGE IS
OF POOR QUALITY

POWERED-LIFT CFD PROGRAM

OBJECTIVE

Develop and validate CFD technologies for the V/STOL field, with particular emphasis on the requirements of the supersonic STOVL program.

TECHNICAL APPROACH

Time-accurate Navier-Stokes solutions on overlapped adapting grids, coupled to thermal, propulsive, controls, and acoustic analyses.

STRATEGY

- Starting from the RFA CFD technology base, develop in-depth expertise in the most critical components of the flow about V/STOL aircraft.
- As required, improve the computational techniques to allow the accurate simulation of these flows.
- Simultaneously, begin complete V/STOL aircraft simulation efforts (e.g., VSRA and E-7), with above "component" efforts contributing required technologies and expertise.

IN A TIMELY MANNER, DEVELOP BOTH IN-DEPTH EXPERTISE AND THE ABILITY TO TREAT COMPLETE V/STOL CONFIGURATIONS.

POWERED-LIFT CHALLENGES & CFD REQUIREMENTS

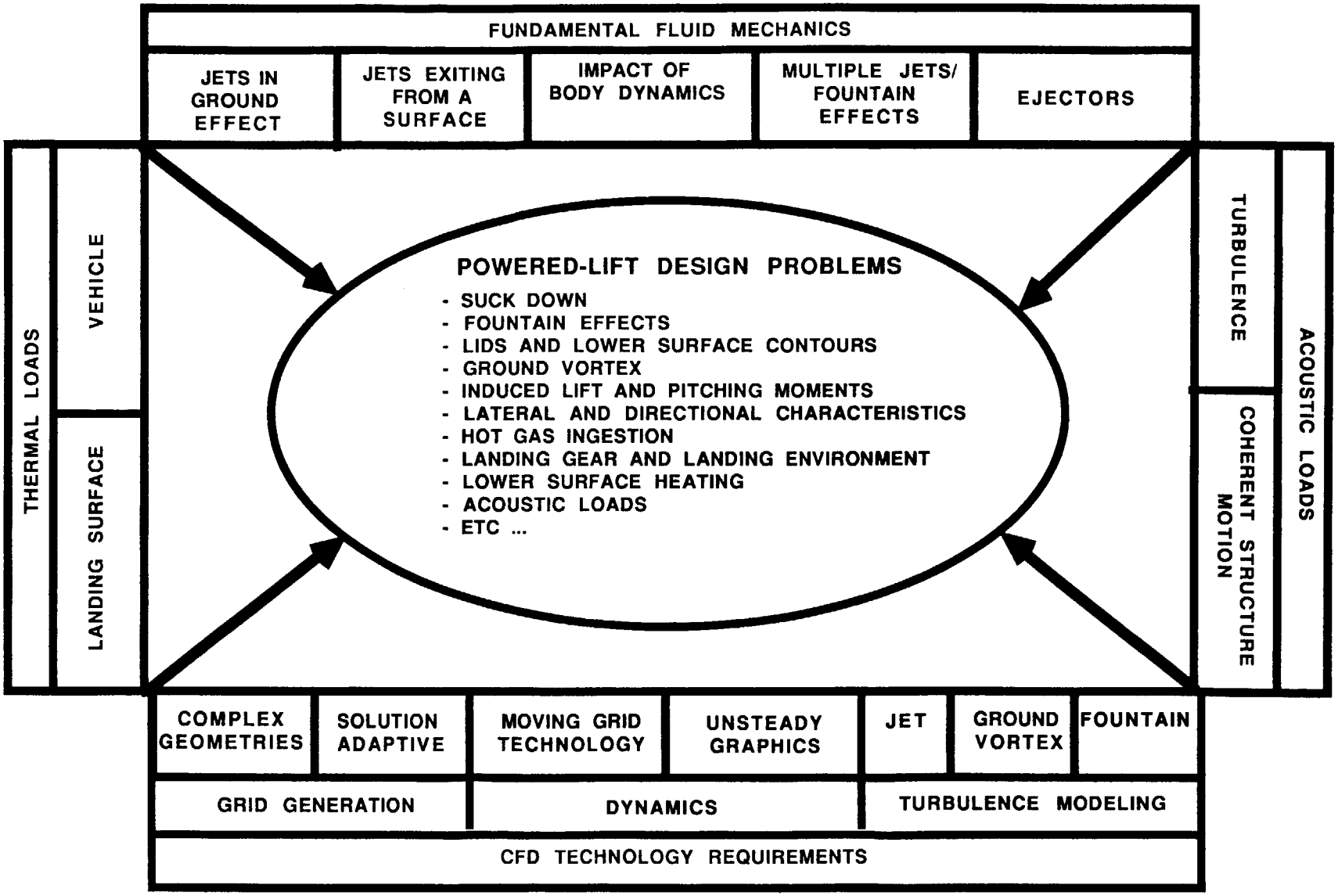

JET IN GROUND EFFECT WITH CROSSFLOW

A fundamental component of STOVL take-off/landing flow physics

- To date, CFD has proved capable of resolving the salient features, and adding to previous understanding:
  - Computed correct ground vortex formation and extent over a range of jet to freestream velocity ratios and jet heights.
  - Allowed a systematic study of the impact of a variety of flow conditions, including jet shape, moving ground board, etc...
  - Simulated ring vortex and shock disc motion, which may be important sources of unexplained intense noise levels
- In the future, will focus on improving our understanding of jet unsteadiness and the existing discrepancies between experimental and full-scale studies.

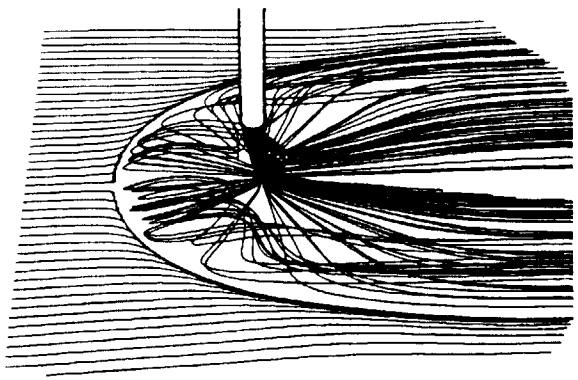

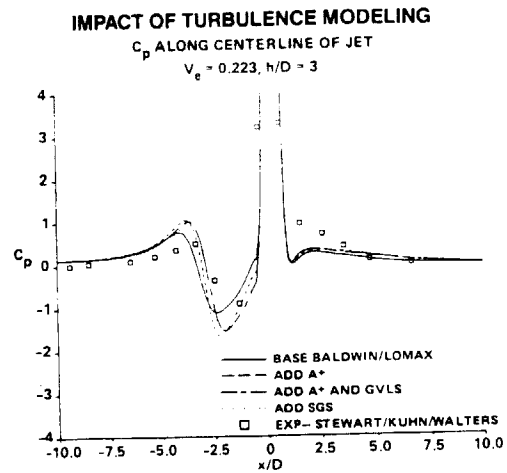

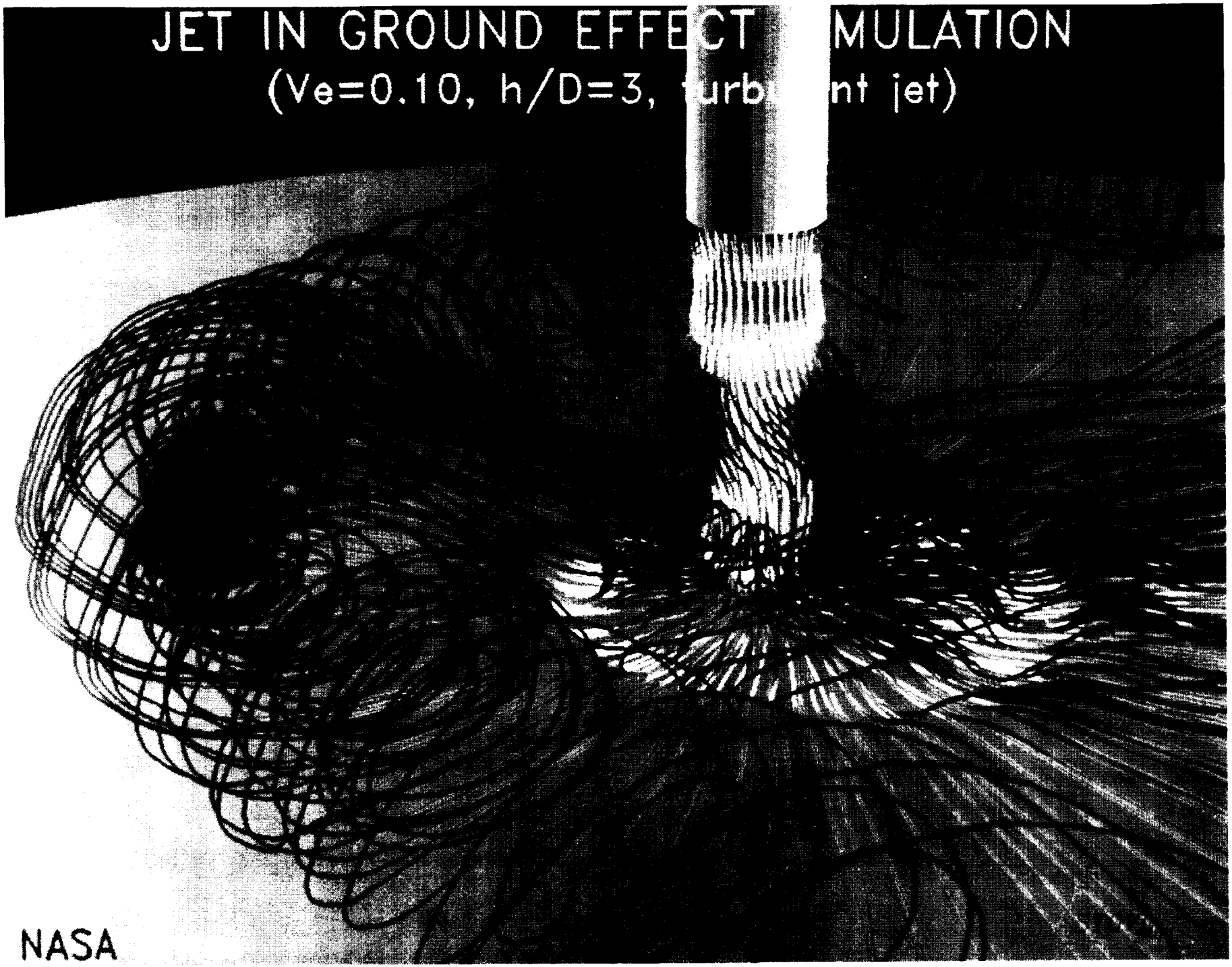
JET IN GROUND EFFECT SIMULATION
(Ve=0.10, h/D=3, turbulent jet)
NASA

UNSTEADY FLOW ANALYSIS

BACKGROUND The unsteady flow about powered-lift vehicles induces significant unsteady loads, hence must be accurately predicted.

Require significant software improvements to deal with unsteady flows on a routine basis.

APPROACH Develop techniques which allow the rapid yet indepth analysis and validation of unsteady flow simulations.

PLOT4D
An "upgraded" version of PLOT3D program which allows the interactive animation and analysis of unsteady data sets.

STREAKER
Produces time-accurate numerical streaklines (smoke) suitable for direct comparison with experimental unsteady flow visualizations.

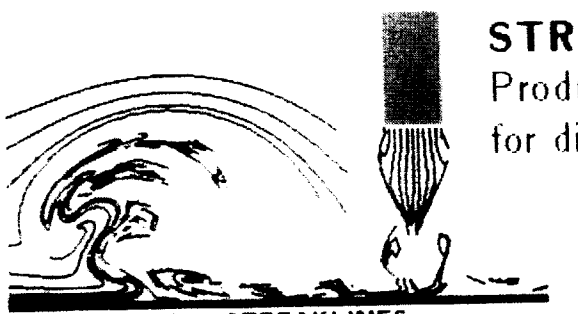

NUMERICAL STREAKLINES

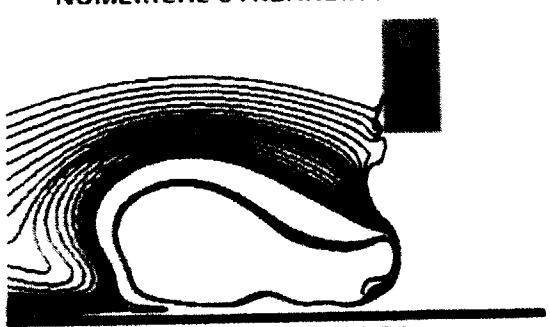

NUMERICAL STREAMLINES

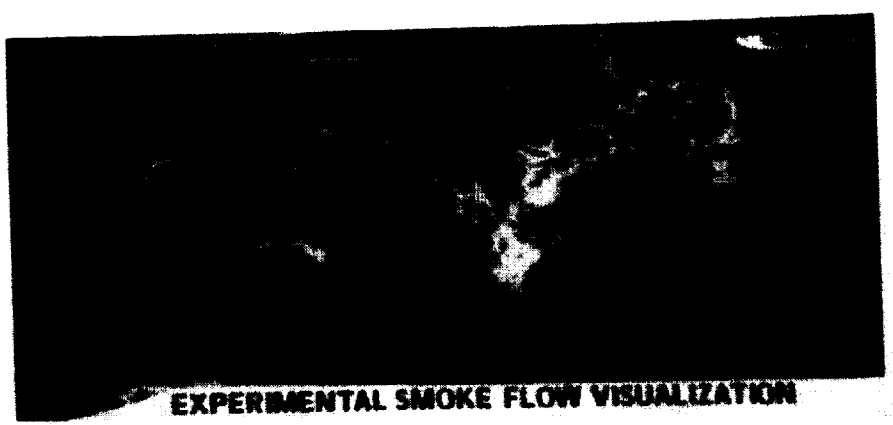

EXPERIMENTAL SMOKE FLOW VISUALIZATION

THERMAL LOADS

PROVEN RISK OF VEHICLE AND LANDING SURFACE DAMAGE (e.g., LPH TRIPOLI DECK BUCKLING) DURING TAKE-OFF/LANDING, AND VEHICLE DAMAGE DURING TRANSITION

- AT PRESENT, EXPENSIVE FULL-SCALE JET ENGINE/MATERIALS TEST (FLUK) ARE ONLY METHOD OF TESTING UNSTEADY THERMAL RESPONSE OF MATERIALS TO ENGINE EXHAUST
- COUPLED UNSTEADY JET FLOW CFD/THERMAL ANALYSIS OF SURFACES MADE OF A VARIETY OF MATERIALS (FROM ALUMINUM AND COMPOSITES, TO CONCRETE) WOULD ALLOW DETAILED ANALYSIS OF V/STOL THERMAL DAMAGE

NAVIER-STOKES EQS.

$$Q_t + E_x + F_y + G_z = Re^{-1}(Ev_x + Fv_y + Gv_z)$$

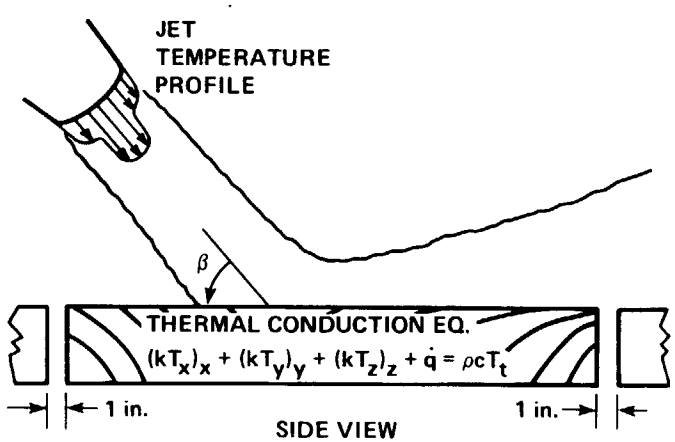

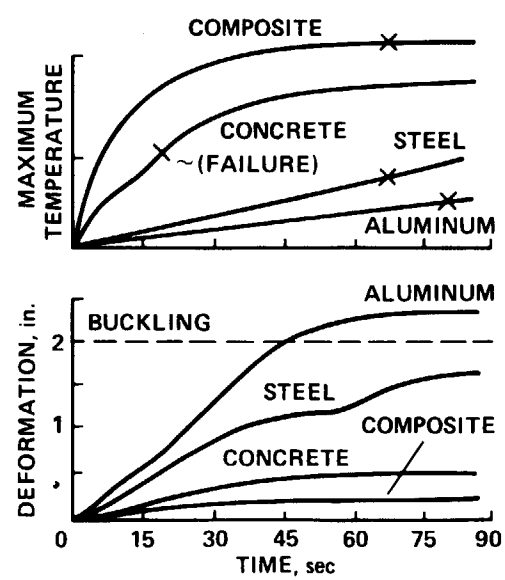

HOT JET THERMAL LOAD

(Ve=0.10, h/D=3, turbulent jet)

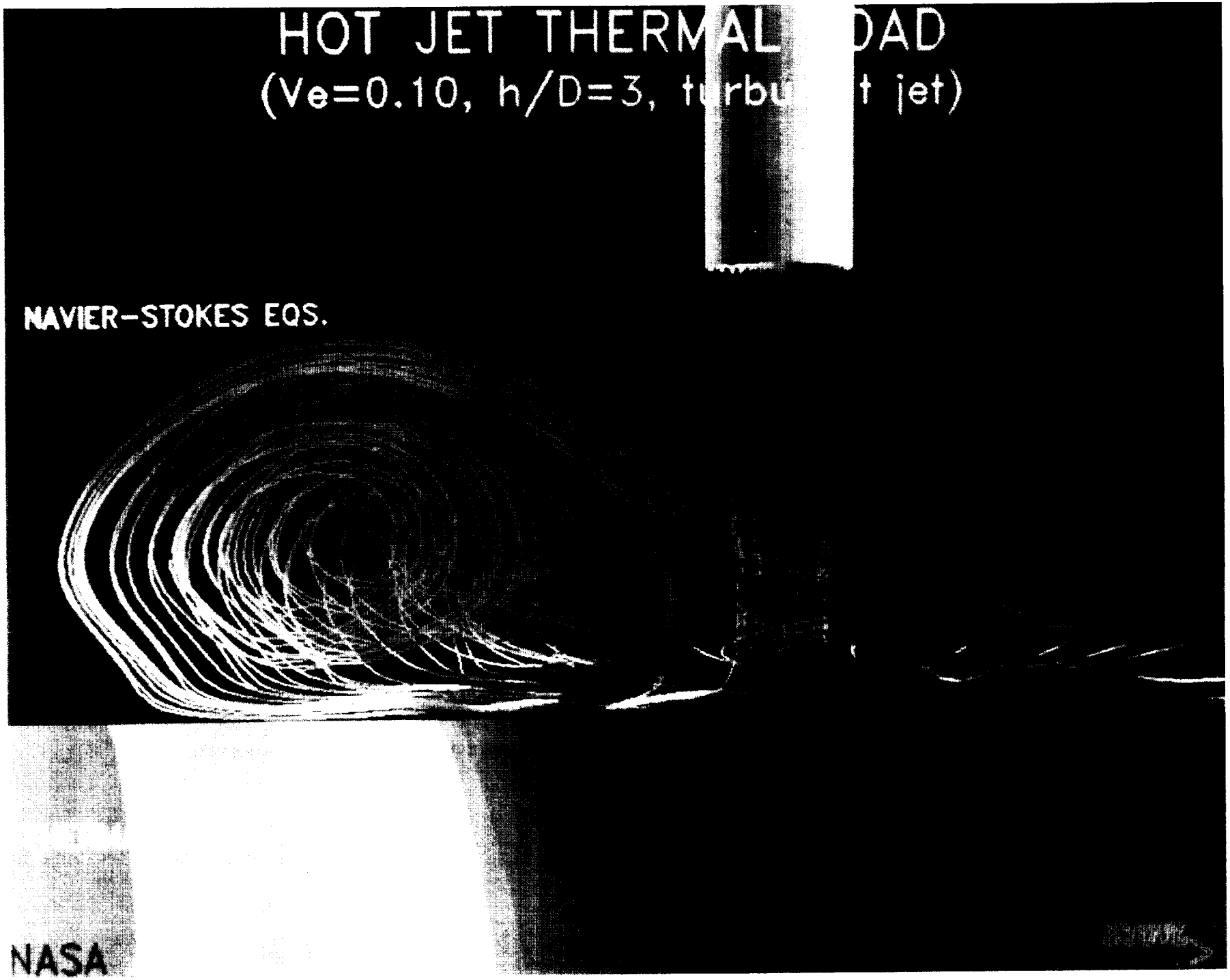

ORIGINAL PAGE IS
OF POOR QUALITY

JET IN A CROSSFLOW

- Isolates physics of aero/propulsive interaction region during transition.
- Navier-Stokes solution captures all critical flow features.
- Quantitative correlation with existing database demonstrated.
- Current efforts focus on computing realistic STOVL geometries.

FLOW PHYSICS

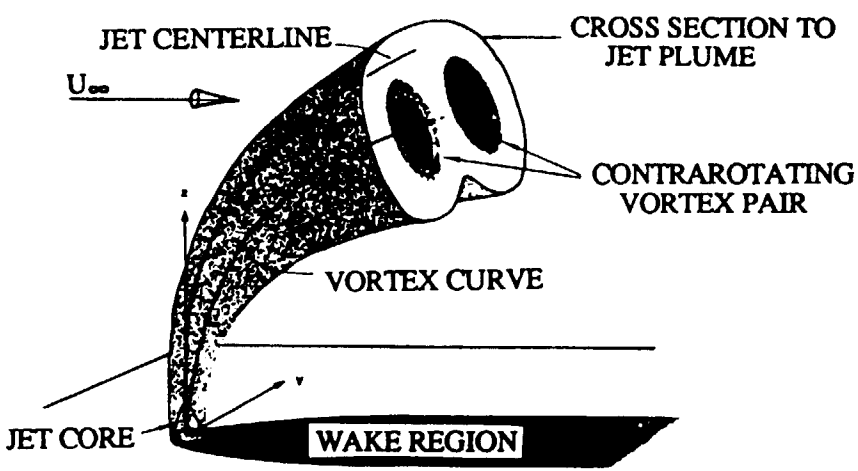

JET CENTERLINE

$M_j/M_\infty = 4.0$, $M_\infty = 0.19$

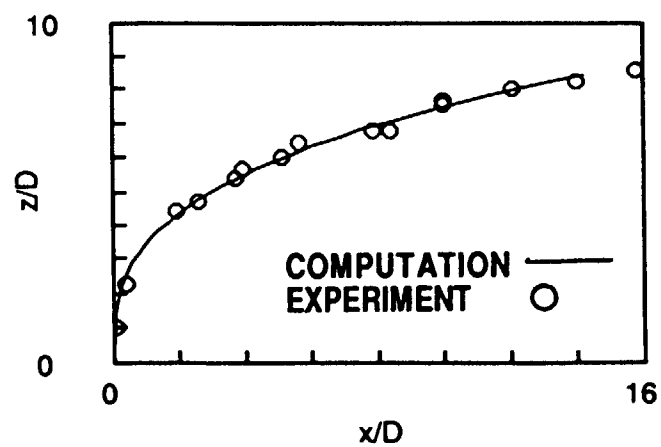

K. Roth, **FFF**

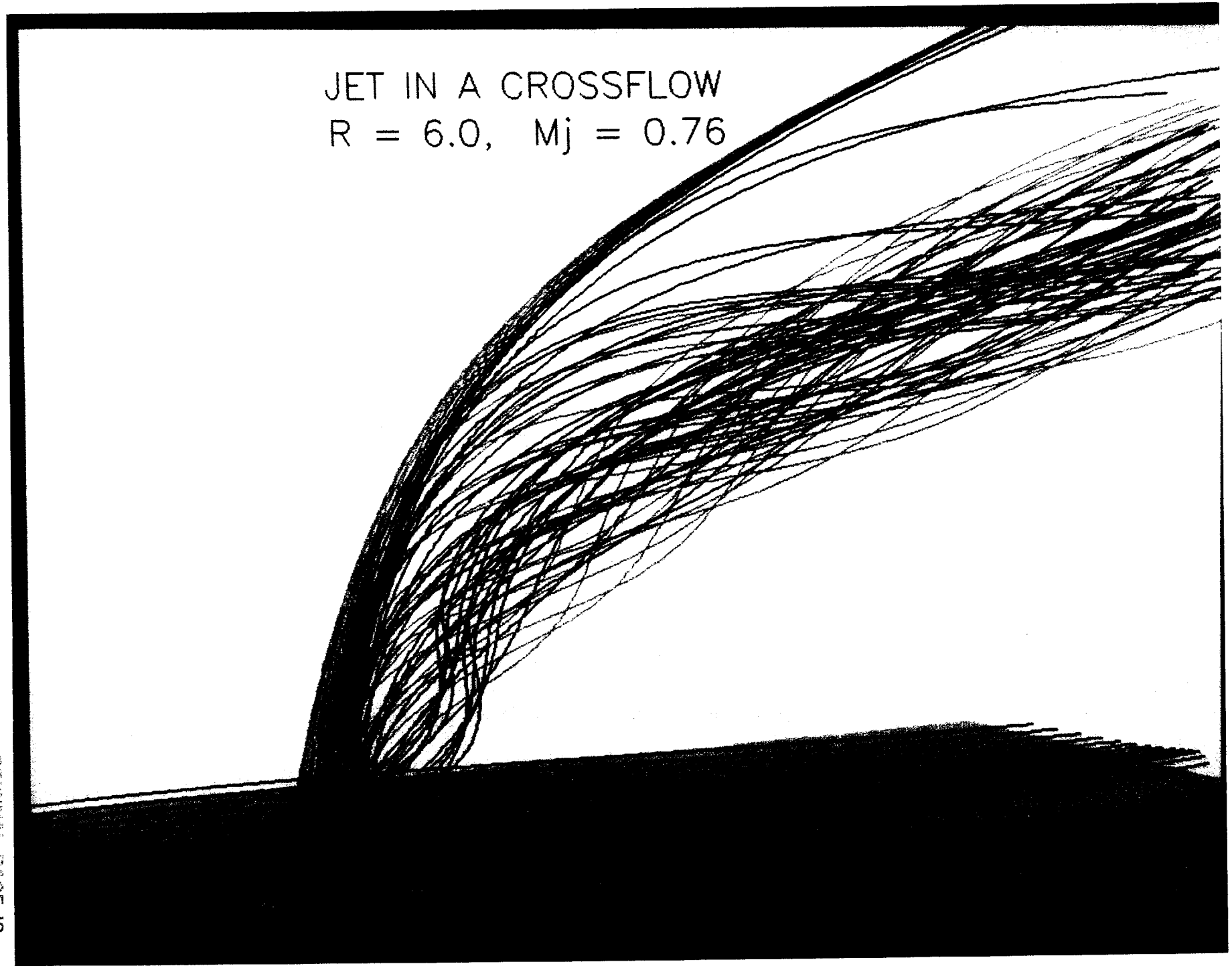

ORIGINAL PAGE IS
OF POOR QUALITY

GROUND EFFECTS

C_l AND C_m OF V/STOL VEHICLES IN GROUND-EFFECT ARE STRONGLY INFLUENCED BY HEIGHT ABOVE GROUND AND RATE OF ASCENT/DESCENT

- DIFFICULT TO STUDY EXPERIMENTALLY, AT PRESENT GOVERNING FLOW PHYSICS IS NOT UNDERSTOOD
- TO DATE, CFD HAS SHED INSIGHT IN TO FLOW PHYSICS OF NEGATIVE C_l AT LOW HEIGHTS, AND WORK IS IN PROGRESS TO STUDY DYNAMIC CASE

$\beta(\alpha, \dot{h}, V_e)$ = EFFECTIVE ANGLE OF ATTACK
α = ANGLE OF ATTACK
$\dot{h}$ = RATE OF DESCENT
$V_e = V_\infty / V_{jet}$

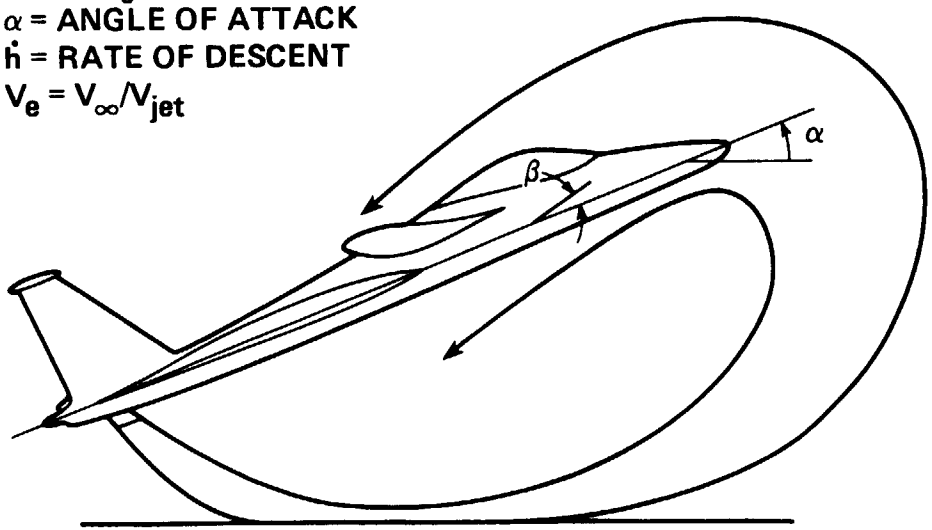

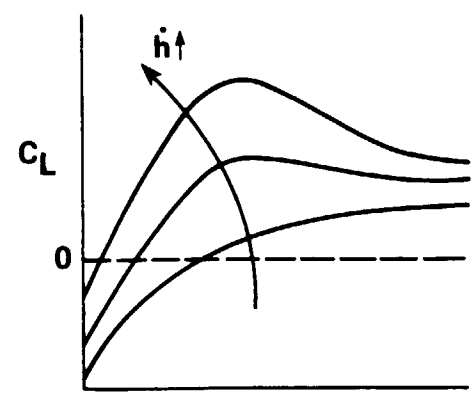

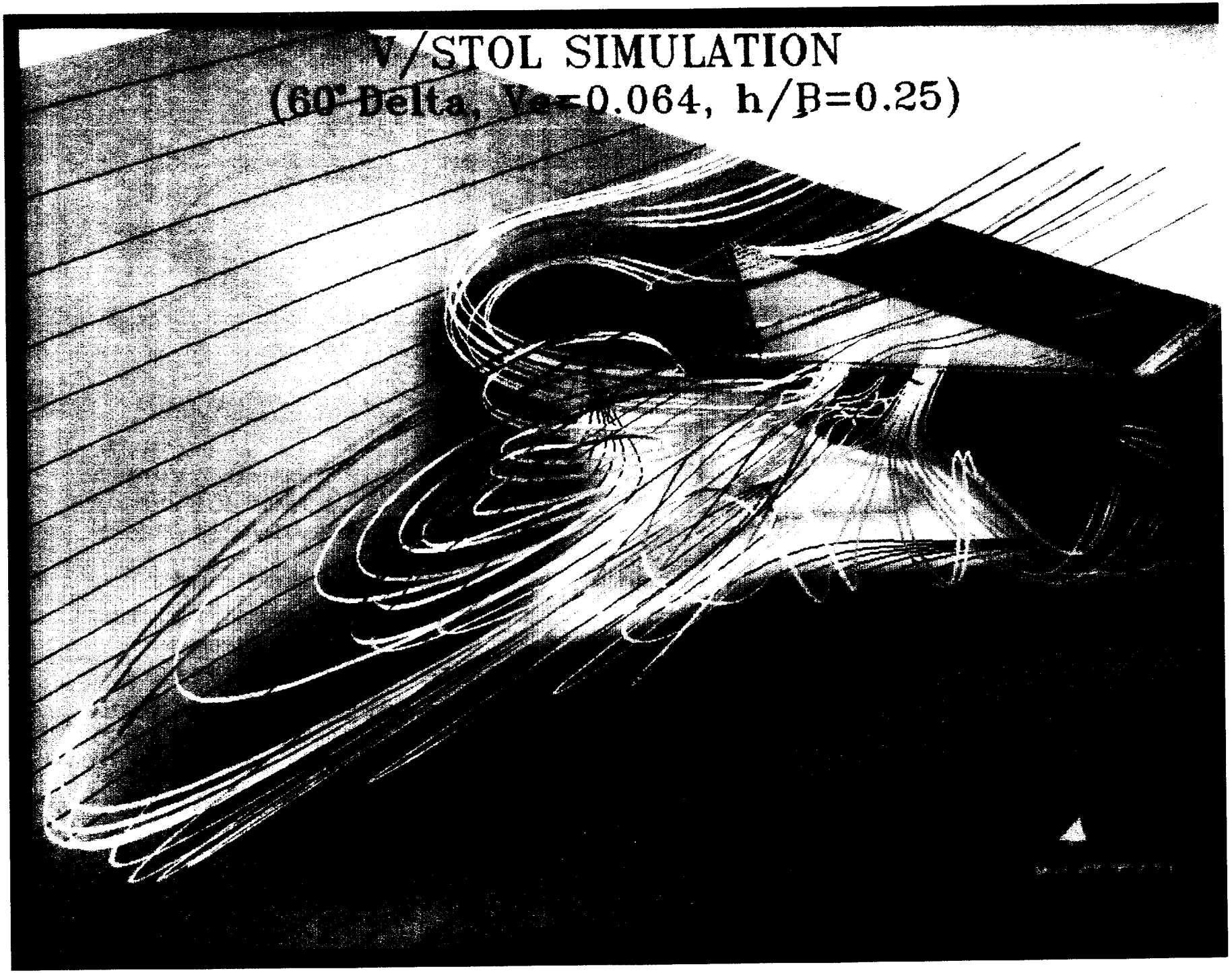

ORIGINAL PAGE IS
OF POOR QUALITY

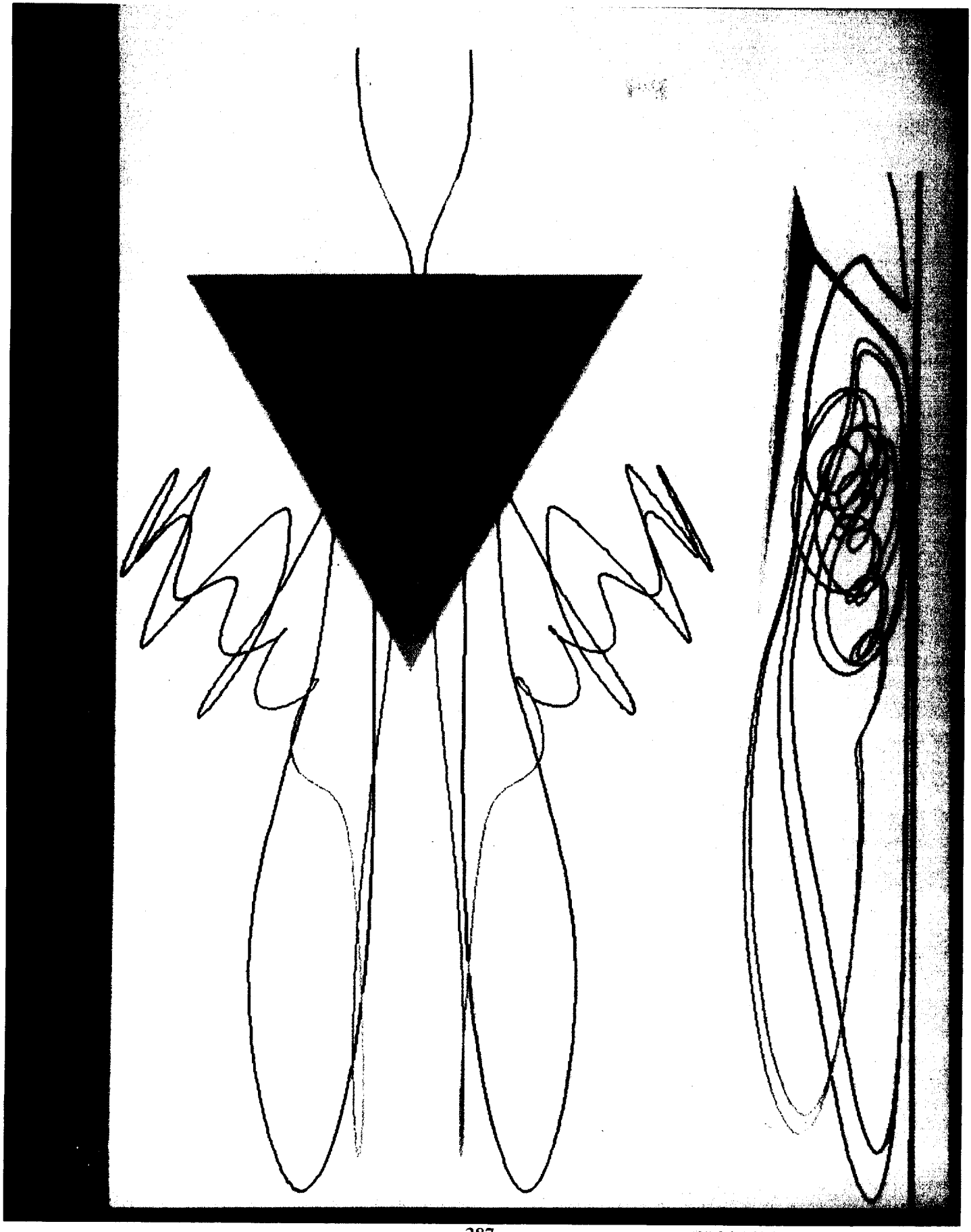

ORIGINAL PAGE IS
OF POOR QUALITY

ORIGINAL PAGE
BLACK AND WHITE PHOTOGRAPH

VSRA COMPUTATION TO FLIGHT PROGRAM
(Preliminary Harrier YAV-8B Surface Definition)

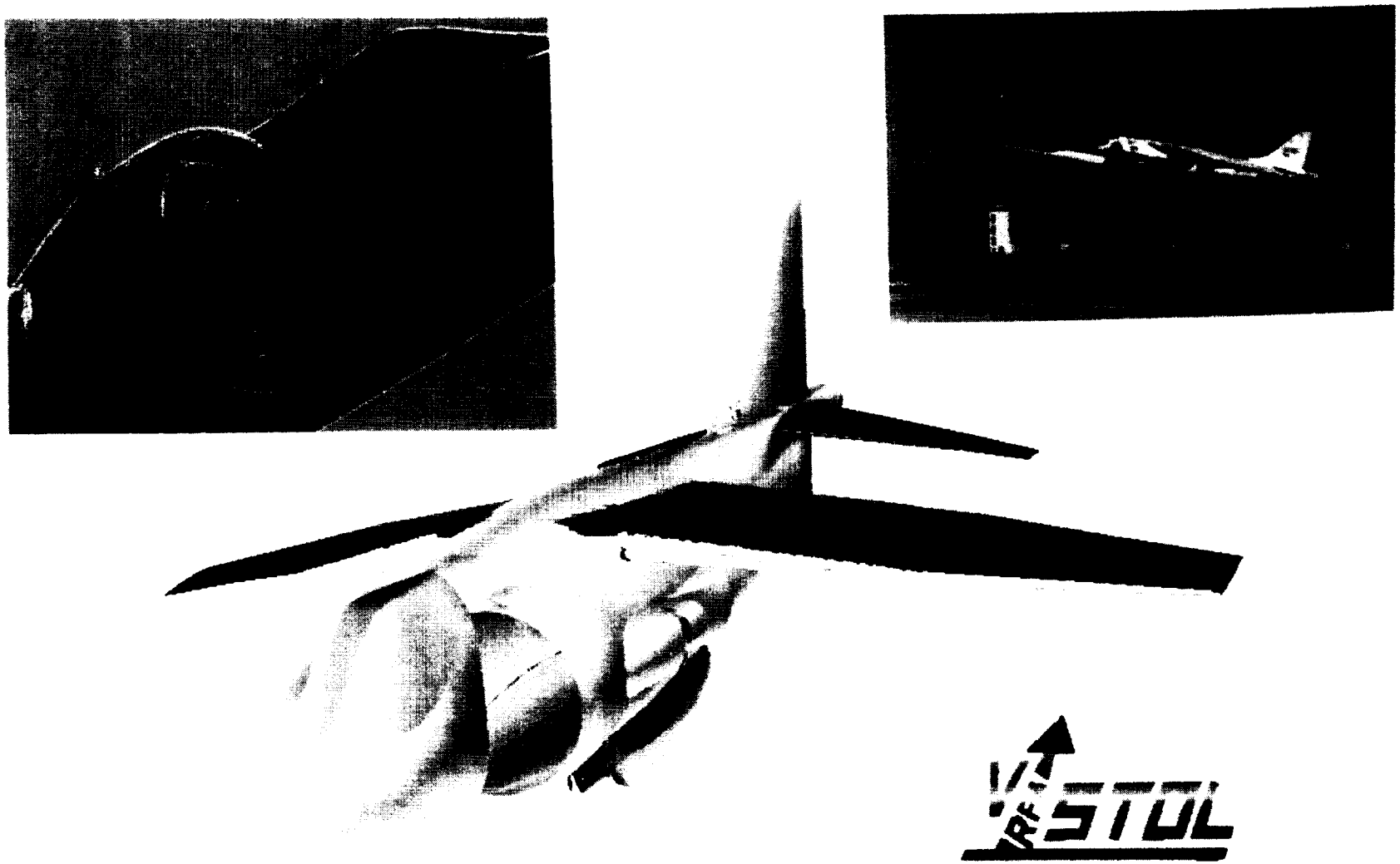

ORIGINAL PAGE IS
OF POOR QUALITY

E-7 COMPUTATION THROUGH FULL-SCALE EXPERIMENT PROGRAM

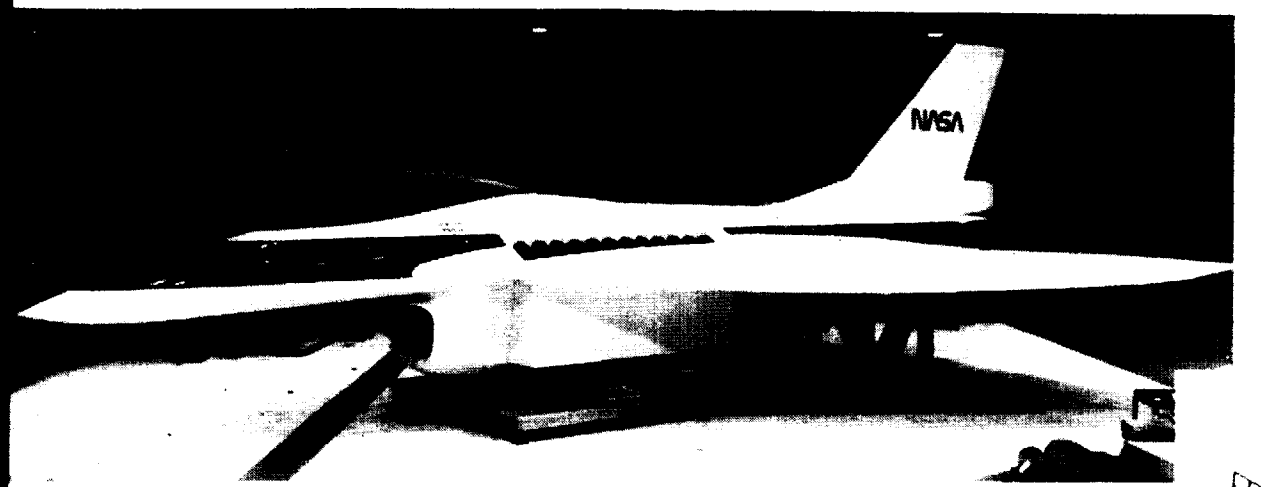

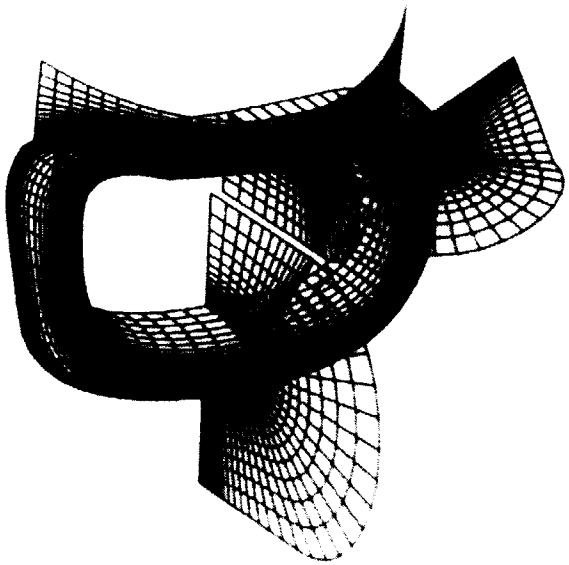

- GRIDS GENERATED BY BOEING
- COMPUTATIONS A JOINT BOEING/NASA-AMES EFFORT

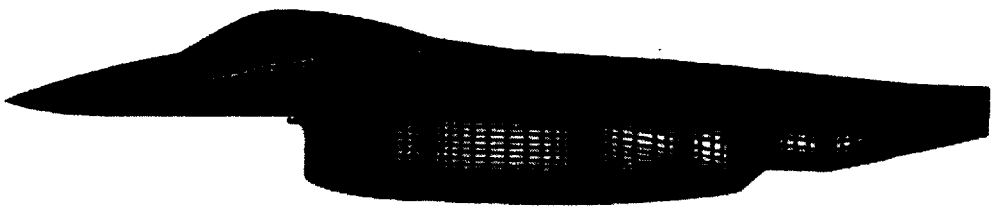

ORIGINAL PAGE
BLACK AND WHITE PHOTOGRAPH

ORIGINAL PAGE IS
OF POOR QUALITY

SUMMARY

- To date, have studied the numerical simulation of the following powered-lift flows:
  - Jet in ground effect with crossflow (including thermal loads)
  - Jet in crossflow
  - Delta with multiple jets in ground effect with crossflow

  Comparison with data indicates that these simulations predict the fundamental flow phenomena and yield quantitative results for many of the observed trends.

- This experience has motivated us towards additional R&D in the following areas:
  - Adaptive gridding
  - Improved turbulence modeling
  - Unsteady flow simulation and analysis

- Presently also working towards simulation of the following "complete" configurations:
  - STOVL CFD Validation model (In cooperation with FFF)
  - YAV-8B Harrier (" FAP to obtain data)
  - E-7 (" Boeing)
  - USB configuration (" FAP)
  - Tiltrotor configuration (" RFA Rotorcraft group)

N91-10887

ORIGINAL CONTAINS
COLOR ILLUSTRATIONS

A Numerical Study of the Hot Gas Environment Around a STOVL Aircraft in Ground Proximity

by

Thomas J. VanOverbeke

and

James D. Holdeman

of

NASA Lewis Research Center

ABSTRACT

The development of Short Take-off Vertical Landing (STOVL) aircraft has been based on empiricism. In this study, a 3-D flow code was used to calculate the hot gas environment around a STOVL aircraft in ground proximity. Preliminary calculations are reported to identify key features of the flowfield, and to demonstrate the capability of a CFD code to calculate the temperature of the gases ingested at the engine inlet for typical flow and geometric conditions.

CALCULATIONS WERE DONE WITH A 3-D TEACH-TYPE CODE TO SOLVE THE TIME-AVERAGED NAVIER-STOKES EQUATIONS

- EQUATIONS ARE SOLVED SEQUENTIALLY
- A PRESSURE CORRECTION EQUATION IS SOLVED USING THE SIMPLE ALGORITM OF PATANKAR
- HYBRID DIFFERENCING WAS USED TO SAVE MEMORY
- A TWO EQUATION TURBULENCE MODEL WAS USED
- CODE WAS USED FOR COMBUSTORS AND DID NOT INCLUDE A DENSITY CORRECTION TERM FOR RAPIDLY VARYING PRESSURE
- EXIT BOUNDARY CONDITIONS WERE CHANGED FOR MODELING THE HOT GAS INGESTION PROBLEM

NASA
C-88-06794

SCHEMATIC OF COMPUTATIONAL DOMAIN

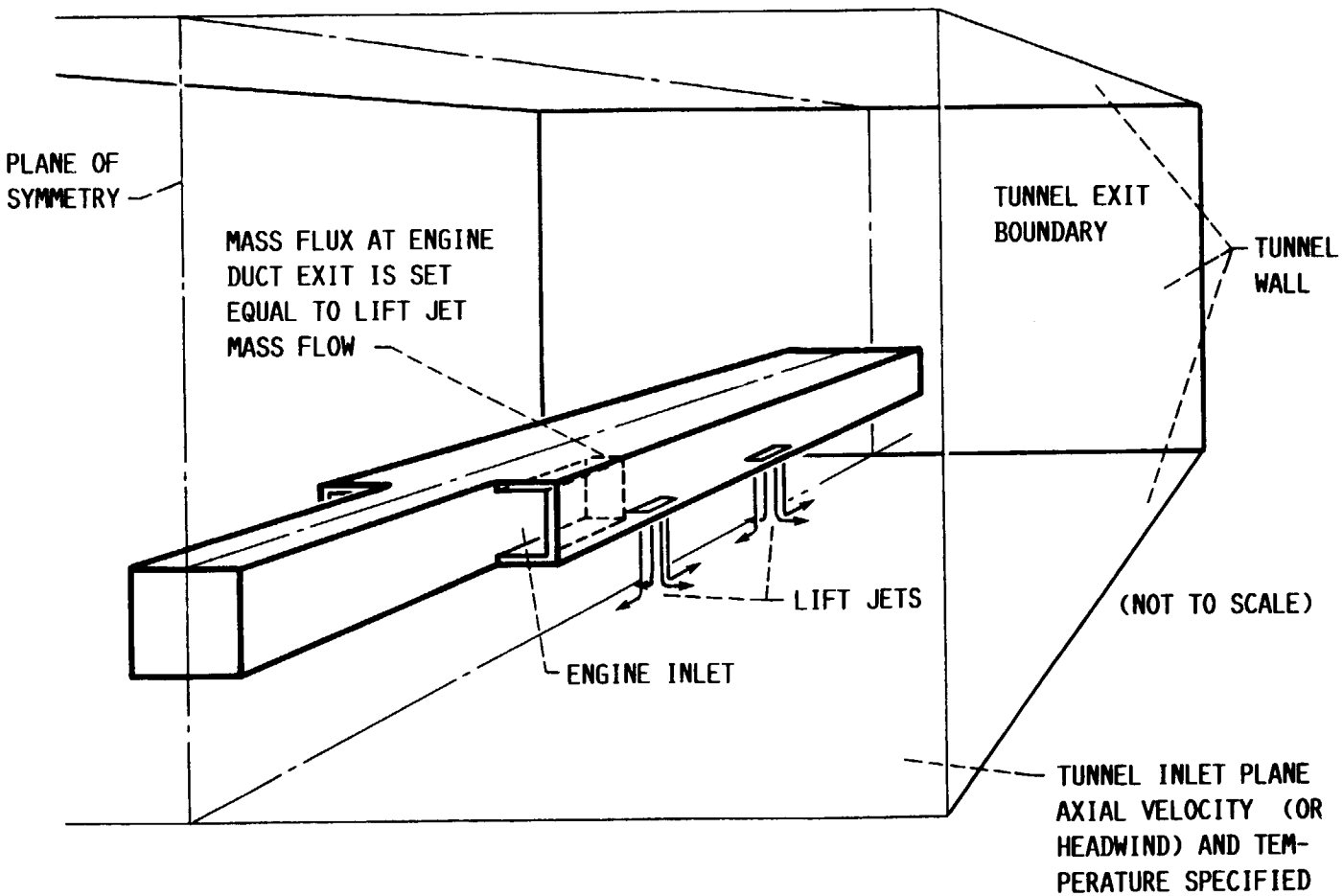

CD-88-34774

NEAR-GROUND PLANE VELOCITY AND TEMPERATURE DISTRIBUTIONS

(H/Dj=4)

U∞/Vj=0.03

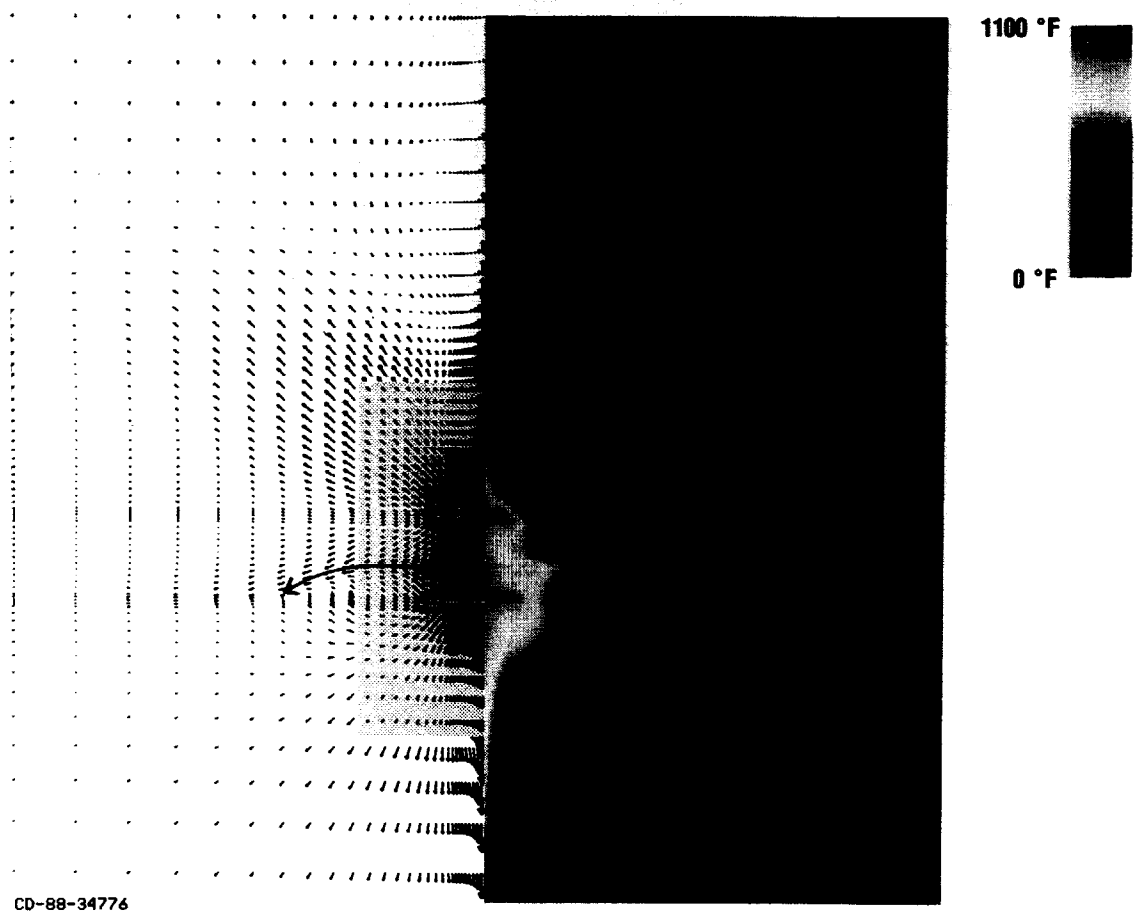

NEAR-GROUND PLANE VELOCITY AND TEMPERATURE DISTRIBUTIONS

(H/Dj=4)

U∞/Vj=0.09

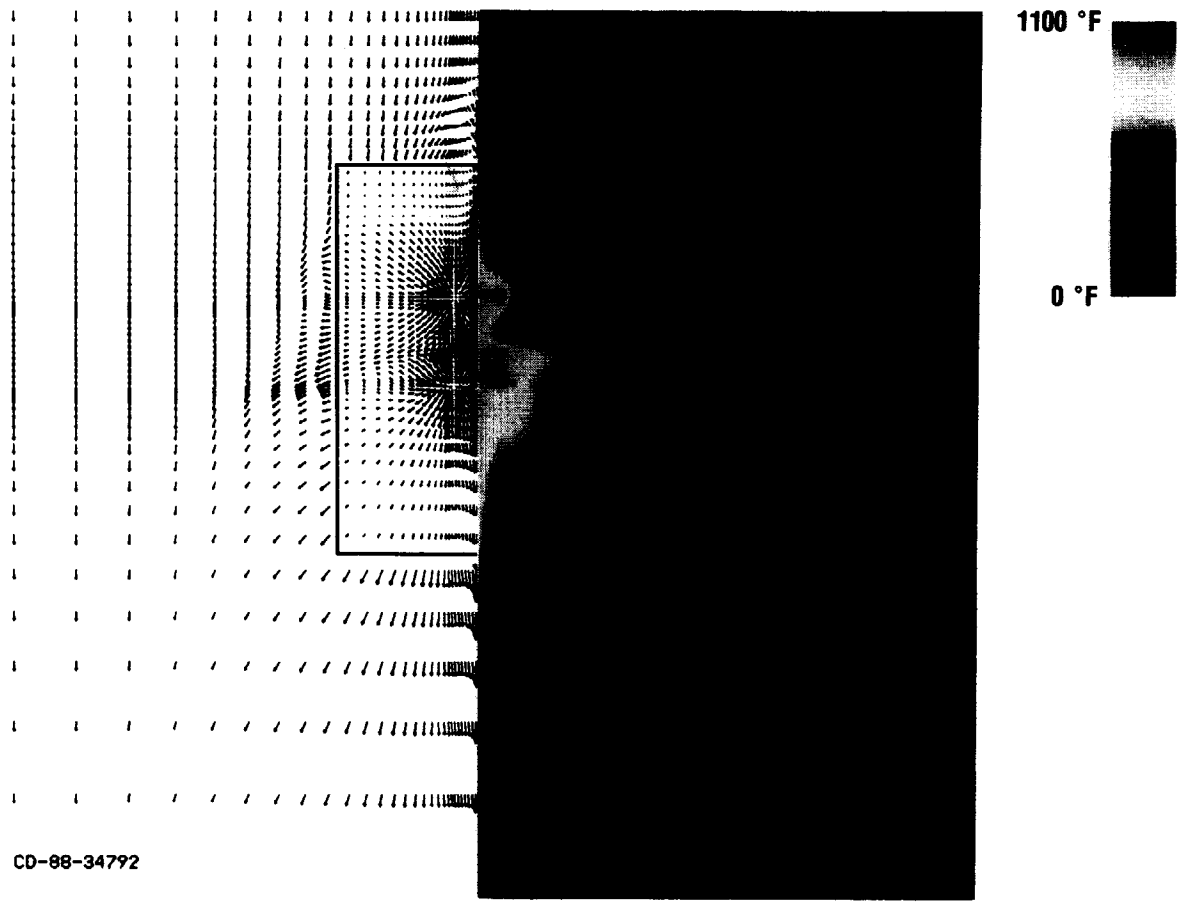

PRECEDING PAGE BLANK NOT FILMED

ORIGINAL PAGE IS OF POOR QUALITY

CALCULATED VELOCITY AND TEMPERATURE DISTRIBUTIONS IN VERTICAL X-Y PLANE THROUGH ENGINE INLET

(H/Dj=4; U∞/Vj=0.03)

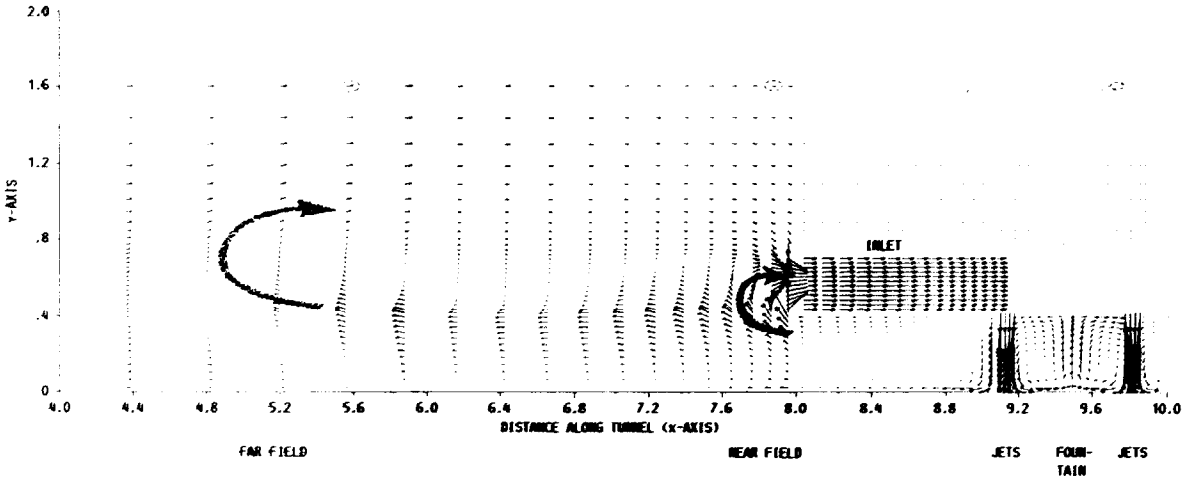

A) VELOCITY

CD-88-34777

B) TEMPERATURE

PRECEDING PAGE BLANK NOT FILMED

ORIGINAL PAGE IS
OF POOR QUALITY

TEMPERATURE DISTRIBUTIONS IN VERTICAL PLANES FROM AIRCRAFT CENTERPLANE TO OUTBOARD OF FUSELAGE

(H/Dj = 4)

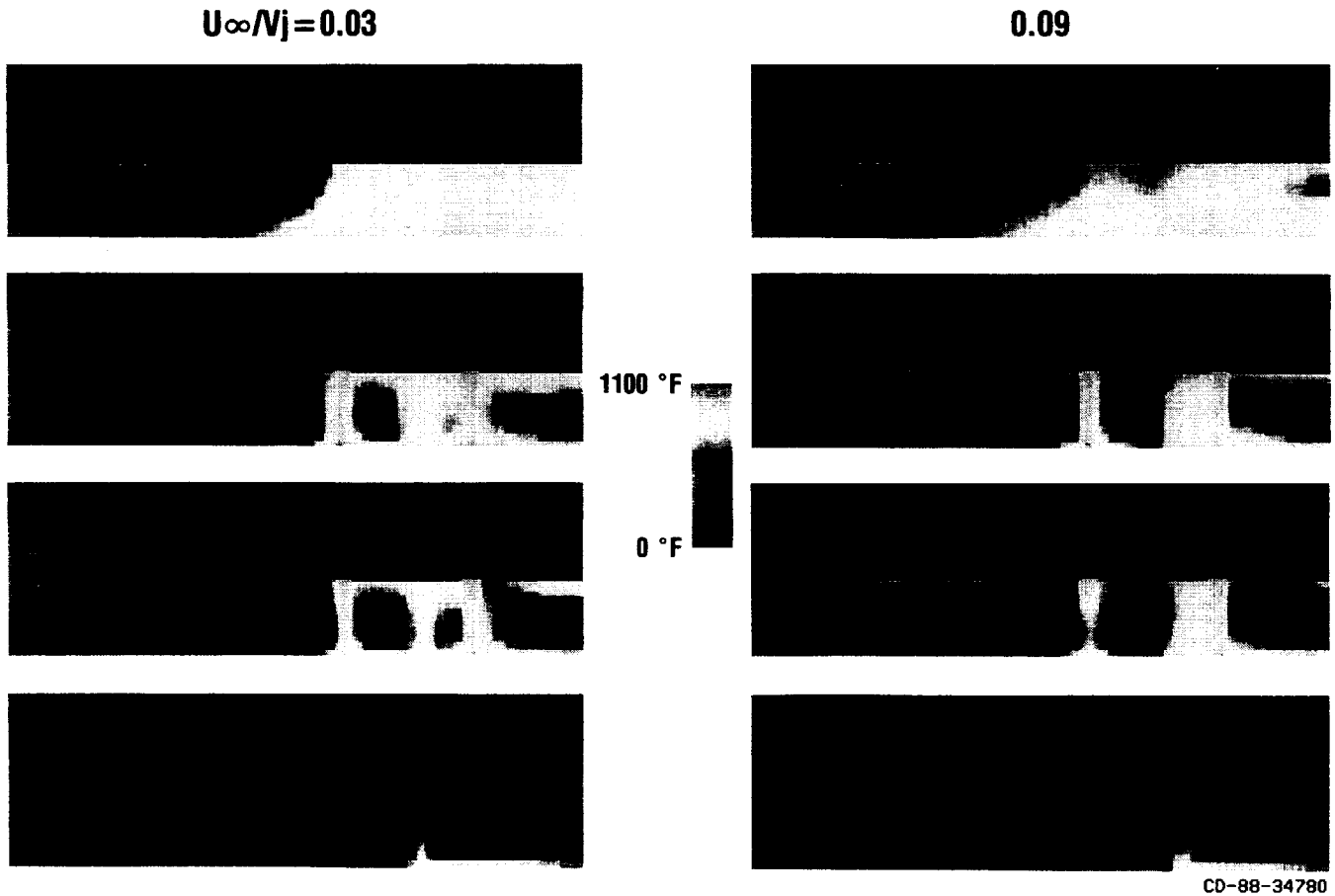

PRECEDING PAGE BLANK NOT FILMED
ORIGINAL PAGE IS OF POOR QUALITY

TEMPERATURE DISTRIBUTIONS IN VERTICAL PLANES FROM AIRCRAFT CENTERPLANE TO OUTBOARD OF FUSELAGE

($U_\infty/V_j = 0.09$)

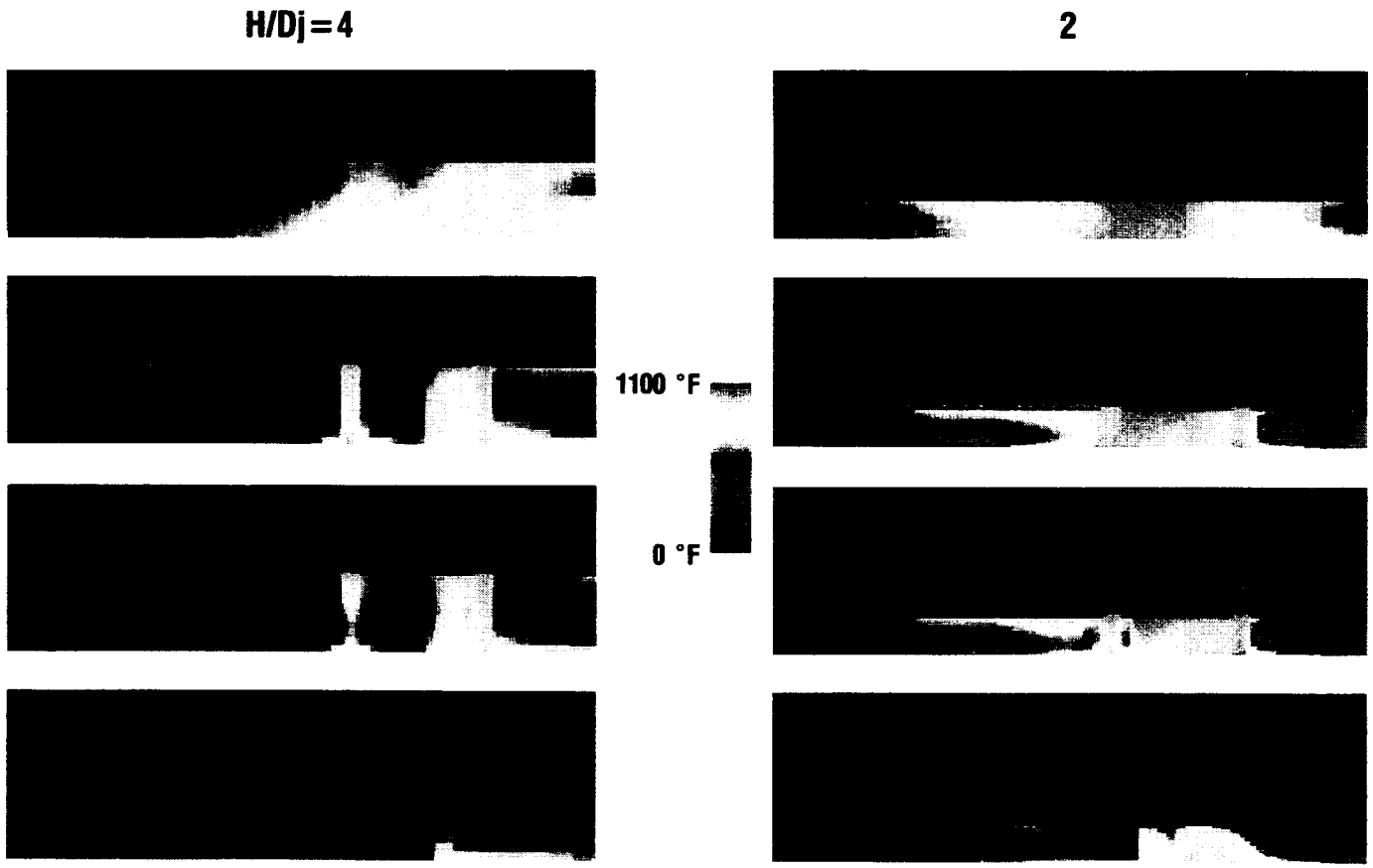

CD-88-34789

PRECEDING PAGE BLANK NOT FILMED

ORIGINAL PAGE IS OF POOR QUALITY

TEMPERATURE DISTRIBUTION IN HORIZONTAL PLANES
EFFECT OF CHANGING HEIGHT

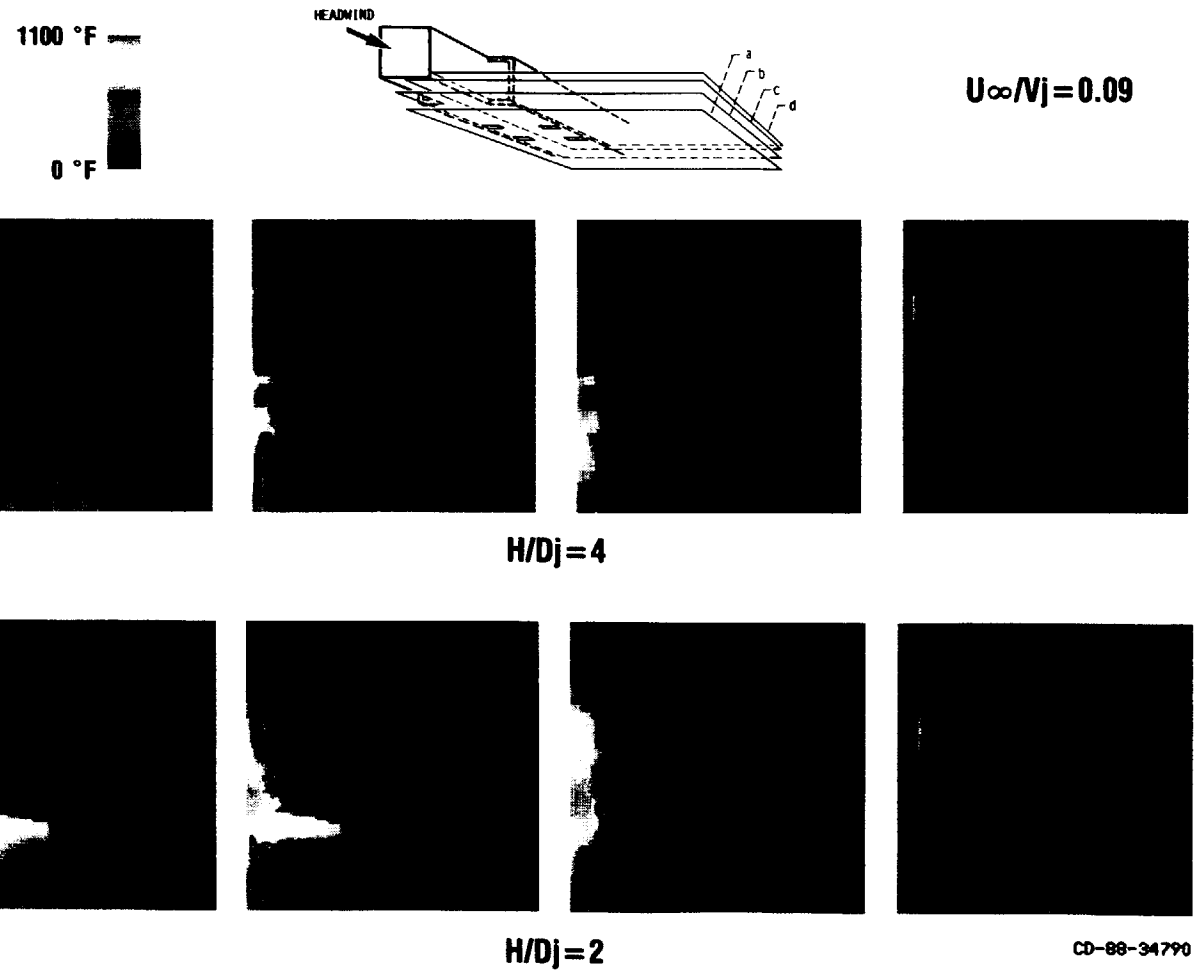

PRECEDING PAGE BLANK NOT FILMED

ORIGINAL PAGE IS
OF POOR QUALITY

PRECEDING PAGE BLANK NOT FILMED

TEMPERATURE DISTRIBUTIONS IN VERTICAL (Y-Z) PLANES THROUGH ENGINE INLET

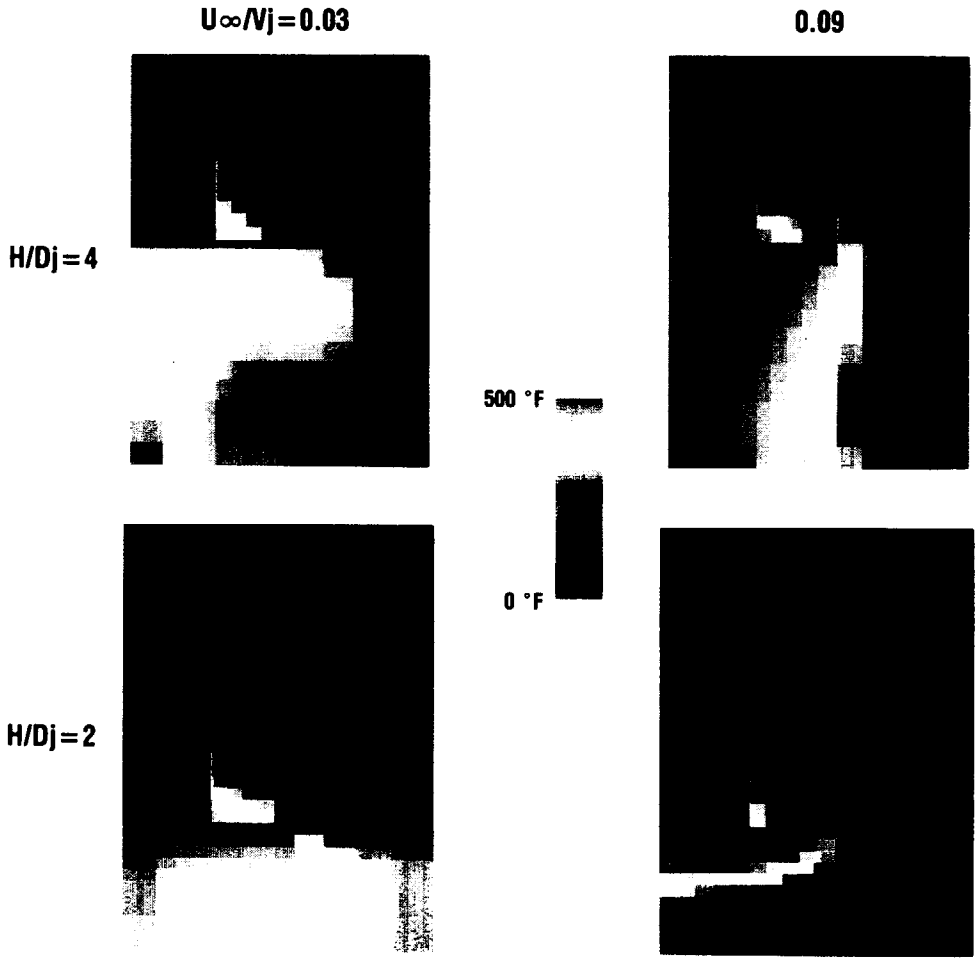

CD-88-34791

ORIGINAL PAGE IS
OF POOR QUALITY

Jet, Ambient, and Inlet
Temperatures for Cases Calculated[a]

U_∞/V_j	H/D_j	U_∞, kn	T_{avg}	T_{max}	T_{min}
0.03	4	17.8	187.7	388.2	109.8
.03	2	17.8	173.5	429.6	72.0
.09	4	53.6	145.1	469.9	61.6
.09	2	53.6	97.6	375.3	62.3

[a]At nozzle pressure ratio of 1.21; T_j = 1000; T_∞ = 70 (all temperatures are degrees F).

Average Inlet Temperatures[a]

Distance from exhaust lift jets to ground plane, H/D_j	Ratio of forward speed of aircraft (or strength of headwind) to exhaust jet velocity, U_∞/V_j	
	0.03	0.09
4	0.13	0.08
2	.11	.03

[a]$(T_{avg} - T_\infty)/(T_j - T_\infty)$

Inlet Temperature Distortion[a]

Distance from exhaust lift jets to ground plane, H/D_j	Ratio of forward speed of aircraft (or strength of headwind) to exhaust jet velocity, U_∞/V_j	
	0.03	0.09
4	0.30	0.44
2	.38	.34

[a]$(T_{max} - T_{min})/(T_j - T_\infty)$

CD-88-34961

PRECEDING PAGE BLANK NOT FILMED

SUMMARY

INTERNAL FLOW CODE CAN BE USED IN PREDICTING STOVL FLOWFIELDS

SIGNIFICANT INGESTION WAS PREDICTED IN ALL CASES CALCULATED

ALL CASES PREDICTED NEAR FIELD INGESTION

WEAKER HEADWINDS ALSO PREDICTED INGESTION BY GROUND VORTEX FLOW

N91-10888

CFD ANALYSIS FOR HIGH SPEED INLETS

Tom Benson

NASA Lewis Research Center

ABSTRACT

The increased national interest in high speed flight has increased research for high speed propulsion components. The highly three-dimensional flows present in supersonic/hypersonic inlets are currently being studied at NASA Lewis both experimentally and computationally using a family of steady PNS and NS solvers and unsteady NS solvers. This paper presents some of the results of these efforts with an emphasis on the comparison of the computational and experimental results.

The flow in high speed inlets typically involves the interaction of compression shock waves and boundary layers on the internal surfaces. The fundamentals of these interactions have been studied experimentally for many years, while more recently, computations have been used to study these complex three dimensional flow fields. Attempts to control the flow through boundary layer bleed are being investigated computationally prior to wind tunnel experiments. The ultimate goal of this research will be the higher performing inlets required for high speed flight.

CFD FOR HIGH SPEED INLETS

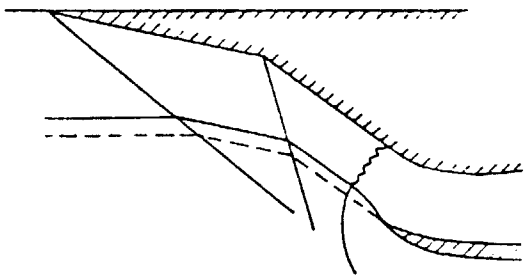

EXTERNAL COMPRESSION

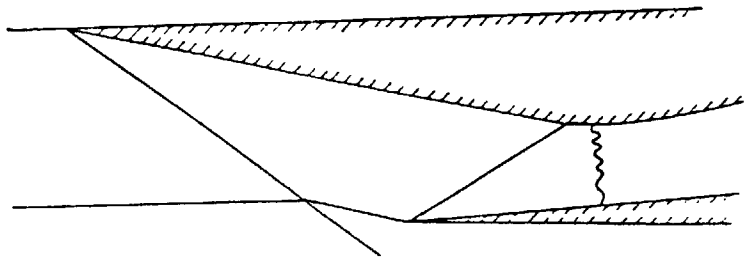

MIXED COMPRESSION

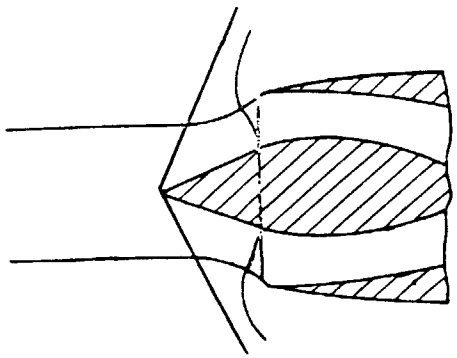

AXI-SYMMETRIC

THRUST DISTRIBUTION FOR SR-71

MACH NO	INLET	ENGINE	EJECTOR
2.2	13%	73%	14%
3. +	54%	18%	28%

CFD FOR HIGH SPEED INLETS

1.3 < MACH < 5.0

PHENOMENA

BUZZ
UNSTART
SHOCK/SHOCK INTERACTION
OBLIQUE SHOCK/BOUNDARY LAYER
NORMAL SHOCK/BOUNDARY LAYER
GLANCING SHOCK/BOUNDARY LAYER
CORNER FLOWS

All of the above with
BOUNDARY LAYER BLEED

CODES

3D PNS (PEPSIS)
- -BRILEY/MCDONALD LBI SCHEME

3D-STEADY NS (PARC)
- -BEAM/WARMING ADI

3D-UNSTEADY NS (PROTEUS)
- -BEAM/WARMING ADI
- -2nd ORDER TIME ACCURATE

CFD FOR HIGH SPEED INLETS

OBLIQUE SHOCK BOUNDARY LAYER INTERACTION

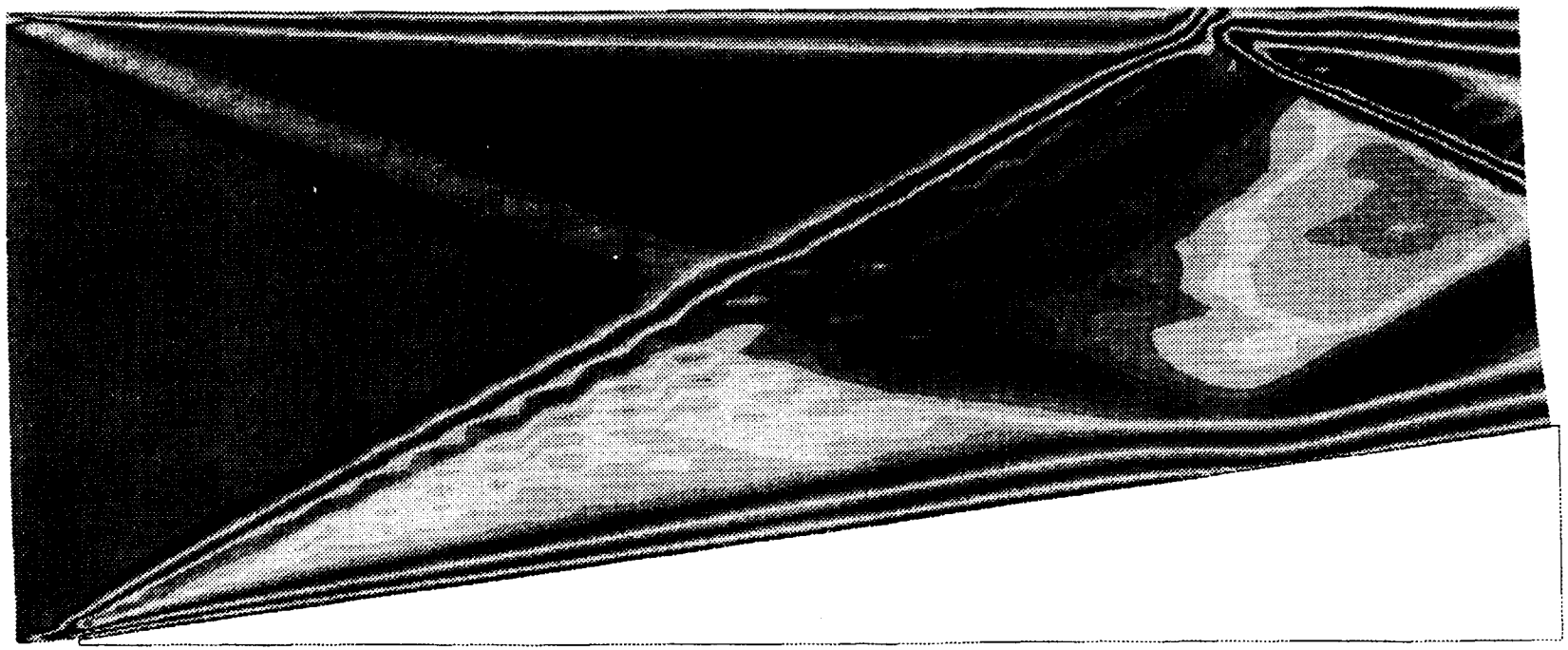

DENSITY GRADIENTS

SHOCK/BOUNDARY LAYER/BLEED INTERACTION
EXPERIMENT/COMPUTATION COMPARISON

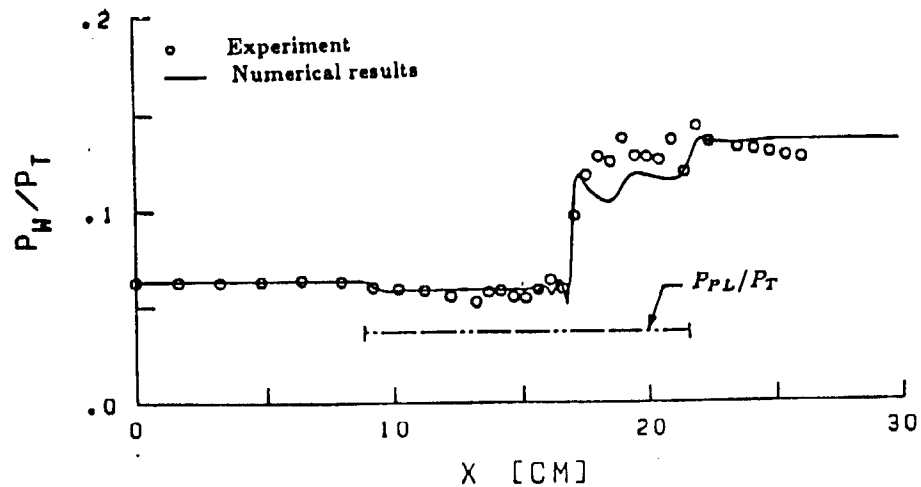

M=2.46

Ang=6.5 deg

WALL PRESSURE DISTRIBUTION

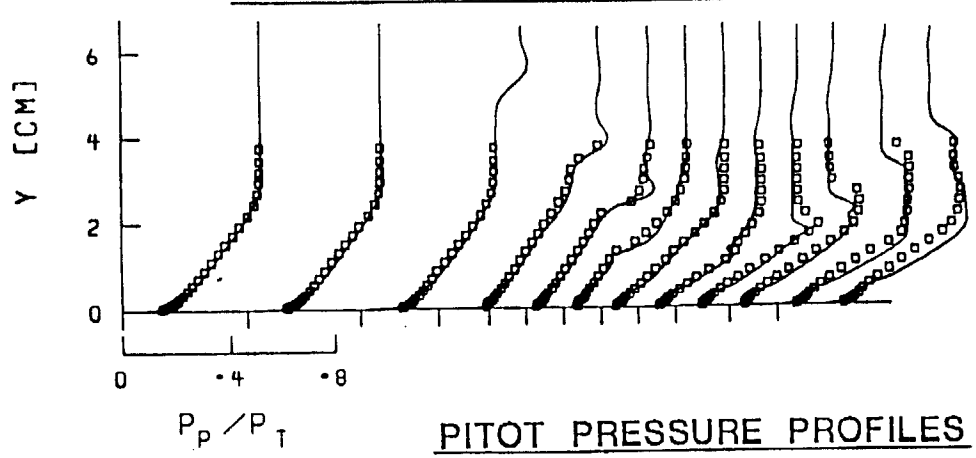

PITOT PRESSURE PROFILES

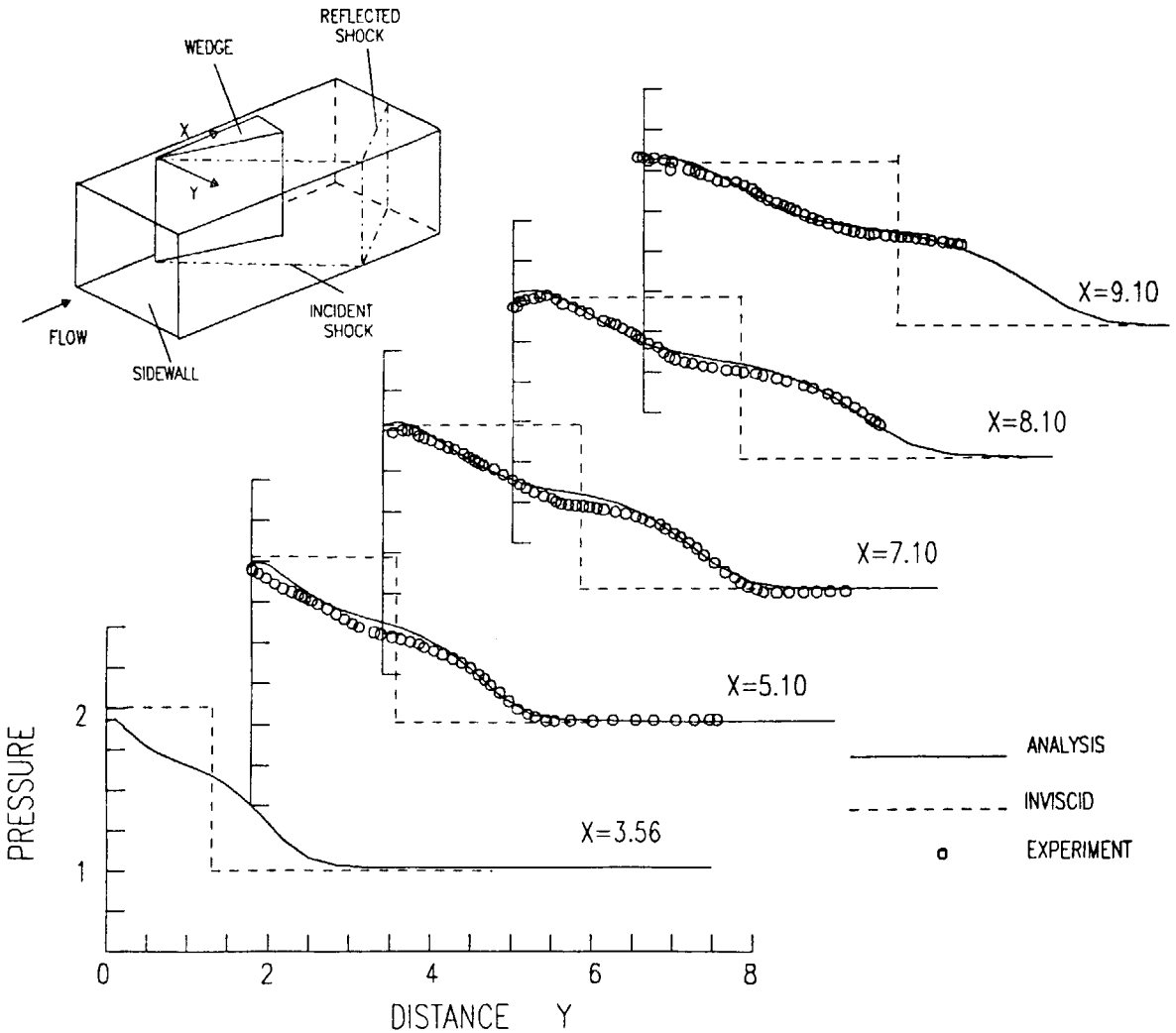
REFLECTED SHOCK
WEDGE
X
Y
FLOW
SIDEWALL
INCIDENT SHOCK
X=9.10
X=8.10
X=7.10
X=5.10
X=3.56
PRESSURE
2
1
0
2
4
6
8
DISTANCE Y
ANALYSIS
INVISCID
EXPERIMENT

CFD FOR HIGH SPEED INLETS

MACH 5.0 INLET
STREAMLINE TRACES

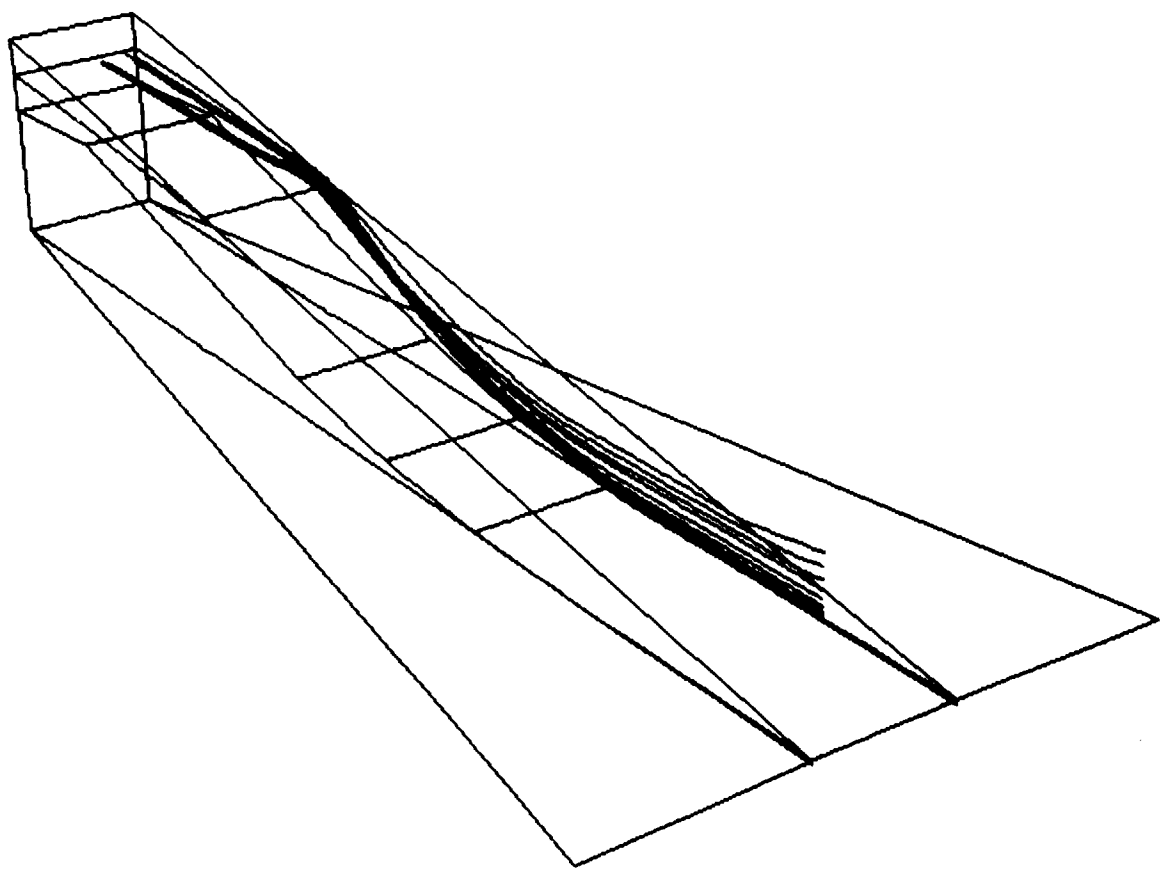

CFD FOR HIGH SPEED INLETS

SUMMARY

Combined computational/experimental investigation has identified importance of 3D shock/boundary layer interactions for rectangular inlets at high speeds

Possible control of glancing shock/boundary layer interaction through bleed now being explored. Little success to date.

Understanding of three dimensional interactions may lead to better methods of flow control in inlets.

ORIGINAL CONTAINS
COLOR ILLUSTRATIONS

N91-10889

THE USE OF A NAVIER-STOKES CODE IN THE WING DESIGN PROCESS

S. Naomi McMillin
NASA Langley Research Center
Hampton, Virginia 23665-5225

Abstract of Paper Presented at the
NASA Computational Fluid Dynamics Conference
NASA Ames Research Center
March 6-9, 1989

An ongoing investigation is being conducted in the Supersonic/Hypersonic Aerodynamics Branch at NASA Langley Research Center to determine the feasibility of incorporating the Navier-Stokes computational code, CFL3D, into the supersonic wing design process. The approach taken in this investigation is of two steps.

The first step was to calibrate CFL3D against existing experimental data sets obtained on thin sharp-edged delta wings. The experimental data identified six flow types which are dependent on the similarity parameters of Mach number and angle of attack normal to the leading edge. The calibration showed CFL3D capable of simulating these various separated and attached-flow conditions.

The second step was to use CFL3D to study the initial formation of leading-edge separation over delta wings at supersonic speeds. This study consisted of examining solutions obtained on a 65° delta wing at Mach number of 1.6 with varying cross-sectional shapes. Reynolds number was held constant at 1000000 and the Baldwin-Lomax turbulence model was used. The study showed that through the use of leading-edge radius and/or camber, the onset of leading-edge separation can be delayed to a higher angle of attack than observed on a flat sharp-edged wing.

Based on the geometries studied, three wind-tunnel models are being designed to verify these results. These models are to be tested over a Reynolds number range of 2×10^6/foot to 8.5×10^6/foot.

NOT FILMED

Fig. 1 The objective and approach for the present investigation.

Fig. 2 CFL3D code characteristics.

Fig. 3 Sketches of the wind-tunnel models tested by Miller and Wood in the Langley Unitary Plan Wind Tunnel (NASA TP-2430).

Fig. 4 The types of flow classified from the Miller and Wood experimental test (NASA TP-2430).

Fig. 5 The computational test matrix at M = 2.8 superimposed on the chart which defines the flow types as functions of α and M normal to the leading edge.

Fig. 6 A comparison of computational results with experimental data for the 75° delta wing at $\alpha = 8^{\circ}$ and M = 2.80 (AIAA 87-2270).

Fig. 7 The major elements of the incipient separation study (second step of approach).

Fig. 8 Computational results which quantify the effects of leading-edge radius at $\alpha = 4^{\circ}$.

Fig. 9 Computational results which quantify the effects of leading-edge radius at $\alpha = 8^{\circ}$.

Fig. 10 Computational results which quantify the effects of camber at $\alpha = 8^{\circ}$.

Fig. 11 A summary on the effects of leading-edge radius and camber on a 65° delta wing at M = 1.6.

Fig. 12 Major element of proposed wind-tunnel test.

Fig. 13 Concluding remarks.

OBJECTIVE

- To determine the feasibility of incorporating the Navier - Stokes computational code, CFL3D, into the supersonic wing design process.

APPROACH

- Calibrate CFL3D with experimental data obtained on flat sharp-edged delta wings at supersonic speeds (AIAA 87-2270). Parameters:
    - leading edge sweep
    - angle of attack
    - Mach number
- Use CFL3D to study the initial formation of leading edge separation on delta wings. Geometric parameters:
    - leading edge radius
    - camber

CFL3D CODE CHARACTERISTICS

- Developed at NASA-LaRC by Jim Thomas
- Unsteady conservation-law form of compressible Navier-Stokes equations (thin layer laminar viscous model)
- Laminar viscous model or Baldwin-Lomax eddy viscosity turbulence model
- Upwind-biased spacial differencing implemented in finite volume form
    - Upwind (flux split) for convective terms and pressure
    - Central for shear stress/heat transfer
    - 2nd order accurate
- Implicit time differencing
    - Streamwise relaxation/cross-flow ADI
    - 1st order accurate
- Conical solutions obtained by 3-D solution
    - Single array of conically constructed volumes
    - Inflow equal outflow
- Grids generated using an elliptic grid generation method, 121 x 93 grid required to resolve details of flow patterns

LEE-SIDE FLOW FLAT DELTA MODELS

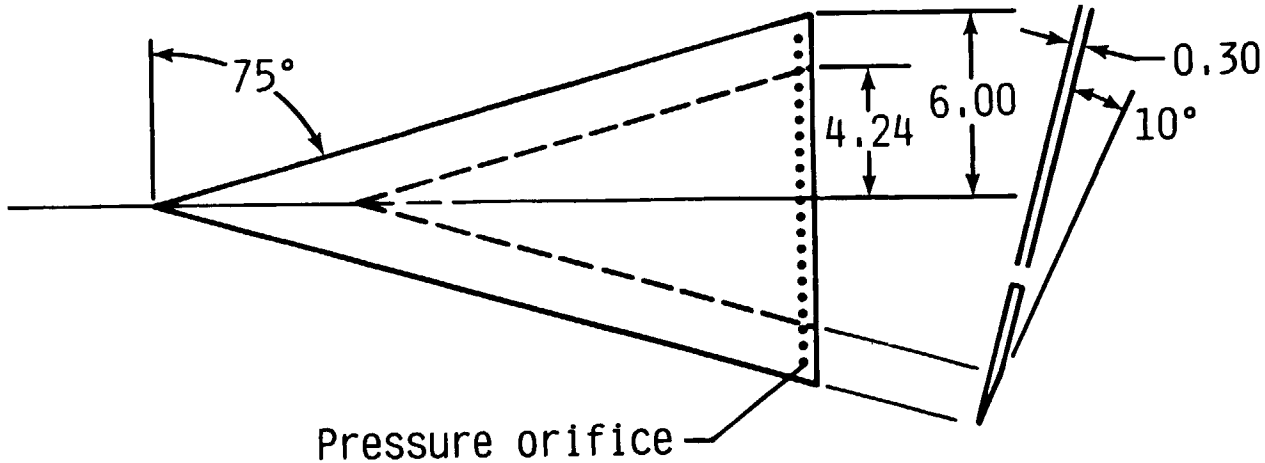

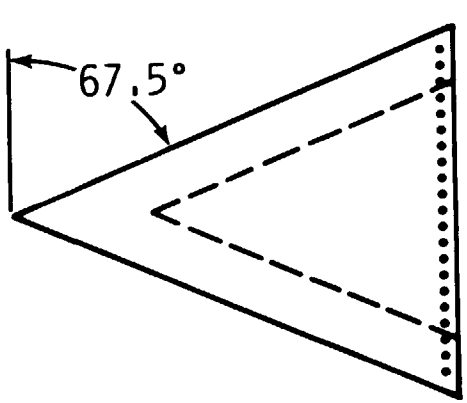

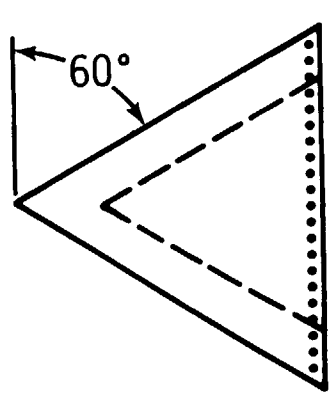

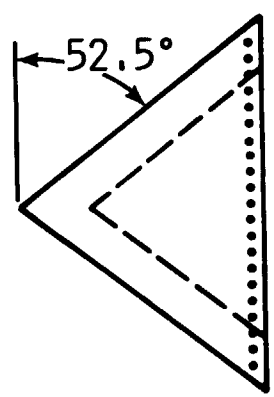

FLOW CLASSIFICATIONS

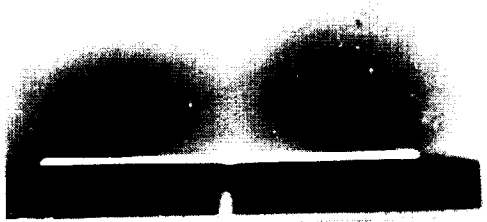

CLASSICAL VORTEX

VORTEX WITH SHOCK

SHOCK-INDUCED SEPARATION

NO SHOCK/NO SEPARATION

SHOCK WITH NO SEPARATION

SEPARATION BUBBLE WITH NO SHOCK

SEPARATION BUBBLE WITH SHOCK

THEORETICAL TEST MATRIX

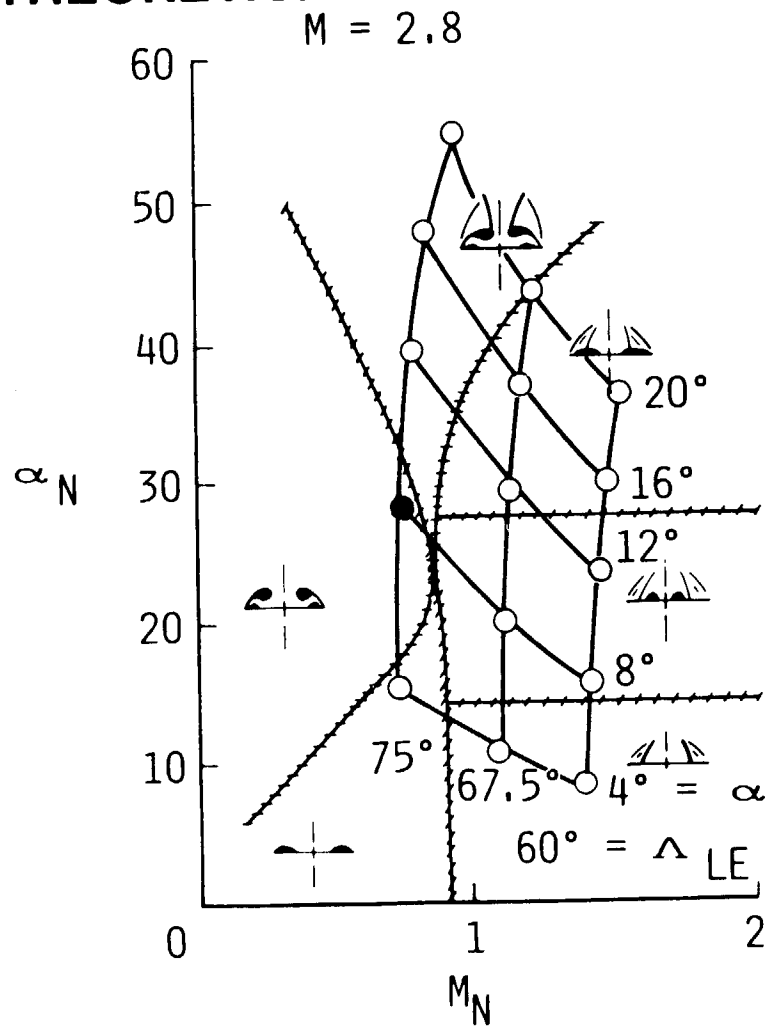

PRECEDING PAGE BLANK NOT FILMED

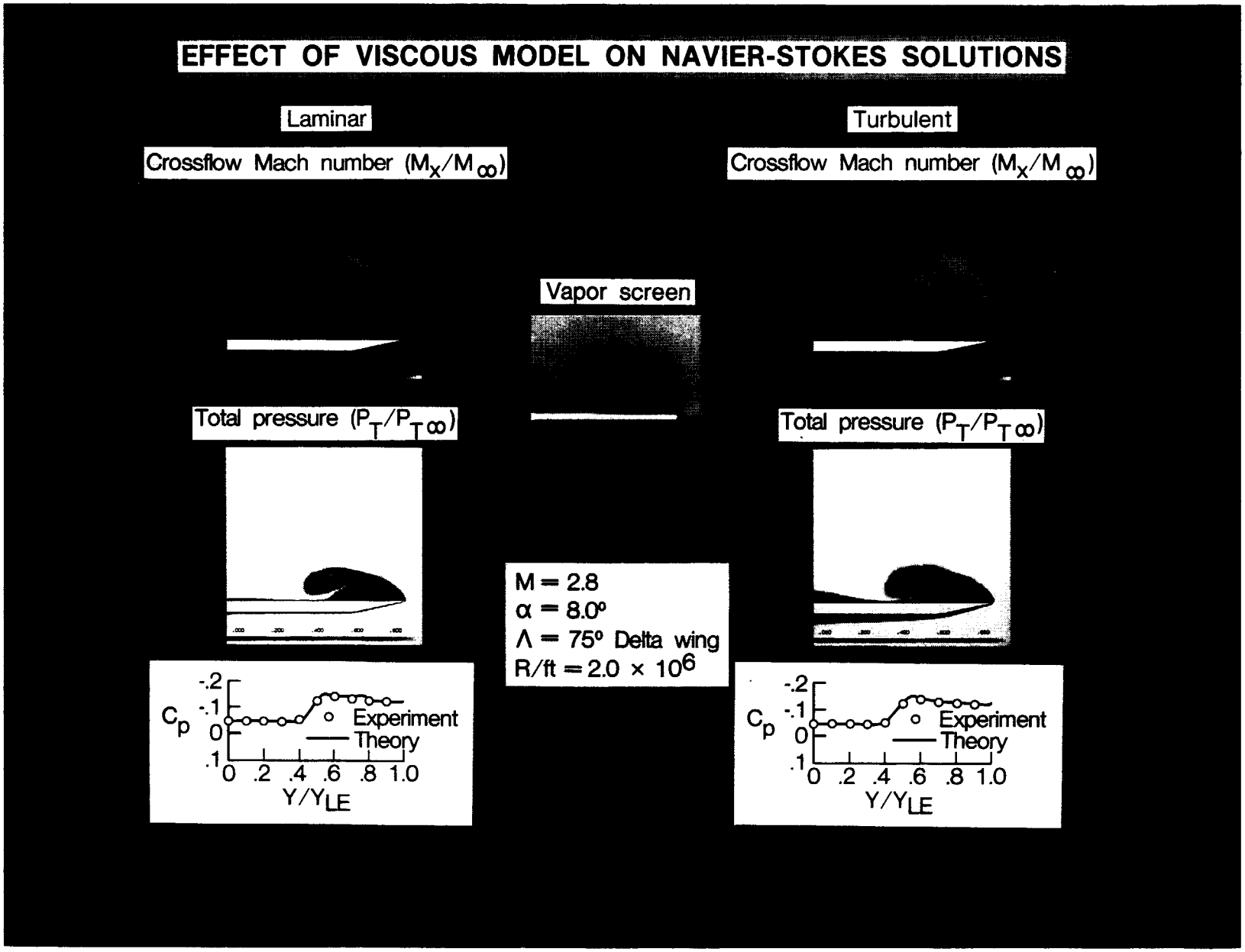

ORIGINAL PAGE IS
OF POOR QUALITY

PRECEDING PAGE BLANK NOT FILMED

INCIPIENT SEPARATION STUDY

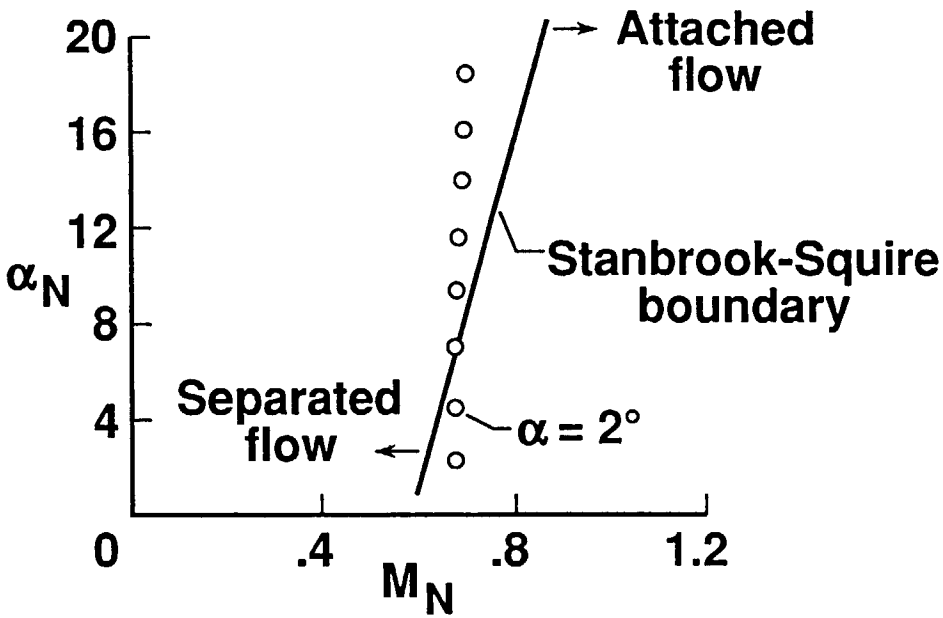

Examine effects of

- Leading edge radius
- Camber
- Angle of attack
- Reynolds number

On the formation of leading edge separation on a conical 65° delta wing at M = 1.6

Parametric cross-sections

Leading edge radius:

Sharp

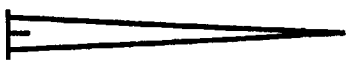

r/(b/2) = 0.0025 (20:1 ellipse)

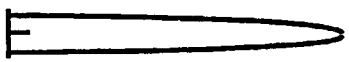

r/(b/2) = 0.0100

Camber (20:1 ellipse)

4° camber

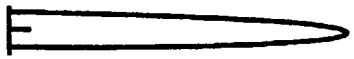

8° camber

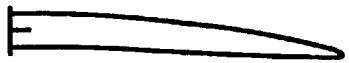

10° camber

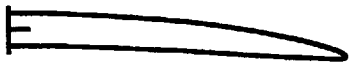

EFFECT OF LEADING EDGE RADIUS

$\alpha = 4°$

$M = 1.6 \quad \Lambda = 65° \quad Re = 1\,000\,000$
Turbulent boundary layer

Sharp	$\frac{r}{b/2} = 0.0025$ (20:1 ellipse)	$\frac{r}{b/2} = 0.01$

Total pressure:

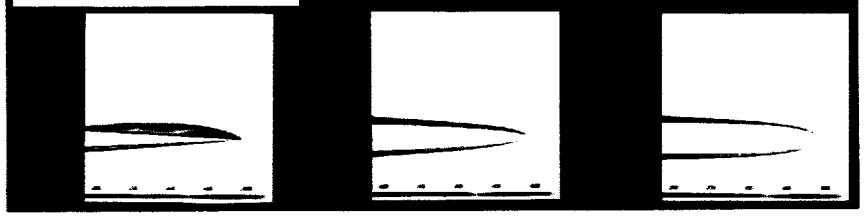

Crossflow Mach number:

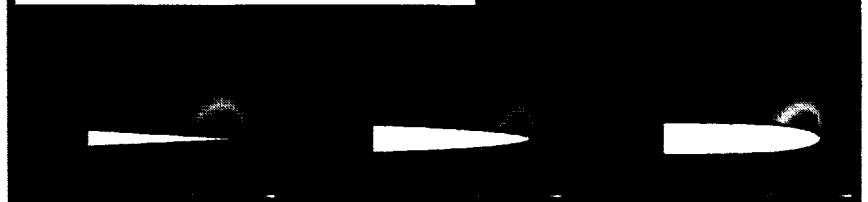

Surface pressure:

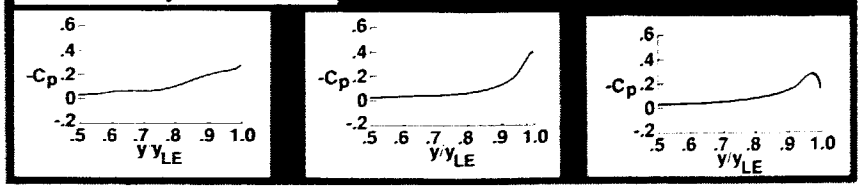

PRECEDING PAGE BLANK NOT FILMED

ORIGINAL PAGE IS
OF POOR QUALITY

EFFECT OF LEADING EDGE RADIUS

$\alpha = 8°$

$M = 1.6 \quad \Lambda = 65° \quad Re = 1\,000\,000$
Turbulent boundary layer

Sharp

$\frac{r}{b/2} = .0025$
(20:1 ellipse)

$\frac{r}{b/2} = .01$

Total pressure:

Crossflow Mach number:

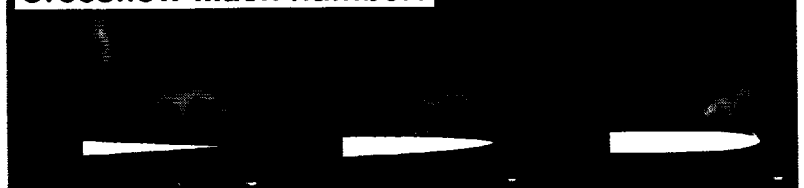

Surface pressure:

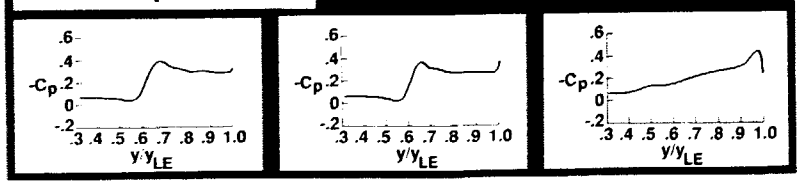

PRECEDING PAGE BLANK NOT FILMED

ORIGINAL PAGE IS
OF POOR QUALITY

PRECEDING PAGE BLANK NOT FILMED

EFFECT OF CAMBER

$\alpha = 8°$

$M = 1.6 \quad \Lambda = 65° \quad Re = 1\,000\,000$
Turbulent boundary layer

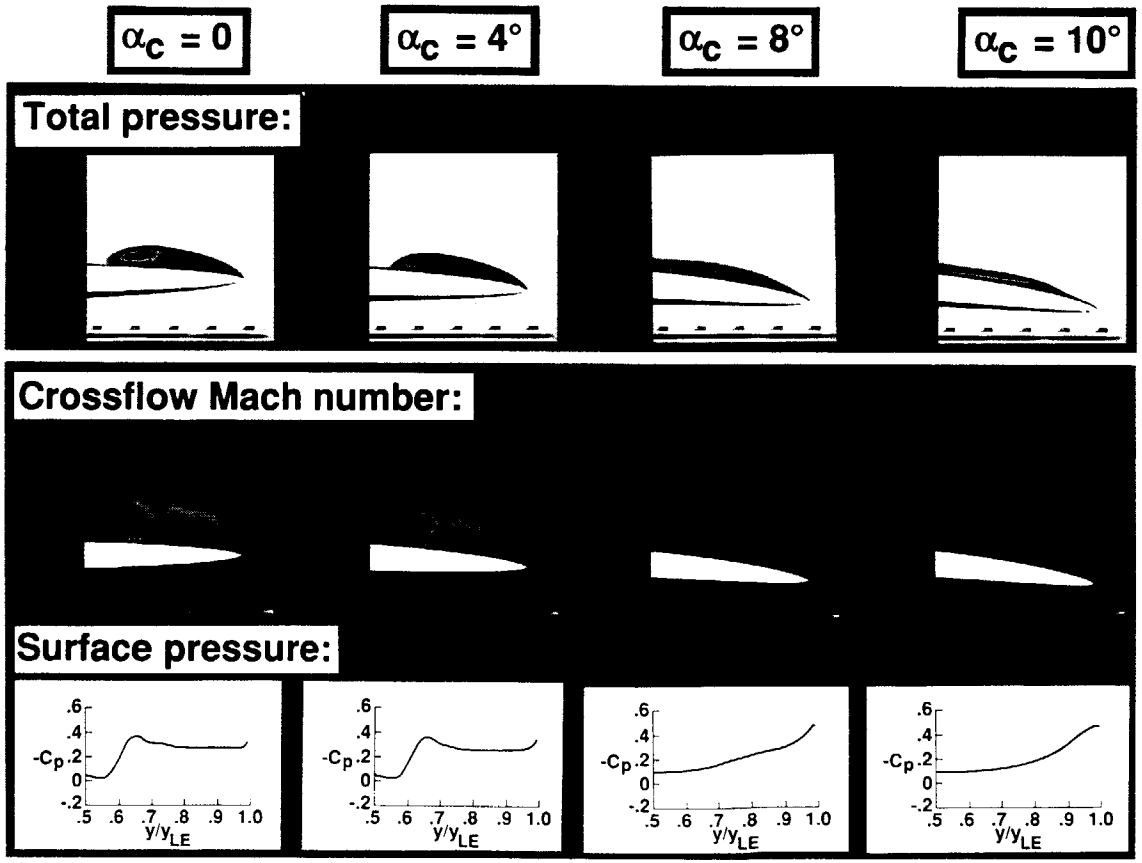

ORIGINAL PAGE IS
OF POOR QUALITY

PRECEDING PAGE BLANK NOT FILMED

INCIPIENT SEPARATION COMPUTATIONAL STUDY

$M = 1.6$, $\Lambda = 65°$, $Re = 1 \times 10^6$
Turbulent boundary layer
color contour plots-crossflow Mach number

Sharp leading edge

Rounded leading edge
no camber

10° camber

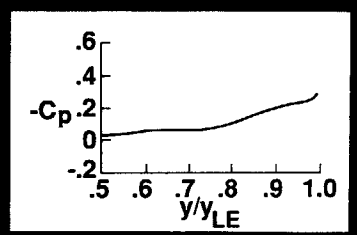

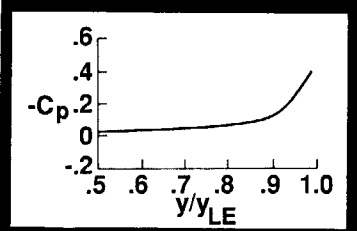

$\alpha = 4°$

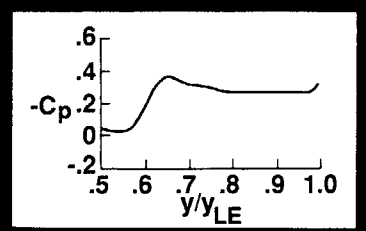

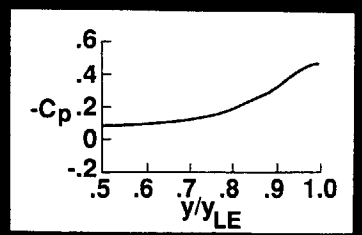

$\alpha = 8°$

PRECEDING PAGE BLANK NOT FILMED

WIND TUNNEL MODELS

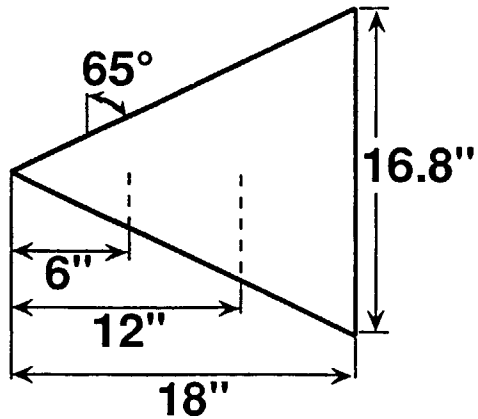

Cross-sections:

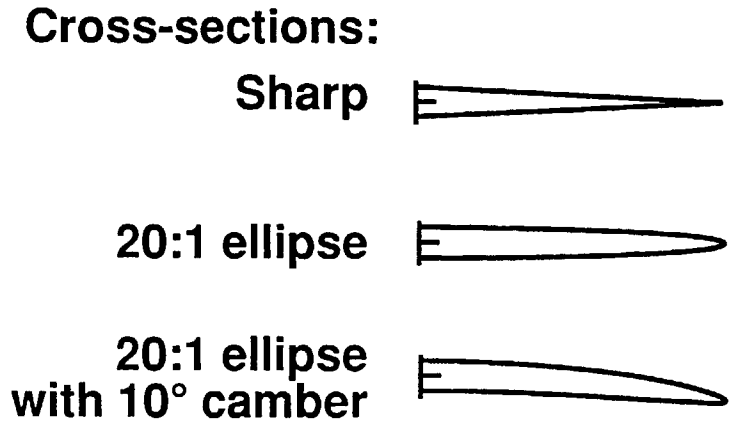

Wind Tunnel Test Description

- M = 1.6; α = 0° to 8° (initial conditions)
- Surface pressure data (~100 ports)
- Vapor screen photographs
- Oil flows
- Unitary Plan Wind Tunnel
  R e = 2 x 10^6 /foot, 5 x 10^6 /foot
- 20" Supersonic Wind Tunnel
  R e = 2 x 10^6 /foot, 8.5 x 10^6 /foot

CLOSING REMARKS

- The six distinct flow types observed over delta wings at supersonic speeds have been computationally reproduced using CFL3D (AIAA 87-2270)

- CFL3D has been used to quantify the effects of leading edge radius and camber on leading edge separation. Wind tunnel test designed to confirm these results.

N91-10890

APPLICATIONS OF A TRANSONIC WING DESIGN METHOD

by

Richard L. Campbell and Leigh A. Smith
NASA Langley Research Center

ABSTRACT

The development of transonic computational fluid dynamic methods over the last fifteen years has had a tremendous impact on the design of airfoils and wings. A variety of approaches to automated design have been developed, such as the hodograph and fictitious gas methods for shock-free design, and inverse, numerical optimization, and predictor/corrector methods for the more general cases. Each of these techniques has advantages as well as limitations, and the designer must choose the one that best suits his specific task.

A method for designing wings and airfoils at transonic speeds using a predictor/corrector approach has been developed. The procedure iterates between an aerodynamic code, which predicts the flow about a given geometry, and the design module, which compares the calculated and target pressure distributions and modifies the geometry using an algorithm that relates differences in pressure to a change in surface curvature. The modular nature of the design method makes it relatively simple to couple it to any analysis method. The iterative approach allows the design process and aerodynamic analysis to converge in parallel, significantly reducing the time required to reach a final design. Viscous and static aeroelastic effects can also be accounted for during the design or as a post-design correction.

Results from several pilot design codes indicated that the method accurately reproduced pressure distributions as well as the coordinates of a given airfoil or wing by modifying an initial contour. The codes were applied to supercritical as well as conventional airfoils, forward- and aft-swept transport wings, and moderate-to-highly swept fighter wings. The design method was found to be robust and efficient, even for cases having fairly strong shocks. Comments from a user in industry indicated that for a specific design problem, this design method was about 25 times faster than a numerical optimization approach that utilized the same aerodynamic analysis code.

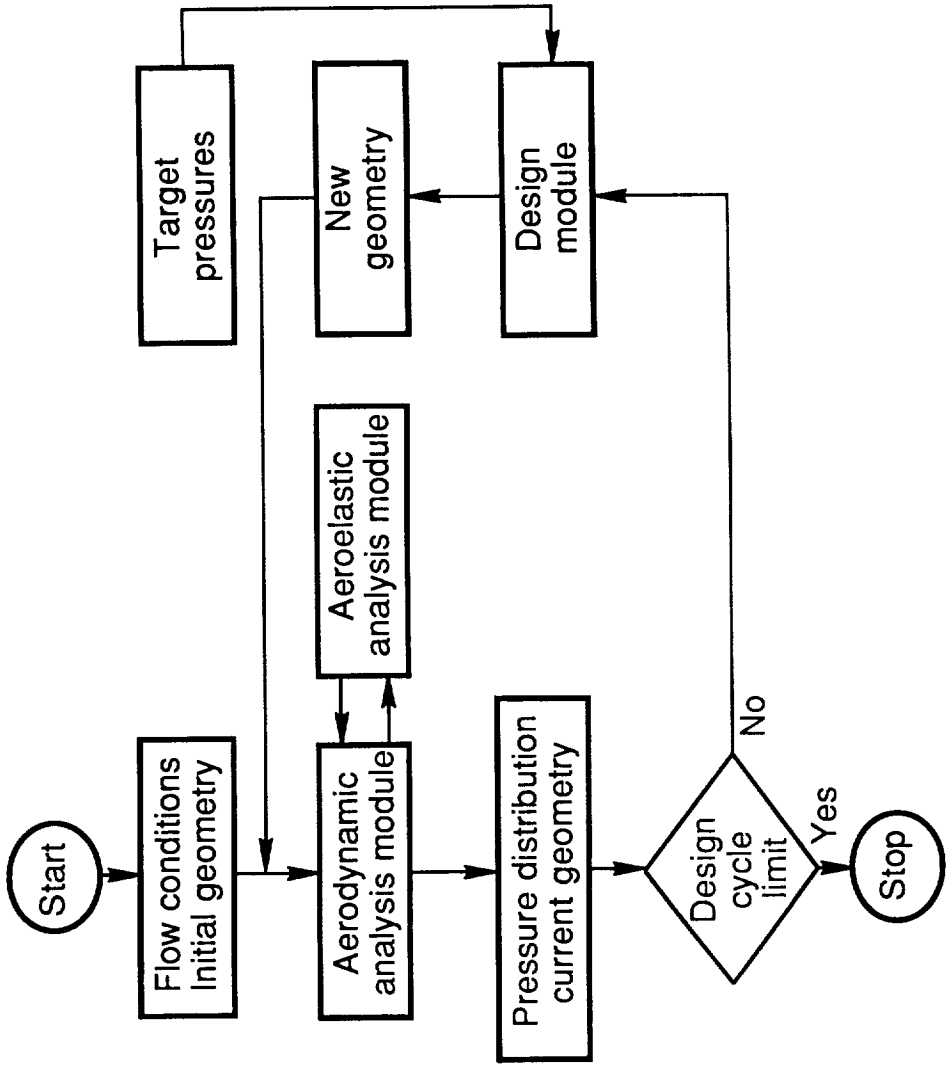
Start
Flow conditions
Initial geometry
Target
pressures
Aerodynamic
analysis module
Aeroelastic
analysis module
New
geometry
Pressure distribution
current geometry
Design
module
Design
cycle
limit
No
Yes
Stop

HYBRID DESIGN ALGORITHM

- Subsonic regions

$$\Delta C = \Delta C_P \; A (1 + C^2)^B$$

- Supersonic regions ($M > 1.15$)

$$\Delta C = \frac{0.05\,A}{(1 + (y')^2)^{1.5}} \frac{d}{dx} (\Delta C_P)$$

SUPERCRITICAL AIRFOIL DESIGN

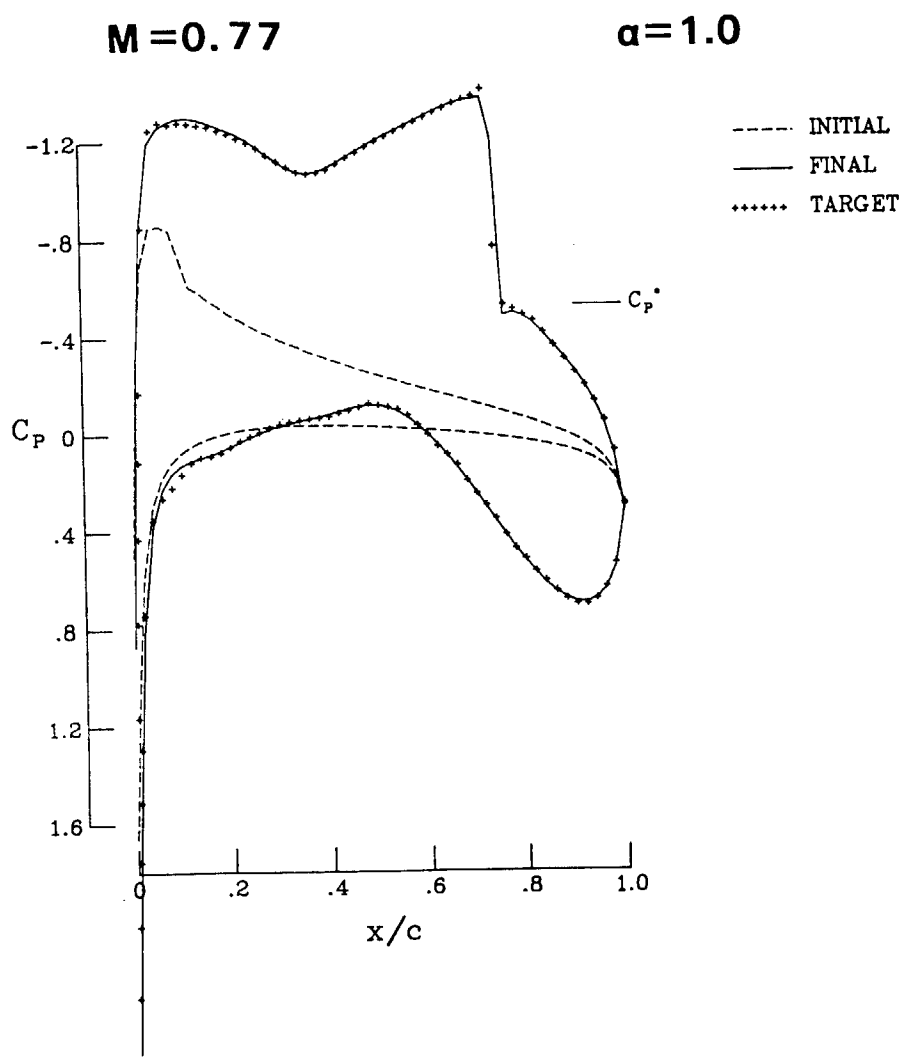

SUPERCRITICAL AIRFOIL DESIGN

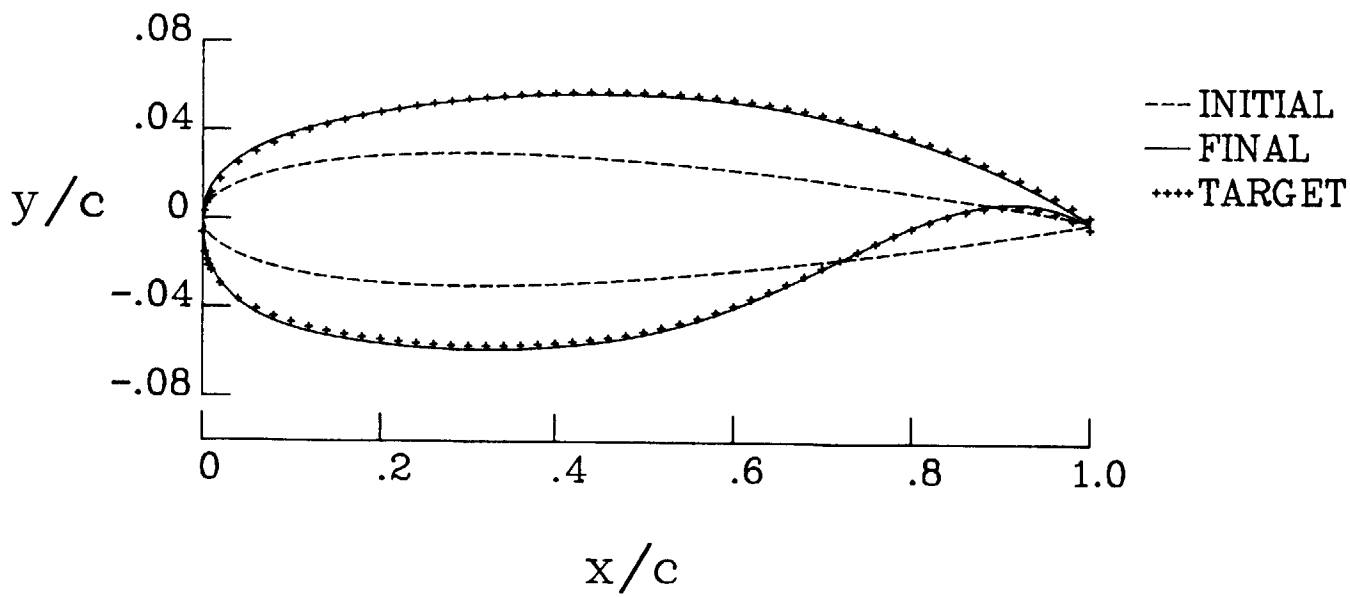

NYU CODE- PARTIAL AIRFOIL MODIFICATION

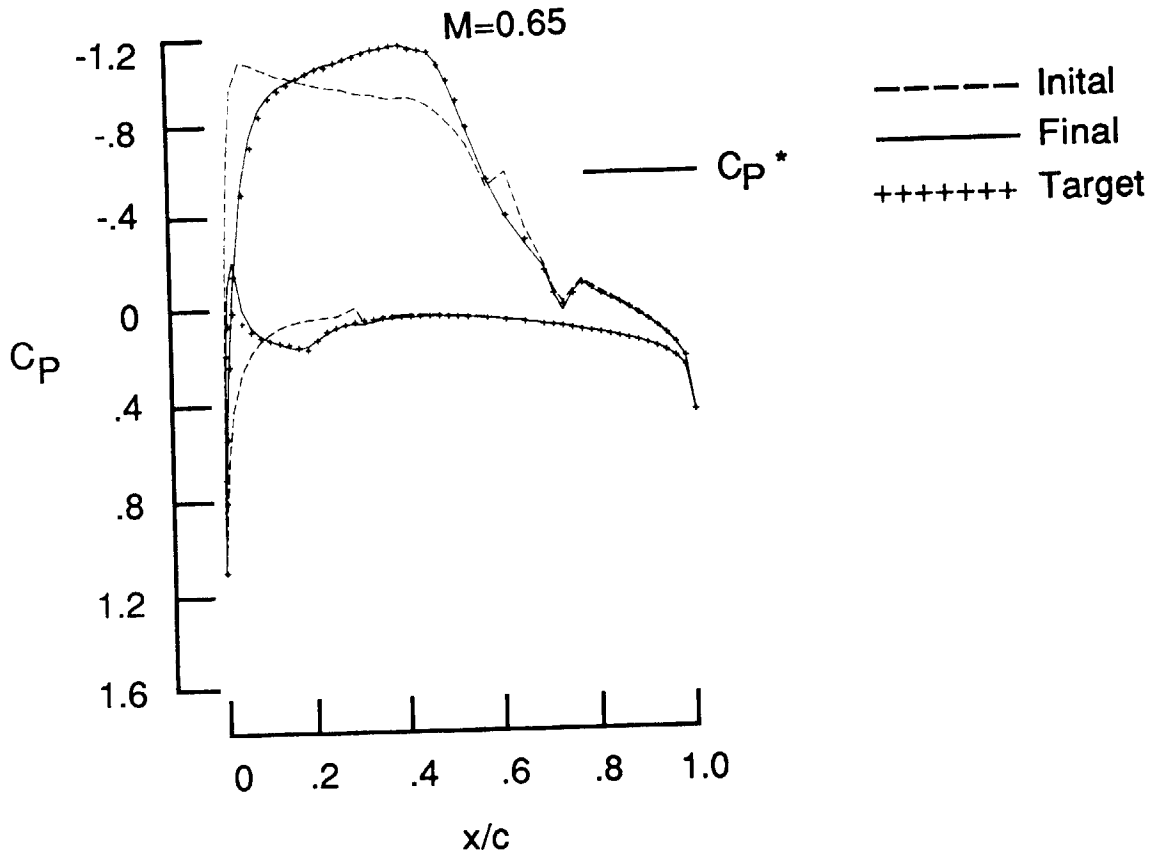

NYU CODE- PARTIAL AIRFOIL MODIFICATION

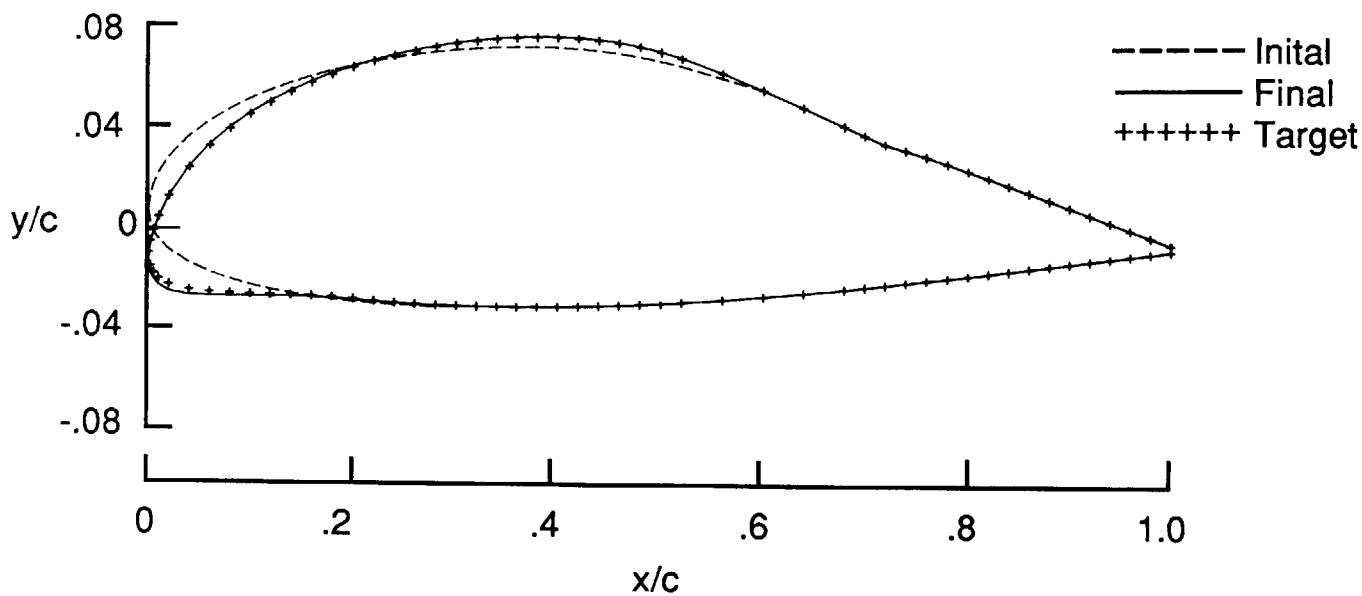

EXECUTIVE JET DESIGN

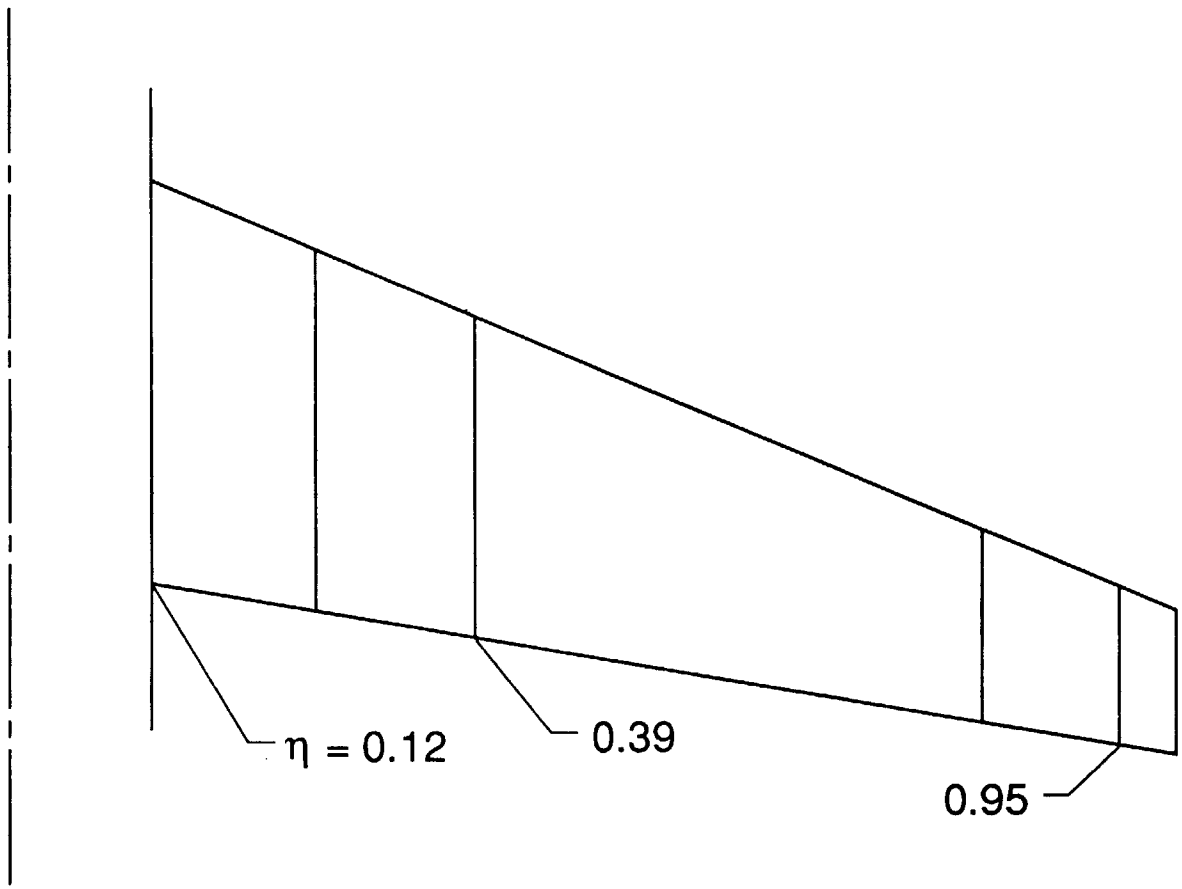

EXECUTIVE JET DESIGN

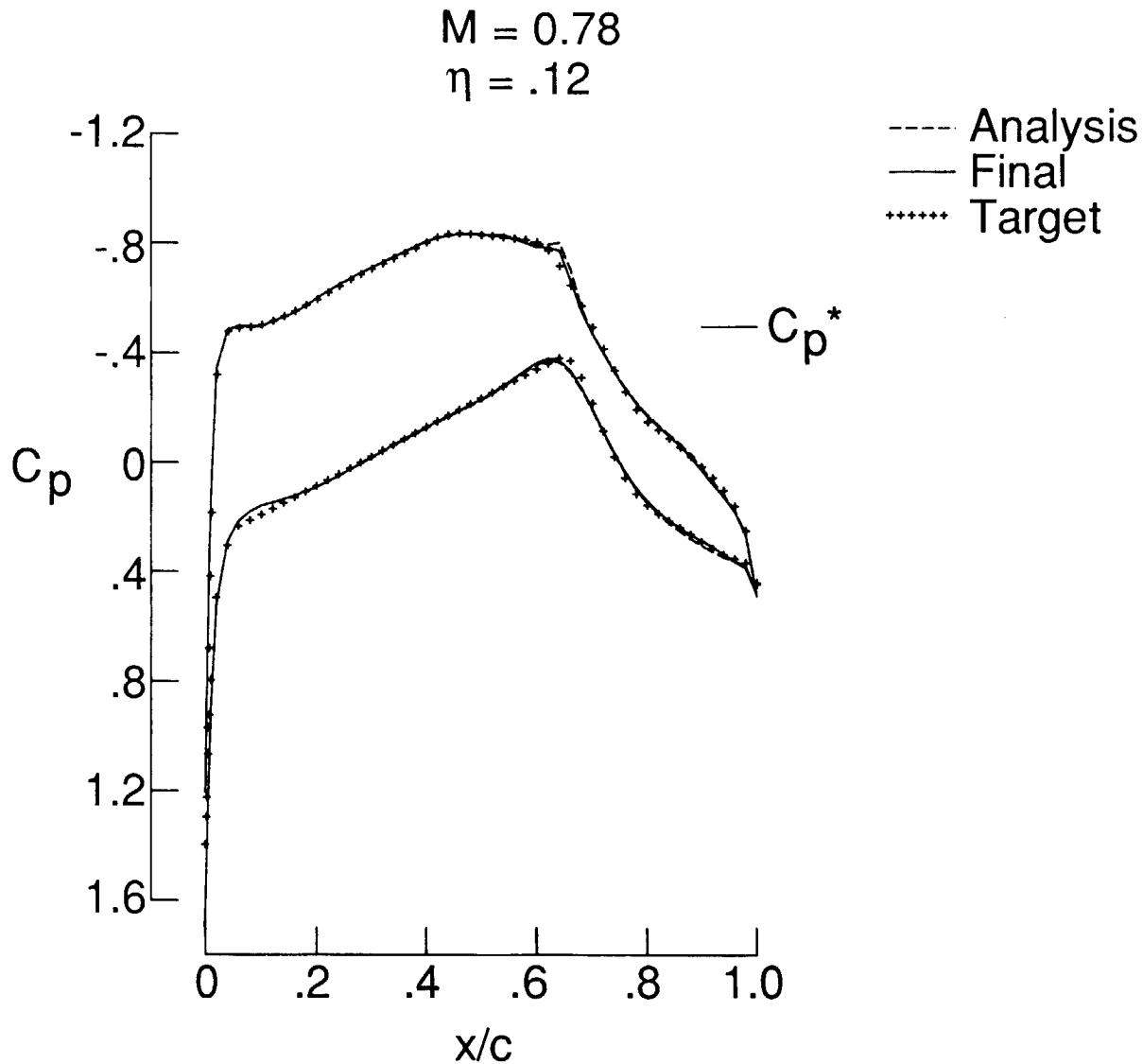

EXECUTIVE JET DESIGN

$M = 0.78$
$\eta = .12$

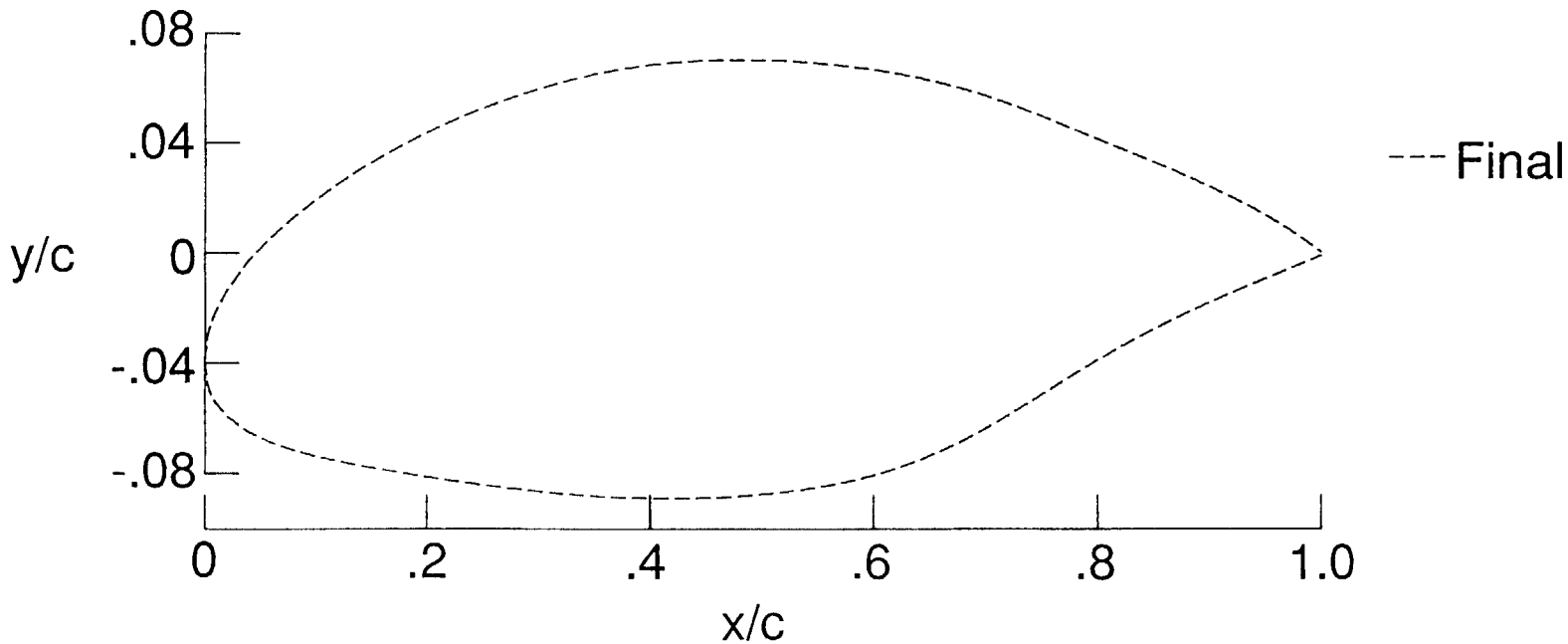

HIGHLY SWEPT FIGHTER WING GEOMETRY

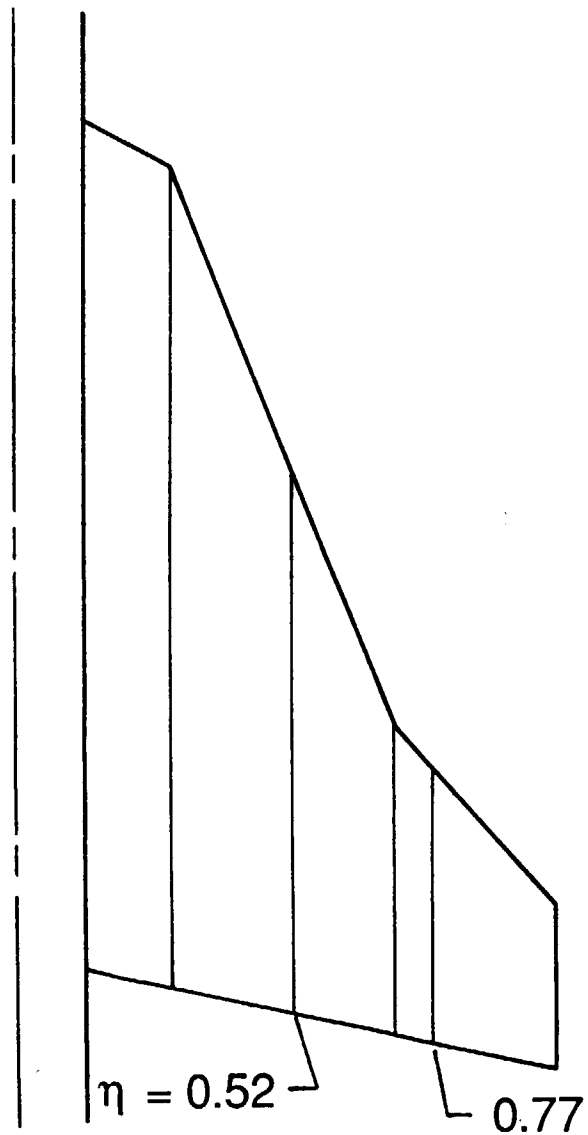

HIGHLY-SWEPT FIGHTER WING CASE

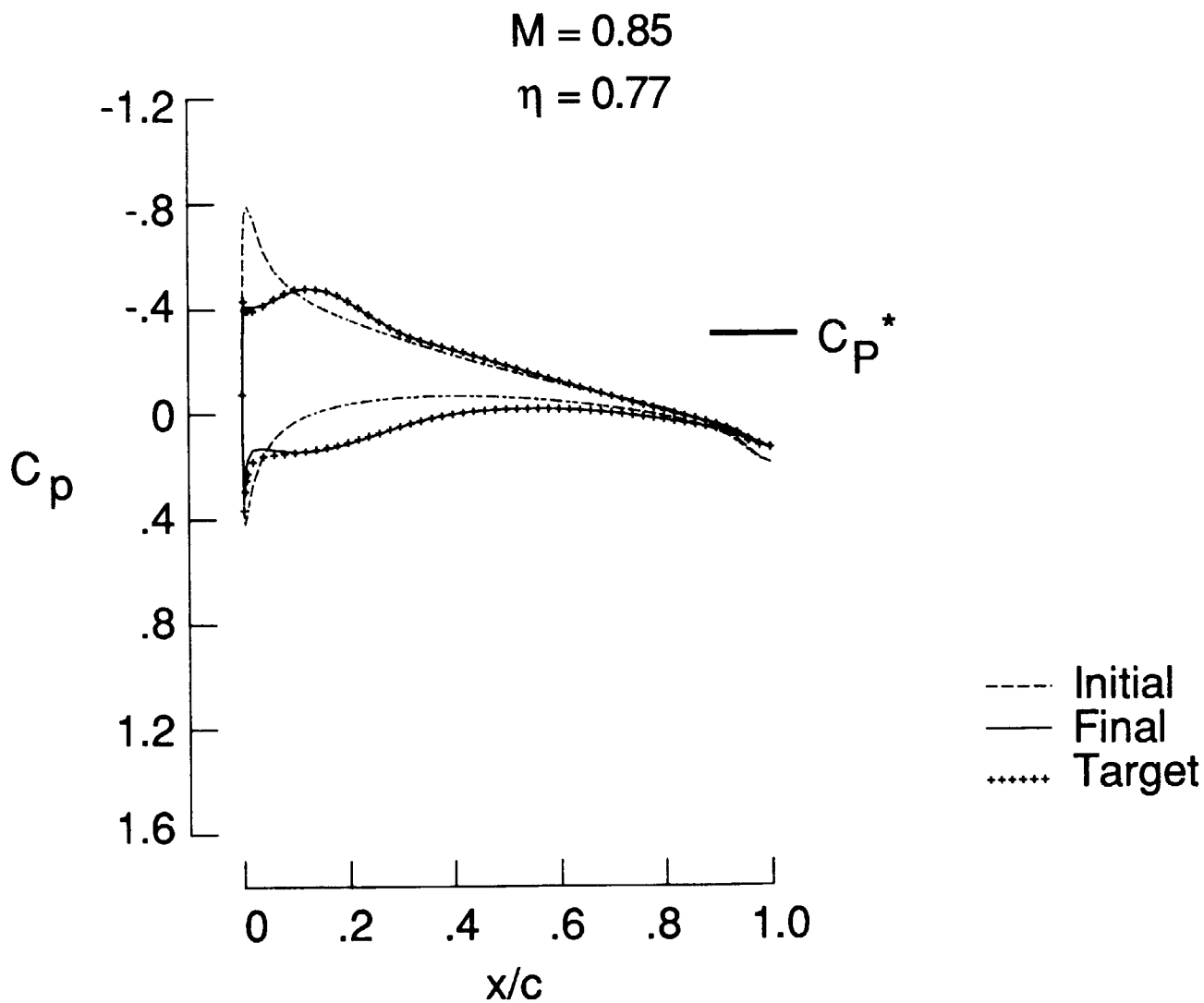

HIGHLY-SWEPT FIGHTER WING CASE

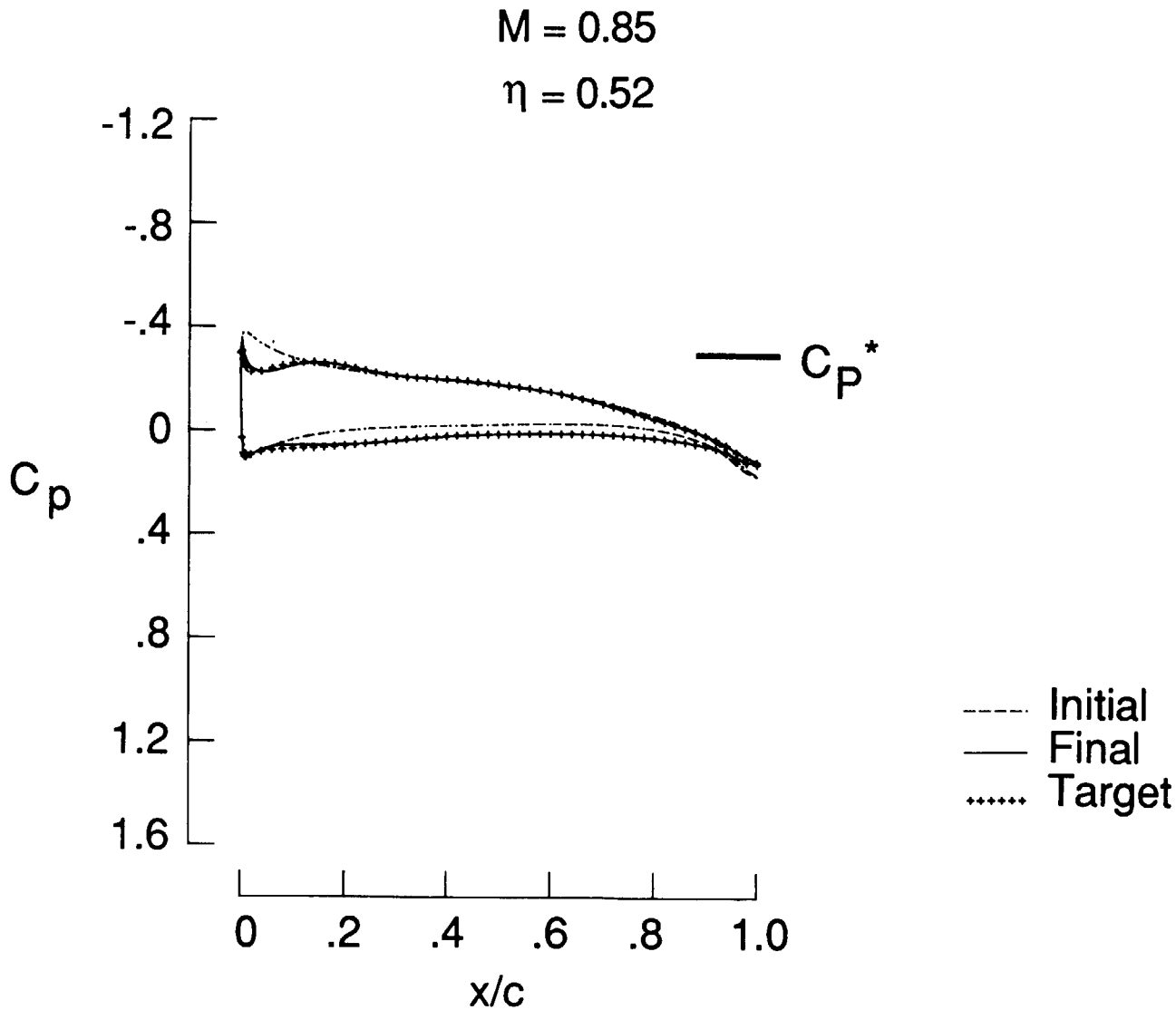

HIGHLY-SWEPT FIGHTER WING CASE

$\eta = 0.77$

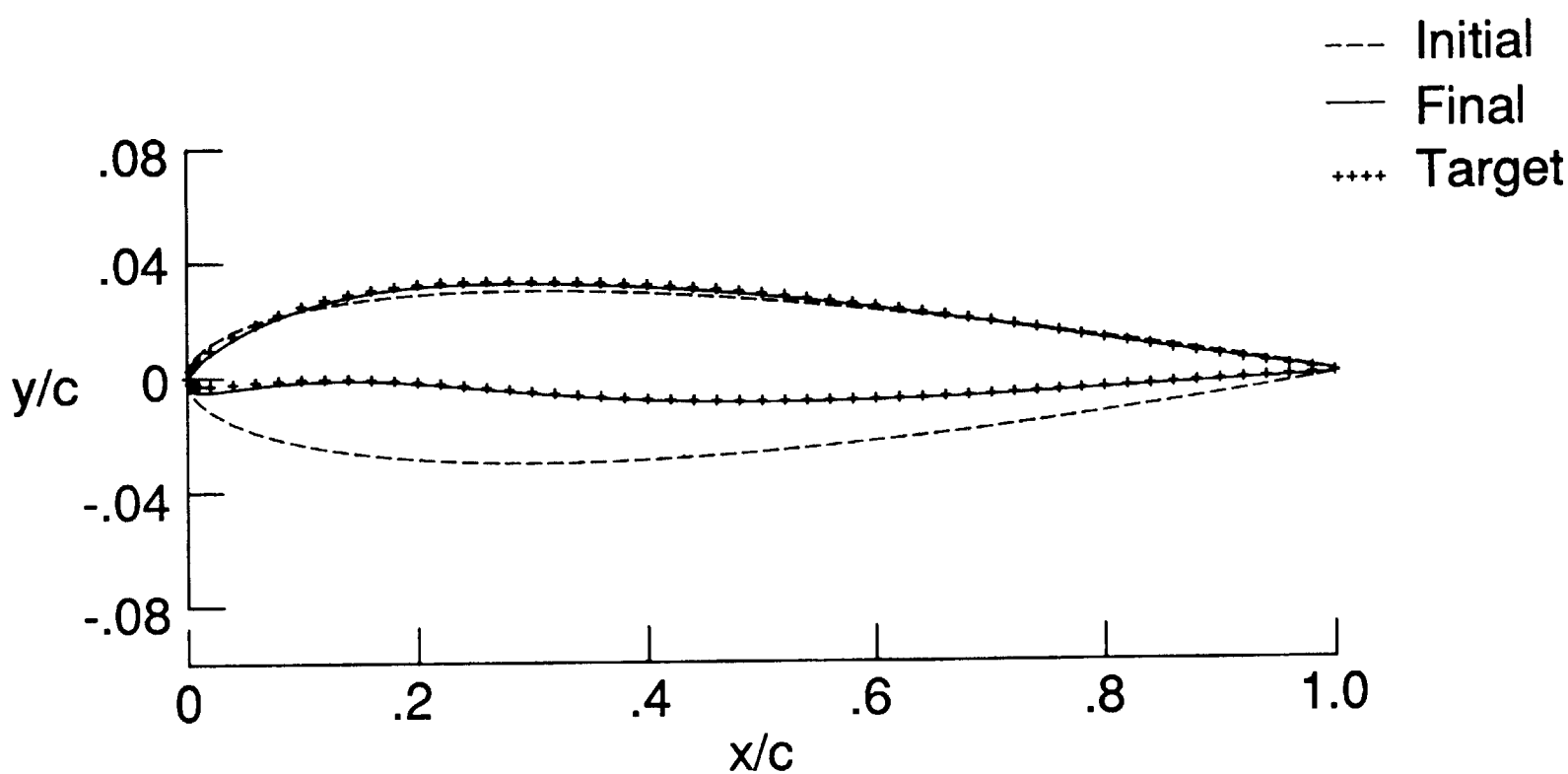

HIGHLY-SWEPT FIGHTER WING CASE

$\eta = 0.52$

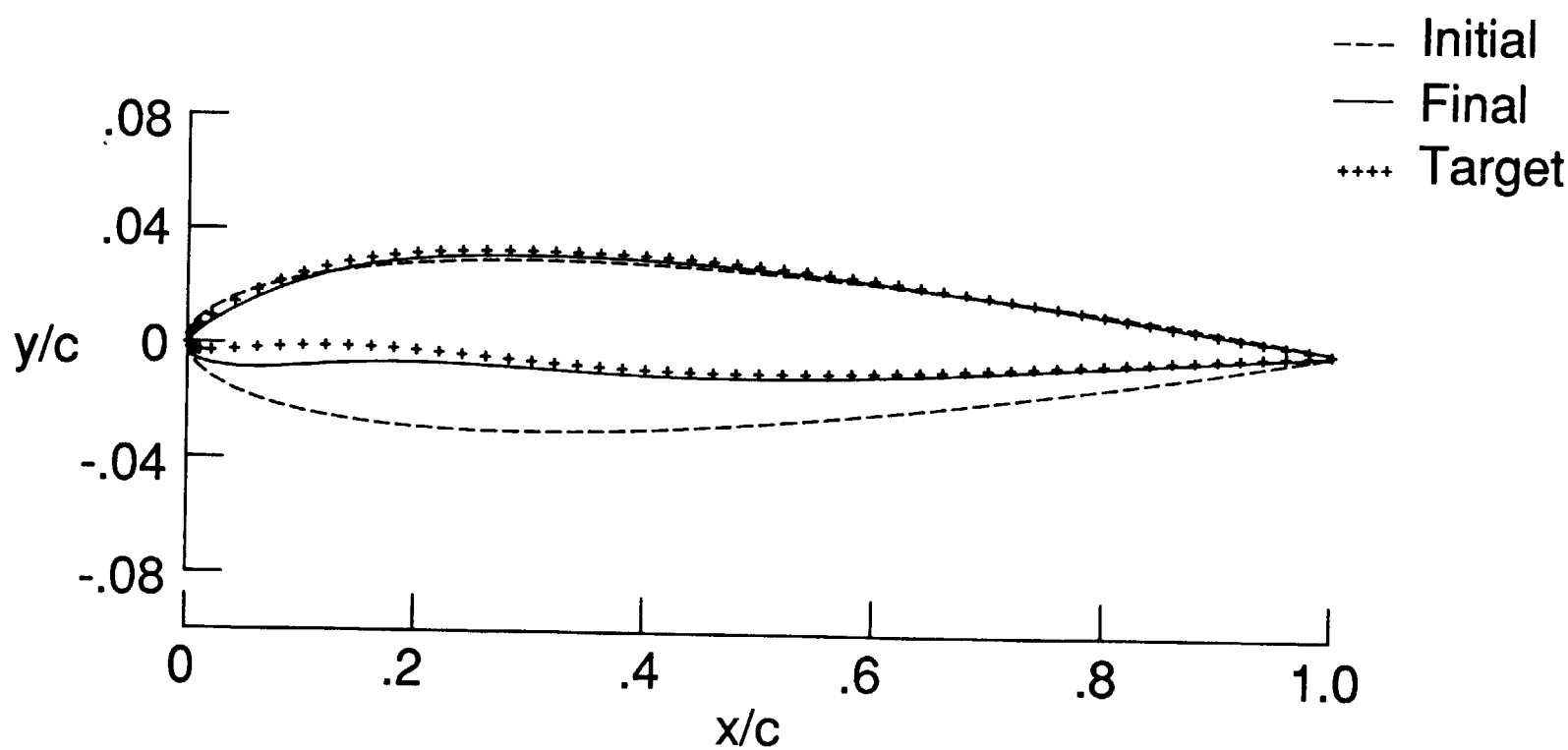

CONCLUDING REMARKS

- A predictor/corrector method for designing airfoils and wings at transonic speeds has been developed
- Hybrid algorithm used in strongly supercritical regions to improve convergence of design process
- Predictor/corrector approach allows geometry constraints to be easily included
- Results from airfoil and wing design pilot codes indicate that the method is robust, efficient, and accurate for a wide variety of configurations
- Techniques for accounting for viscous and aeroelastic effects have been included

SESSION XI

ALGORITHMS AND TOOLS

Chairman:
Joseph L. Steger
Senior Staff Scientist
Fluid Dynamics Division
NASA Ames Research Center

PRECEDING PAGE BLANK NOT FILMED

PRECEDING PAGE BLANK NOT FILMED

An Embedded Grid Formulation Applied to Delta Wings

James L. Thomas
NASA Langley Research Center, Hampton, Virginia
Sherrie L. Krist
Vigyan Research Associates, Inc., Hampton, Virginia

An embedded-grid algorithm for the Euler/Navier-Stokes equations is developed and applied to delta wings at high angles of attack in low-speed flow. The Navier-Stokes code is an implicit, finite-volume algorithm, using flux-difference-splitting for the convective and pressure terms and central differencing for the viscous and heat transfer terms. Calculations are compared with detailed experimental results over an angle of attack range up to and beyond the maximum lift coefficient, corresponding to vortex breakdown at the trailing edge, for a delta wing nominally of unit aspect ratio. The results indicate that the overall flowfield, including surface pressures, surface streamlines, and vortex trajectories, can be simulated accurately with the global grid version of the present algorithm. However, comparison of computed velocities and vorticity with experimentally measured off-body values at an angle of attack of 20.5 degree indicates the core region is substantially more diffuse in the computations than that measured with either a five-hole probe or a laser velocimeter.

Embedded grids, used in the present work to improve the numerical discretization in the core region, are formulated within the framework of the implicit, upwind-biased multi-grid algorithm. Structured levels of local nested refinements are made. The refinements, which should be based on the local truncation error of the solution, are currently based on the location of the vortex core trajectory. The embedded grid boundary data are determined through linear interpolation of the coarser underlying grid. The values of flow variables in the coarser grid cells underlying finer grids are determined by a volume-weighted restriction of the finer grid values. To compensate for the limited extent of the implicit operators in the embedded grids, each level of grid refinement uses corrections from coarser grids, which can be either embedded or global grids, to accelerate the convergence to the steady state of the embedded blocks.

Three-dimensional results for both Euler and Navier-Stokes calculations are shown, with up to 3 levels of embedded refinement. The embedding procedure was effective in eliminating a crossflow secondary separation produced in the Euler solutions on coarse grids. The core velocities in the Euler solutions are substantially higher than in the viscous solutions and in both, the embedded grids can efficiently reduce the numerical diffusion in the flowfield. The computed core velocities in the viscous calculations are increased on the embedded grids but are lower than the measured values with the grids used in the present study.

N91-10891

LIST OF CHARTS

Chart 1. Introduction.

Chart 2. Outline of presentation.

Chart 3. Global grid algorithm.

Chart 4. Comparisons with experiments.

Chart 5. Secondary and tertiary separation lines.

Chart 6. AR=1 delta wing, Cl vs. alpha plot.

Chart 7. Embedded grid scheme.

Chart 8. Embedded grid scheme with V-cycle.

Chart 9. Crossflow embedded grids.

Chart 10. Particle traces.

Chart 11. Euler solution for 76 degree delta wing; U-velocity.

Chart 12. Grid refinement effect plot.

Chart 13. 3-D Navier-Stokes results.

Chart 14. Streamwise U-velocity contours.

Chart 15. Concluding remarks.

INTRODUCTION

Motivation :

Performance and stability of aircraft at high angles of attack are dominated by the nonlinear interaction of shed vortices

Present objective :

Compare predictions of Navier-Stokes code with detailed experimental data for delta wings with both global and embedded grid schemes

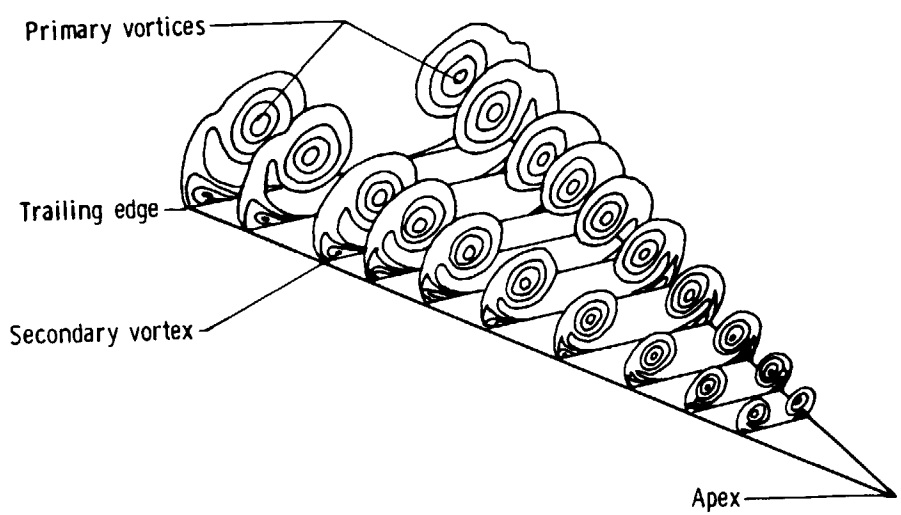

OUTLINE OF PRESENTATION

- Introduction
- Global grid scheme
  - Computational algorithm
  - Comparisons with experiment
- Embedded grid scheme
  - Spatial differencing
  - Time advancement
- Computational results
  - Euler
  - Navier-Stokes
- Concluding remarks

GLOBAL GRID ALGORITHM

Upwind-biased Navier-Stokes code CFL3D

$$\frac{\partial \widehat{Q}}{\partial t} + \frac{\partial \widehat{F}}{\partial \xi} + \frac{\partial \widehat{G}}{\partial \eta} + \frac{\partial (\widehat{H} - \widehat{H}_v)}{\partial \zeta} = 0$$

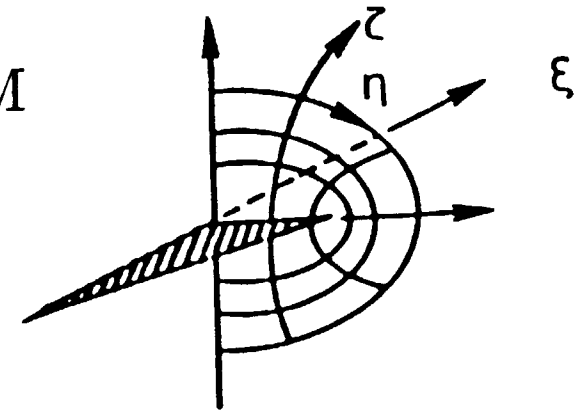

- Time-dependent conservation law form of compressible Navier-Stokes equations
- Implicit (diagonalized) time advancement algorithm
- Upwind-biased spatial differencing
  - o Flux difference splitting for convective/pressure terms
  - o Central differencing for shear stress/heat transfer terms
- Thin-layer with algebraic turbulence model
- Semi-discrete finite-volume implementation
- Zonal (patched) grids

COMPARISONS WITH EXPERIMENTS

Delta wings at high alpha in low speed flow

- Hummel (DFVLR) AR=1 wing
  - $R_L = 0.95 \text{ x } 10^6$
  - Force and moment
  - Surface oil flows
- Kjelgaard and Sellers (BART) $\Lambda = 75^\circ$wing
  - $R_L = 0.5 - 1.5 \text{ x } 10^6$
  - Surface oil flows
  - Flowfield measurements (5-hole probe / LDV)

SECONDARY AND TERTIARY SEPARATION LINES

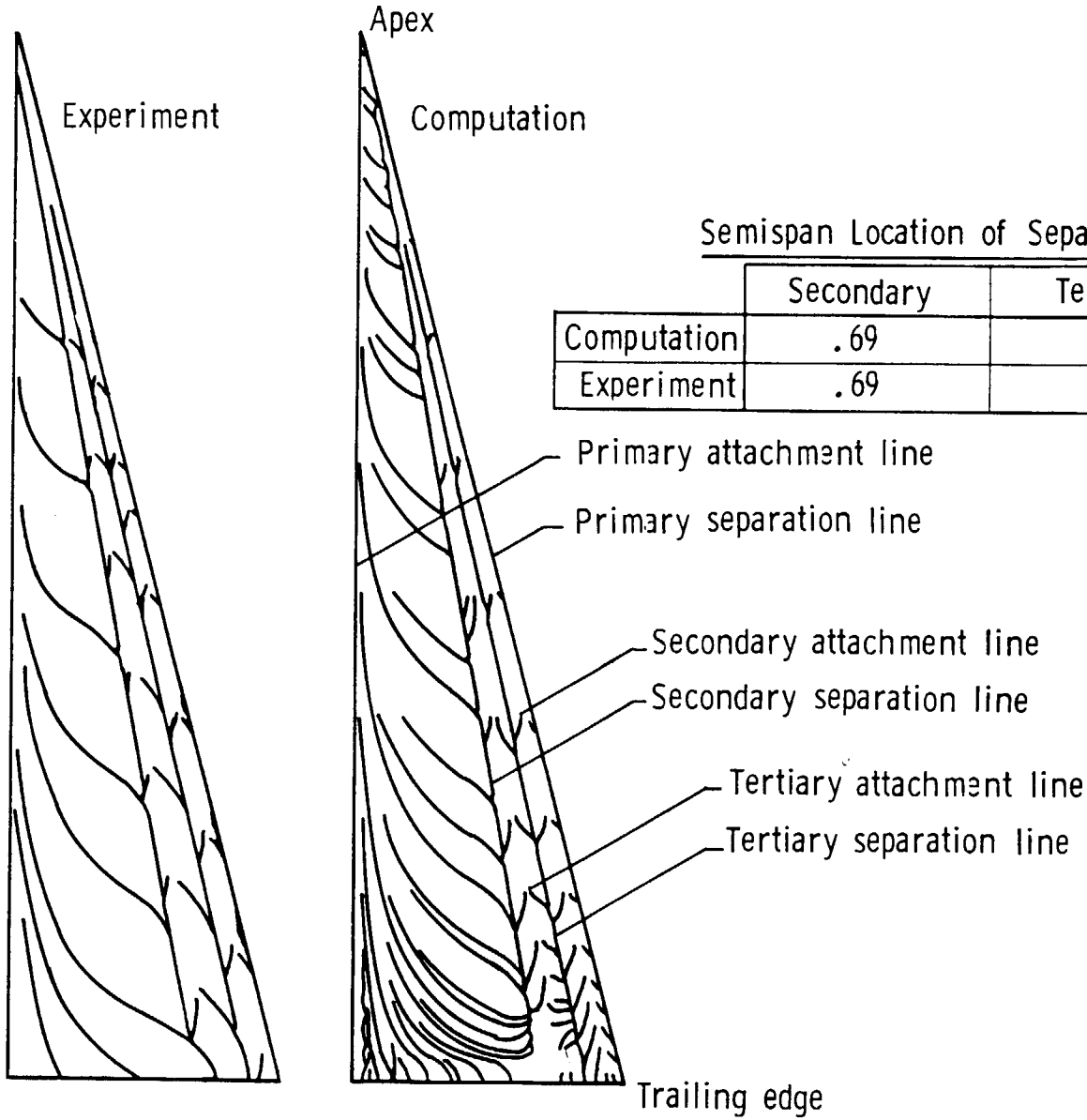

Semispan Location of Separation Lines

	Secondary	Tertiary
Computation	.69	.87
Experiment	.69	.88

AR = 1 DELTA WING

$Re_L = 0.95 \times 10^6$

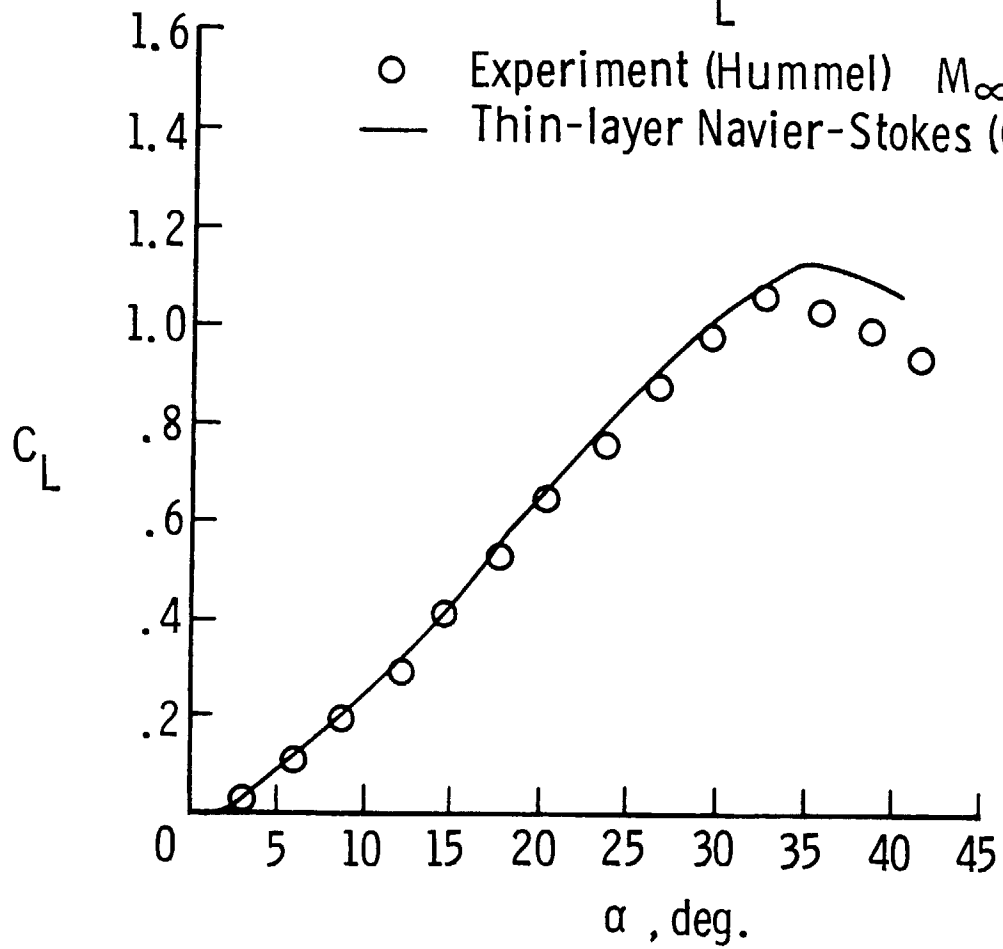

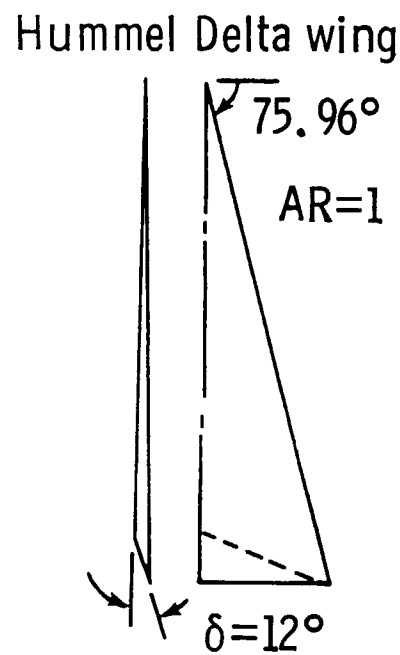

Embedded Grid Scheme

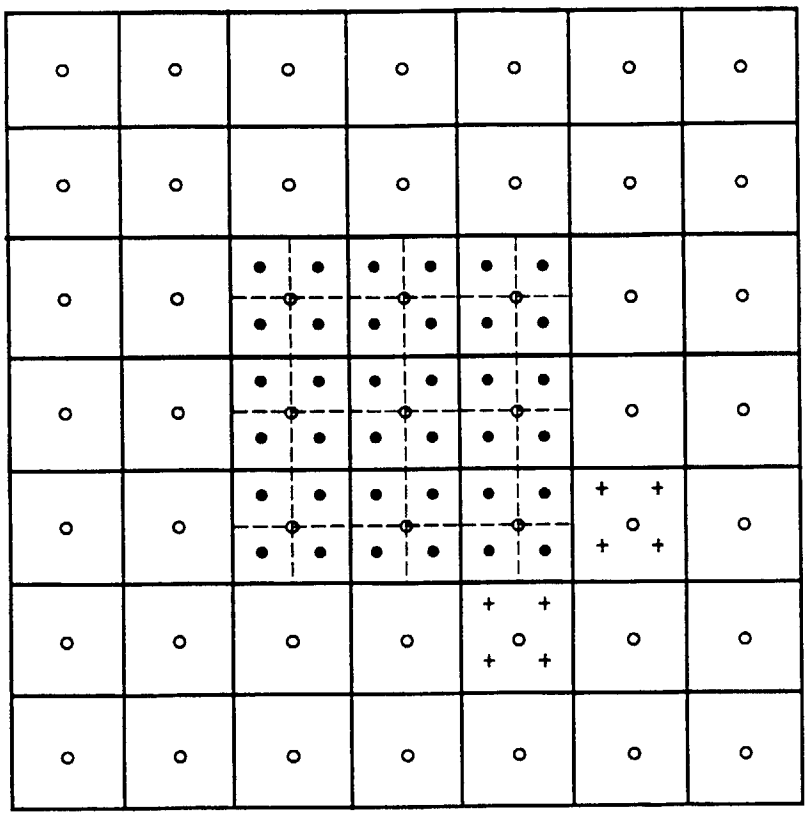

—— Coarse grid

------ Fine grid

- Volume-weighted restriction of finer grid to coarser grid cells
- Linear interpolation for projections of finer grid cells into coarse grid

Embedded Grid Scheme

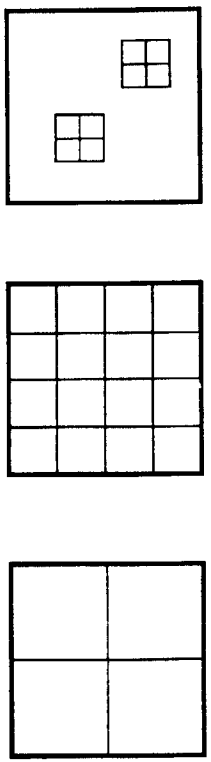

Level

Embedded Grid

Global Grid

Global Grid

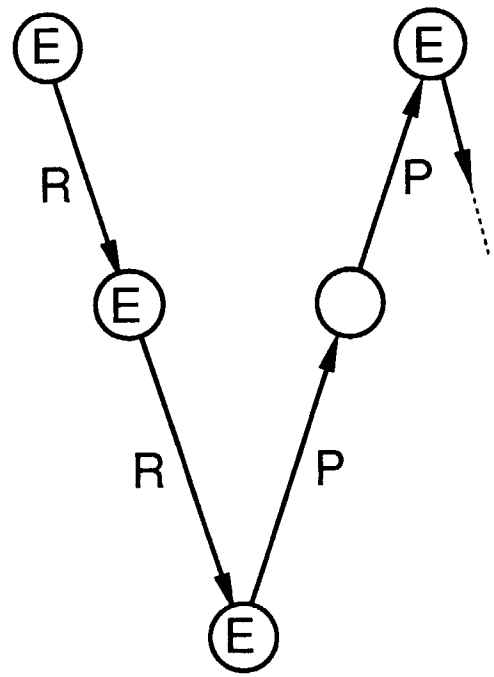

E: Navier-Stokes Calculation
R: Restriction of Residual and Q
P: Prolongation of Correction

CROSSFLOW EMBEDDED GRIDS

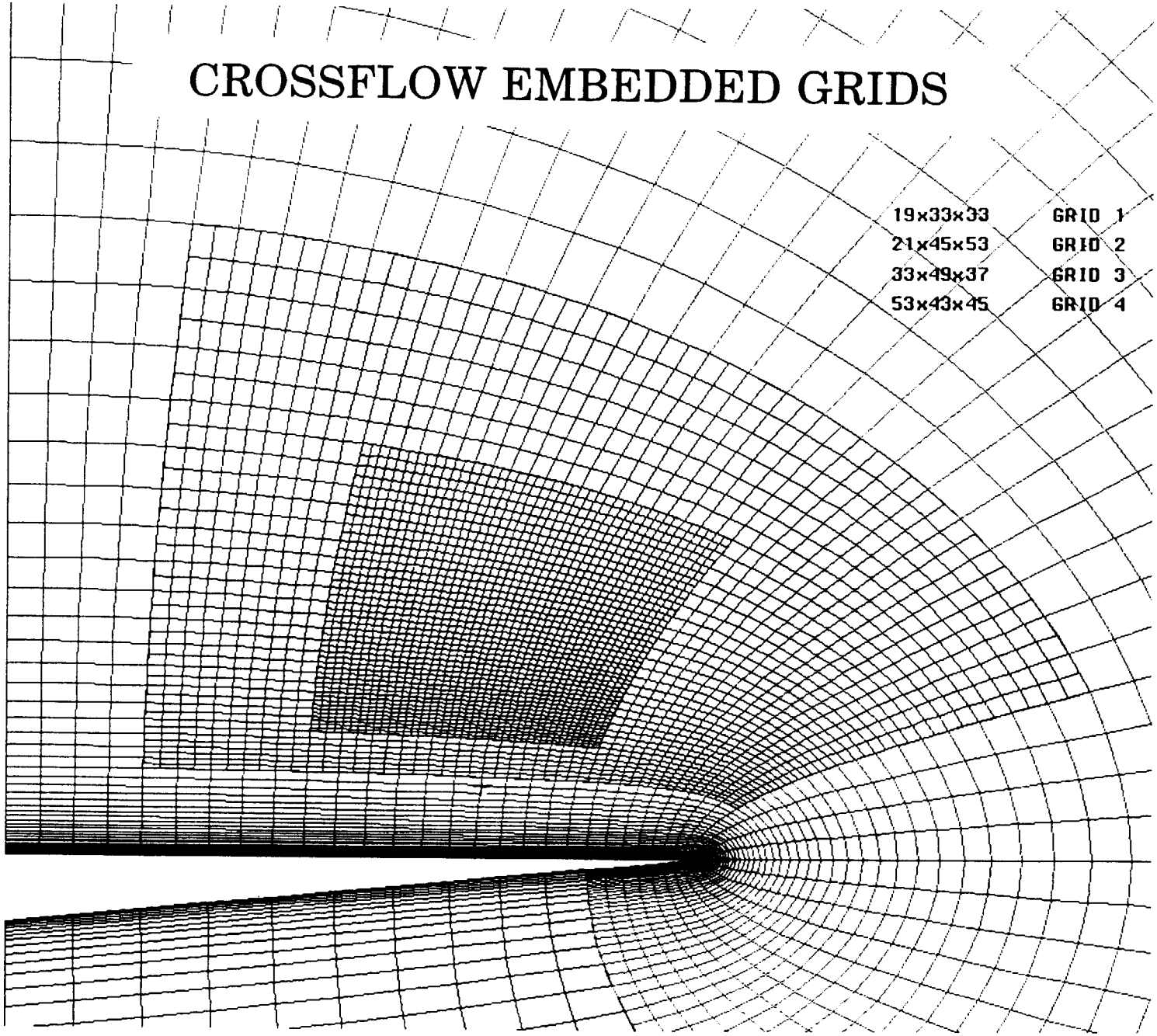

PARTICLE TRACES

33x33x19 Mesh

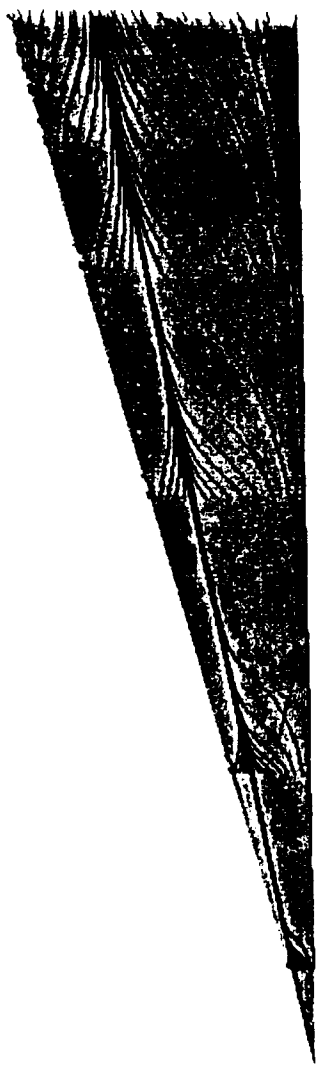

w/Grid Embedding

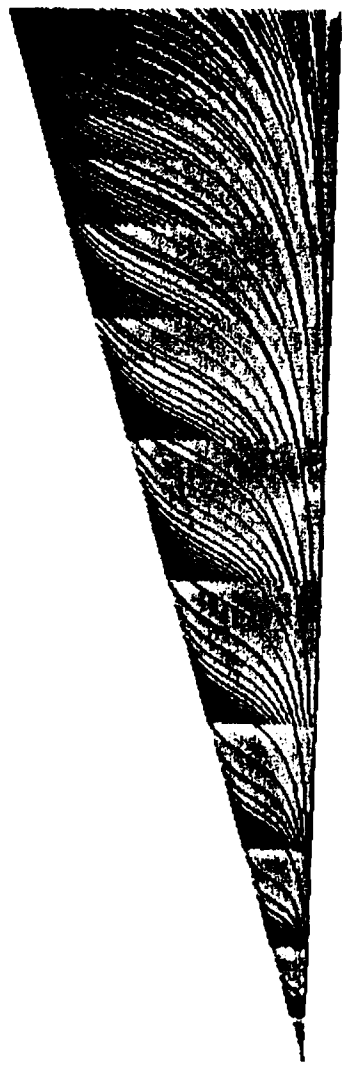

EULER SOLUTION FOR 76 DEGREE DELTA WING
u velocity component

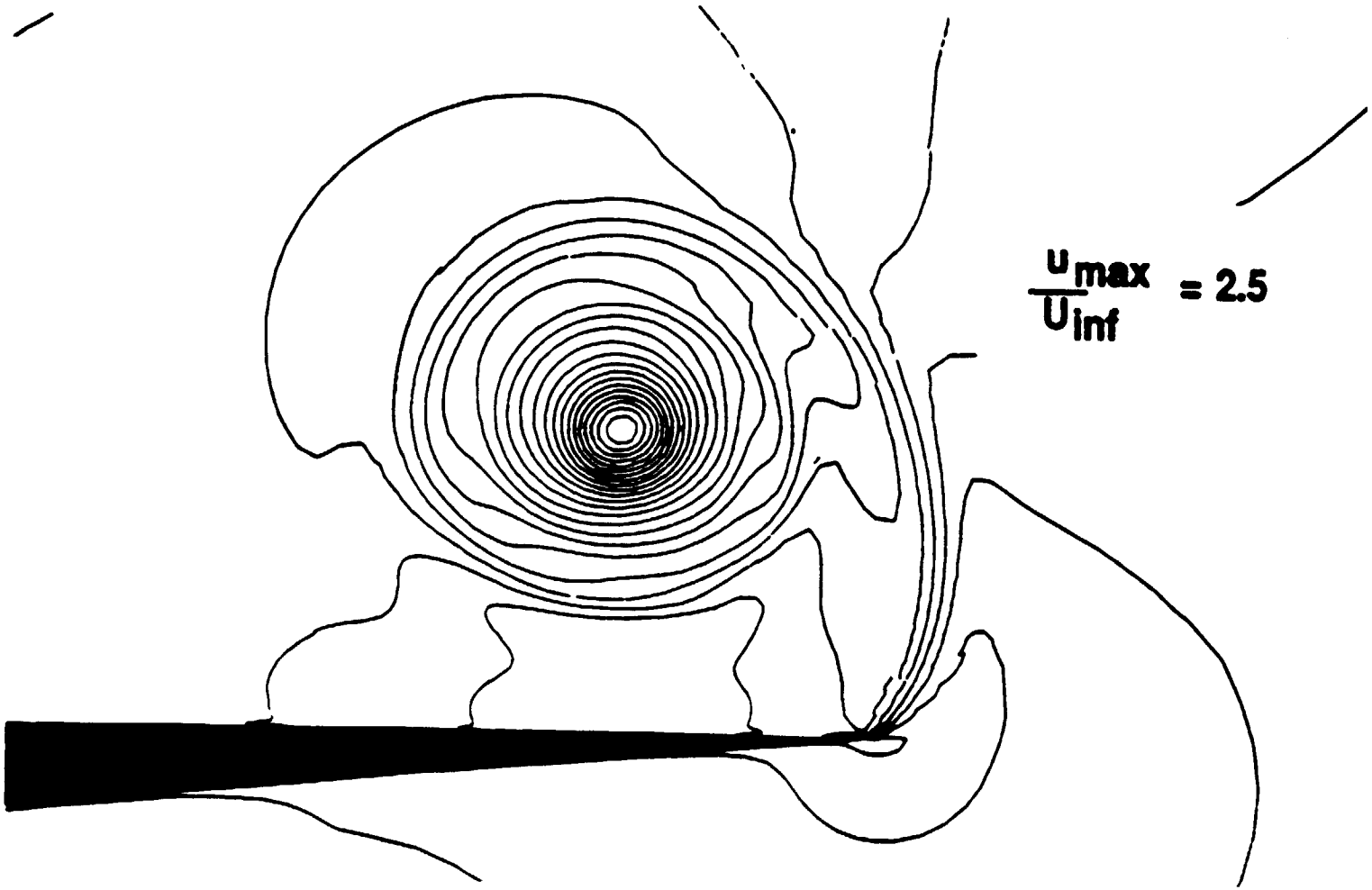

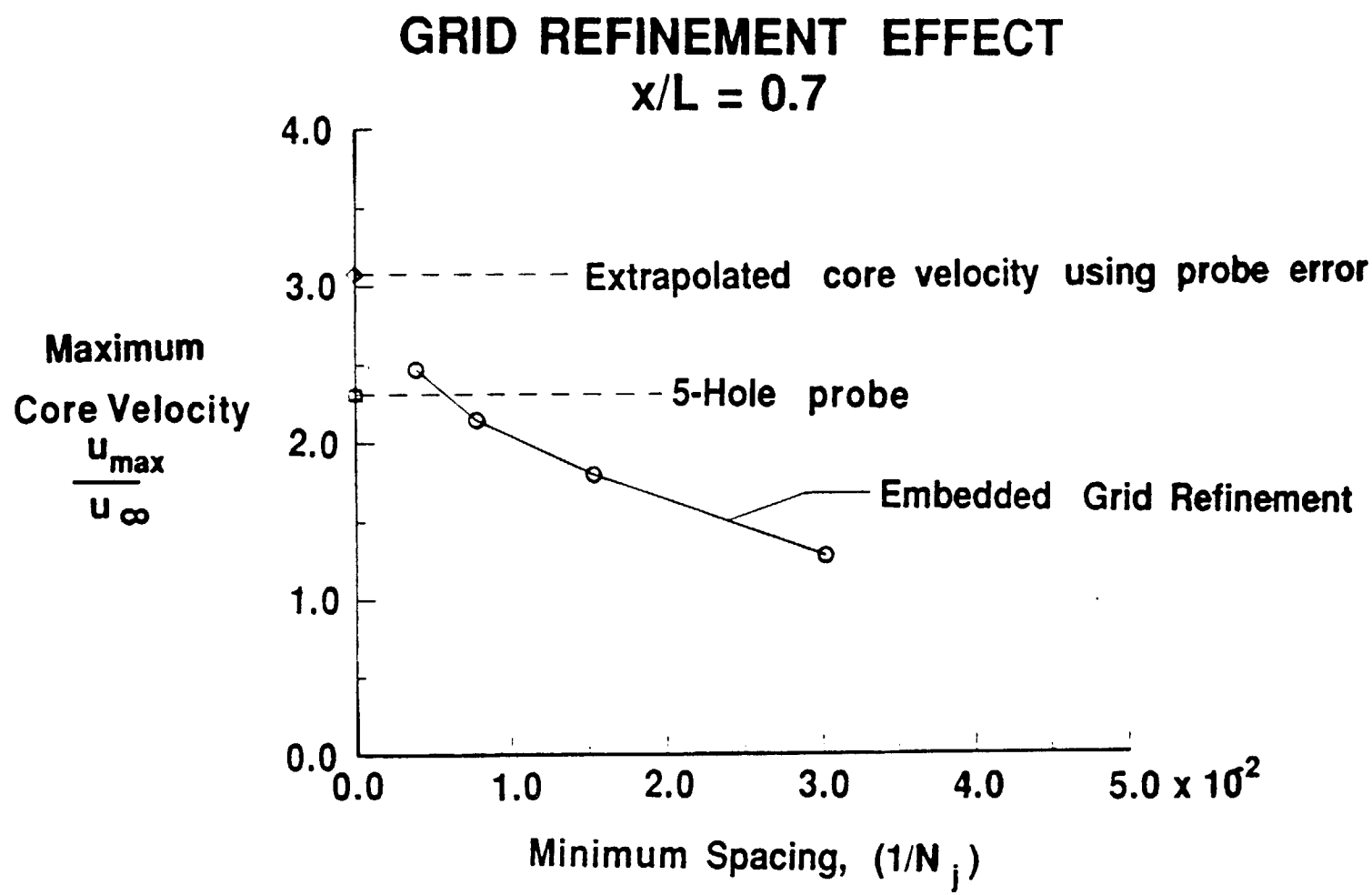
GRID REFINEMENT EFFECT
x/L = 0.7
Maximum
Core Velocity
u_{max} / u_∞
4.0
3.0
2.0
1.0
0.0
Extrapolated core velocity using probe error
5-Hole probe
Embedded Grid Refinement
0.0
1.0
2.0
3.0
4.0
5.0 x 10^2
Minimum Spacing, (1/N_j)

3-D NAVIER STOKES RESULTS

$\alpha = 20.5\ ^{\circ}$; $\Lambda = 75\ ^{\circ}$; $R_L = 0.5 \text{ x } 10^6$

Mesh	Grid points	u_{max}/u_{∞} @ x/L = 0.7
33x33x19 global	20,691	1.20
33x33x19 global w/ 3 embedded levels	233,160	1.80
65x65x37 global	156,325	1.55
65x65x37 global w/ 1 embedded level	512,770	1.92

STREAMWISE VELOCITY CONTOURS

$x/L = 0.7$; $\alpha = 20.5$

Experiment

$u_{max}/u_\infty = 2.25$

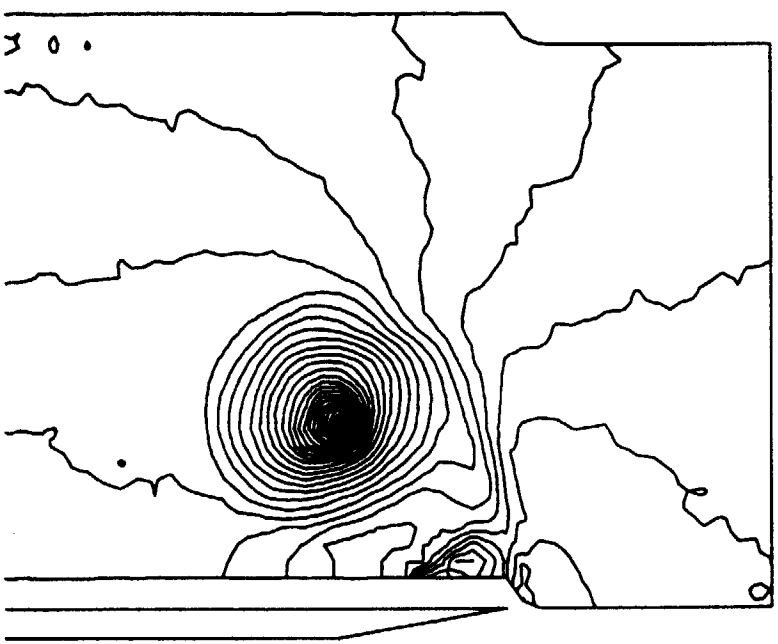

Navier-Stokes

$u_{max}/u_\infty = 1.92$

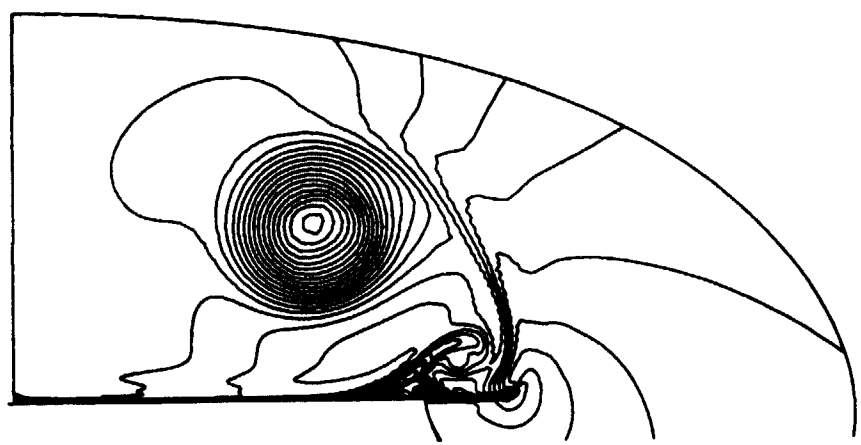

CONCLUDING REMARKS

- Global grid algorithm predicts overall flow topology and surface characteristics of delta wings in good agreement with experiment
  - Force and moment
  - Surface oil flows
  - Vortex trajectories
- Embedded grid algorithm provides efficient way to predict local off-surface flows
  - Vortex core velocities
  - Downstream interactions

N91-10892

Unstructured Mesh Solution of the Euler and Navier-Stokes Equations

Timothy J. Barth

CFD Branch
NASA Ames Research Center
Moffett Field, CA 94035

Mesh generation procedures as well as solution algorithms for solving the Euler and Navier-Stokes equations on unstructured meshes are presented. The solution algorithms discussed utilize approximate Riemann solver, upwind differencing to achieve high spatial accuracy. Numerical results for Euler flow over single and multi-element airfoils are presented.

PRECEDING PAGE BLANK NOT FILMED

Motivation/Requirements

- Generality
  - Mesh Generation of Complex Geometries
  - Inviscid/Viscous, Subsonic/Transonic Flows
- Accuracy
  - High Spatial Accuracy for Smooth Flows
    - Mesh Adaptation
  - Shock Capturing for Discontinuous Flows
    - Generalized Upwind Scheme
- Efficiency
  - Edge Data Structure
    - Edge and Face "Coloring"

Mesh Generation

- Structured
  - Algebraic, Elliptic, Hyperbolic, Parabolic, ...
- Delaunay Triangulation
  - $O(n \log n)$
  - Maximize Minimum Angle
- Advancing Front
  - Probably $O(n \log n)$

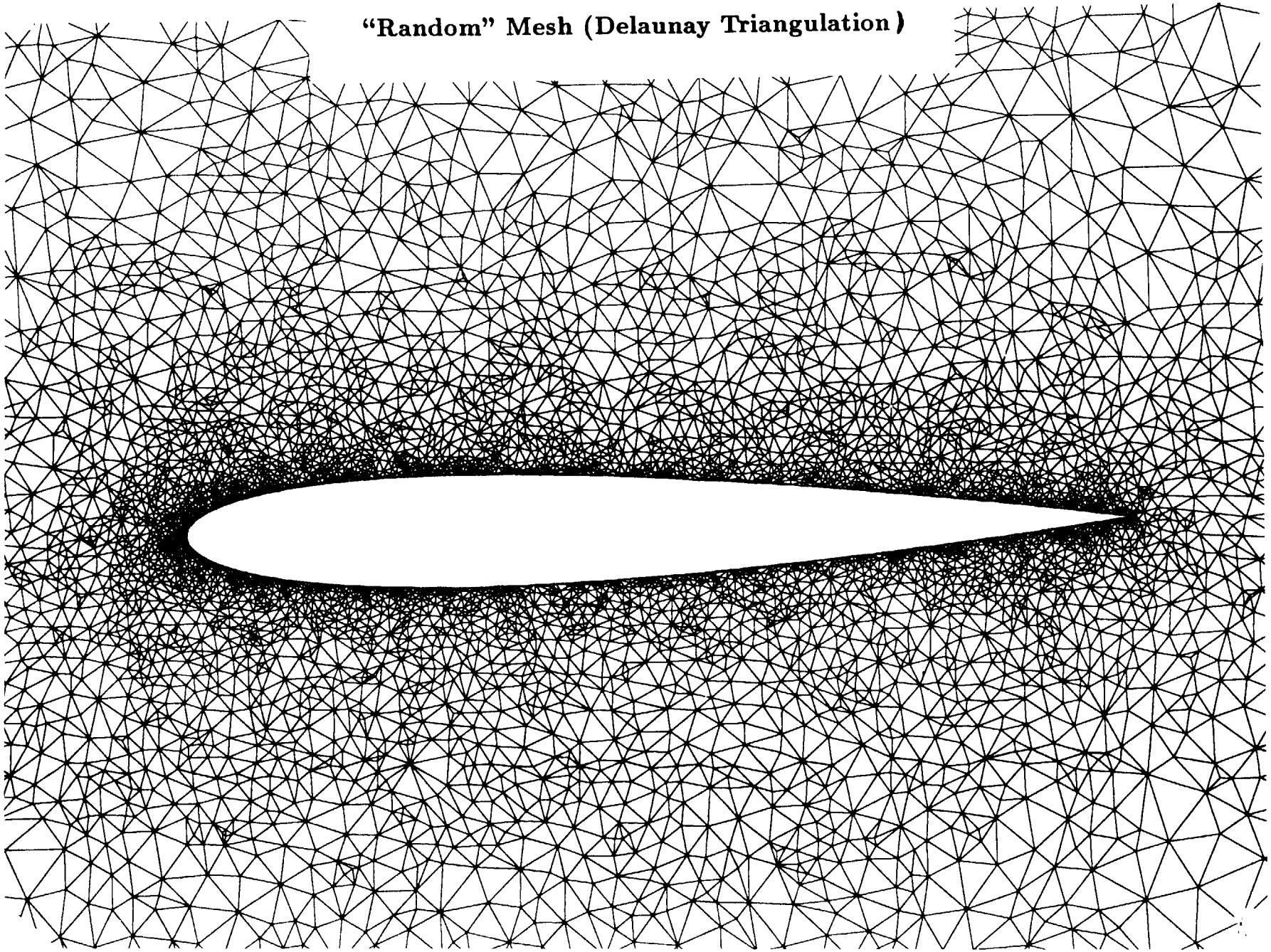
"Random" Mesh (Delaunay Triangulation)

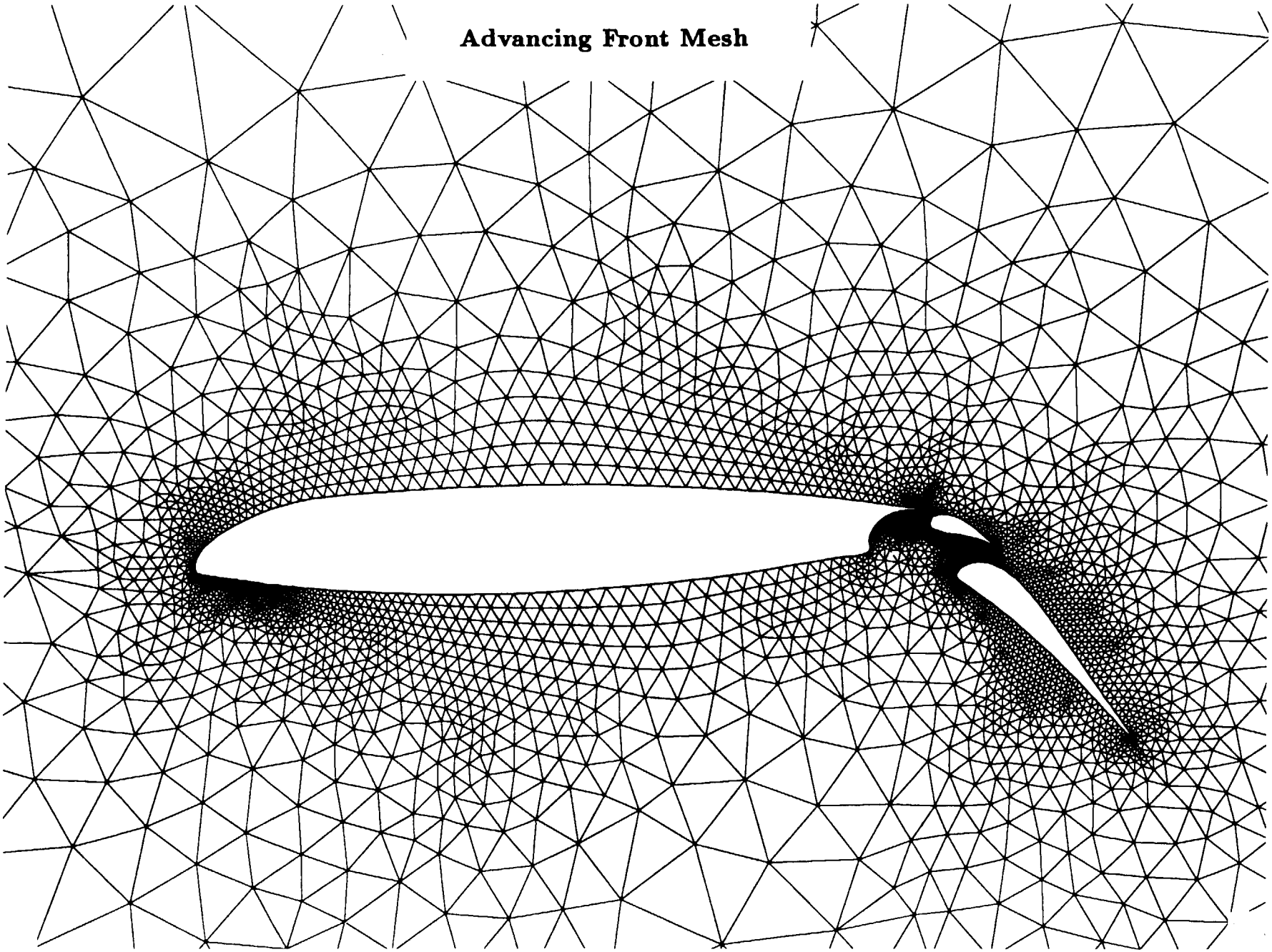
Advancing Front Mesh

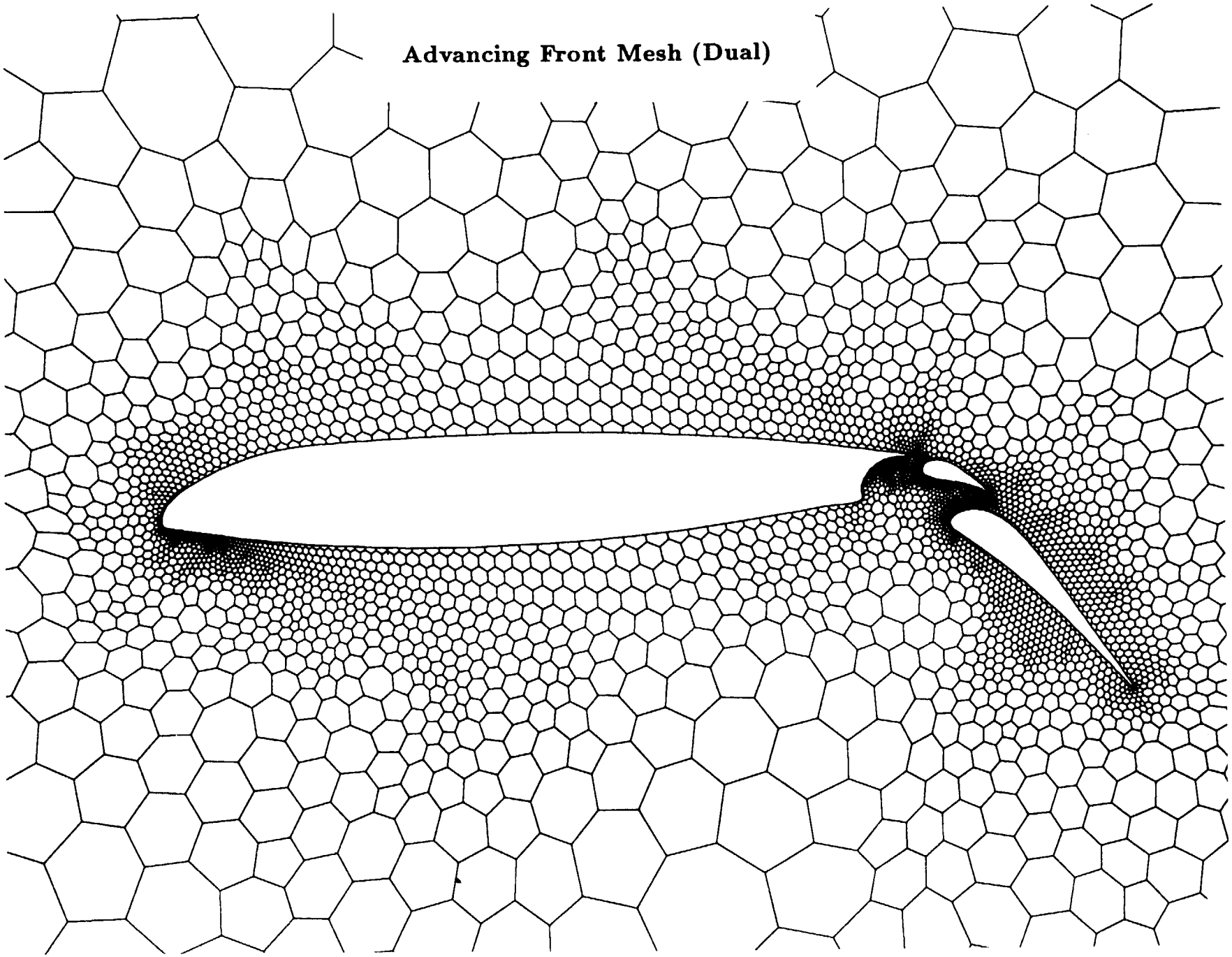
Advancing Front Mesh (Dual)

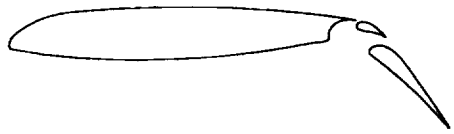

Fig. 2.1a) Three-component configuration.

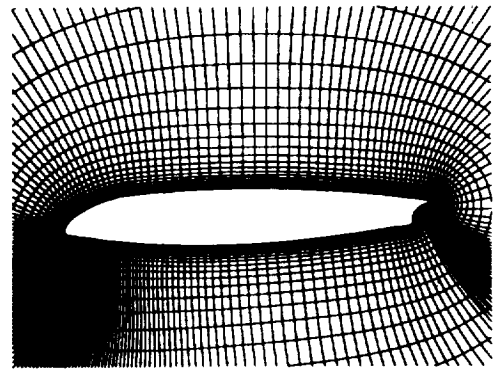

Fig. 2.1b) Grid about main element.

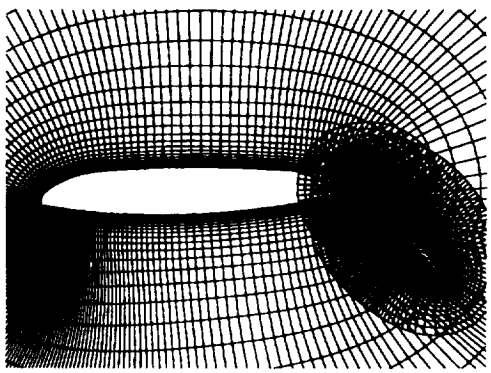

Fig. 2.1c) Grids plotted atop one another.

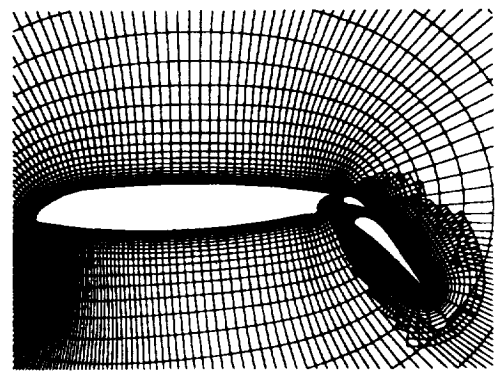

Fig. 2.1d) Grid after elimination of unwanted pts.

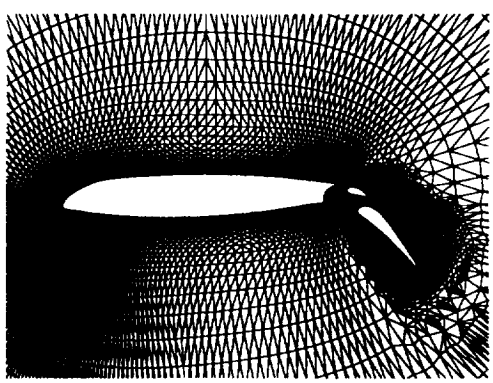

Fig. 2.1e) Grid after reconnection of points.

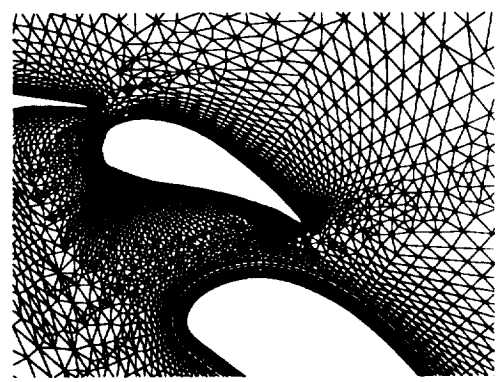

Fig. 2.1f) Grid after reconnection, detail.

Figure (2.1) Mesh generation synthesis of 3 element airfoil.

Finite-Volume Spatial Scheme

Euler equations in integral form:

$$\frac{\partial}{\partial t}\int_{\Omega} \mathbf{u}\, da + \oint_{\partial\Omega} \overline{\mathbf{f}}(\mathbf{n})\, dl = 0$$

where $\overline{\mathbf{f}}(\mathbf{n}) = n_x\mathbf{f} + n_y\mathbf{g}$

Numerical approximation about polygonal face:

$$\frac{\partial}{\partial t}\int_{\Omega_{f_j}} \mathbf{u}\, da = -\sum_{i=1}^{d(f_j)} \Delta l_i\ \mathbf{h}(\overline{\mathbf{u}}_i^+, \overline{\mathbf{u}}_i^-; \mathbf{n}_i), \quad j = 1, n(f)$$

Roe Flux Function:

$$\begin{aligned}\mathbf{h}(\mathbf{u}^+, \mathbf{u}^-; \mathbf{n}) =& \frac{1}{2}(\overline{\mathbf{f}}(\mathbf{u}^+; \mathbf{n}) + \overline{\mathbf{f}}(\mathbf{u}^-; \mathbf{n})) \\ &- \frac{1}{2}|A(\mathbf{u}^+, \mathbf{u}^-; \mathbf{n})|(\mathbf{u}^+ - \mathbf{u}^-)\end{aligned}$$

Reconstruction - Evolution

- Solution Reconstructions
  - Piecewise Constant
  - Piecewise Linear $\overline{u}(x,y) = u(x_0,y_0) + \Phi \nabla u \cdot \Delta\ \mathbf{r}$
    - Gradient Estimation in each face, $\nabla u = \frac{1}{a_\Omega} \int_{\partial\Omega} u\mathbf{n}\ dl$
    - Monotonicity Enforcement
      - Limiting (Multidimensional), $\Phi \in [0,1]$

- Solution Evolution
  - Three Stage Runge-Kutta Time-Stepping

Numerical Examples

- NACA 0012 airfoil ($M_\infty = .8, \alpha = 1.25°$)
  - Subdivided Structured Mesh (193x33)
  - Irregular Mesh
- 3 Element Airfoil ($M_\infty = .2, \alpha = 0.0°$)

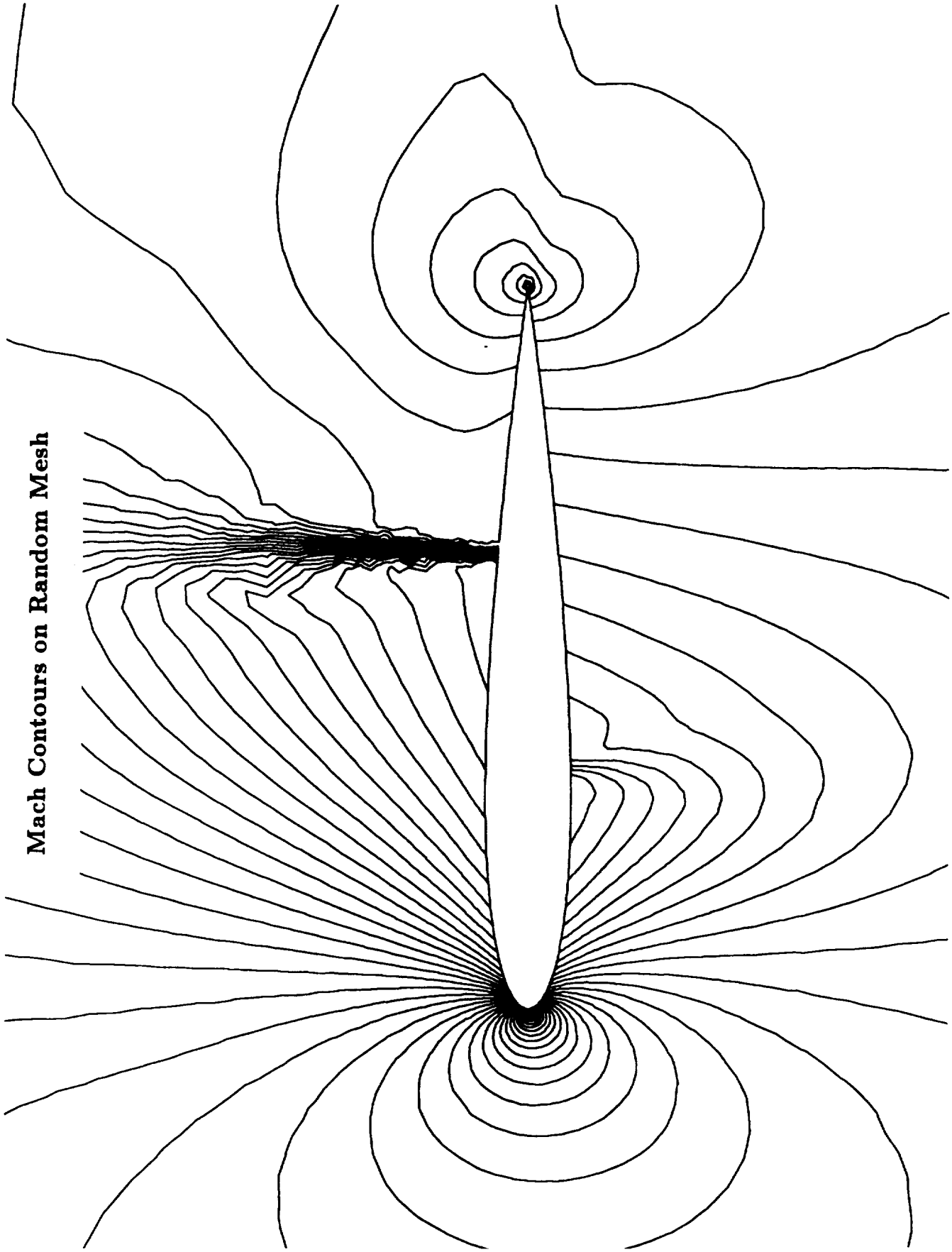
Mach Contours on Random Mesh

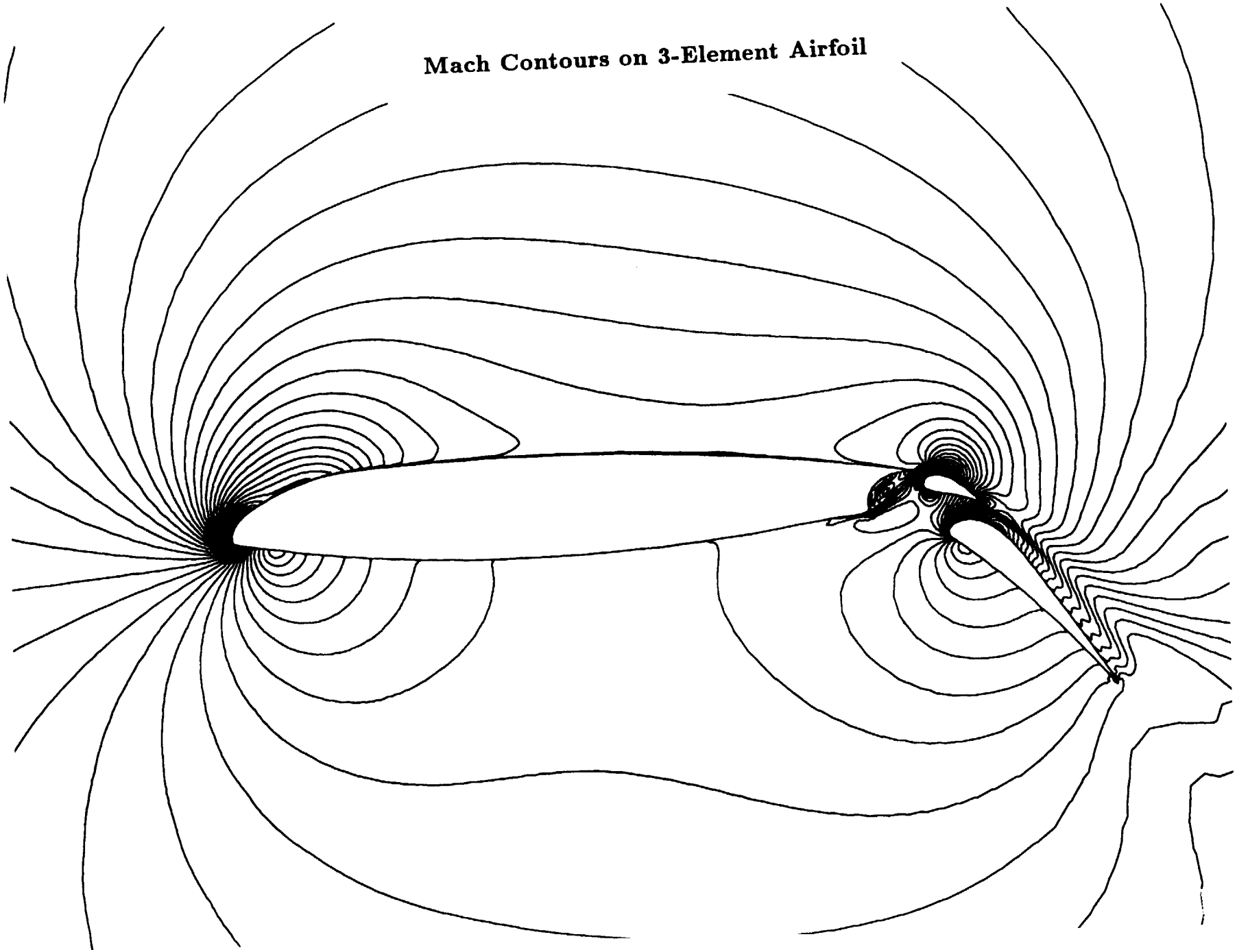
Mach Contours on 3-Element Airfoil

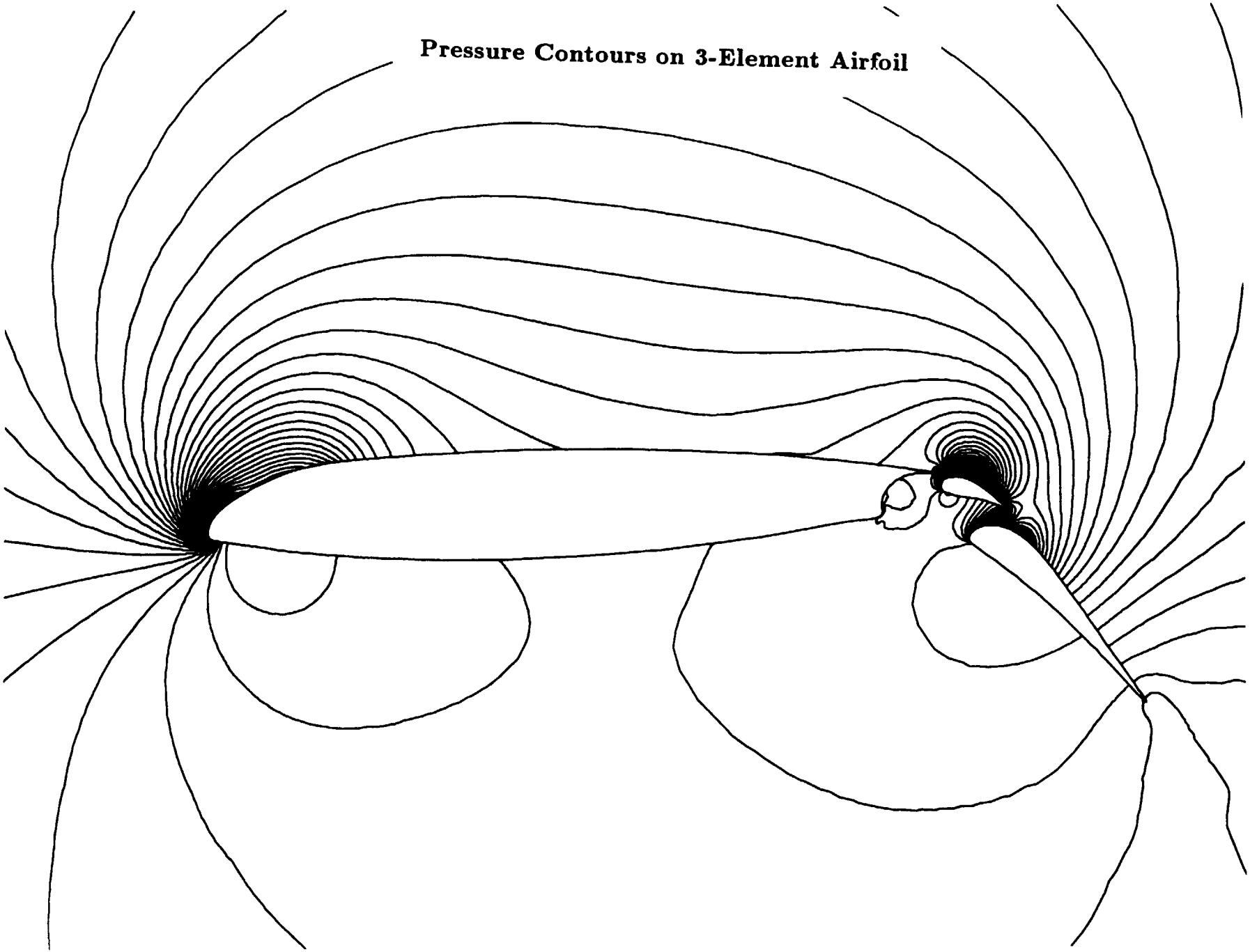
Pressure Contours on 3-Element Airfoil

3-Element Airfoil Cp Distribution

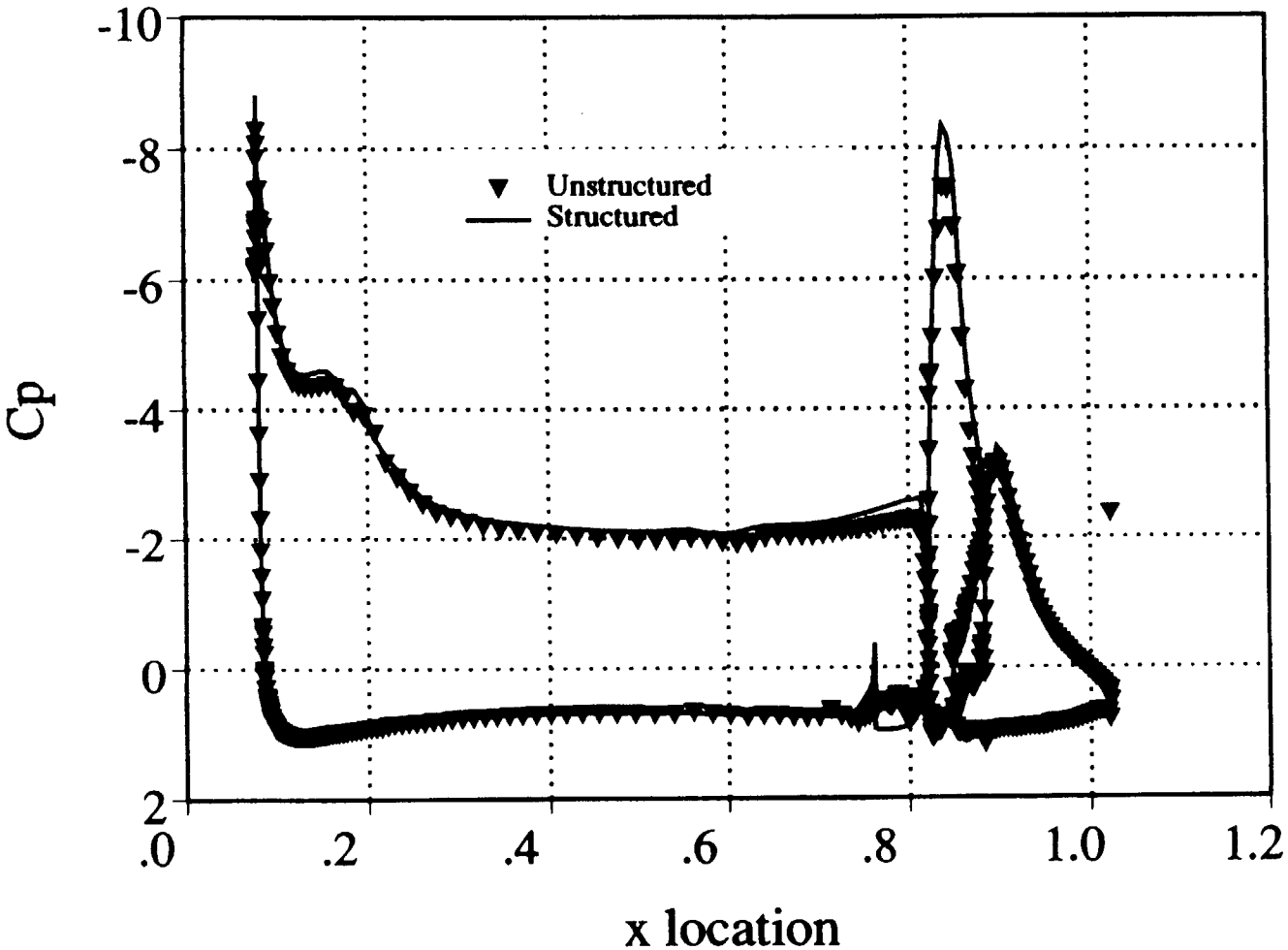

Current and Future Directions

- Quadratic Reconstructions
- Viscous Calculations with Turbulence Modelling
- Adaptive Mesh Refinement

ORIGINAL CONTAINS
COLOR ILLUSTRATIONS

N91-10893

3–D UNSTRUCTURED GRIDS FOR THE SOLUTION OF THE EULER EQUATIONS

C. Gumbert
NASA Langley Research Center

P. Parikh, S. Pirzadeh
Vigyan Research Associates

R. Löhner
George Washington University

NASA CFD Conference
NASA Ames Research Center
March 7–9, 1989

PRECEDING PAGE BLANK NOT FILMED

Advancing Front Grid Generator

The advancing front technique is being used to develop a code to generate grids around complex three dimensional configurations for use in computing the invisid flow solutions by the Euler equations. By the advancing front technique points are introduced concurrently with the connectivity information so that a separate library is not required. The generation of a 3–D grid is accomplished in several steps. First the boundaries of the domain to be gridded must be described by two-, three– or four-sided surface patches. Next, a background mesh is required to control the grid spacing and stretching throughout the domain. This coarse tetrahedral grid is not required to conform to any of the boundaries. Next, each of the patches is mapped to 2–D, triangulated by the advancing front technique and mapped back to 3–D. These triangles form the initial front for the generation of the final tetrahedral mesh.

ADVANCING FRONT GRID GENERATOR

- The field points are introduced *while* grid is generated.
  - Does not require a separate library to introduce points before grid generation.
  - Allows adaptive regeneration of grids easily.
- Generation Steps:
  - Define boundaries of the domain using surface patches.
  - Set up background grid to control local grid characteristics.
  - 2-D triangulation of patches

  ⇒ Initial Front
  - Advancing front in 3-D to fill region with tetrahedra.

Advancing Front in 2–D

The figure is a schematic showing the advancing front technique in 2–D. The initial front is a set of line segments called faces. In 3–D a face is a triangle. In succession, each face of the front is deleted and a new point in the field is introduced. As in the center figure, if the new point is close to an existing point, then the existing one is used instead. The front advances until it closes in on itself at which point the region is fully gridded.

ADVANCING FRONT IN 2-D

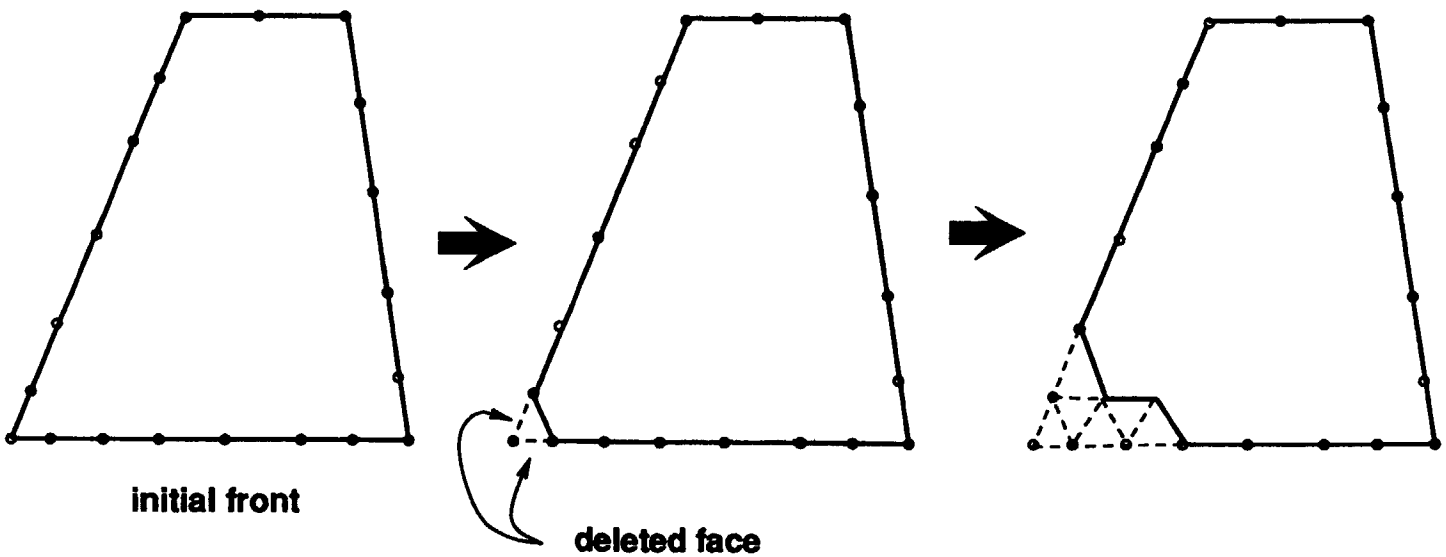

Surface Grid for F-18 Configuration

The figure shows the surface grid for an F-18 fighter configuration. The grid was generated for only one half of the configuration but it has been mirrored in the picture. The grid consists of 367,000 tetrahedrons using nearly 66,000 points of which 10,000 lie on the 75 surface patches defining the airplane and the computational box. It required about 400 seconds on the NAS CRAY-2 computer.

PRODUCED FROM BEST AVAILABLE FILMED

Finite Element Flow Solver

The flow solver developed in conjunction with the grid generator uses a two-step Taylor Galerkin finite element method for the Euler equations cast in Arbitrary Lagrangian-Eulerian (ALE) form. The Galerkin weighted residual method is used to perform the spatial discretization. Timestepping options are available for steady-state or transient problems. Accurate solutions without spurious over/undershoots can be obtained using Flux Corrected Transport (FCT) techniques. Second order pressure or Lapidus damping is used near shocks. Adaptive mesh refinement is used to better capture sharp gradients. This technique has not been fully implemented in 3–D.

PRECEDING PAGE BLANK NOT FILMED

FINITE ELEMENT FLOW SOLVER

- Two-step Taylor-Galerkin scheme
- Spatial discretization performed via Galerkin weighted residual method using linear elements
- Options for:

  Global/local timestepping

  Second order pressure or Lapidus damping

  Flux Corrected Transport (FCT)

  Adaptive H-refinement

Results In 2–D

As a means of determining the accuracy of this code, results are presented for two 2–D flow calculations. The first case is the transonic flow calculation for an NACA 0012 airfoil at $M_\infty = .80$ and $\alpha = 1.25°$. Comparison is made with results from FLO52, a finite volume method calculated on an O-type grid.

The second case is the flow field around a 20° ramp at $M_\infty = 3.0$. The exact solution is known and can be compared. This case also illustrates the use of adaptive mesh refinement.

RESULTS IN 2–D

- **Comparison of NACA 0012 airfoil**

  at $M_\infty = .80, \quad \alpha = 1.25°$

  FEFLO27 (unstructured mesh, Finite Element solver)

  FLO52 (O-grid, finite volume method)

- **20° ramp flow**

  at $M_\infty = 3.0$

  adaptive mesh refinement

Grid for NACA 0012 Airfoil

The figure shows the unstructured grid used for the calculation. There are nearly 5000 points in the grid of which 266 points lie on the airfoil surface. This is similar to the 193 points in the structured grid of FLO52.

Pressure Coefficient Comparison for NACA 0012 Airfoil

The pressure coefficient distributions are compared in the figure. The results of the calculation made on the structured grid are designated by diamonds connected by straight lines. The results of the calculation on the unstructured grid are designated by filled circles. The solutions are very similar. The location and strength of the normal shock on the upper surface are nearly identical. The finite element solver captured the shock more sharply than did FLO52. The finite element solution shown was obtained in 4000 steps which used 1.9×10^{-3} seconds/point/timestep on a Convex C2 computer.

PRECEDING PAGE BLANK NOT FILMED

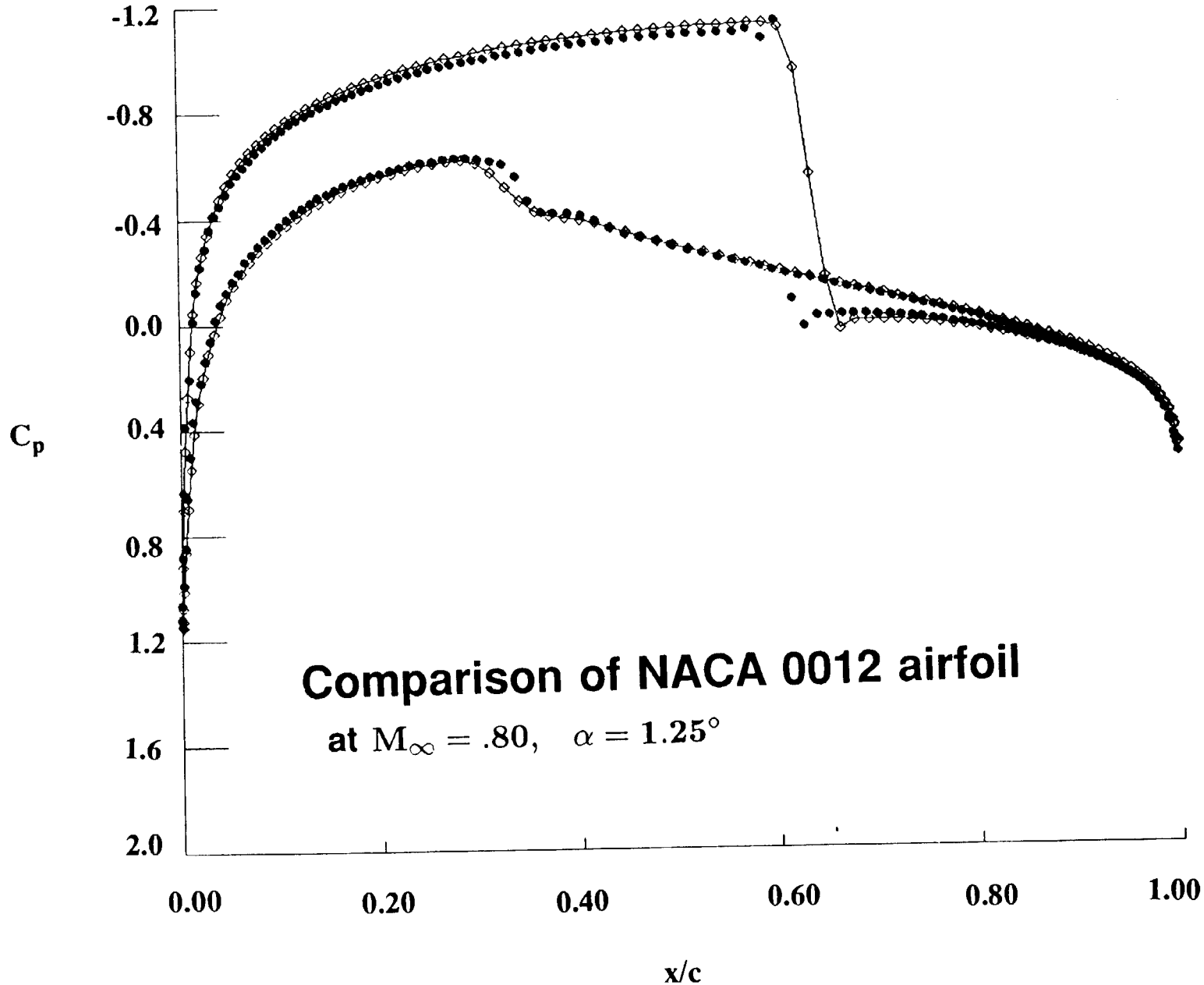
Comparison of NACA 0012 airfoil
at $M_\infty = .80, \quad \alpha = 1.25°$
C_p
-1.2
-0.8
-0.4
0.0
0.4
0.8
1.2
1.6
2.0
0.00
0.20
0.40
0.60
0.80
1.00
x/c

Exact Solution For Supersonic Flow Over A Ramp

This figure shows a schematic of the second case, supersonic flow over a 20° wedge. The exact solution is shown for the regions designated 1, 2, and 3.

EXACT SOLUTION FOR SUPERSONIC FLOW OVER RAMP

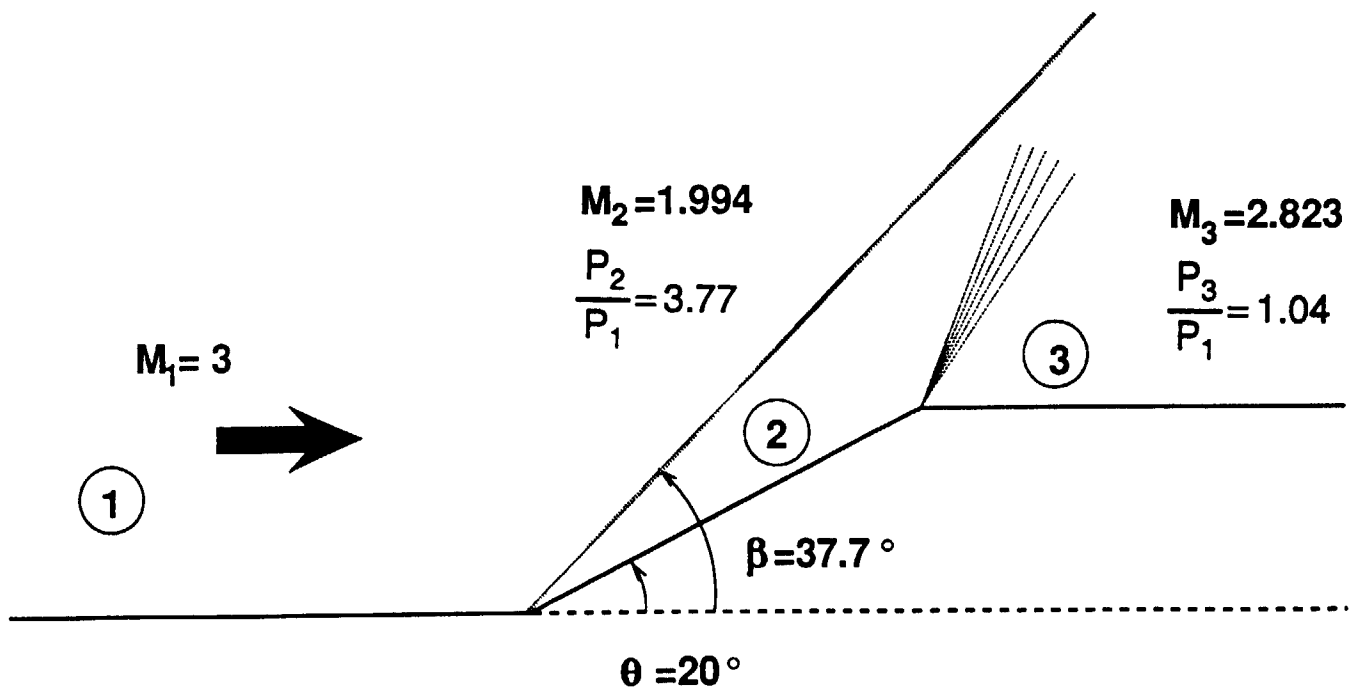

Grid Adaptation for 20° Ramp

This figure shows the final adapted grid for the solution. The levels of adaptation are shown by different colors.

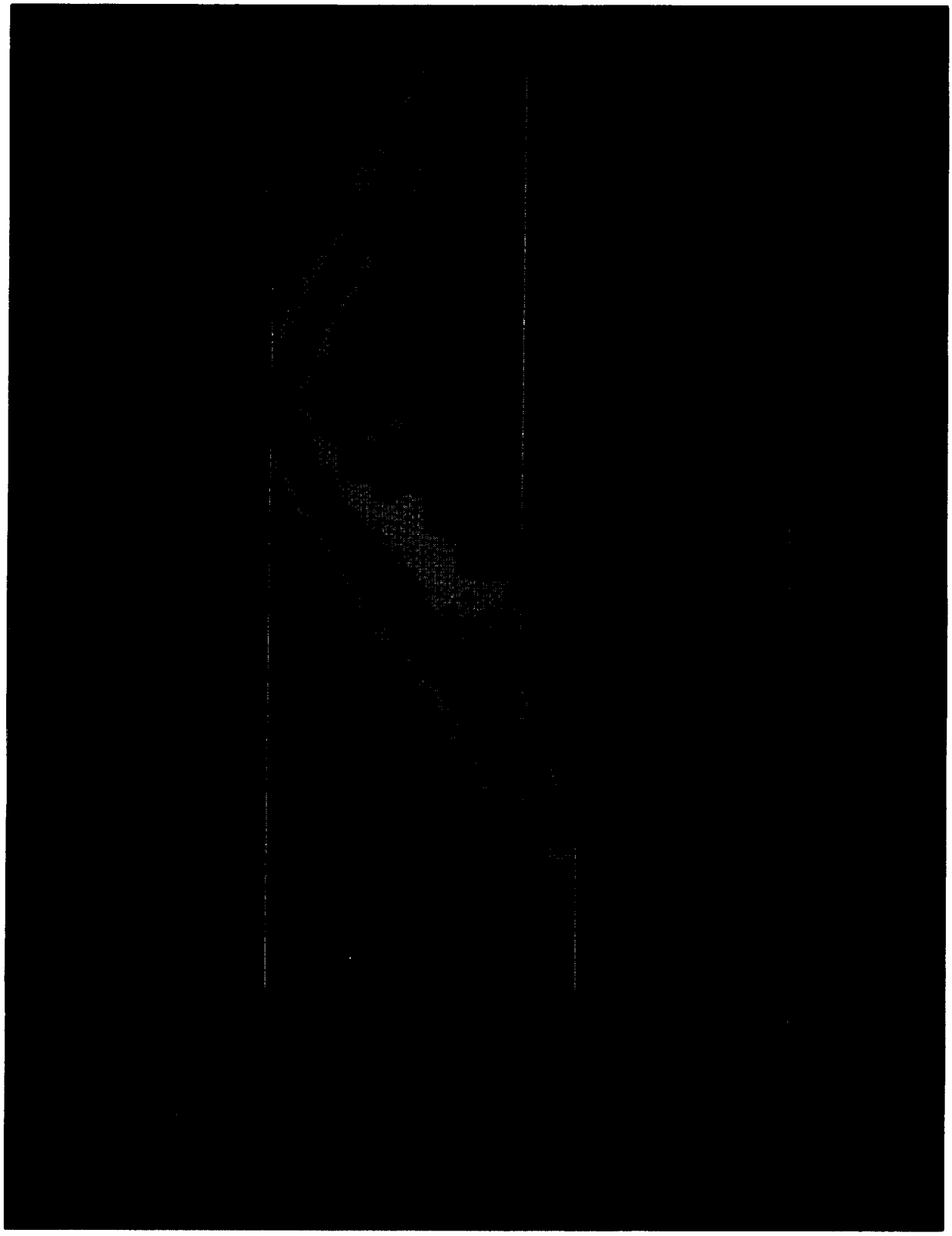

PRECEDING PAGE BLANK NOT FILMED

ORIGINAL PAGE IS
OF POOR QUALITY

Mach Number and Pressure Contours for 20° Ramp

The calculated Mach number and pressure are shown in the following figures. The shock angle and the conditions in the regions designated 1, 2, and 3 are predicted accurately. The figure also shows the interaction of the oblique shock with the expansion fan and the reflection of the shock off the straight wall.

PRECEDING PAGE BLANK NOT FILMED

PRECEDING PAGE BLANK NOT FILMED

ORIGINAL PAGE IS
OF POOR QUALITY

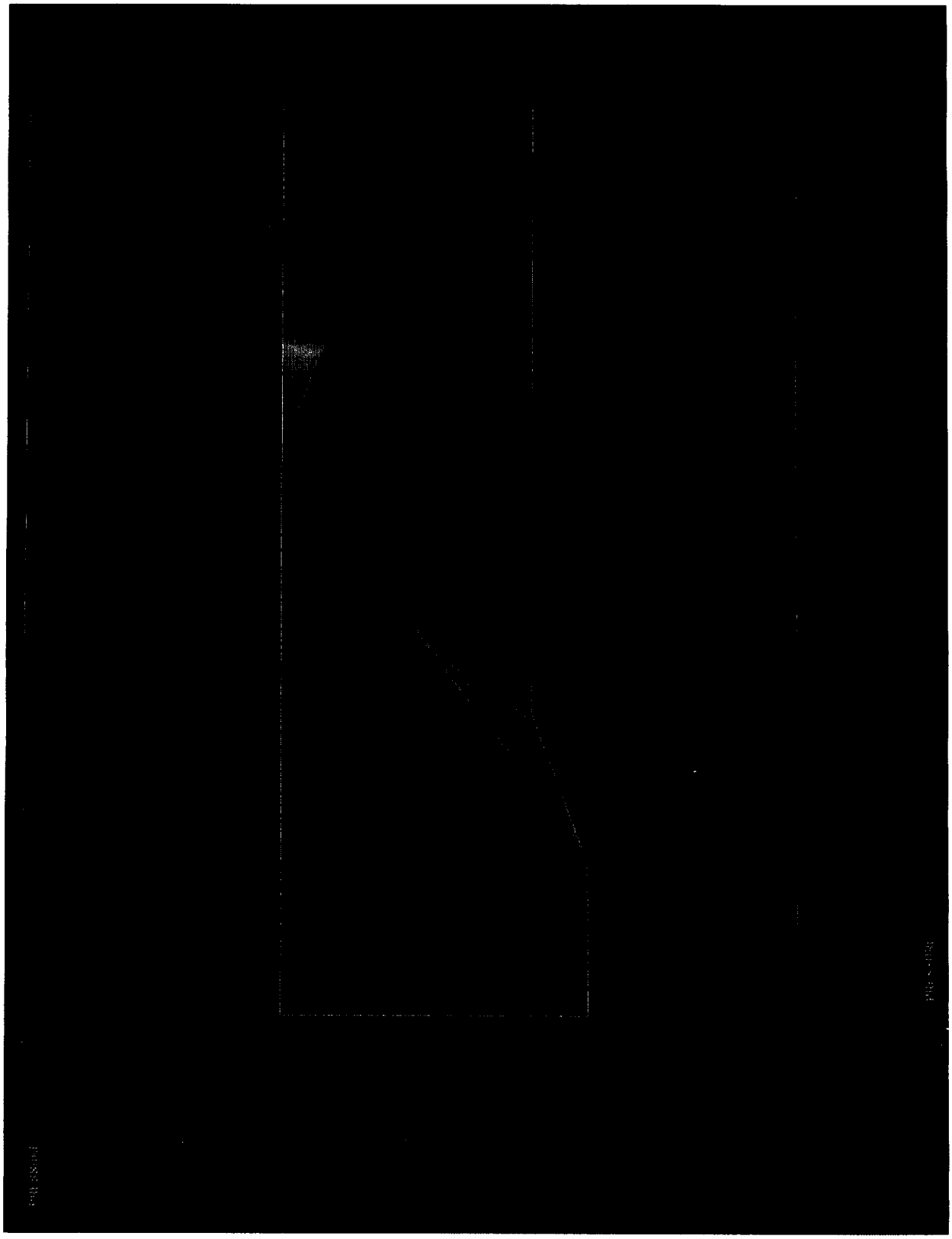

PRECEDING PAGE BLANK NOT FILMED

ORIGINAL PAGE IS
OF POOR QUALITY

Surface Pressure Contours on F-18 Aircraft

The figure shows the pressure contours on the surface of an F-18 aircraft configuration at $M_\infty = 0.3$ and $\alpha = 15°$. The solution was calculated on a grid for which the engine inlet and nozzle were blocked. This solution was run 600 iterations in 159 minutes on the NAS CRAY-2 computer to decrease the maximum residual by two orders of magnitude.

PRECEDING PAGE BLANK NOT FILMED

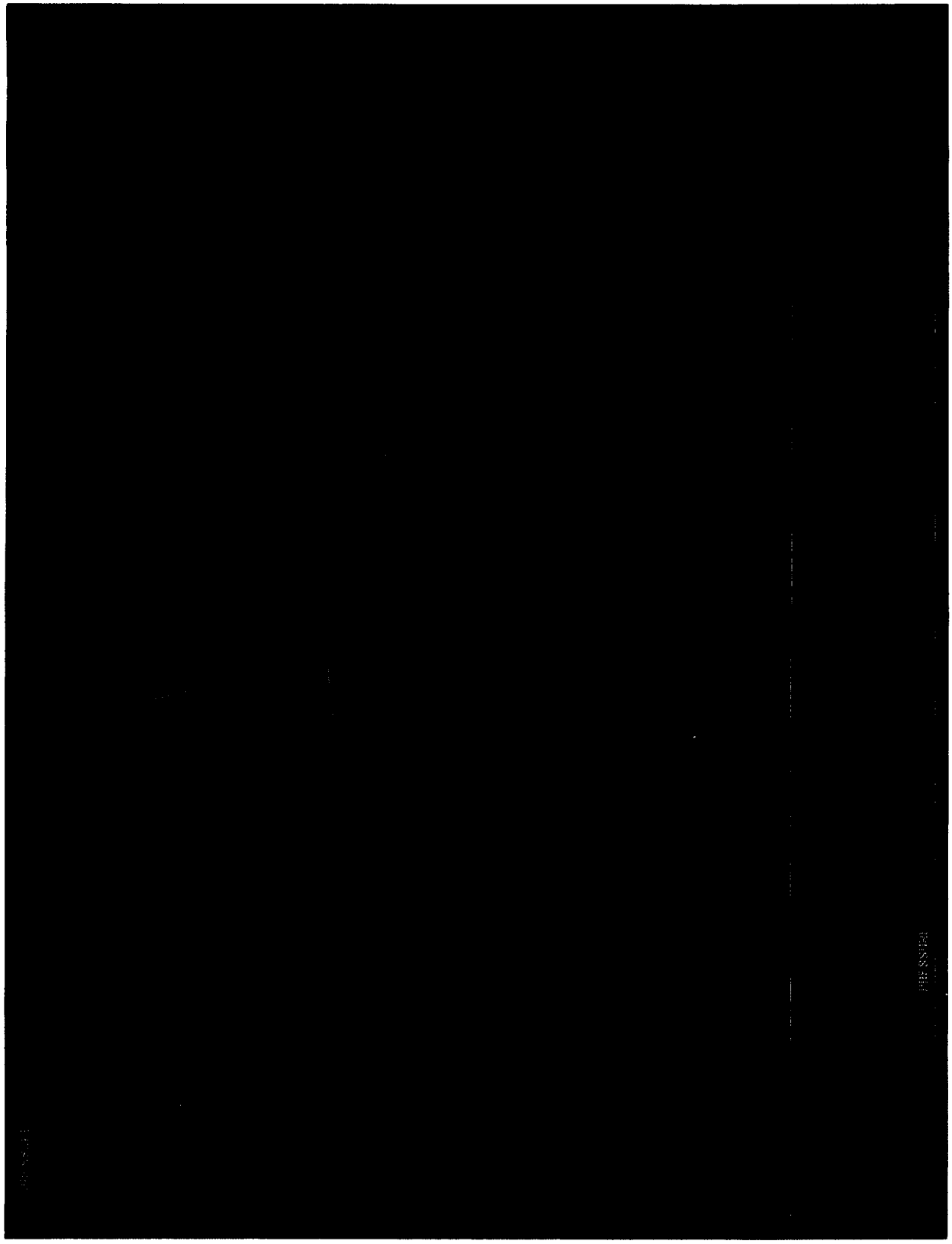

PRECEDING PAGE BLANK NOT FILMED

ORIGINAL PAGE IS
OF POOR QUALITY

Pressure Contours For Shock Emanating From A Corner

Sharp gradients in density and pressure were imposed at the intersection of three perpendicular walls as the initial conditions for a transient flow calculation. The figures show the pressure contours on the walls at two different time steps. The grid on the three walls is also shown. Additional grid points were added during the calculation to better capture the sharp gradients. No derefinement was done after the large gradients had passed.

PRECEDING PAGE BLANK NOT FILMED

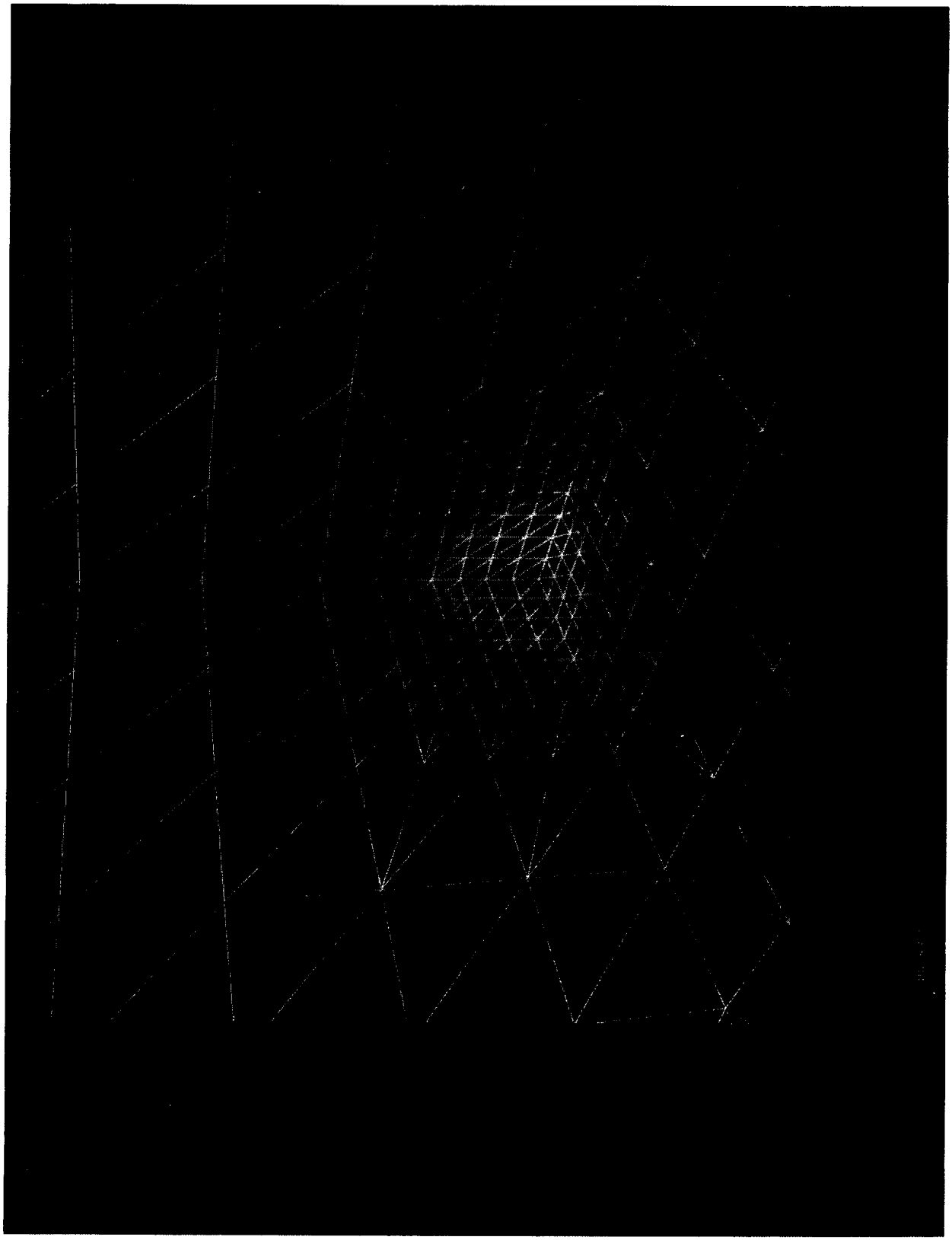

PRECEDING PAGE BLANK NOT FILMED

ORIGINAL PAGE IS
OF POOR QUALITY

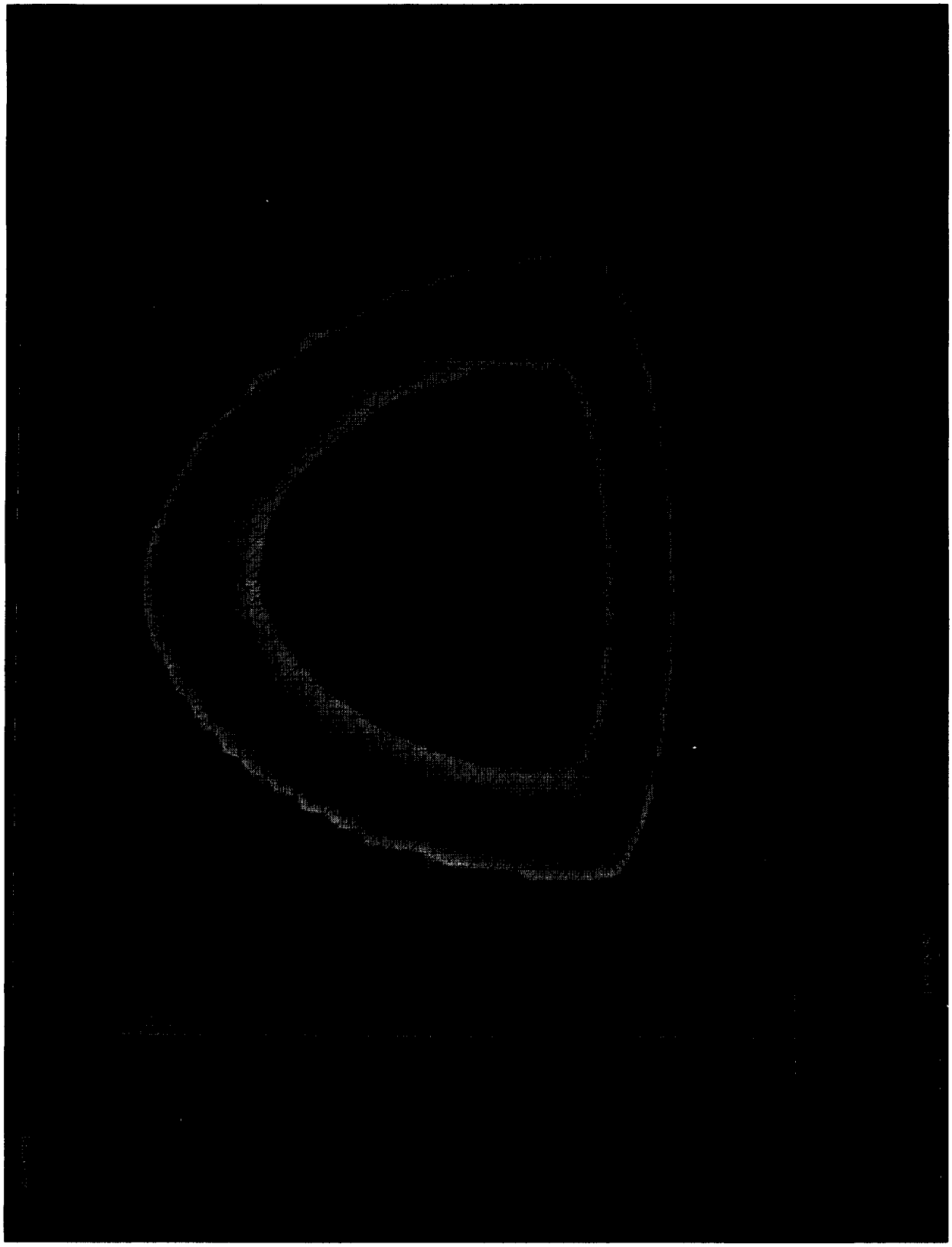

Future Plans

Further development of the grid generator will tend along three paths: (1) implementation of existing CAD sytem for faster and easier surface definition, (2) enhancement of the surface element library to allow slope continuity across surface patch boundaries and (3) faster and better ways of defining the background grid.

Further development of the flow solver is expected to involve incorporation of the viscous terms into the flow equations, use of implicit or semi-implicit algoriths and implementation on parallel computers.

FUTURE PLANS

- For the grid generator:
  - Link to commercial CAD/CAM systems for faster and more accurate surface definition.
  - Faster and better ways to input background grid information.
  - Enhancement of surface element library.
- For the flow solver:
  - Incorporation of viscous terms.
  - Implicit or semi-implicit flow solver for transient problems.
  - Implementation on parallel computers.

FLUX SPLITTING ALGORITHMS FOR TWO-DIMENSIONAL VISCOUS FLOWS WITH FINITE-RATE CHEMISTRY

Jian-Shun Shuen
Sverdrup Technology, Inc.
NASA Lewis Research Center, Cleveland, Ohio 44135

Meng-Sing Liou
NASA Lewis Research Center, Cleveland, Ohio 44135

N91-10894

ABSTRACT

The Roe flux-difference splitting method has been extended to treat two-dimensional viscous flows with nonequilibrium chemistry. The derivations have avoided unnecessary assumptions or approximations. For spatial discretization, the second-order Roe upwind differencing is used for the convective terms and central differencing for the viscous terms. An upwind-based TVD scheme is applied to eliminate oscillations and obtain a sharp representation of discontinuities. A two-stage Runge-Kutta method is used to time integrate the discretized Navier-Stokes and species transport equations for the asymptotic steady solutions. The present method is then applied to two types of flows: the shock wave/boundary layer interaction problems and the jet in cross flows.

OBJECTIVES

1. To develop a numerical algorithm for real gases which is robust for high Mach number flows and has the ability to accurately capture strong shocks and other types of discontinuities.

2. To include nonequilibrium chemistry in the formulation.

3. To make the formulation consistent and simple.

GOVERNING EQUATIONS

The 2-D, thin layer Navier-Stokes and species equations for a chemically reacting gas of N species:

$$\frac{\partial \mathbf{U}}{\partial t} + \frac{\partial \mathbf{F}(\mathbf{U})}{\partial x} + \frac{\partial \mathbf{G}(\mathbf{U})}{\partial y} - \frac{\partial \mathbf{W}(\mathbf{U}, \mathbf{U_y})}{\partial y} = \mathbf{S},$$

where

$$\mathbf{U} = \begin{pmatrix} \rho \\ \rho u \\ \rho v \\ \rho E \\ C_1 \\ C_2 \\ \cdot \\ \cdot \\ C_{N-1} \end{pmatrix}, \quad \mathbf{F} = \begin{pmatrix} \rho u \\ \rho u^2 + p \\ \rho u v \\ u(\rho E + p) \\ u C_1 \\ u C_2 \\ \cdot \\ \cdot \\ u C_{N-1} \end{pmatrix}, \quad \mathbf{G} = \begin{pmatrix} \rho v \\ \rho u v \\ \rho v^2 + p \\ v(\rho E + p) \\ v C_1 \\ v C_2 \\ \cdot \\ \cdot \\ v C_{N-1} \end{pmatrix},$$

$$\mathbf{W} = \begin{pmatrix} 0 \\ \mu u_y \\ \frac{4}{3}\mu v_y \\ \mu u u_y + \frac{4}{3}\mu v v_y + k T_y - \sum_{i=1}^{N} C_i h_i \tilde{v}_i \\ -C_1 \tilde{v}_1 \\ -C_2 \tilde{v}_2 \\ \cdot \\ \cdot \\ -C_{N-1} \tilde{v}_{N-1} \end{pmatrix}, \quad \mathbf{S} = \begin{pmatrix} 0 \\ 0 \\ 0 \\ 0 \\ S_1 \\ S_2 \\ \cdot \\ \cdot \\ S_{N-1} \end{pmatrix}.$$

THERMODYNAMIC AND TRANSPORT MODELS

Equation of State

$$p = p(\rho, e, C_1, C_2, ...C_{N-1})$$

$$p = R_u T \sum_{i=1}^{N} \frac{C_i}{W_i}$$

Physical Properties

- Mass diffusion is approximated by Fick's law. Binary mass diffusivity obtained from Chapman-Enskog theory.
- For the individual species: C_p, k, and μ are determined by fourth-order polynomials of temperature.
- For the gas mixture: C_p obtained by mass concentration weighting of each species. k and μ obtained using Wilke's mixing rule.

Chemistry Model of Air

- Five (5) species (O_2, N_2, O, N, NO) and eleven (11) elementary reaction steps.
- Neglecting ionization as well as thermal nonequilibrium.

SOLUTION METHOD

1. Two-stage Runge-Kutta method for time integration of the governing equations.

2. Chemical source terms treated implicitly so that the stiffness associated with the source terms will not upset numerical stability.

3. Second-order upwind differencing for convective terms, central differencing for viscous terms.

4. Upwind-based TVD scheme to eliminate oscillations and to obtain a sharp representation of discontinuities.

UPWIND DIFFERENCING

- Good Property for Capturing Discontinuities.

- Flux-Vector Splittings
  - ✓ Steger-Warming Splitting
  - ✓ Van Leer Splitting

- Flux-Difference Splittings
  - ✓ Roe Splitting
  - Osher Splitting

ROE FLUX-DIFFERENCE SPLITTING

To construct Roe flux-difference splitting, one usually defines an average state $\hat{\mathbf{U}}$ such that

$$\Delta\mathbf{F} = \hat{\mathbf{A}}\Delta\mathbf{U}, \qquad \Delta\mathbf{G} = \hat{\mathbf{B}}\Delta\mathbf{U}, \qquad \Delta(\cdot) = (\cdot)_{\mathbf{R}} - (\cdot)_{\mathbf{L}},$$

$$\hat{\mathbf{A}} = \mathbf{A}(\hat{\mathbf{U}}), \qquad \hat{\mathbf{B}} = \mathbf{B}(\hat{\mathbf{U}}), \qquad \hat{\mathbf{U}} = \hat{\mathbf{U}}(\mathbf{U_L}, \mathbf{U_R})$$

The eigenvalues of the Jacobian A are (for N=5):

$$\lambda(\mathbf{A}) = u, \quad u, \quad u-a, \quad u+a, \quad u, \quad u, \quad u, \quad u$$

A is diagonizable

$$\mathbf{A} = \mathbf{S}_{\Lambda}\Lambda_{\Lambda}\mathbf{S}_{\Lambda}^{-1}, \qquad diag\ \Lambda_{\Lambda} = \lambda(\mathbf{A}).$$

Splitting of the diagonal matrix Λ_{Λ} results in the splitting of $\mathbf{A}^{\pm}$:

$$\mathbf{A} = \mathbf{A}^{+} + \mathbf{A}^{-}, \qquad \mathbf{A}^{\pm} = \mathbf{S}_{\Lambda}\Lambda_{\Lambda}^{\pm}\mathbf{S}_{\Lambda}^{-1}$$

Thus, the splitting of the flux difference $\Delta\mathbf{F}$:

$$\Delta\mathbf{F} = \Delta\mathbf{F}^{+} + \Delta\mathbf{F}^{-}, \qquad \Delta\mathbf{F}^{\pm} = \mathbf{A}^{\pm}(\hat{\mathbf{U}})\Delta\mathbf{U}.$$

Goal: Find the average state $\hat{\mathbf{U}} = \hat{\mathbf{U}}(\mathbf{U_L}, \mathbf{U_R})$.

ROE'S AVERAGE STATE

- $\Delta \mathbf{F} = \mathbf{A}(\hat{\mathbf{U}})\Delta \mathbf{U}$
- **For a calorically perfect gas:** the Roe average state is easily obtained.
- **For a real gas:** the simplicity is lost.

Choose the set of average quantities

$$(\hat{\rho}, \hat{u}, \hat{v}, \hat{e}, \hat{H}, \hat{Y}_{i,i=1,4}, \hat{p}_\rho, \hat{p}_e, \hat{p}_{C_{i,i=1,4}})$$

Define the Roe-average operator μ,

$$\hat{f} = \mu(f) = \frac{f_R + d\, f_L}{1+d}, \qquad d = (\rho_L/\rho_R)^{\frac{1}{2}}, \qquad f = u, v, e, H, Y_i, \qquad \hat{\rho} = \rho_R d.$$

The condition left to be satisfied is:

$$\Delta p = \hat{p}_\rho \Delta\rho + \hat{p}_e \Delta e + \sum_{i=1}^{N-1} \hat{p}_{C_i} \Delta C_i. \qquad (A)$$

Condition (A) contains N+1 variables for only one equation.

ROE'S AVERAGE STATE (cont'd)

$$\bar{Q} \equiv (\bar{p}_e, \bar{p}_\rho, \bar{p}_{C_i}), \qquad \bar{p}_\rho = p_\rho(\hat{\rho}, \hat{e}, \hat{C}_i), \quad etc.$$

$$\hat{Q} \equiv (\hat{p}_e, \hat{p}_\rho, \hat{p}_{C_i})$$

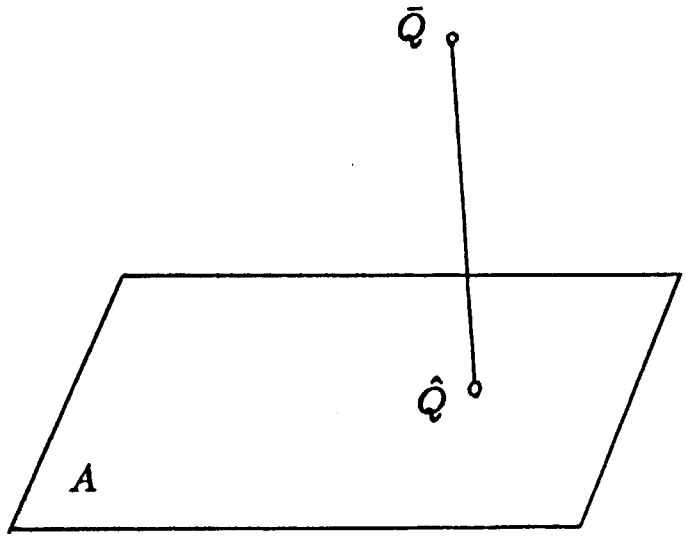

- $(\hat{p}_e,\ \hat{p}_\rho,\ \hat{p}_{C_i}) = (\bar{p}_e,\ \bar{p}_\rho,\ \bar{p}_{C_i})$ for a calorically perfect gas.

NUMERICAL TEST

- Constituent elements of the present flux-splitting method validated by comparison with exact solutions or experimental data in our previous work on 1-D Euler equations for reacting gases, and 2-D Navier-Stokes equations for ideal gases.

- Direct comparison of the present 2-D reacting flow N-S calculations with experimental data is hindered by the lack of suitable data for high Mach number reacting flows.

Two classes of problems are considered in the following:

(1) shock wave/laminar boundary layer interaction problems.

(2) jet in cross flow problems.

SHOCK WAVE/BOUNDARY LAYER INTERACTION

WALL PRESSURE AND TEMPERATURE

$M_\infty = 8.0, \quad \beta = 22°, \quad R_e = 1.57 \times 10^6$

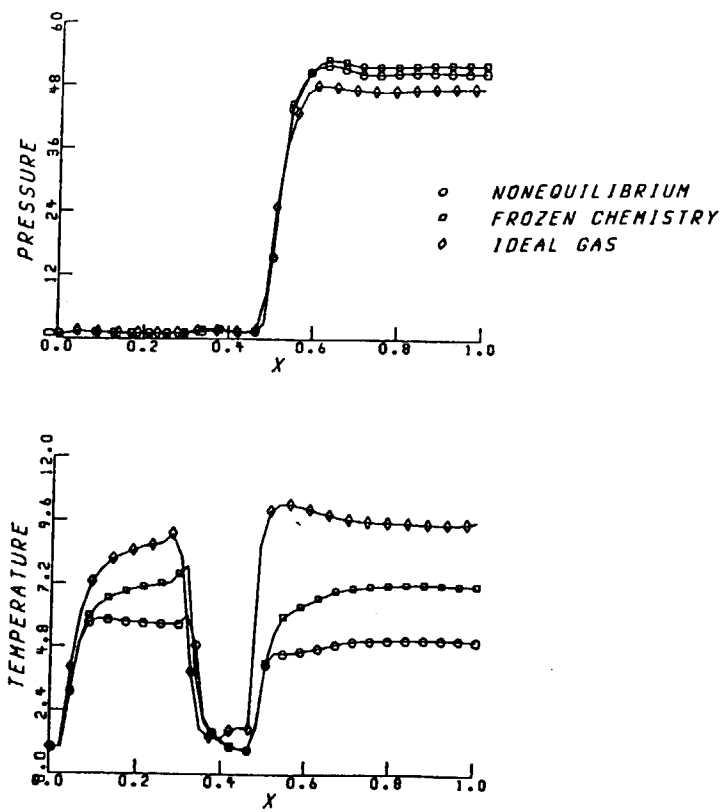

JET-IN-CROSS FLOW

VELOCITY VECTORS AND WALL PRESSURE

$M_\infty = 6.0, \quad R_e = 3.21 \times 10^6$

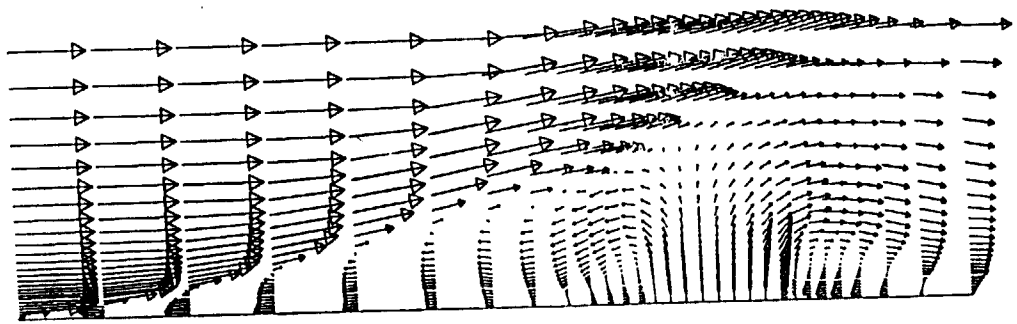

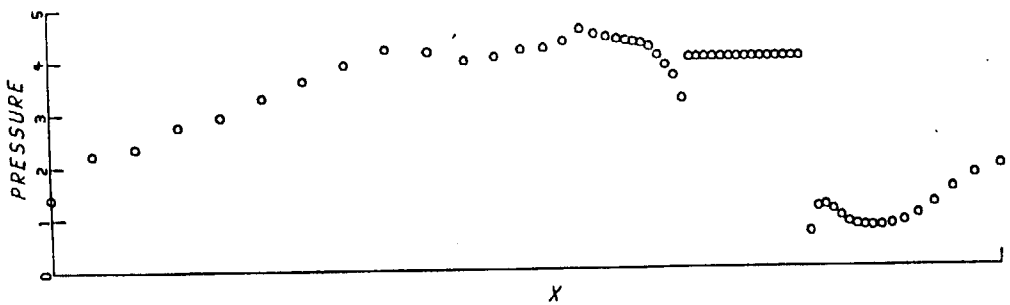

DUAL JETS-IN-CROSS FLOW

VELOCITY VECTORS AND WALL PRESSURE

$M_\infty = 6.0, \quad R_e = 3.21 \times 10^6$

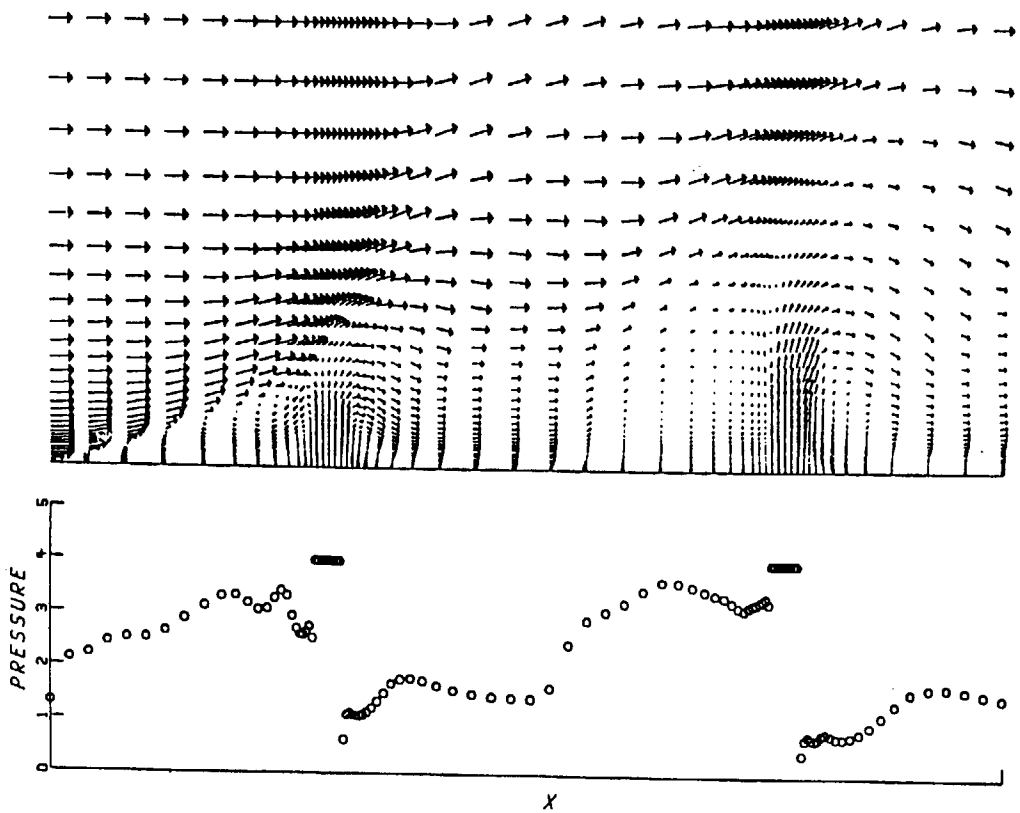

SUMMARY

1. New average state of Roe's splitting for chemical reacting gases is proposed.
2. A numerical method based on Roe flux-splitting for solving the Navier-Stokes and species equations for chemical nonequilibrium gases has been developed.
3. Numerical results show the present method has the potential for calculating high Mach number flows with nonequilibrium chemistry and complex wave structure.
4. Implementation of an implicit time solver is in progress.
5. Thermal nonequilibrium is being considered in the next stage of code development.
6. Work for further code validation is needed.

N91-10895

Visualization of Fluid Dynamics at NASA Ames

Val Watson
NASA Ames Research Center

The hardware and software currently used for visualization of fluid dynamics at NASA Ames is described. The software includes programs to create scenes (for example particle traces representing the flow over an aircraft), programs to interactively view the scenes, and programs to control the creation of video tapes and 16mm movies. The hardware includes high performance graphics workstations, a high speed network, digital video equipment, and film recorders.

With the current workstations, a scientist can interactively view flow over simplified objects, such as the flow over a circular cylinder. For complex objects, such as an aircraft, the workstation creates each picture too slowly to gain a sense of the dynamics of the flow. Therefore, each picture is stored frame by frame on a video tape or 16mm film and then the video or movie is played back at normal speed to illustrate the flow dynamics.

The upgrade in workstations planned for this year is expected to permit moderately complex pictures (pictures that can be represented by 10,000 polygons or less) to be created at a rate of 10 frames per second --- fast enough to gain a sense of the flow dynamics. Therefore, these workstations should permit interactive viewing of the flow over complete aircraft rather than just simple objects. Upgrades planned this year for software should provide a more effective interface for controlling the interactive viewing.

A comparison of the upgrades planned this year with an ideal simulation and visualization environment shows that there is still potential for major improvements in both software and hardware. The greatest potential for improving the environment is the development of software to extract and illustrate the essence of very complex phenomena.

Results presented by other scientists during this conference clearly demonstrate the effectiveness of the current visualization tools for assisting in the understanding of complex simulations, but it is also clear that we are a long way from utilizing visualization tools to their full extent.

Outline

NASA's current visualization tools

Capabilities with the current tools

Upgrades planned for this year

Potential for further improvements

Conclusions

Visualization Hardware

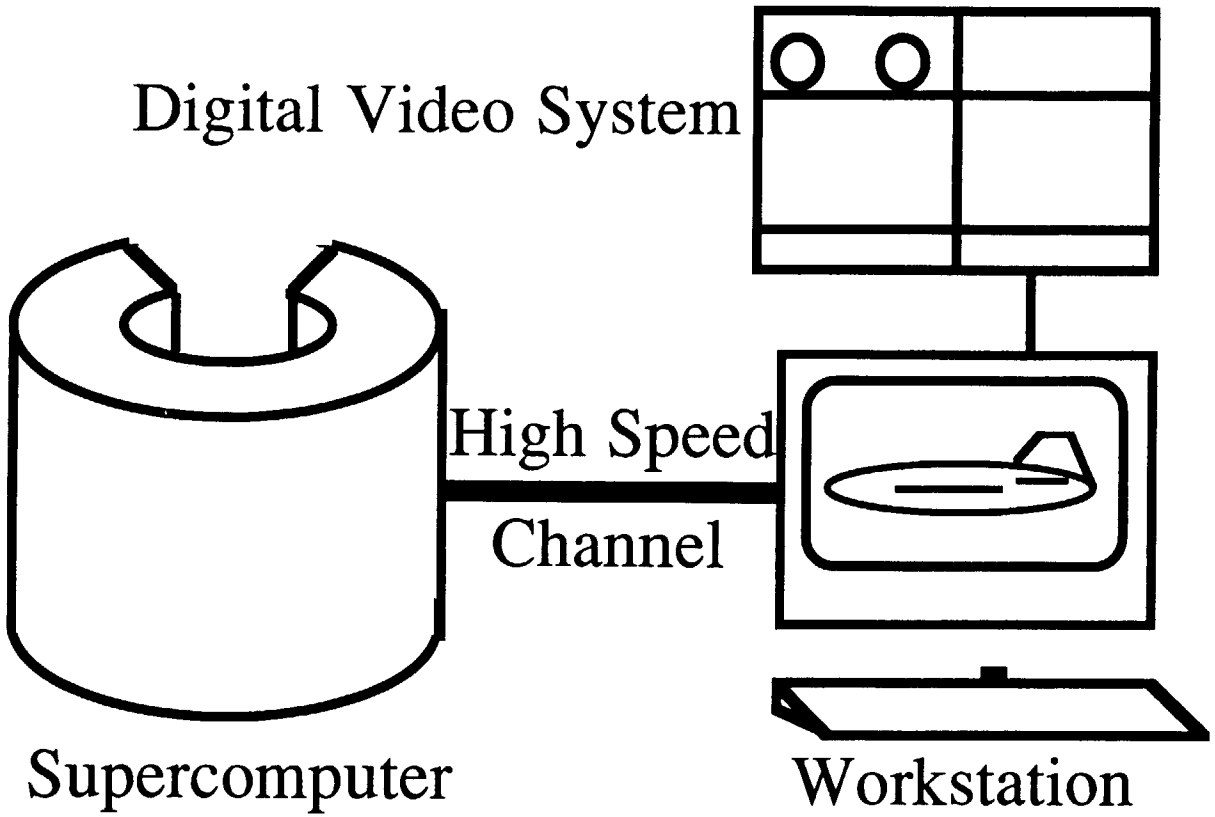

Video Recording System

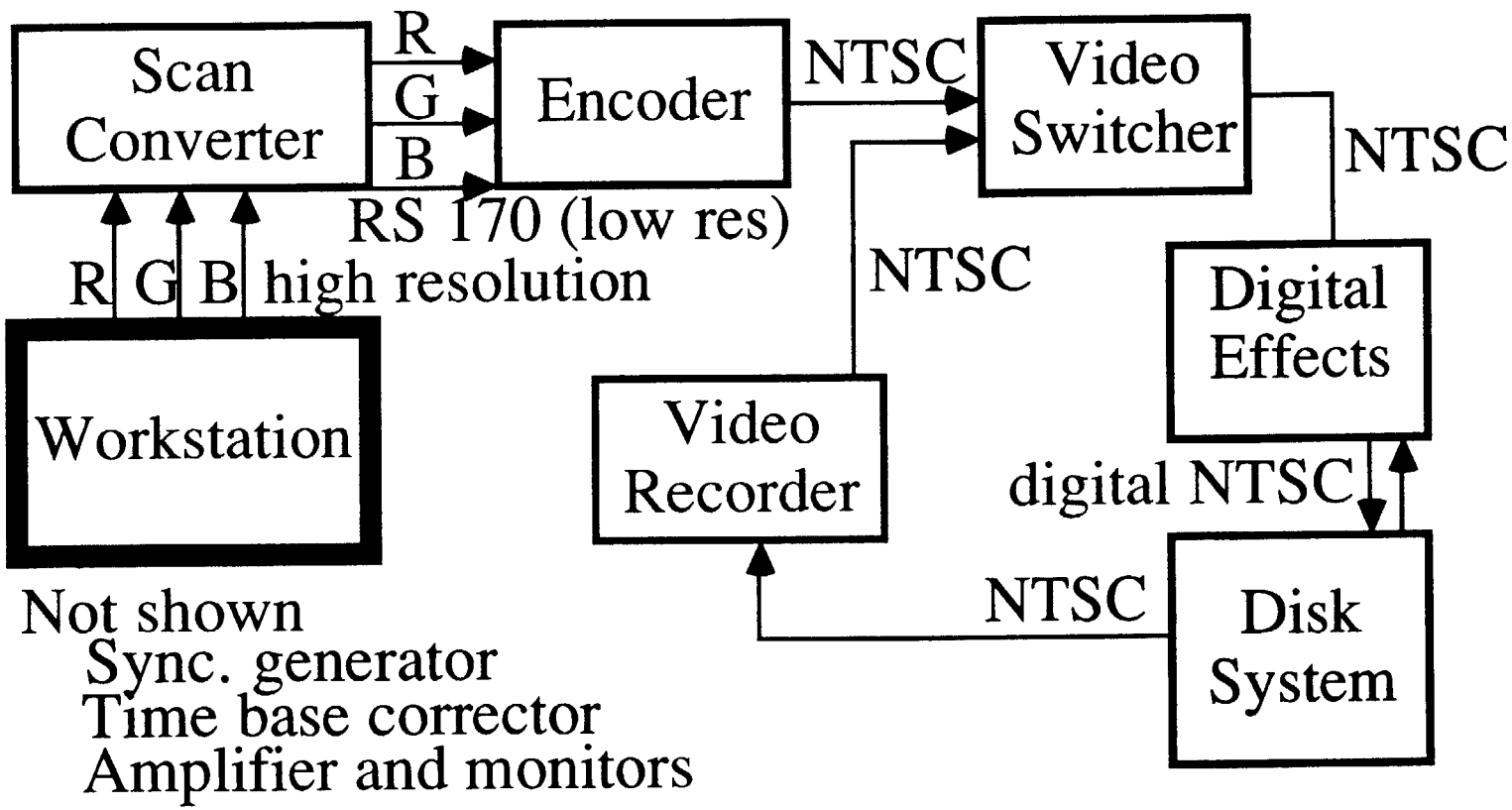

Software

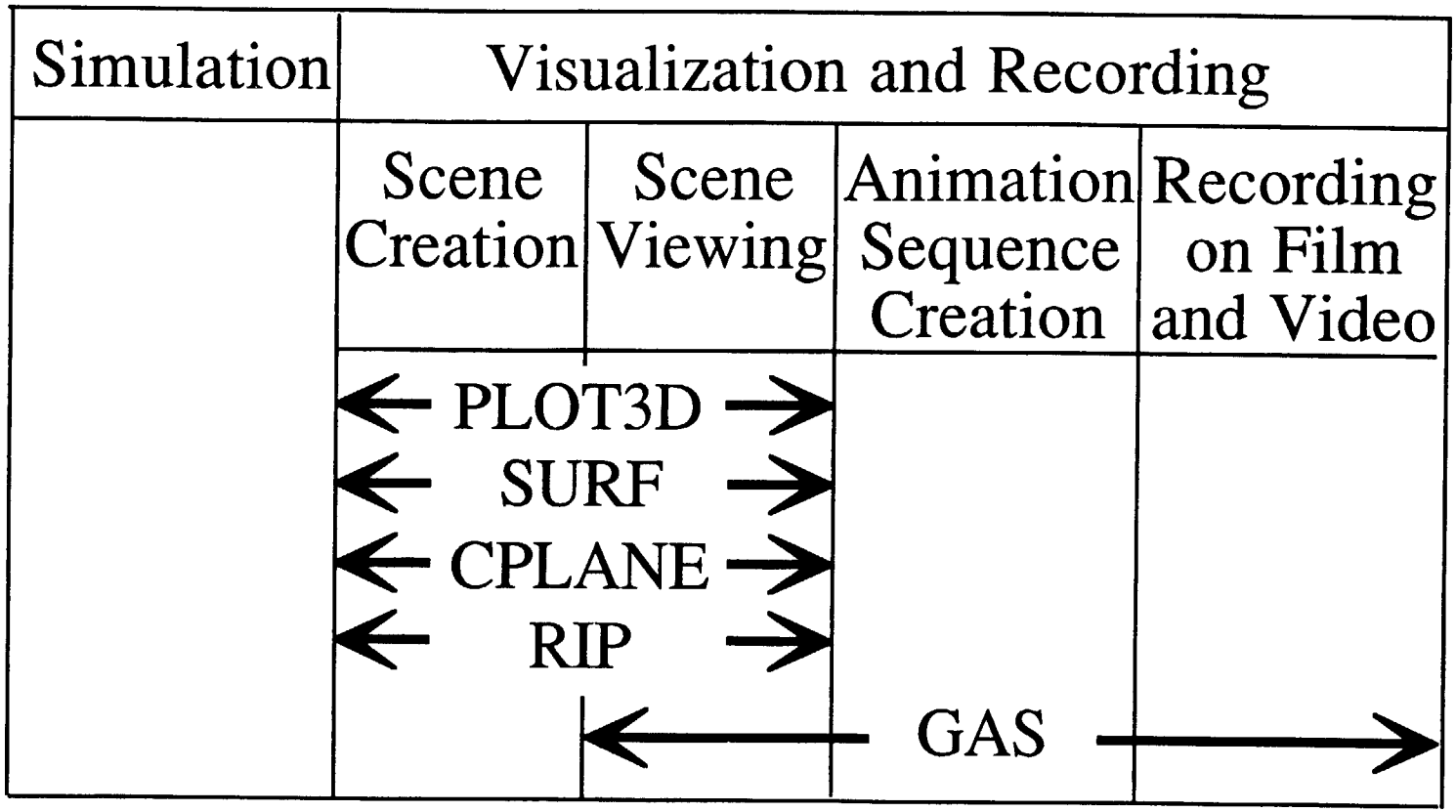
Simulation
Visualization and Recording
Scene Creation
Scene Viewing
Animation Sequence Creation
Recording on Film and Video
PLOT3D
SURF
CPLANE
RIP
GAS

Current Capabilites in Visualization

Interactive viewing with workstations

- Dynamic illustration of wire frame objects
- Dynamic illustration of simple solid objects
- Static illustration of complex solid objects

Playback viewing with video or film

- Dynamic illustration of complex solid objects

Upgrades in Workstations Planned this Year

Basic Workstation features

Central processor	from 2600 to 2000 Dhrystones
Arith processor	from 0.1 to 6.0 MFLOPS
Primary memory	from 4 to 32 MBytes
Secondary mem.	from 474 to 1000 MBytes

Graphics Features

3D coord. transf.	from 80K to 800K coord./sec
Solids rendering	from 0.5K to 100K polygons/sec

(= 10,000 polygons at 10 frames/sec)

Upgrades in Software Planned this Year

Combination of old modules into a single program

Changes to take advantage of new workstations

Changes to make visualization more interactive

Comparison of Current Capabilities with "Ideal" for Vision

Feature	Current	"Ideal"
spatial res.	1 minute of arc	of the same order
color res.	16 million colors	of the same order
freq. resp.	(scene dependent)	15 frames/sec
field of view	1/5 steradian	5 steradians

Comparison of the Ideal vs Current Field of View

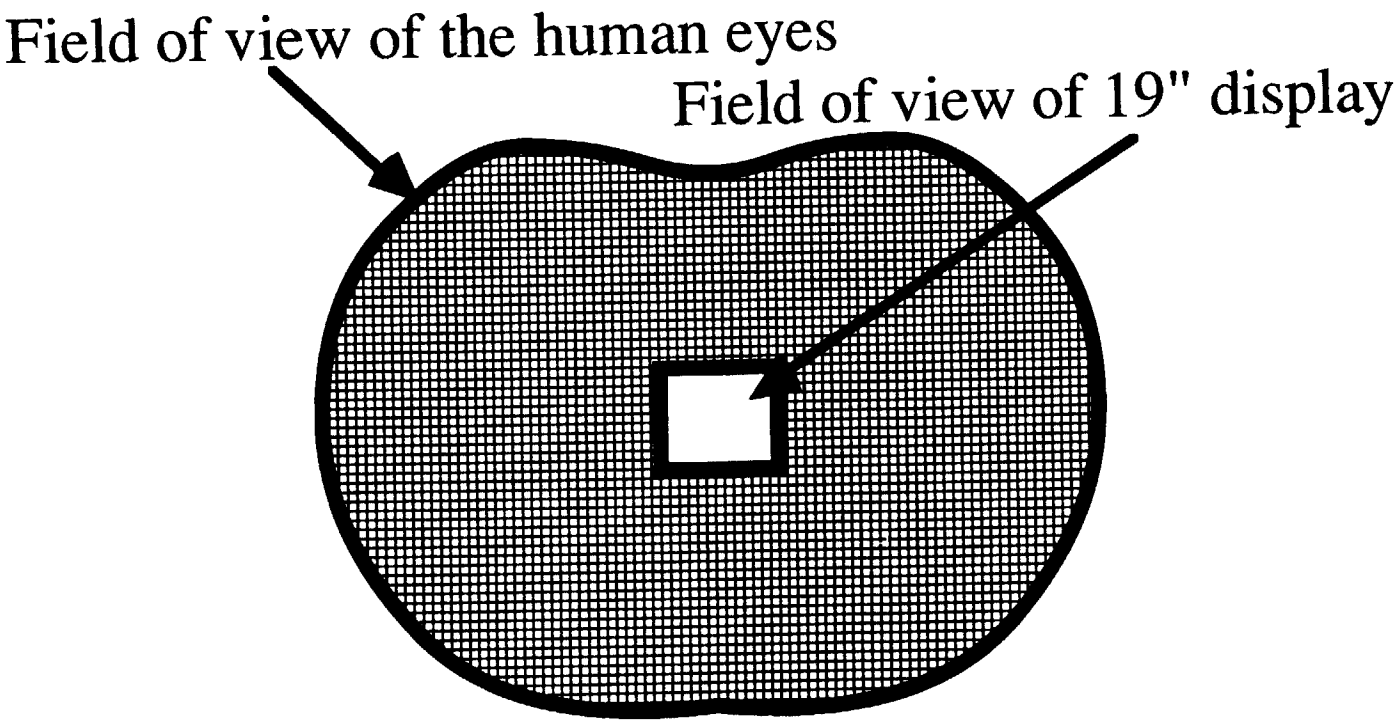

Comparison of Current Capabilities with "Ideal" for Interactive Control

Current

- mouse and keyboard

"Ideal"

- 6-degree of freedom control
- voice recognition

Potential for Improvements in Software

Tools for extraction of critical features

Tools for highlighting critical features and suppressing less important features

CONCLUSIONS

The NAS decision to invest in visualization tools has been justified by improved analysis capabilities

The most effective use of vis. tools is the *routine* interactive viewing of solutions *and techniques*

Current workstations permit interactive viewing of the flows over simple shapes

Workstations to be procurred should permit interactive viewing of flows over complex shapes

CONCLUSIONS (continued)

A new generation of software is being developed
- to take advantage of new workstation capabilties
- to make the visual analysis more interactive

The most critical task is overcoming visual clutter
- developing techniques to extract the "essence"
- developing techniques to illustrate the "essence"

We are a long way from utilizing our present visualization tools completely

For Further Information

NAS procurement for the new workstations

Rosemary Buchanan
Mail Stop 258-6
NASA Ames Research Center
Moffett field, CA 94035
(415) 694-4610

Scientific visualization materials

Stanford report on automated feature extraction
1988 CFD Highlights video
Stereo slides

Pat Mumford Elson
Mail Stop 258-2
NASA Ames Reseach Center
Moffett Field, CA 94035
(415) 694-4463

N91-10896

COMPUTATIONAL FLUID DYNAMICS ON A MASSIVELY PARALLEL COMPUTER

Dennis Jespersen, CFD Branch, NASA/Ames
and
Creon Levit, NAS Applied Research Branch, NASA/Ames

Abstract. We have implemented a finite-difference code for the compressible Navier-Stokes equations on the Connection Machine, a massively parallel computer. The code is based on the ARC2D/ARC3D program and uses the implicit factored algorithm of Beam and Warming. The code uses odd-even elimination to solve linear systems. We give timings and computation rates for the code, and compare with a Cray XMP.

PRECEDING PAGE BLANK NOT FILMED

COMPUTATIONAL FLUID DYNAMICS ON A MASSIVELY PARALLEL COMPUTER

Dennis Jespersen, CFD Branch NASA/Ames
and
Creon Levit, NAS Applied Research Branch, NASA/Ames

- Goal: implement a real CFD code (ARC2D/ARC3D) on a massively parallel computer, the Connection Machine.
  - > Implicit

- Is Connection Machine useful for CFD?

OUTLINE

- CM architecture
- ARC2D
- *Lisp
- Odd-even elimination
- Current status and results
- Problems and prospects

CM ARCHITECTURE

- Very large number of physical processors (up to 64K)
- SIMD
- Single-bit processors
- 2K words (32 bits each) memory per processor
- Floating point accelerator available
- Context bit (each processor on or off)
- Peak performance (computational kernels) 2–4 Gflops

CONNECTIONS

- 16 processors per chip
- Chips wired in 12-dimensional hypercube
  - > If distance=power of 2, communication in 2 hops
- General router
- Nearest-neighbor (NEWS) available and fast
  - > (Reminiscent of ILLIAC)
- Wrap-around at edges

VIRTUAL PROCESSORS

- Each physical processor can be configured as $1, 2, 4, 8, \ldots$ virtual processors.

VP ratio	1	2	4	8	16	32	64
memory/processor (words)	2K	1K	512	256	128	64	32

- Transparent to user.
- Arithmetic slows down (slightly slower than linear)
- Communication relatively faster
  > Memory references that were off-chip may become on-chip.

ARC2D

- 2D Compressible Navier-Stokes

$$\partial_t Q + \partial_\xi E + \partial_\eta F = \mathrm{Re}^{-1}(\partial_\xi E_v + \partial_\eta F_v)$$

- Central space differencing, implicit Euler in time, factored, delta form:

$$(I + \Delta t \delta_\xi A^n - \Delta t \frac{1}{\mathrm{Re}} \delta_\xi R^n)(I + \Delta t \delta_\eta B^n - \Delta t \frac{1}{\mathrm{Re}} \delta_\eta S^n)\Delta Q^n$$

$$= -\Delta t(\delta_\xi E^n + \delta_\eta F^n - \frac{1}{\mathrm{Re}}(\delta_\xi E_v^n + \delta_\eta F_v^n))$$

- Pulliam-Chaussee diagonal form:

$$T_\xi(I + \Delta t \delta_\xi \Lambda_\xi - \Delta t \frac{1}{\mathrm{Re}} \delta_\xi \Lambda_{\xi,v})$$

$$N(I + \Delta t \delta_\eta \Lambda_\eta - \Delta t \frac{1}{\mathrm{Re}} \delta_\eta \Lambda_{\eta,v}) T_\xi^{-1} \Delta Q^n = \mathrm{rhs}$$

ARC2D on CM

- One grid point per (virtual) processor.
- Write in *Lisp
  - > No line-by-line translation
- Shear-layer
- Cylinder
- Typical size 128×64 (8K processors, VP ratio = 1)
- CM well-suited for explicit time-step methods (e.g., Runge-Kutta)

IMPLICIT SOLVER: ODD-EVEN ELIMINATION

- Closely related to cyclic reduction
- One row corresponds to one processor
- Communication is always to processors 2^k distant
- $2^n \times 2^n$ system solvable in n stages
- Algorithm makes no sense on uniprocessor machines
- Stability not a problem in practice
  - > Some stability results provable, e.g. $B(-\Delta t, 1, \Delta t)$

ODD-EVEN ELIMINATION: ALGORITHM

$Ax = y$

$$\begin{pmatrix} b_1 & c_1 & & & \\ a_2 & b_2 & c_2 & & \\ & \ddots & \ddots & \ddots & \\ & & a_{n-1} & b_{n-1} & c_{n-1} \\ & & & a_n & b_n \end{pmatrix}$$

For $k = 0, 1, \ldots, \log_2 n - 1$,

$$m = 2^k$$

$$a_i \leftarrow a_i / b_i$$

$$c_i \leftarrow c_i / b_i$$

$$y_i \leftarrow y_i / b_i$$

$$b_i \leftarrow 1 - a_i c_{i-m} - c_i a_{i+m}$$

$$y_i \leftarrow y_i - a_i y_{i-m} - c_i y_{i+m}$$

$$a_i \leftarrow -a_i a_{i-m}$$

$$c_i \leftarrow -c_i c_{i+m}$$

ODD-EVEN ELIMINATION:PERIODIC

- Same code
- Same cost
- Periodic solves no more costly than nonperiodic solves

PROGRESS

- 2D Explicit (Runge-Kutta)
- 2D Implicit (scalar and block tridiagonal)
  - > Shear layer
  - > Cylinder (low Re)
- 3D Explicit (Runge-Kutta)

TIMINGS

- Timings, Mflop rates (16k processors, implicit scalar tridiagonal algorithm)

Grid size	VP ratio	Mflops	sec/step	XMP time/CM time
128×128	1	58	0.43	0.66
256×128	2	86	0.60	0.75
512×512	16	106	4.2	0.86

- Timings, Mflop rates (16k processors, explicit algorithm)

Grid size	VP ratio	Mflops	sec/step	XMP time/CM time
128×128	1	63	0.43	0.69
256×128	2	123	0.44	1.34
512×512	16	241	1.8	2.62

TIMINGS: 2D BLOCK IMPLICIT AND 3D

- 2D Timings, 16k processors, block tridiagonal algorithm

Grid size	VP ratio	sec/step	XMP time/CM time
128×128	1	2.61	0.23
256×128	2	3.21	0.37
256×256	4	4.84	0.49
512×256	8	9.66	0.49

- 3D Timings, 8k processors, explicit algorithm

Grid size	VP ratio	sec/step
$32 \times 32 \times 16$	2	1.94
$64 \times 32 \times 32$	8	3.80
$64 \times 64 \times 32$	16	6.53

PROBLEMS AND PROSPECTS

- Memory limitation
- Communication bottleneck?
- Boundary conditions
  - > Complicated boundary conditions – inefficient?
- Future plans:
  - > 3D Implicit

SESSION XII

HYPERSONICS/AFE

Chairman:
Chien P. Li
Advanced Programs Office
NASA Johnson Space Center

PRECEDING PAGE BLANK NOT FILMED

N91-10897

Conservation Equations and Physical Models for Hypersonic Air Flows Over the Aeroassist Flight Experiment Vehicle

Peter A. Gnoffo

NASA Langley Research Center
Hampton, VA 23665
Mail Stop 366

Abstract

The code development and application program for the Langley Aerothermodynamic Upwind Relaxation Algorithm (LAURA), with emphasis directed toward support of the Aeroassist Flight Experiment (AFE) in the near term and Aeroassisted Space Transfer Vehicle (ASTV) design in the long term is reviewed. LAURA is an upwind-biased, point-implicit relaxation algorithm for obtaining the numerical solution to the governing equations for three-dimensional, viscous, hypersonic flows in chemical and thermal nonequilibrium. The algorithm is derived using a finite-volume formulation in which the inviscid components of flux across cell walls are described with Roe's averaging and Harten's entropy fix with second-order corrections based on Yee's Symmetric Total Variation Diminishing scheme. Because of the point-implicit relaxation strategy, the algorithm remains stable at large Courant numbers without the necessity of solving large, block tri-diagonal systems. A single relaxation step depends only on information from nearest neighbors. Predictions for pressure distributions, surface heating, and aerodynamic coefficients compare well with experimental data for Mach 10 flow over an AFE wind tunnel model. Predictions for the hypersonic flow of air in chemical and thermal nonequilibrium (velocity = 8917 m/s, altitude = 78 km.) over the full scale AFE configuration obtained on a multi-domain grid are discussed.

PRECEDING PAGE BLANK NOT FILMED

SIMULATION CAPABILITIES

PROGRAM LAURA (LANGLEY AEROTHERMODYNAMIC UPWIND RELAXATION ALGORITHM)

I. PHYSICS

Navier -Stokes Or Thin-Layer Navier-Stokes Equations

Steady Or Unsteady

Laminar (Turbulent Boundary Layer)

Chemical Nonequilibrium (11 Species, 2 Chemical Kinetic Models)

Thermal Nonequilibrium (Two-Temperature Model)

Documented In NASA TP 2867

II. NUMERICS

Finite Volume, Roe's Averaging, STVD Limiters

Fluid Mechanics And Chemistry Strongly Coupled

Point Implicit Relaxation, Freeze Inverse Jacobian

Multi-Domain Capability, Structured Grids

Ideally Suited For Parallel, Asynchronous Iteration Using Unstructured Grids

COMPUTATIONAL GRID 0N SURFACE AND PLANE OF SYMMETRY FOR AFE WIND TUNNEL MODEL

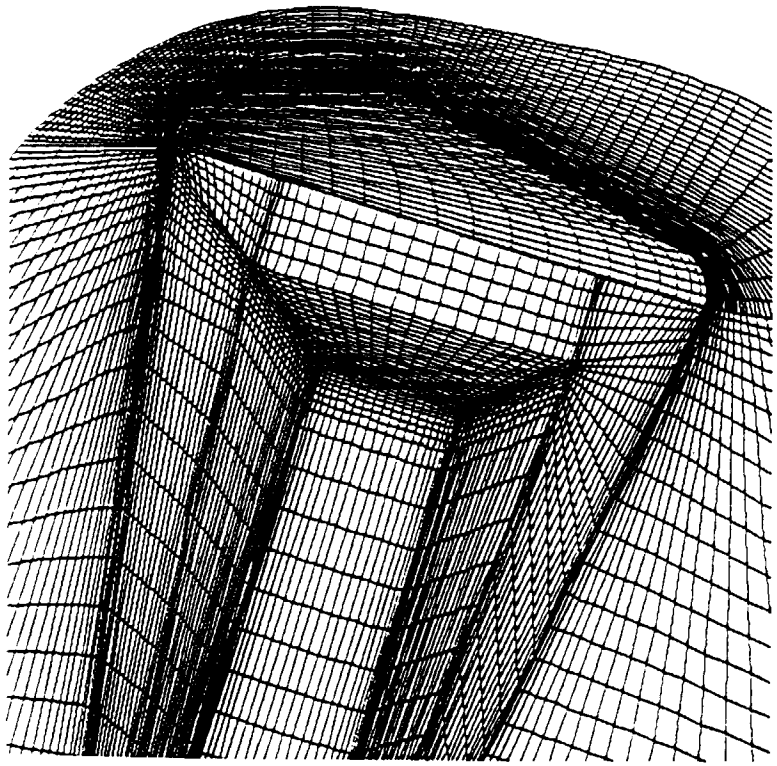

PRESSURE AND HEATING DISTRIBUTION FOR AFE

Mach 10 $\alpha = 5^{\circ}$

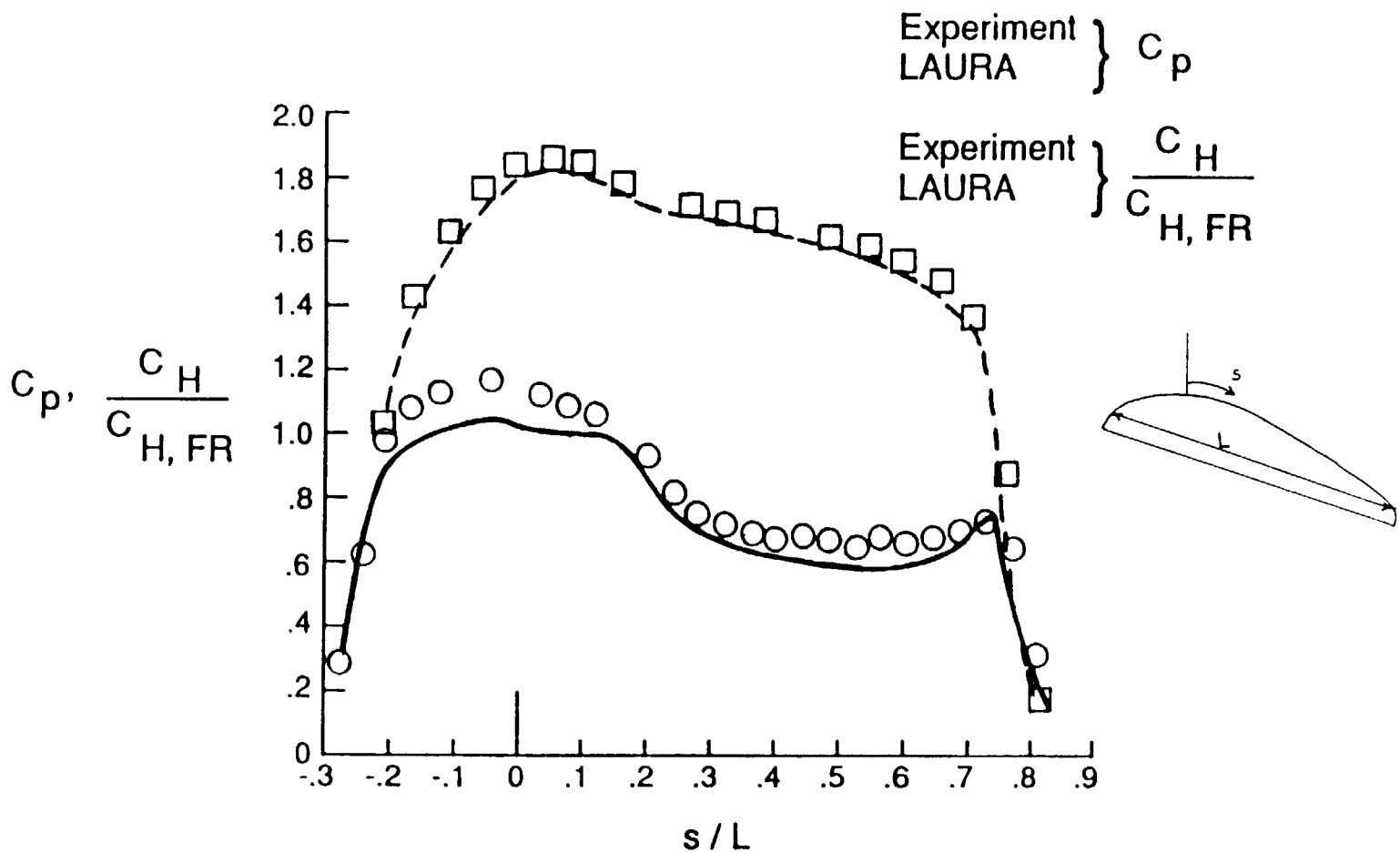

PRESSURE AND HEATING DISTRIBUTION FOR AFE

Mach 10 $\alpha = 0^\circ$

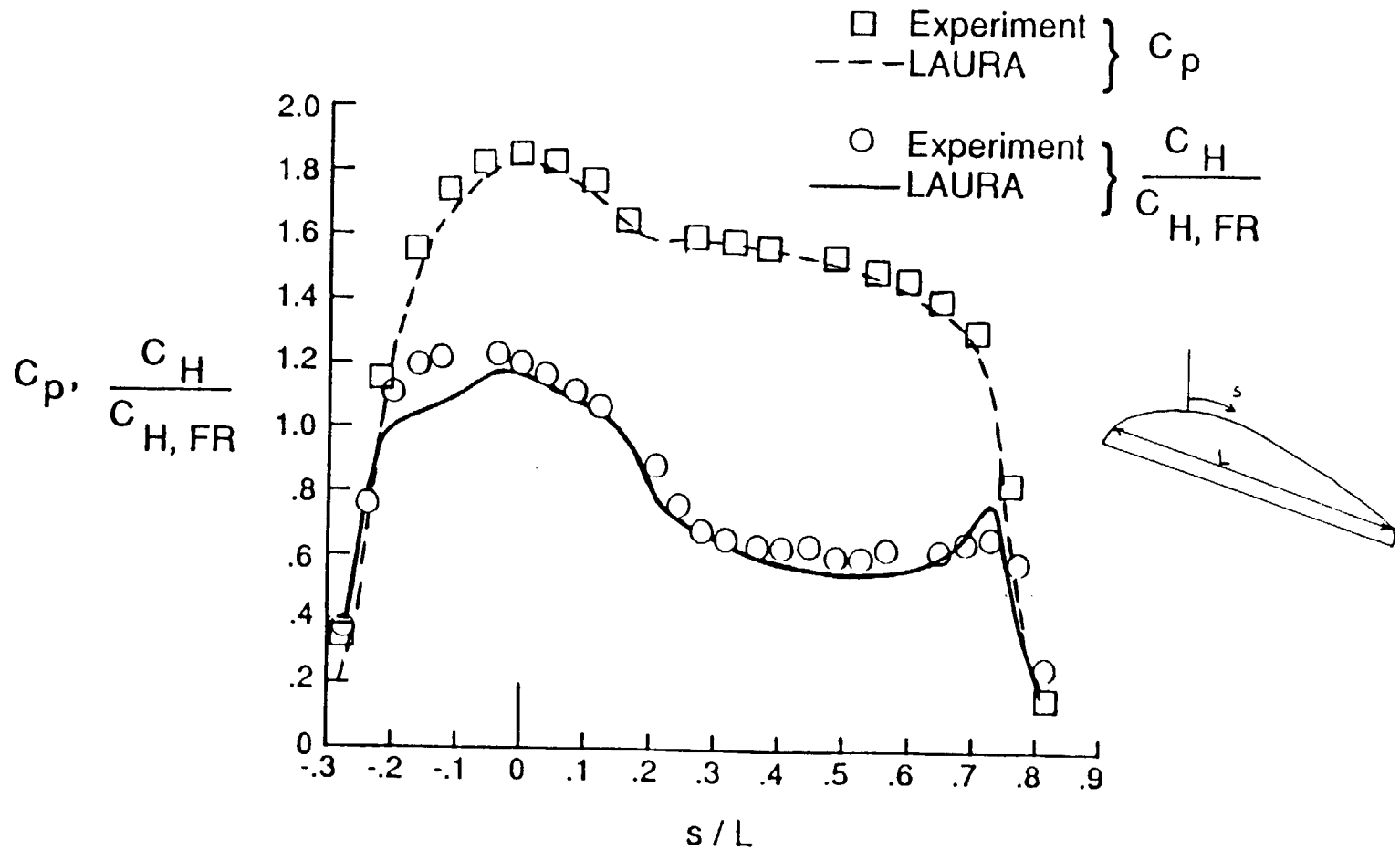

PRESSURE AND HEATING DISTRIBUTION FOR AFE

Mach 10 $\alpha = -5°$

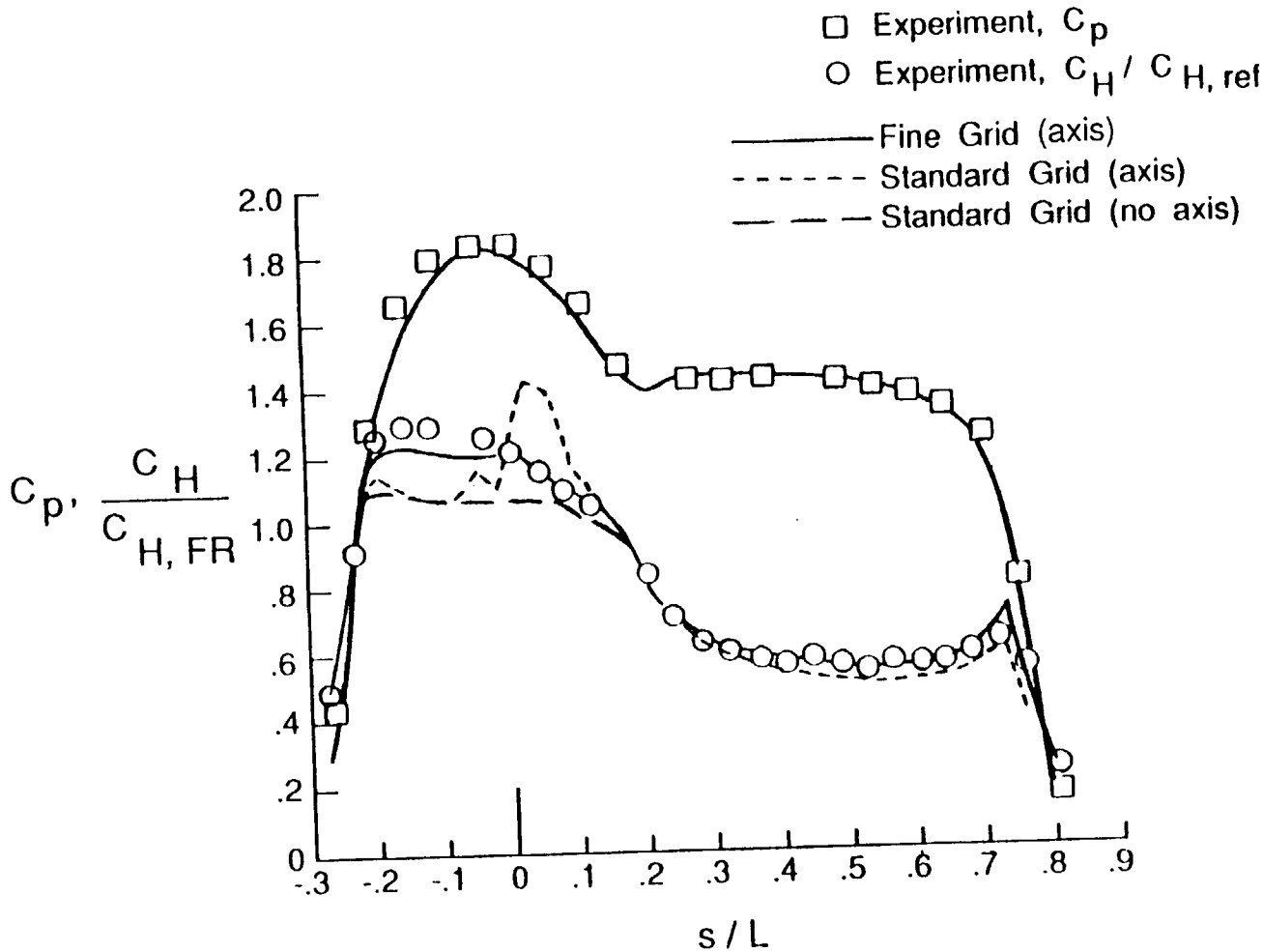

DETAIL OF AXIS AND N0 AXIS GRIDS

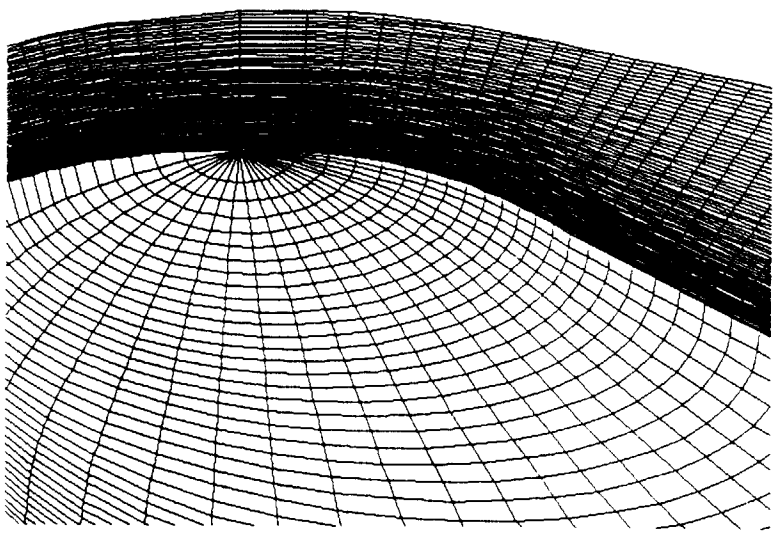

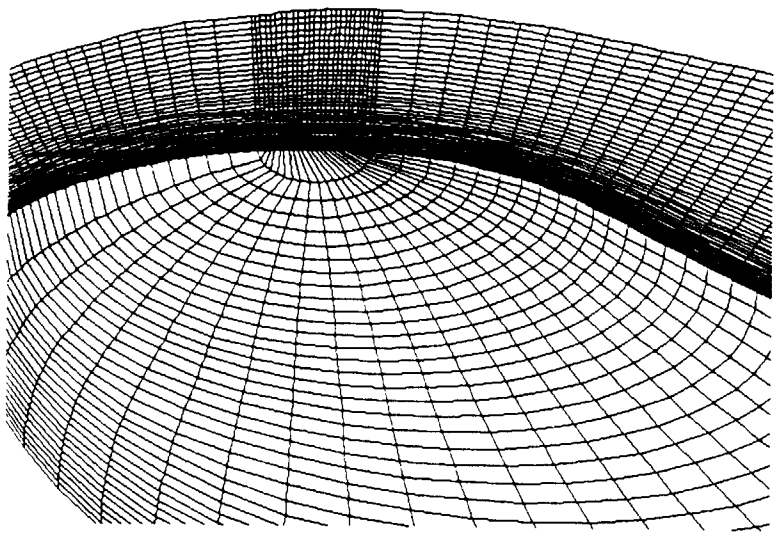

HEATING DISTRIBUTIONS FOR AFE STING

Mach 10 $\alpha = 0^{\circ}$

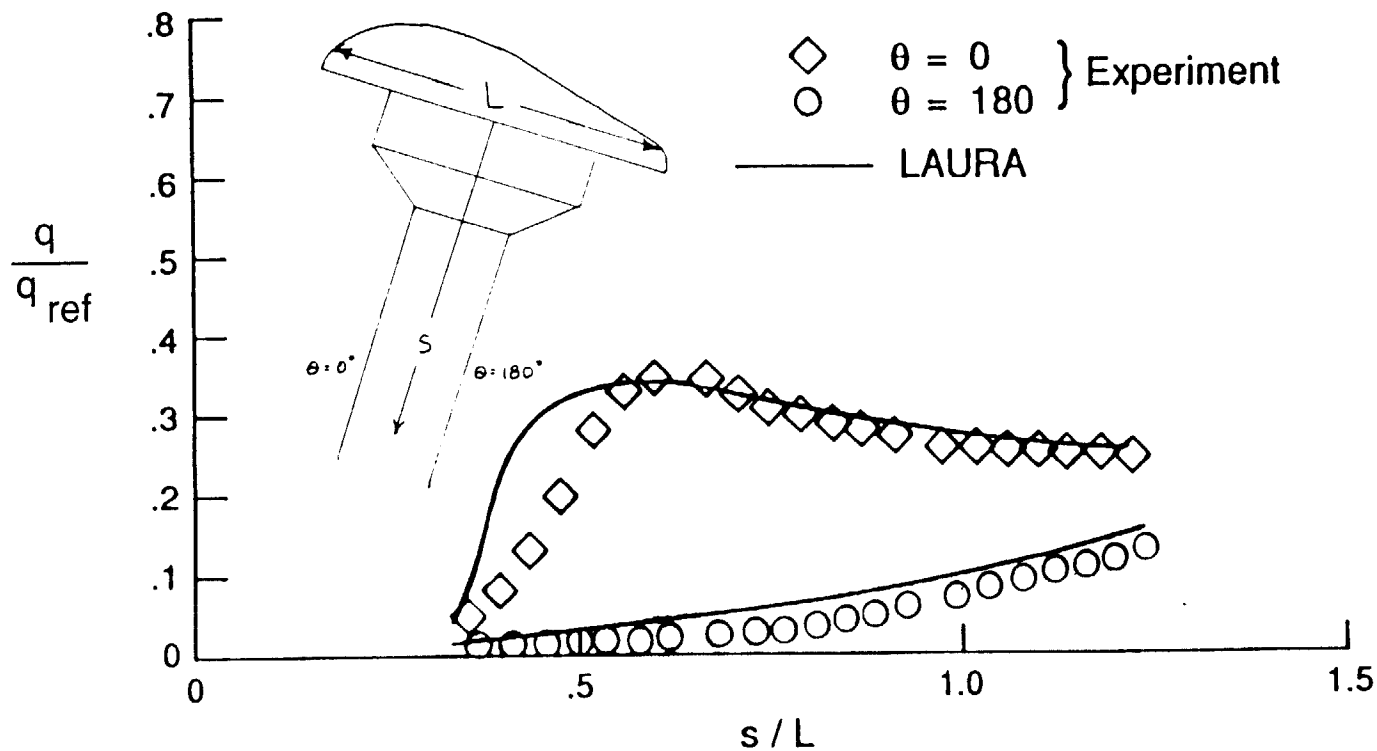

HEATING DISTRIBUTIONS FOR AFE STING

Mach 10 $\alpha = -5^\circ$

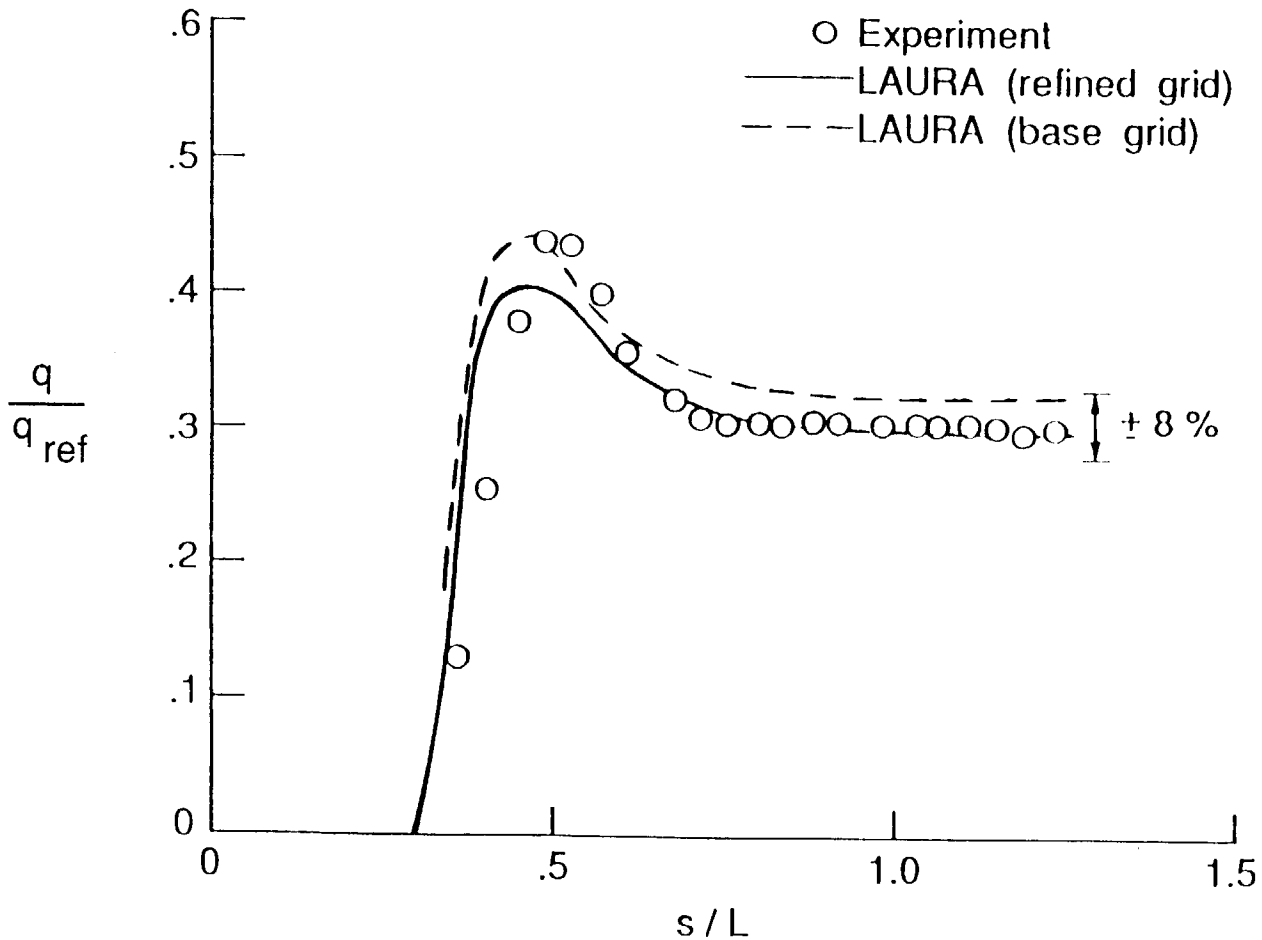

PRESSURE CONTOURS IN THE PLANE OF SYMMETRY

$M_\infty = 10 \qquad \alpha = -5^\circ$

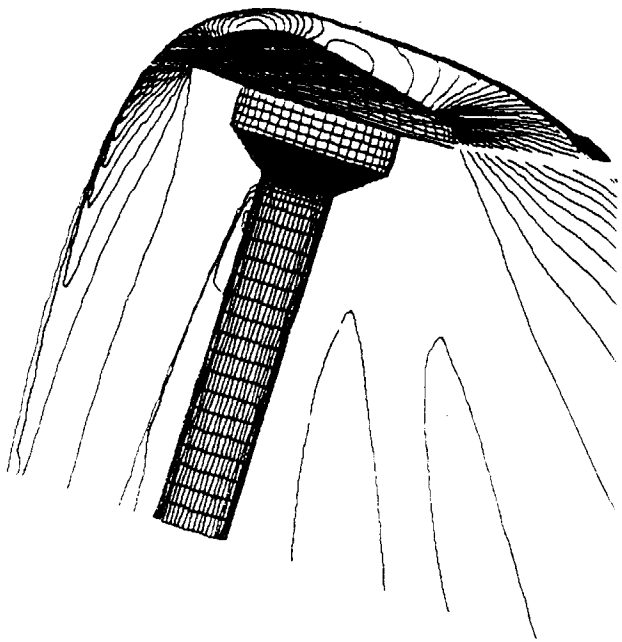

MACH NUMBER CONTOURS IN THE PLANE OF SYMMETRY

$M_\infty = 10 \qquad \alpha = -5^\circ$

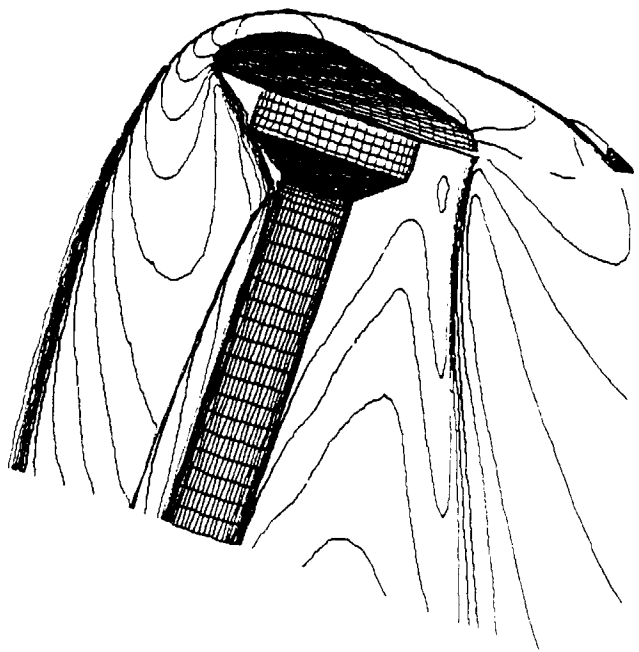

COMPUTATIONAL GRID ON SURFACE AND PLANE OF SYMMETRY FOR AFE

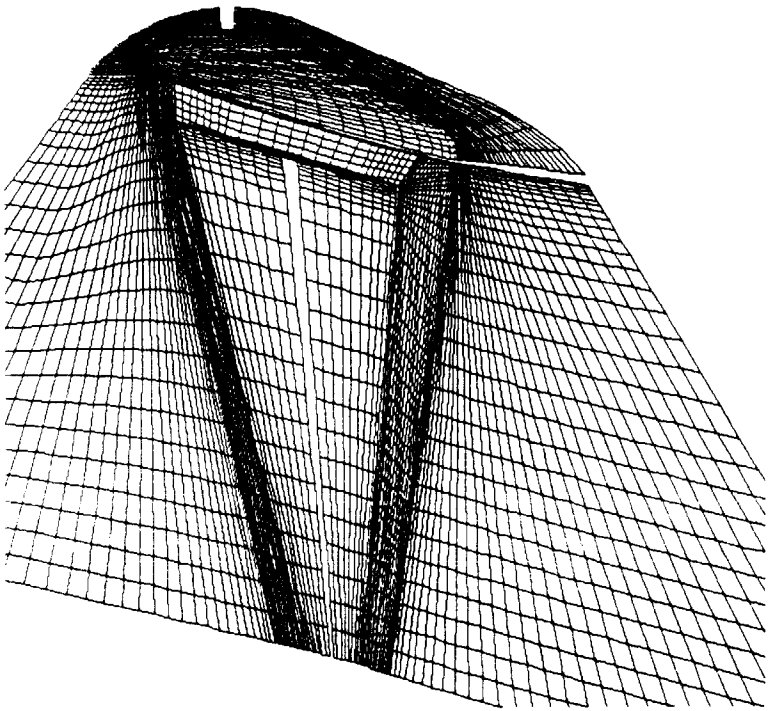

TRANSLATIONAL TEMPERATURE CONTOURS IN THE PLANE OF SYMMETRY

$M_\infty = 32$ $h = 78$ km

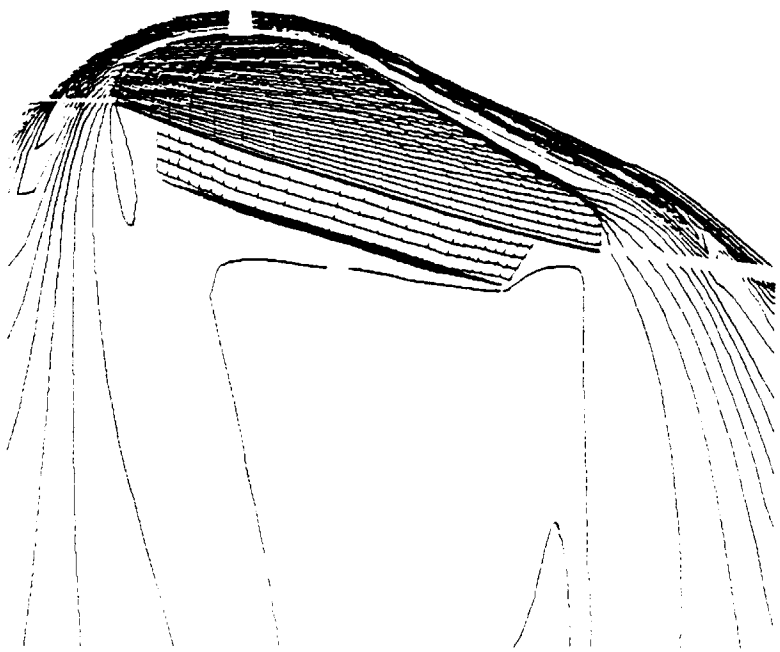

VIBRATIONAL TEMPERATURE CONTOURS IN THE PLANE OF SYMMETRY

$M_\infty = 32$ $h = 78$ km

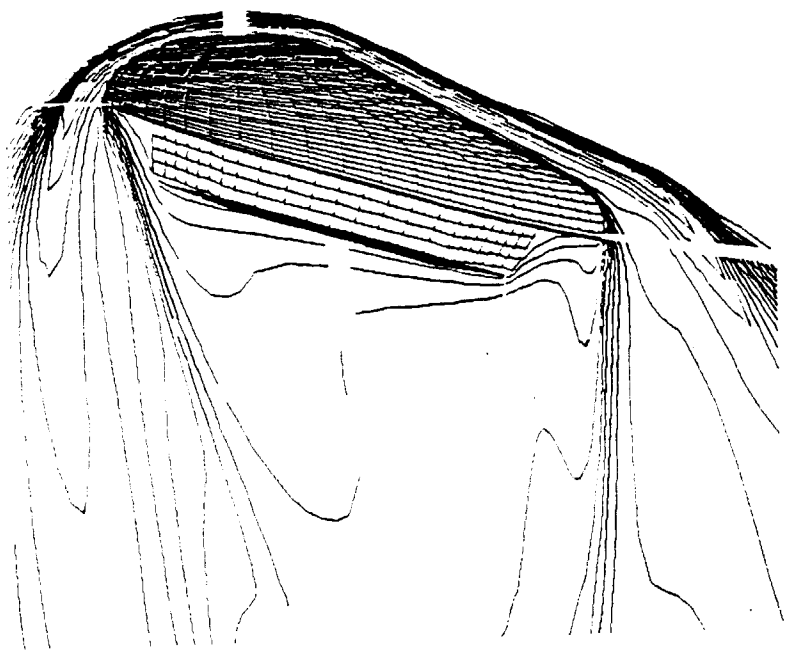

ELECTRON NUMBER DENSITY CONTOURS IN THE PLANE OF SYMMETRY

$M_\infty = 32$ $h = 78$ km

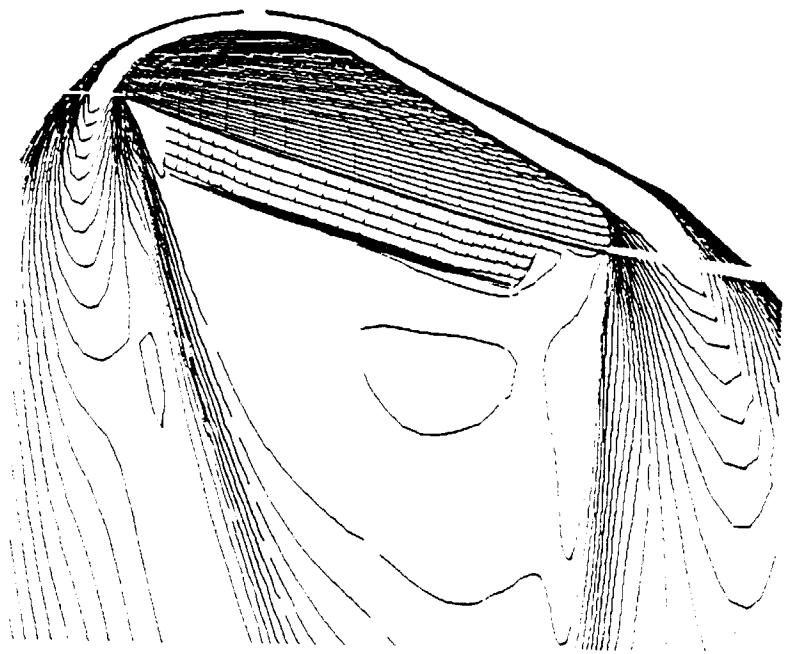

TEMPERATURE DISTRIBUTION ACROSS THE SHOCK LAYER

COMPARISON TO DSMC

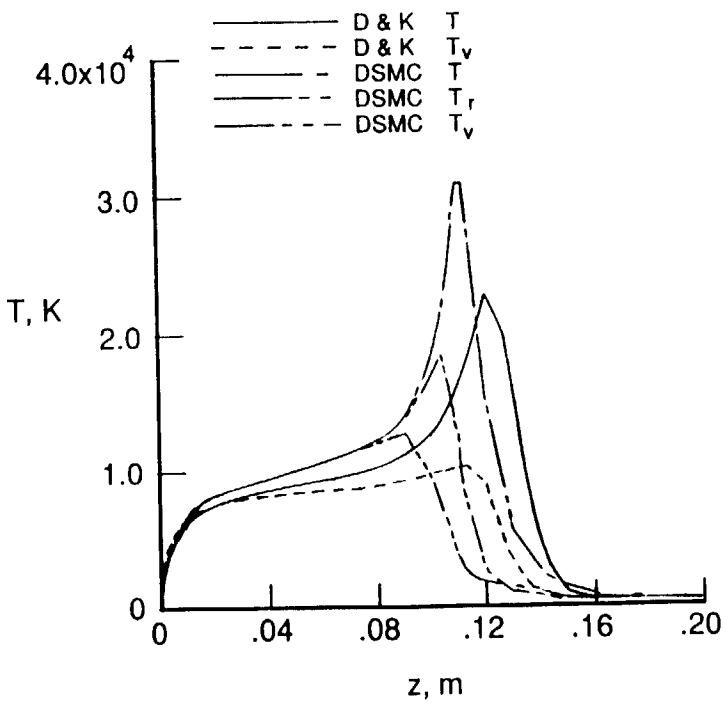

GRID REFINEMENT STUDY

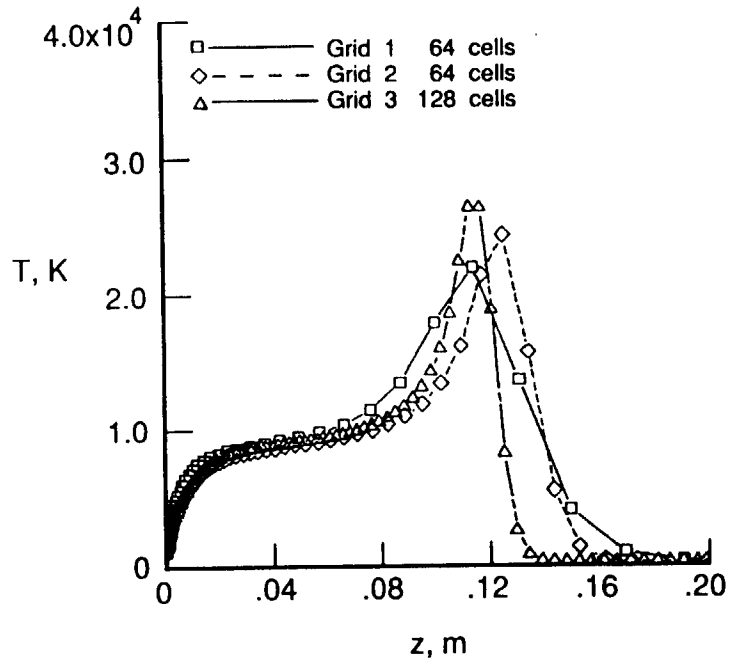

N91-10898

THE COMPUTATION OF THERMO-CHEMICAL NONEQUILIBRIUM HYPERSONIC FLOWS

Graham Candler
Aerothermodynamics Branch
MS 230-2, 415-694-4227
NASA Ames Research Center
Moffett Field, CA 94035

Several conceptual designs for vehicles that would fly in the atmosphere at hypersonic speeds have been developed recently. For the proposed flight conditions the air in the shock layer that envelops the body is at a sufficiently high temperature to cause chemical reaction, vibrational excitation, and ionization. However, these processes occur at finite rates which, when coupled with large convection speeds, cause the gas to be removed from thermo-chemical equilibrium. This non-ideal behavior affects the aerothermal loading on the vehicle and has ramifications in its design.

A numerical method to solve the equations that describe these types of flows in two dimensions has been developed. The state of the gas is represented with seven chemical species, a separate vibrational temperature for each diatomic species, an electron translational temperature, and a mass-averaged translational-rotational temperature for the heavy-particles. The equations for this gas model are solved numerically in a fully coupled fashion using an implicit finite volume time-marching technique. Gauss-Seidel line-relaxation is used to reduce the cost of the solution and flux-dependent differencing is employed to maintain stability.

The numerical method has been tested against several experiments. The calculated bow shock wave detachment on a sphere and two cones was compared to those measured in ground testing facilities. The computed peak electron number density on a sphere-cone was compared to that measured in a flight test. In each case the results from the numerical method were in excellent agreement with experiment. The technique has been used to predict the aerothermal loads on an Aeroassisted Orbital Transfer Vehicle including radiative heating. These results indicate that the current physical model of high temperature air is appropriate and that the numerical algorithm is capable of treating this class of flows.

Research Objectives

- Study flows with thermo-chemical nonequilibrium
  - multiple temperatures: $T \neq T_v \neq T_e$
  - chemical state not in equilibrium at local e, ρ
- Primary application to blunt re-entry vehicles in air
  - other nonequilibrium problems are possible, *e.g.* NASP
  - could be used with other gases, *e.g.* H_2 – Air
  - steady-state
  - two-dimensional or axisymmetric
  - laminar
- Demonstrate feasibility of numerical solutions to reacting flows
  - stiff equations
  - large source terms

Justifications

- Proposed hypersonic vehicles:
  - AOTV/AFE
  - NASP
  - Mission to Mars
- Ground-based testing is difficult
- Nonequilibrium effects important:
  - force coefficients
  - convective and radiative heating
- Study high-temperature air physics:
  - effects of thermo-chemical nonequilibrium
  - develop new modeling techniques

Technical Approach – Thermodynamic Model

- Translational-rotational equilibrium assumed
- One vibrational temperature for each diatomic species
- Electron-electronic temperature
  - free-electron and electronic temperatures equal
- Model finite-rate energy transfer modes

Technical Approach – Conservation Equations

- Governing equations in two dimensions:

$$\frac{\partial U}{\partial t} + \frac{\partial F}{\partial x} + \frac{\partial G}{\partial y} = W$$

- For a gas with n species, m diatomic:

$$U = \left(\rho_1,\ \rho_2,\ \ldots,\ \rho_n,\ \rho u,\ \rho v,\ E_{v_1},\ \ldots,\ E_{v_m},\ E_e,\ E\right)^T$$

Technical Approach – Equations of State

- Pressure and temperature:

$$T = \frac{1}{\rho c_v}\left(E - \sum_{s=1}^{m} E_{v_s} - E_e - \frac{1}{2}\rho(u^2 + v^2) - \sum_{s=1}^{n} \rho_s h_s^\circ - \sum_{s\neq e}^{n} \rho_s e_{\mathrm{el}\,s}\right),$$

$$p = \sum_{s\neq e}^{n} \frac{\rho_s}{M_s} RT + p_e, \qquad c_v = \sum_{s\neq e}^{n} \frac{\rho_s}{\rho} c_{v_s}.$$

- Electron pressure and temperature:

$$T_e = \frac{1}{\rho_e c_{ve}}\left(E_e - \frac{1}{2}\rho_e(u^2 + v^2)\right), \qquad p_e = \rho_e \frac{R}{M_e} T_e.$$

- Vibrational temperature:

$$E_{v_s} = \rho_s \frac{R}{M_s} \frac{\theta_{vs}}{e^{\theta_{vs}/T_{vs}} - 1}.$$

Technical Approach – Chemical Model

- Air is modeled with seven species:

$$N_2,\ O_2,\ NO,\ NO^+,\ N,\ O,\ \text{and}\ e^-.$$

- Possible reactions:

$$\begin{aligned} N_2 + M &\rightleftharpoons 2N + M \\ O_2 + M &\rightleftharpoons 2O + M \\ NO + M &\rightleftharpoons N + O + M \\ N_2 + O &\rightleftharpoons NO + N \\ NO + O &\rightleftharpoons O_2 + N \\ N + O &\rightleftharpoons NO^+ + e^-, \end{aligned}$$

  - use two-temperature reaction rate (TT_v) model of Park

Technical Approach – Numerical Algorithm

- Equations solved in fully coupled fashion:
  - nonequilibrium directly influences solution
- Gauss-Seidel line-relaxation technique of MacCormack (1985)
- Fully implicit:
  - large time steps for rapid convergence
  - rapid reactions do not slow convergence appreciably
  - many computations required per time step
- Gauss-Seidel line-relaxation reduces cost of implicit method
- Flux-splitting:
  - stability in subsonic and supersonic regions
  - capture bow shock wave

Validation – Peak Electon Number Density

- Sphere–9° Cone in air. $u_\infty = 7.65\,\mathrm{km/s}$, $\mathcal{M}$=25.9, $Re = 6280$.

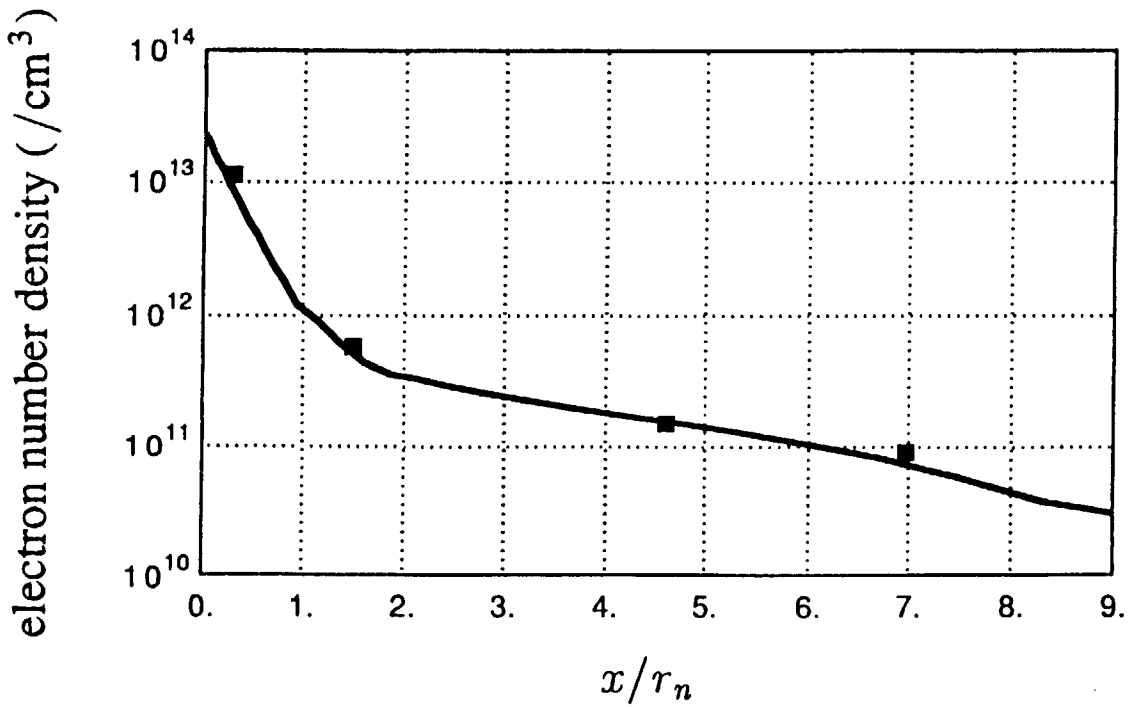

Results – Axisymmetric AOTV

- Shadowgraph of an axisymmetric AOTV model in air.

$u_\infty = 4.02\,\mathrm{km/s}$, $\mathcal{M}_\infty = 11.6$, $Re = 343000$, $\psi = 180$.

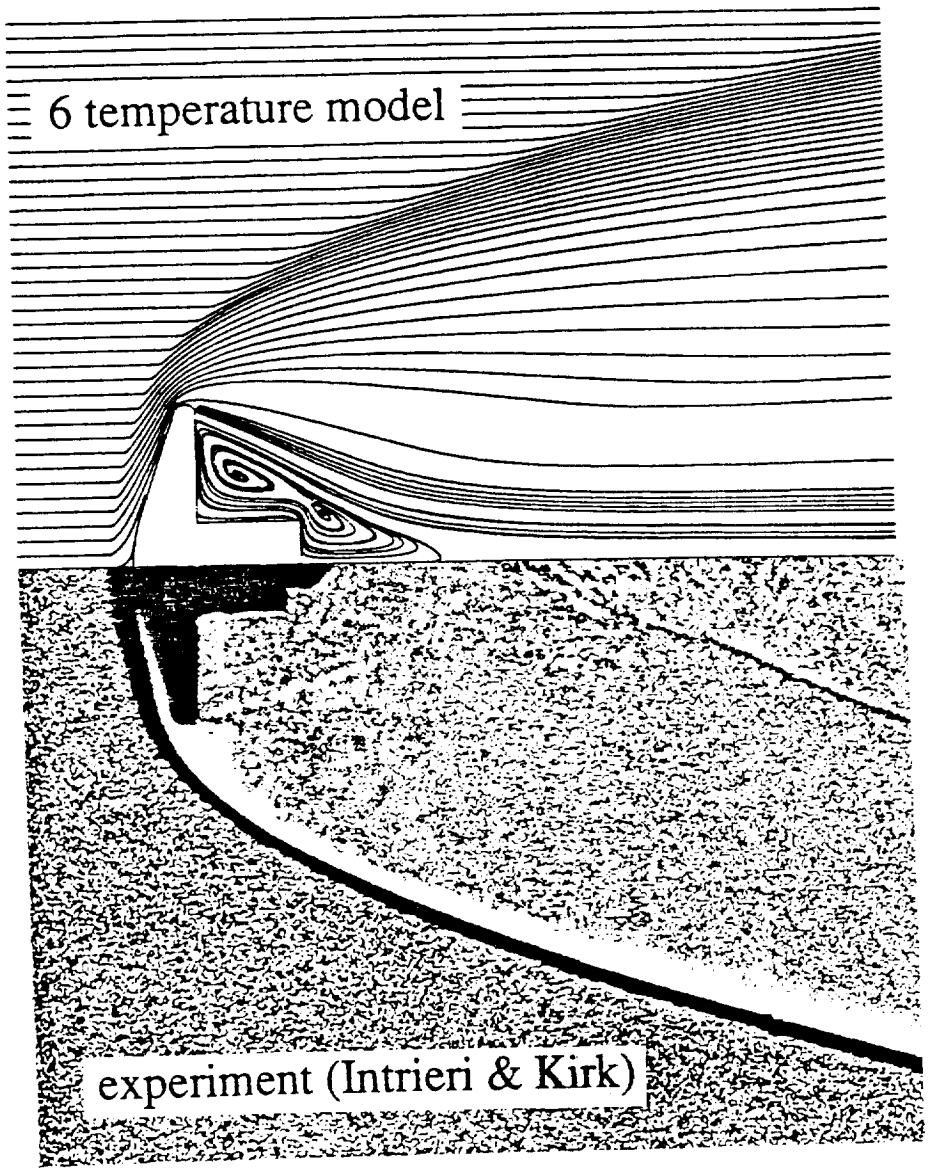

ORIGINAL PAGE IS
OF POOR QUALITY

Results – Cylinder

- Interferogram of 2 inch diameter cylinder in N_2 and N.

  $u_\infty = 5.59\,\mathrm{km/s}$, $\mathcal{M}_\infty = 6.1$, $Re = 12000$, $\psi = 5.5$.

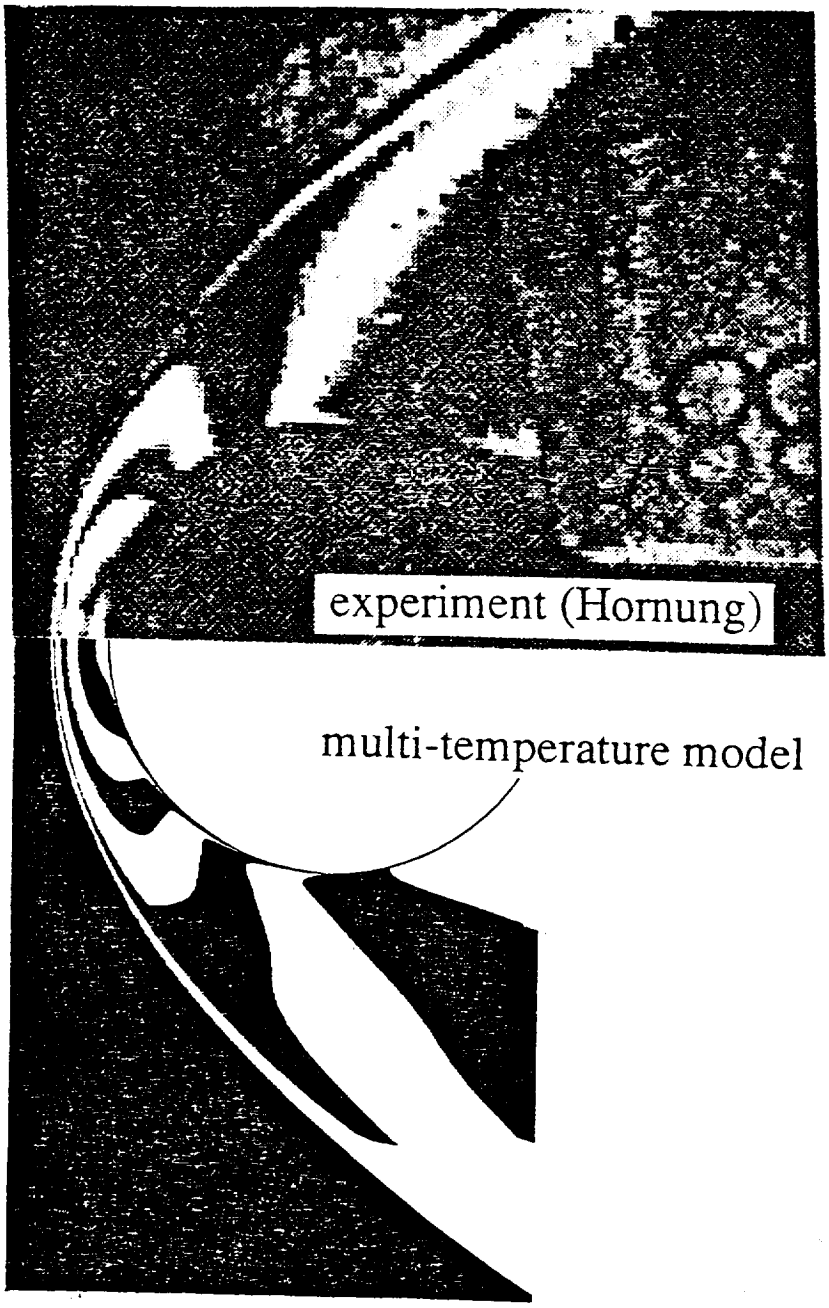

ORIGINAL PAGE IS
OF POOR QUALITY

Status of Computer Code

- Current status:
  - basically a research code
  - not vectorized (26 mflops on Cray X-MP)
  - code being used outside of Ames
  - typical solution takes 1.5 hours of Cray X-MP CPU
- Near-term improvements:
  - vectorized version
  - more efficient physical modelling
  - anticipate factor of 5 speedup
  - other gas models

Conclusions

- Algorithm for thermo-chemical nonequilibrium flow developed:
  - seven species, six temperatures
  - complete viscous terms (binary diffusion, laminar)
  - implicit numerical method
  - fully coupled equation set
  - results compared to experiment
- Future work:
  - three-dimensions
  - better models for high temperature air
  - larger degree of ionization

N91-10899

Aerodynamic Stability and Heating Analyses for the Aeroassist Flight Experiment Vehicle

J. McGary and C. P. Li
Lockheed Engineering and Science Company, Houston, Tx 77058
Johnson Space Center, Houston, Tx 77058
FTS 525-4684

Since ground based flow simulations are presently unable to model flight conditions expected for AOTVs (Aeroassist Orbital Transfer Vehicle) and other hypersonic space vehicles, computer codes are being developed to provide design parameters necessary for structure, guidance, and control aspects. Over the past four years, VRFLO (Viscous Reactive Flow) has been written to model finite-rate chemistry and viscous effects for a variety of aerobrake bodies. VRFLO includes a number of unique features that are summarized as follows:

1. Grid generation is an integral part of the code for several aerobrake configurations which includes the wake flow region.
2. The formulation is valid for three air chemical models.
3. An ADI central difference technique is used to solve the Navier-Stokes and species continuity equations in split groups.
4. Grid density and numerical damping are minimized by shock-fitting and conformal mapping of body points.

Currently, the AFE (Aeroassist Flight Experiment) project requires critical input parameters for the design development, and to aid its progress, aerodynamic forces and heating rates are calculated at a specified trajectory point of maximum heating. The code was calibrated against Mach 10 measurements taken at the Langley Continuous-Flow Hypersonic Tunnel to determine grid sensitivity and reliability estimates for flight calculations. Aerodynamic forces and moment coefficients (lifts, drags, and pitching moments) were calculated at five angles of attack to determine the basic coefficient behavior as a function of angle for stability analysis. Wind tunnel simulations were modeled by calculating the flowfield about the complete body assuming an inviscid, perfect gas which resolved the non-linear behavior in the pitching moment measured from wind tunnel experiments. Inviscid, reacting air calculations, for flight conditions at Mach 32, show a linear pitching moment that agrees with calculations performed at Langley Research Center which considered inviscid, equilibrium air with forebody geometry. Preliminary, not fully converged, viscous, reacting flow calculations at the same flight conditions reveal a slight non-linear relation between pitching moment and angle of attack. In each case, the base pressure contributions are examined by considering the forebody and complete body separately.

Considering that heat-transfer measurements are accurate within ±7% and an equal amount of uncertainty is associated with CFD results, the convective heat flux calculations are in fairly good agreement with the Langley Mach 10 wind tunnel measurements. While the calculated surface pressure distribution demonstrates excellent agreement with measurement, the heat-transfer coefficient exhibits similar surface behavior to the data but varies in value. Incident angle studies show that the maximum heating decreases with increasing attack angle without modifying the overall distribution shape. Calculations for flight conditions show similar trends observed from wind tunnel simulations but have a more pronounced peak at the stagnation region. Fully catalytic calculations indicate that the heat-transfer coefficients are about 25% larger in general than those in the non-catalytic solutions; the actual fluxes expected for flight conditions will be bounded by the two extremes.

PRECEDING PAGE BLANK NOT FILMED

Wind Tunnel Axis System for Aerocoefficients

$\alpha = 0°$

$$C_L = \frac{L}{q\,S}$$

$$C_D = \frac{D}{q\,S}$$

$$C_M = \frac{M}{q\,S\,L'}$$

$$S = \frac{\pi\,W\,L'}{4}$$

$$q = \frac{1}{2}\rho_\infty V_\infty^2$$

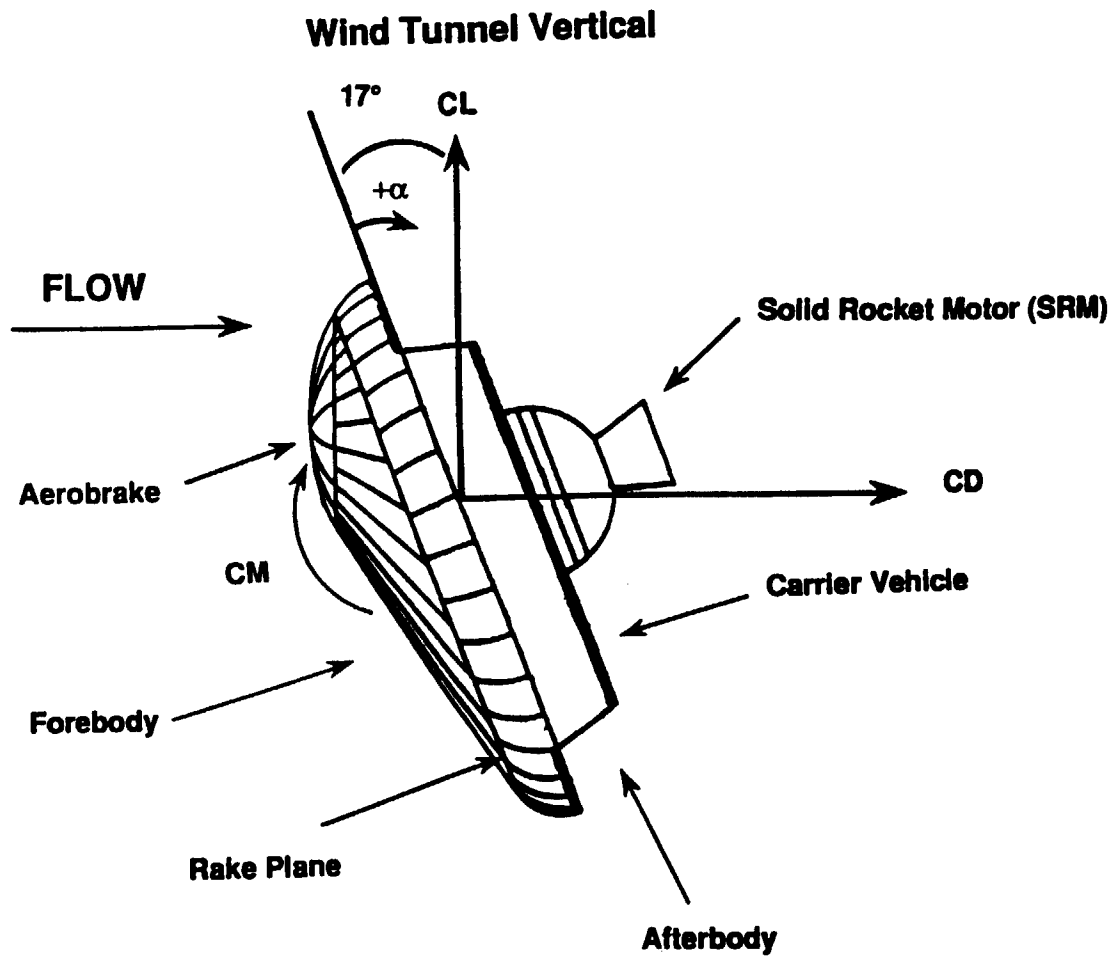

Shock Shape Variations with Angle of Attack

Inviscid, Mach 10

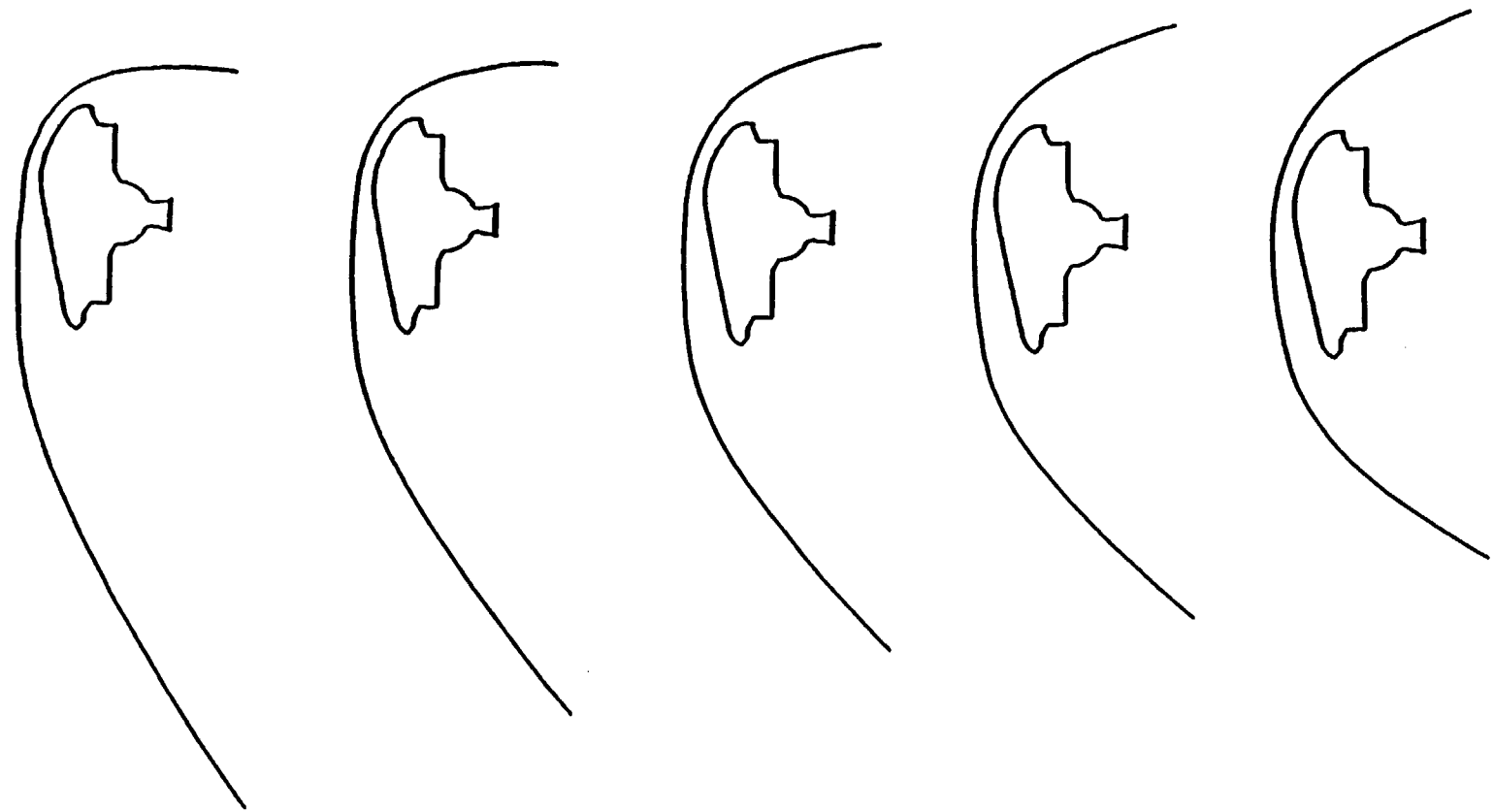

Pressure Distribution Along AFE Body

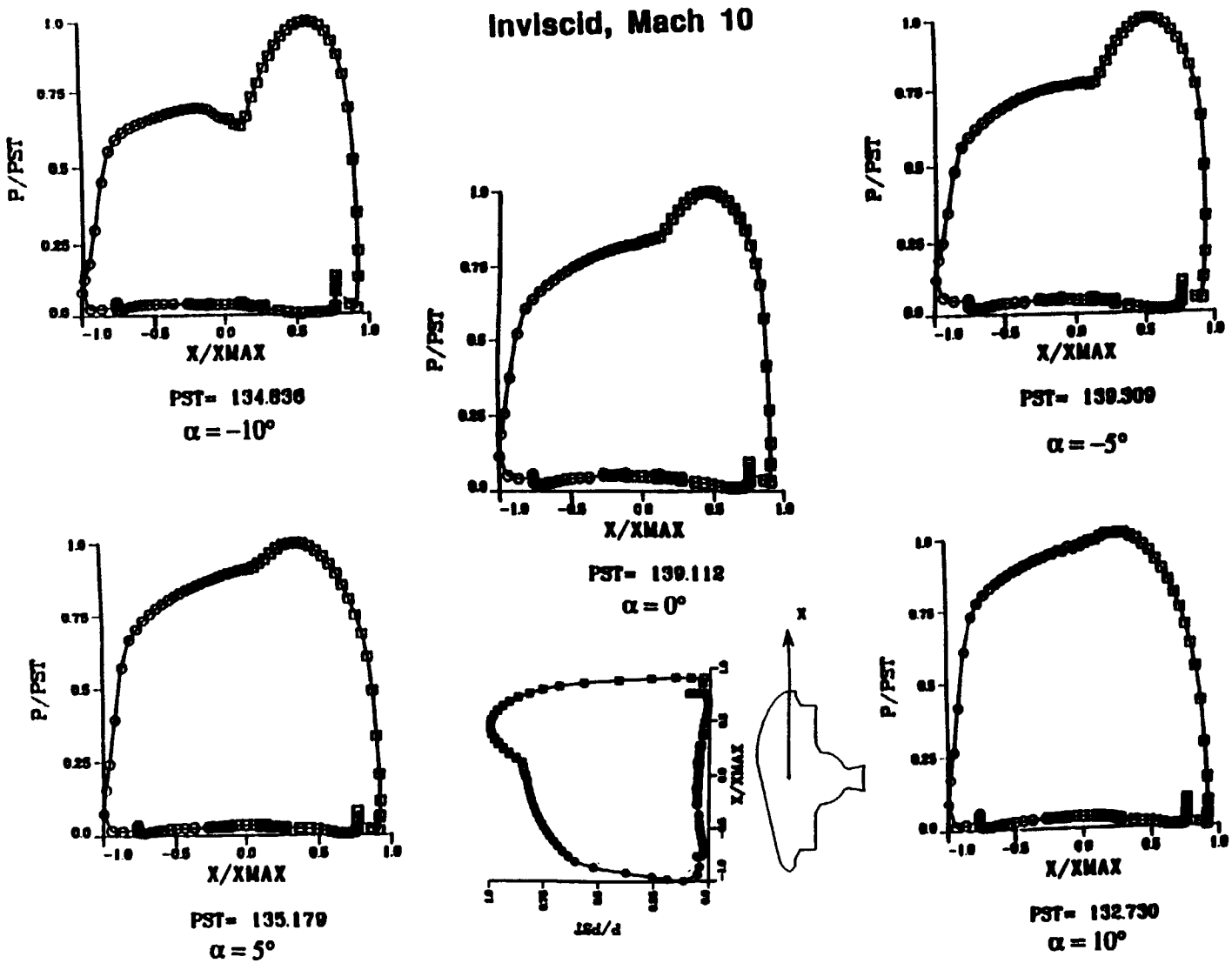

ORIGINAL PAGE IS
OF POOR QUALITY

Grid Variations
Inviscid, Mach 10

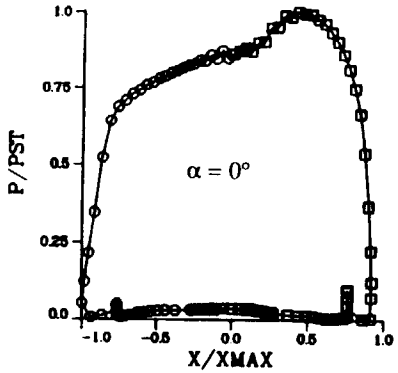

12x60x9 PST= 133.579

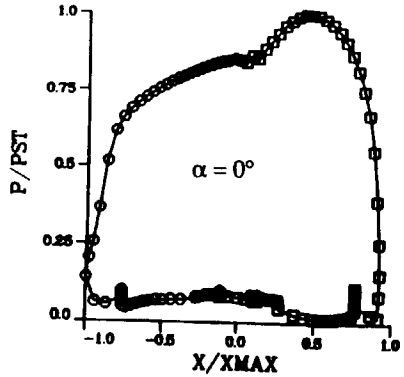

12x60x25 PST= 134.846

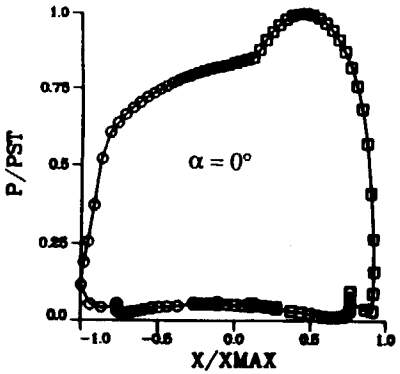

30x60x25 PST= 139.112

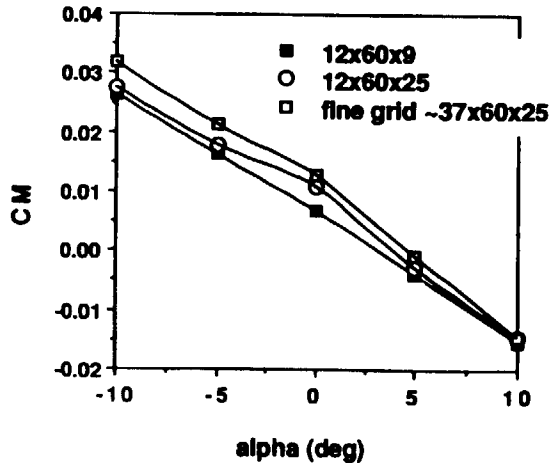

NxMxL , where

N = number of points from AFE body to boundary

M = number of points from forebody to afterbody

L = number of points around body in plane normal to pitch plane

ORIGINAL PAGE IS
OF POOR QUALITY

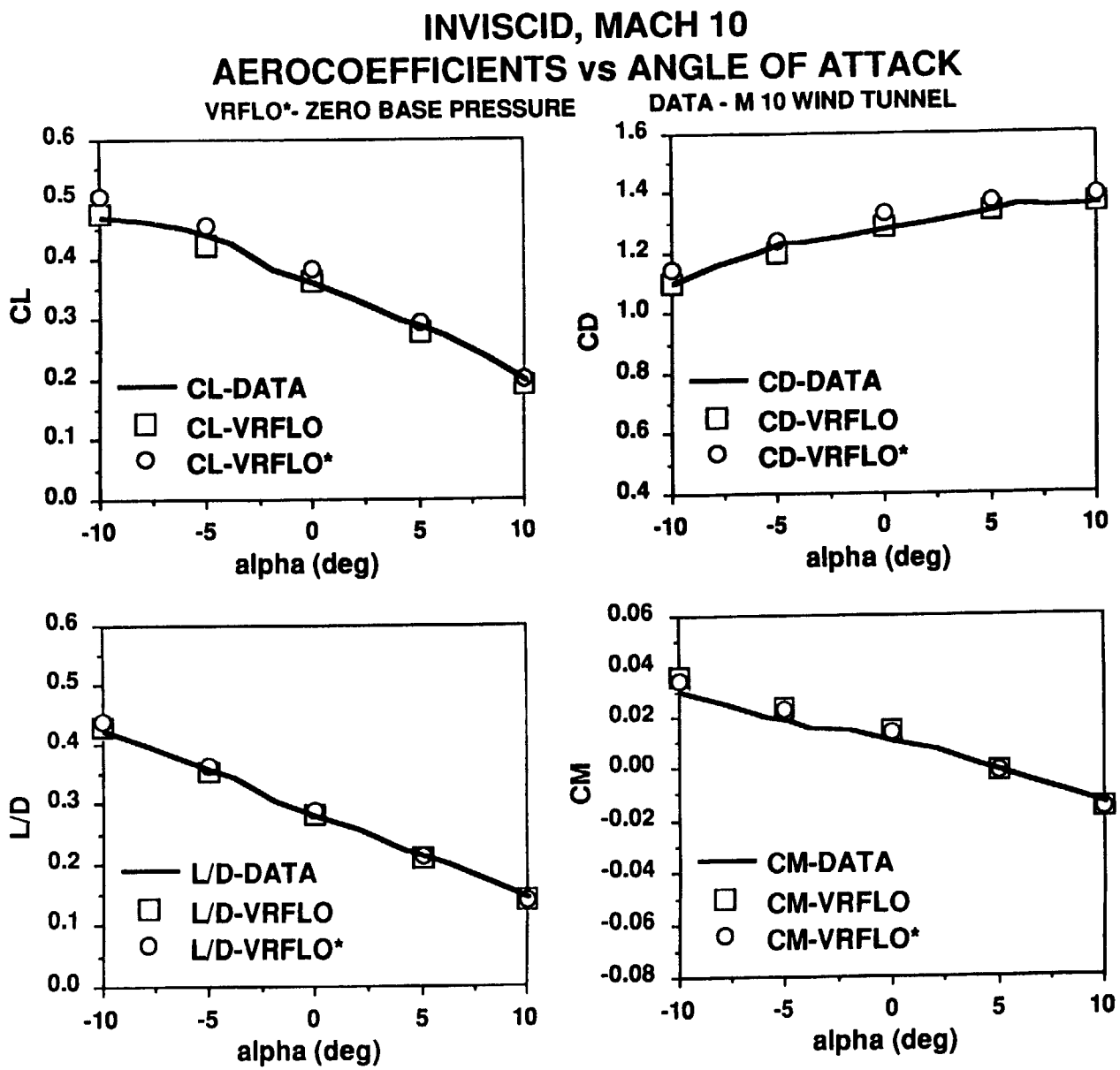
INVISCID, MACH 10
AEROCOEFFICIENTS vs ANGLE OF ATTACK
VRFLO*- ZERO BASE PRESSURE
DATA - M 10 WIND TUNNEL
CL
CL-DATA
CL-VRFLO
CL-VRFLO*
CD
CD-DATA
CD-VRFLO
CD-VRFLO*
L/D
L/D-DATA
L/D-VRFLO
L/D-VRFLO*
CM
CM-DATA
CM-VRFLO
CM-VRFLO*
alpha (deg)

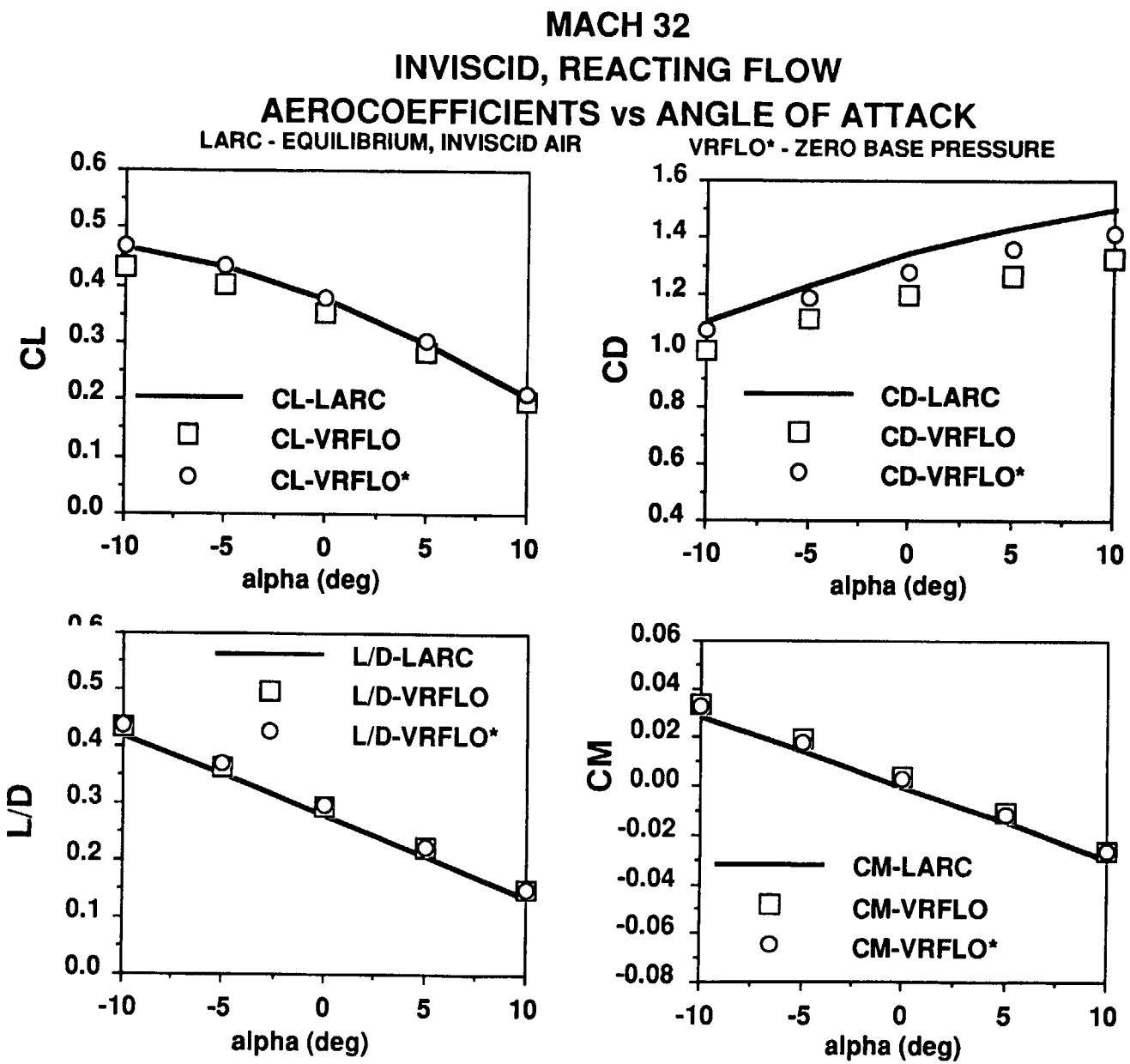
MACH 32
INVISCID, REACTING FLOW
AEROCOEFFICIENTS vs ANGLE OF ATTACK
LARC - EQUILIBRIUM, INVISCID AIR
VRFLO* - ZERO BASE PRESSURE
CL
CL-LARC
CL-VRFLO
CL-VRFLO*
CD
CD-LARC
CD-VRFLO
CD-VRFLO*
L/D
L/D-LARC
L/D-VRFLO
L/D-VRFLO*
CM
CM-LARC
CM-VRFLO
CM-VRFLO*
alpha (deg)

MACH 32
VISCOUS, REACTING FLOW
AEROCOEFFICIENTS vs ANGLE OF ATTACK

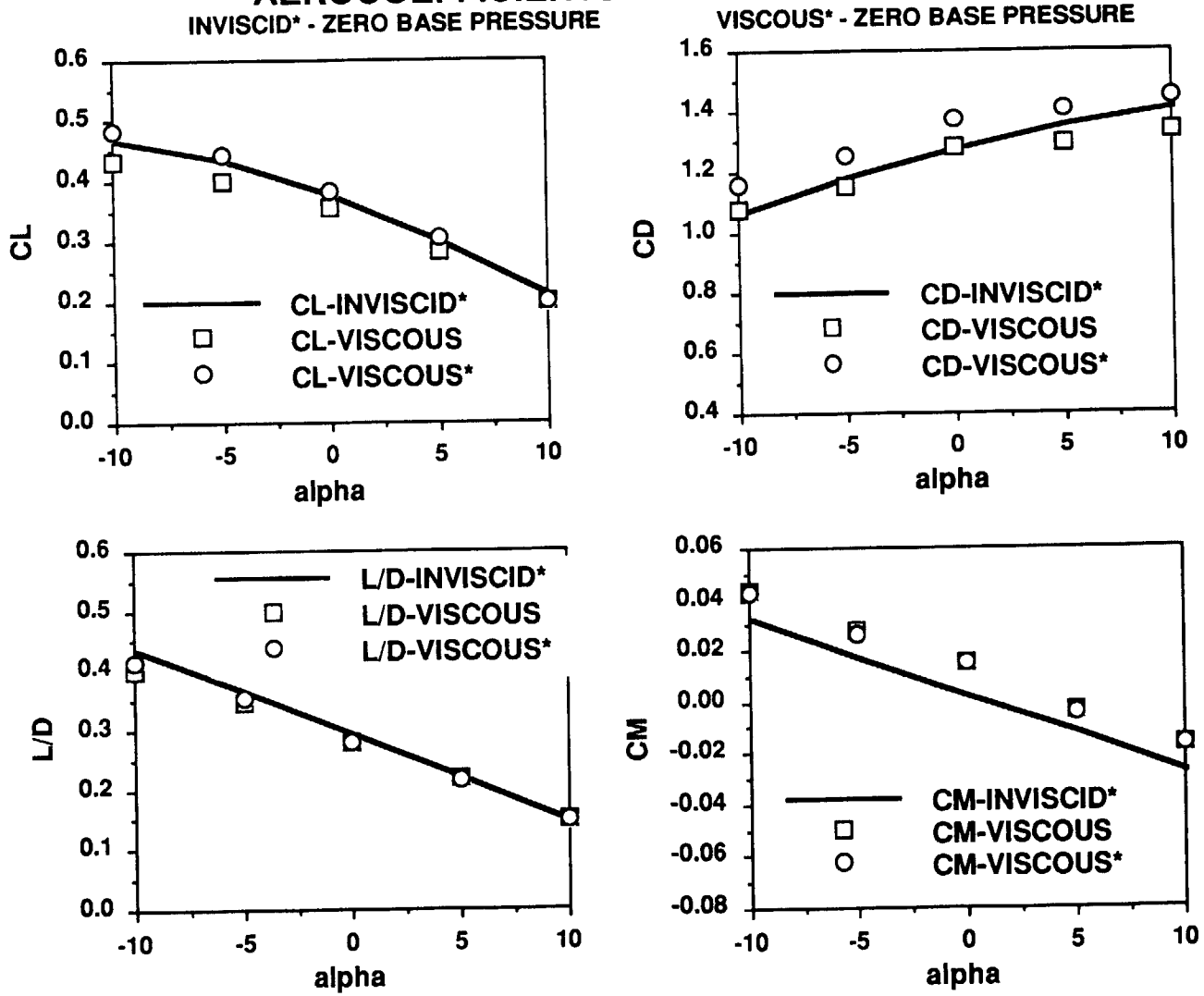

MACH 32
INVISCID / VISCOUS COMPARISONS

$\alpha = 0°$

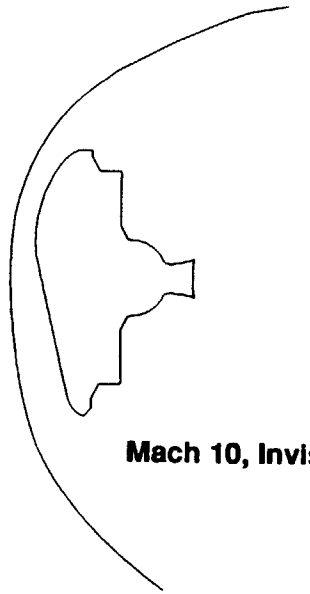

Mach 10, Inviscid

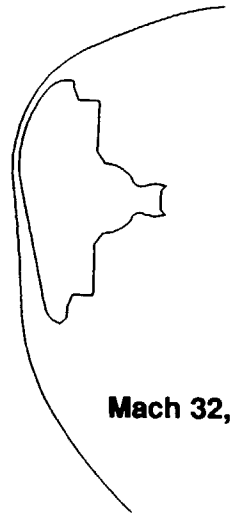

Mach 32, Inviscid

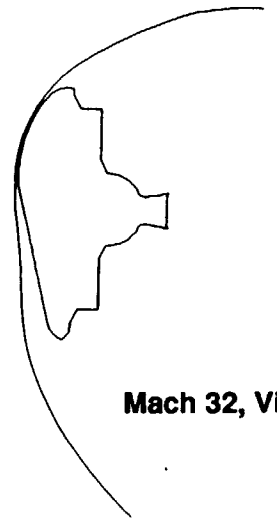

Mach 32, Viscous

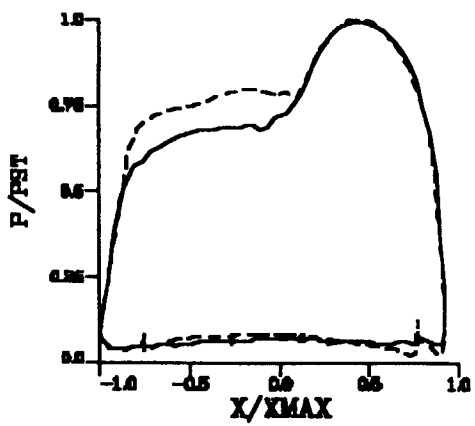

----- Inviscid —— Viscous

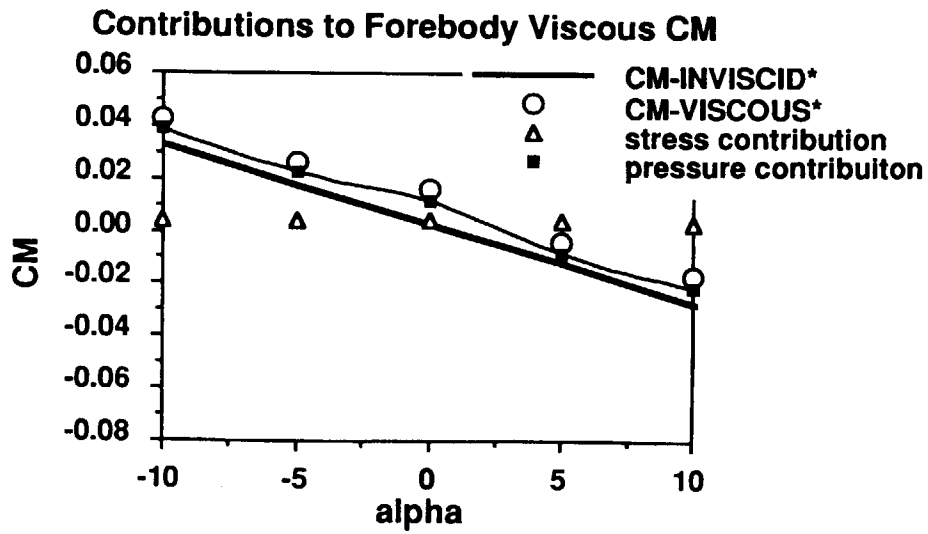

Comparisons of Pressures and Heat Transfer

α = 10°, 0°, -10°

MACH 10

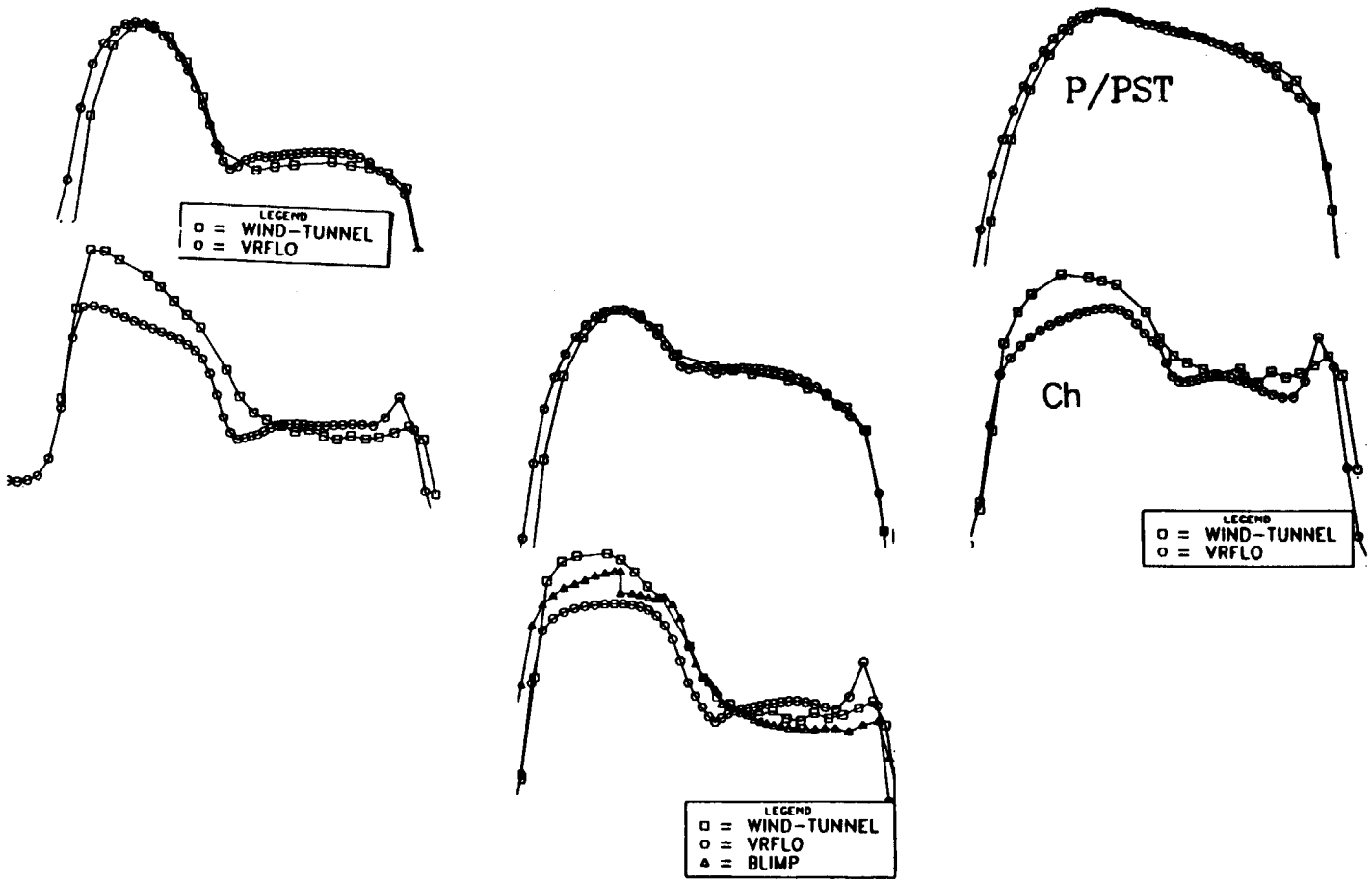

Effects of Gas Models on Pressure and Heating
MACH 35

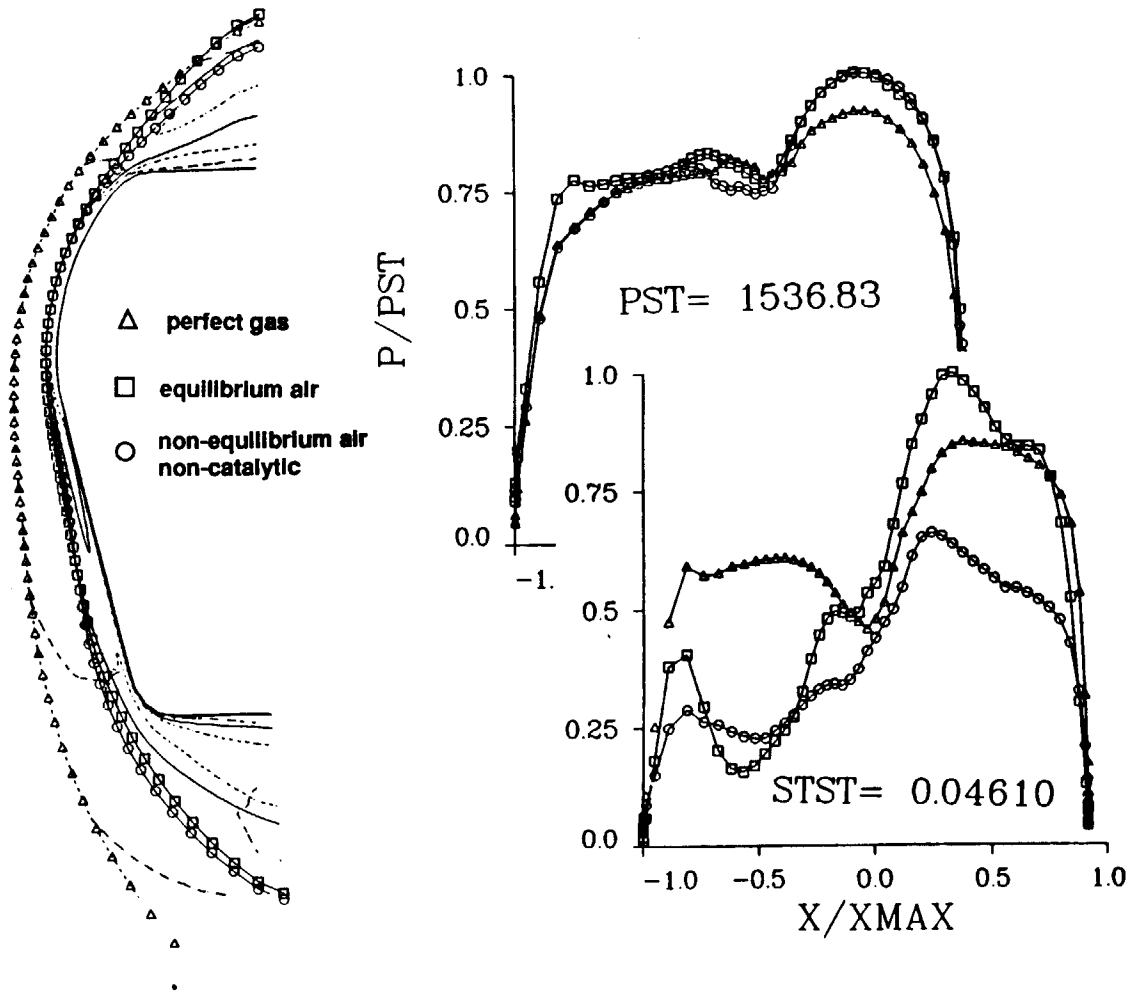

Wall Catalytic Effects on Pressure and Heating
MACH 35

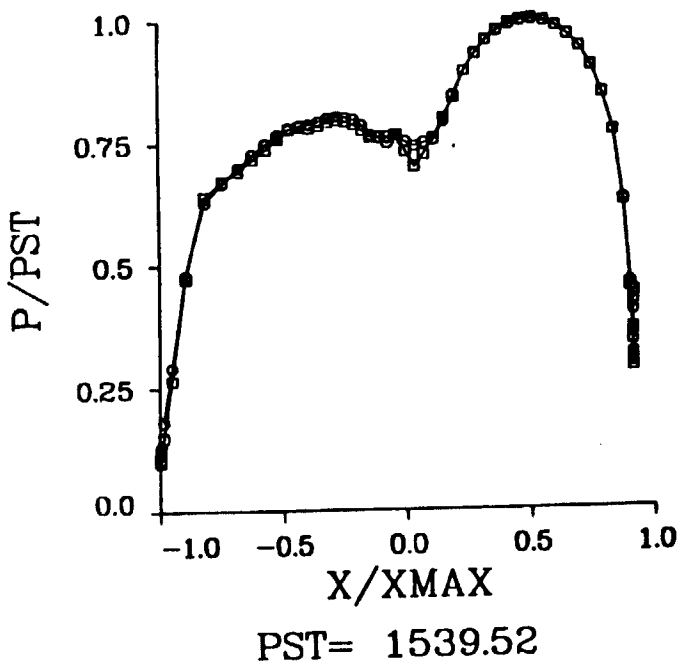

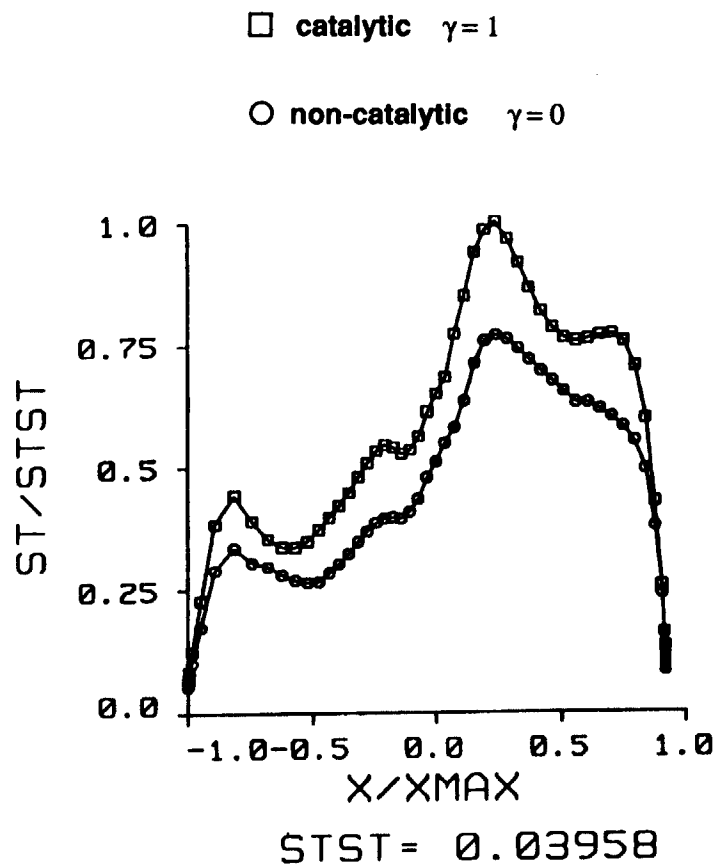

Comparisons of Heating Rates
Boundary Layer and Navier Stokes Codes
MACH 35

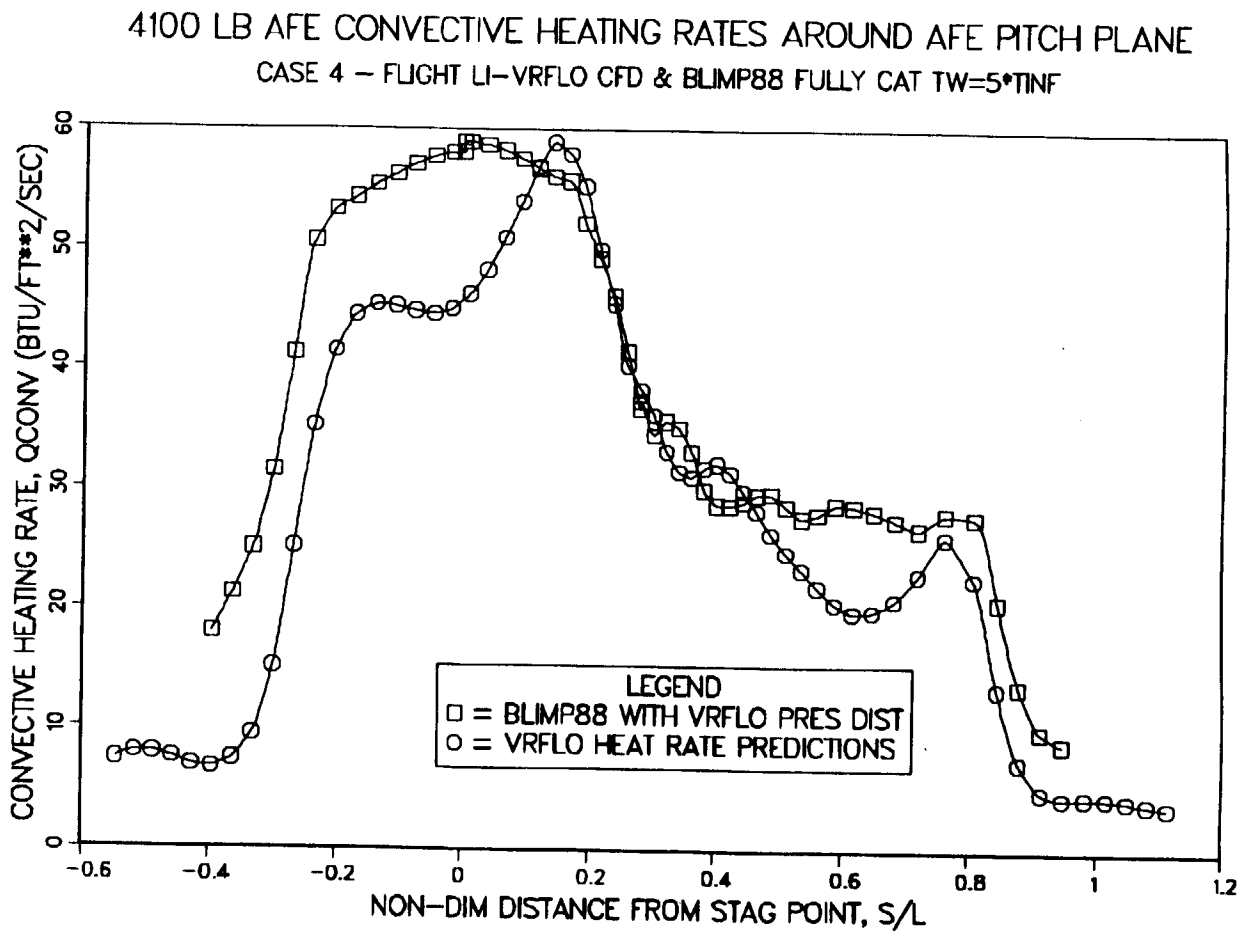

Heat Transfer Distribution on AFE
Chemically Reactive Computation

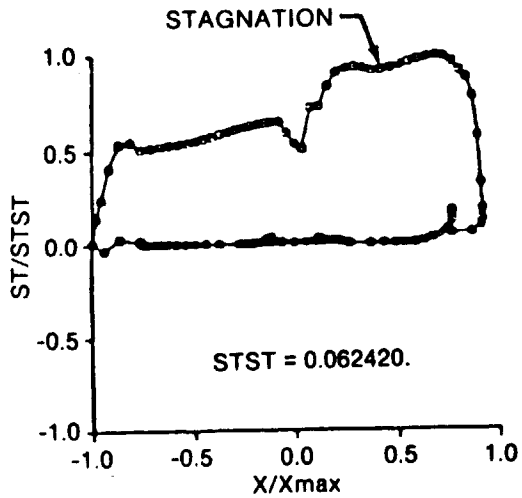

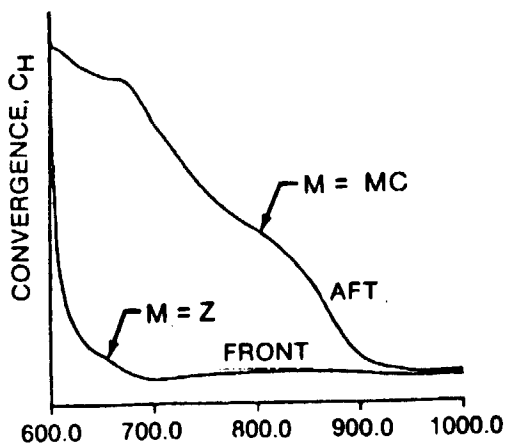

A 7.00E - 02
B 6.55E - 02
C 6.09E - 02
D 5.64E - 02
E 5.18E - 02
F 4.73E - 02
G 4.27E - 02
H 3.82E - 02
I 3.36E - 02
J 2.91E - 02
K 2.45E - 02
L 2.00E - 02

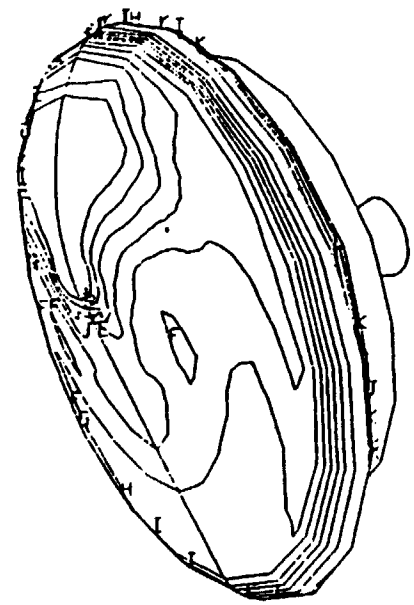

ORIGINAL CONTAINS
COLOR ILLUSTRATIONS

N91-10900

AEROASSIST FLIGHT EXPERIMENT AERODYNAMICS AND AEROTHERMODYNAMICS

Edwin B. Brewer, NASA/MSFC

Abstract

The problem is to determine the transitional flow aerodynamics and aerothermodynamics, including he base flow characteristics, of the Aeroassist Flight Experiment (AFE). The justification for the CFD Application stems from MSFC's system integration responsibility for the AFE. To insure that the AFE objectives are met, MSFC must understand the limitations and uncertainties of the design data.

Perhaps the only method capable of handling the complex physics of the rarefied high energy AFE trajectory is Bird's Direct Simulation Monte Carlo (DSMC) technique. The three-dimensional code used in this analysis is applicable only to the AFE geometry. It uses the Variable Hard Sphere (VHS) collision model and five specie chemistry model available from Langley Research Center.

The code will be benchmarked against the AFE flight data and used as an Aeroassisted Space Transfer Vechicle (ASTV) design tool. Meanwhile, the code is being used to understand the AFE flow field and verify or modify existing design data. Continued application to lower altitudes is testing the capability of the Numerical Aerodynamaic Simulation Facility (NASF) to handle three-dimensional DSMC and its practicality as an ASTV/AFE design tool.

AFE AEROTHERMODYNAMIC LOADS

OBJECTIVE:

DEVELOP A CODE TO CALCULATE THE AERODYNAMICS AND AEROTHERMODYNAMICS OF THE AFE IN HYPERSONIC RAREFIED NONEQUILIBRIUM FLOW WITH CHEMICAL REACTIONS.

APPROACH:

THE DIRECT SIMULATION MONTE CARLO (DMSC) IS THE ONLY TECHNIQUE WHICH CAN HANDLE THE TRANSITIONAL FLOW ENVIRONMENT. THE VARIABLE HARD SPHERE (VHS) COLLISION MODEL OF G.A. BIRD IS BEING USED IN THIS DEVELOPMENT.

COMPUTER RESOURCES:

500 HOURS ON THE NUMERICAL AERODYNAMIC SIMULATION (NAS) FACILITY AT NASA'S AMES RESEARCH CENTER WAS USED DURING THE NAS OPERATIONAL YEAR (MARCH 1988 THROUGH FEB. 1989).

IMPACT:

NASA'S AFE GOAL IS TO OBTAIN THE PHYSICAL DATA BASE REQUIRED TO BENCHMARK COMPUTATIONAL CODES APPLICABLE TO THE DESIGN OF THE AERO ASSISTED SPACE TRANSFER VEHICLE (ASTV). AFE DESIGN IS RELYING ON CFD CALCULATIONS TO AN UNPRECEDENTED EXTENT DUE TO THE LACK OF WIND TUNNEL FACILITIES WHICH SIMULATE THE RAREFIED/REAL GAS PHYSICS.

5-3121-8-39

ORGANIZATION: ED32	MARSHALL SPACE FLIGHT CENTER	NAME: E. BREWER
CHART NO.:	**AFE AEROPASS CONFIGURATION SIDE VIEW**	DATE:

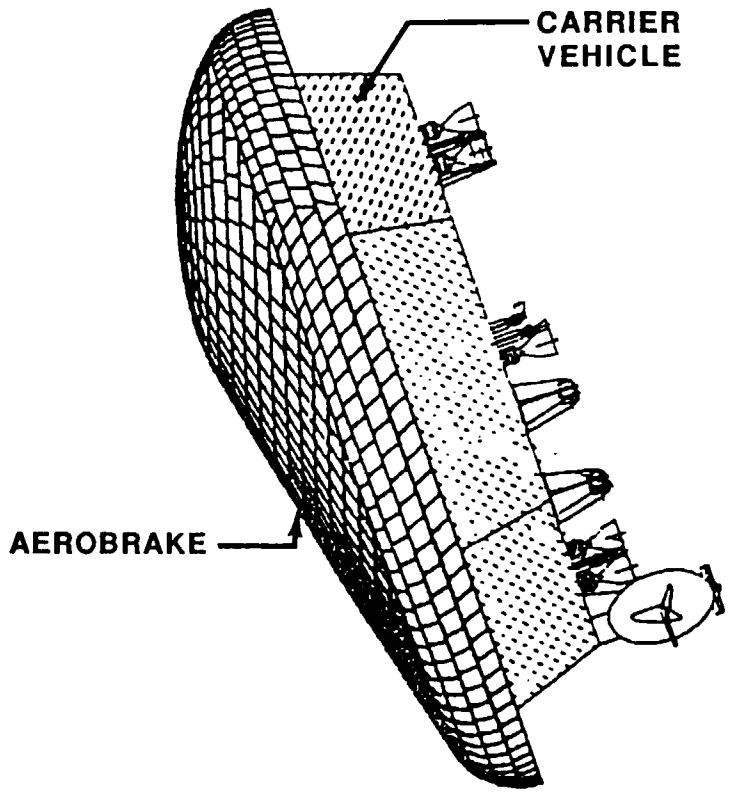

ED6614
5-1587-9-100

AFE Aerobrake Surface Grid

(22 x 12)

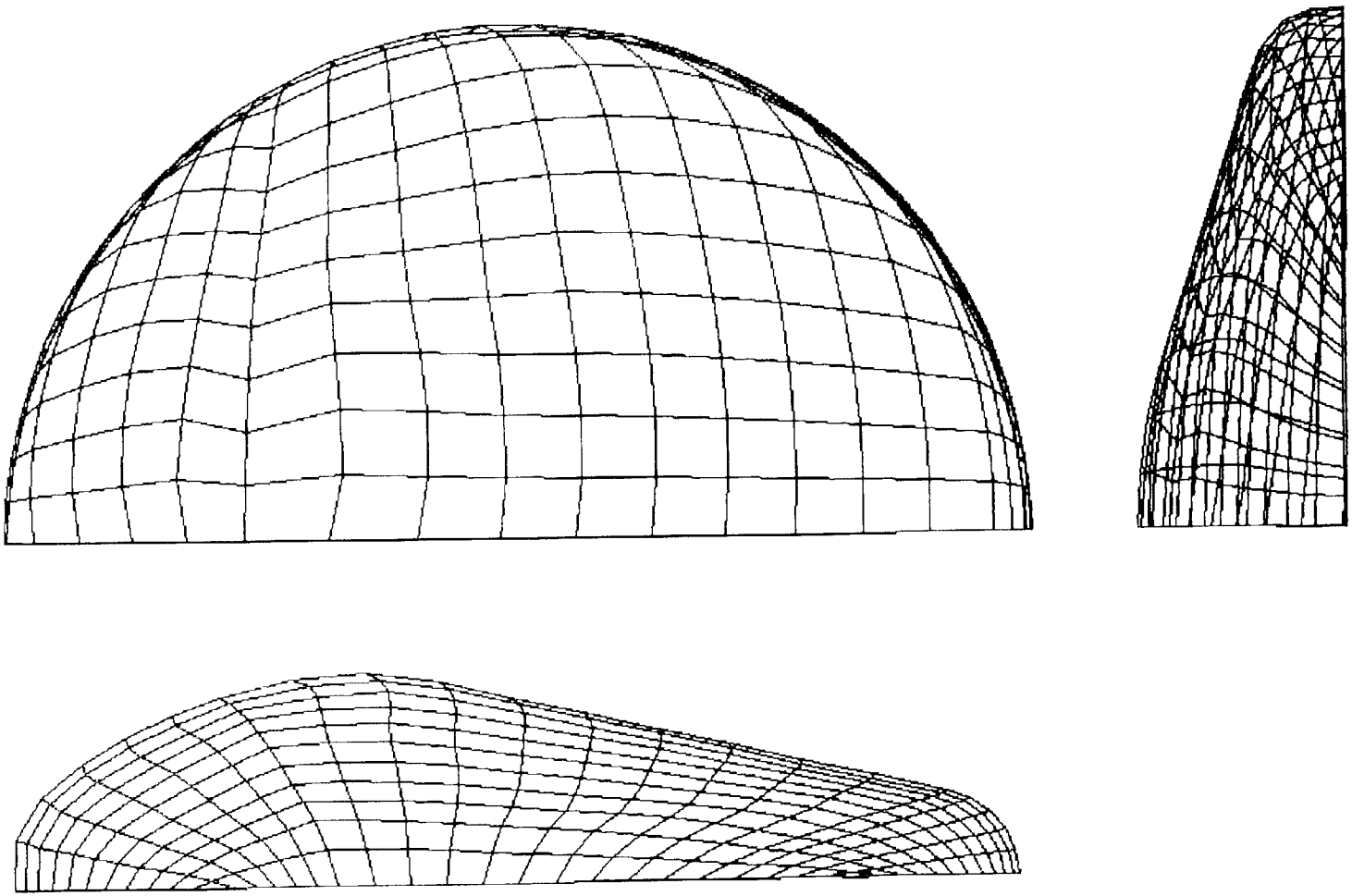

BODY AND WALLS

BODY FITTED GRID IN AFE PLANE OF SYMMETRY

68x40x32 GRID

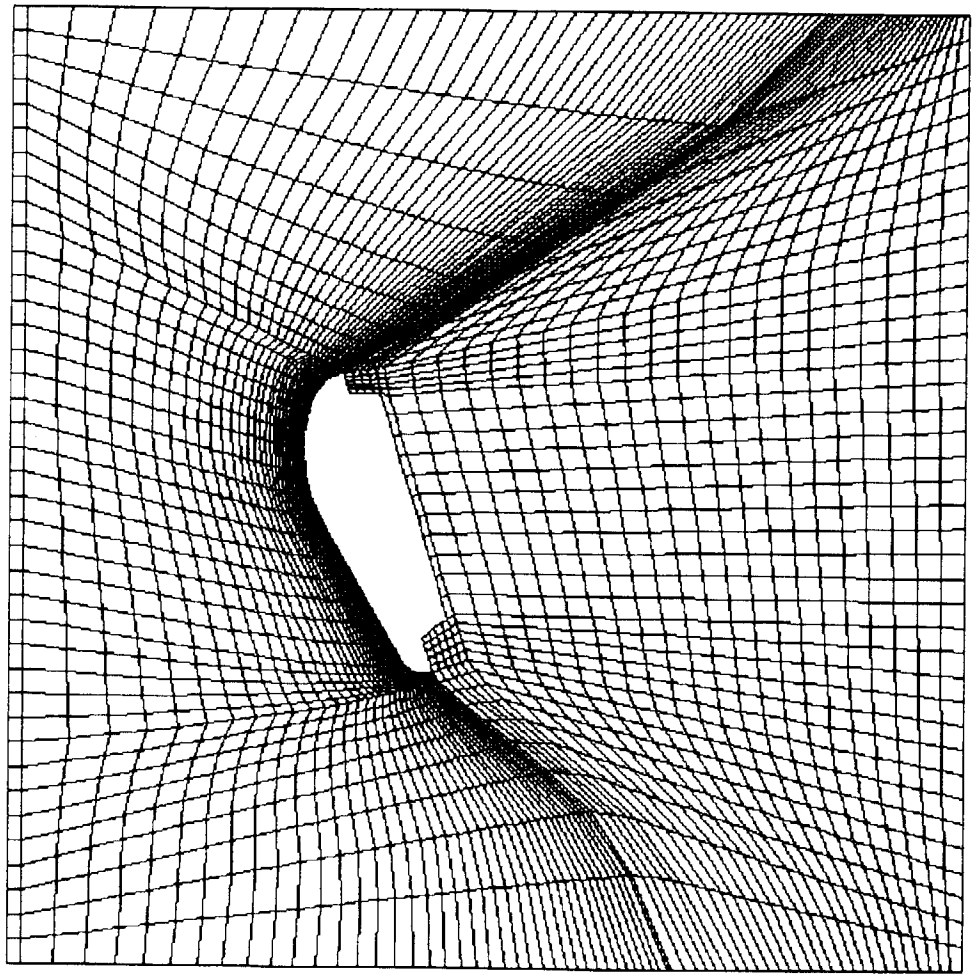

PRECEDING PAGE BLANK NOT FILMED

AEROASSIST FLIGHT EXPERIMENT

VELOCITY MAGNITUDE

0.000x10 0
500.000
1000.000
1500.000
2000.000
2500.000
3000.000
3500.000
4000.000
4500.000
5000.000
5500.000

6500.000
7000.000
7500.000
8000.000
8500.000
9000.000
9500.000
10000.000

Kn = 0.015

Altitude = 95 km

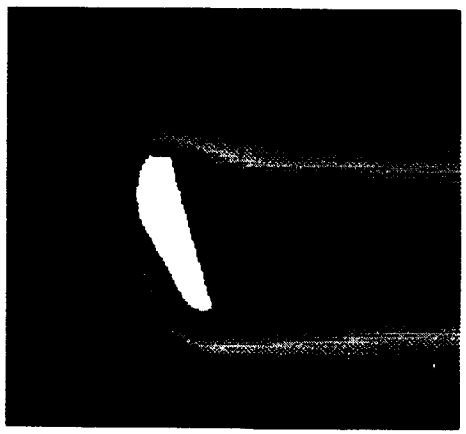

Kn = 0.2

Altitude = 110 km

Kn = 1.0

Altitude = 120 km

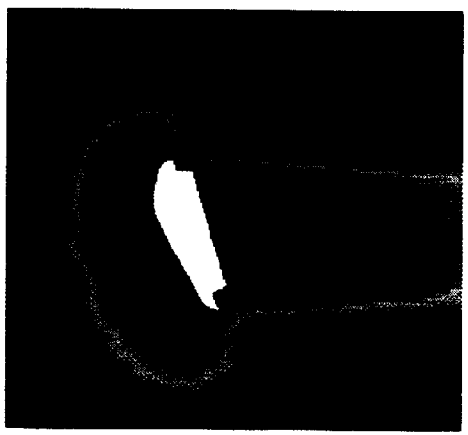

ORIGINAL PAGE IS
OF POOR QUALITY

PRECEDING PAGE BLANK NOT FILMED

AFE TRANSITIONAL FLOW AERODYNAMICS DETERMINED BY DSMC

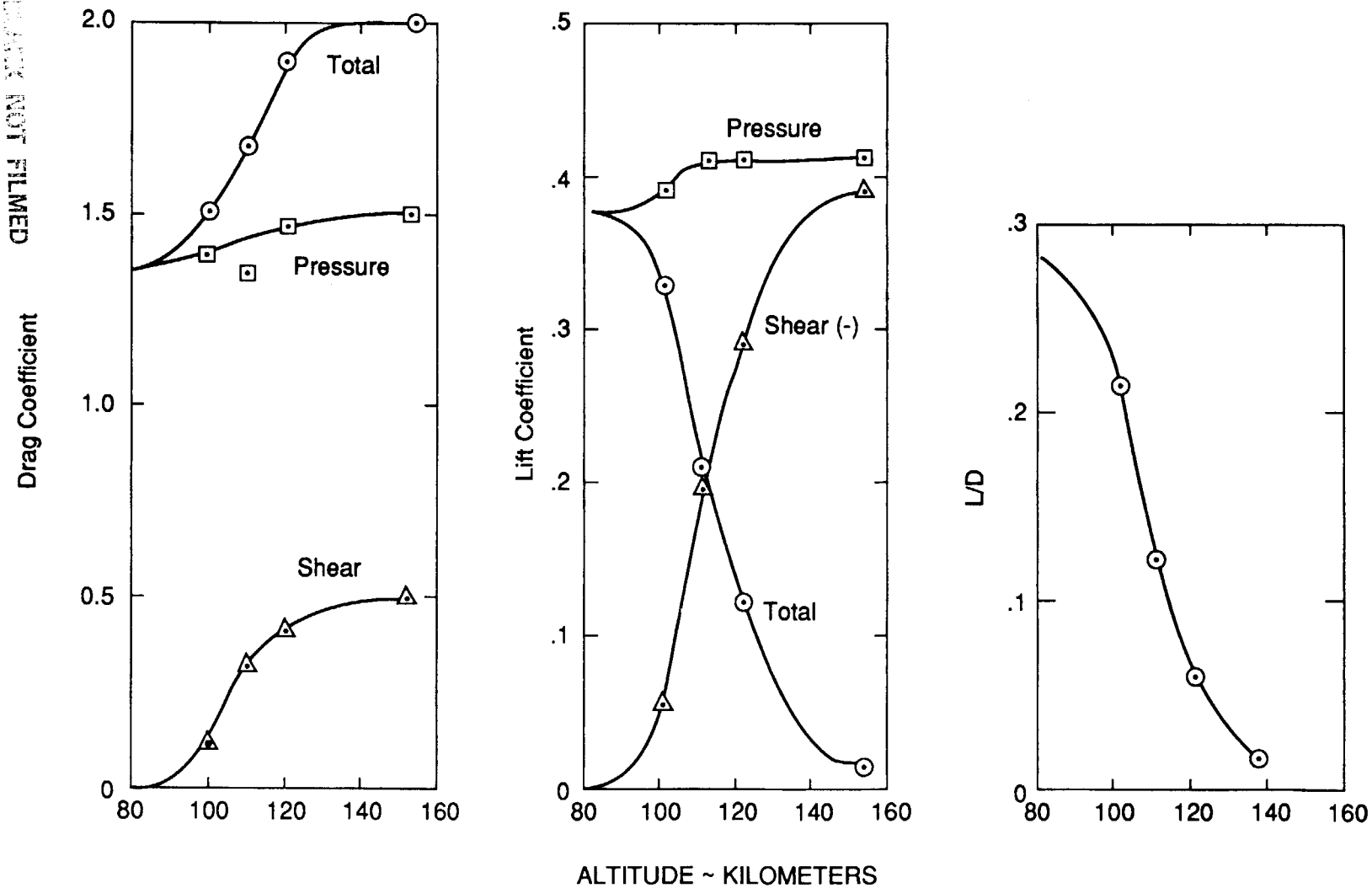

5-1590-9-100

AFE SURFACE HEATING RATE DISTRIBUTION IN PLANE OF SYMMETRY

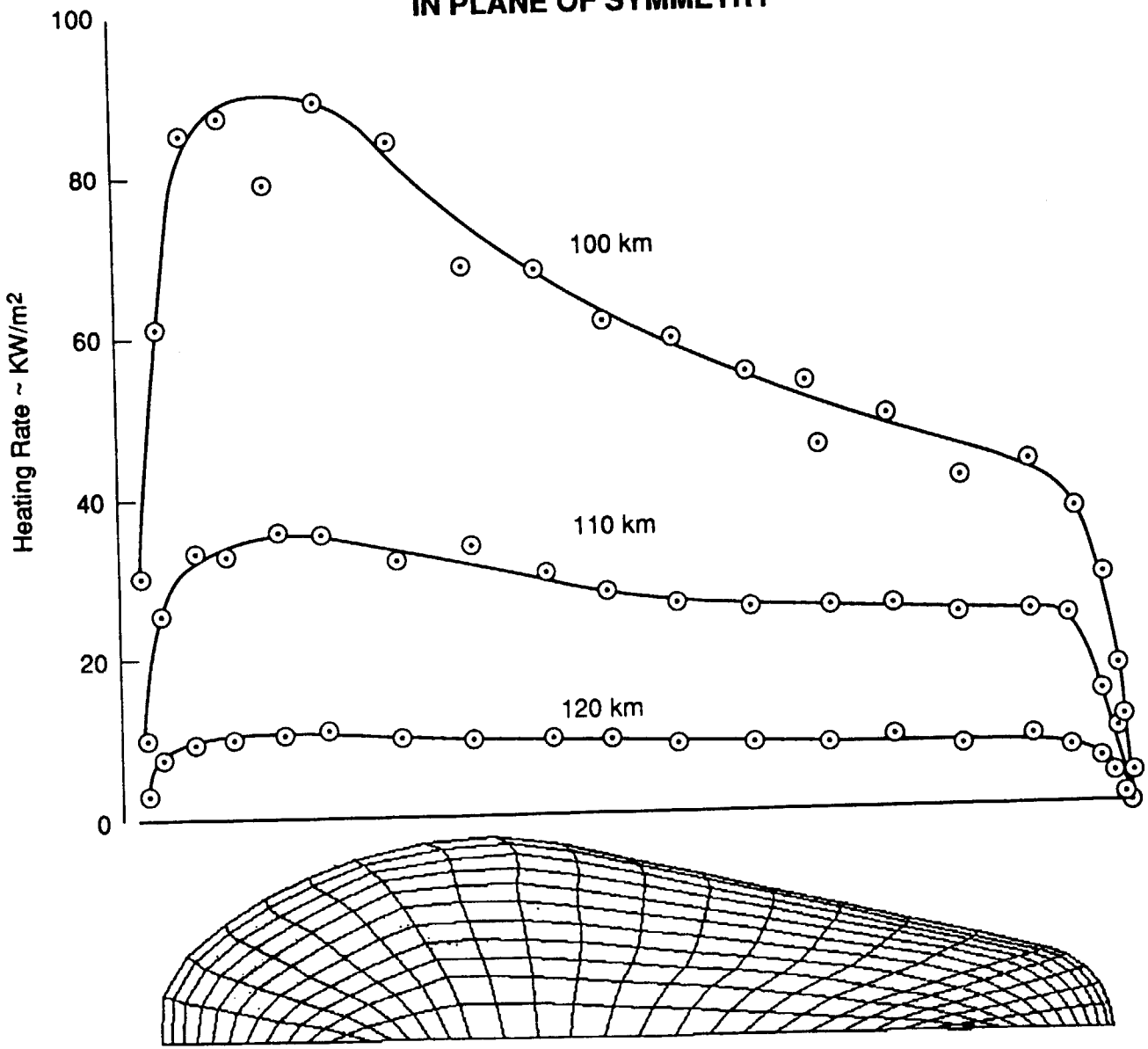

ED6615
5-1588-9-100

AFE SURFACE HEATING RATE DISTRIBUTION IN LATERAL DIRECTION

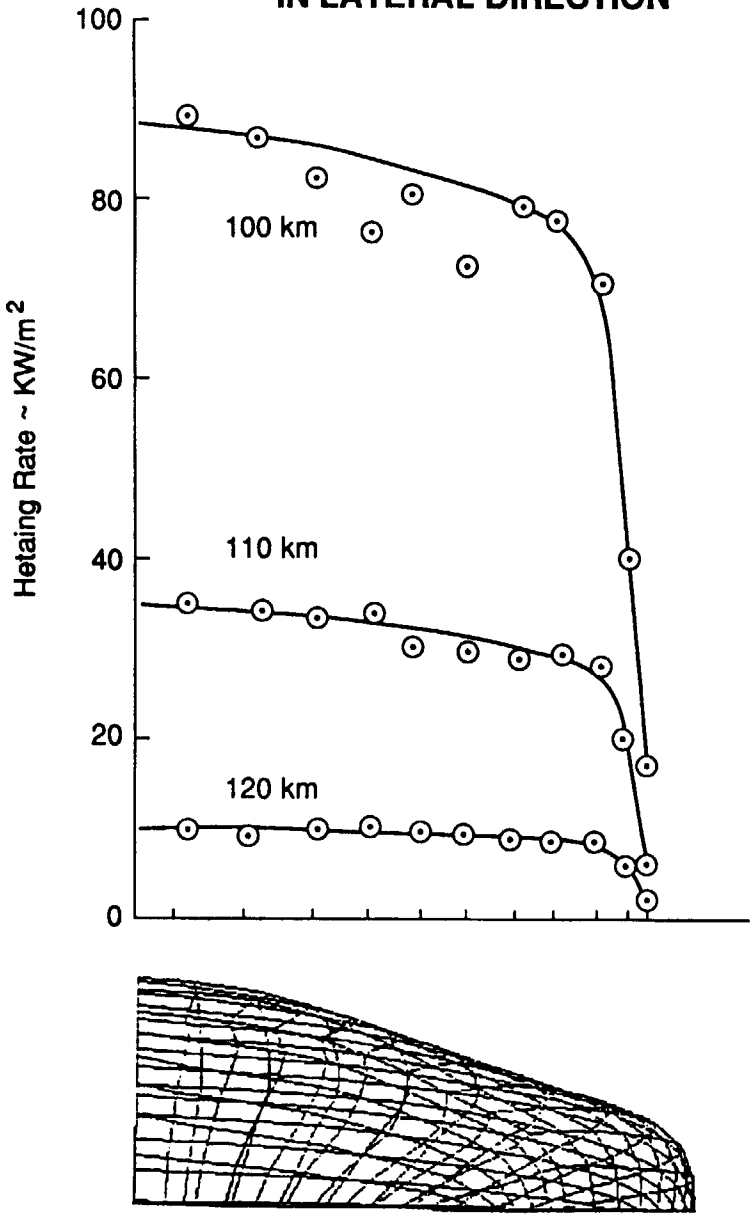

ED6616
5-1589-9-100

SUMMARY OF AFE ENTRY AERODYNAMIC COEFFICIENTS CALCULATED BY DSMC

ALTITUDE	TOTAL			PRESSURE		SHEAR	
~(Km)	CL	CD	L/D	CL	CD	CL	CD
100	0.334	1.530	0.218	0.392	1.402	–0.058	0.128
110	0.214	1.688	0.127	0.413	1.363	–0.199	0.325
120	0.125	1.904	0.065	0.414	1482	–0.289	0.422
152.4	0.019	2.007	0.010	0.415	1.506	–0.396	0.501

5-1628-9-103

ATMOSPHERIC CONDITIONS USED BY DSMC (1976 US STD ATM)

ALTITUDE	DENSITY	TEMPERATURE	PRESSURE	SPECIES NO. DENSITY		
Km	Kg/m**3	Kelvin	Pascal	N2	O2	O
95	0.1393E–05	189.9	0.7596E–01	.7835	.2014	.0151
100	0.5604E–06	195.0	0.3201E–01	.7811	.1824	.03645
110	0.9708E–07	240.0	0.7104E–02	.7692	.12285	.10795
120	2.2220E–08	360.0	2.5380E–03	.7316	.0863	.1821
152.4	1.8200E–09	650.3	4.1070E–04	.5932	.05135	.3554

AFE ENTRY TRAJECTORY USED BY DSMC

ALTITUDE	VELOCITY	KNUDSEN NO.	MEAN-FREE-PATH	WALL TEMP	TWALL/TINF
Km	m/s		Meters	Kelvin	
95	9908	0.0136	0.0579	1000	5.266
100	9911	0.0334	0.142	866	4.441
110	9911	0.1855	0.788	500	2.083
120	9897	0.7794	3.31	295	0.819
152.4	9897	8.4768	37.	295	0.4536

5-1627-9-103

CONCLUSION

- THE AERODYNAMICS AND AEROTHERMODYNAMICS OF THE AFE HAVE BEEN OBTAINED IN THE TRANSITIONAL FLOW REGIME USING DIRECT SIMULATION MONTE CARLO. THESE CALCULATIONS ARE FOR A FIVE SPECIE REACTING AIR CHEMISTRY MODEL INCLUDING THERMAL NONEQUILIBRIUM.

- DSMC IS A VERY POWER TOOL EVEN FOR COMPLEX THREE-DIMENSIONAL GEOMETRY. THIS HAS BEEN MADE FEASIBLE BY THE LARGE MEMORY AVAILABLE ON THE NAS CRAY-2. THREE-DIMENSIONAL NONVECTORIZED DSMC DOES REQUIRE TOO MUCH COMPUTER TIME TO CONDUCT PARAMETER STUDIES.

5-1591-9-100

AEROASSIST FLIGHT EXPERIMENT

VELOCITY MAGNITUDE

0.000x10 0
500.000
1000.000
1500.000
2000.000
2500.000
3000.000
3500.000
4000.000
4500.000
5000.000
5500.000
6000.000
6500.000
7000.000
7500.000
8000.000
8500.000
9000.000
9500.000
10000.000

Kn = 0.015

Altitude = 95 km

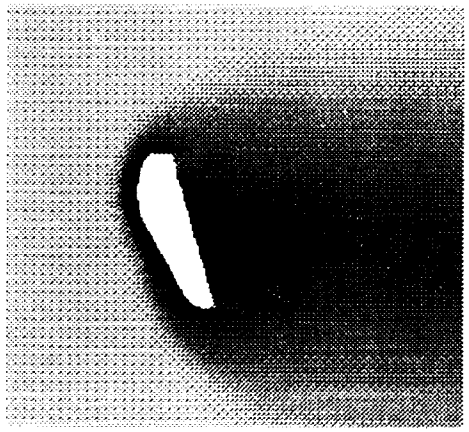

Kn = 0.2

Altitude = 110 km

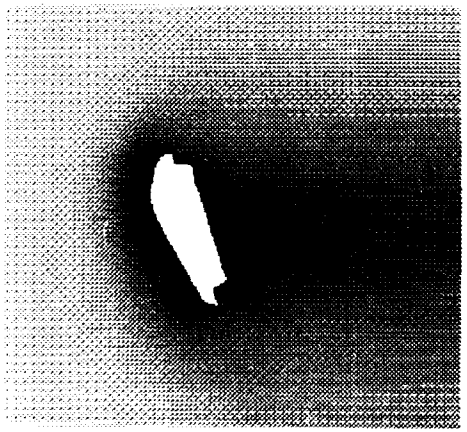

Kn = 1.0

Altitude = 120 km

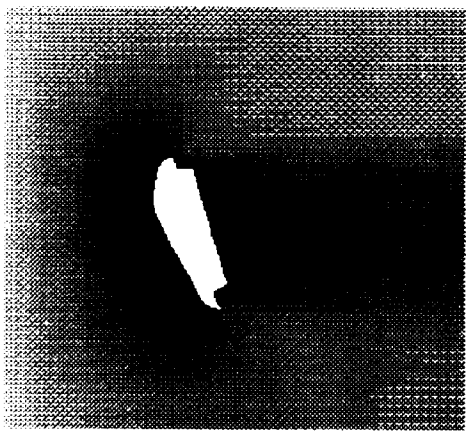

ORIGINAL PAGE IS
OF POOR QUALITY

N91-10901

DIRECT SIMULATION OF RAREFIED HYPERSONIC FLOWS

James N. Moss
NASA Langley Research Center
Hampton, Virginia 23665-5225

As the capability of the space transportation vehicles (STV's) expand to meet the requirements for future space exploration and utilization, the effects of rarefied hypersonic flows will play a more significant role in defining the aerodynamic and aerothermodynamic performance of STV's. This is particularly true of the low lift/drag aeroassisted STV's where aerobraking occurs at relatively high altitudes and high velocity. Because of the limitations of the continuum description as expressed by the Navier-Stokes equations and the difficulties of solving the Boltzmann equation, the particle or molecular approach has been developed over the last three decades for modeling rarefied gas effects. The direct simulation Monte Carlo (DSMC) method of Bird is the most used method today for simulating rarefied flows. The DSMC method provides a direct physical simulation as opposed to a numerical solution of a set of model equations. This is accomplished by developing phenomenological models of the relevant physical events. The DSMC method accounts for translational, thermal, chemical, and radiative nonequilibrium effects. The present discussion will review the general features of the DSMC method, the numerical requirements for obtaining meaningful results, the modeling used to simulate high temperature gas effects, and applications of the method to calculate the flow about an aeroassist flight experiment vehicle (AFE). The AFE simulates a geosynchronous return while entering the Earth's upper atmosphere at approximately 10 km/s. Results obtained using a general 3-D code are presented for the more rarefied portion of the atmospheric encounter (altitudes of 200 to 100 km) emphasizing surface, flowfield, and aerodynamic characteristics of the AFE. Finally, results obtained using axisymmetric and 1-D versions of the code are presented for lower altitude conditions.

PRECEDING PAGE BLANK NOT FILMED

KNUDSEN - NUMBER LIMITS ON GAS FLOW MODELS

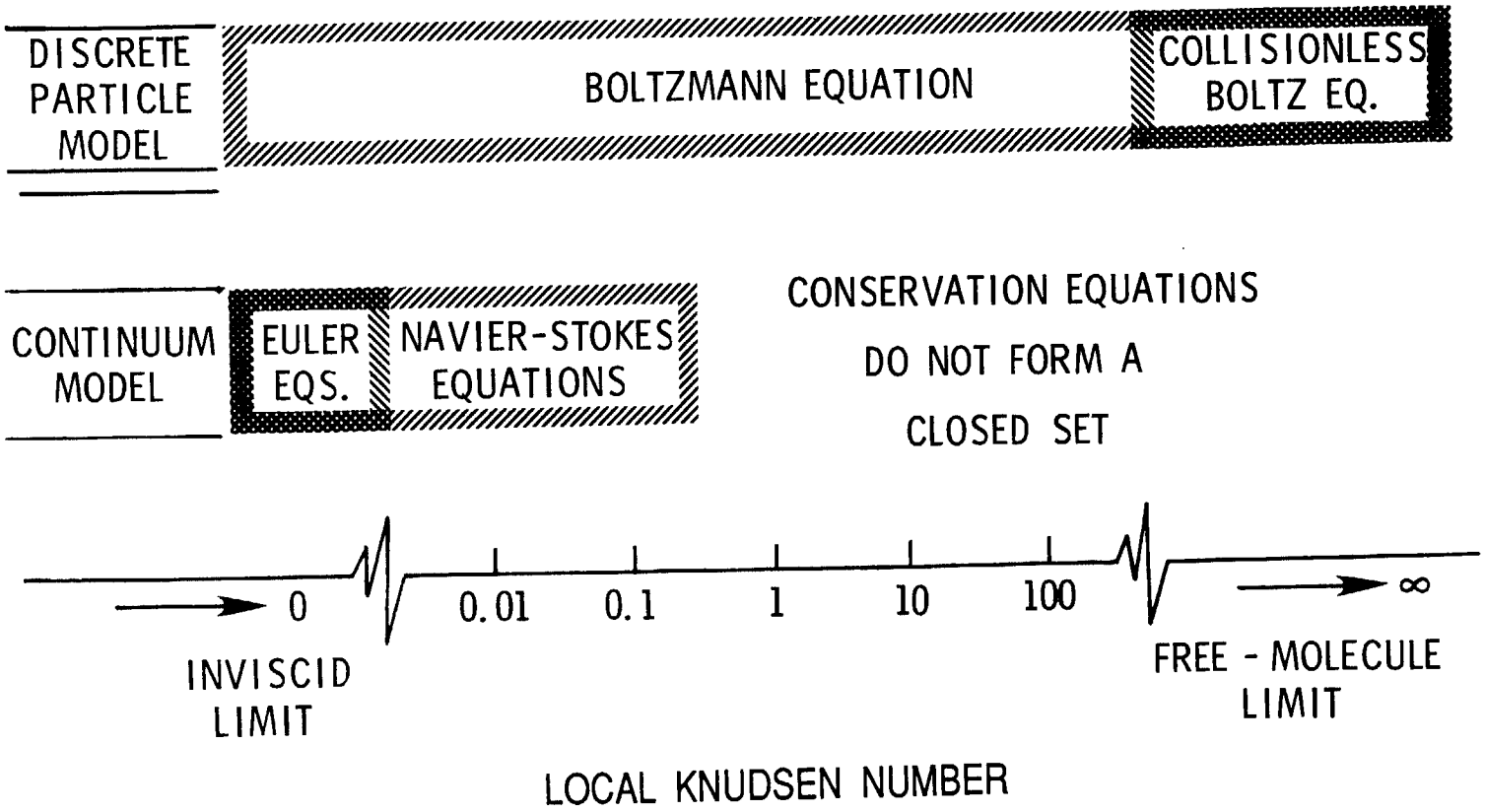

DIRECT SIMULATION MONTE CARLO METHOD

- The Real Gas Flow Is Modeled By Some Thousands Of Simulated Molecules

- The Position Coordinates And Velocity Components Are Stored In The Computer

- The Molecules Are Simultaneously Followed Through Representative Intermolecular Collisions And Boundary Interactions In Simulated Physical Space

DSMC METHOD

- Each simulated molecule represents a large number of real molecules.
- The molecular motion and collisions are uncoupled over a small time step.
- The relative locations of molecules in physical space cells are disregarded in the selection of collision pairs.
- The computational time can be directly proportional to the number of simulated molecules.

COMPUTATIONAL DOMAIN

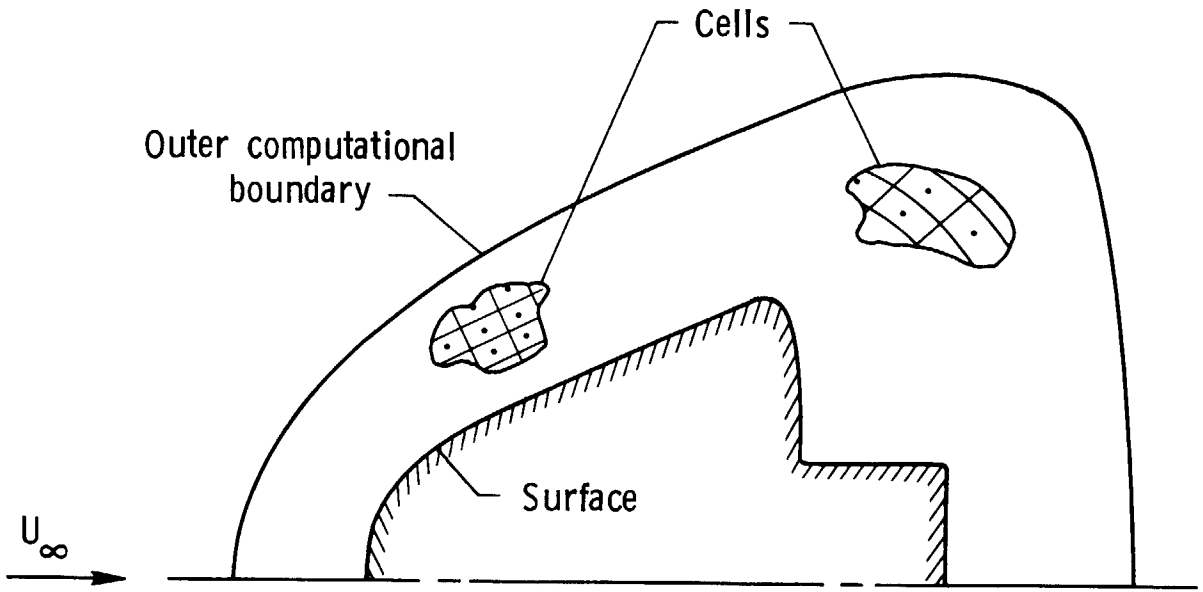

REAL AIR MODEL

- Elastic collisions
  Variable diameter Hard Sphere (VHS)

- Rotation and vibration
  Larsen-Borgnakke model

- Chemical reactions
  Collision theory with reactive cross sections from continuum rate constants

- Thermal radiation (bound-bound)
  Electronic state distribution from analog of Larsen-Borgnakke method. Mean radiative lifetime from data. Finite absorption cross-section

AFE FLIGHT CONFIGURATION

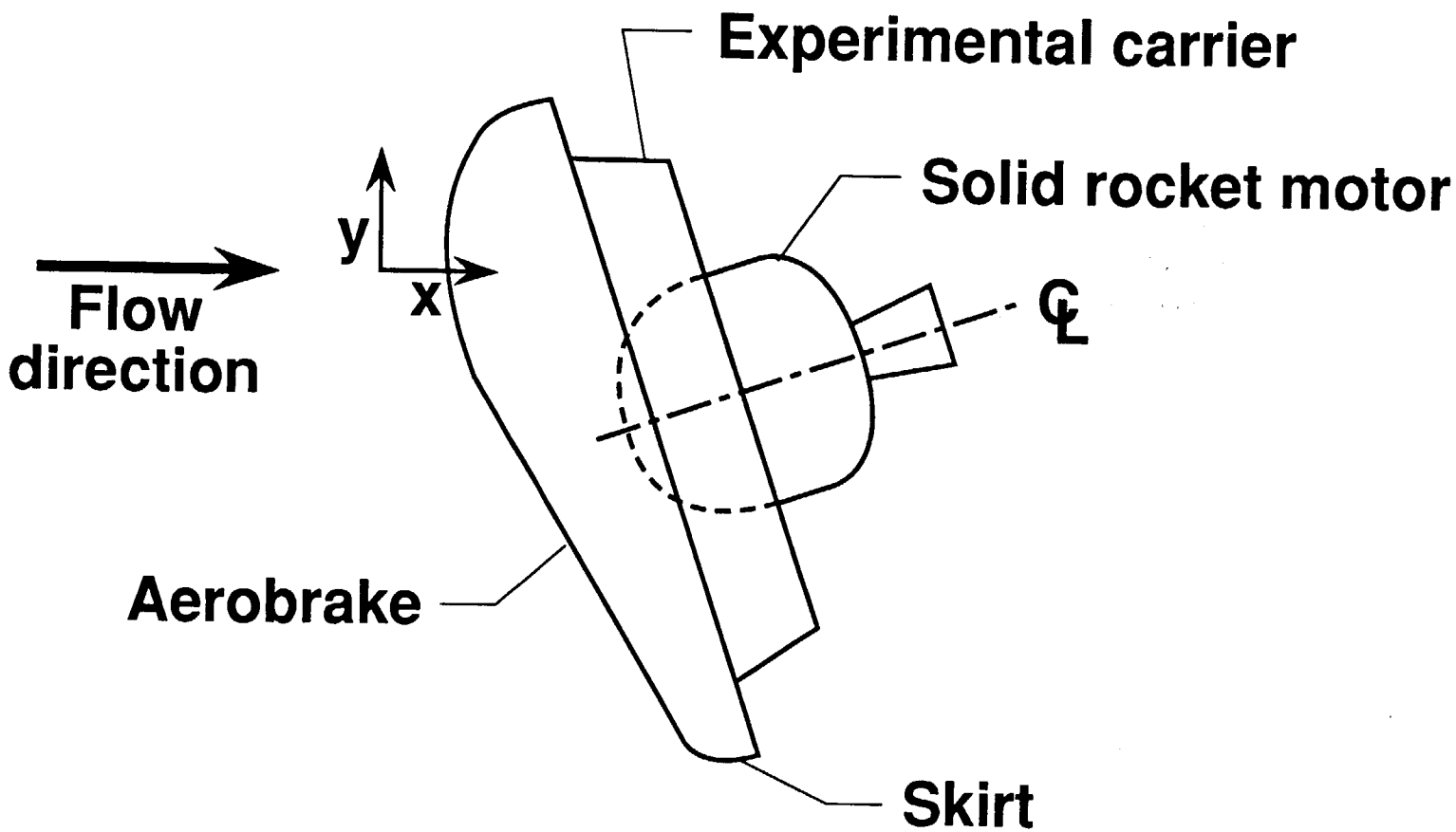

COMPUTATIONAL GRID

Alt = 120 km

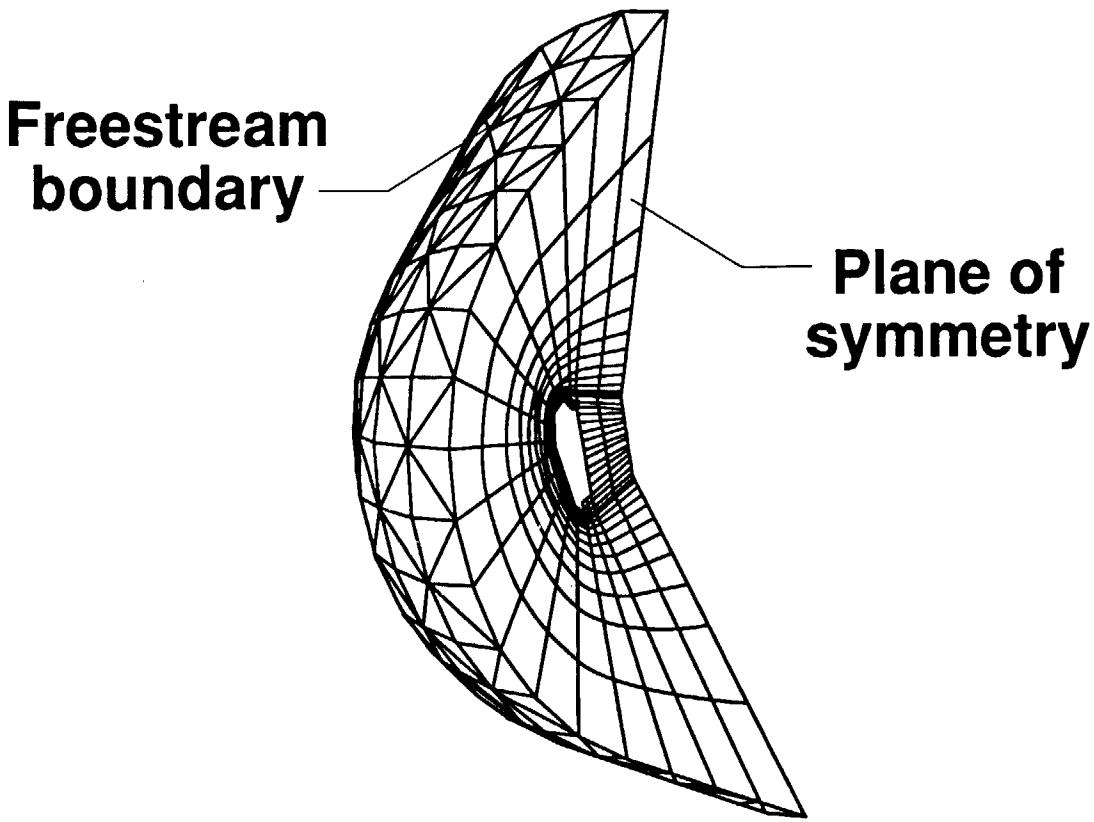

SURFACE HEAT TRANSFER RATE DISTRIBUTIONS

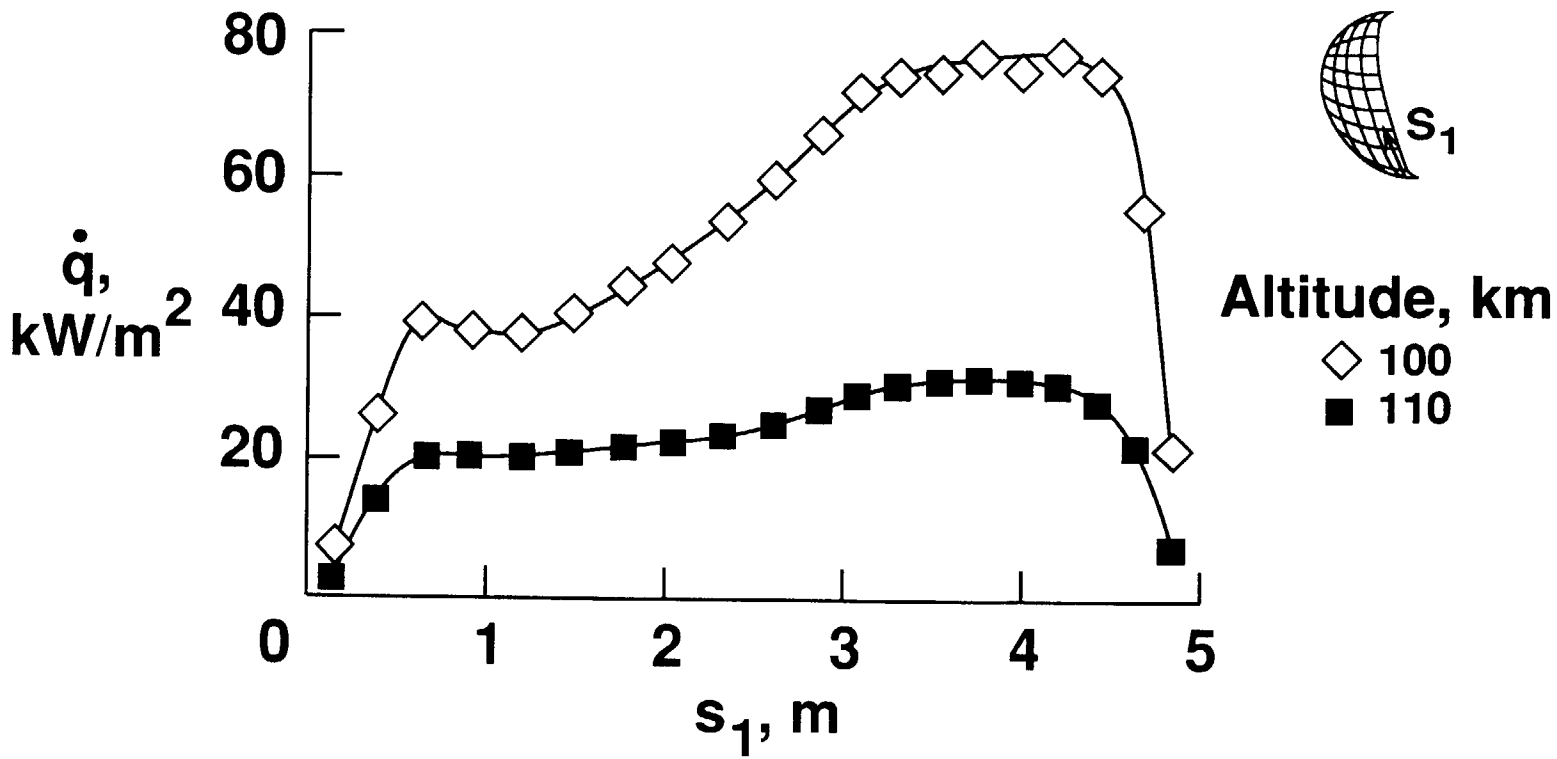

TRANSLATIONAL TEMPERATURE CONTOURS FOR AFE FLOWFIELD

Alt = 120 km

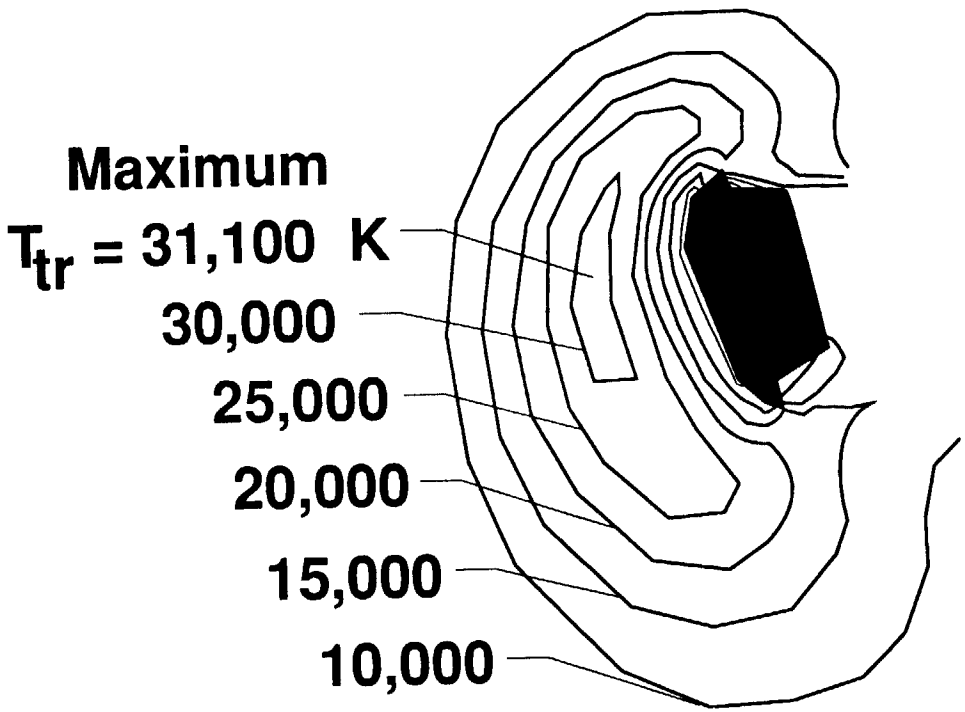

INTERNAL TEMPERATURE CONTOURS FOR AFE FLOWFIELD

Alt = 120 km

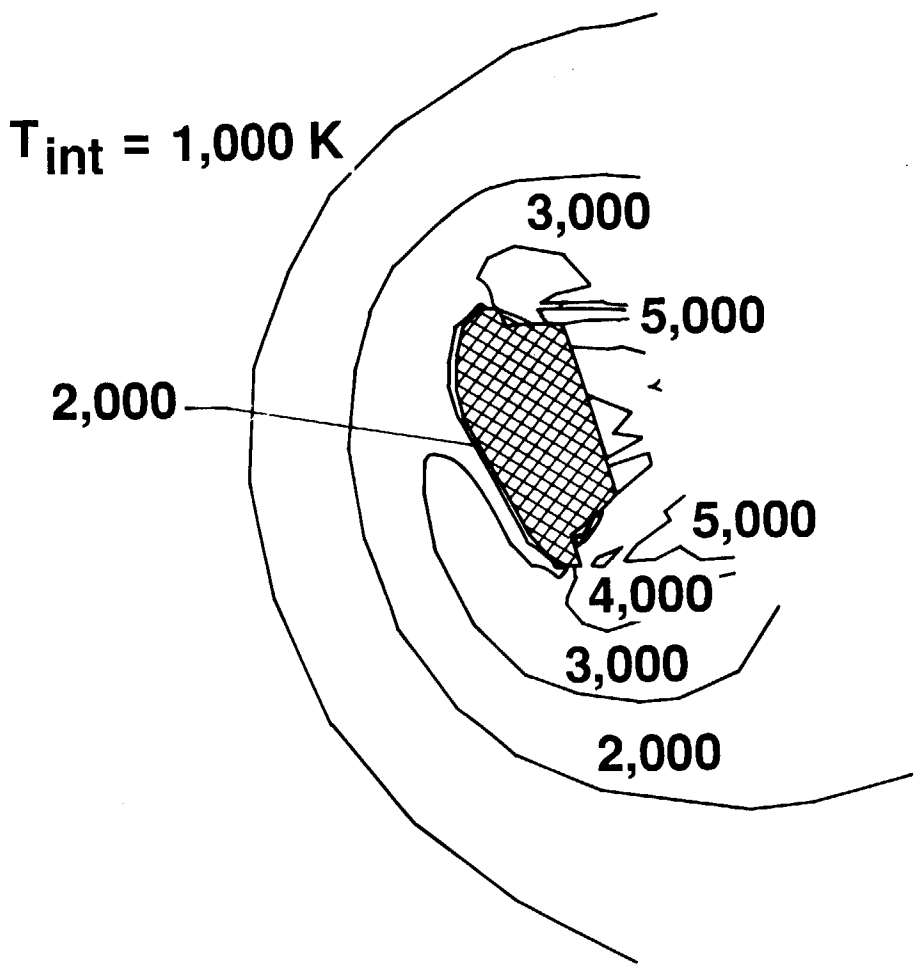

L/D VARIATION

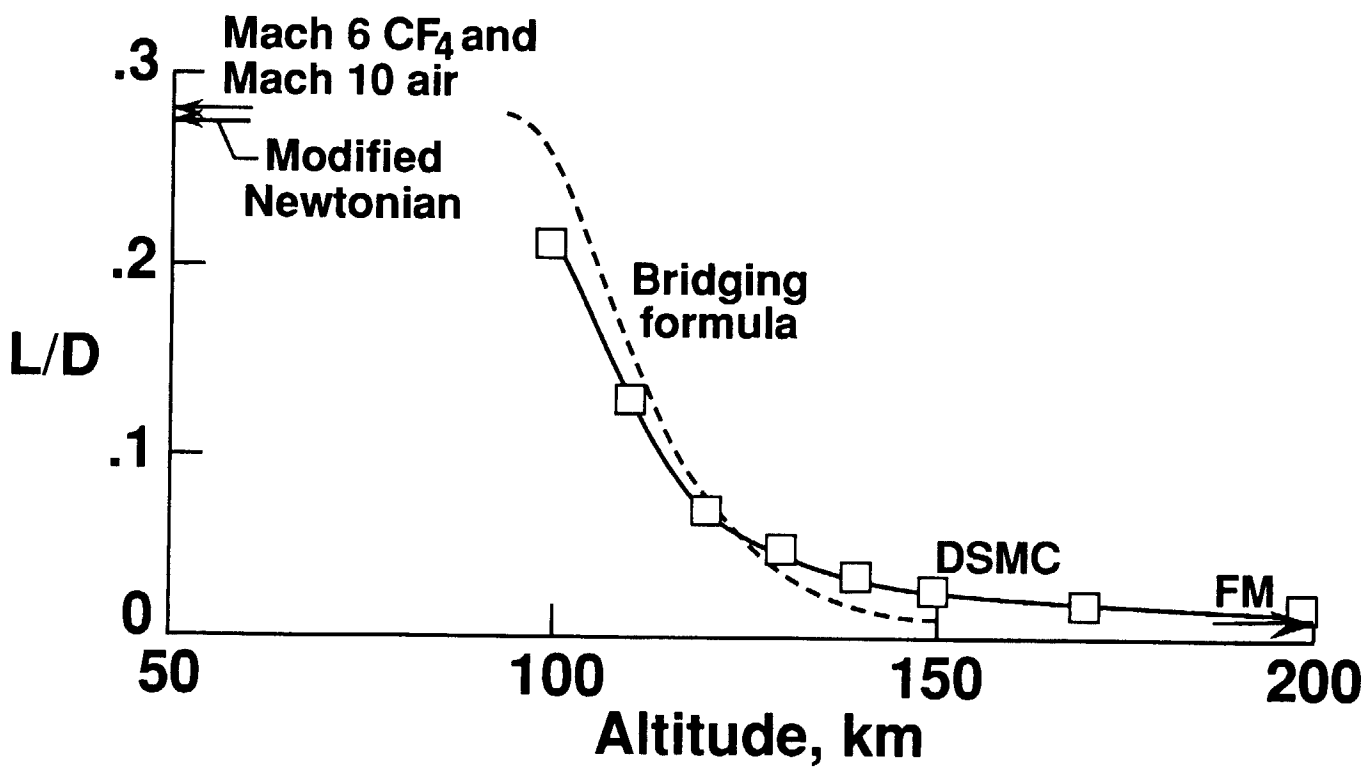

TEMPERATURE PROFILES

Alt = 78 km, U_∞ = 9.1 km/s

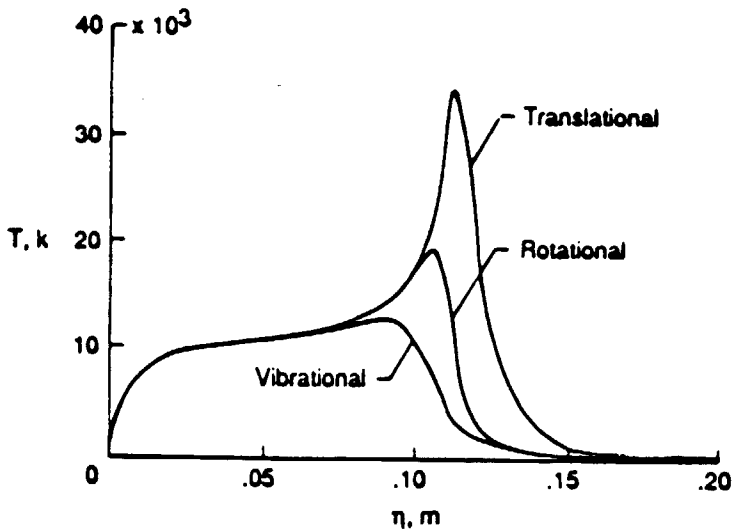

Alt = 90 km, U_∞ = 9.9 km/s

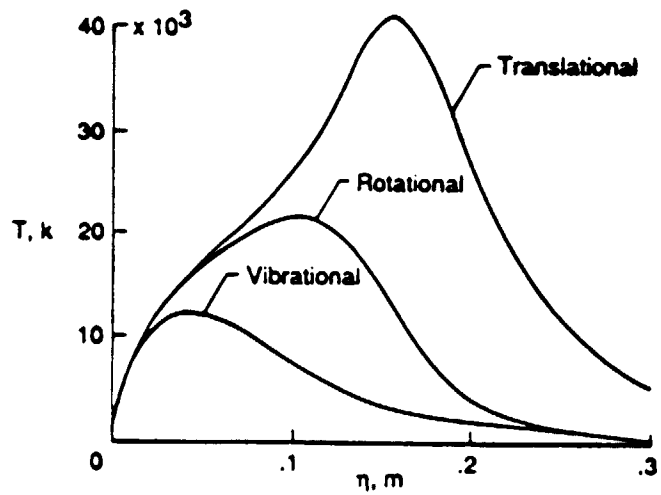

ORIGINAL PAGE IS
OF POOR QUALITY

MOLE FRACTION DISTRIBUTIONS

Alt = 78 km, U_∞ = 9.1 km/s

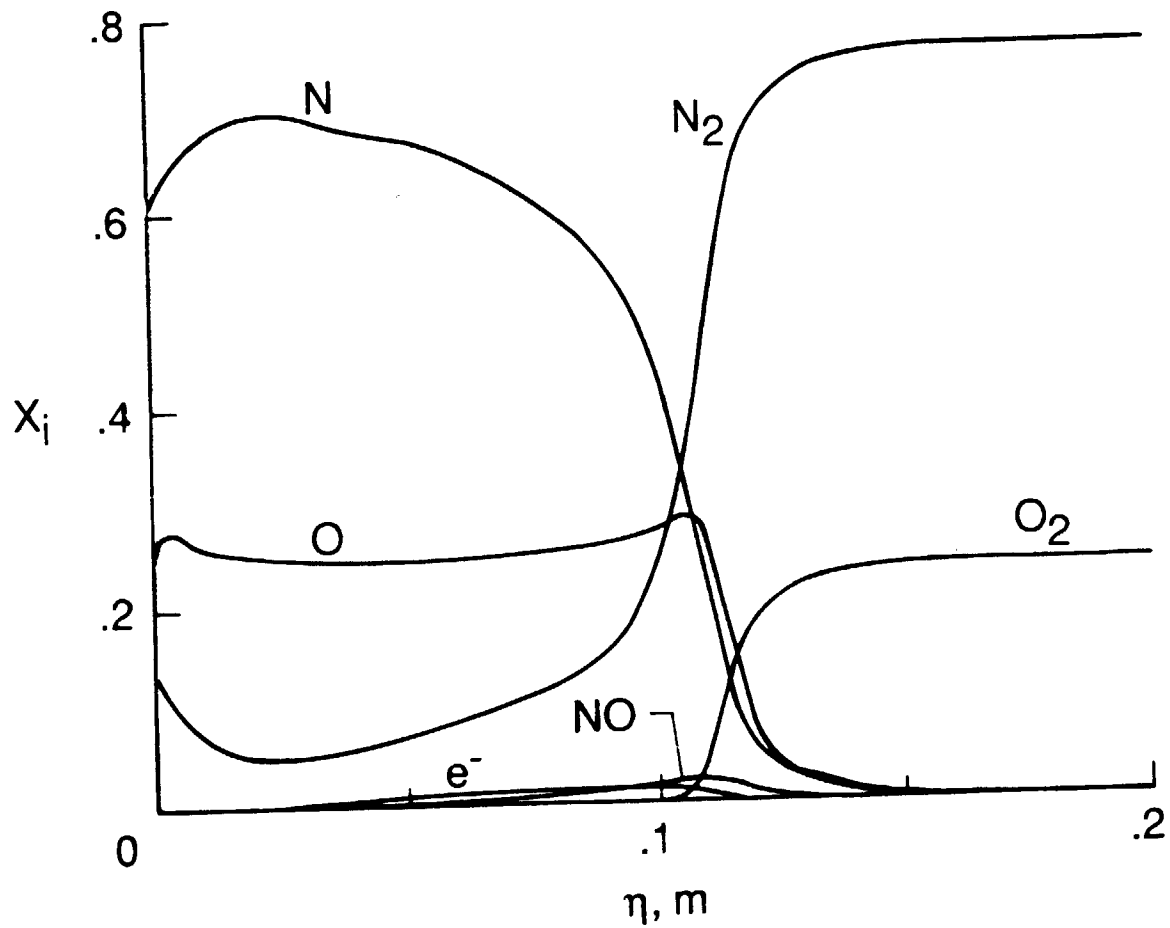

APPENDIX

LIST OF ATTENDEES

John J. Adamczyk
NASA Lewis Research Center
MS 5-9
Cleveland, OH 44135

Ramesh K. Agarwal
McDonnell Douglas
Research Laboratories
P.O. Box 516
Department 222, Building 110, MS4
St. Louis, MO 63166

James A. Albers
NASA Ames Research Center
MS 200-3
Moffett Field, CA 94035

Chris Atwood
MCAT Institute
NASA Ames Research Center
MS 258-1
Moffett Field, CA 94035

James D. Baeder
NASA Ames Research Center
MS 258-1
Moffett Field, CA 94035

Don Bai
NASA/MSFC
Mail Code ED55
Huntsville, AL 35812

Bala Balakrishnan
MCAT Institute
NASA Ames Research Center
MS 258-1
Moffett Field, CA 94035

Daniel W. Barnette
Sandia National Laboratories
P.O. Box 5800, Organization 1556
Albuquerque, NM 87185

Tim Barth
NASA Ames Research Center
MS 202A-1
Moffett Field, CA 94035

Richard A. Batchelder
McDonnell Douglas
Space Systems Co.
5301 Bolsa Avenue
Station 13-3
Huntington Beach, CA 92647

John T. Batina
NASA Langley Research Center
MS 173
Hampton, VA 23665

Oktay Baysal
NASA Langley Research Center
MS 170
Hamtpon, VA 23665

Brad Bennett
MCAT Institute
NASA Ames Research Center
MS 258-1
Moffett Field, CA 94035

Thomas J. Benson
NASA Lewis Research Center
MS 5-7
Cleveland, OH 44135

Robert F. Bergholz
GE Aircraft Engines
1 Neumann Way
Cincinnati, OH 45215

John Bertin
DFAN
U. S. Air Force Adacemy, CO 80840

Ishwar C. Bhateley
General Dynamics
Fort Worth Division
P. O. Box 748, Mail Stop 28-70
Fort Worth, TX 76101

Sedat Birigen
University of Colorado–Boulder
College of Engineering and Applied Science
Boulder, CO 80309

F. G. Blottner
Sandia National Laboratories
P. O. Box 5800, Organization 1556
Albuquerque, NM 87185-5800

Thomas C. Blum
Boeing Advanced Systems
P.O. Box 3707, MS 33-18
Seattle, WA 98124-2207

Brian Bochsch
General Dynamics/Convair
P.O. Box 85357
MS 36-1240
San Diego, CA 92138

Edwin Brewer
NASA/MSFC
Mail Code ED32
Huntsville, AL 35812

David L. Burrus
G.E. Aircraft Engines
1 Neumann Way
Cincinnati, OH 45215

Richard J. Busch, Jr.
Northrop Aircraft Division
One Northrop Avenue
MS 3731/89
Hawthorne, CA 90250

George Callas
NASA Ames Research Center
MS 233-14
Moffett Field, CA 94035

Richard L. Campbell
NASA Langley Research Center
MS 294
Hampton, VA 23665

Graham Candler
NASA Ames Research Center
MS 230-2
Moffett Field, CA 94035

Graham Carey
University of Texas at Austin
CFD Laboratory
ASE-EM Department, WRW 305
Austin, TX 78712

Mark H. Carpenter
NASA Langley Research Center
MS 156
Hampton, VA 23665

James E. Carter
United Technologies Research Center
MS 20 - Silver Lane
East Hartford, CT 06108

Steve Caruso
Nielsen Engineering
510 Clyde Avenue
Mountain View, CA 94043

Neal M. Chaderjian
NASA Ames Research Center
MS 258-1
Moffett Field, CA 94035

Denny S. Chaussee
NASA Ames Research Center
MS 258-1
Moffett Field, CA 94035

Kalpana Chawla
MCAT Institute
NASA Ames Research Center
MS 258-1
Moffett Field, CA 94035

C. S. Chen
NASA Ames Research Center
MS T031
Moffett Field, CA 94035

Lee-Tzong Chen
McDonnell Douglas
3855 Lakewood Blvd.
Long Beach, CA 90846

Lester Cheng
Boeing Military Company
P.O. Box 7730, MS K13-00
Wichita, KS 67277-7730

Bob Childs
Nielsen Engineering
510 Clyde Avenue
Mountain View, CA 94043

Roderick V. Chima
NASA Lewis Research Center
21000 Brookpark Road, MS 5-11
Cleveland, OH 44135

Tawit Chitsomboon
NASA Langley Research Center
MS 168
Hampton, VA 23665

Ing-Tsau Chiu
NASA Ames Research Center
MS 258-2
Moffett Field, CA 94035

Lynn C. Chou
NASA/MSFC
Mail Code ED32
Huntsville, AL 35812

Wei J. Chyu
NASA Ames Research Center
MS 227-6
Moffett Field, CA 94035

Thomas J. Coakley
NASA Ames Research Center
MS 229-1
Moffett Field, CA 94035

Stuart D. Connell
General Electric Co.
Mail Drop A323
8500 Govenors Hill Drive
Cincinnati, OH 45249

Gary B. Cosentino
NASA Ames Research Center
MS 227-6
Moffett Field, CA 94035

Russell M. Cummings
NASA Ames Research Center
MS 258-1
Moffett Field, CA 94035

Leo Dadone
Boeing Vertol Company
P.O. Box 16858, MS Pd32-74
Philadelphia, PA 19142

Carol Davies
NASA Ames Research Center
MS 230-3
Moffett Field, CA 94035

Sanford Davis
NASA Ames Research Center
MS 260-1
Moffett Field, CA 94035

George S. Deiwert
NASA Ames Research Center
MS 230-2
Moffett Field, CA 94035

Robert A. Delaney
GMC Allison Gas Turbine Division
P.O. Box 420 (Speed Code S46)
Indianapolis, IN 46206

D. Doran
NASA/MSFC
Mail Code Ed32
Huntsville, AL 35812

Henry S. Dresser
Rockwell International
125 Ruby Avenue
Balboa Island, CA 92662

Douglas L. Dwoyer
NASA Langley Research Center
MS 256
Hampton, VA 23665

Gordon Erlebacher
NASA Langley Research Center
MS 156
Hampton, VA 23665

Ian Fejtek
NASA Ames Research Center
MS T-031
Moffett Field, CA 94035

Jolen Flores
NASA Ames Research Center
MS 258-1
Moffett Field, CA 94035

James A. Franklin
NASA Ames Research Center
MS 211-2
Moffett Field, CA 94035

Douglas M. Friedman
McDonnell Douglas
3855 Lakewood Boulevard, MS 36-81
Long Beach, CA 90846

Robert Garcia
NASA/MSFC
Mail Code ED32
Huntsville, AL 35812

Sharad Gavali
Amdahl
1250 E. Arquez Avenue.
MS 265, P.O. Box 3470
Sunnyvale, CA 94088-3470

Steve Gegg
NASA Ames Research Center
MS 258-1
Moffett Field, CA 94035

Michael W. George
Rockwell International Corporation
201 N. Douglas Street
P.O. Box 92098, MS-GB12
Los Angeles, CA 90009

Farhad Ghaffari
NASA Langley Research Center
MS 294
Hampton, VA 23665

Leslie Glatt
TRW
One Space Park, MS R1/1038
Redondo Beach, CA 90278

Peter Gnoffo
NASA Langley Research Center
MS 366
Hampton, VA 23665-5225

Tahir Gokcen
Stanford University
Department of Aeronautics and Astronautics
Stanford, CA 94305

John Goodrich
NASA Lewis Research Center
MS 5-7
Cleveland, OH 44135

Peter M. Goorjian
NASA Ames Research Center
MS 258-1
Moffett Field, CA 94035

Randolph A. Graves, Jr.
NASA Headquarters
Code RF
Washington, DC 20546

Michael Green
NASA Ames Research Center
MS 258-1
Moffett Field, CA 94035

Lisa Griffin
NASA Marshall Space Flight Center
Mail Code ED32
Huntsville, AL 35812

Anthony R. Gross
NASA Ames Research Center
MS 258-3
Moffett Field, CA 94035

Clyde Gumbert
NASA Langley Research Center
MS 159
Hampton, VA 23665

Guru P. Guruswamy
NASA Ames Research Center
MS 258-1
Moffett Field, CA 94035

Raimo Hakkinen
McDonnell Douglas Research Laboratories
Department 222, Building 110
P.O. Box 516
St. Louis, MO 63166

Dean C. Hammond, Jr.
General Motors Research Laboratories
FM/57, 30500 Mound Road
Warren, MI 48090-9055

Taeyoung Han
General Motors Research Laboratories
FM/57, 30500 Mound Road
Warren, MI 48090-9055

H. A. Hassan
North Carolina State University
Mechanical and Aerospace Engineering
Raleigh, NC 27695-7910

Bob Henke
Boeing Commercial Airplane Company
P.O. Box 3707
Seattle, WA 98124-2207

Kristin A. Hessenius
NASA Ames Research Center
MS 200-4
Moffett Field, CA 94035

Paul Hickey
Gulfstream Aerospace Corporation
P.O. Box 2206, D-04 Department 895
Savannah, GA 31402-2206

Terry L. Holst
NASA Ames Research Center
MS 258-1
Moffett Field, CA 94035

James Horling
Naval Air Propulsion Center
P. O. Box 7176
Trenton, NJ 08628

Tsuying Hsieh
Naval Surface Weapons Center
R44 White Oak, MD

Yu-Kao Hsu
University of Maine
Illinois Avenue
Bangor, ME 04401

Mark Huebler
General Motors Research Laboratories
FM/57, 30500 Mound Road
Warren, MI 48090-9055

Dennis L. Huff
NASA Lewis Research Center
21000 Brookpark Road, MS 77-6
Cleveland, OH 44135

Danny P. Hwang
NASA Lewis Research Center
MS 100-5, 21000 Brookpark Road
Cleveland, OH 44135

Mamoru Inouye
NASA Ames Research Center
MS 202A-1
Moffett Field, CA 94035

David A. Jacqmin
NASA Lewis Research Center
MS 5-7
Cleveland, OH 44135

Zakaria Jalamani
NASA Ames Research Center
MS 258-1
Moffett Field, CA 94035

Antony Jameson
Princeton University
Mechanical and Aerospace
Engineering Department
Princeton, NJ 08544

Mohan Jayaram
IBM Corporation
MS 276 Neighborhood Road
Kingston, NY 12401

Dennis Jespersen
NASA Ames Research Center
MS 202A-1
Moffett Field, CA 94035

Jeffrey L. Johnson
Sterling Software
NASA Ames Research Center
MS 221-6
Moffett Field, CA 94035

Dennis A. Johnson
NASA Ames Research Center
MS 229-1
Moffett Field, CA 94035

Gary M. Johnson
North Carolina Supercomputing Center
P.O. Box 12732
Research Triangle Park, NC 27709

Max Kandula
Lockheed Engineering and Management
Services Company
2400 NASA Road 1
Houston, TX 77058

Charles Kang
General Dynamics/Convair
P.O. Box 85357, MS 36-1240
San Diego, CA 92138

Lyndell S. King
NASA Ames Research Center
MS 260-1
Moffett Field, CA 94035

John Kreatsoulas
Digital Equipment Corporation
Four Results Way
MR04-2/H19
Marlboro, MA 01752

Sherrie Krist
NASA Langley Research Center
MS 128
Hampton, VA 23665

Thomas Kropp
Sterling Software
1121 San Antonio Road
Palo Alto, CA 94303

Paul Kutler
NASA Ames Research Center
MS 258-3
Moffett Field, CA 94035

C. Lee
NASA Marshall Space Flight Center
Mail Code ED33
Huntsville, AL 35812

Ki D. Lee
University of Illinois
104 South Mathews Avenue
Urbana, IL 61801

Johnson Lee
Sterling Software
NASA Ames Research Center
MS 258-1
Moffett Field, CA 94035

Jerry L. Lee
Boeing Commercial Airplane Company
P.O. Box 3707
MS 7C-36
Seattle, WA 98124-2207

Chien Li
NASA Johnson Space Center
Mail Code ED311
Houston, TX 77058

R. T. Ling
Northrop Aircraft Division
One Northrop Avenue
Department 3811/82
Hawthorne, CA 90250

Meng Liou
NASA Lewis Research Center
MS 5-7
Cleveland, OH 44135

Amalia R. Lopez
Sandia National Laboratories
P.O. Box 5800, Organization 1556
Albuquerque, NM 87185

Paula Lovely
Sterling Software
NASA Ames Research Center
MS 221-6
Moffett Field, CA 94035

Raymond Luh
MCAT Institute
NASA Ames Research Center
MS 258-1
Moffett Field, CA 94035

Robert W. MacCormack
Stanford University
Department of Aeronautics and Astronautics
Stanford, CA 94305

Nateri K. Madavan
Sterling Software
NASA Ames Research Center
MS 258-2
Moffett Field, CA 94035

Mike Madson
NASA Ames Research Center
MS 227-2
Moffett Field, CA 94035

John B. Malone
Bell Helicopter Textron
P.O. Box 482
MS 012681-14
Fort Worth, TX 76101

J. F. Mangus
Northrop Aircraft Division
One Northrop Avenue
Department 3811/82
Hawthorne, CA 90250

Reda Mankbadi
NASA Lewis Research Center
MS 5-11
Cleveland, OH 44135

Fred Martin
NASA Ames Research Center
MS 258-1
Moffett Field, CA 94035

Joseph G. Marvin
NASA Ames Research Center
MS 229-1
Moffett Field, CA 94035

Douglas R. McCarthy
Boeing Commercial Airplane Company
P.O. Box 3707
MS 7C-36
Seattle, WA 98124-2207

William J. McCroskey
U.S. Army
NASA Ames Research Center
MS 258-1
Moffett Field, CA 94035

Susan McMillin
NASA Langley Research Center
MS 170
Hampton, VA 23665

Rabi Mehta
NASA Ames Research Center
MS 260-1
Moffett Field, CA 94035

Unmeel B. Mehta
NASA Ames Research Center
MS 202A-1
Moffett Field, CA 94035

Keith Meintjes
General Motors Research Laboratories
FM/57, 30500 Mound Road
Warren, MI 48090-9055

Robert E. Melnik
Grumman Aerospace Corporation
A08-Plant
35 Corporate Research Center
Bethpage, NY 11714

John Melton
NASA Ames Research Center
MS 227-6
Moffett Field, CA 94035

Joel P. Mendoza
NASA Ames Research Center
MS 227-6
Moffett Field, CA 94035

Clark D. Mikkelsen
USAMICOM
AMSMI-RD-SS-AT
Redstone Arsenal, AL 35898-5252

Brent A. Miller
NASA Lewis Research Center
MS 5-3
21000 Brookpark Road
Cleveland, OH 44135

Kenichi Miura
Fujitsu America, Inc.
MS B2-7
3055 Orchard Drive
San Jose, CA 95134

Greg Molvik
MCAT Institute
NASA Ames Research Center
MS 258-1
Moffett Field, CA 94035

Marianne Mosher
NASA Ames Research Center
MS T031
Moffett Field, CA 94035

James Moss
NASA Langley Research Center
MS 170
Hampton, VA 23665

Shohei Nakazawa
MARC Analysis Research Corporation
260 Sheridan Avenue.
Palo Alto, CA 94306

Jim C. Narramore
Bell Helicopter Textron
P.O. Box 482
MS 012681-14
Fort Worth, TX 76101

Ejike Ndefo
Aerospace Corporation
P.O. Box 92957 (M4/964)
Los Angeles, CA 90009-2957

Charles J. Nietubicz
U. S. Army Ballistic Research Laboratory
Computational Aerodynamics Branch
Aberdeen Proving Ground, MD 21005

Shigeru Obayashi
NASA Ames Research Center
MS 258-1
Moffett Field, CA 94035

Stephen Owen
Sikorsky Aircraft
MS B101B
6900 Main Street
Stratford, CT 06601-1381

Michael Papadakis
Wichita State University
Department of Aeronautical Engineering
Wichita, KS 67208

Blaine E. Pearce
CALSPAN Corporation
P.O. Box 400
Buffalo, NY 14225

E. W. Perkins
NASA Ames Research Center
MS 227-6
Moffett Field, CA 94035

Victor L. Peterson
NASA Ames Research Center
MS 200-4
Moffett Field, CA 94035

M. Potapczuk
NASA Lewis Research Center
MS 86-7
Cleveland, OH 44135

Louis A. Povinelli
NASA Lewis Research Center
21000 Brookpark Road
MS 5-3
Cleveland, OH 44135

Thomas Pulliam
NASA Ames Research Center
CFD Branch
Moffett Field, CA 94035

Man Mohan Rai
NASA Ames Research Center
MS 258-1
Moffett Field, CA 94035

Rich Raiford
Northrop Aircraft Division
One Northrop Avenue
Department 3811/82
Hawthorne, CA 90250

Pradeep Raj
Lockheed Aeronautical Systems Group
D/75-52, B/63
Burbank, CA 91520-7552

Pamela Richardson
NASA Langley Research Center
MS 156
Hampton, VA 23665

Michael Riger
Utra Network Technologies
101 Daggett Drive
San Jose, CA 95134

Michael D. Rivers
Stellar Computer Inc.
920 Hillview Court
Suite 180
Milpitas, CA 95035

Arthur W. Rogers
Hughes Aircraft Company
P. O. Box 35085
Los Angeles, CA 90035

Stuart Rogers
Sterling Software
NASA Ames Research Center
MS 258-1
Moffett Field, CA 94035

Richard Roloff
Alliant Computer Systems
One Monarch Drive
Littleton, MA 01460

Harold Rosenstein
Boeing Vertol Company
P. O. Box 16858
MS P32-74
Philadelphia, PA 19142

Karl P. Rowley
Evans and Sutherland
1808 N. Shoreline Blvd.
Mountain View, CA 94043

Paul E. Rubbert
The Boeing Company
MS 7C-36
P.O. Box 3707
Seattle, WA 98124-2207

David H. Rudy
NASA Langley Research Center
MS 156
Hampton, VA 23665

Leonidas Sakell
AFOSR/NA
Bolling AFB
Wahington, DC 20332-6448

Manuel D. Salas
NASA Langley Research Center
MS 159
Hamtpon, VA 23665-5225

Jose M. Sanz
NASA Lewis Research Center
21000 Brookpark Road
MS 5-11
Cleveland, OH 44135

Dale Satran
NASA Headquarters
Code RF
Washington, Dc 20546

Michael J. Schuh
NASA Ames Research Center
MS 227-6
Moffett Field, CA 94035

Catherine H. Schulbach
NASA Ames Research Center
MS 233-14
Moffett Field, CA 94035

Luke A. Schutzenhofer
NASA Marshall Space Flight Center
Mail Code ED 32
Huntsville, AL 35812

Joseph Shang
Air Force Wright Aeronautical Laboratories
AFWAL/FIMM
Wright-Patterson AFB, OH 45433

Vijaya Shankar
Rockwell International Science Center
1049 Camino Dos Rios
Thousand Oaks, CA 91360

Chih-Fang Shieh
Rohr Industries, Inc.
P.O. Box 878
Foot of H Street
Chula Vista, CA 92012

Munir M. Sindir
Rockwell International Corporation
Rocketdyne Division
6633 Canoga Avenue, MS AC56
Canoga Park, CA 91303

Jeff Slotnick
Lockheed Engineering and Sciences Company
2400 NASA Road 1
Houston, TX 77058

Leigh Ann Smith
NASA Langley Research Center
MS 125
Hampton, VA 23665

Robert E. Smith
NASA Langley Research Center
MS 125
Hampton, VA 23665

Jerry C. South, Jr.
NASA Langley Research Center
MS 103
Hampton, VA 23665

Sharon Stanaway
MCAT Institute
NASA Ames Research Center
MS 258-1
Moffett Field, CA 94035

Joseph Steger
NASA Ames Research Center
MS 258-1
Moffett Field, CA 94035

Daniel Strash
Analytical Methods, Inc.
2133 152nd Avenue N.E.
Redmond, WA 98052

Paul M. Stremel
NASA Ames Research Center
MS TR31
Moffett Field, CA 94035

Robert M. Stubbs
NASA Lewis Research Center
21000 Brookpark Road
MS 5-11
Cleveland, OH 44135

S. V. Subramanian
AVCO Lycoming - Textron
550 Main Street
Stratford, CT 06497

Richard L. Sun
Chrysler Motors Corporation
(Aero. Department)
15863 W. 11 Mile Road, #108
Southfield, MI 48076

Daniel Y. Sung
Sterling Software
NASA Ames Research Center
MS 221-6
Moffett Field, CA 94035

Julie M. Swisshelm
NASA Ames Research Center
MS 258-5
Moffett Field, CA 94035

Kan Szalai
NASA Ames Research Center
MS 200-1
Moffett Field, CA 94035

Choon S. Tan
Massachusetts Institute of Technology
MS 31-267
77 Massachusetts Avenue
Cambridge, MA 02139

Yehuda Tassa
Lockheed Missiles & Space Company
3251 Hanover Street
Palo Alto, CA 94304

Michael E. Tauber
NASA Ames Research Center
MS 230-2
Moffett Field, CA 94035

Jim Thomas
NASA Langley Research Center
MS 128
Hampton, VA 23665

Scott Thomas
Sterling Software
NASA Ames Research Center
MS 258-1
Moffett Field, CA 94035

Kevin Thompson
NASA Ames Research Center
MS 245-3
Moffett Field, CA 94035

Edward N. Tinoco
The Boeing Company
P.O. Box 3707, MS 7C-36
Seattle, WA 98124-2207

David Alan Treiber
Boeing Advanced Systems
P.O. Box 3707, MS 33-17
Seattle, WA 98124-2207

Wei W. Tseng
Naval Air Develoment Center
Code 6051
Warminster, PA 18974-5000

Kenji Uenishi
General Electric Aircraft Engines
A304 - 1 Neumann Way
Cincinnati, OH 45215-6301

Johannes M. Van Aken
University of Kansas
NASA Ames Research Center
MS TR031
Moffett Field, CA 94035

William R. Van Dalsem
NASA Ames Research Center
MS 258-1
Moffett Field, CA 94035

U.S. Government Printing Office
1989-785-524

NASA
National Aeronautics and Space Administration

Report Documentation Page

1. Report No. NASA CP-10038	2. Government Accession No.	3. Recipient's Catalog No.
4. Title and Subtitle NASA Computational Fluid Dynamics Conference Volume 2: Sessions VII-XII		5. Report Date September 1989 6. Performing Organization Code
7. Author(s)		8. Performing Organization Report No. A-89160 10. Work Unit No. 505-60-01
9. Performing Organization Name and Address Ames Research Center Moffett Field, CA 94035		11. Contract or Grant No.
12. Sponsoring Agency Name and Address National Aeronautics and Space Administration Washington, DC 20546-0001		13. Type of Report and Period Covered Conference Publication 14. Sponsoring Agency Code

15. Supplementary Notes

Point of Contact: Dale Satran, NASA Headquarters, Code RF, Washington, D.C. 20546
(202) 453-2828 or FTS 453-2828

16. Abstract

This publication is a collection of the presentations given at the NASA Computational Fluid Dynamics (CFD) Conference held at NASA Ames Research Center, Moffett Field, California, March 7-9, 1989. The objectives of the conference were to disseminate CFD research results to industry and university CFD researchers, to promote synergy among NASA CFD researchers, and to permit feedback from researchers outside of NASA on issues pacing the discipline of CFD. The focus of the conference was on the application of CFD technology but also included fundamental activities. The conference was sponsored by the Aerodynamics Division, Office of Aeronautics and Space Technology (OAST), NASA Headquarters, Washington, D.C. 20546.

The conference consisted of twelve sessions of papers representative of CFD research conducted within NASA and three non-NASA panel sessions. For each panel session, the panel membership consisted of industry and university CFD researchers. A summary of the comments made during the panel sessions has been included in this publication.

Volume 1 contains the papers given in Sessions I-VI. Volume 2 covers Sessions VII-XII.

17. Key Words (Suggested by Author(s)) Computational fluid dynamics Numerical methods Computational aerodynamics Supercomputing	18. Distribution Statement Unclassified-Unlimited Subject Category -02

19. Security Classif. (of this report) Unclassified	20. Security Classif. (of this page) Unclassified	21. No. of Pages 593	22. Price A25

NASA FORM 1626 OCT 86

For sale by the National Technical Information Service, Springfield, Virginia 22161